THE BIOMECHANICS OF THE ACETABULUM AND ACETABULAR REPLACEMENT

Philip C. Noble

This thesis is submitted in partial fulfillment of the requirements for a degree of Doctor of Philosophy in the Bioengingeering Unit

University of Strathclyde
Glasgow
April 1995

DECLARATION

ACKNOWLEDGMENTS

The work described in this thesis was performed in the Orthopedic Laboratory at the Methodist Hospital in Houston and supported with funding from the Department of Orthopedic Surgery, the Dove Foundation and Howmedica Inc.

The author wishes to express his appreciation for the support and understanding of his wife, Kathy, and his children David and Katherine. He also wishes to acknowledge the guidance of Professor John Paul and Dr. A. C. Nicol of the University of Strathclyde in Glasgow whose support and encouragement was critical to the ultimate success of this work in the face of numerous experimental difficulties.

The optimization technique used to predict muscle forces was developed in cooperation with Mr. Emir Kamaric who wrote the computer program. Mr. Kamaric also performed the measurements of cup micromotion with the assistance of Mr. Vibor Paravic, Mr. Jerry Alexander and Mr. Matthew Collier.

The author is grateful to Mr. Jerry Alexander and Mr. Matthew Collier for their technical assistance with many aspects of the study, primarily data collection and analysis. The author is also indebted to Ms. Mirena Paravic and Ms. Judy Davis for their assistance with the preparation of the manuscript.

The ongoing support of Howmedica Inc. and its employees is greatly appreciated, especially the assistance and encouragement of Mr. Peter van Syckle, Mr. Glen Kashuba, Mr. Matt Poggie, Mr. Tom McCarthy and Mr. Jon Klippel.

ABSTRACT

This thesis describes studies performed to measure the deformation of the human acetabulum during weight bearing. This work is then extended to measure the effect of three surface coatings on the relative motion between the pelvis and cementless acetabular cups.

The soft-tissue and bony anatomy of the hip joint is described with particular attention to the muscles controlling joint motion. An additional chapter is devoted to the biomechanics of gait and electromyographic measurement of muscular activity during normal walking. This is followed by a review of the biomechanics of the hip joint and the contribution of studies performed using instrumented hip prostheses. The author then presents a new approach to the prediction of muscle forces during walking. A conventional engineering analysis is presented relating the intersegmental components of force and moment acting across the hip joint to forces developed by individual muscles during the early stance phase of the gait cycle. Various strategies are employed to solve this indeterminate mechanical problem using data derived from quantitative electromyography, the kinematics and biomechanics of gait and intravital recordings of hip joint forces. Through use of mathematical optimization, a solution is found that is consistent with both the engineering analysis and quantitative electromyographic data.

Experiments are reported utilizing four cadaveric specimens in which the position and loading of the hip joint were recreated using instrumented cables and loading fixtures. Measurements of acetabular deformation are reported at 11 sites on each specimen. These data are recorded on a computer disk which accompanies this thesis. The overall pattern of deformation is found to be consistent with biaxial bending of the pelvis over a fulcrum formed by the femoral head.

The second part of the thesis describes an experiment performed to determine whether external coatings influence the stability of cementless acetabular cups implanted in the acetabulum. A standard design of an acetabular cup is developed on the basis of anatomic studies of cadaveric pelves. Experiments are described using cups with three external coatings: spherical Co-Cr beads, plasma-sprayed titanium and

hydroxyapatite. These components were implanted into the acetabuli of five fresh cadaveric pelves and loaded in three-point bending. Interface motion was measured at the dome, the acetabular floor and the cotyloid notch of each specimen during loading to 2000 N. The results of this study are recorded on a computer disk (see Appendix). These data showed that the surface coating dramatically influences the interface motion of acetabular cups. Implant motion was found to be site-specific and appeared to be determined, primarily, by the interaction of elastic deformation of the pelvis and frictional conditions at the shell/bone interface.

TABLE OF CONTENTS

COMPUTER DISK: INSTRUCTIONS FOR ACCESSING DATA FILES

Experimental data describing measurements of the deformation of the pelvic specimens and the acetabular analogue are contained on the computer disk that accompanies this thesis. All data are contained within the following files:

1. Acetabular Analogue Deformation.

   This file contains measurements describing the deformation of the acetabular analogue. Transducer measurements are reported at 15 sites on the surface of the analogue for transacetabular hole diameters of 0, 3, 5 and 7 mm. The corresponding values of deformation and effective strain are also tabulated. Further details appear in chapter 9.

2. Pelvic Deformation

   This file contains all measurements of deformation recorded using fresh cadaveric pelves. The data are reported at 11 measurement sites in four specimens. Values of transducer output, deformation and effective strain are also tabulated. Further details appear in chapter 6.

All data are stored in spreadsheet files within Microsoft Excel 5.0 (Macintosh version).

INTRODUCTION

The pelvis and acetabulum posses unique morphologic and biomechanical properties due to the large forces supported by the hip joint during walking and the unusual sandwich construction of the pelvis. There have been surprisingly few experimental studies of the load-bearing response of the acetabulum, in part, because of the complexity of muscle loading and the theoretical difficulties associated with simulating the loads supported by the hip joint during financial activities. Nonetheless, several investigators have developed cadaveric models of the hip with representation of the weight of the trunk and several muscle forces sufficient to develop static equilibrium.

Information concerning the loading and deformation of the acetabulum would be invaluable to our understanding of several fundamental orthopedic problems. Previous authors have speculated that the acetabulum is relatively flexible and undergoes deflections of several hundred microns during normal activities, though proof of these speculations are elusive. Nonetheless, experimental studies of the biomechanics of load transmission across the hip joint suggests an interplay is present between the inherent incongruity of the acetabulum and the femoral head and deformation of the acetabulum with load-bearing.

In early experiments of the etiology of osteoarthritis, Radin and coworkers showed that degenerative changes in the cartilage of the hip joint were related to sclerosis of the subchondral bone of the acetabulum with changes in its structural stiffness. This suggests that acetabular deformation and the health of the articular cartilage may be interrelated. Surgical reconstruction of the hip joint is also influenced by our understanding of acetabular loading patterns. Operative procedures performed to stabilize acetabular fractures, increase coverage of the femoral head or to repair bony defects of the acetabular rim all depended upon an appreciation of the direction and magnitudes of forces crossing the hip joint.

Prosthetic replacement of the hip joint is also critically affected by the response of the acetabulum to load-bearing. Due to the mixed results

experienced with cemented fixation of acetabular cups, cementless acetabular fixation has become predominant, especially in the United States. However, it is now becoming apparent that some long term complications of this mode of fixation, especially the osteolytic response of the acetabulum to polymeric wear debris, is influenced by the presence of fibrous tissue at the cup/bone interface. As the type of tissue surrounding cementless prostheses is determined by the magnitude of implant/bone motion, the elasticity of the acetabulum may significantly impact the longevity of these prosthetic devices.

This thesis is a compilation of several investigations that were performed in an attempt

(i) to develop an experimental model to simulate the loading of the pelvis during walking

(ii) to determine the magnitude and distribution of deformation of the acetabulum during the stance phase of the gait cycle

(iii) to determine the magnitude and distribution of relative motion between the acetabulum and a prosthetic component, and

(iv) to investigate whether the micromotion of acetabular prostheses can be attributed to the 'physiologic' flexibility of the pelvis

CHAPTER 1. THE ANATOMY OF THE PELVIS AND THE HIP JOINT

1.1 THE DESIGN OF NATURAL JOINTS

Natural joints consist of several different biological structures acting in concert to perform the functions of load-bearing and motion. Joints allow bones to support loads and still move with minimal frictional loss and virtually no wear of the articulating surfaces. This remarkable performance is achieved through a composite skeletal structure. The primary, load-bearing function of each bone is performed by a tubular cortex consisting of a hard elastic matrix of calcified collagen. This mineralized framework is deposited in response to the dynamic strain field developed within the tissue in order to achieve the most efficient engineering structure for transmission of loads. At the ends of each bone, a hard external shell is internally supported by cancellous (spongy) bone, consisting of a network of trabeculae aligned with the local principal stress direction; this again results in the most efficient distribution of bone mineral and reduced total skeletal weight. To enable joints to move smoothly while transmitting large loads, the articulating surfaces at the ends of each bone are coated with a layer of cartilage, lubricated with synovial fluid. This results in an articulation which moves with minimal friction under a broad range of conditions of varying joint loads and sliding speeds.

The function of joints can be compromised by numerous factors, including trauma, disease processes and abnormal loading. Degeneration of the joint or osteoarthrosis is one of the commonest conditions leading to joint replacement and is associated with progressive restriction of joint movement, stiffness and severe pain on movement. This condition becomes increasingly common with advancing age. Numerous palliative methods are available to treat the symptoms of joint degeneration, but once relief is no longer obtained from non-operative measures, prosthetic replacement of the articulating surfaces is often recommended to restore the pain-free function which the patient desires. This definitive method of treating the symptoms of osteoarthrosis has become extremely popular, to the extent that over 400,000 total joint arthroplasties are performed throughout the world each year.

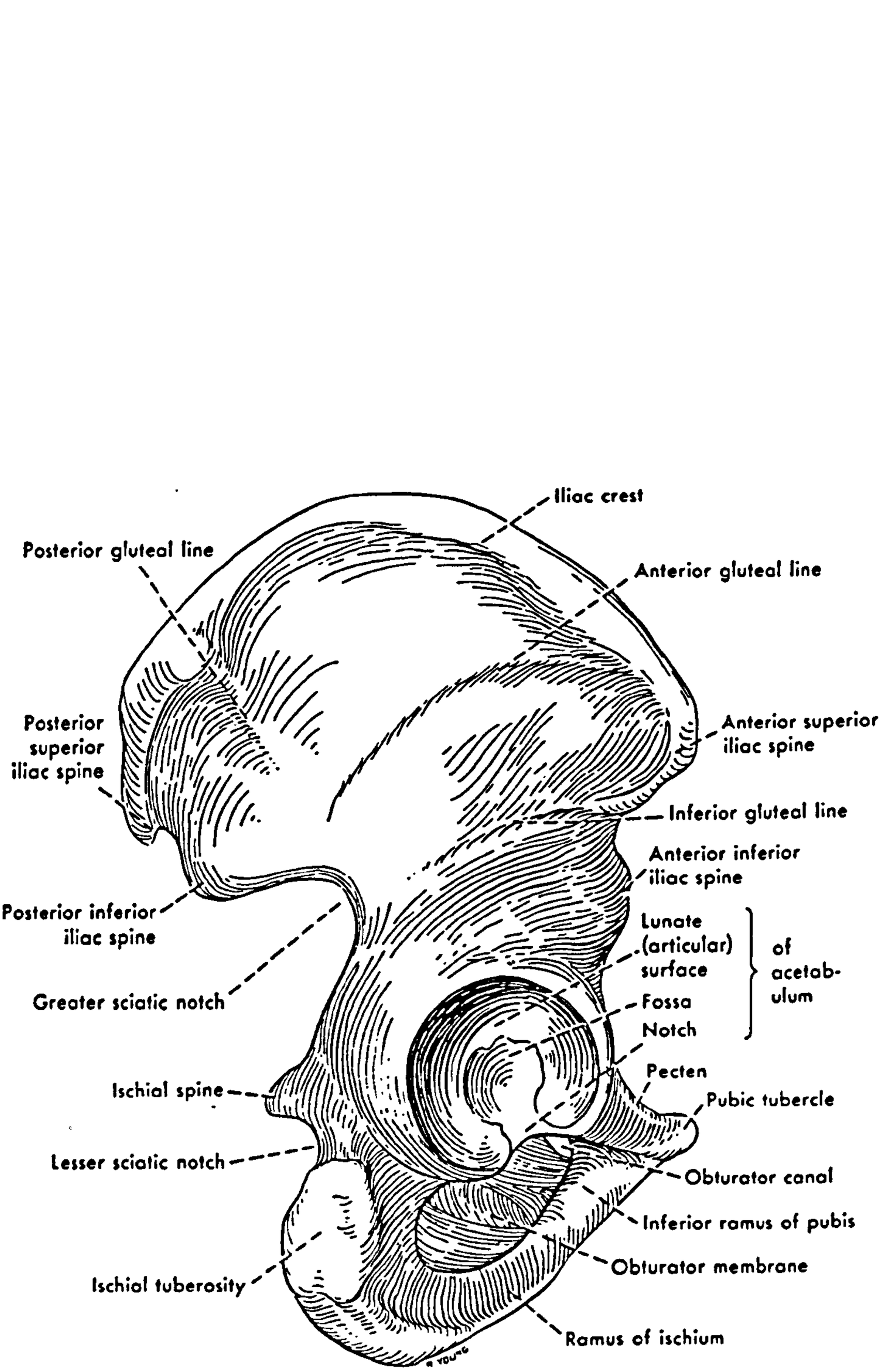

Figure 1.1 The lateral (outer) surface of the right coxa of the pelvis, showing bony landmarks (from Hollinshead and Rosse, 1985).

1.2 THE BONY STRUCTURES OF THE HIP JOINT

The essential mechanical function of the pelvic girdle is to transmit forces from the axial skeleton to the lower extremities through the hip joints. The pelvis itself consists of four bones: the right and left innominate bones or coxae, the sacrum and the coccyx (Hollinshead, 1969). The sacrum forms the posterior part of the pelvic ring and is connected to the lumbar vertebrae and the spinal column superiorly and the innominate bones on either side through the saddle shaped sacro-iliac joints. The coxae form the anterior arch of the pelvic ring and is connected to the lumbar vertebrae and the spinal column superiorly and the innominate bones on either side through the saddle shaped sacro-iliac joints. The coxae form the anterior arch of the pelvic ring and articulate with the right and left femora. During growth, each coxa forms from three bones, the ilium (superior), the ischium (inferior) and pubis (antero-medial), which fuse at the acetabulum, the hemispherical socket which articulates with the head of the femur. The ischium and ilium are also joined inferiorly to form a bony ring which surrounds an opening called the obturator foramen (figs. 1.1 and 1.2).

The acetabulum itself consists of a concave bony bowl, with a raised edge which extends around approximately 300 degrees of a circle (Oberlander, 1973). The weight-bearing surface is formed by a layer of cartilage which covers a cortical shell, the subchondral plate; the subchondral plate does not cover the entire concavity, but forms a horse-shoe shaped ring of approximately spherical geometry which is termed the fascies lunata or lunate surface and extends from the outer margin to approximately 60 degrees toward the base of the socket (Tillmann, 1969; Oberlander et al, 1978). Inferiorly, a break is present in the acetabular rim which is termed the acetabular or cotyloid notch (or incisura). On either side of the notch, the lunate surface forms two facets termed the cornu anterius and posterius, the posterior facet being the larger. Within the center of the acetabulum, a depression called the acetabular fossa is present which joins the acetabular notch for the passage of blood vessels and nerves into the joint. The fossa is normally covered by a fat pad which occupies the space between the base of the acetabulum and the spherical lunate surface, a distance of 4-7 mm (Yochum and Rowe, 1987).

The bony rim of the acetabulum is augmented by a number of soft tissue structures. A layer of fibro-cartilage covers the rim

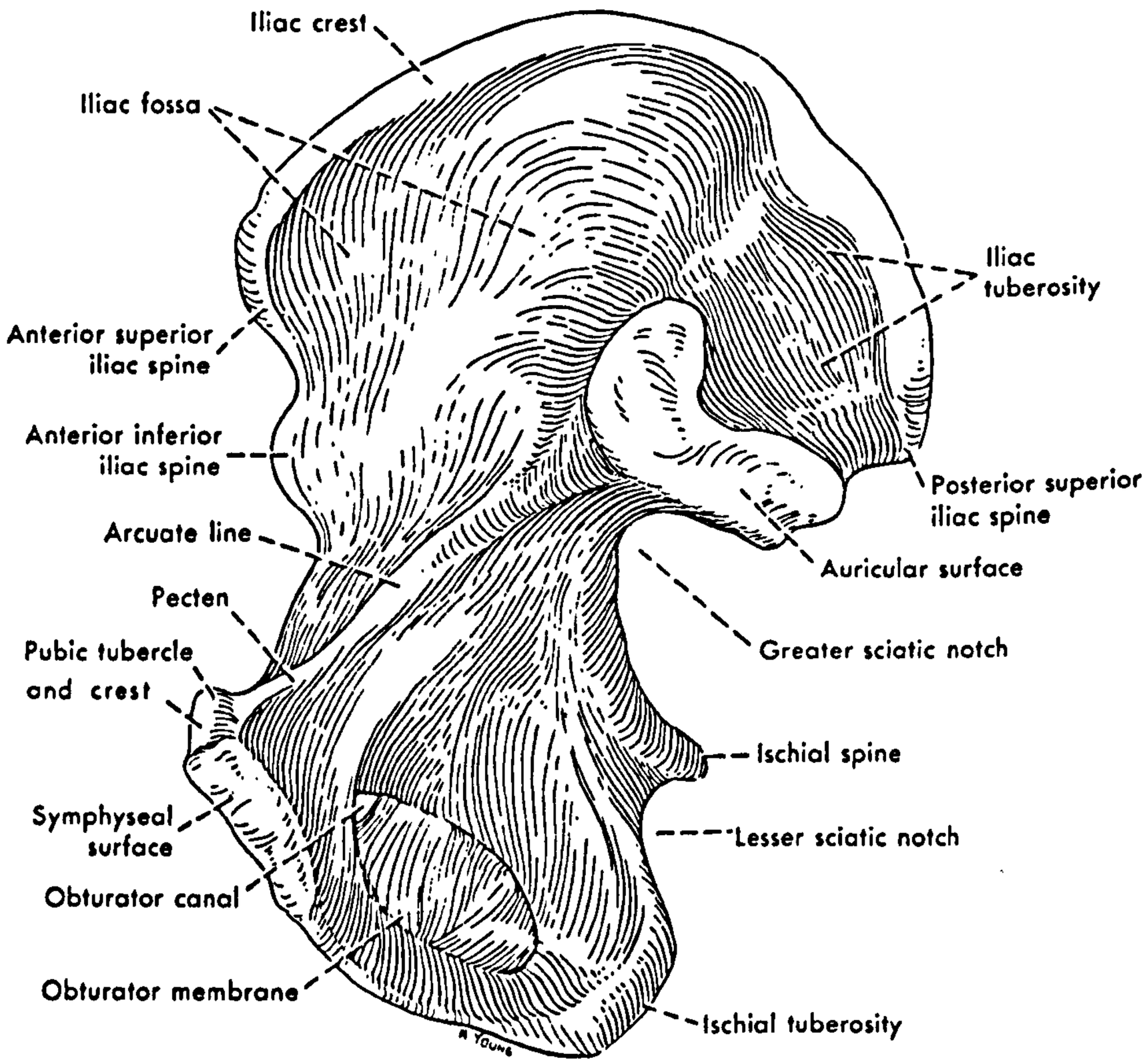

Figure 1.2 The medial (inner) surface of the right coxa of the pelvis, showing bony landmarks.

circumferentially forming the acetabular labrum which increases the coverage of the femoral head and thus the mechanical stability of the hip joint. The trans-acetabular ligament joins the acetabular facets and provides continuity to the acetabular rim by covering the outer surface of the notch while leaving sufficient space at its base for the passage of vessels and nerves into the joint.

The orientation of the acetabulum within the bony pelvis is of functional and clinical significance (McKibbin, 1970; Armbuster et al, 1978; Lewinnek et al, 1978; Ghelman, 1979; Woo and Morrey, 1982; Murray, 1993). The acetabular rim does not face directly laterally, but is oriented somewhat anteriorly and inferiorly to increase the range of useful motion of the hip joint while still maintaining joint stability. The anterior inclination or anteversion of the rim ranges from 15 to 35 degrees and is most readily appreciated in a vertical or apical projection. The acetabulum is also tilted in the coronal plane, the inclination of the rim to the vertical ranging from 23 to 59 degrees with an average value of 38 to 40 degrees (Armbuster et al, 1978; Terver et al, 1982)).

Although the lunate surface and the head of the mating femur have been characterized as a ball and socket joint of spherical geometry, several authors have demonstrated that neither articulating surface is precisely spherical in shape (Schmid, 1874; Bullough et al, 1968; Cathcart, 1971, 1972; Clarke and Amstutz, 1975). This issue and was initially studied by Schmid using wax replicas of the freshly dissected hip joint. He found that the femoral head was slightly ellipsoidal, being elongated in the direction of the femoral neck by 0.8 to 3.5 mm in comparison with the anteroposterior head diameter. Clark and Amstutz reported values of 2.9 mm in males and 0.9 mm in females whereas Cathcart (1972) reported an overall value of 1.4 mm, based on measurements of 45 fresh human specimens. Little definitive data exist concerning the shape of the acetabulum. Clarke and Amstutz measured the shape of 13 acrylic replicas of human acetabuli and reported that they were identical to the shape of the corresponding femoral head, however no specific data were reported. Others have noted that the adult acetabulum becomes more spherical and more congruent with the head of the femur with aging (Bullough et al, 1968).

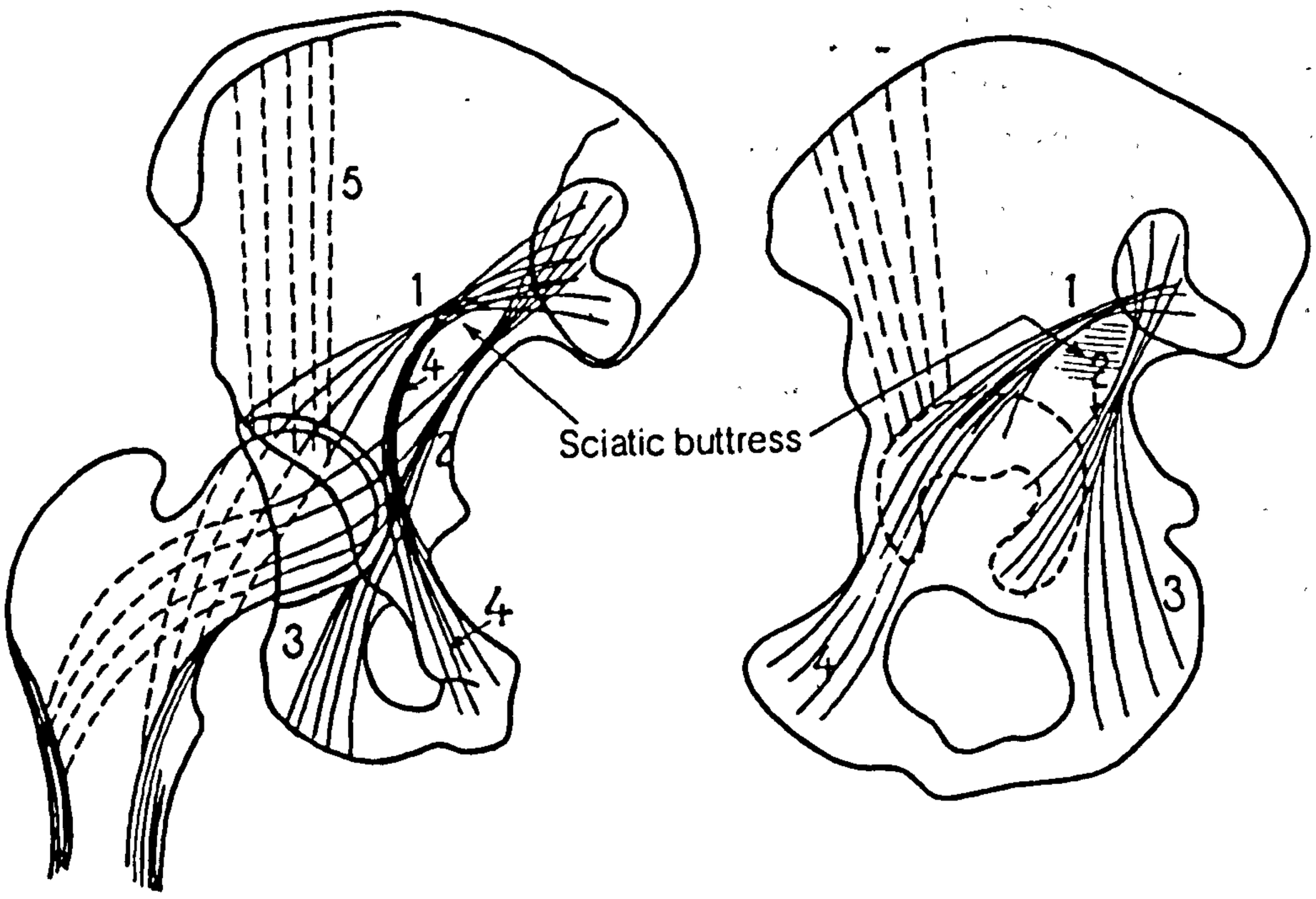

Figure 1.3 Internal structure of the innominate bone (Campanacci, 1967). Trabeculae of the anterior column: 1 sacro-acetabular, 4 sacro-pubic, 5 ilio-acetabular. Trabeculae of the posterior column: 2 sacro-acetabular, 3 sacro-ischial. There is an overlap between these groups.

1.3 THE CANCELLOUS STRUCTURE OF THE PELVIS

Within the pelvis, the acetabulum is essentially supported by two bony limbs or columns: the posterior (ilio-ischial) column, which extends from the sciatic notch to the ischial tuberosity, and the anterior (ilio-pubic) column, which is formed by the anterior part of the ilium, the anterior half of the acetabulum and the superior pubic ramus (Letournel & Judet, 1981; Rubenstein et al, 1982a, 1982b; Howie, 1985). The strength and rigidity of each column is determined by the thickness of the outer and inner cortical walls, the separation of the cortices themselves and the density of the cancellous bone in between. The anterior column consists of three principal arcades or systems of cancellous bone: the anterior sacro-acetabular arcade, the sacro-pubic arcade and the ilio-acetabular arcade (fig. 1.3). The anterior sacro-acetabular trabeculae extend laterally from the inferior part of the sacro-iliac joint along the ilio-pectineal line into the superior pubic ramus. The ilio-acetabular trabeculae descend almost vertically from the wing of the ilium to the superior margin of the anterior acetabulum. The posterior column is reinforced by the sacro-ischial arcade which joins the sacro-acetabular trabeculae above the level of the acetabulum in the vicinity of the sciatic notch (Kapanji, 1987). In this way the pelvis is reinforced so that it can support the loads imposed by standing, sitting and ambulation.

As a consequence of the crossing and fanning out of these trabeculae, the density and strength of the cancellous bone supporting the acetabulum varies greatly, the strongest bone being situated immediately beneath the subchondral plate and the acetabular rim, and superior and anterior to the greater sciatic notch in area called the "sciatic buttress" where the principal trabeculae are in close proximity (Letournel & Judet, 1981). The trabecular arcades of the pelvis perform three basic mechanical functions (Rubenstein et al, 1981; Brand et al, 1982; Saks, 1986):

(i) they support the cortical shell and maintain the separation of the inner and outer walls of the pelvis,

(ii) they connect the joints of the coxae and so transfer load from the acetabulum to the sacro-iliac joint and the pubic symphysis, and

(iii) they transfer forces from the principal areas of muscle attachment to the acetabulum. For example, the ilio-acetabular arcade within the anterior column connects the origin of the

anterior part of gluteus medius to the anterior limb of the lunate surface. Similarly, the sacro-ischial arcade of the posterior column extends from the origin of the hamstring muscles (semimembranosus, semitendinosus and biceps femoris) to the sacro-iliac joint via the posterior wall of the acetabulum (fig. 1.3).

1.4 PATHOLOGIC CHANGES IN PELVIC ANATOMY

With aging, degenerative changes occur within the bone and cartilage of the hip joint which compromise its ability to function painlessly and with minimal friction and wear. Most commonly, osteophytes form around the fovea and the outer margin of the femoral head and over the inner and outer margins of the lunate surface of the acetabulum. Changes in cartilage have been recorded by numerous observers and may be classified as being "limited" or "progressive". In the earliest stages, fibrillation of the cartilaginous surface is observed which can progress to regions of frank ulceration. Limited degeneration typically occurs over the ends of the articular facets, at the junction between the labrum and the articular cartilage and along the inner border of the lunate surface. Progressive degeneration is less common, but involves the entire surface of the inferior half of the acetabulum.

While the etiology of osteoarthritis is not fully understood, a key factor in the degenerative process is localized mechanical breakdown of the articulation resulting in loss of concentricity of the joint and abnormal wear of the cartilage layer. This dysfunctional process is termed osteoarthrosis. Other changes also occur, including biochemical alterations within the cartilage matrix causing softening and fragmentation and, ultimately, remodeling of the joint surface themselves. Some investigators have postulated that joint degeneration occurs once areas of articular cartilage which do not normally support significant contact stresses are recruited into weight-bearing through changes in the shape of the articulating surfaces (Bullough et al, 1973). This hypothesis is borne out in the acetabulum which becomes increasingly spherical with advancing years, causing the nonweight-bearing area of the superior dome to bear weight event though it is normally covered with fibro-cartilage which is not adapted for weight bearing.

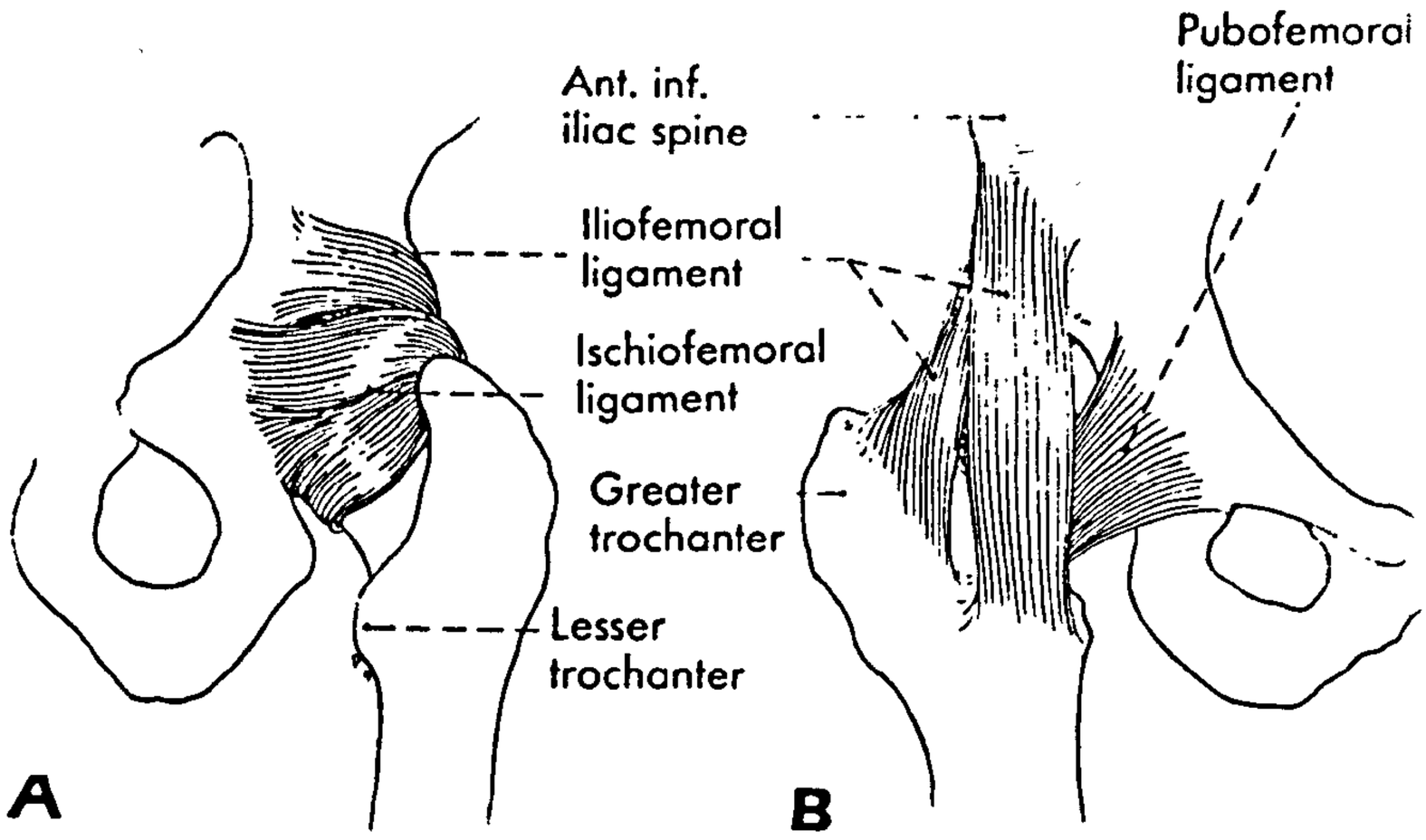

Figure 1.4 The ligaments of the hip joint (Hollinshead and Rosse, 1985).

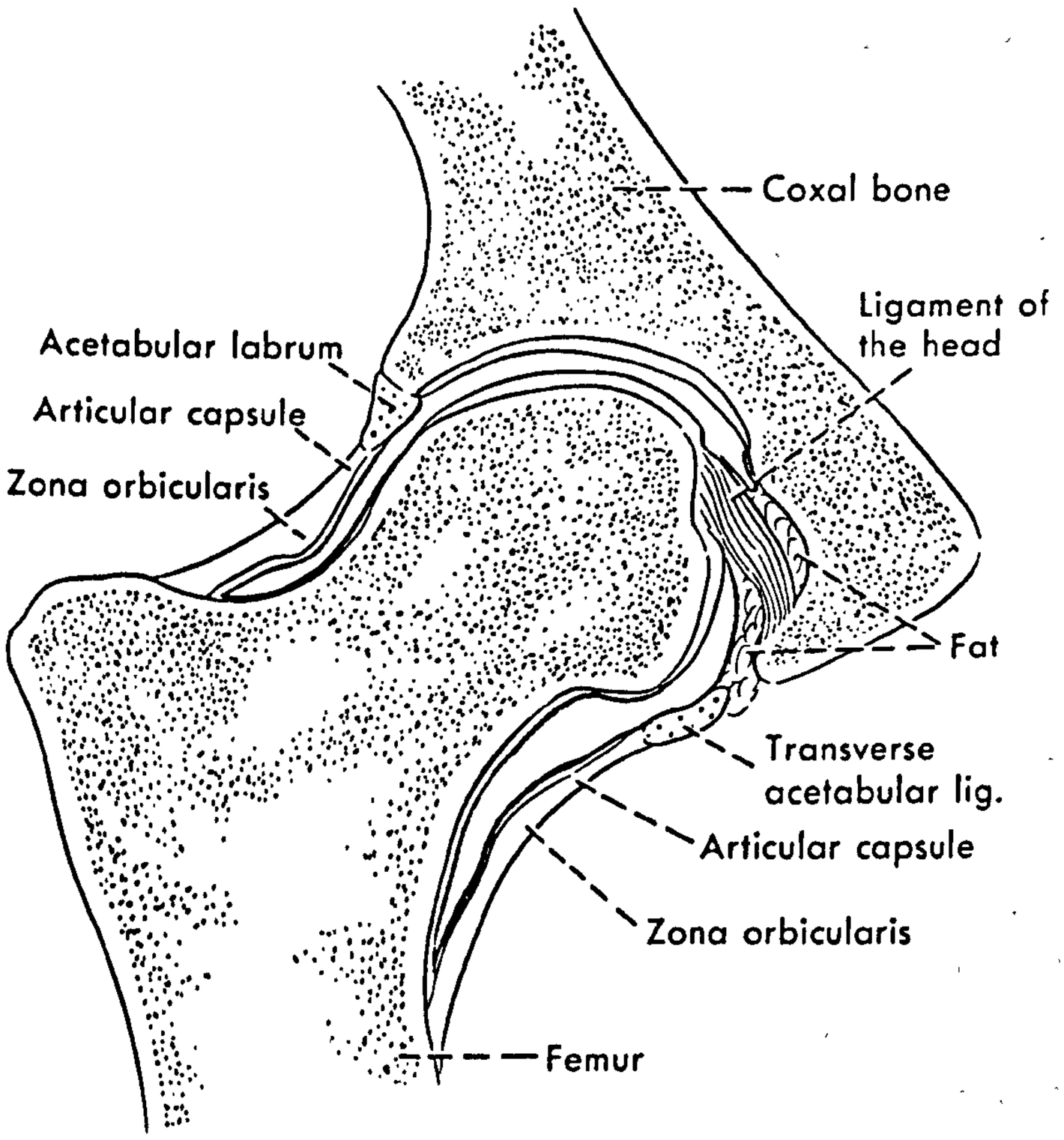

Figure 1.5 Mid coronal section through the hip joint showing the relationship between bony and soft tissue structures.

1.5 THE LIGAMENTOUS STRUCTURES OF THE HIP JOINT

The ligamentous and muscular tissues of the hip joint contribute significantly to its function and stability. The primary role of the ligaments is to stabilize the joint at its extremes of motion by restricting excessive movements which would otherwise lead to subluxation or frank dislocation (Kapandji, 1987; Hollinshead, 1969). The hip joint is surrounded by a cylindrical sleeve of ligamentous tissue called the capsular ligament which is attached to the acetabular rim, the acetabular ligament and the peripheral surface of the labrum, medially, and to the base of the femoral neck, laterally. The capsular ligament shows three prominent thickenings which are described as discrete ligaments. These include:

(a) The ilio-femoral ligament, the largest ligament of the hip joint and one of the strongest in the body. Anteriorly, it is present as two bands which extend from the anterior-inferior iliac spine medially to two sites along the inter-trochanter line laterally (fig. 1.4). Because the ligament expands from its origin to its insertion, it adopts the appearance of an inverted "Y", and so has been referred to as the "Y" ligament of Bigelow. The major function of this structure is control of hyperextension of the joint, though it also limits internal rotation.

(b) The pubofemoral ligament is also anterior and arises from the body and superior ramus of the pubis. It inserts into the anterior surface of the femoral neck after blending with the lower limb of the ilio-femoral ligament. The function of the pubofemoral ligament appears to be to limit abduction and external rotation.

(c) Posteriorly, the thin ischio-femoral ligament is present, running almost horizontally across the posterior surface of the femoral neck form the acetabular rim and the labrum to the inner surface of the greater trochanter. Its primary function appears to be to limit internal femoral rotation.

Within the hip joint itself, a ligamentous structure is present called the ligamentum teres (fig. 1.5). This ligament arises from the fovea of the femoral head and inserts into the floor of the acetabulum where it lies embedded in a fat pad surrounded by a tube of synovial membrane. Part of the ligamentum teres also inserts outside the acetabulum after passing beneath the transverse acetabular ligament. The primary role of

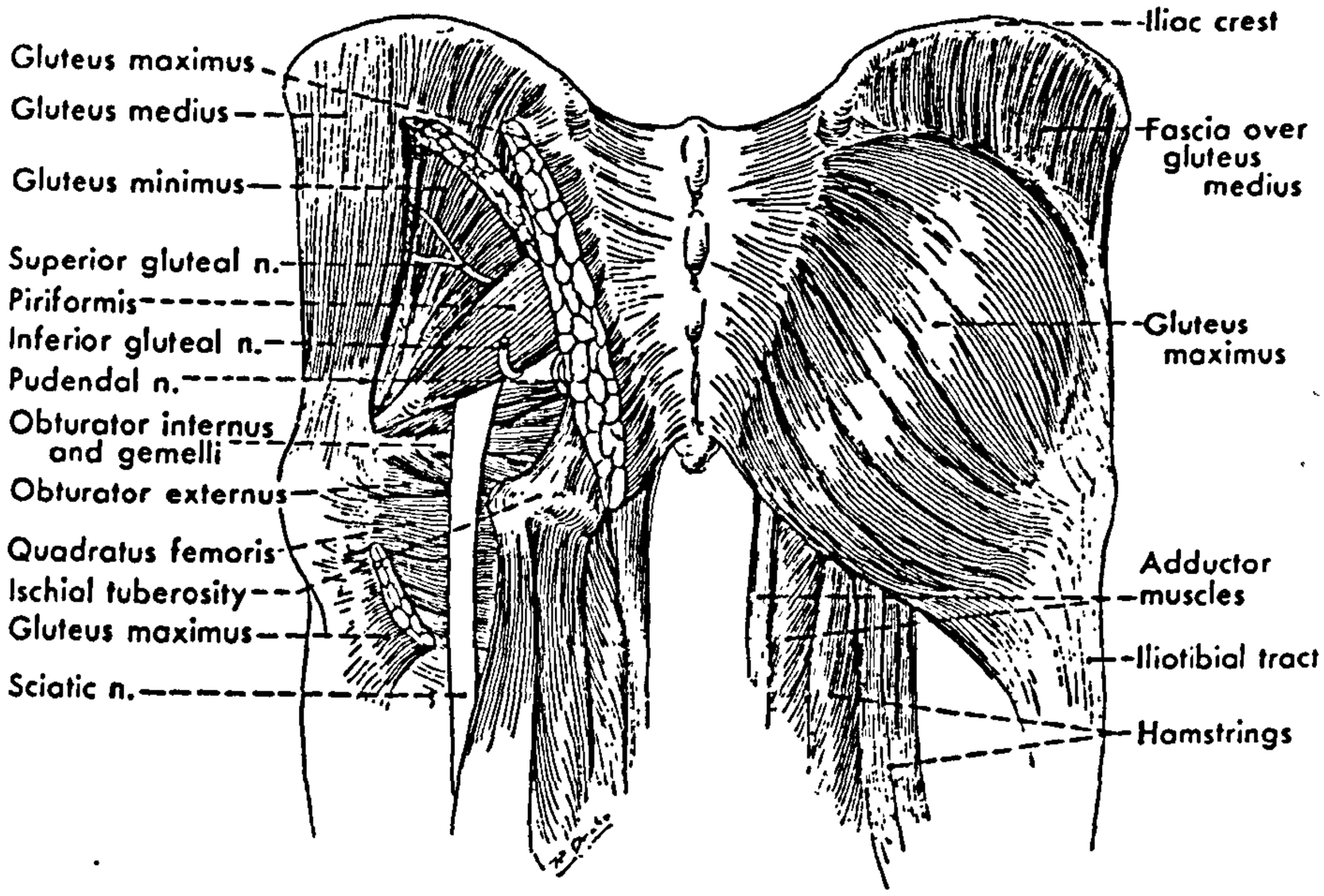

Figure 1.6 Muscles arising from the posterior surface of the pelvis (from Hollinshead and Rosse, 1985).

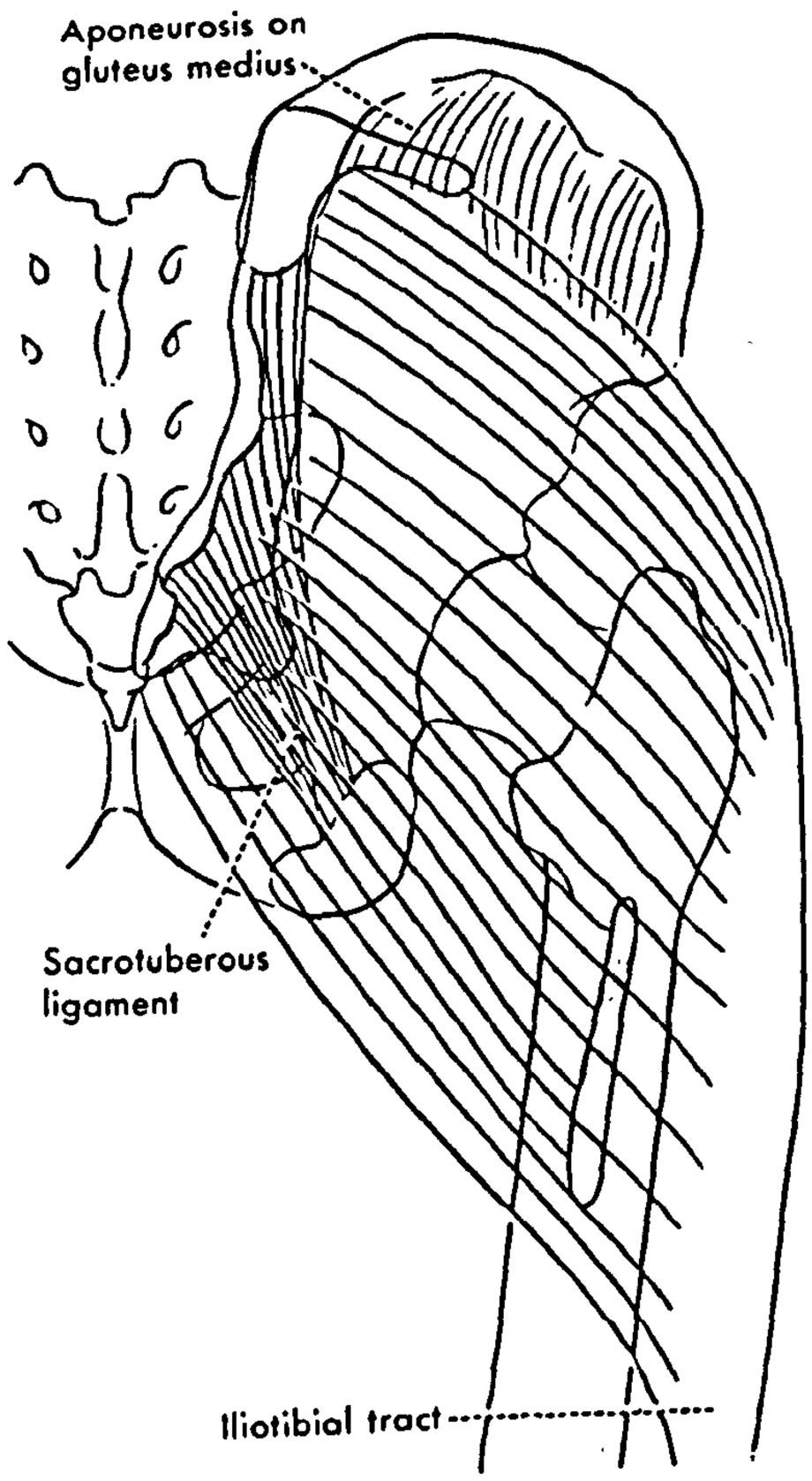

Figure 1.7 The attachments of the gluteus maximus (from Hollinshead and Rosse, 1985).

ligamentum teres is to contribute to the vascular supply of the femoral head. In the adult, it appears to play no mechanical role, however it may perform a significant function in stabilizing the joint in the fetus and the newborn (Hollinshead & Rosse, 1985).

1.6 THE MUSCLES OF THE HIP JOINT

The hip joint is actively moved and stabilized through the action of some 22 different muscles which may be conveniently classified in terms of their principal functions, although most muscles cause compound motions of the joint due to their orientation with respect to the principal anatomic axes.

1.6.1 The Extensors

Extension of the hip joint is generated by two main muscle groups, gluteus maximus and the hamstrings. Gluteus maximus covers most of the buttock and is the largest and most powerful muscle of the body. Due to its size, its origin is distributed over several structures, including the outer surface of the ilium, the dorsal surface of the sacrum and coccyx and the sacro-tuberous ligament (figs. 1.6 and 1.7). Approximately three quarters of the muscle inserts into the ilio-tibial tract; the remainder, the deep portion of the lower part of the muscle, inserts directly into the gluteal tuberosity of the posterior femur.

The hamstring muscles consist of biceps femoris, semitendinosus and semimembranosus and are also capable of developing a powerful extension moment. However, as the hamstrings are biarticular muscles, their effectiveness is dependent upon the position of the knee. All three hamstring muscles arise form the ischial tuberosity, although biceps femoris has dual origins: its long head shares it origin with semitendinosus and its short head arises from the lower half of the linea aspera (fig. 1.8). Although both parts of biceps femoris unite in the lower third of the thigh, only the long head crosses the hip joint. Biceps femoris forms a tendon of insertion which attaches to the head of the fibula after crossing the poster-lateral aspect of the knee joint. The tendon of insertion of semitendinosus passes behind the knee and then courses anteriorly where it inserts into the medial aspect of the proximal tibia. Semimembranosus follows a similar course, however it inserts into the posteromedial side of the medial tibial condyle.

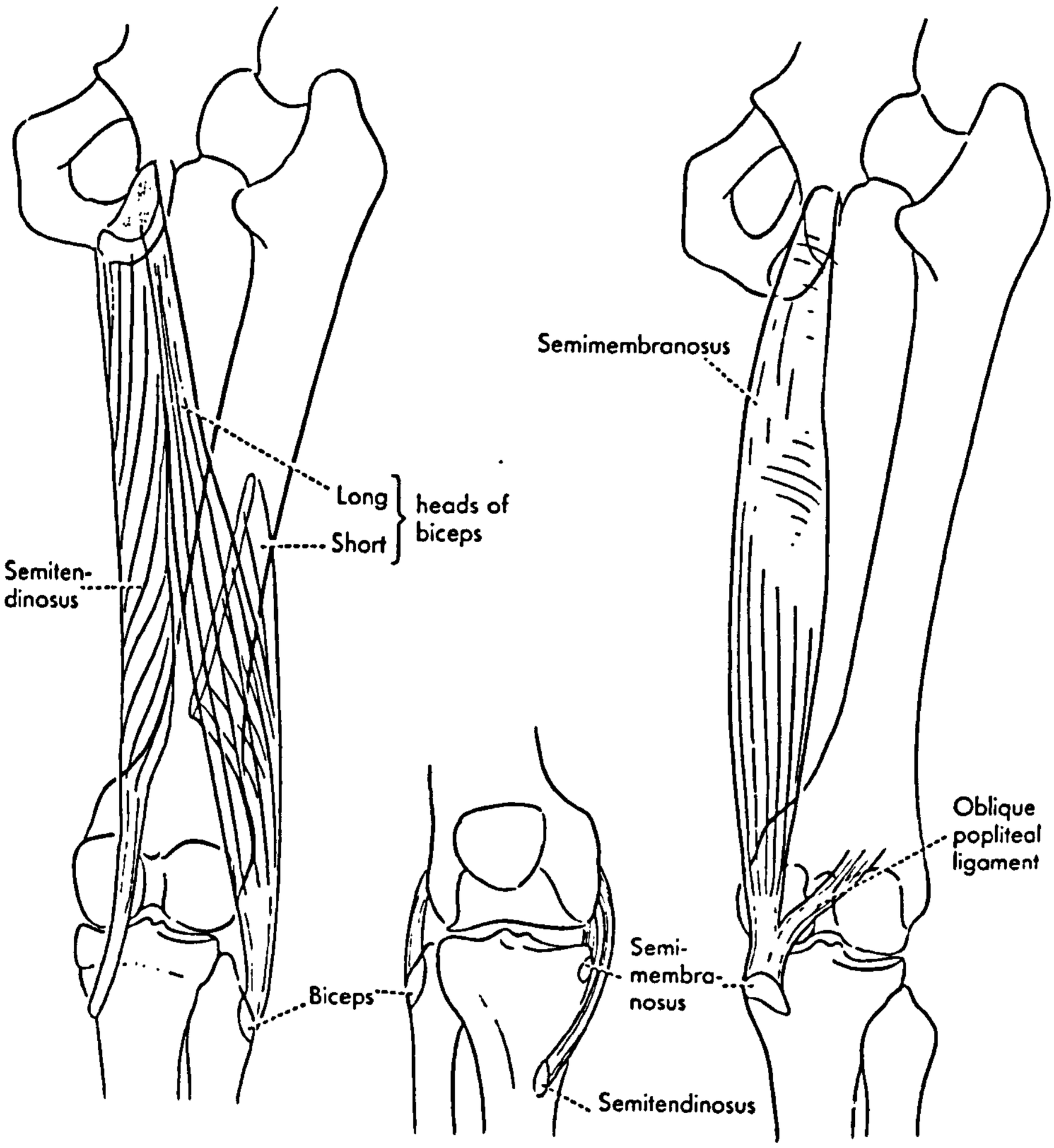

Figure 1.8 The origins and insertions of the hamstring muscles (from Hollinshead and Rosse, 1985).

1.6.2 The Flexors

The primary flexors of the hip joint are ilio-psoas, rectus femoris and tensor fascia lata. The ilio-psoas muscle is formed by the psoas major and iliacus muscles which have separate origins but blend to form one muscle at about the level of the inguinal ligament (fig. 1.9). The psoas major arises from the 12th thoracic to the 4th lumbar vertebrae and their adjacent intervertebral disks, whereas iliacus, a fan shaped muscle, has its origin over a broad area of the anterior surface of the ilium. Ilio-psoas, the most powerful of the muscles of the hip, passes across the anterior surface of the joint and then bends sharply before inserting into the lesser trochanter.

Rectus femoris is a biarticular muscle which forms part of the quadriceps femoris, a group of four muscles which provide extension of the knee joint (fig. 1.10). In crossing the hip as well as the knee, rectus femoris serves both as a hip flexor and a knee extensor. It has a double tendinous origin from the ilium, the straight or major tendon arising from the anterior-inferior iliac spine and a thinner, reflected tendon passing over the posterior femoral neck after arising from the ilium immediately above the acetabular margin. Both parts of the muscle insert into the upper border of the patella and through the patellar tendon to the tibial tubercle. The mechanical effectiveness of rectus femoris is enhanced by simultaneous extension of the hip and flexion of the knee as this allows the muscle to contract within the favorable range of its length/tension relationship.

Another biarticular hip flexor is the tensor fascia lata which arises from the anterior part of the iliac crest near the anterior superior iliac spine (fig. 1.11). Tensor fascia lata runs obliquely, both posteriorly and inferiorly, to insert into the ilio-tibial tract, which is part of a dense tissue sheath called the fascia lata which envelops the entire thigh (fig. 1.12). The ilio-tibial tract runs down the lateral surface of the thigh and, with tensor fascia lata and gluteus maximums, forms the "deltoid" of the hip joint. The anterior pull of the tensor fascia lata is opposed by the superficial fibers of gluteus maximus which insert into the posterior border of the ilio-tibial tract. Coordinated contraction of the tensor fascia lata and the gluteus maximus can result in pure abduction of the hip joint, allowing tensor fascia lata to act both as a flexor and an abductor.

Several other muscles play a minor role as hip flexors. One is

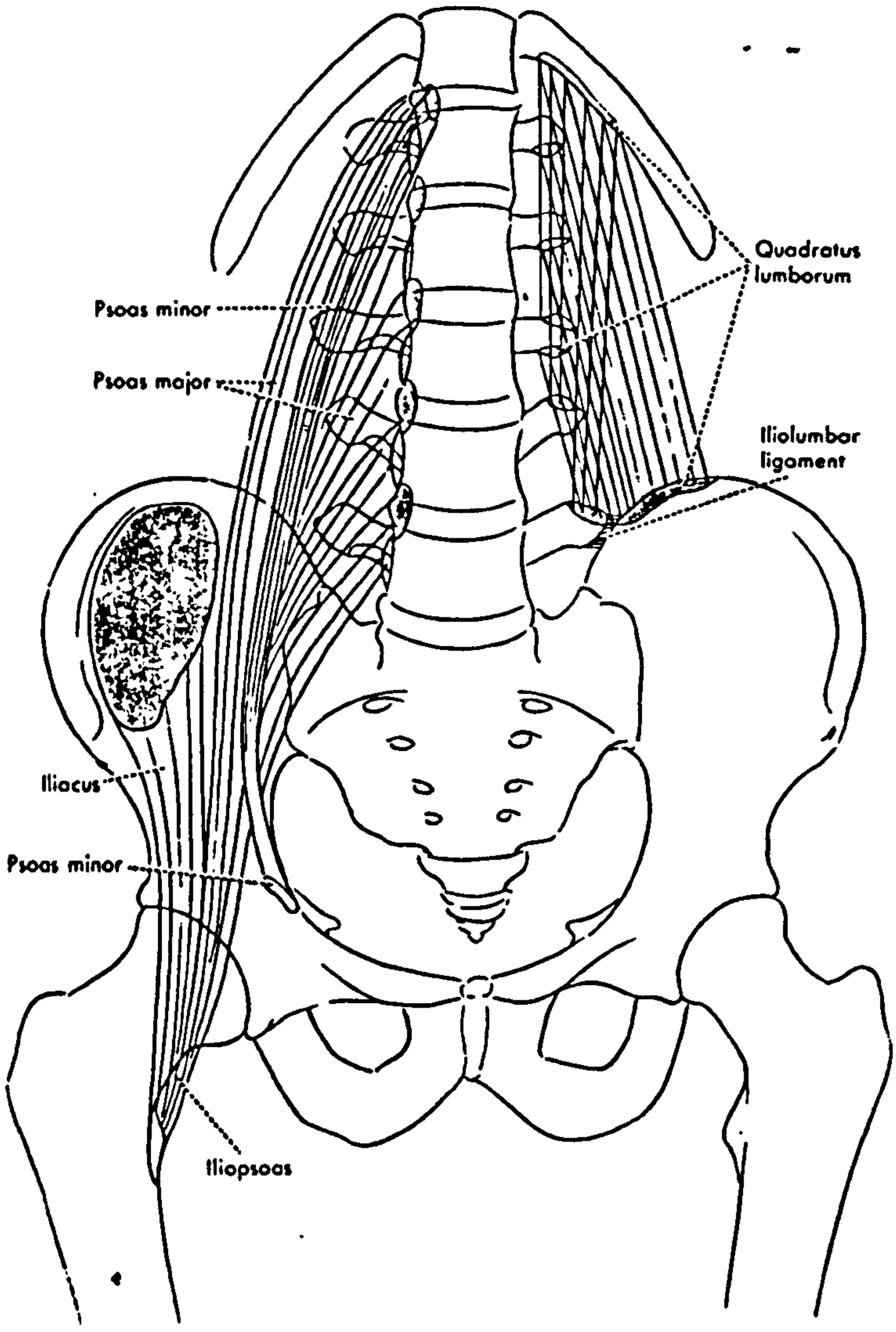

Figure 1.9 The attachments of iliopsoas and quadratus lumborum (from Hollinshead and Rosse, 1985).

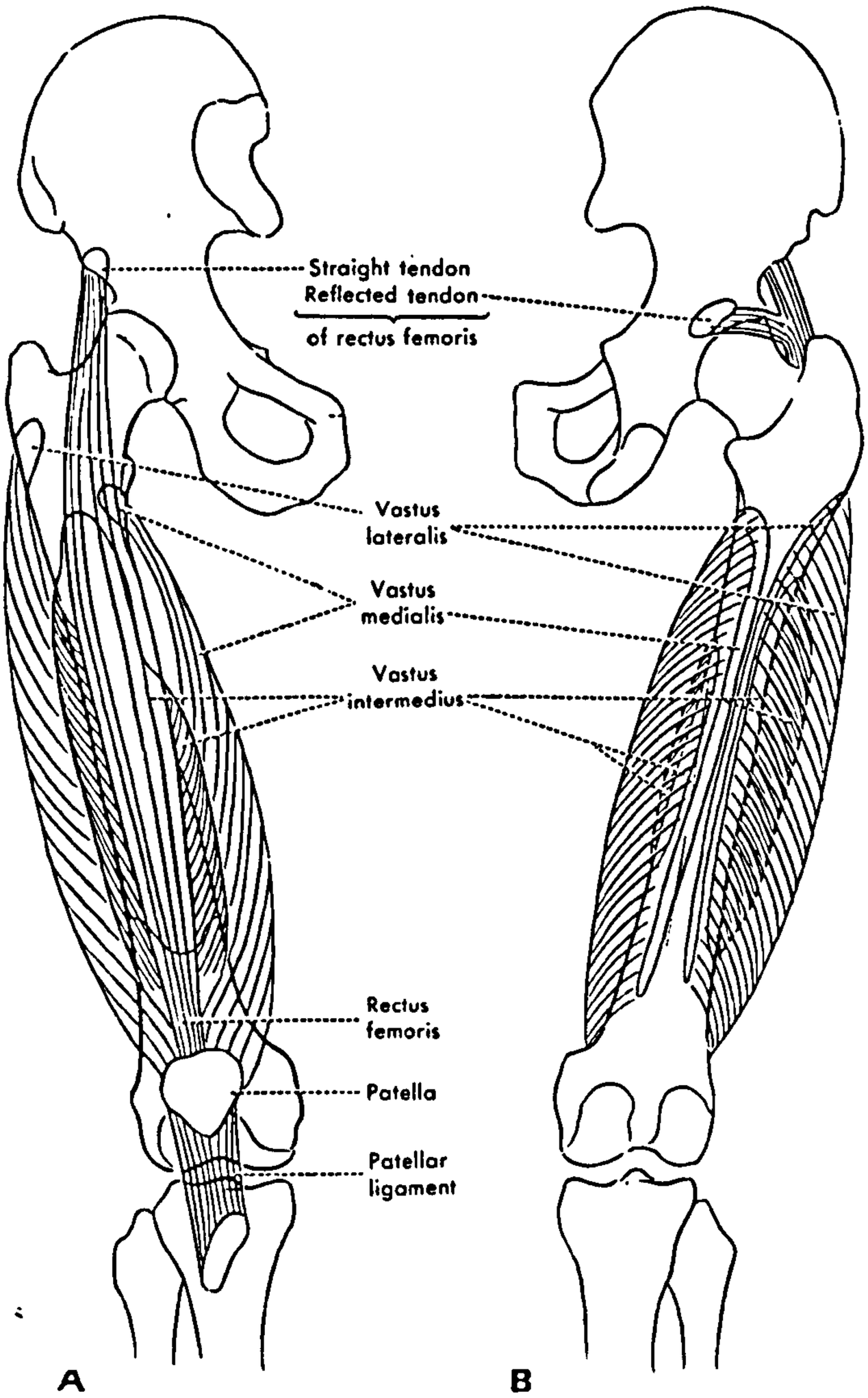

Figure 1.10 Anterior (left) and posterior (right) views of the components of the quadriceps mechanism (from Hollinshead and Rosse, 1985).

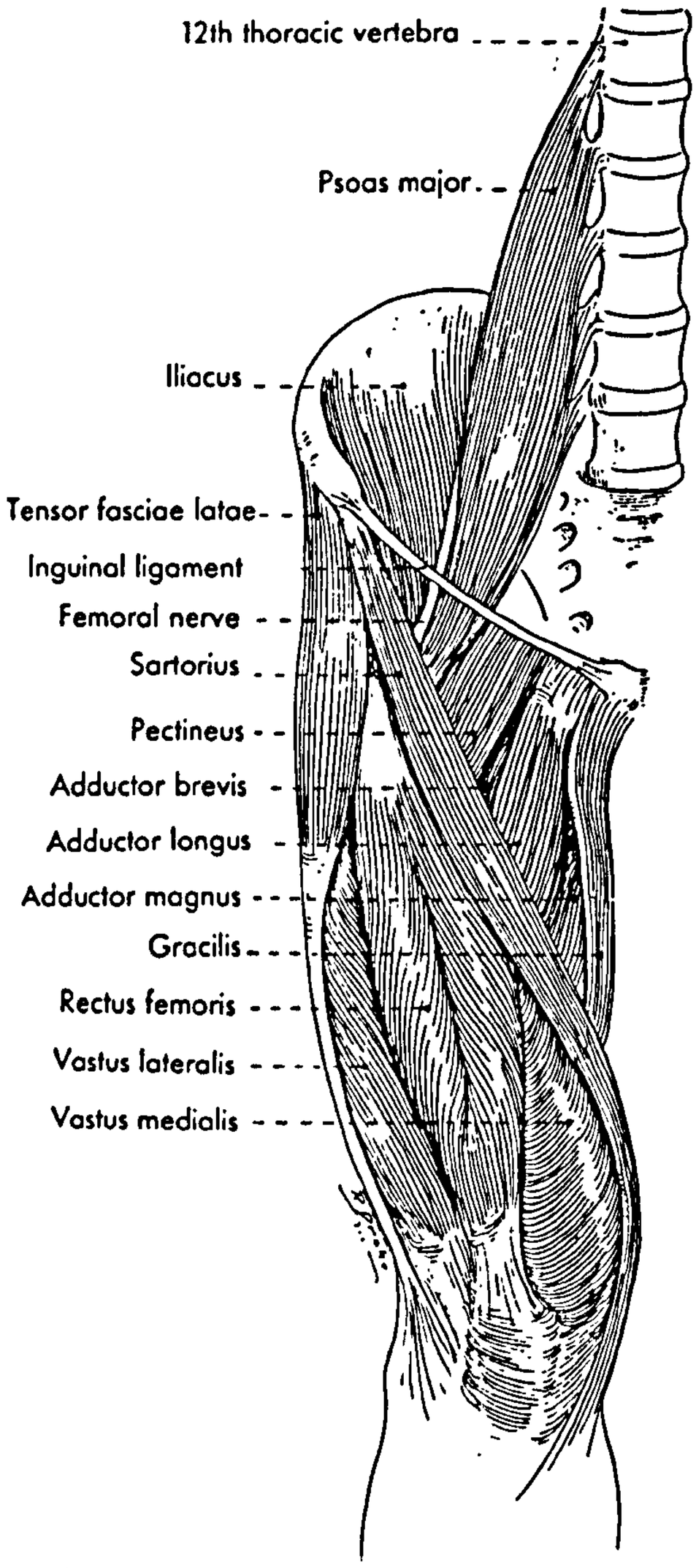

Figure 1.11 The muscles of the anterior surface of the thigh (from Hollinshead and Rosse, 1985).

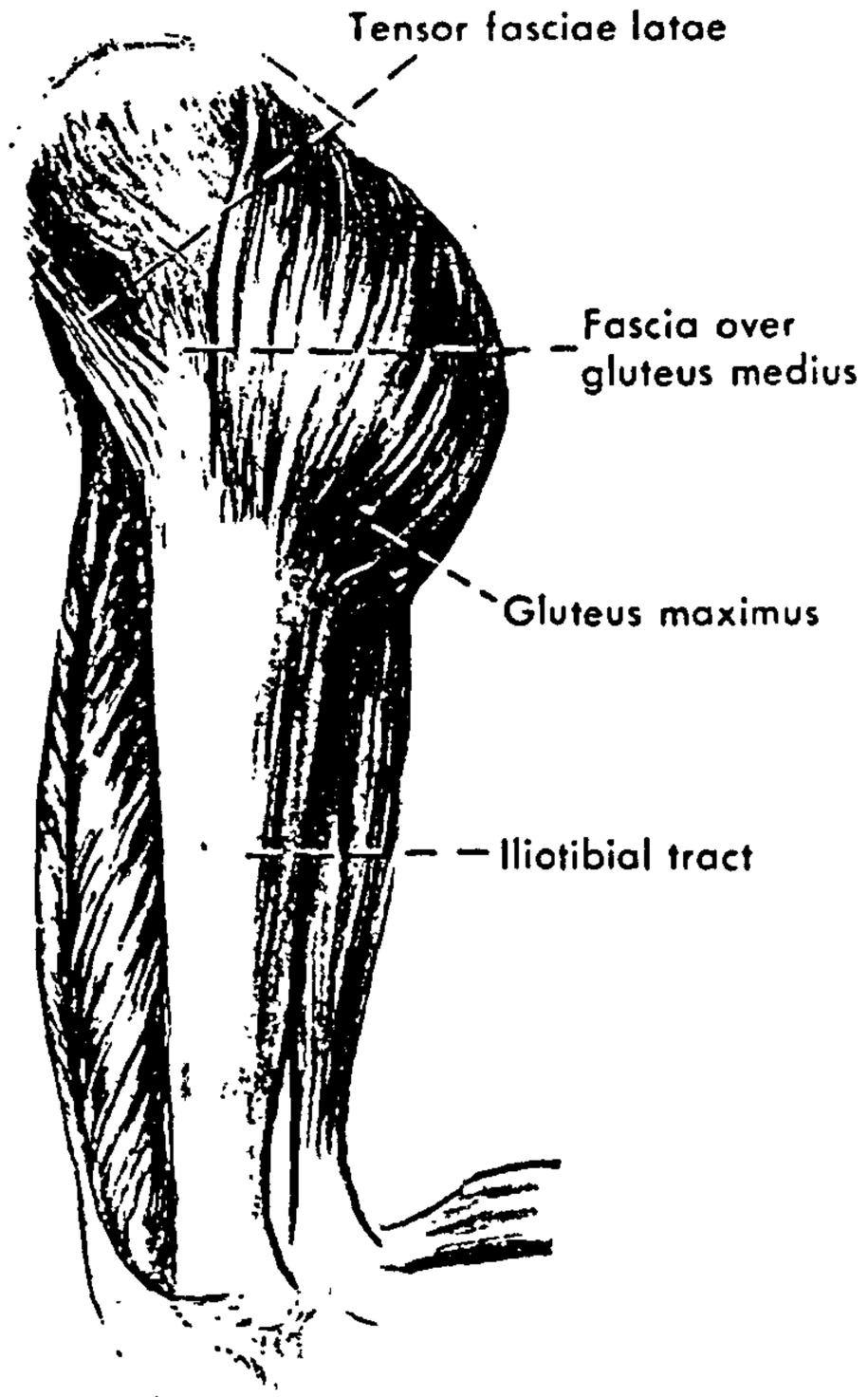

Figure 1.12 The ilio-tibial tract and the deltiod of the hip joint (from Hollinshead and Rosse, 1985).

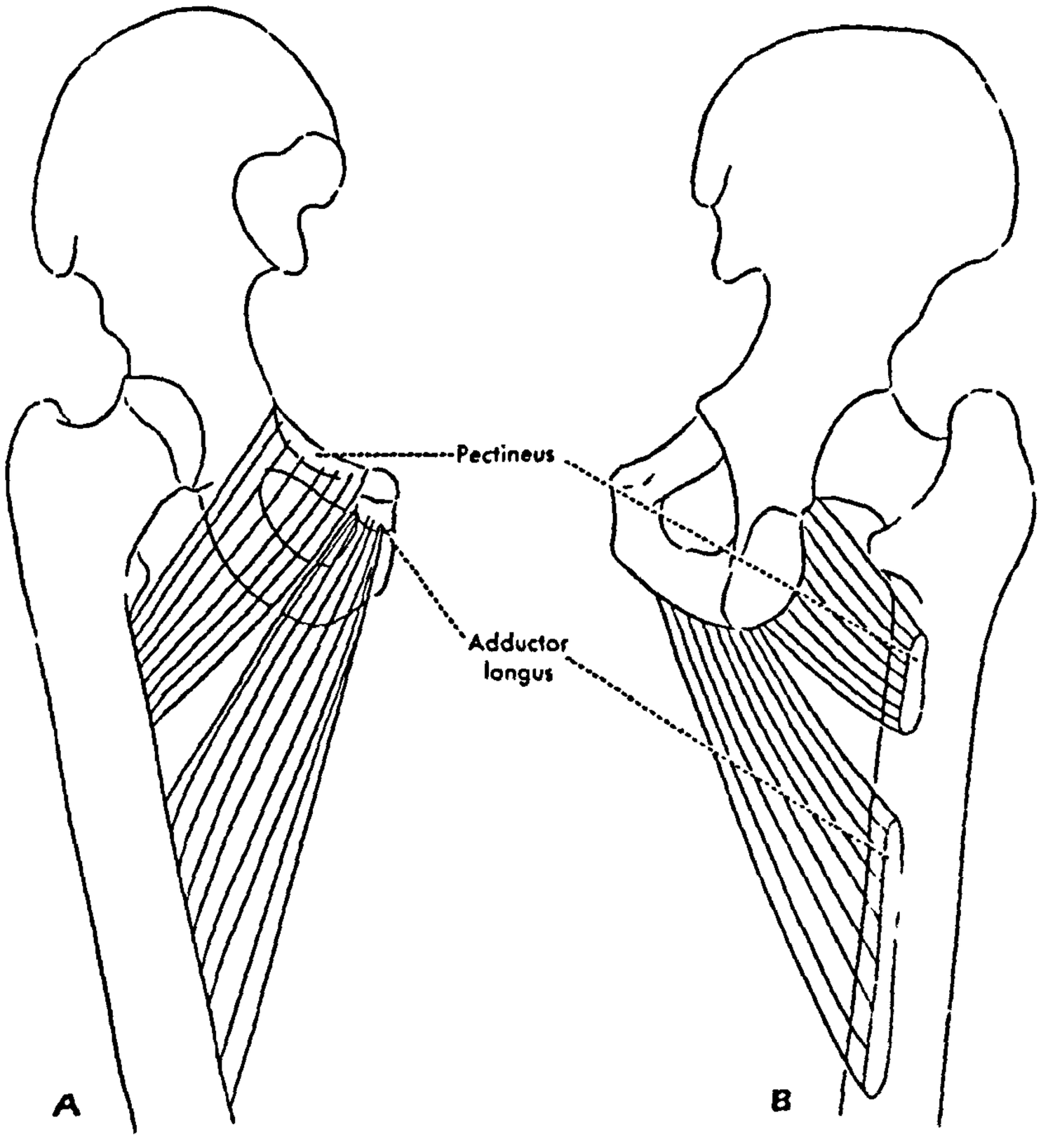

Figure 1.13 Origin and insertion of pectineus and adductor longus (Hollinshead and Rosse, 1985).

sartorius which is a long, strap-like muscle which extends obliquely from the anterior to the medial side of the thigh (fig. 1.11). It arises from the anterior-superior iliac spine and passes in front of the hip joint and medial to the knee joint where it inserts in the antero-medial surface of the upper tibia, close to the insertion of semitendinosus. Sartorius also acts to produce secondary abduction and external rotation of the hip.

Pectineus is another secondary flexor of the hip joint. This short, flat muscle runs from the pectin of the pubis on the superior pubic ramus to insert in the femur on the pectineal line immediately below the lesser trochanter (fig. 1.13). Due to its anatomic placement, pectineus strongly resembles a hip adductor, however it functions primarily as a flexor in coordination with tensor fascia lata, although it also produces adduction and internal rotation of the hip joint.

1.6.3 The Abductors

Abduction of the hip is mainly generated by contraction of gluteus medius and minimus and the balanced action of other muscles which act secondarily as abductors during normal contraction. The main abductor of the hip is gluteus medius which is a fan shaped muscle which owes its effectiveness in abducting the hip to the fact that its moment arm is almost perpendicular to its direction of action. Gluteus medius arises from the wing of the ilium between the anterior and posterior gluteal lines and inserts into the posterior aspect of the upper surface of the greater trochanter (figs. 1.6 and 1.14). Similarly, gluteus minimus, another fan shaped muscle, lies deep to gluteus medius, close to the capsule of the hip joint (fig. 1.15). It has its origin on the wing of the ilium between the anterior and inferior gluteal lines and inserts onto the anterior border of the greater trochanter.

Additional abduction is generated by the contraction of tensor fascia lata and sartorius which act primarily as hip flexors.

1.6.4 The Adductors

In order to perform the action of adduction at the hip joint, the body is equipped with particularly powerful muscles, namely adductor magnus, adductor longus, adductor brevis and gracilis. The most significant of these is adductor magnus which arises from the inferior ramus of the pubis, the ramus of the ischium and the ischial tuberosity

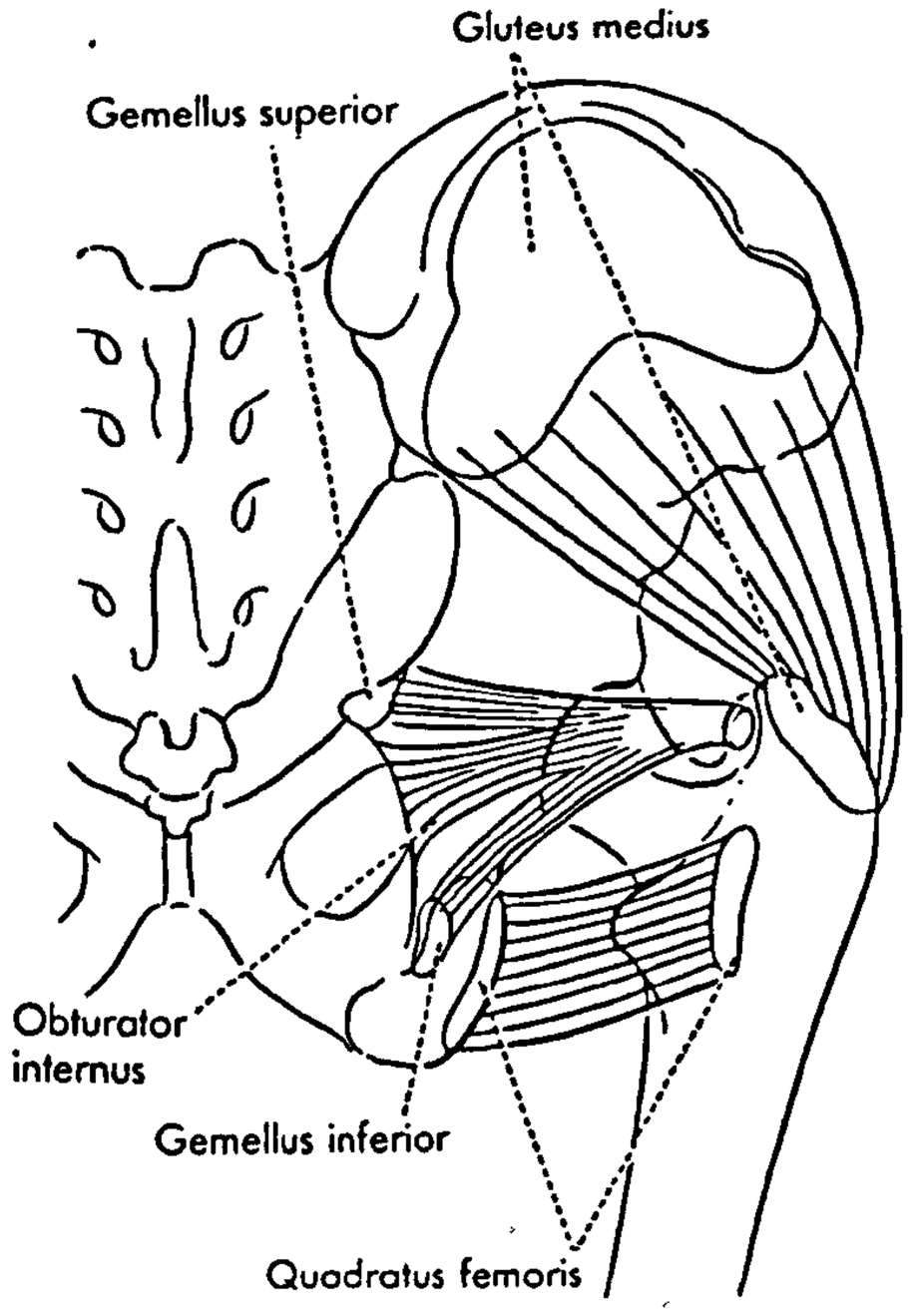

Figure 1.14 Attachment of the gluteus medius, the gemelli and the quadratus femoris (from Hollinshead and Rosse, 1985).

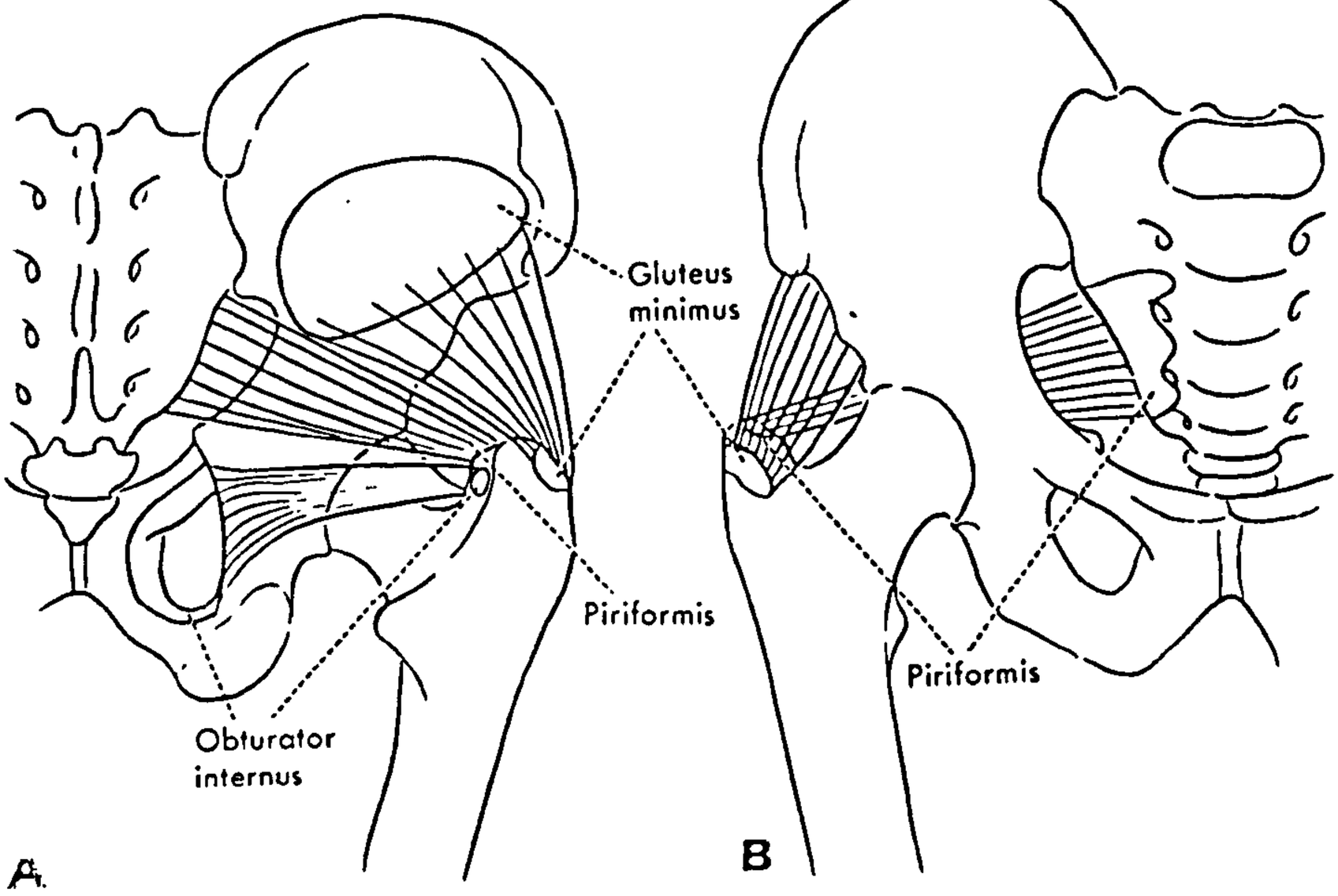

Figure 1.15 Attachments of gluteus minimus, piriformis and obturator internus (from Hollinshead and Rosse, 1985).

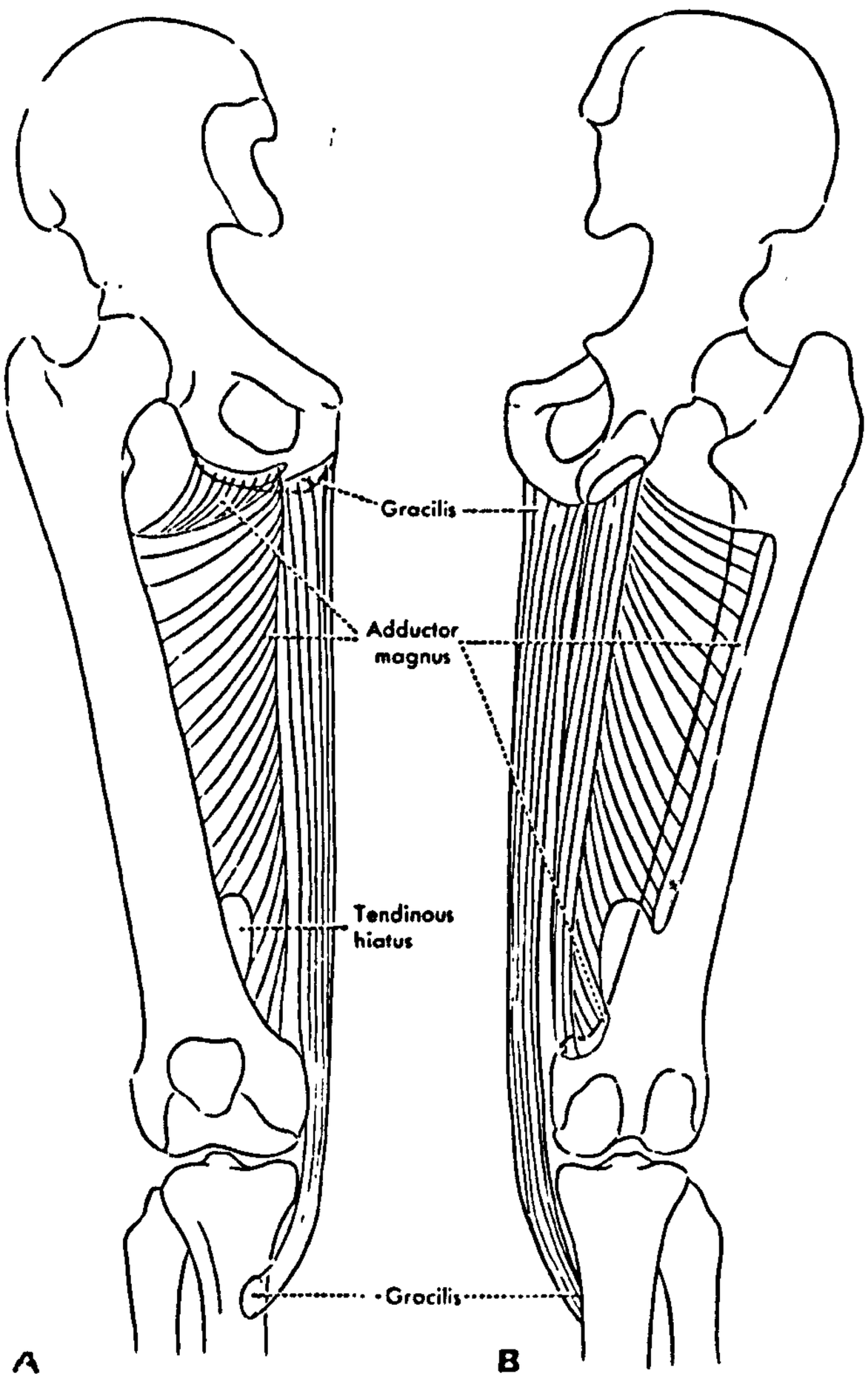

Figure 1.16 Attachments of adductor magnus and gracilis, as seen from the anterior (left) and posterior (right) views (from Hollinshead and Rosse, 1985).

and inserts along the entire length of the linear aspera of the posterior femur and the adductor tubercle of the medial femoral condyle (fig. 1.16). The next most significant adductor is adductor longus which is the most anteriorly placed of the adductors, arising from a tendinosus origin at the front of the body of the pubis and inserting in the middle half of the linea aspera (fig. 1.13). Adductor longus is bordered by adductor brevis which arises from the body and inferior ramus of the pubis and fans out to insert into the upper part of the linea aspera (fig. 1.17). Gracilis is a biarticular muscle and is the most inferiorly placed adductor of the hip. It runs almost vertically down the medial side of the thigh from its origin over the body and inferior ramus of the pubis, to its tendinosus insertion between sartorius and semitendinosus on the antero-medial surface of the tibia (fig. 1.16).

1.6.5 The Rotators

External rotation of the hip joint is controlled by a set of short muscles which are located in the posterior gluteal region beneath gluteus maximus. These muscles include the obturator internus, the piriformis, the superior gemellus and the inferior gemellus, all of which are inserted into the greater trochanter and have origins on the posterior part of the coxae and the sacrum (figs. 1.14, 1.15 and 1.17). Additionally, quadratus femoris, a short broad muscle extends almost horizontally form the ischial tuberosity to the inter-trochanteric crest of the femur. Axial rotation of the femur is also generated by obturator externus which twists around the femoral neck from the margins of the obturator foramen anteriorly to the superior surface of the femoral neck in the trochanteric fossa, where it has its insertion.

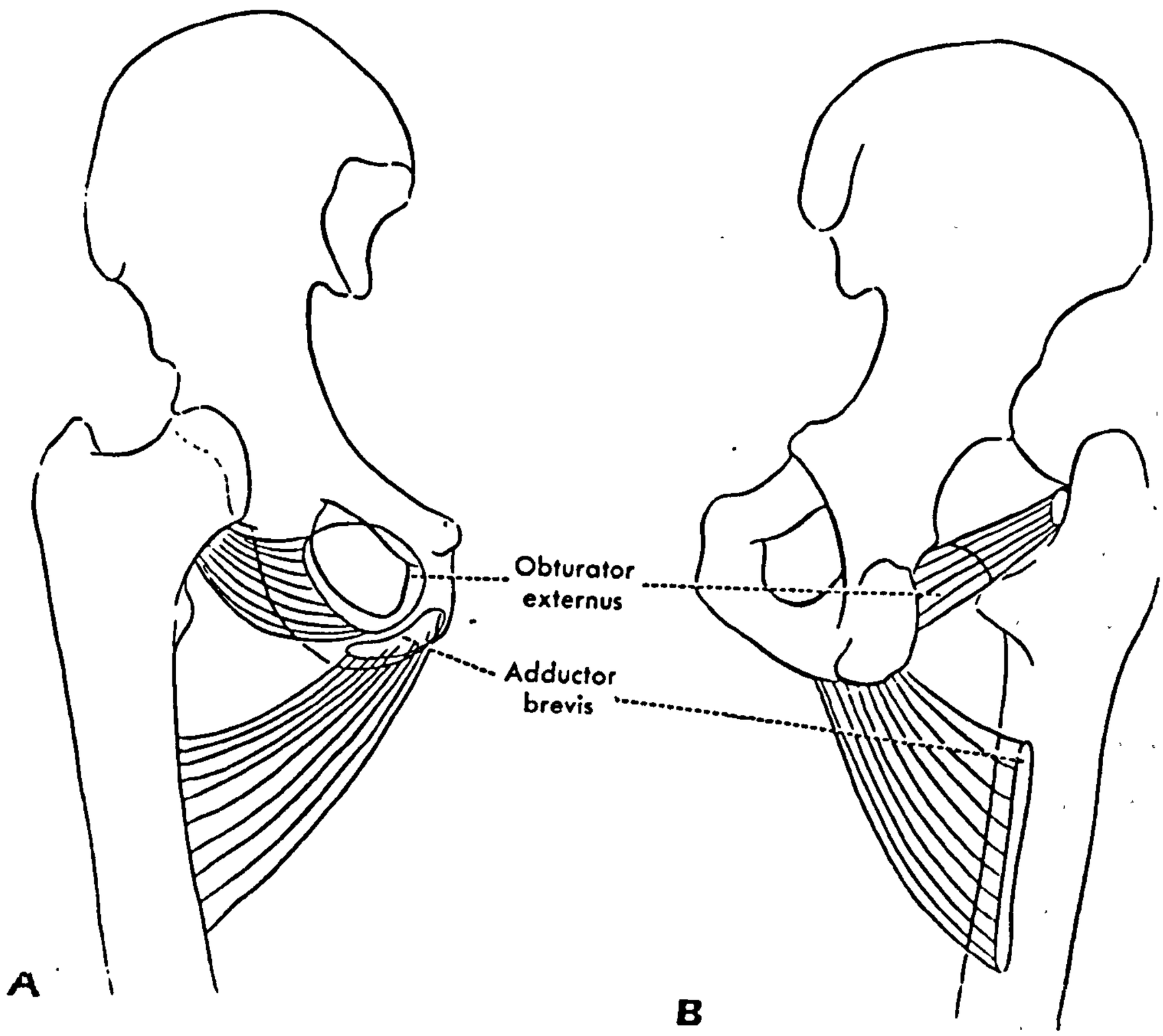

Figure 1.17 Attachments of adductor brevis and obturator externus, seen from the anterior (left) and posterior (right) views of the hip joint (from Hollinshead and Rosse, 1985).

CHAPTER 2. THE BIOMECHANICS OF THE PELVIS AND ACETABULUM

2.1 THE LOADING OF THE HIP JOINT

Any real understanding of the biomechanics of the acetabulum and the pelvis must be based upon knowledge of the mechanics of loading and load transmission at the hip joint.

2.1.1 Theoretical Analysis

Numerous authors have studied the loading of the hip joint during single-legged stance and normal ambulation, leading to estimates of the joint reaction force from measurements of kinematic and biomechanical parameters. Foremost in these studies is the work of Paul (1967) who presented a fundamental analysis of the forces acting on the weight-bearing extremity during walking. Paul calculated the forces at the hip joint throughout the gait cycle by combining kinematic data derived from cinematographic recordings of subjects taken during walking, with simultaneous measures of the components of the reaction force developed between the ground and the foot. This analysis took into account the contributions to joint loading made by the weight of the body supported by the hip joint, inertial forces developed by acceleration of the body, and the muscle forces generated to control joint motion.

The magnitude of the joint reaction force was estimated to reach a maximum of approximately 5 times body weight at two points during stance phase, at approximately 10% and 50% of the gait cycle. This was found to correspond at the points of transition between single and double support, at the moment of toe-off and heel strike of the contralateral foot. At mid-stance, when the body has its maximum vertical acceleration, it was calculated that the joint force would drop by up to half of its peak value, depending upon the speed of ambulation. Paul also calculated the variation in the orientation of the hip joint force and found that although the component acting in the vertical (superoinferior) direction was largest components of up to 1.0 times body-weight also acted along the anteroposterior and mediolateral directions, especially at 50% of the gait cycle.

2.1.2 Intravital Force Measurements

Intravital measurements of hip joint forces have been reported by several authors following implantation of instrumented prostheses. This field was pioneered by Rydell (1964, 1966) who implanted instrumented hemiarthroplasties in two patients and recorded hip joint forces during standing, walking, stair-climbing and a variety of other activities. Rydell's hip prostheses were of a Moore-type design with a hollow modular neck and a modular head, all made of stainless steel. Both implants were manufactured with a fixed head diameter of 47.2 mm. All components were assembled prior to implantation and fixed in place with epoxy adhesive. Strain gages were attached to the inner surface of the neck and wired to a cable which passed out of the bone of the head and was joined to a connector, implanted within the fascia of each patient. Due to the alignment of the strain gages within the neck of the implant, all forces were reported in an axis system defined with respect to plane of the prosthesis and not the femur or the body of the patient. Thus, forces were reported acting along the axis of the neck of the prosthesis, and in two directions orthogonal to the neck, one within the plane of the implant (i.e. approximately within the mid-coronal plane of the femur), and the other normal to the plane of the prosthesis (ie. anterior-posterior, in approximately the mid-sagittal plane through the hip joint).

The first patient was a 51 year old man (body mass: 76 kg) who had his hip replaced following a femoral neck fracture in an automobile accident. The operation was performed four weeks after the initial injury. At surgery, fit of the prosthetic ball within the acetabulum was considered acceptable, even though it was 3 mm smaller than the contralateral femoral head. The prosthesis was implanted without cement in 8 degrees more anteversion and 10 degrees lower neck-shaft angle than the contralateral femur. The patient was allowed to commence weight-bearing at four weeks post-operatively. Electromyographic studies performed at six months post-operatively showed normal patterns for all hip muscles except gluteus maximus. Although the patient did not walk with a noticeable limp, the operated leg was 10 mm shorter than the contralateral limb.

One complication of the Rydell prosthesis was the need to directly connect the implant to an external power-source and recording instruments via a percutaneous cable. This necessitated a second

operation as the connector attached to the instrumented prosthesis was left buried within the fascia for six months following implantation. However, as Rydell and his co-workers feared that the direct connection between the cable and the prosthesis might result in an infection, recordings were started at only two days following the second operation and were terminated four days later. This introduced the possibility that discomfort of the operative site may have affected the gait of the patient although Rydell states that the percutaneous passage of the recording cable did not cause discomfort after the first post-operative day.

Rydell's second patient was a small, 56 year-old woman (body-mass: 44 kg) who fractured her femoral neck during a fall. The instrumented prosthesis was implanted without cement, and, in this case, there was an exact match between the diameter of the prosthetic ball and the original head of the femur. Despite the presence of coxa valga of both femora (neck-shaft angle: 140°), the proximal femur was reconstructed with an endoprosthesis with a neck-shaft angle of only 120°. Both femora also had rotational deformities: the anteversion of the femur was 38° on the contralateral side and 35° on the prosthetic side in contrast to the normal range of 5-25°. Although Rydell did not report whether the patient's leg lengths were equal after the operation, an EMG examination at seven months post-operatively revealed functional abnormalities of gluteus medius and maximus. The adductors and rectus femoris were normal although the patient had "a decreased ability to externally rotate" the operated hip.

Both patients walked on instrumented platforms which measured components of the foot/ground reaction force directed vertically and in the direction of gait. Simultaneously, a film of each subject was recorded at a speed of 64 frames/second to allow the stages of the gait cycle to be reconciled with the recordings of foot/ground reaction force. In the first subject, marked irregularities were observed in the foot/ground reaction force and in the relative duration of the stance and swing phases. These irregularities were more common at slower speeds (0.7 m/s) where the stance/swing ratio was 1.60 for the prosthetic limb vs. 2.57 for the opposite side (normal value: 1.06 ± 0.07). The second patient showed no abnormalities and had a stance/swing ratio of 1.04 ± 0.07. Rydell suggested that the cause of the abnormal gait in his first patient was either

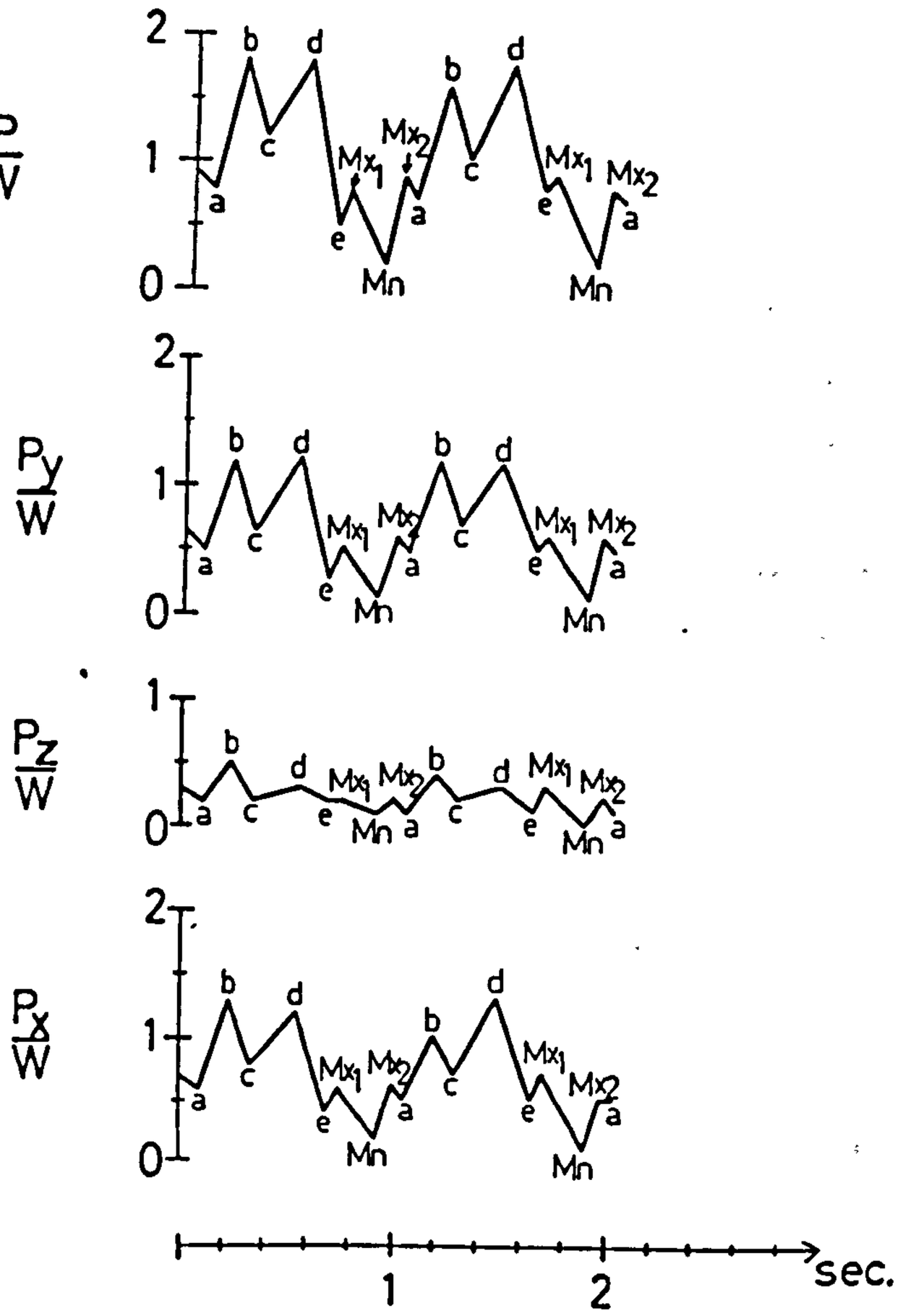

Figure 2.1 Typical data reported by Rydell (1966), of his first patient during level walking. The joint reaction force, P, is reported with its components Py, Pz, and Px with respect to the mass of the body at rest (75 kg).

the mismatch between the femoral head and the acetabulum or loosening of the prosthesis within the femur.

The data reported by Rydell for normal walking at six months post-operation showed two distinct maxima of the hip joint reaction force during each gait cycle, as predicted by Paul's analysis of kinematic and force plate data. During level walking at a self-selected speed (1.3 - 1.4 m/s), Rydell measured joint forces of up to 1.80 times body-weight (BW) in his first patient (fig 2.1) and 3.3 BW in his second patient (fig 2.2). In the second patient, the hip force rose to 4.3 BW during running (2.5 m/s) and 3.4 BW during stair-climbing. The considerable difference in the data from these two patients may be attributed to a variety of factors, including large differences in the body-weight, walking speed and stride lengths of both subjects. The use of a hemi-prosthesis with a significantly undersized head may have also led to some inaccuracy in the force measurements performed in the first patient. Nonetheless, Paul (1976) has demonstrated that Rydell's data are reasonably consistent with his own predictions of hip forces, if the differences in body weight and stride length of the two subjects are taken into account (fig 2.3).

In the United Kingdom, English and Kilvington (1979) recorded forces acting along the axis of the femoral neck using a specially designed femoral prosthesis with reduced medial offset. The neck of the prosthesis was oriented at 25 degrees to the shaft to minimize the errors associated with the in-plane and out-of-plane components of the hip joint force. Data were recorded from one patient for a period of 42 days postoperatively. The prosthesis was implanted in a valgus orientation with the greater trochanter osteotomized and grafted in a laterally offset position to reduce the hip reaction force. Even so, "axial" forces of up to 2.56 times body weight were recorded during slow walking (0.44m/s). This report is informative and allows a lower bound to be placed on the magnitude of the joint reaction force; however, as the orthogonal components of the force acting on the neck of the prosthesis were not measured by the authors, the joint reaction force cannot be calculated from the recorded data.

Another instrumented implant was developed at Case Western Reserve University in Cleveland. In this design, strain gages bonded to the neck of a prosthesis allowed the loading of the hip joint to be recorded for up to 500 hours via an integral telemetry system (Davy et al 1988;

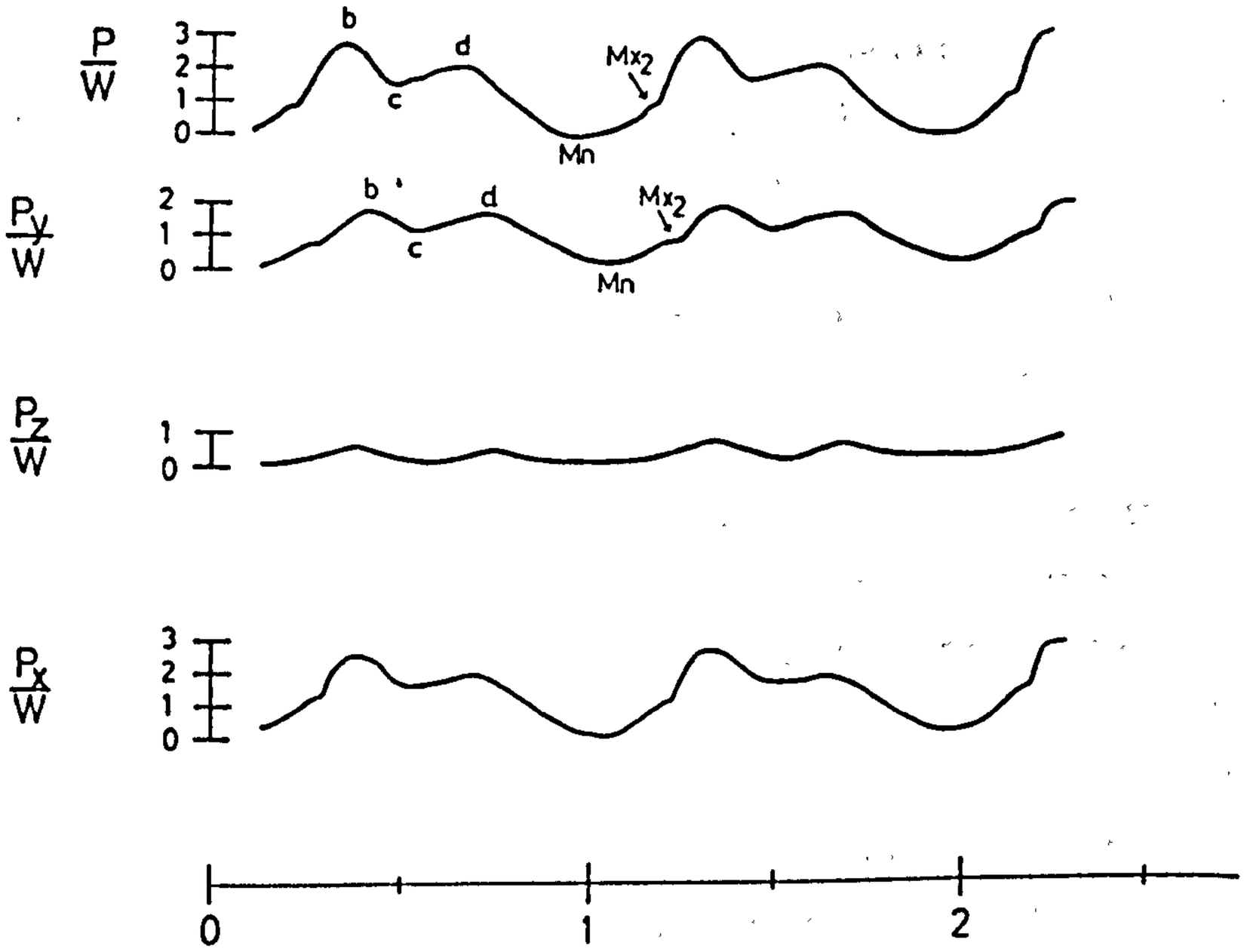

Figure 2.2 Experimental data reported by Rydell (1966) for his second patient (body mass [W] = 44 kg).

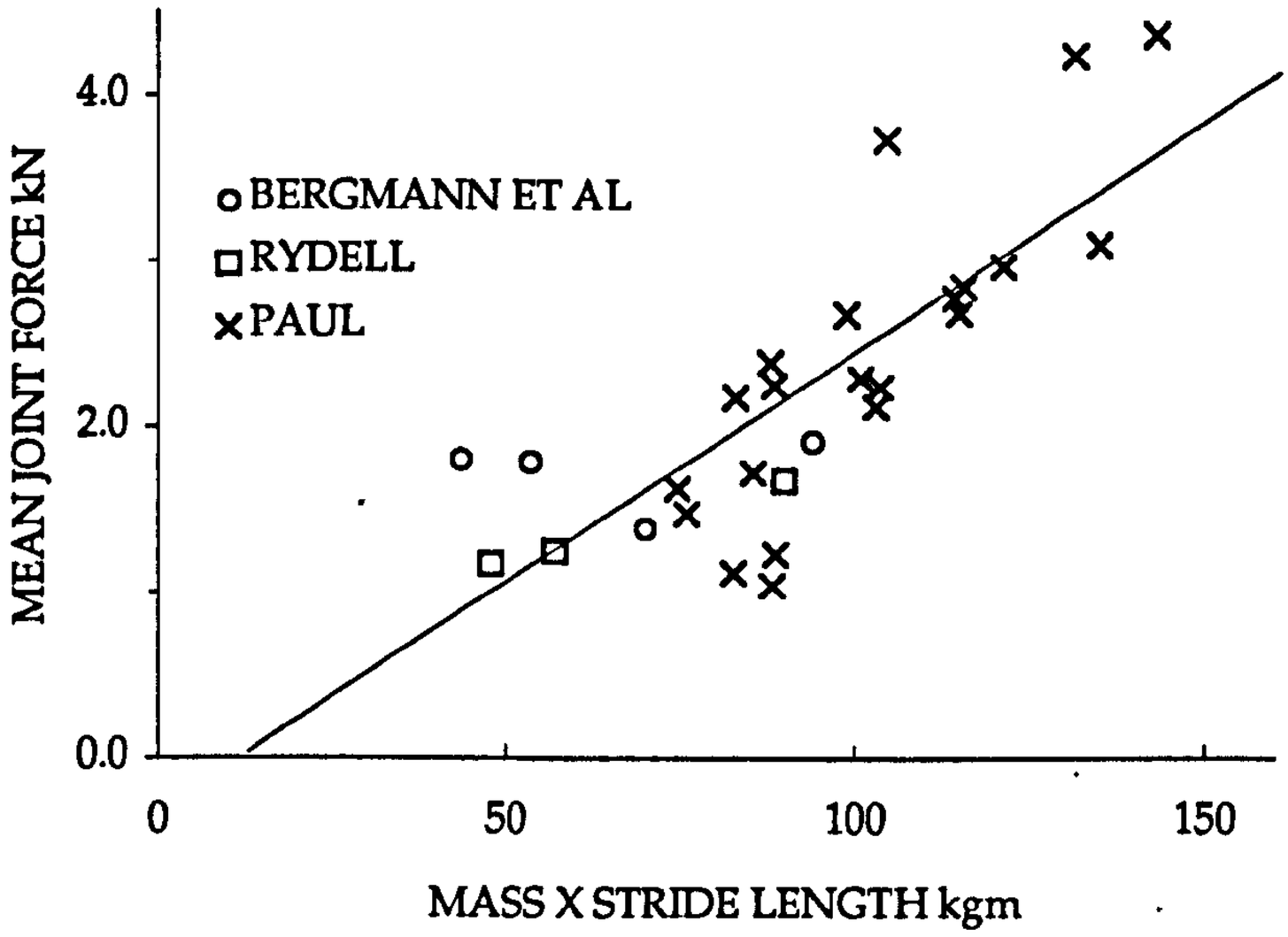

Figure 2.3 Average of the two maxima of the joint reaction force occurring during early and terminal stance for each subject of Rydell (1967), Paul (1967) and Bergmann et al (1993). All values are plotted as a function of the quantity body mass x stride length.

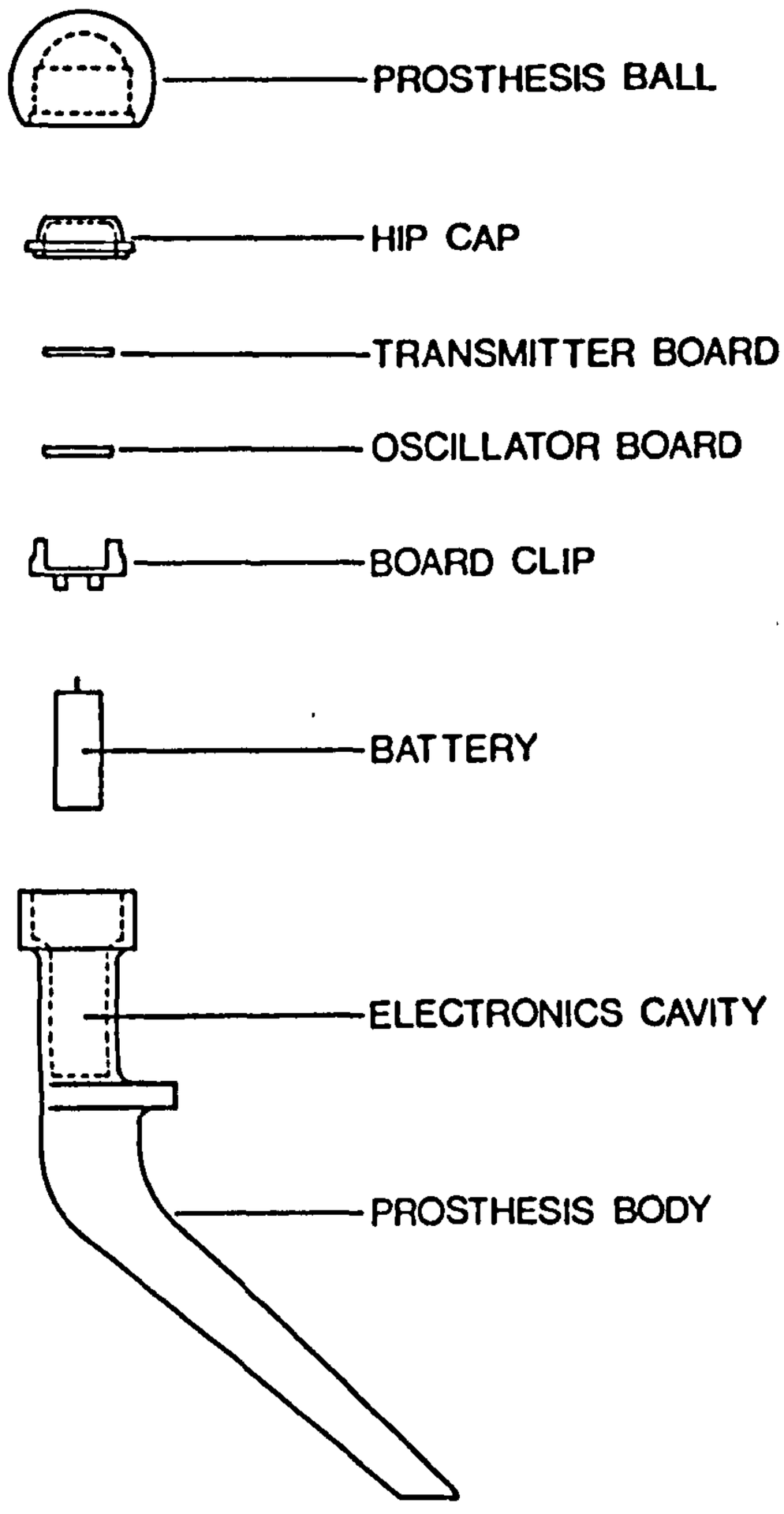

Figure 2.4 The major components of the telemetric prosthesis of Davy et al (1988). The electronic components were pre-assembled and inserted in the neck of the prosthesis as a single unit.

Brown et al 1985; Goldberg et al, 1988) (fig 2.4). Two implantations were performed using devices of this design, one in a female patient in 1984, from whom data were recorded for 31 days, and a second in a male patient in 1987, from whom 44 days of data were collected (Davy et al, 1988; Brown et al, 1985; Goldberg et al, 1988). All data were reported with respect to the neck of the prosthesis using an axis system similar to that of Rydell. The total joint reaction force was approximately 2.7 BW for slow walking and varied little in terms of its direction with respect to the implant.

In 1989, Bergmann and coworkers from Berlin reported long term measurements of hip forces obtained from a very active, 82 year old male patient performing a wide range of activities. Their system consisted of an array of semiconductor strain gages fixed to the inner surface of a prosthesis with a hollow neck and an integral telemetry system. All data from these experiments were reported with respect to a coordinate system based upon the orientation of the femoral shaft and not the neck of the prosthesis as in earlier studies (fig 2.5).

Using this device, the total hip joint force was found to be 2.7-3.4 BW with very slow walking (0.3 m/s), increasing to 3.3-4.3 BW at normal walking speed (1.3 m/s). Surprisingly, the joint reaction force was found to be inclined at 25 degrees to the femoral axis within the coronal plane; this was in contrast to 10-20 degrees in previous intravital studies and 14-21 degrees in the theoretical studies of Pauwels and Maquet. Bergmann's data suggest that the lateral component of the reaction force exceeds the weight of the body for much of the duration of stance phase of the gait cycle, whereas the posterior component varies from near zero for slow gait up to only 38% of body-weight at normal walking speeds (fig 2.6). Even larger forces were measured during common activities, especially rising out of a chair. This causes a considerable component of the hip reaction force to act at right angles to the femoral shaft, generating a large torsional moment about the femoral axis.

The intravital data reported within the literature demonstrate that the relative magnitude of the components of the joint reaction force acting perpendicular to the femoral axis increase with walking speed (table 2.1). This is probably due to the increase in hip flexion that occurs with increased walking speed. In addition, many of the slow speed studies were performed early in the post-operative recovery period, so it

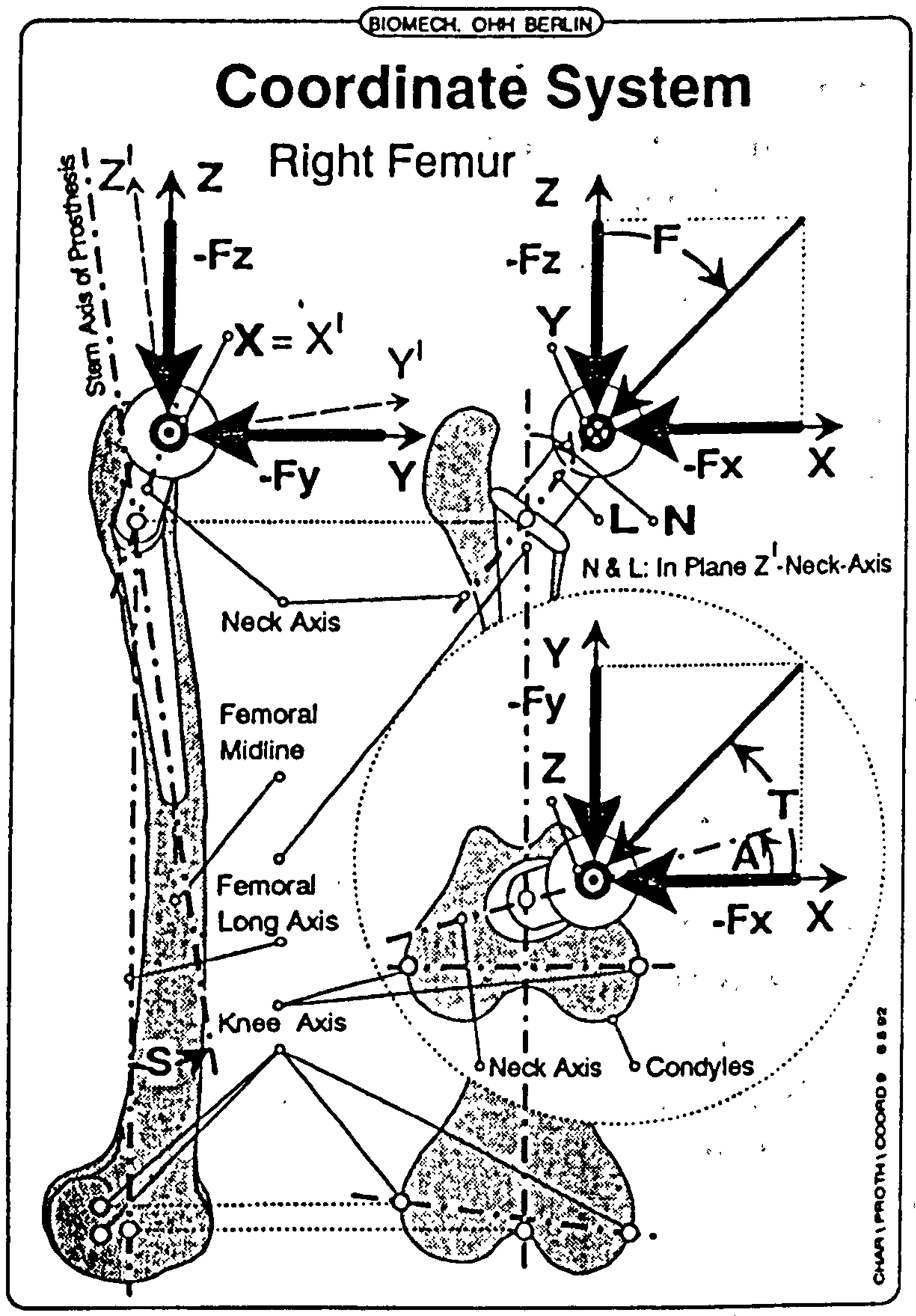

Figure 2.5 Diagrammatic representation of the coordinate system of Bergmann et al (1989), derived with respect to the anatomic axes of the femur.

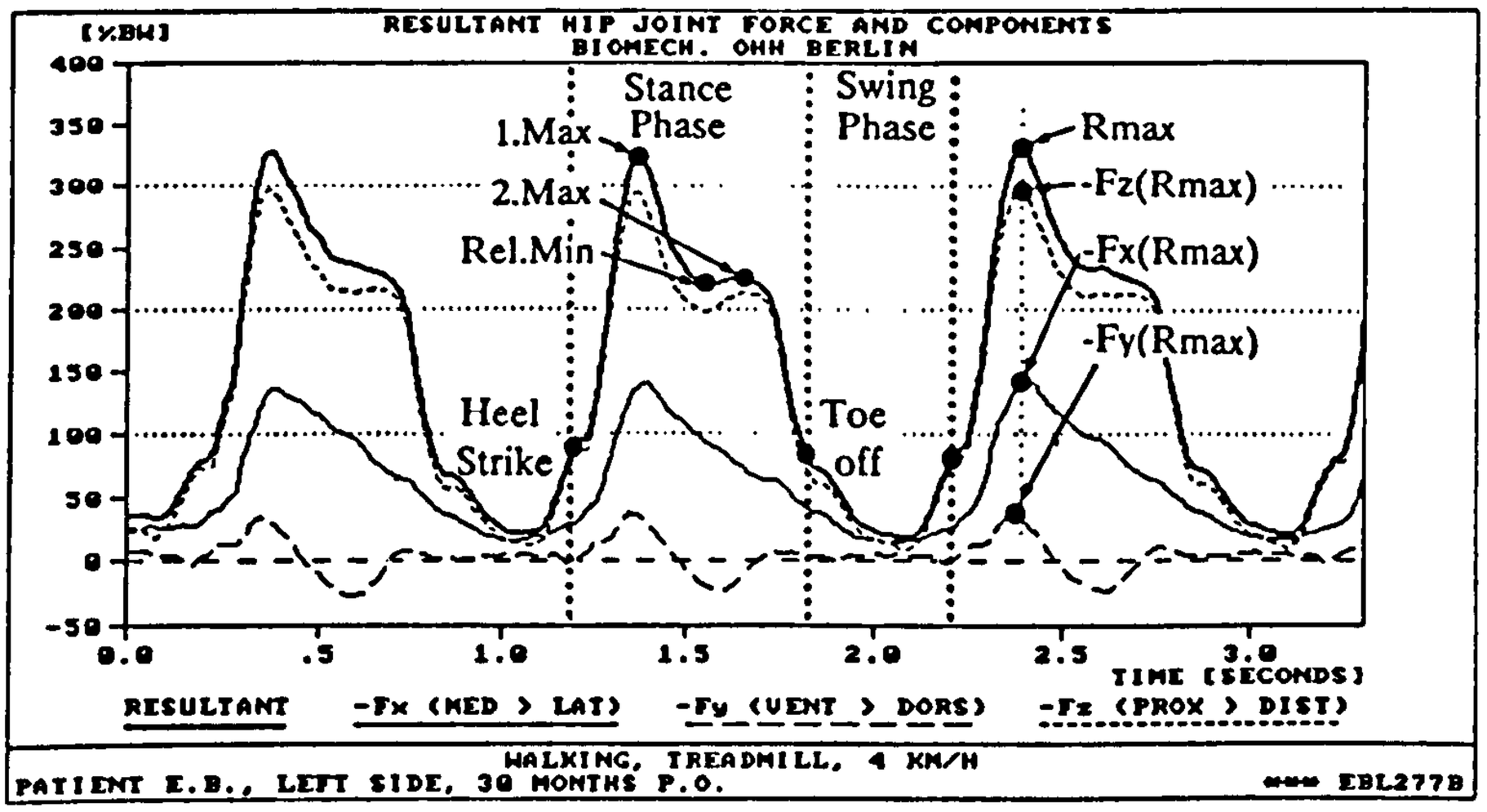

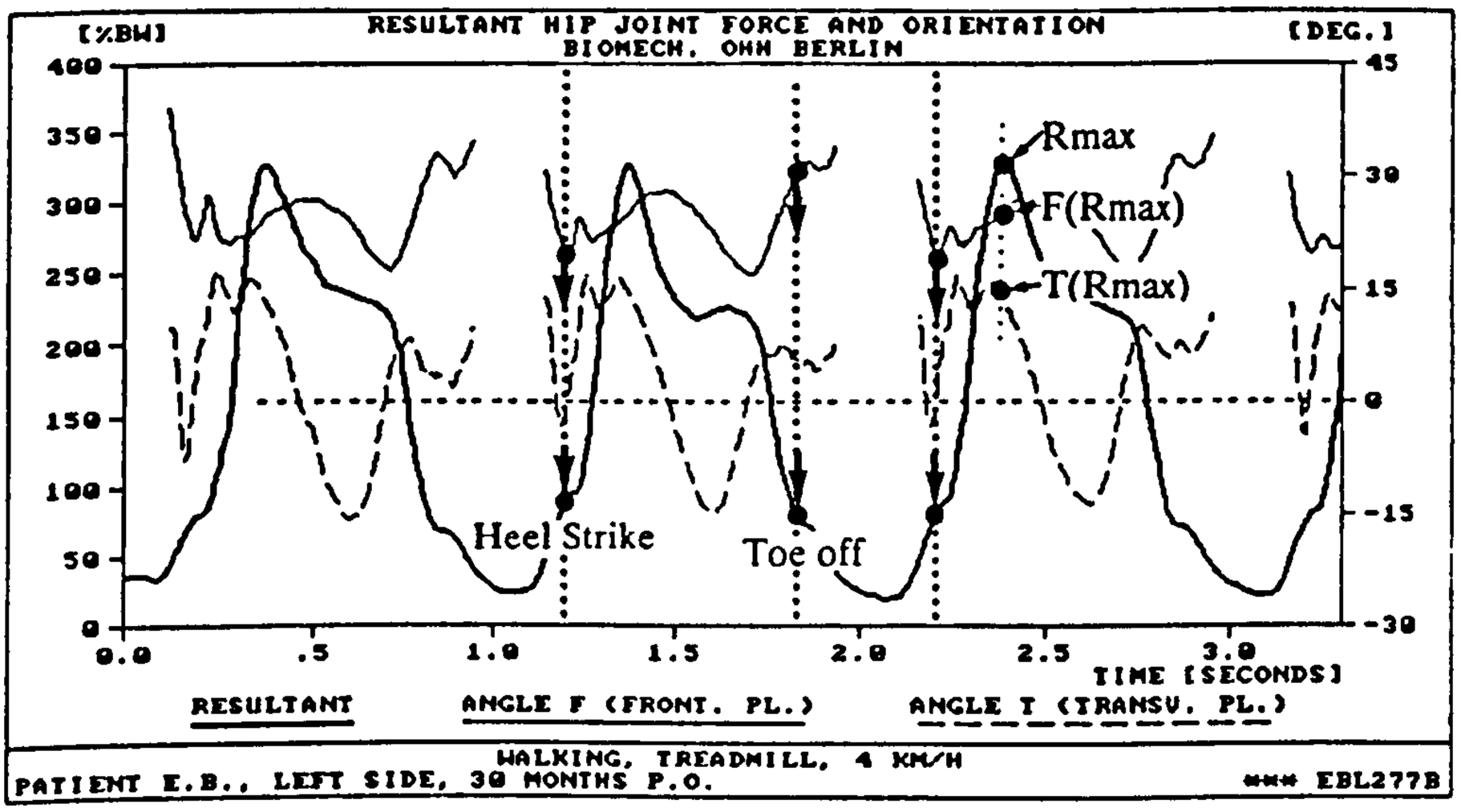

Figure 2.6 Typical data reported by Bergmann et al (1989) for the left hip of their first patient, walking at 4 km/h. In the upper diagram, the resultant joint force and its components are displayed during three walking cycles. In the lower diagram, the resultant force is superimposed on the direction of the resultant acting in the frontal (angle F) and transverse planes (angle T).

Study	Patient No.	Gait Velocity (m/s)	$-F_X$ (% F_R)	$-F_Y$ (% F_R)	$-F_Z$ (% F_R)	F_R
Rydell (1966)	1	0.9	0.42 (28%)	0.21 (14%)	1.43 (95%)	1.51
	2	1.1	0.96 (33%)	0.92 (31%)	2.64 (89%)	2.95
	1	1.3	0.43 (24%)	0.34 (19%)	1.71 (95%)	1.8
	2	1.4	1.07 (33%)	0.98 (30%)	2.93 (90%)	3.27
Davy et al (1988)	1	0.7	0.47 (17%)	0.33 (12%)	2.65 (98%)	2.71
		0.7	0.47 (18%)	0.39 (15%)	2.56 (97%)	2.63
Bergmann et al (1989)	1	0.3	1.18 (41%)	-0.09 (-3%)	2.64 (91%)	2.9
		1.1	1.53 (40%)	0.38 (12%)	3.14 (88%)	3.57
Range of Data		**0.7-1.4**	**(18-42%)**	**(9-31%)**	**(89-95%)**	

Table 2.1 Summary of published data for intra-vital hip forces. All values are expressed in the coordinate system of Bergmann et al which is defined by the frontal plane of the femur and the medullary axis.

X: medial, Y:anterior, Z:superior

is likely that much of the reported data reflect the fact that as patients regained their ability to walk freely during the post-operative period, flexion and adduction of the hip increased and the gait pattern became more natural. These changes necessitate recruitment of muscles which control the horizontal component of the joint reaction force in order to provide necessary stability to the hip joint. Thus, it is not surprising that early in the rehabilitative phase, measurements of the vertical component of hip force range from 95-98% of the total force whereas, later in recovery, values of around 90% appear typical and indicative of normal function.

The data from Bergman's patient seem to be abnormal in the context of the other studies and previous theoretical analyses. In this case, the total joint force is unusually high, not so much because of a larger vertical component but because of the large lateral component, reported to average 1.75 times body weight at normal walking speeds. Although the high joint reaction force may be explained on the basis of a longer than average stride length, an alternative explanation is that in this patient, extraordinary co-contraction of antagonistic muscle groups was necessary due to some instability of the hip following joint replacement. This may be due to some abnormality of the position of the prosthesis (e.g. reduced medial offset or a change in the anteversion of the femoral head) or could have been caused by loss of normal function in one or more muscle groups secondary to the operative procedure. Another peculiarity of this patient's gait was the attenuation of the second maximum of the hip reaction force, which one would have expected to be of similar magnitude to the first. This may be due to the presence of a flexion contracture which would have prevented normal extension of the hip at the end of stance phase. Unfortunately, data on these points are not presently available.

An underlying assumption in the use of instrumented prostheses to study human gait is that the implantation procedure and the presence of the hip prosthesis itself does not alter the loading of the hip joint. This issue can be examined through detailed kinematic measurements on patients after unilateral hip replacement by comparing ground force reaction patterns and kinematic parameters describing the function of prosthetic and contralateral hips. Alternatively, the gait parameters of patients following joint replacement may be compared to normal

controls. It is surprising how few published studies have quantified gait following hip replacement. Brown et al (1984) used gait analysis and a biomechanical study to predict the joint reaction forces of 14 subjects with unilateral hip disease who underwent total hip replacement and eleven healthy subjects without evidence of hip disease. Two different designs of hip implants had been implanted in the joint replacement patients, the Charnley round-backed prosthesis (8 patients) and the CAD Muller prosthesis (6 patients). A fundamental difference in these two prostheses was their relative head offset and neck-shaft angle; the CAD Muller stem was designed with a more vertical neck and one third less medial head offset than the Charnley design in an attempt to reduce lateral stresses and protect against stem breakage.

The results of Brown et al (1984) showed that both prosthetic devices caused significant changes in the magnitude and duration of loading of the hip joint. The first maximum of the joint reaction force (early stance phase) was 4.0 times body weight at a self-selected speed of gait in the normal subjects, compared to 3.4 BW in the CAD-Muller group and 2.7 BW in the Charnley group. There was little difference between the three groups in terms of the inclination of the joint reaction force in the lateral view which ranged from 6-10 degrees towards posterior (with respect to the axis of the implant). In the coronal plane, the joint reaction force was inclined at an average of 26 degrees lateral to the mechanical axis of the femur in the normal subjects in comparison to only 16 degrees in the Charnley group and 14 degrees in the CAD-Muller group. These differences indicate that the forces borne by the prosthetic hip and the normal joint may be quite different so that data derived from instrumented prostheses may only provide a first approximation of the load being transmitted by the normal hip joint.

2.1.3 Load Transfer across the Hip Joint

Few studies have directly measured the distribution of contact between the acetabulum and the femoral head in the normal joint. In 1968, Bullough and Goodfellow studied load transfer in the hip joint by manually loading cadaveric specimens and using dye transfer to indicate articular contact. In younger specimens it was found that a triangular area of the acetabular surface in the dome of the acetabulum did not bear weight with loading but that in older specimens virtually complete load

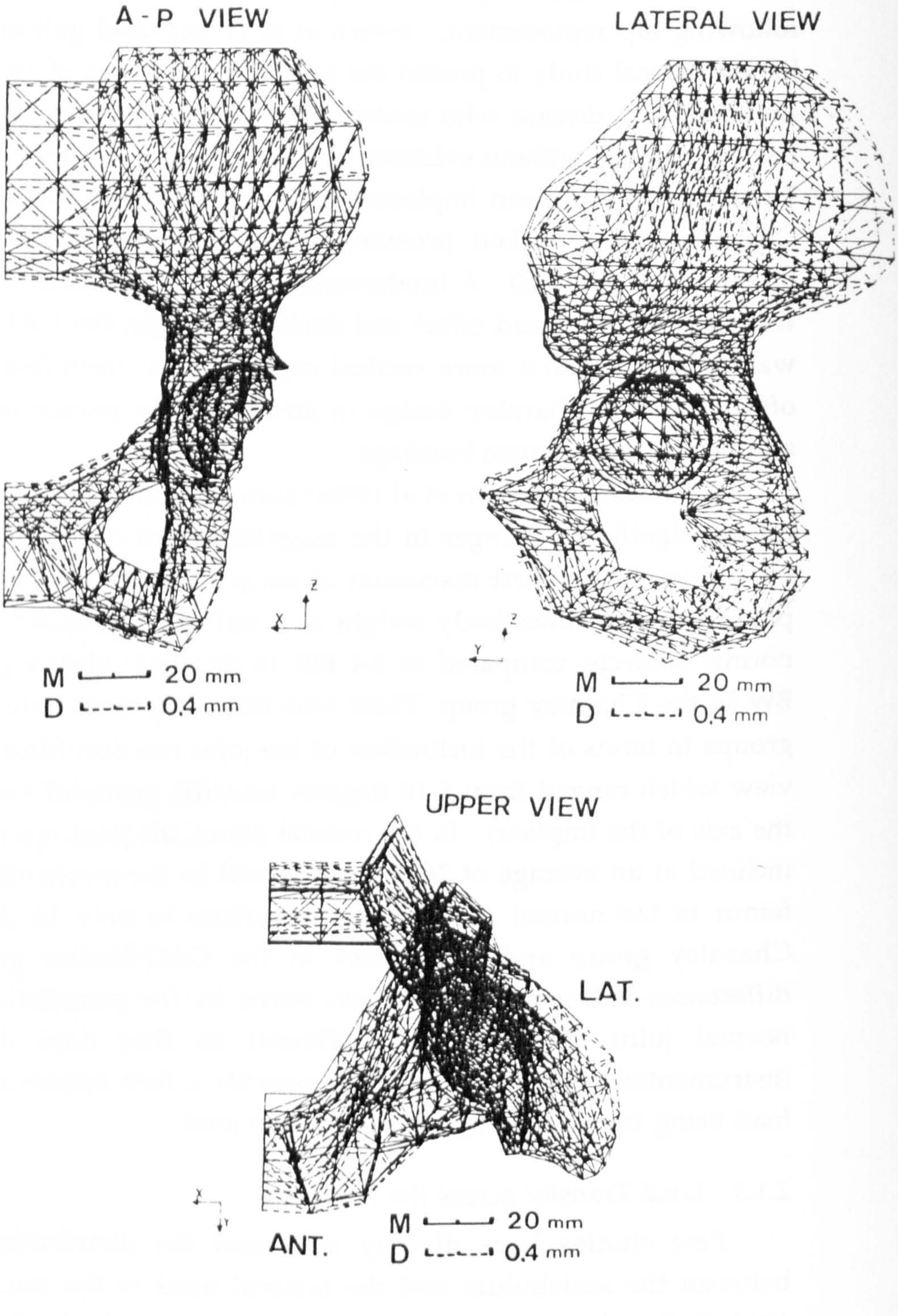

Figure 2.7 Summary of the pelvic displacement predicted by the finite-element model of Oonishi et al (1983) for unilateral weight bearing.
M: dimensions of the original model.
D: magnitude of model displacements.

transfer was present over the entire lunate surface. These results were contested by Greenwald (1972) and Greenwald and O'Connor (1971) who found that the size and location of contact areas in the hip joint varied with the magnitude and direction of the applied force due to the incongruity of the acetabulum and the femoral head. These conclusions were based on measurements of the weight-bearing areas of 51 normal adult hips using an apparatus that loaded the joint in various positions simulating the orientation of the hip at different stages of the gait cycle. Under normal joint loads it was concluded that the entire surface of the acetabulum was weight-bearing, whereas at lower loads, corresponding to the swing phase of the gait cycle, load transfer was restricted to the anterior and posterior areas of the articular surface.

The work of Byers et al (1970) has shown that the dome of the acetabulum is lined with fibrocartilage as load transfer in the young, healthy joint is predominantly anterior and posterior and not superior. As fibrocartilage has a lower compressive modulus than articular cartilage, it appears that the normal distribution of compressive stress between the femoral head and the acetabulum is nonuniform, with low compressive stresses within the dome. However, in older individuals, as the joint surfaces become more congruent, this area may be forced to bear greater pressures during gait, leading ultimately to osteoarthritic degeneration. A factor entirely unexplored in any of these studies is the possible role of the stiffness of the bony acetabulum in the etiology of osteoarthritis as elastic deformation controls the peak contact stress and the distribution of load transfer between the femoral head and the acetabulum.

2.2 DEFORMATION OF THE PELVIS

2.2.1 Theoretical Studies

In several published accounts, the stresses developed within peri-acetabular bone during weight-bearing have been predicted using finite element methods (FEM). Oonishi et al (1983) developed a three-dimensional model of the entire pelvis based upon detailed measurements of one cadaveric specimen (fig 2.7). Their model assumed right-left symmetry; the pelvis was modeled with triangular and quadrilateral membrane elements representing a cortical shell of 1 mm

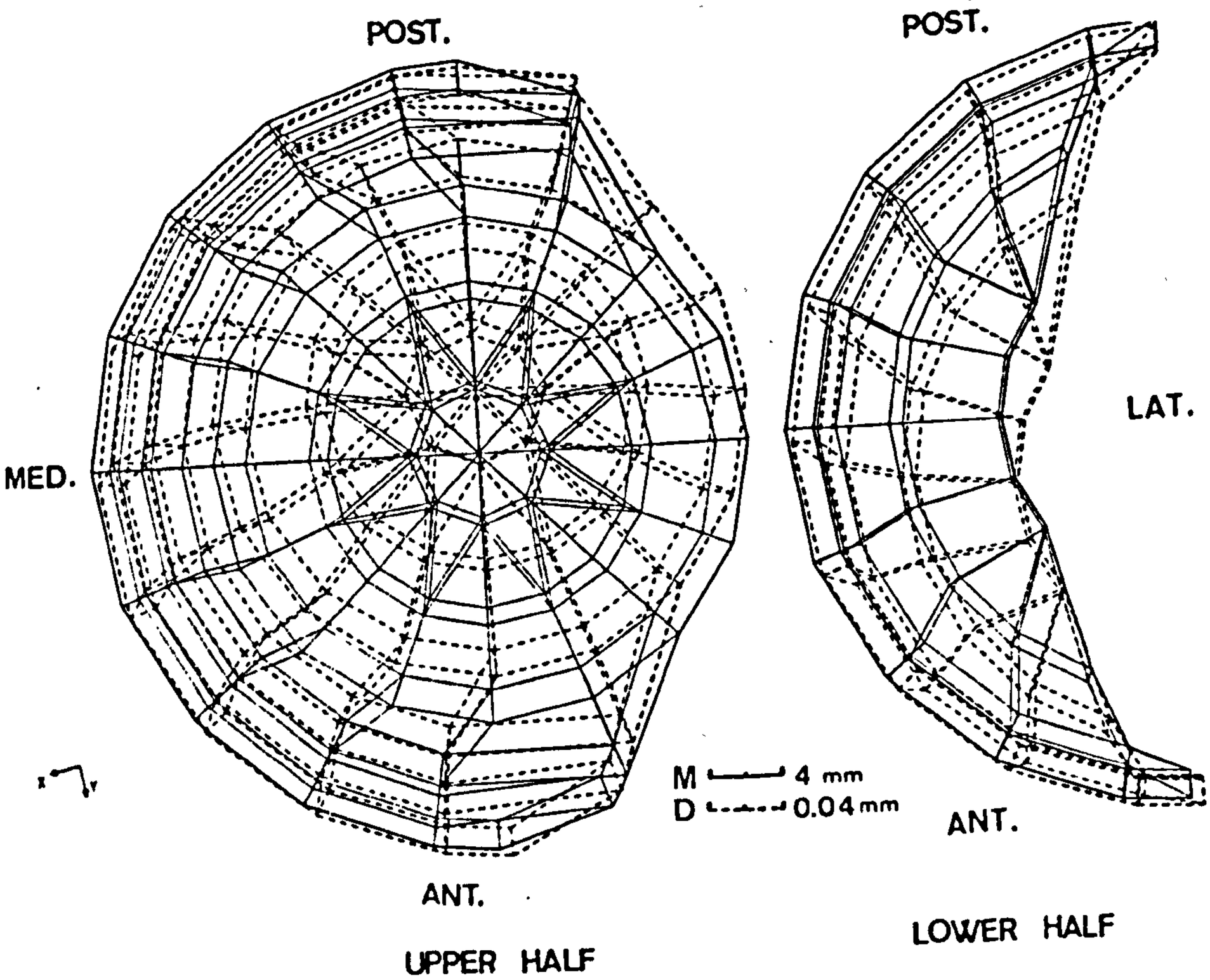

Figure 2.8 Acetabular displacement as predicted by the analysis of Oonishi et al (1983).

thickness filled with solid elements representing cancellous bone. An attempt was made to replicate the loading of the hip joint during single-legged stance, using the muscle forces predicted by Crowninshield et al (1978) at the first maximum of the joint reaction force. Flange elements were used to represent six muscle groups: the glutei, tensor fascia lata, the hamstrings and the adductors, each muscle having one fixed point of insertion and an origin distributed over 28 nodal points. It was assumed that during unilateral stance, the same muscles contract on the loaded and unloaded sides of the pelvis, but that the force of contraction of each muscle on the loaded side was 5 times that of its contralateral counterpart.

Boundary conditions for the model were imposed at the vertical plane of symmetry of the pelvis and within the hip joint. Two separate solutions were derived assuming that the pelvis was constrained vertically and then horizontally along the mid-plane of the sacrum and the pubic symphysis. Superposition of both solutions was performed to predict the total displacement of each node. Within the hip joint, acetabular displacement was restrained in a direction normal to the articular surface over the superior weight-bearing dome.

This analysis predicted that the predominant mode of deformation of the pelvis consists of bending about a fulcrum formed by the femoral head. It was predicted that the anterior and posterior walls of the acetabulum would deflect by approximately 20 μm in a superior direction during weight-bearing, whereas, in the transverse plane, stretching of the inferior half of the lunate surface would occur with most of the acetabulum shifting anteriorly by 15-20 μm (fig 2.8). This was accompanied by posterior displacement of the superior half of the acetabulum by approximately 30 μm. It was predicted that little deformation of the rim of the acetabulum would occur in either the anterior-posterior or superior-inferior directions during normal loading.

Some difficulties are encountered in applying the results of this analysis of the entire pelvis to the relatively small area of the acetabulum and their peri-acetabular bone stock as the mesh employed in the model was relatively coarse in comparison with the dimensions of the acetabulum and the thickness of the acetabular walls. To simplify this model, highly generalized assumptions were made concerning the elastic properties of the peri-acetabular bone, despite the variability of the density of the cancellous bone and the thickness of the cortical shell. A further

criticism is the representation of the acetabulum by a series of shells with an irregular, anatomically-contoured boundary. In practice it is expected that the complex geometry of the acetabular notch, the fascies lunata and the inferior facets would also significantly influence the distribution of stress and the bulk deformation of the biologic specimen.

A more realistic representation of the loading, geometry and material properties of the acetabulum was presented by Koeneman et al (1989) and by Hansen and Koeneman (1989) who developed a three-dimensional finite element model of the hip joint consisting of 5500 solid and membrane elements. This model was based upon data from a computer-assisted tomography study which demonstrated that the thickness of the cortical shell varied considerably at different points around the acetabulum, though typically it was less than 0.5 mm and not 1 mm as Oonishi et al (1983) had assumed. Two activities were simulated using this model: one-legged stance and rising from a chair. Four muscles were included in order to obtain static equilibrium: gluteus maximus, medius and minimus, and tensor fascia lata. The ratio of muscle forces was fixed in proportion to the bulk of each muscle, independent of the functional activity being modelled. Material properties were represented by three densities of cancellous bone and three forms of cortical bone (solid cortex, thin cortical membrane and subchondral plate).

One of the interesting features of this model was the use of the Specified Boundary Displacement Method to increase the resolution of features of interest in the vicinity of the acetabulum. Using this technique, the displacement constraints of a boundary enclosing the acetabulum were predicted using a coarse model of the bulk structure. A sub-model of fine mesh size was then developed within the boundary using the predicted boundary conditions. This model allowed the anatomic features and discontinuities in the geometry and material properties of the acetabulum to be represented with greater accuracy than was possible in earlier models in which the entire pelvis was represented by elements of approximately similar size.

The stresses within cancellous bone predicted by Hansen and Koeneman's model were less than those predicted previously using two dimensional FEM models but greater than those predicted by axisymmetric representations of acetabular geometry. Under loading, it

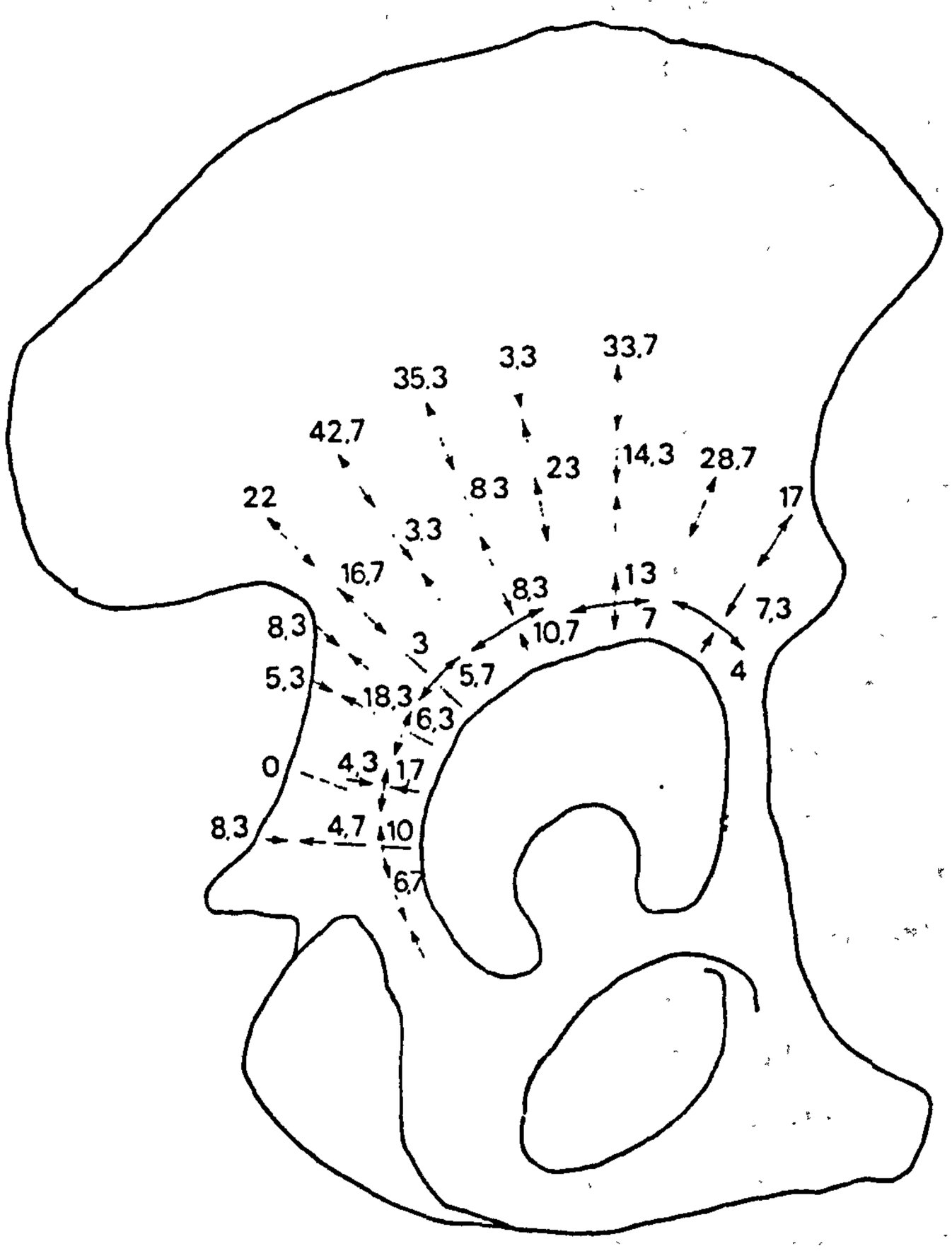

Figure 2.9 Deformation (in microns) of the lateral cortex of the ilium as reported by Rabischong et al (1977).

was predicted that the wings of the ilium would bend laterally and inferiorly. Considerable deformation was predicted within the acetabulum, of the order of 200 μm in one-legged stance and 500 μm during rising from a chair. Loading of the hip joint was shown to be concentrated over the superior dome during standing, causing a gap to appear inferiorly between the femoral head and the acetabulum. In rising from a chair, it was predicted that load transfer would be situated more inferiorly, and that the separation of the anterior and posterior columns would be reduced, causing "lateral pinching" of the femoral head by the acetabulum.

2.2.2 Experimental Studies

Several authors have attempted to measure the deformation of the pelvis during load-bearing. Rabischong et al (1977) describe experiments using embalmed pelves loaded with bilateral femoral support in which the action of the glutei, the tensor fascia lata and the ilio-psoas were simulated using nylon cables. A body-weight of up to 600 N was employed in a variety of postures representing single and double limb stance. During these experiments, the deformation of the periacetabular bone was measured using metal strips, formed into semicircular clips and attached at each end to the lateral cortex. Strain gages attached to the curved surface of each clip allowed the elongation of the underlying bone to be monitored.

Several significant observations were made in this study (fig 2.9). Although the authors report results obtained from only one specimen and though the precise orientation of the specimen is difficult to deduce from their report, elongations of 2-10 μm were observed circumferentially around the acetabular margin. Radially, the deformation of the cortex varied from 4.3 μm of compression to 13 μm of tension in no systematic pattern. At sites located further from the acetabular rim, generally larger values were measured with elongations of 20-40 μm being reported across the base of the ilium. Assuming that the gage length of each transducer was approximately 20 mm, these values correspond to strains of 100-500 microstrain around the acetabular rim and 1000-2000 microstrain on the surface of the ilium.

It is surprising that Rabischong et al reported tensile strains within the lateral cortex of the ilium in the presence of abductor loading.

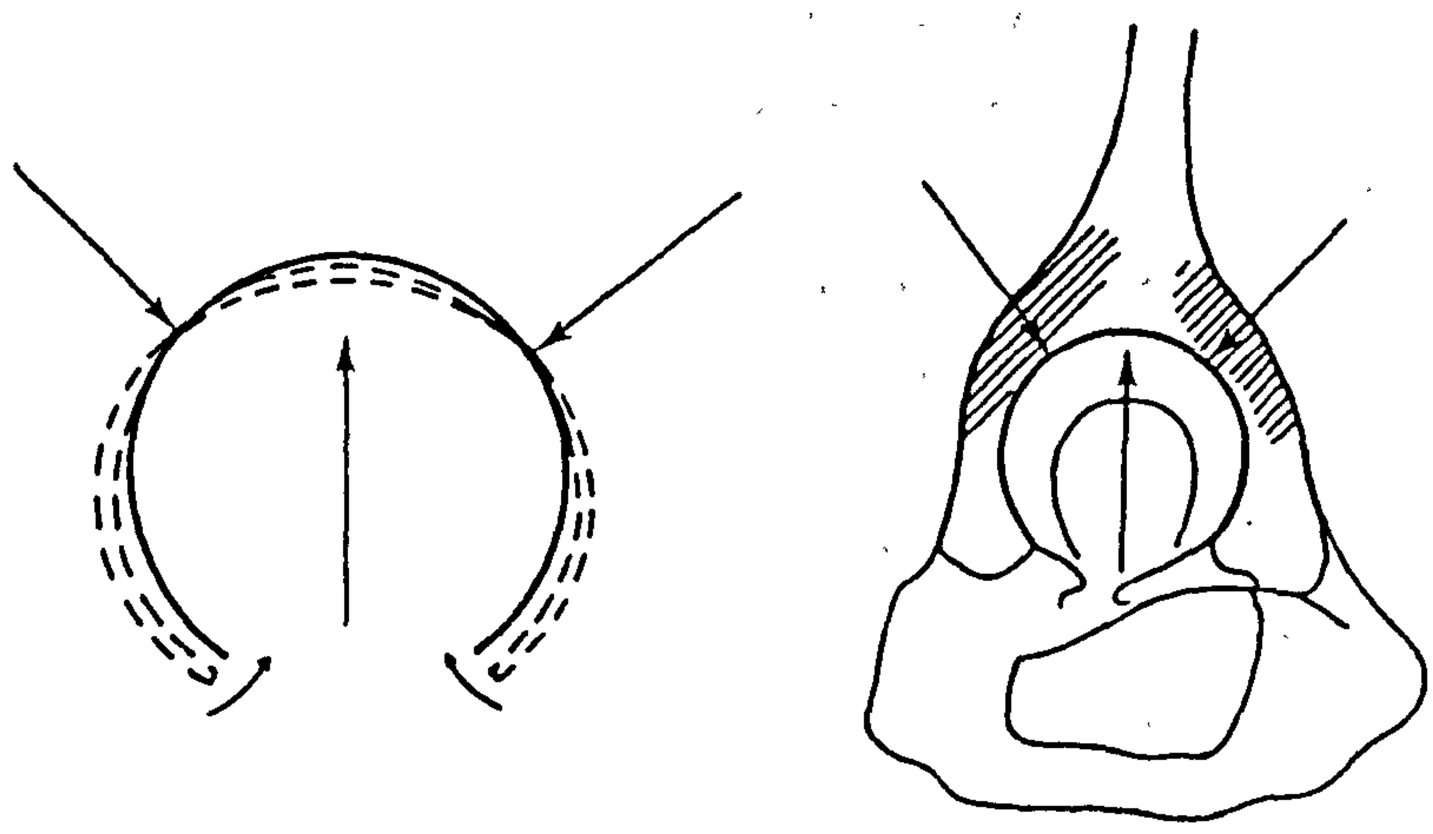

Figure 2.10 Schematic representation of the deformation of the acetabulum with loading, according to Teinturier et al (1984).

However, they did note that the displacement of the acetabulum, the sacro-iliac joint and the pubic symphysis was altered by variations in the magnitude of the gluteal muscle force. The displacements of the cotyloid facets were lowest in bipedal stance without muscle forces (22 μm) and with loads simulating the glutei and the tensor fascia lata (25 μm). These deformations were doubled (48 μm) in conditions simulating single leg stance which necessitated the addition of 350N of gluteal force to maintain joint equilibrium. Again, as data from only one experiment were reported, it is not possible to assess the significance or reproducibility of these data.

A similar study has been reported by Teinturier et al (1983), also within the French literature. In this paper the authors discuss experiments which they performed to measure the deformation patterns of the acetabulum before and after joint replacement but only report their findings in qualitative and philosophical terms. Much of this work is difficult to follow due to its inexact description, however the authors mention that photoelastic and extensometric studies were performed to allow measurement of the deformation of the acetabulum in cadaveric specimens. To simulate bipedal support, loads of up to 1250-1500N were applied to the spine at the L4 body using an hydraulic jack. They do not mention whether muscle forces were simulated or the specific method employed to measure the deformation of the cadaveric acetabula during loading. However, based upon their observations, Teinturier and co-workers concluded that, with abduction and anteversion of the femoral head, the acetabulum elongates slightly in the superior-inferior direction and narrows in the anterior-posterior direction.

In these experiments, the greatest acetabular displacement was observed inferiorly corresponding to narrowing of the acetabular notch with increasing load (fig 2.10). Two stationary points were identified, situated at approximately 45° anterior and posterior to the axis of the iliac wing about which the walls of the socket appeared to bend during loading. The magnitudes of these deformations were only reported in terms of the relative motion of the cotyloid facets. With increasing load, the width of the acetabular notch in one specimen was reduced by approximately 50 μm under a joint load of 305 N and 100 μm at 600 N (fig 2.11). These experiments were repeated to determine the effects of femoral anteversion on acetabular deformation. It was found that with

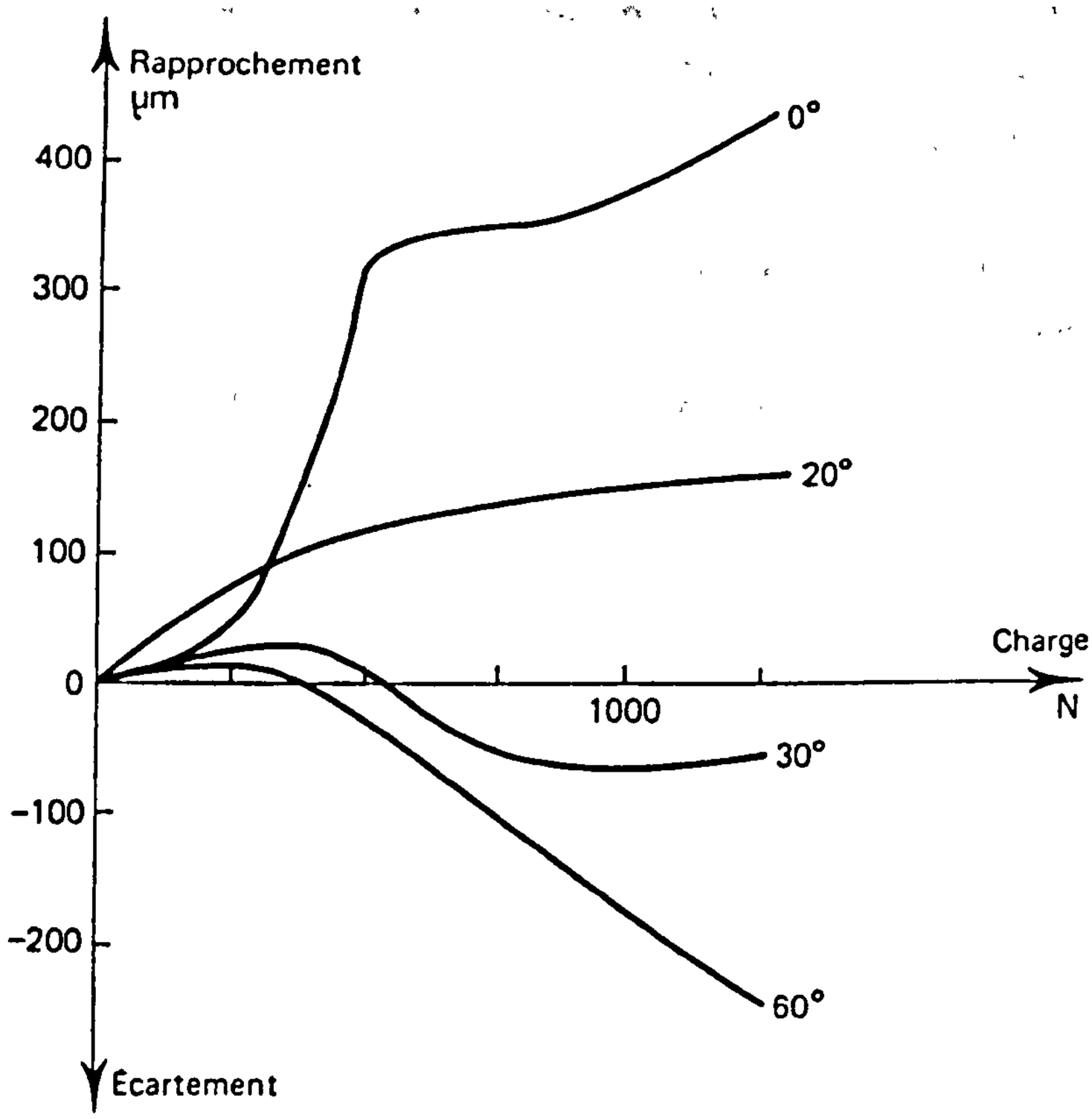

Figure 2.11 Results reported by Teinturier et al (1984) illustrating the displacement of the cotyloid facets as a function of axial load and the anteversion of the femoral neck.

internal rotation of the femur, the deformation of the acetabulum increased dramatically with the separation of the facets decreasing by up to 400 μm under joint loads of 500-600 N. Conversely, with external rotation of the femur, the width of the acetabular notch increased by 70 μm with 30 degrees and 180 μm with 60 degrees of external rotation.

Teinturier et al also reported their results as a function of the age of the donor of each pelvic specimen; they suggested that acetabular deformation decreased with age, possibly because of the increasing sphericity of the femoral head and the lunate surface. Thus they surmised that the primary cause of deformation of the acetabulum with loading was adjustment of the incongruity of the femoral head and the acetabulum, and not stretching of a congruent socket in response to axial load.

Experimental measurements of the strains developed over the cortical surface of the loaded pelvis and acetabulum have been reported in a number of studies. Jacob et al (1976) prepared epoxy replicas closely simulating the morphology of the human pelvis (fig 2.12). Initially, a solid epoxy model was instrumented with 80 triaxial strain gages attached to various points on the medial and lateral surfaces of the ilium, the dorsal surface of the ischium behind the acetabulum, the body of the ischium and the posterior wall of the acetabulum. Additional gages were attached to the lunate surface beneath a polymeric layer simulating normal articular cartilage. The model was intended to represent the loading of the pelvis in mid-stance; cables were used to simulate the action of gluteus medius and minimus, tensor fascia lata and gravitational forces. To more accurately represent the composite structure of the human pelvis, a second model was developed consisting of a solid cortex of epoxy resin with an inner core of epoxy foam. To compensate for the lower strength of the epoxy shell and core compared to cortical and cancellous bone, the authors applied a load of only 80 N to their model and assumed that a direct relationship existed between the recorded strains and those developed in the body under normal physiologic loading.

These experiments demonstrated that most of the load in the normal human pelvis is transmitted by the cortical shell; the role of the cancellous bone within the composite construction appeared to be to maintain the separation of the membrane elements and thus the rigidity

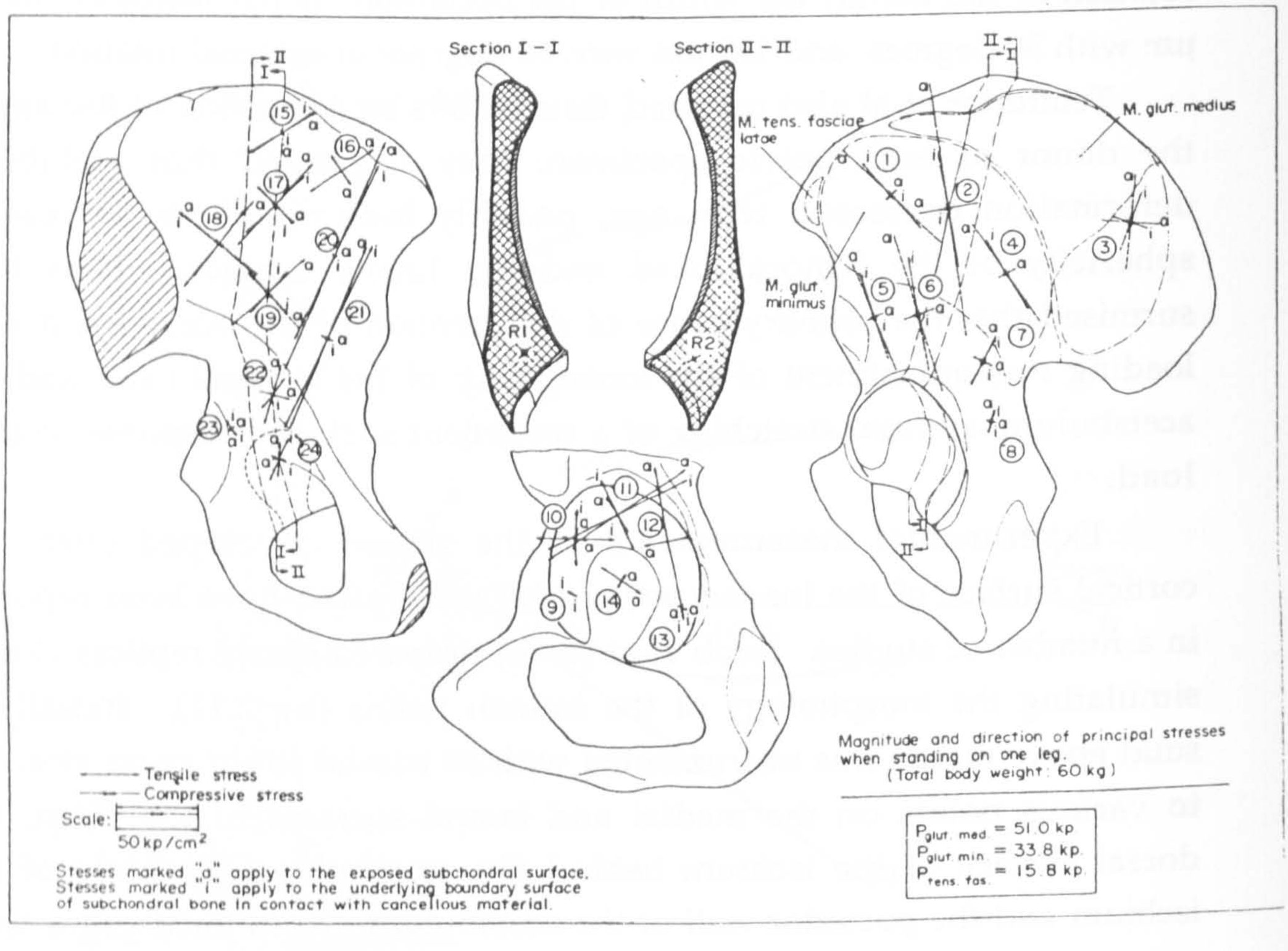

Figure 2.12 The results of Jacob et al (1976), derived from a strain gauged composite model of the pelvis.

of the composite structure. During loading, the femoral head acts as a fulcrum over which the pelvis bends under the action of the abductor muscles laterally and the weight of the body medially. Consequently, large compressive strains were measured over the lateral cortex of the ilium in the direction of the abductor muscle fibers with even larger tensile strains over the medial cortex, along the ilio-pectineal line and over the anterior surface of the ilium. Predominantly tensile stresses were also measured over the subchondral surface of the acetabulum corresponding to stretching of the acetabulum over the articular surface of the femoral head.

A number of authors have measured strains within the acetabulum and pelvis before and after implanting an acetabular prosthesis. Lionberger et al (1985) applied rosette gages at five sites on the pelvis and measured cortical strains during loading. All acetabuli were loaded in axial compression with the iliac wing embedded in a block of plaster. In all, ten acetabuli from five different pelves were tested using a load of 1336 N (300 lb) with the pelvis inclined at 16 degrees to the vertical in the frontal plane. Loads were applied in three positions of the hip joint: 30 degrees of flexion, neutral and 30 degrees of extension. The strain data derived from these experiments were found to vary considerably between specimens, although the directions of the principal strains were reasonably consistent. During normal stance (neutral flexion), the strains measured over the dome of the acetabulum were much lower than those over the posterior rim. However, with flexion of the hip joint, the compressive strains generated over the posterior rim were almost doubled while those along the ilio-pectineal line were halved. In both cases, the tensile stresses were virtually unchanged. In extension, the pattern was reversed; the highest compressive strains were recorded anteriorly whereas almost no strain was present on the posterior cortex.

The data of Lionberger et al (1985) are consistent with the interpretation that during gait, most of the load transmitted by the hip joint passes through the anterior and posterior areas of the lunate surface, depending upon the degree of flexion or extension of the joint. During most activities, the contact force passes posteriorly, hence the concentration of strong cancellous and cortical bone within the posterior column of the pelvis. It would also appear that little of the joint load passes directly superiorly, consistent with the observations of Greenwald

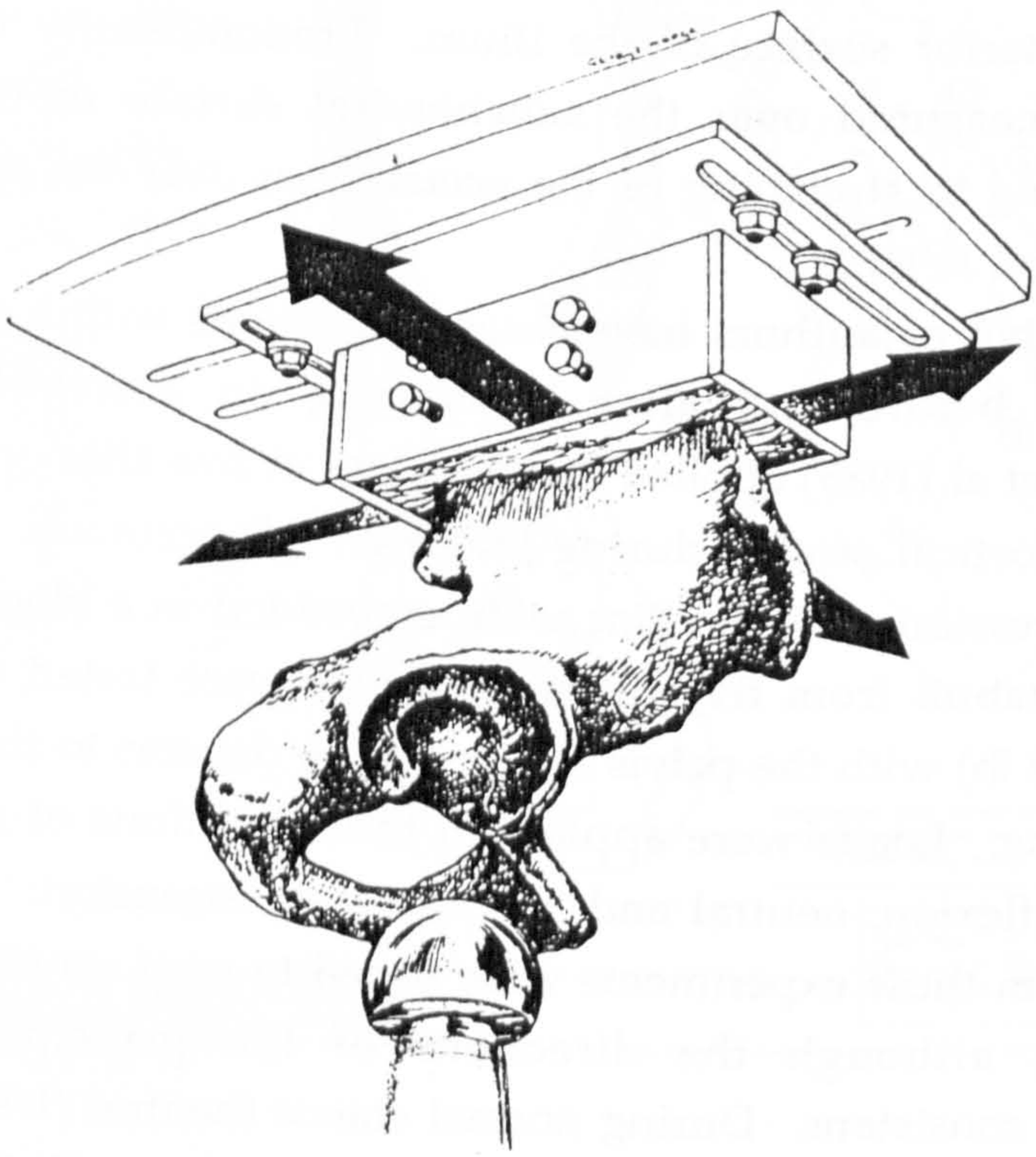

Figure 2.13 Schematic representation of the mechanical fixture of Finlay et al (1986a).

and others that the primary areas of load transfer are the anterior and posterior limbs of the lunate surface with the dome of the acetabulum playing a secondary role.

A very comprehensive study of strains developed in the pelvis with weight-bearing was undertaken by Finlay and co-workers (1986a). Seven embalmed human pelves were instrumented with 25 strain gage rosettes and mounted with the iliac wing embedded in a plaster block in the same manner as the studies of Lionberger et al (1988) (fig 2.13). Each specimen was loaded via the natural femoral head with a static force of 2,500 N without simulation of muscle forces. Strains were measured within the acetabular fossa, around the rim of the acetabulum, over the medial aspect of the pelvis including the anterior column and the quadrilateral surface, and over much of the lateral surface of the ilium (fig 2.14).

A number of surprising results were reported from these experiments. Athough the overall strain pattern was consistent with uniaxial bending, strains over the lateral surface of the ilium were almost entirely tensile. Conversely, compressive strains were observed along the ilio-pectineal line and over much of the medial aspect of the pelvis, superior to the acetabulum. Although consistent with the work of Lionberger et al, the sign and magnitude of many of the strains reported are completely contrary to the findings of Jacob et al (1976). The most reasonable interpretation is that the boundary conditions adopted to simulate normal loading of the pelvis critically affect the cortical strain distribution. Thus, experiments in which the ilium is embedded in a solid block and loaded without simulation of musce forces are likely to generate erroneous and misleading strain data. Given the geometry of the iliac wing, and the line of action of the glutei and tensor fascia lata with respect to the hip joint center, substantial moments are generated by muscle contraction to balance the adducting moment acting on the hip. The bending moment acting on the ilium during the gait cycle is expected to be quite significant, leading to cortical strains far larger than those directly generated by the compressive load applied to the acetabulum by the femoral head.

It is surprising that the studies of Finlay et al (1986b) and Jacob et al (1976) differ with regard to strains within the subchondral plate. In this area, Finlay et al report low strains consisting of radial compression and circumferential tension (hoop stress), whereas Jacob et al measured large

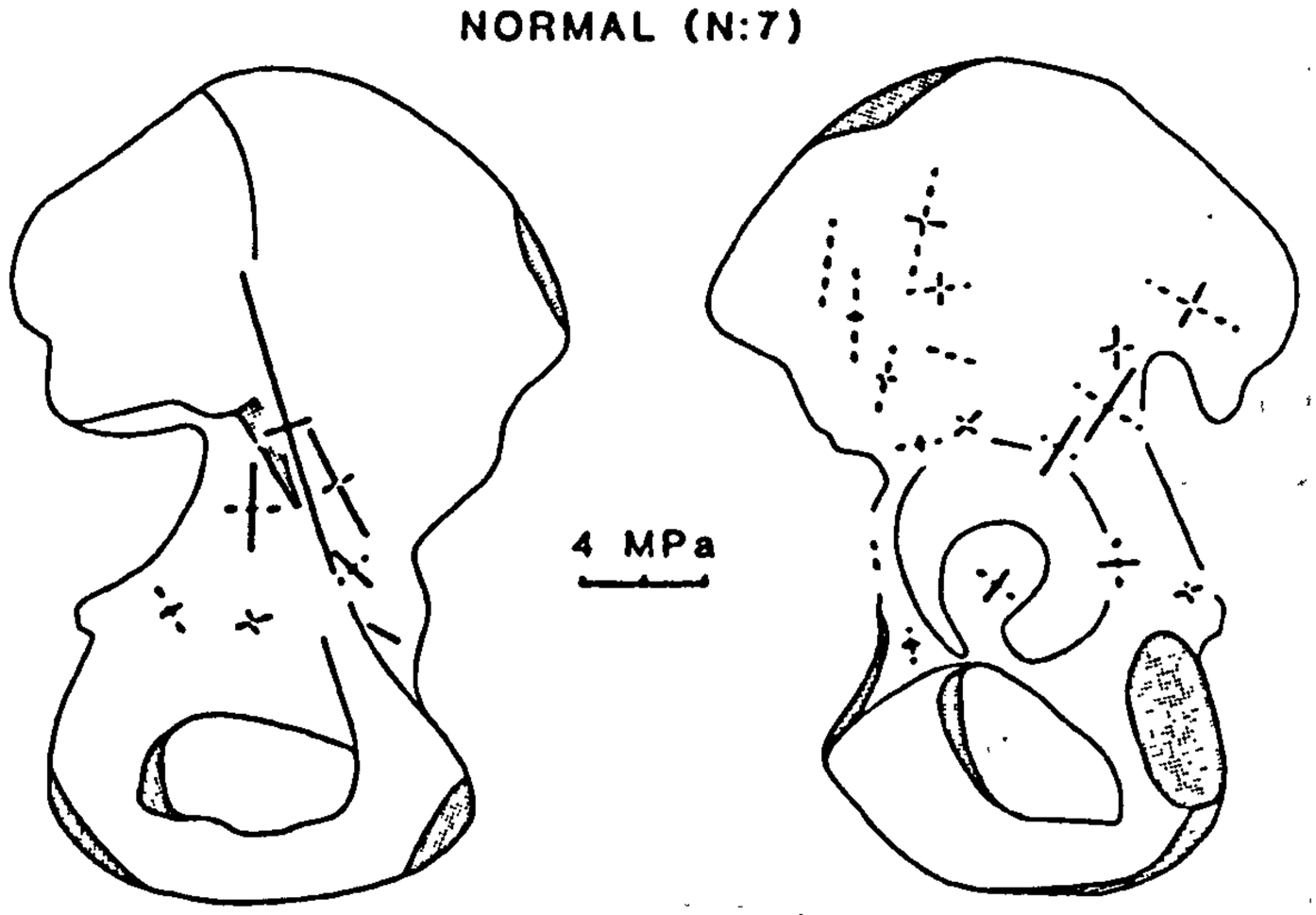

Figure 2.14 Distribution of average stresses on the cortices of the pelvis, developed through loading to 2.5 kN, in contact with the femoral head (n = 7), as reported by Finlay (1986a).

biaxial tensile strains at all acetabular measurement sites. This discrepancy may have arisen through differences in frictional conditions at the joint surfaces of the two experimental models.

CHAPTER 3. THE DETERMINATION OF MUSCLE ACTIVITY DURING WALKING

3.1 INTRODUCTION

As muscle contraction is the greatest source of joint loading during ambulation, information concerning the activity of individual muscles is vital to the development of an accurate mechanical model of the hip joint. Within the literature, there is a great deal of qualitative information concerning the patterns of muscle contraction occurring during functional activities (Basmajian & DeLuca, 1985). Moreover, numerous authors have reported the results of electromyographic (EMG) experiments performed on subjects during a variety of ambulatory activities. These have included normal gait at a variety of speeds, ambulation with variations in posture (eg. leaning forward or backward, walking with the feet closer together or further apart) and stair climbing and descent. In many studies, recordings have been performed using surface electrodes attached to the skin, either through reference to surface landmarks or through direct palpation of the muscles under study. These data are basically qualitative in nature and indicate whether a muscle is active or quiescent at different stages of the gait cycle. However, traces of electrical activity do not allow us to estimate directly the force of contraction of individual muscles.

3.2 QUANTITATIVE ELECTROMYOGRAPHY

Several investigators have attempted to make EMG data more quantitative by normalizing signals with respect to the maximum integrated voltage recorded during gait (Murray et al, 1984). Others have standardized their recordings by measuring EMG signals during standardized maneuvers designed to elicit the maximum voluntary contraction of each muscle (Arsenault et al., 1986). Another approach is to calibrate the EMG electrode in a manner akin to a force transducer by relating dynamometric measurements of joint torque to the integrated EMG signal. These attempts are of great potential significance to mechanical modeling of the extremity, as the hip joint is a mechanically indeterminate structure due to the large number of muscles contributing to the joint reactive force. Thus any method which can provide quantitative or even ordinal data concerning the force developed by

individual muscles may facilitate the derivation of physiologically realistic representations of the loaded extremity.

It is not possible to directly relate muscle force to the integrated EMG signal because of a variety of factors. Firstly, data derived from surface electrodes are susceptible to artifacts and often reflect the electrical activity of several muscles in the vicinity of an electrode. Consequently, EMG data obtained using surface electrodes tend to be unreliable if a muscle is small in cross-section or is deep to the surface of the skin even for qualitative assessment of muscle activity. Moreover, in some instances, several muscles in close proximity may be electrically active and so attribution of the recorded signal to a specific muscle can be difficult, if not impossible (Koh & Grabiner, 1992). These problems can be overcome through the use of fine wire electrodes directly inserted into the belly of each muscle. This allows the electrical activity of an individual muscle to be recorded, regardless of its position with respect to the skin.

Secondly, as several muscles generally perform the same function around the joint and many muscles have more than one function (e.g. in the hip joint, "adductors" typically generate a combination of adduction, flexion and external rotation), it is not always possible to accurately predict the force developed by individual muscles during standardized, isometric exercises. In almost all activities, several muscles will participate in resisting applied moments so that even if pure moments and forces are applied to the joint under rigorously controlled conditions, it is difficult to accurately estimate the force of contraction of each individual muscle. However, it is possible to employ isometric exercises to elicit the maximum attainable EMG signal from any muscle using fine wire electrodes and to use that signal, defined as the maximum voluntary contraction (MVC), for subsequent normalization of EMG data.

It is also possible to obtain an estimate of the maximum isometric contraction of a muscle from Hill's equation (Hill, 1953; Abbott & Wilkie, 1953; Pedotti et al, 1978) or, more simply, by relating average values of the physiologic cross-sectional area of a muscle to the maximum activation coefficient (ie. the force per unit area) typically defined as 30-60 N/cm^2. Unfortunately, the cross-sectional areas of muscles are known to vary considerably between subjects and physiologic cross-sectional areas are not easily measured. Moreover, it is not known exactly what value of the activation coefficient corresponds to the maximum isometric contraction

of most muscles. Thus, this method can only provide rough estimates of the maximum force developed by each muscle, even if its EMG signal is known.

3.3 MUSCLE ACTIVITY DURING NORMAL GAIT

A comparative study of many of the previous texts and published papers discussing "normal" EMG activity during gait reveals significant variations between different studies. These are probably due to a variety of factors, particularly:

(i) the experimental methodology, especially the care taken in the placement of electrodes and whether measurements were performed with a surface, needle or fine wire electrode;

(ii) whether the investigator was attempting to measure the activity of specific muscles or whether it was assumed a priori, that different muscles performing the same function were similar enough to have their EMG patterns averaged;

(iii) whether the investigator was attempting to study variations in the EMG pattern from subject to subject or had decided, from the outset, than an "average" or "normal" pattern of EMG activity was present;

(iv) the method of recording and standardizing the walking speed of each subject, as both the rate of ambulation and attempts to regulate gait velocity can significantly alter the patterns of muscle recruitment and activity;

(v) the method of representing and reporting variations between subjects. In many studies, "typical" data are reported and are said to be "consistent" with that of all subjects on the basis of the subjective impressions of the investigator. Recent studies have demonstrated that profound variations exist between the EMG patterns of different subjects during normal walking and even recordings obtained from the same subjects on different days (Winter & Martiniuk, 1986; Kadaba et al, 1989).

Despite the variability of published reports, some consistent patterns of muscle recruitment have been reported during free walking at normal speed. The available data suggest that in functional terms, muscle activity during the gait cycle may be summarized as follows:

(i) During stance phase, the hip muscles oppose the large

adducting and flexing/extending moments generated by the motion of the center of gravity of the supported body over the fixed position of the planted foot. Because the body is positioned medial to the point of plantar support, the abductors (gluteus medius, gluteus minimus and tensor fascia lata) are active for the entire period of single limb support. Similarly, as the body progresses forward over the femoral head, the hip extends from its initial position of maximum flexion. During the first 20% of the gait cycle, an external flexing moment is present as the ground reaction force vector passes anterior to the hip joint. This is opposed by activity of the extensor muscles, notably, gluteus maximus, biceps femoris (long head), semitendinosus and semimembranosus. Beyond this point in the gait cycle, the ground reaction force moves posterior to the hip joint, thus generating an external extending moment. This necessitates activity of the hip flexors, notably iliopsoas and, to some degree, rectus femoris, to maintain equilibrium.

(ii) Much of the activity of the muscles of the hip joint occurs during the transition from single to double stance and then back to single stance on the contralateral extremity. These activities necessitate coordinated motion and thus careful control of both the pelvis and trunk as well as the weight-bearing limbs. Consequently, most muscles are active at heel strike, suggesting stabilization of both the hip and also the knee joint through significant antagonistic muscle activity. At this point, both the abductors and adductors (notably gluteus medius and adductor magnus) and the flexors and extensors (iliacus, rectus femoris and gluteus maximus and the hamstrings) are observed to be active.

(iii) Less muscle activity is present at toe-off as, at this stage of the gait cycle, loading of the limb is decreasing rapidly with the major functional groups being the flexors (iliopsoas, gracilis) and the adductors (adductor magnus, adductor brevis, and adductor longus).

(iv) The swing phase of gait generates little loading of the hip joint as the extremity is non weight-bearing, however muscle activity is needed to flex the hip and to accelerate the limb forward to

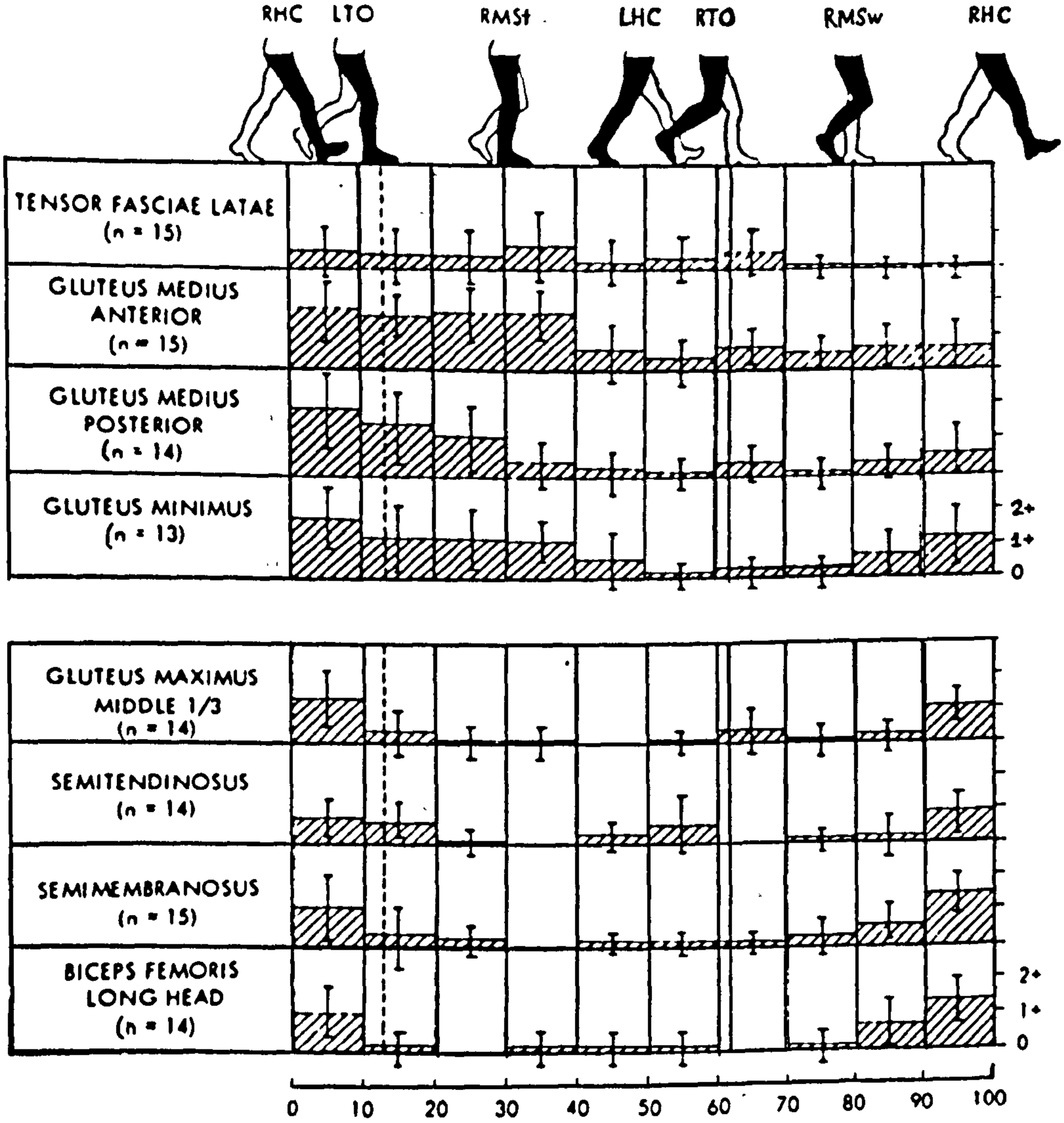

Figure 3.1 The EMG activity of hip muscles during one cycle at medium cadence, reported in terms of the mean and standard deviation on a rating scale of 0 (no activity) to 3 (maximum activity). From Basmajian (1976).

accept the weight of the body at heel strike. Thus the flexors of the hip (iliopsoas, gracilis) and the knee (hamstrings) are active throughout most of this period.

3.4 THE ACTIVITY OF INDIVIDUAL MUSCLES DURING GAIT

The following specific conclusions may also be drawn concerning the activity of individual muscles during the early and terminal stance periods of stance phase:

3.4.1 Gluteus Maximus:

Gluteus maximus is the primary single-joint extensor of the hip and often contracts during activities requiring unusual demands, notably ascending and descending stairs, bending forwards and straightening from toe touching. In functional terms, gluteus maximus consists of three parts, an upper part which abducts the joint and middle and lower parts which extend the joint. During normal gait, all parts are active at the end of swing phase and at heel strike. Accounts vary as to when activity then ceases. Lyons et al (1983) studied eleven normal subjects using fine wire electrodes and found no activity after 10% of the gait cycle whereas, Basmajian (1976) found that this period of muscle action extended until approximately 20% of the gait cycle (fig 3.1). This observation is consistent with the experiments of Battye and Joseph (1966) who measured the activity of many muscles during gait in a group of 14 healthy subjects. Using surface electrodes, they found that gluteus maximus was active in twelve subjects (86%) at 15% of the gait cycle and remained active in half of the subjects until 20% of the gait cycle. Similarly, Paul (1971) showed gluteus maximus active to 20% of the gait cycle in his study of 17 normal subjects.

One additional source of confusion may be the effect of walking speed on muscle activity, which many earlier studies largely ignored. In a study of seven normal women walking at slow, free and fast speeds, Murray et al, (1984) found that the average EMG signal of gluteus maximus increased three-fold in intensity as the walking speed increased from 0.67 to 2.0 m/s. Moreover, six of the seven subjects displayed a continuous, low level signal over most of stance phase at all walking speeds.

Another possible source of contradiction is the assumption that,

gluteus maximus functions as only one muscle with all of its parts acting in phase during normal activities. This is contrary to the observations of Basmajian & DeLuca (1985) who have shown that the upper, middle and lower parts of the muscle act quite differently. Whereas the upper and lower parts display a biphasic pattern during the gait cycle, with activity at heel strike and near the end of swing phase, the middle part exhibits three phases of activity, with its most intense contraction at toe-off. Although detailed studies have not been published to corroborate the findings it is likely that in the earlier studies of Eberhart et al, (1954), Battye and Joseph, and Paul, the single electrode used to measure activity of the "gluteus maximus" was only placed in or upon the middle part of the muscle. This would explain the observation that the muscle was active during single stance, even though the upper and lower parts of the muscle may have been silent following toe-off of the contralateral limb. In terms of the intensity of muscle activity, Basmajian (1976) reports a value of 10-15% of maximum voluntary contraction for the middle part of gluteus maximus during pre-stance.

On the basis of these data, a consensus appears to be that the middle part of gluteus maximus shows some activity during pre-stance, but that no activity is present during terminal stance.

3.4.2. Gluteus Medius

The action of gluteus medius has been studied in detail by Soderberg and Dostal (1978) who examined the onset, duration and intensity of activity of the anterior, middle and posterior segments of the muscle using fine wire electrodes. Recordings made of ten normal subjects during walking showed that all three parts of the muscle were active at early stance but were inactive in terminal stance phase in all but one subject. These observations have been corroborated by a number of other workers, including Battye and Joseph, Shiavi et al (1981), and Lyons et al, (1983). Battye and Joseph placed electrodes "over the mass" of gluteus medius and found that activity was maximal just after heel strike but decayed rapidly between 35% and 45% of the gait cycle. Data for the intensity of muscle contraction during pre-stance vary considerably: Basmajian reports values of around 50% of maximum contraction, compared with only 15% in the work of Lyons et al.

3.4.3. Gluteus Minimus

Few studies have examined gluteus minimus in particular, as it has commonly been assumed that its activity mirrors that of gluteus medius. This assumption is confirmed by a number of reports, including the original work of Inman et al at the University of California (Inman et al, 1951) and the later studies of Crowninshield et al, 1978. Basmajian & DeLuca (1985) reported more prolonged activity of gluteus minimus than the posterior segment of gluteus medius during stance phase. His measurements showed 40% of maximum activity at pre-stance and 15% during terminal stance.

3.4.4 Tensor Fascia Lata

Tensor fascia lata functions as a flexor, medial rotator and abductor of the hip joint. During the stance phase, this muscle has been reported to act very similarly to gluteus medius and minimus, with most activity between heel strike and 40% of the gait cycle (Inman et al, 1951; Basmajian, 1976; Basmajian & DeLuca 1985; Shiavi, 1990. However, these reports are contradicted by the work of Lyons et al (1983) in which minimal activity was recorded during ambulation, and then only between 25 and 40% of the gait cycle. Information concerning the intensity of contraction of tensor fascia lata is scarce, however Basmajian (1976) reports values of 15% MVC during pre-stance and 5-10% during terminal stance (fig 3.1).

3.4.5 Semitendinosus and Semimembranosus

As part of the hamstrings, both semitendinosus and semimembranosus are active during extension of the hip joint and flexion and external rotation of the knee joint. Although these muscles are most active in supporting the trunk against gravity when the body is leaning forward, activity is also reported during normal gait, at the transition from swing to stance phases. This period of contraction extends from heel strike until 20-40% of the gait cycle (Paul,1971; Battye & Joseph, 1966). Consistent activity is not observed during terminal stance. During pre-stance, Basmajian (1976) reports that the rectified EMG signal for semimembranosus is 5-10% of maximum voluntary contraction whereas the value of semitendinosus is approximately 10% (fig 3.1).

3.4.6. Biceps Femoris

Biceps femoris, the third part of the hamstrings, is active during the end of swing phase and during heel strike and double limb support. The short head remains active for very little of stance phase, however, the activity of the long head appears to last until 10-15% of the gait cycle (Inman et al, 1951; Basmajian, 1976; Crowninshield et al, 1978; Lyons et al, 1983; Arsenault et al, 1986; Shiavi, 1990). The variability of the activity of biceps femoris has been studied by Arsenault et al who found profound differences between subjects in the last 25% and first 10% of the gait cycle. During early stance, activity was usually minimal and averaged only 5% of maximum voluntary contraction. Small signals were also measured during terminal stance.

3.4.7 Ilio-psoas

As the principal flexor of the hip joint, ilio-psoas appears to be active around heel strike and during the stance to swing transition when a net extensor moment is acting on the hip joint. Some confusion has arisen in the literature due to accounts which show antagonistic activity of ilio-psoas for the first 15-20% of the gait cycle (Paul, 1971; Battye & Joseph, 1966). During this period, a large flexion moment is acting on the hip joint, so significant activity by ilio-psoas, although possibly providing rotational stability, would simply increase the burden placed on the hip joint extensors and increase energy consumption in ambulation. For this reason, it is more likely that the studies of Inman et al (1951), and Basmajian (1976) are correct in stating that ilio-psoas is not active for much of the initial part of stance phase. It is likely that Paul, and Battye & Joseph attributed the activity of gracilis or tensor fascia lata to ilio-psoas on the basis of their surface electrode recordings. Another possible interpretation is that in some individuals, psoas is active in stance phase in order to stabilize the spine and the sacro-iliac joint, even though its action at this point is antagonistic at the hip joint. All studies concur that ilio-psoas is active during terminal stance at 45-50% of the gait cycle.

3.4.8 Rectus Femoris

As a flexor of the hip and an extensor of the knee, the activity of rectus femoris is determined by the relative position and loading of both joints, movement of either joint necessitating contraction of the entire

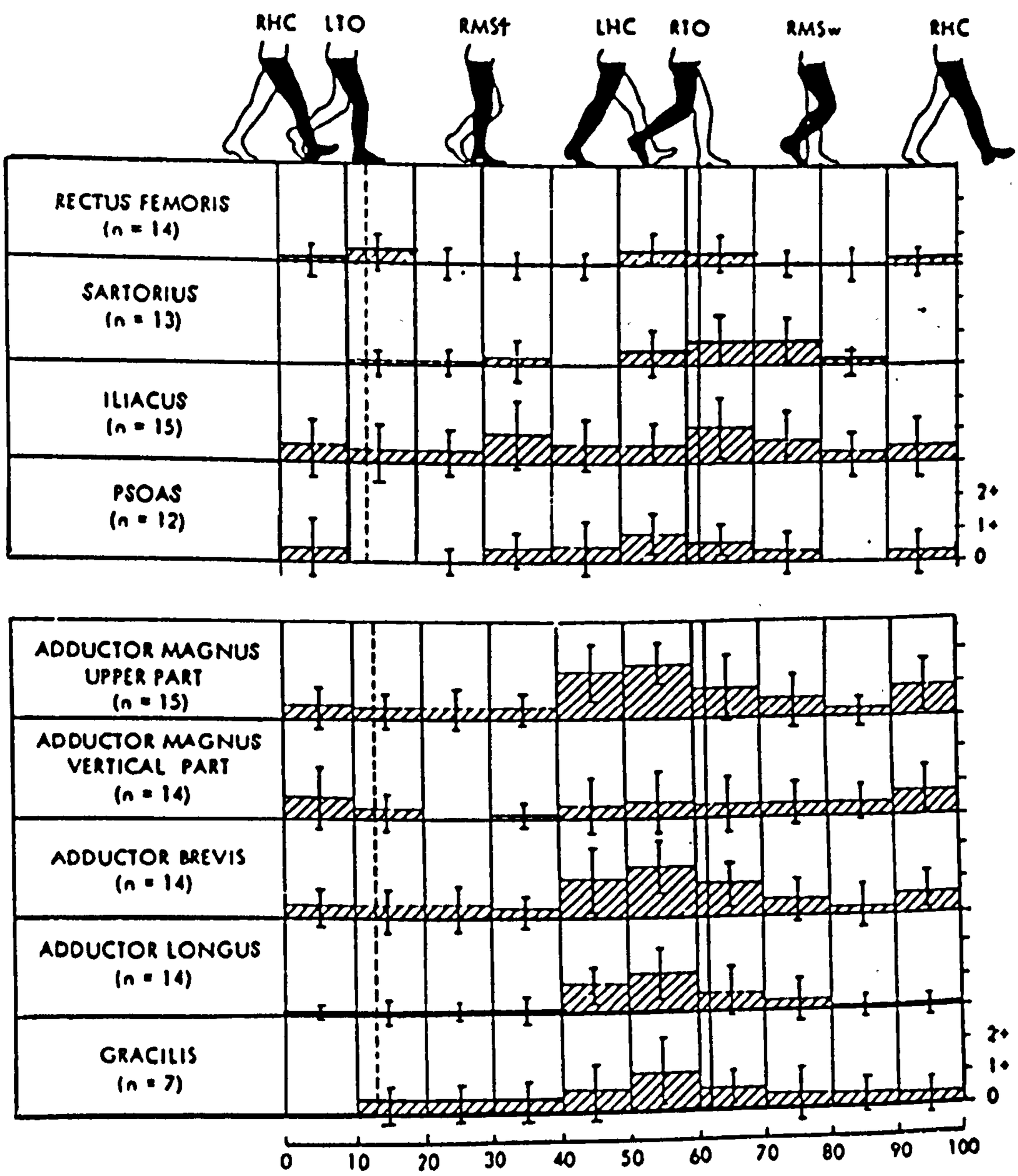

Figure 3.2 Continuation of figure 3.1 showing EMG data for some hip muscles as reported by Basmajian (1976).

muscle (Basmajian, 1976). During gait, biphasic activity has been recorded in a majority of subjects (Eberhart, et al, Shiavi et al, Joseph & Battye, Paul, Inman et al) the principal contraction occurring at the start of stance phase (0-15% of gait cycle). This period of activity ends at the point when the opposite limb leaves the ground (van der Straaten et al, 1975) and is necessary to resist the external flexing moment generated at the knee as the ground reaction force passes posterior to the knee joint. However, at the hip joint, an external flexing moment is present for the first 20% of the gait cycle and thus contraction of rectus femoris causes this flexion moment to increase still further. This necessitates antagonistic activity of the extensors with correspondingly greater joint reaction forces.

Rectus femoris is also active, during the stance-swing transition when the leg is accelerating forward, though to a lesser extent than at the start of stance phase. This period starts at 40% of the gait cycle, concludes near 60% and becomes more significant with increasing walking speed (Shiavi et al, 1981). The studies of Arsenault et al have shown that the recruitment of rectus femoris varies greatly from subject to subject and averages only 7 ± 5% of maximum voluntary contraction at pre-stance of the gait cycle and 3 ± 2% at terminal stance.

3.4.9 The Adductors (Adductor Longus, Brevis and Magnus)

The published accounts of the activity of the adductor muscles are contradictory. Basmajian (1976) reports that, with the exception of the vertical part of adductor magnus, all the adductors show significant activity from the stance-swing transition, until 40 to 70% of the gait cycle (fig 3.2). Some additional activity, particularly of adductor magnus, is also recorded around heel strike over the last 10% and first 10% of the gait cycle. These results are supported by the work of Murray et al (1984); Crowninshield et al (1978); and Shiavi et al (1981), although the original work of Inman showed only a single phase of activity for adductor longus and magnus (upper and lower parts), which extended from approximately 50 to 70% of the gait cycle. In contrast, Lyons et al (1983), found no activity in the upper part of adductor magnus late in stance phase but reported activity during the swing-stance transition. This variability is consistent with the view that the adductors do not act as primary moving or balancing muscles during ambulation, but "fine-tune" the equilibrium of the extremity in response to postural reflexes (Janda and Stava, 1965).

This conclusion is supported by the work of Green & Morris, (1970), who specifically examined the role of the adductors in postural control of the hip joint during normal activities. They found that during normal ambulation, adductor magnus (upper part) was only active during double stance whereas adductor longus showed activity both during double stance and at the commencement of swing phase at the initiation of hip flexion. This correlates well with the observation that during postural movements, the electrical activity of adductor longus was considerably greater in flexion and external rotation than pure adduction. Conversely, the upper part of adductor magnus was most active during adduction and activities requiring extension and hip rotation. Green and Morris also showed that the intensity and duration of activity of adductor magnus could be substantially increased if their subjects leaned forward during walking or if they walked with their feet closer together, thereby accentuating pelvic rotation and adduction. Conversely, walking with a broad based gait or leaning backwards reduced muscle activity. Adductor longus responded similarly; reduced foot spacing led to almost continuous activity throughout the gait cycle.

On the basis of this study, it is concluded that, during normal ambulation, the adductors probably do not contribute to significant loading of the hip joint during early stance and terminal stance. However, it is conceivable, that in studies in which subjects walk carefully with conscious control or regulation of their ambulation, the adductors may be recruited.

3.4.10 Gracilis

Though a two-joint muscle, gracilis has traditionally been assumed to act similarly to adductor longus, although contradictory accounts are present within the literature. The UCLA group (Inman et al, 1951) reported uniphasic activity extending from the latter part of swing phase to just beyond heel strike, a pattern also reported by Shiavi, (1990). Similarly, Jonsson and Steen (1965), in a detailed electromyographic study, found that the activity of gracilis was greatest during flexion of the hip joint, with most activity occurring in swing phase. It is assumed that gracilis does not demonstrate significant activity during early stance or terminal stance.

A consensus of reports concerning the activity of the muscles of the

Muscle	Early Stance Phase (15% of gait cycle)
Gluteus Maximus (3 parts)	Some activity (10 - 15% MVC) in middle part of muscle
Gluteus Medius (3 parts)	All parts active (15 - 50% MVC)
Gluteus Minimus	Active (40% MVC)
Tensor Fascia Lata	Active (20% MVC)
Semitendinosus	Active (25% MVC)
Semimembranosus	Slight activity (10% MVC)
Biceps Femoris	Slight activity (5% MVC)
Ilio-Psoas	Not active
Rectus Femoris	Slight activity (5 - 10% MVC)
Adductors	Not active
Gracilis	Not active

Table 3.1 Summary of muscle activity during early stance phase.
MVC: Maximum Voluntary Contraction of each muscle

hip joint during early stance phase is presented in Table 3.1, complete with estimates of the strength of contraction of each muscle.

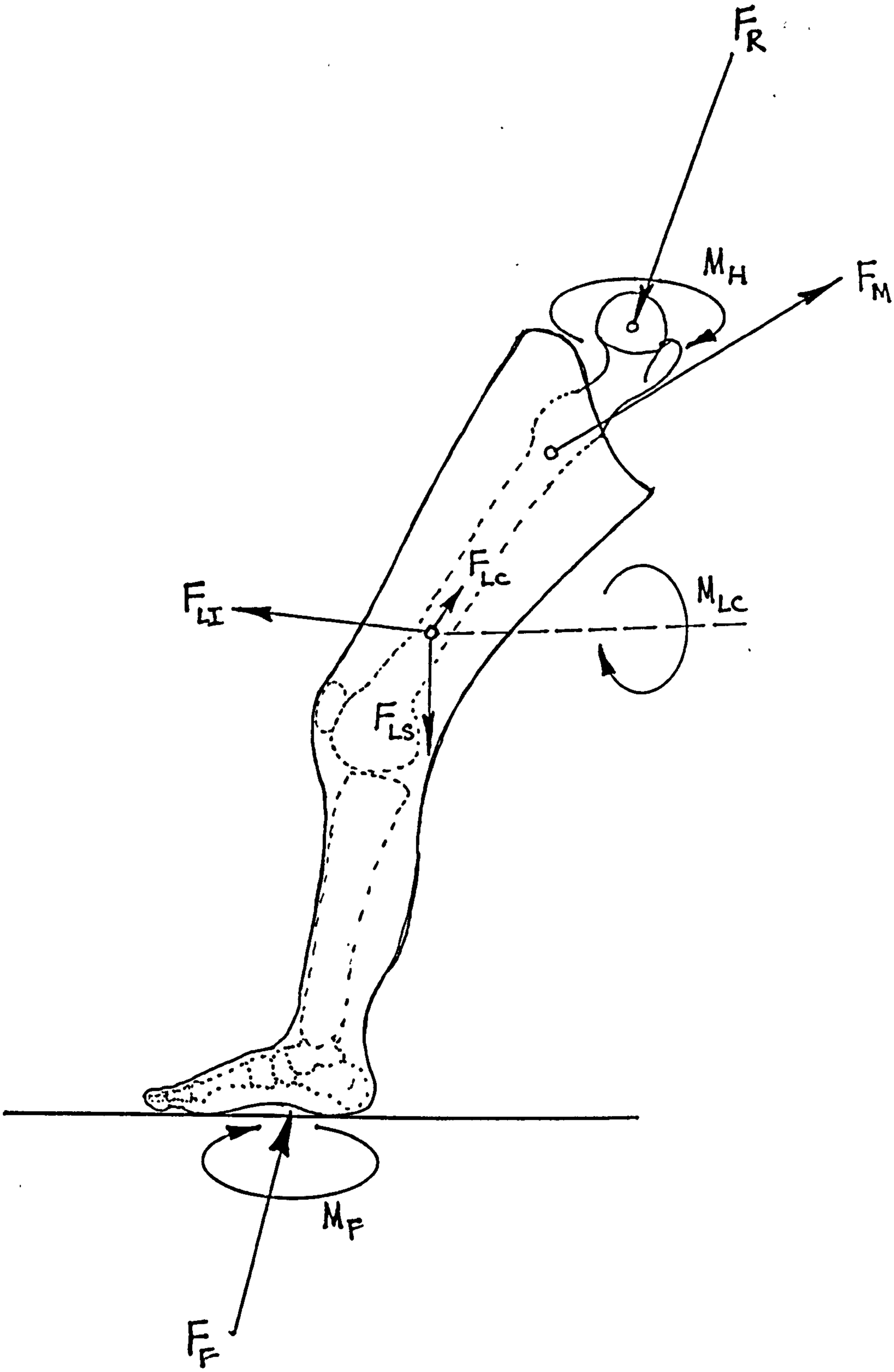

Figure 4.1 Free-body diagram illustrating the forces and moments acting on the weight-bearing lower extremity.
Note: All forces and moments have components in 3-dimensions.

CHAPTER 4. DEVELOPMENT OF A METHOD TO PREDICT MUSCLE FORCES ACTING ACROSS THE HIP JOINT

4.1 INTRODUCTION

To perform experiments to measure the deformation of the pelvis and acetabulum during walking, it is necessary to determine the position of the femur and the pelvis at key stages of the gait cycle and the forces acting across the hip joint. The forces acting on the hip can be predicted from kinematic and biomechanical measurements performed in the gait analysis laboratory. However, the forces generated by the contraction of individual muscles during gait are estimated less readily as the large number of muscles acting during the gait cycle makes these forces mathematically indeterminate using a conventional mechanical analysis. Another confounding factor is the variation in the electrical activation of each muscle during the gait cycle. As a first step in the development of a cadaveric model of the hip, a method of predicting muscle forces was developed. This was achieved by combining direct measurements of the hip joint reaction force reported in previous studies utilizing instrumented prostheses with a conventional engineering analysis of the forces and moments developed by muscles acting across the hip joint.

4.2 THE DYNAMIC FORCE EQUILIBRIUM ABOUT THE HIP JOINT

The forces exerted by each of the muscles acting across the hip joint may be estimated by solving the force and moment equations that represent the balance between:

(i) F_{LS}: the static weight of the extremity
(ii) F_{LI}: the inertial force generated by the change in linear momentum of the extremity
(iii) F_{LC}: the force generated by the change in angular momentum of the extremity
(iv) F_F: the ground reaction force
(v) F_M: the forces generated by the muscles crossing the hip joint
(vi) F_R: the joint reaction force acting between the acetabulum and the femoral head

To simplify calculations and to minimize the influence of unknown variables, a free-body diagram was developed (fig 4.1). In this analysis, it is assumed that forces supported by the contribution of passive structures

Study	Patient No.	Gait Velocity (m/s)	$-F_X$ (% F_R)	$-F_Y$ (% F_R)	$-F_Z$ (% F_R)	F_R
Rydell (1966)	1	0.9	0.42 (28%)	0.21 (14%)	1.43 (95%)	1.51
	2	1.1	0.96 (33%)	0.92 (31%)	2.64 (89%)	2.95
	1	1.3	0.43 (24%)	0.34 (19%)	1.71 (95%)	1.8
	2	1.4	1.07 (33%)	0.98 (30%)	2.93 (90%)	3.27
Davy et al (1988)	1	0.7	0.47 (17%)	0.33 (12%)	2.65 (98%)	2.71
		0.7	0.47 (18%)	0.39 (15%)	2.56 (97%)	2.63
Bergmann et al (1989)	1	0.3	1.18 (41%)	-0.09 (-3%)	2.64 (91%)	2.9
		1.1	1.53 (40%)	0.38 (12%)	3.14 (88%)	3.57
Consensus*		**1.1 m/s**	**1.13 (33%)**	**0.79 (23%)**	**3.1 (91%)**	**3.4**
Range of Data		**0.7-1.4**	**(18-42%)**	**(9-31%)**	**(89-95%)**	

Table 4.1: Summary of published intra-vital measurements of the first maximum of the joint reaction force (in early stance phase) and its components. All components are defined within the coordinate system of Bergmann et al which is defined by the frontal plane of the femur and the medullary axis.

X: medial, Y: anterior, Z: superior

*Values calculated by assuming a total joint force of 3.4 body weight at 1.3m/s, based upon an average value of the inclination of the joint reaction force of 20° in the coronal plane and 14° in the sagittal plane (see Table 4.2). Resultant values are then calculated based upon the average distribution of the resultant force reported in all three intra-vital series.

(e.g. the capsule, ligaments, and non-contractile parts of muscles) to the inter-segmental forces and moments at the hip joint are negligible, given that the joint is not acting at the extremes of normal motion at either early stance or terminal stance. In the range of hip flexion observed in normal gait this assumption is supported by previous experimental investigations (Yoon & Mansour, 1982; Vrahas et al, 1990).

Dynamic force equilibrium of the weight-bearing limb is achieved if

$$F_R + F_M + F_{LS} + F_{LI} + F_{LC} + F_F = 0 \qquad (4.1)$$

where all forces are assumed to be vectorial quantities as indicated in Fig. 4.1. As the leg is virtually stationary, it may be assumed that the inertial and centripetal forces generated by the limb will be negligible, i.e. $F_{Li} = F_{LC} = 0$. Assuming that $F_{LS} = 0.19\ F_{BW}$, where F_{BW} = the weight of the entire body, equation (1) may be rearranged to yield:

$$F_M = -F_R - 0.19\ F_{BW} - F_F \qquad (4.2)$$

In order to calculate F_M, values for the joint reaction force may be estimated from published intra-vital measurements obtained with instrumented joint prostheses (tables 4.1 and 4.2). Simultaneous foot/floor reaction forces are not reported in each of the intravital studies and so typical values must be derived from other published studies (table 4.3).

4.3 INTRAVITAL HIP FORCES

Intravital hip force data from three different studies were previously discussed in Chapter 2 and may be normalized with respect to the peak hip reaction force recorded in early stance. A set of 'consensus' or best guess estimates can then be formulated by selecting:

(a) a value for the peak reaction force during unrestricted gait at a speed typical for a joint replacement patient (1.1 m/s), and

(b) the relative magnitude of the three components of hip reaction force.

These values are set forth in table 4.1; corresponding directions of the joint reaction force in the sagittal and coronal planes are presented in table 4.3. These data formed the basis of the subsequent biomechanical analysis of muscle forces.

Two new reports of intra-vital hip force measurements have appeared within the literature since this analysis was performed. The first was by Bergmann and co-workers who went on from their first

Study	Patient No.	Gait Velocity (m/s)	Coronal Angle* (deg)	Sagittal Angle** (deg)
Rydell (1966)	1	0.9	16°	8°
	2	1.1	20°	19°
	1	1.3	14°	11°
	2	1.4	20°	18°
Davy et al (1988)	1	0.7	10°	7°
		0.7	10°	9°
Bergmann et al (1989)	1	0.3	24°	-2°
	Left Hip	1.1	26°	7°
Consensus		**1.1**	**20°**	**14°**

Table 4.2: Direction of the joint reaction force acting on the femoral head at early stance from published intravital hip force recordings.

* Angle from vertical towards medial.
** Angle from vertical towards posterior.

Author	N	F_X (Medial)	F_Y (Anterior)	F_Z (Superior)
Chao et al (1983)	Males 52	-0.048 ± 0.022	-0.174 ± 0.042	1.13 ± 0.08
	Females 55	-0.046 ± 0.022	-0.157 ± 0.047	1.08 ± 0.08
Gilbert et al (1984)	12	NA	-0.22	1.25
Bresler and Frankel (1950)	4	0	-0.13	1.03
Rohrle et al (1984)	Males 17	-0.02	-0.19 ± 0.04	1.10 ± 0.08
Consensus Values	**Females 5**	**-0.05**	**-0.16**	**1.11**

Table 4.3: Reported values of the three components of the foot/ground reaction force at early stance (15% of the gait cycle), expressed as a multiple of body weight.

Study	Patient No.	Gait Velocity (m/s)	$-F_x$ (%F_r)	$-F_Y$ (%F_R)	$-F_Z$ (%F_R)	F_R
Bergmann et.al. (1993)	1 Right hip	1.1	1.40 (37%)	0.60 (16%)	3.50 (93%)	3.8
	2	1.1	1.42 (36%)	0.11 (3%)	3.75 (94%)	4.0
Brand et. al. (1994)	1	1.2	–	0.65 (27%)	–	2.4

Table 4.4 Intravital hip force data reported since the analysis of muscle forces described in this dissertation.

experimental study to implant two further prostheses of the same design (Bergman et al, 1993). One prosthesis was implanted in the contralateral (right) hip of their original patient, an 82 year-old male (height: 168 cm, body mass: 65 kg) and the second was implanted in the right hip of a 69 year-old female patient, (height: 160 cm, body mass: 47 kg) with unilateral avascular necrosis of the femoral head. Hip joint forces were recorded from both patients performing a variety of activities, including walking and jogging at speeds of up to 8 km/hr (2.2 m/s). The results of these measurements are presented in table 4.4 in the same format as table 4.1

Another case reported within the recent literature was a 72 year-old male (body mass: 66 kg) who received an instrumented prosthesis during revision hip arthroplasty at Case Western Reserve University in Cleveland. This device was of a similar design to that previously utilized by Davy et al. Although a comprehensive report of the data collected from this patient has not been published to date, some data were cited by Brand et al (1994) in comparing intravital measurements of hip forces with predictions based on biomechanical and kinematic data describing the gait of the instrumented patient. Hip force data were recorded during slow unassisted gait (0.86 - 1.01 m/s) and free unassisted gait (1.11 - 1.37 ms^{-1}) at 58 and 90 days post-operatively. Brand et al only reported the resultant force and its out-of-plane (approximately anterior-posterior) component for six gait cycles recorded as the subject walked at a self-selected speed. Under these conditions, the peak force ranged from approximately 2.0 to 2.9 BW (average: 2.4 BW), while its out-of-plane component ranged from 0.58 to 0.76 BW (average: 0.65 BW).

It is unclear why the peak resultant force measured in this patient is lower than values reported by previous investigators for subjects walking at the same speed; these values have ranged from 2.64 BW (Rydell) to 4.00 BW (Bergmann). It is likely that the reasons for these differences are multi-factorial, but that kinematic data, including the angle of flexion and adduction of the hip in early stance, and the position of the trunk during the gait cycle would reveal significant differences between each of these subjects.

It is interesting to compare the relative magnitudes of the anterior-posterior components of the peak joint reaction force reported in the two recent studies. The data from the right and left hips of Bergmann's first patient were very similar; both had relatively small components of the

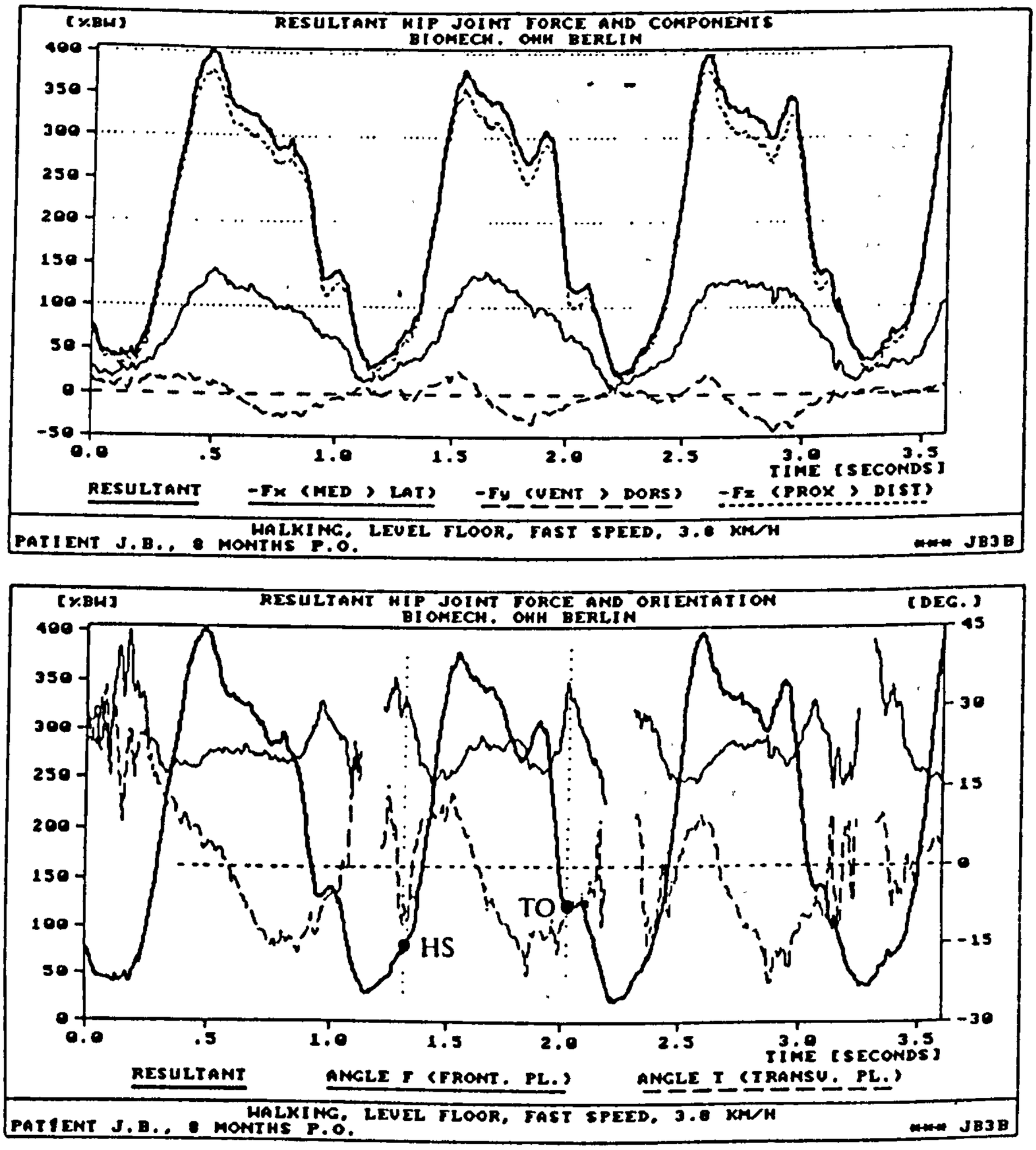

Figure 4.2 Intravital hip force data reported by Bergmann et al (1993) for their second patient during walking at 4 km/h. The components of the hip reaction force and the force resultant are shown in the upper figure. In the lower figure, the direction of the resultant in the frontal and transverse planes is graphically displayed.

posteriorly directed components which amounted to only 12% and 16% of the total joint reaction force. This supports the conclusion that differences between data obtained from this patient and the others reported in the literature are not due to malfunctioning or misalignment of the prosthesis, but might be attributable to idiosyncrasies in the gait or muscular activity of this individual.

Bergmann's second patient had virtually no posterior component of the hip force, moreover, the curves describing the temporal variation of each force component during mid-stance were of markedly different shape than those of the patients of previous studies reported in the literature (fig 4.2). The largest abnormality was the absence of the normal minimum in the joint reaction force during mid-stance. In some cycles, the anterior/posterior component did not have a distinct maximum in early stance phase, but remained relatively stable until its reversal of direction during mid-stance. These characteristics suggest that the patient had some hesitancy during early stance and that co-contraction of additional muscle groups was necessary to stabilize the hip joint. This would have led to elevation of the vertical and medial/lateral components of the joint reaction force. Other kinematic abnormalities may have been present, however, a complete description of this patient's gait has yet to be published.

Despite the paucity of the data reported by Brand et al, the relative magnitude of the peak anterior/posterior force component (0.27 F_R) is very consistent with the data obtained from other patients walking at freely selected speeds (i.e. 1.1 - 1.4 m/s). Under these conditions, both of the Rydell's patients generated peak components of around 0.3 body weight. This suggests that the selection of 23% of the total joint reaction force as the "consensus" value for the anterior/posterior force component was appropriate, given the significantly lower values of 12%, 10% and 3% reported in the studies of Bergmann et al.

4.4 THE MOMENT EQUILIBRIUM OF THE HIP JOINT

With the exception of the joint reaction force, each of the forces acting on the weight-bearing limb will generate a moment about the hip joint, resulting in a net transfer of moment from the limb to the trunk via the muscles acting on the pelvis. In general terms, the moment equilibrium of the lower limb may be formulated as:

Source	No. of Subjects	Adducting Moment (Nm)	Flexing Moment (Nm)	Internally Rotating Moment (Nm)
Cappozzo (1986)	8	43 (31-56)	49 (37-66)	5 (2-10)
Paul (1971)	17	47 (27-74)	47 (19-80)	6 (1-14)
Bresler and Frankel (1950)	4	74 (57-91)	17 (0-47)	NA
Andriacchi and Strickland (1985)	29	61	62	12
Consensus		**55**	**45**	**8**
Range		**(43-74)**	**(17-62)**	**(5-12)**

Table 4.5: Reported values for the net hip joint moment in abduction, extension and axial rotation at 15% of the gait cycle.

$$M_H = M_F + F_F \times r_F + F_{LS} \times r_{LS} + M_M + M_{LI} + M_{LC} \quad (4.3)$$

Where

(i) M_H The moment transmitted across the hip joint

(ii) M_F: The transverse foot/floor moment resisting rotation of the foot

(iii) F_F: The ground reaction force

(iv) r_F: The displacement vector from the hip joint center to the centroid of the ground reaction force

(v) F_{LS}: The weight of the weight-bearing extremity

(vi) r_{LS}: The displacement vector from the hip joint center to the center of mass of the extremity

(vii) M_M: The net moment generated by muscle forces

(viii) M_{LI}: The inertial moment generated by the change in linear momentum of the extremity

(xi) M_{LC}: The inertial moment corresponding to the change in angular momentum of the extremity.

As the hip joint is assumed to be frictionless, M_H is assumed to be zero. Moreover, during stance phase, as the foot is in contact with the ground, the inertial moment generated by linear and angular acceleration of the limb will be minimal (i.e. M_{LI}, M_{LC} = 0). Thus, the internal moment generated by muscle contraction (M_M) may be calculated as:

$$M_M = - M_F - F_F \times r_F - F_{LS} \times r_{LS} \quad (4.4)$$

Thus, the net moment acting at the hip joint may be calculated if the position of the centroid of the foot/floor contact force distribution is known with respect to the center of the hip joint and if the center of gravity and weight of the lower limb can be estimated. These calculations have been performed in several previous studies of the biomechanics of the hip during gait (table 4.5). The average values reported are relatively consistent, particularly for abduction/adduction, although in every study considerable variation is reported between different subjects (fig 4.3). Much of this variation is due to differences in the age of the experimental subjects, the speed of walking, the footwear worn by the subjects and the method of normalization of the moment data employed by each investigator (Ramakrishnan et al, 1990). In the case of flexion/extension, the moment developed between the trunk and the leg is highly

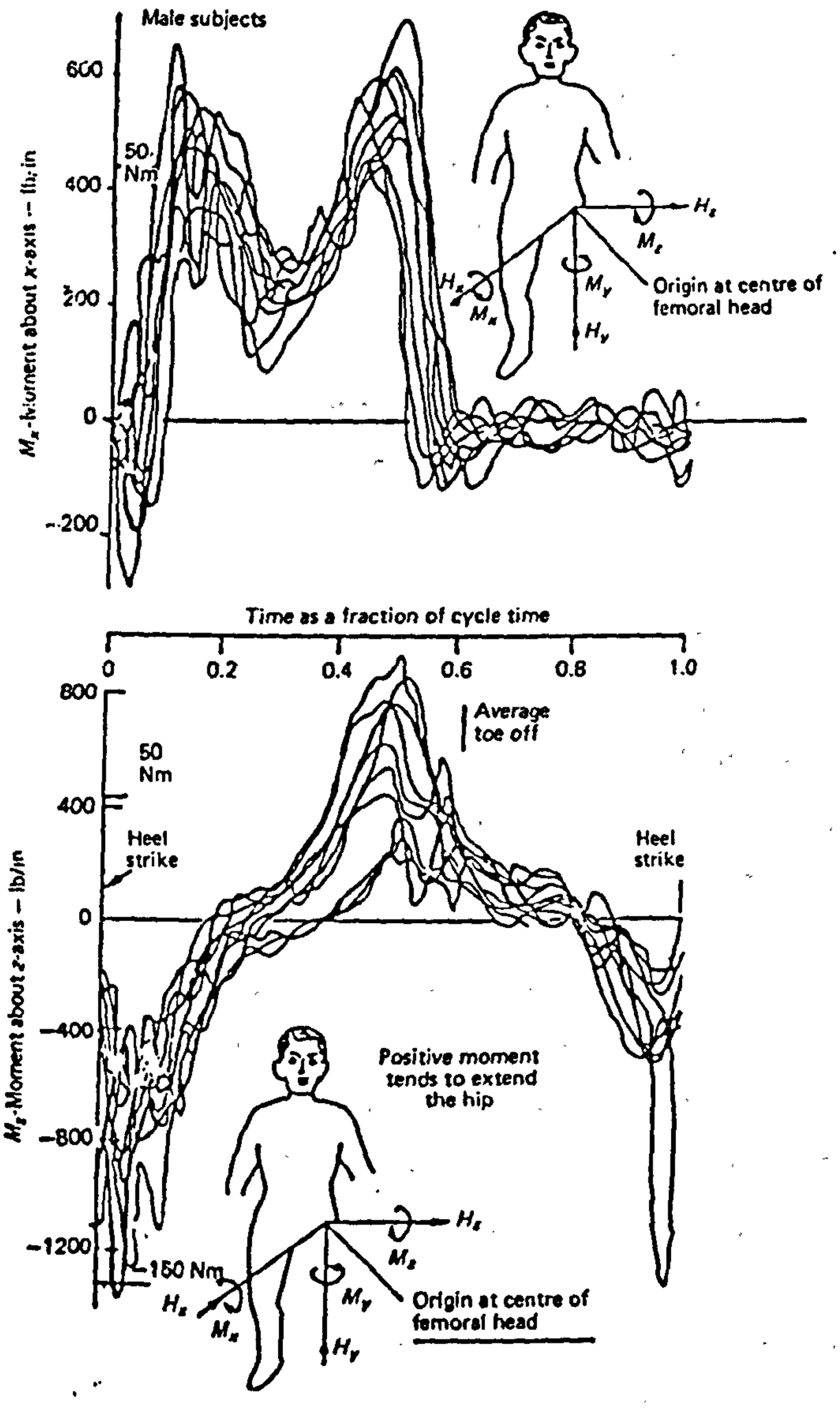

Figure 4.3 Moments transmitted to the trunk by one leg during normal gait (from Paul, 1971).

dependent upon stride length and the speed of ambulation (Andriacchi and Strickland, 1985) and so the reported values tend to be more variable. Substantial variability is also reported in transverse plane moments (internal and external rotation), although all subjects are observed to display the same characteristic pattern of variation of this component during the gait cycle.

4.5 A METHOD OF CALCULATION OF MUSCLE FORCE COMPONENTS:

The average speed of ambulation of older individuals (60 years of age and older) is 1.1 m/s during free gait (Ramakrishnan , 1990). Based upon the data of table 4.1, a reasonable estimate of the magnitude of the first maximum of the total joint reaction force at this walking speed is 3.4 times body weight. Under these conditions, the average direction of hip joint reaction force may be assumed to be 20^{o} to the vertical in the coronal plane and 14^{o} to the vertical in the sagittal plane (table 4.3). This corresponds to the following components of the joint reaction force, defined within the coordinate system of Bergmann et al (fig 2.5):

F_X (medial): -1.13 BW
F_Y (anterior): -0.79 BW
F_Z (superior): -3.11 BW
F_R (total): 3.4 BW

These data may be transferred to an external, anatomically-based coordinate system if the three-dimensional position of the femur is known. Many studies have been performed in which the positions of the femur, the pelvis and the hip joint have been measured during gait (tables 4.6, 4.7, 4.8). Although there is some variation between studies, primarily due to the measurement technique and the definition of a zero position, there is sufficient agreement to develop a set of 'consensus' values.

After applying the coordinate transformation derived in Appendix 4.1, the joint reaction force is resolved into the following components within the external reference frame:

F_X (medial): -0.63 BW
F_Y (anterior): 0.77 BW
F_Z (superior): -3.25 BW
F_R(total): 3.4 BW

Reference	Subjects	Gait Velocity	Flextion	Abduction*	Rotation
Lamoreux (1971)	2 2	1.0 ms^{-1} 1.5/1.6 ms^{-1}	7° 10°	NR NR	5° IR 4° IR
Gore (1984)	73 (males)	1.3 - 1.7 ms^{-1}	18°	-5° ± 4°	7° IR
Smidt (1971)	31 (males)	0.91 ms^{-1} 1.34 ms^{-1}	22° ± 5°	-4° -3°	4° IR 4° IR
Kadeba (1987)	35	"normal speed"	17° 27°	-7° ± 5°	7° IR 7°
Johnson (1974)	1	not stated	35° ± 5°	-3°	
Murray (1964)	60 (males)	"free cadence walking"	24°		12° IR
Sutherland and Hagy (1972)	8		25° ± 5°		
Consensus			**25°**	**-6°**	**5° IR**

Table 4.6 Literature values for the position of the hip joint at 15% of the gait cycle.
* Zero degrees of abduction of the hip joint is assumed during standing at rest. In this position, the femoral shaft is adducted by 5-7 degrees.

Reference	No. of Subjects	Gait Velocity	Flexion	Abduction	Internal Rotation
Lamoreux 1971)	1 1	1.0 m/s 1.5/1.6 m/s	1° -4°	+1° +2°	1° 3°
Sutherland (1972)	9	not stated	–	–	6° ± 5°
Kadeba (1987)	35	"normal speed"	-11° ± 4° **	3° ± 3°	3° ± 3°
Murray (1964)	60 (males)	"free cadence walking"	-2° ± 2°	–	3° ± 3°
Levens (1948)	10 (males)	not stated	–	–	4°
Consensus			**-2°**	**4°**	**3°**

Table 4.7 Literature values for the position of the pelvis at 15% of the gait cycle.

Note:
Pelvic Abduction is defined as occurring when the weight-bearing joint is higher than the non-weight bearing joint. Internal pelvic rotation denotes that the weight-bearing joint is further forward in the direction of gait than the non-weight bearing joint.

* Zero rotation is assumed to occur at 30% of the gait cycle.
** Data of doubtful validity due to definition of zero pelvic tilt (not stated).

	Component of Motion		
	Flexion	Abduction	Internal Rotation
Hip	25°	-6°	5°
Pelvis	-2°	3°	3°
Femur	27°	-9°	8°

Table 4.8 Calculated position of femur in early stance phase with respect to an external coordinate system based on consensus values for the positions of the hip joint and the pelvis.

The components of the total muscle force crossing the hip joint (F_M) may be calculated using the reported values for the ground reaction force at 15% of the gait cycle (table 4.2): from equation 4.2 ($F_M = -F_R - 0.19\,F_{BW} - F_F$). This leads to the following estimates of the unknown force components:

The joint reaction force (F_R) = {-0.63, +0.77, -3.25}

Foot/floor reaction force (F_F) = {-0.05, -0.16, 1.11}

Weight of leg (0.19 F_{BW}) = {0, 0, -0.19}

Resultant Muscle force (F_M) = {+0.68, -0.61, 2.33}

Thus, for an assumed body mass of 70kg, it is estimated that the components of the net muscle force acting on the femur would be 476 N medially, 427 N posteriorly and 1631 N superiorly.

4.6 CALCULATION OF INDIVIDUAL MUSCLE FORCES

The components of the net force and net moment developed by muscle contraction may be described by a set of six equations of the form:

$$\sum a_{ij} F_j = b_i \qquad (4.5)$$

Where

a_{ij} = a coefficient derived from the direction of action or moment arm of each muscle.

F_j = the force developed by the jth muscle, and

b_i = the component of net force or moment.

Electromyographic data indicate that eight of the muscles crossing the hip joint are active during the early stance phase of the gait cycle, although the intensity of the integrated EMG signal varies considerably between the different muscles (table 4.9). As there are only six components of force and moment, it is only possible to predict the forces in six of these muscles.

The estimated direction of the force of contraction of all eight of the muscles active in the early stance phase (15% of the gait cycle) are presented in table 4.10. These data were derived from a radiographic study which was performed in two parts. The first part of the study was performed to enable the origin and insertion of each muscle to be

Muscle	Early Stance Phase (15% of gait cycle)
Gluteus Maximus (3 parts)	Some activity (10 - 15% MVC) in middle part of muscle
Gluteus Medius (3 parts)	All parts active (15 - 50% MVC)
Gluteus Minimus	Active (40% MVC)
Tensor Fascia Lata	Active (20% MVC)
Semitendinosus	Active (25% MVC)
Semimembranosus	Slight activity (10% MVC)
Biceps Femoris	Slight activity (5% MVC)
Ilio-Psoas	Not active
Rectus Femoris	Slight activity (5 - 10% MVC)
Adductors	Not active
Gracilis	Not active

Table 4.9 Summary of Muscle Activity in Early Stance Phase based upon the work of Basmajian (1976).

MVC: Maximum Voluntary Contraction

Muscle	Force	θ	ϕ	Fx	Fy	Fz	Fxy	Fxz	Fyz
Gluteus Maximus	F1	33	20	0.521	0.292	0.802	0.597	0.956	0.854
Gluteus Medius									
anterior	F2	5	-8	0.086	-0.139	0.987	0.163	0.990	0.996
middle	F3	10	4	0.173	0.060	0.983	0.183	0.998	0.985
posterior	F4	30	24	0.468	0.352	0.810	0.586	0.936	0.884
Gluteus Minimus	F5	22	20	0.355	0.320	0.879	0.478	0.948	0.935
Tensor Fascia Lata	F6	8	-8	0.129	-0.138	0.982	0.189	0.990	0.992
Semi Tendinosus	F7	-6	30	-0.091	0.498	0.862	0.506	0.867	0.996
Semi Membranosus	F8	-6	29	-0.092	0.483	0.871	0.491	0.876	0.996
Biceps Femoris	F9	1	35	0.007	0.574	0.819	0.574	0.819	1.000
Rectus Femoris	F10	20	27	0.308	0.432	0.848	0.531	0.902	0.951

Table 4.10 Average orientation (θ, ϕ) and direction cosines of the hip muscles active during early stance phase.

θ : Angle of muscle force vector from the vertical in the coronal plane.

ϕ : Angle of muscle force vector from the vertical in the sagittal plane.

Muscle	Coronal Plane			Sagittal Plane			Transverse Plane		
	Muscle Force (N)	Moment Arm (mm)	Moment (Nm)	Muscle Force (N)	Moment Arm (mm)	Moment (Nm)	Muscle Force (Nm)	Moment Arm (mm)*	Moment (Nm)
Gluteus Maximus	0.956 F1	-22	-0.021 F1	0.854 F1	43	0.037 F1	0.597 F1	19.8	0.012 F1
Gluteus Medius									
anterior	0.990 F2	62	0.061 F2	0.996 F2	15	0.015 F2	0.163 F2	-49.4	-0.008 F2
middle	0.998 F3	60	0.060 F3	0.985 F3	18	0.018 F3	0.183 F3	38.3	0.007 F3
posterior	0.936 F4	41	0.038 F4	0.884 F4	21	0.019 F4	0.586 F4	32.8	0.019 F4
Gluteus Minimus	0.948 F5	42	0.040 F5	0.935 F5	13	0.012 F5	0.478 F5	7.5	0.004 F5
Tensor Fascia Lata	0.990 F6	72	0.071 F6	0.992 F6	-25	-0.025 F6	0.189 F6	-67.2	-0.013 F6
Semi Tendinosus	0.867 F7	-19	-0.016 F7	0.996 F7	59	0.059 F7	0.506 F7	-38.4	-0.019 F7
Semi Membranosus	0.876 F8	-13	-0.011 F8	0.996 F8	47	0.047 F8	0.491 F8	-34.5	-0.017 F8
Biceps Femoris	0.819 F9	-24	-0.020 F9	1.000 F9	59	0.059 F9	0.574 F9	-24.1	-0.014 F9
Rectus Femoris	0.902 F10	29	0.026 F10	0.951 F10	-30	-0.029 F10	0.531 F10	27.9	0.015 F10

Table 4.11 Muscle force and moment components within the Coronal, Sagittal and Transverse planes for each of the 10 muscles active during early stance phase.
* Calculated

identified from AP and lateral radiographs of the pelvis and femur. A cadaveric hemipelvis and femur were mounted on a board and fixed in the average orientation of the hip joint during early stance. The origin and insertion of each muscle on the surface of the pelvis and the femur were identified through reference to anatomic texts and skeletal specimens. In the cases of several muscles, (gluteus maximus and gluteus minimus (origin and insertion) and rectus femoris (origin)), two fresh cadavers were dissected to allow each muscle to be identified throughout its length. Wires were passed through the belly of each muscle and around its fibers at its points of origin and insertion. AP and lateral radiographs prepared of each specimen allowed the line of action of each muscle and its origin and insertion to be identified on subsequent radiographs.

The origin and insertion of every muscle was defined by a single point referenced to anatomic landmarks. Gluteus medius was represented by three parts (anterior, middle and posterior) with origins at points along the iliac crest. On the AP radiograph, the direction of action of each muscle was defined with respect to a vertical line which bisected the sacrum and was aligned perpendicular to the tangent to both ischial tuberosities. On the lateral view, it was assumed that the vertical axis of the body ran parallel to the tangent to the pubic symphysis and the anterior edge of the iliac crest.

In the second part of the study, AP and lateral radiographs were prepared of five specimens. On each radiograph, the predicted origin and insertion of each muscle was marked, and the corresponding line of action of each muscle was measured with reference to the vertical axis of the body. The average of the set of five values was used in further calculations and appears in table 4.9, with the corresponding components of muscle force, calculated in the coordinate system defined by the pelvis.

In order to calculate the moment generated about the hip joint by each muscle, the moment arms of all muscles were measured in the sagittal (flexion/extension), coronal (abduction/adduction) and transverse (internal/external rotation) planes on each of the five sets of radiographs. The moments generated by each muscle are expressed in terms of the force of contraction in table 4.11. Note that the moments developed in the transverse plane were calculated from the coronal and sagittal plane data. The transverse component of the moment arm was calculated by

dividing the transverse component of moment (M_{yz}) by the muscle force acting in the transverse plane (F_{yz}).

Based upon the data of tables 4.10 and 4.11, the following six equations were derived relating the external components of force and moment to the 10 unknown muscle forces:

Medial/Lateral Force:
$$0.521F_1 + 0.086F_2 + 0.173F_3 + 0.468F_4 + 0.355F_5 + 0.129F_6 - 0.091F_7 - 0.092F_8 + 0.007F_9 + 0.308F_{10} = 476N \quad \textbf{(4.6)}$$

Anterior/Posterior Force:
$$0.292F_1 - 0.139F_2 + 0.060F_3 + 0.352F_4 + 0.320F_5 - 0.138F_6 + 0.498F_7 + 0.483F_8 + 0.574F_9 + 0.432F_{10} = 427N \quad \textbf{(4.7)}$$

Superior/Inferior Force:
$$0.802F_1 + 0.987F_2 + 0.983F_3 + 0.810F_4 + 0.879F_5 + 0.982F_6 + 0.862F_7 + 0.871F_8 + 0.819F_9 + 0.848F_{10} = 1631N \quad \textbf{(4.8)}$$

Coronal Plane Moments:
$$-0.021F_1 + 0.061F_2 + 0.060F_3 + 0.038F_4 + 0.040F_5 + 0.071F_6 - 0.016F_7 - 0.011F_8 - 0.020F_9 + 0.026F_{10} = 55\ Nm \quad \textbf{(4.9)}$$

Sagittal Plane Moments:
$$0.037F_1 + 0.015F_2 + 0.018F_3 + 0.019F_4 + 0.012F_5 - 0.025F_6 + 0.059F_7 + 0.047F_8 + 0.059F_9 - 0.029F_{10} = 45\ Nm \quad \textbf{(4.10)}$$

Transverse Plane Moments:
$$0.012F_1 - 0.008F_2 + 0.007F_3 + 0.019F_4 + 0.004F_5 + 0.013F_6 - 0.019F_7 - 0.017F_8 - 0.014F_9 - 0.015F_{10} = 8Nm \quad \textbf{(4.11)}$$

To render these equations determinate, strategies were explored to pool different muscle force components in order to reduce the number of unknown forces. A natural strategy was to combine muscles which perform similar functions or which develop similar contraction forces per unit cross-sectional area. To this end, gluteus minimus and the three parts of gluteus medius were combined (i.e. it was assumed that $F_2 = F_3 = F_4 = F_5$). Semimembranosus and semi-tendinosus were also combined (ie. $F_7 = F_8$), as both muscles have virtually identical lines of action with the same force and moment coefficients, even though the cross-sectional

Muscle Grouping	Fn	PCSA (cm2)	Predicted Force (N)	Predicted Activation Cooefficient (N/cm2)
Gluteus Maximus	F1	22.2	1436	64.7
Gluteus Medius and Gluteus Minimus	F2	39	39	1.0
Tensor Fascia Lata	F3	5	-289	-57.8
Semitendinosus and Semimembranosus	F4	22	1891	86.0
Biceps Femoris	F5	14	-3554	-253.9
Rectus Femoris	F6	15	299	23.0

Table 4.12 Muscle forces predicted by solution of six equations with six unknowns.

areas and intensities of activation of the muscles are distinctly different. The six resulting equations with six unknowns were solved using standard matrix methods. The algebraic solution is reported in table 4.12.

The predicted muscle forces were not physiologically reasonable as the forces in two muscles, tensor fascia lata and biceps femoris, were negative and, as a result, it was predicted that gluteus maximus, semitendinosus and semimembranosus would develop absurdly large forces, corresponding to an activation coefficient (ie. force per unit cross-sectional area) in excess of the normal physiologic range (0 - 40 N/cm^2).

To explore the sensitivity of the solution set of the six equations to errors in b_i, the fixed values of the components of force and moment, the magnitude of the six components were varied in a systematic fashion (table 4.13). The solution set to the six equations was found to be unstable and susceptible to extreme variations due to relatively small changes in the predicted components of force and moment. This instability was due to a number of factors, especially the fact that many of the forces were oriented in directions close to the vertical with relatively small direction cosines in the medial and anterior directions. Moreover, the data used to generate the values of force and moment are generally very variable and susceptible to significant inaccuracies. In addition, gluteus maximus makes a large contribution to the moment generated in the transverse plane and yet the true insertion of this muscle is difficult to estimate as relatively little of gluteus maximus directly inserts into the femur itself, most of it being connected to the fascia lata. A further factor is that the equations ignore the contributions of the short rotators of the hip which probably make significant contributions to the moment generated in the transverse plane.

There have been many previous attempts to predict muscle forces during gait using optimization techniques (Seireg & Arvikar, 1973, 1975; Crowninshield, 1978; Hardt, 1978; Pedotti et al, 1978; Crowninshield & Brand, 1981; Patriarco et al, 1981). In these studies, a simple static analysis has generally led to predictions of negative force values in muscles known to be actively contracting during the relevant phase of the gait cycle. This may be accommodated by assuming that muscles predicted to be acting in compression are inactive, however, such an assumption can lead to predictions of muscle activity which are inconsistent with published electromyographic studies.

Condition						Solution					
Fx (N)	Fy (N)	Fz (N)	Mx (Nm)	My (Nm)	Mz (Nm)	F1	F2	F3	F4	F5	F6
416	427	1631	55	45	8	1436	39	-289	1891	-3554	299
436	467	1631	55	45	8	1396	41	-391	2058	-3834	378
516	387	1631	55	45	8	1475	38	-188	1725	-3274	220
476	427	1631	65	35	8	1259	39	-171	1626	-3044	382
476	427	1631	45	55	8	1613	40	-407	2157	-4064	216
476	427	1631	55	45	3	1184	32	25	1209	-2089	180
516	387	1631	65	35	8	1299	37	-70	1459	-2764	303
476	427	1631	65	35	3	1008	32	143	944	-1579	264

Table 4.13 Effect of changes in the magnitude of the components of force and moment acting across the hip joint on the predicted values of the muscle forces (in Newtons).

In some cases, muscles which are not active at particular phases of the gait cycle are predicted to be active to maintain the force and moment equilibrium (e.g. gluteus medius at mid-stance in the model of Crowninshield and Brand, 1981). Conversely, forces in other muscles are predicted to be negligible or non-existent, despite the EMG evidence (eg. rectus femoris and gluteus minimus in early stance in the model of Hardt, 1978).

In an attempt to reduce the sensitivity of the predicted muscle forces to the inherent uncertainty of the force and moment components, three changes were made to the original formulation of the mathematical model:

(i) the number of equations was reduced by lumping together more physiologically similar muscles. In the case of muscles spanning two joints, this process is somewhat arbitrary as muscle activity may be determined by the position of the knee rather than the hip. For example, although rectus femoris is a flexor at the hip, its activity is primarily determined by the demand placed on the knee extensor mechanism. Similarily, tensor fascia lata plays an important role in providing lateral stability to the knee in addition to flexing the hip. Nonetheless, in order to facilitate calculation of hip muscle forces tensor fascia lata and rectus femoris were pooled in view of their common function as flexors of the hip; semi-tendinosus was placed in a separate group; and semi-membranosus and biceps femoris were pooled as both function as extensors of the hip and flexors of the knee.

(ii) the force developed by each muscle was expressed as the product of its physiologic cross-sectional area and its activation coefficient during contraction (α), expressed in units of force per unit area (N/cm^2). Thus equation 4.5 became:

$$\sum a_{ij}\,\alpha_j\,PCSA_j = b_i \qquad \textbf{(4.12)}$$

where α_j = activation coefficient of jth muscle

$PCSA_j$ = Physiologic cross-sectional area of jth muscle

(iii) Equation 4.7, describing the moments generated in the transverse plane was not utilized in the analysis.

Muscle	PCSA (cm^2)	Activation Coefficient (N/cm^2)	Fx (Med) (N)	Fy (Ant) (N)	Fz (Sup) (N)
Gluteus Maximus	22.2	α1	11.56 α1	6.48 α1	17.81 α1
Gluteus Medius					
anterior	10.4	α2	0.90 α2	-1.44 α2	10.26 α2
middle	5.2	α2	0.90 α2	0.31 α2	5.11 α2
posterior	10.4	α2	4.87 α2	3.66 α2	8.43 α2
Gluteus Minimus	13.0	α2	4.61 α2	4.16 α2	11.42 α2
Tensor Fascia Lata	5.0	α3	0.65 α3	-0.69 α3	4.91 α3
Semi Tendinosus	8.0	α4	-0.73 α4	3.98 α4	6.90 α4
Semi Membranosus	14.0	α5	-1.28 α5	6.76 α5	12.19 α5
Biceps Femoris	14.0	α5	0.10 α5	8.03 α5	11.47 α5
Rectus Femoris	13.0	α3	4.01 α3	5.61 α3	11.02 α3

Table 4.14: Force components of muscles active in early stance phase expressed as the product of the activation coefficients of muscle contraction (α_n) and the physiologic cross-sectional area (PCSA).

Values for the derivation of an average PCSA for each muscle appear in Appendix 4.2.

The resulting components of force and moment appear in tables 4.14 and 4.15.

The solution to the five equations produced by this simplification is presented in table 4.16. This still led to one negative force (semimembranosus and biceps femoris) and an unphysiologic value of the activation coefficient of semitendinosus (α = 51.4 N/cm^2). This situation was worsened when the muscles were regrouped by combining all of the hamstring muscles (semitendinosus, semimembranosus and biceps femoris) and leaving tensor fascia lata in a group of its own (table 4.17). The corresponding solution indicated that tensor fascia lata would be loaded at a physiologically unreasonable level (α = 102 N/cm^2) and gluteus medius and minimus would undergo virtually no contraction (α = 0.6 N/cm^2).

Much more promising results were obtained once the number of equations was reduced to four by combining all muscles of relatively small cross-section or low electrical activity (tensor fascia lata, semimembranosus, biceps femoris, and rectus femoris) (table 4.18). The predicted values of the activation coefficients of gluteus maximus and the less active muscles varied substantially with the selection of different sets of force and moment equations. The average value of the predicted activation coefficients for gluteus maximus was 8.1 N/cm^2 which is both reasonable and consistent with the quantitative EMG data. Nonetheless, for the six cases considered, the individual values of the activation coefficient ranged from -0.8 to 12.4 N/cm^2. In the case of the less active muscles, the predicted values of the activation coefficient averaged only 0.2 N/cm^2 and ranged from -2.6 to 4.3 N/cm^2. The average values predicted for semitendinosus (38.3 N/cm^2) and gluteus medius and minimus (34.5 N/cm^2), were surprisingly constant, and although physiologically feasible, contradicted the observed EMG data in terms of their relative magnitude.

4.7 PREDICTION OF MUSCLE FORCES BY OPTIMIZATION

The approach described above has several inherent deficiencies, despite the fact that the predicted activation coefficients are within the physiologic range. Firstly, the relative magnitudes of the activation coefficients of different muscles should bear some resemblance to the percentage of maximum voluntary contraction developed by the muscle

Muscle	PCSA (cm2)	Activation Coefficient (N/cm2)	Coronal Moment (Nm)	Sagittal Moment (Nm)	Transverse Moment (Nm)
Gluteus Maximus	22.2	α1	-0.467 α1	0.815 α1	0.262 α1
Gluteus Medius					
anterior	10.4	α2	0.639 α2	0.155 α2	-0.084 α2
middle	5.2	α2	0.311 α2	0.092 α2	0.037 α2
posterior	10.4	α2	0.399 α2	0.193 α2	0.200 α2
Gluteus Minimus	13.0	α2	0.517 α2	0.158 α2	0.047 α2
Tensor Fascia Lata	5.0	α3	0.357 α3	-0.124 α3	-0.064 α3
Semi Tendinosus	8.0	α4	-0.132 α4	0.470 α4	-0.152 α4
Semi Membranosus	14.0	α5	-0.159 α5	0.655 α5	-0.237 α5
Biceps Femoris	14.0	α5	-0.275 α5	0.826 α5	-0.194 α5
Rectus Femoris	13.0	α3	0.340 α3	-0.371 α3	0.192 α3

Table 4.15 Coronal, Sagittal and Transverse components of moments generated by the muscles active in early stance phase expressed in terms of activation coefficients.

PCSA: Physiologic cross-sectional area

Muscle Grouping	α	Activation Coefficient (N/cm2)	Predicted Force (N)
Gluteus Maximus	α1	10.2	226
Gluteus Medius and Gluteus Minimus	α2	34.3	1338
Tensor Fascia Lata and Rectus Femoris	α3	0.7	13.5
Semitendinosus	α4	51.4	411
Semimembranosus and Rectus Femoris	α5	-5.2	-146

Table 4.16 Predicted values of the force of contraction and average activation coefficient, derived from five equations with five values of the activation coefficient, with pooling of tensor fascia lata and rectus femoris.

Muscle Grouping	α	Activation Coefficient (N/cm2)	Predicted Force (N)
Gluteus Maximus	α1	35.9	798
Gluteus Medius and Gluteus Minimus	α2	0.6	22
Tensor Fascia Lata	α3	102	508
Semitendinosus, Semimembranosus and Biceps Femoris	α4	4.5	162
Semimembranosus and Rectus Femoris	α5	-0.1	-1.5

Table 4.17. Activation coefficients and muscle forces predicted by solution of five equations with five unknown values of a, with pooling of semimembranosus and rectus femoris

Case	Force/Moment* Components	Gluteus Maximus	Gluteus Medius and Minimus	Semi Tendinosus	Less Active Muscles **
1	Fx,y,z;Mx	10.1	35.5	44.1	-2.6
2	Fx,y,z;My	9.2	35.3	36.1	-0.6
3	Fy,z;Mx,y	11.1	34.7	33.1	-0.5
4	Fz,Mx,y,z	6.7	33.6	37.1	1.8
5	Fy,z;My,z	-0.8	38.2	51.3	-1.4
6	Fx,z;My,z	12.4	29.9	27.2	4.3
Average		**8.1**	**34.5**	**38.3**	**0.2**

Table 4.18: Activation Coefficients predicted by solution of sets of four of the force and moment equations with four muscle groups.

* Force and Moment equations solved to obtain muscle forces.
** Semimembranosus, Tensor Fascia Lata, Rectus Femoris, Biceps Femoris.

Activation Coefficient	Muscle Activity (% MVC)*	Muscles
α1	0-10%	Semimembranosus Rectus Femoris Biceps Femoris
α2	10-25%	Gluteus Maximus Tensor Fascia Lata Semitendinosus
α3	25-50%	Gluteus Medius Gluteus Minimus

Figure 4.19: Rationale for stratification of activation coefficients.

* % MVC: Percent of maximum voluntary contraction of each muscle as reported by Basmajian, 1976.

during gait. This is not possible if muscles exhibiting different levels of activity (eg. tensor fascia lata and biceps femoris) are lumped together for purposes of analytical convenience. Secondly, the elimination of some of the force and moment equations for the sake of simplification may result in loss of significant information despite the uncertainty of some of the data upon which these equations are based. Consequently, a new approach was developed to find a solution which was consistent with the quantitative EMG data by weighting the relative contribution of the six force and moment equations according to the uncertainty of the data from which they were derived.

An algorithm was developed on the basis of numerical optimization theory to derive a solution to the equations of force and moment under the following constraints:

(i) it was assumed that the force of contraction of all muscles could be described by three values of the activation coefficient: α_1, α_2, or α_3. Assignment of an activation coefficient to each muscle was determined by the percentage of the maximum voluntary contraction of each muscle reported in the EMG studies (Basmajian, 1976). All muscles developing less than 10% of the maximum force of voluntary contraction (MVC) were assigned a single activation coefficient, α_1. Similarly, muscles contracting at 10-25% MVC were assigned α_2, and those greater than 25% MVC, α_3 (table 4.19).

(ii) For any predicted values of the muscle forces to be physiologically reasonable, the corresponding values of the activation coefficients would have to satisfy the condition $0 < \alpha_1 < \alpha_2 < \alpha_3$

(iii) Although it was evident that an exact solution was not present which would satisfy the six force and moment equations and the activation coefficient constraint, it was assumed that the values of b_i, the components of force and moment could be adjusted, provided that the values chosen were within the range reported within the literature.

As an initial step in the algorithm, three of the equations of force and moment were solved to yield initial estimates of the activation coefficients (α_1, α_2, and α_3). The three remaining force and moment equations were then solved using these values of the activation

Initial Values	Method of Solution	Activation Coefficients (N/cm^2)		
		α_1	α_2	α_3
$F_X = 476N, F_Y = 427N, F_2 = 1631N$	Direct	7.2	4.4	35.5
	Optimized	4.7	12.5	31.1
$M_X = 55$ Nm, $M_Y = 45$ Nm, $M_Z = 8$Nm	Direct	-1.9	23.8	32.5
	Optimized	4.8	12.3	31.2

Table 4.20: Values of the activation coefficient, predicted by direct solution of three equations and solution of all six equations using the optimization method. `Direct' refers to the direct solution for the activation coefficients using three equations with three unknowns and the initial values of force or moment.

coefficients to yield estimates of the three corresponding components of force and moment. These estimates are generally at variance with the six initial values of b_i which were assumed in equations 4.6 through 4.11 on the basis of the published data.

To guide the optimization routine, the differences between the predicted and initial values of the components of force and moment (Δb_i) were calculated. These differences were normalized to allow for the different levels of uncertainty in the published values of b_i. For example, the magnitude of the moment developed in the transverse plane (b_6) was assumed to be 8 Nm, however, literature values vary by approximately ± 6 Nm from 1 to 13 Nm. Thus, the deviation of any predicted value from 8 Nm was normalized by dividing it by 6 Nm and expressing it as a percentage of the reported range. This process was repeated for all six components which were then summed to form the following objective function:

$$F = \sum_{i=1}^{6} \left(\frac{\Delta b_i}{r_{bi}} \right) \quad \textbf{(4.13)}$$

where r_{bi} = the range of values of b_i reported within the literature.

Using the Simplex method, the values of b_i were varied until the minimum value of the objective function (F) was determined. At each step of the program, the value of the objective function was heavily weighted if the conditions $0 < \alpha_1 < \alpha_2 < \alpha_3$ were violated. Using this technique, a set of activation coefficients and force and moment components were derived, corresponding to the minimum value of the objective function, and thus the least possible deviation of all six values of force and moment from the consensus data derived from the literature. This algorithm was developed in cooperation with Mr. E. Kamaric, an expert in optimization theory, who wrote the corresponding computer program (See Appendix 4.3).

The equations of force and moment were solved using a variety of initial conditions. Initially, the three equations describing the components of force (F_X, F_Y, F_Z) were utilized as the starting point for the routine. The process was then repeated using the three components of moment (M_X, M_Y, M_Z) (tables 4.20 and 4.21). This procedure was undertaken as optimization techniques are known to be sensitive to the initial conditions, especially where several solutions exist corresponding

Muscle	1	2	3	4	Consensus
1 Gluteus Maximus	12.5	12.5	10.4	10.8	11
2 Gluteus Medius					
Anterior	31.2	31.2	29.8	30	30
Middle	31.2	31.2	29.8	30	30
Posterior	31.2	31.2	29.8	30	30
3 Gluteus Minimus	31.2	31.2	29.8	30	30
4 Tensor Fascia Lata	12.5	12.3	18.9	17.7	17
5 Semitendinosus	12.5	12.3	18.9	17.7	17
6 Semimembranosus	4.7	4.8	5	5	5
7 Biceps Femoris	4.7	4.8	5	5	5
8 Rectus Femoris	4.7	4.8	5	5	5

Table 4.22: Values of the activation coefficient for the eight muscles active during early stance, predicted using the optimization method.

Boundary Conditions:

(1) F_X, F_Y, F_Z set initially, muscles pooled by degree of activation (3 values).

(2) M_X, M_Y, M_Z set initially, muscles pooled by degree of activation (3 values).

(3) F_X, F_Y, F_Z set initially, activation coefficient of least active muscles set at $5N/cm^2$.

(4) M_X, M_Y, M_Z set initially, activation coefficient of least active muscles set at $5N/cm^2$.

Muscle	Activation Coefficient (N/cm^2)	Muscle Force (N)
1. Gluteus Maximus	11	244
2. Gluteus Medius		
Anterior	30	312
Middle	30	156
Posterior	30	312
3. Gluteus Minimus	30	390
4. Tensor Fascia Lata	17	136
5. Semitendinosus	17	85
6. Semimembranosus	5	70
7. Biceps Femoris	5	70
8. Rectus Femoris	5	70

Table 4.23: Values of the activation coefficient and muscle forces predicted by optimization, using the consensus values of the activation coefficient from Table 4.22.

APPENDIX 4.1 TRANSFORMATION OF MUSCLE FORCES

The coordinate system of Bergmann et al, 1989, is based upon the medullary axis of the femur, which may be assumed to be oriented with respect to the external coordinate system by an angle α in the coronal plane, corresponding to adduction of the femur and an angle ß in the sagittal plane corresponding to flexion of the hip joint. In the Bergmann system, the coronal plane is defined by an axis passing through the femoral epicondyles and so, as a first approximation, it may be assumed that the coronal plane of Bergmann coincide with the frontal plane of the external frame of reference of the body standing at rest. Thus, if the anteversion of the femur is ignored, no transformation is necessary due to internal or external rotation of the femur.

To calculate the transformation matrix to convert the Bergmann coordinate system to the external reference system, assume that the joint reaction force F consists of components F_{bx}, F_{by} and F_{bz} in the Bergmann system and F_x, F_y and F_z in the external system. Adduction through an angle α will cause the components F_{bz} and F_{bx} to be rotated in the XZ plane.

Thus,

$$F_X = F_{bx} \cos \alpha - F_{bz} \sin \alpha \quad \text{(A1.1)}$$

$$F_Y = F_{by} \quad \text{(A1.2)}$$

$$F_Z = F_{bx} \sin \alpha + F_{bz} \cos \alpha \quad \text{(A1.3)}$$

Flexion through an angle of ß will cause the components of F lying in the YZ plane to be rotated. Thus,

$$F_X = F_{bx} \cos \alpha - F_{bz} \sin \alpha \quad \text{(A1.4)}$$

$$F_Y = -F_{bx} \sin \alpha \sin ß + F_{by} \cos ß - F_{bz} \cos \alpha \sin ß \quad \text{(A1.5)}$$

$$F_Z = F_{bx} \sin \alpha \cos ß + F_{by} \sin ß + F_{bz} \cos ß \quad \text{(A1.6)}$$

At the early stance phase of the gait cycle, consensus values of α and ß are 9 and 27 degrees respectively, ie. the femur is flexed to 27 degrees to the vertical and is adducted to 9 degrees in the frontal plane (3 degrees more than in standing). Substitution of these values leads to the equations:

$$F_X = 0.988\ F_{bx} - 0.156\ F_{bz} \quad \text{(A1.7)}$$

$$F_Y = -0.071\ F_{bx} + 0.891\ F_{by} - 0.448\ F_{bz} \quad \text{(A1.8)}$$

$$F_Z = 0.139\ F_{bx} + 0.454\ F_{by} + 0.880\ F_{bz} \quad \text{(A1.9)}$$

For sake of completeness and analysis of possible errors due to anteversion or retroversion of the prosthetic component, the coordinate transformation may be extended to the case of rotation of the coordinate system about the femoral axis. As this rotation occurs within the femur based system and not the external coordinate system, the Bergmann components must be initially transformed through a rotation of γ in the X_bY_b plane, i.e.

$$F_b{}^1{}_x = F_{bx} \cos\gamma - F_{by} \sin\gamma \quad \text{(A1.10)}$$

$$F_b{}^1{}_y = F_{bx} \sin\gamma + F_{by} \cos\gamma \quad \text{(A1.11)}$$

$$F_b{}^1{}_z = F_{bz} \quad \text{(A1.12)}$$

Substitution of $F_{bx}{}^1$, $F_b{}^1{}_y$ and $F_b{}^1{}_z$ for F_{bx}, F_{by} and F_{bz} in equations A1.4, A1.5 and A1.6, then leads to:

$$F_x = F_{bx} \cos\alpha \cos\gamma\, F_{by} \sin\gamma \cos\alpha - F_{bz} \sin\alpha \quad \text{(A1.13)}$$

$$F_y = (F_{bx} (\cos ß \sin\gamma - \sin\alpha \sin ß \cos\gamma) + F_{by} (\sin\alpha \sin\gamma \sin ß + \cos ß \cos\gamma) - F_{bz} \cos\alpha \sin ß \quad \text{(A1.14)}$$

$$F_z = F_{bx} (\sin\alpha \cos ß \cos\gamma + \sin ß \sin\gamma) + F_{by} (\sin ß \cos\gamma - \sin\gamma \sin\alpha \cos ß) + F_{bz} \cos\alpha \cos ß \quad \text{(A1.15)}$$

Muscle	Sex	Number of Subjects	CSA (cm2)	Source	Consensus Value
1. Gluteus maximus	Male	12	63.7 ± 18.3	1	
	Female	12	43.7 ± 10.8	1	
	?	?	66.6	2	
	Male	2	60.5	3	66 cm2
2. Gluteus medius	Male	9	26.8 ± 4.5	4	
	Male	5	25.4 ± 4.1	5	
	Female	9	23.8 ± 4.5	4	26 cm2
3. Gluteus minimus	Male	9	11.1 ± 5	4	
	Male	5	14.7 ± 3.0	5	
	Female	9	7.1 ± 3	4	13 cm2
4. Tensor fascia lata	Male	9	4.1 ± 1.9	4	
	Male	5	5.1 ± 2.7	5	
	?	?	8.4	2	
	Male	2	7.9	3	5 cm2
5. Rectus femoris	?	?	28.9	2	
	Male	3	12.9	6	
	?	?	13	7	
	Male	5	6.6 ± 3.5	5	13 cm2
6. Biceps femoris	Male	12	17.4 ± 5.0	1	
	Male	3	13.1 ± 6.8	5	
	?	?	14.3	2	
	Male	3	12.9	6	
	?	?	14	7	14 cm2
7. Semimembranosus	?	?	14.6	2	
	?	?	13	7	
	Male	3	14.3	5	14 cm2
8. Semitendinosus	?	?	7.7	2	
	?	?	13	7	
	Male	3	6.2 ± 1.7	5	
	Male	2	5.3	6	8 cm2
9. Iliopsoas	?	?	27	7	
	Male	12	12.1 ± 2.8	1	
	Male	4	21.5 ± 6.1	5	21 cm2

Table A2.1: Literature values for cross-sectional areas of selected hip muscles.

APPENDIX 4.2: DATA PERTAINING TO THE HIP MUSCULATURE

In order to predict muscle forces on the basis of the activation coefficient, it is necessary to know the physiologic cross-sectional area of each muscle which, for a fusiform muscle, is defined as the cross-sectional area of the belly of the muscle perpendicular to the direction of its fibers when the muscle is midway between complete elongation and complete shortening. There is little published data on the morphologic characteristics of the muscles of the hip joint and even less on the physiologic cross-sectional area of specific muscle groups. For this reason, data on the cross-sectional areas of muscles have been used as an estimate of physiologic values. This information has been collected from a wide variety of sources, including anatomic atlases, physiology texts and more recently, studies of muscular degeneration and disease using computerized axial tomography. Where little numerical data could be found, direct measurements were made from transverse preparations of cadavers by tracing the outline of each muscle in question and calculating the cross-sectional area. These values appear in table A2.1 with the consensus values which were assumed for subsequent derivation of muscle force data.

References:

1. Termote et al, 1980

2. The data of Fick (1911), as presented by Lehmkuhl & Smith, 1983.

3. Brand et al, 1982

4. Clark and Haynor, 1987

5. Direct measurements performed from published studies of the cross-sectional anatomy of the lower extremities (Wagner & Lawson, 1982; Koritke & Sick, 1983; Cahill & Orland, 1984; Gerhardt & Frommhold, 1988; Bo et al, 1990; Cahill et al, 1990)

6. Wickewicz et al, 1983

7. Pedotti et al, 1978

APPENDIX 4.3: OPTIMIZATION METHOD FOR CALCULATION OF MUSCLE FORCES

An algorithm consisting of the following steps was developed to calculate acceptable values for the muscle forces:

Step 1. The six equations of force and moment were written in terms of three levels of muscle force activation α_1, α_2, and α_3 (4.12).

Step 2. Three of these equations were selected to start the computational process. Assuming initial values for the components of b_i, these equations were solved for the corresponding values of α_1, α_2, and α_3. These values of α_n were entered into the three remaining equations to calculate new values for the components of force and moment, b_i.

Step 3. An objective function was calculated, based upon the deviation of the calculated values of b_i from the initial values. The deviation was weighted by the range of values of b_i reported in the literature. The objective function was also heavily weighted for solutions that were not consistent with the condition $\alpha_1 > \alpha_2 > \alpha_3$.

Step 4. Using the Simplex method, the values of α_3, α_2, and α_1 were varied to find the minimum value of the objective function that corresponded to the least possible deviation from the initial values b_i. Once the minimum condition was met, the corresponding values of α_1, α_2 and α_3 and b_i, b_2, b_3, b_4, b_5 and b_6 are calculated.

Step 5. The forces of contraction of each muscle were then predicted from the product of the corresponding values of physiological cross-sectional area and activation coefficient.

CHAPTER 5. A CRITICAL EVALUATION OF THE EXPERIMENTAL METHOD DEVELOPED TO PREDICT MUSCLE FORCES

5.1 PREVIOUS APPROACHES

The method described to predict muscle forces during early stance offers many theoretical benefits. Its greatest asset is that it provides data which are both physiologically and biomechanically consistent, in contrast to many earlier approaches that have yield solutions which may be described as being "mechanically equivalent" to reality. The simplest approach to this problem has been to develop a robotic model of the human body in which the muscles are treated as idealized uniaxial actuators capable of developing unlimited force of contraction (Seireg & Arvikar, 1973, 1975; Hardt, 1978). In these models, it has been assumed that any muscle can contract at any time to generate joint motion which is kinematically equivalent to that observed during gait. Not surprisingly, the muscle forces predicted using this approach have often exceeded values which are physiologically reasonable.

Some authors have compared the predictions of such models with EMG recordings of hip muscles recorded during gait (Seireg & Arvikar, 1973, 1975; Hardt, 1978; Pedotti et al, 1978; Crowninshield & Brand, 1981; Crowninshield, 1978; Patriarco et al, 1981). While there is some resemblance of the predicted muscle forces to the EMG traces, there are also dramatic contradictions. For example, the mathematical model of Crowninshield and Brand (1981) predicted that only the glutei would be active during early stance phase and that gluteus medius would contract strongly for the duration of stance phase, despite EMG evidence to the contrary. Although the analysis of Hardt (1978) predicts muscle contractions which generally correspond with EMG recordings, rectus femoris must contract in mid-stance to maintain equilibrium of the lower extremity. Similarly, Crowninshield (1978) predicted that gluteus maximus would be active for almost all of stance phase and tensor fascia lata would only contract from mid stance until toe-off, again in contradiction of the EMG data.

An inherent deficiency of mechanical models of the hip joint has been ambiguous representation of the anatomic course of the hip musculature. While the position of origin and insertion of each muscle

may be approximated by one or more discrete points, generally located on the pelvis and the femur or on adjacent soft tissue structures (e.g. the origin and insertion of parts of gluteus maximus), the true course of each muscle is further constrained by a number of factors. In contrast to a line element in a computer model (i.e. a uniaxial actuator), the physical bulk of real muscles dictates that the line of action of adjacent muscles must be separated by a distance approximated by half the sum of the thickness of both muscles during contraction. The muscles of the hip are present in planes which limit their relative position with respect to the joint center. Thus, deep muscles will always lie closer to the hip joint than those that are superficial. Consequently, within any mechanical model, the predicted lines of action of deep and superficial muscles should not cross, particularly in extreme positions of joint motion.

The presence of the femoral head and the joint capsule also means that no muscles can pass closer than 30 - 35mm to the center of rotation of the hip joint. Some of the muscles of the hip, e.g. gluteus maximus and ilio-psoas, do not pass in a straight line from their origin to their insertion but wrap around other structures that have bursae to distribute the reaction force developed by the change in direction of action. These effects can become critical in modeling muscle actions during activities performed near the extremes of the joint position, eg. rising from a chair. These pitfalls in mathematical modeling tend to occur when the line of action of individual muscles has not been measured from actual specimens but has been predicted through extrapolation from one standard position of the joint to other positions within its range of motion. These errors may be minimized by developing models directly from cadaveric preparations or radiographic data (CT or MRI scans) in which all structures are visualized with the joint held at the position of interest.

A common feature of approaches to estimating individual muscle forces during gait is the use of numerical optimization to find a minimum value of an objective function derived from the force of contraction of each muscle (Seireg & Arvikar, 1973, 1975; Pedotti et al, 1978; Crowninshield et al, 1978; Hardt, 1978; Crowninshield, 1978; Penrod et al, 1974; Patriarco et al, 1981; Crowninshield & Brand, 1981). This approach is necessary because the biomechanical model of the hip is indeterminate, especially when every muscle is assumed to be active at

each point in the gait cycle!

Optimization techniques have been employed to find muscle force solutions satisfying a wide variety of constraints, including the lowest energy of contraction, the least total muscle force, the lowest force per unit area in each muscle. An underlying assumption of this approach is that the activation patterns of muscles have evolved in order to minimize some physical quantity, e.g. energy, force, stress. However, there is no empirical or experimental evidence to show that this is indeed the case and some authors have argued that some muscle forces predicted by common formulations of the optimization problem are not consistent with reality (Barbenel, 1983).

The most promising formulations of optimization functions have been based upon the effective stress generated by each muscle (i.e. contraction force per unit cross-sectional area) as these functions appear to provide the most reasonable predictions of muscle forces (Crowninshield & Brand, 1981; Challis & Kerwin, 1993). However, as none of these approaches includes, a priori, the observed patterns and intensities of muscle contraction occurring during gait, the best that could be expected from this approach is an "optimized, mechanically equivalent" model of the hip joint during ambulation.

5.2 SOURCES OF ERROR IN PREDICTED MUSCLE FORCES

The method of predicting muscle forces developed in this study imposes the conditions that any acceptable solution must be consistent with gait kinematics and quantitative EMG, as well as satisfying equations derived from a biomechanical model of the hip joint. Moreover, the biomechanical model itself is constrained by the use of values for hip joint forces and moments actually measured by instrumented prostheses and not deduced from motion analysis and force plate data. While each of these considerations makes this approach attractive and ensures that the forces predicted will have a significant resemblance to reality, it presents a number of problems in implementation, as all of the inputs to the theoretical model are subject to a large degree of variability between individual subjects.

While it is possible to measure simultaneously foot/ground forces, hip joint forces, EMG and gait kinematics using patients with instrumented prostheses, comprehensive data of this type has not been

reported in the literature. This necessitates use of average values of quantities which can be highly variable and are not always precisely defined, even in studies of individual patients. Fortunately, these sources of variation primarily influence the distribution of forces between muscle groups rather than the total muscle force acting during gait.

Taken separately, the following considerations affect the accuracy of the sources of data utilized to predict muscle forces in this study:

(i) Ground/Foot Forces. As seen from Table 4.3, there are large variations in the reported values of the medial/lateral and anterior/posterior components of the foot/ground reaction force. Typically, these data have a coefficient of variation (i.e. (standard deviation x 100) /mean) of 45% (medial/lateral) and 27% (anterior/posterior) respectively. Fortunately, the vertical component is much less variable (CV = 7%); it has the greatest effect on the calculated value of the total muscle force.

(ii) Hip Joint Forces. Data derived from the few published reports of intravital hip forces are relatively variable. Moreover, the methods, and even the coordinate systems, utilized in each study are different, making the comparability of the results of different investigators an issue. Nonetheless, as Tables 4.1 and 4.4 show, there is some consistency within the data, especially if the speed of ambulation is standardized and all data are normalized with respect to the peak joint reaction force. Moreover, the large range of values for the anterior/posterior and medial/lateral components of hip force are similar to the variation in published values of the components of the foot/ground reaction forces. The impact of this source of error on the ultimate predictions of muscle forces is minimized through the use of the optimization procedure.

(iii) EMG Data. There is reasonable agreement between different studies of the EMG activity of the hip muscles during walking, though some differences exist with respect to the exact period of action of individual muscles. Undoubtedly, some earlier data were affected by artifacts due to the design of electrodes and detection of activity in adjacent muscles. Variations must also exist because of differences in the precise placement of the surface and wire electrodes utilized in different studies.

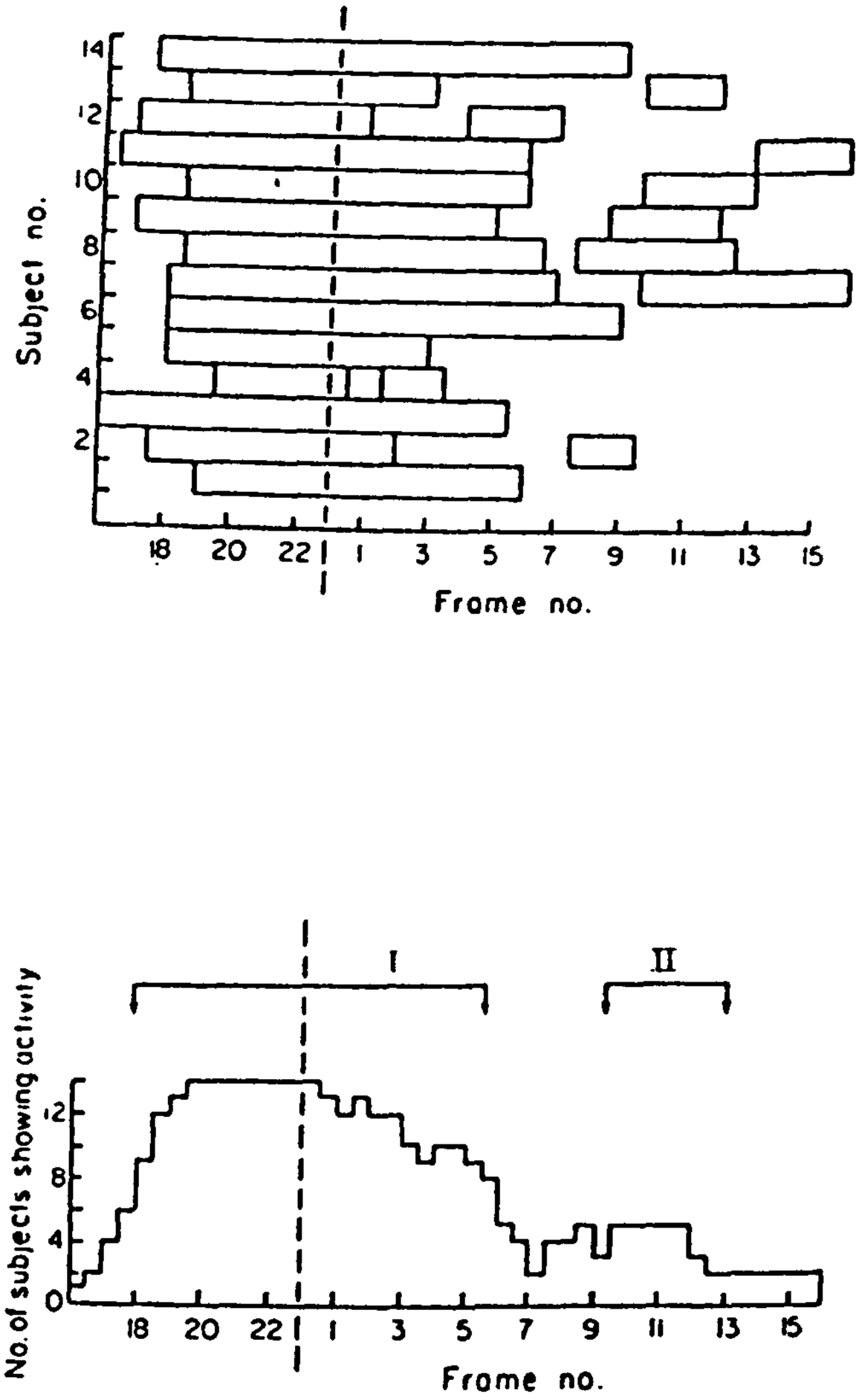

Figure 5.1 Typical variation in EMG activity of the hamstrings in 14 different subjects during normal gait. All subjects show activity prior to heel strike (frame no. 0). After heel strike, activation patterns are highly variable, with approximately one-third of subjects showing activity late in stance phase (from Battye and Joseph, 1966).

Moreover, it is often difficult to demonstrate that signals are being obtained from the belly of the correct muscle with absolute certainty, especially when the muscle lies deep to the surface of the skin.

Another confounding factor is the inherent variability of the pattern and intensity of electrical activation of muscles during ambulation (figs 5.1 and 5.2). In an interesting study, Kadaba et al (1989) examined the repeatability of EMG data recorded in 40 normal subjects on three separate occasions during the same day and on three different days. All measurements were performed by investigators with extensive experience in electromyography and motion analysis, though the EMG data were recorded using surface electrodes, which may have contributed to some of the variability. The multiple correlation coefficient for the magnitude of the integrated and rectified EMG signals ranged from 0.746 to 0.899 for recordings performed on the same day, and 0.661 to 0.860 for recordings performed on different days. Typically, measurements performed on superficial hip muscles had correlation coefficients of 0.85 for recordings made on the same day and 0.82 for recordings made on different days. During early stance phase, (15% of the gait cycle) the coefficient of variation (standard deviation/mean) of the EMG signals of most of the muscles studied exceeded 50%, slightly larger than the variability reported by Winter and York (1987).

Key features of the analytical method presented in this dissertation are the assumptions that each muscle is not equally activated during the gait cycle and that the intensity of activation of each muscle can be derived from published data. In this respect, the quantitative EMG studies of Basmajian and co-workers are extremely useful and instructive. However, these data show that considerable variation is present from subject to subject. Moreover, values reported are not entirely consistent with the reports of other investigators using similar experimental methods (Lyons et al, 1983).

A weakness of this approach is that the relationship between the integrated EMG signal and the force of contraction

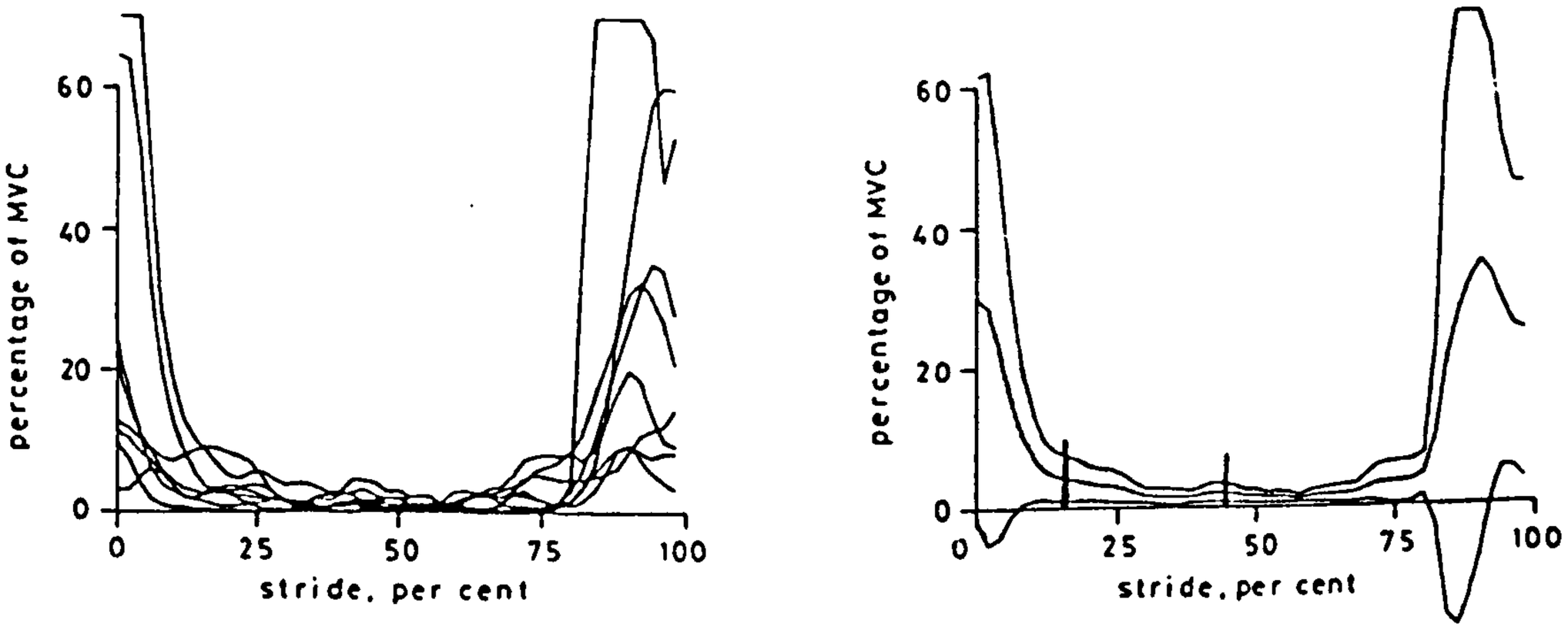

Figure 5.2 EMG activity of biceps femoris recorded in eight subjects during the gait cycle and normalized with respect to the EMG signal for maximum voluntary contraction (MVC). The graph on the left shows average values for each subject while the average of all subjects (± 1 sd) is displayed on the right (from Arsenault et al, 1986).

of each muscle of the hip joint is not truly known (Hof & Van den Berg, 1981a, 1981b, 1987). During voluntary isometric contraction of muscles, a linear relation has been reported between muscle force and the rectified and integrated EMG signal. However, the force developed by each muscle varies with its pennation angle, resting length, fiber type and speed of contraction (Hill, 1953; Abbott & Wilkie, 1953; Pedotti et al, 1978). Bigland-Ritchie et al (1980) showed that linear force/EMG relations accurately described the action of muscles of predominantly uniform fiber type (e.g. soleus). In contrast, muscles consisting of approximately equal proportions of fast and slow fibers (e.g. biceps) displayed a non-linear relationship between force and EMG with a discontinuity at about 30% MVC, the level above which only fast fibers are recruited. In view of these observations, precise values of the activation coefficient of each muscle were not used in the present study. Rather, muscles were ranked in terms of the estimated strength of stimulation and then grouped as weak, mild, or moderately activated for inclusion in the subsequent analysis.

(iv) Gait Kinematics. As with most other quantities describing gait, the position of the leg and the body during walking varies significantly from person to person. Fortunately, several comprehensive studies have reported average values which are reasonably consistent, although variations of ± 10 degrees are possible in the extremes of hip flexion with somewhat less variation in the position of the hip in early stance. This variability can become pronounced if data from individuals of different ages or walking speed are pooled, especially when peak values of adduction and internal rotation are being compared at the maximum value of the foot/floor reaction force. This severely limits the interpretation and generalization of intravital hip force data as relatively slight changes in adduction lead to a large reduction in the abductor forces needed to stabilize the hip joint.

One form of adaptation to hip replacement during gait is reduction of the maximum flexion of the hip joint with increased adduction and internal rotation of the lower

extremity. This reinforces the necessity for simultaneous recordings of kinematic and biomechanical data to allow adequate interpretation of joint forces measured with instrumented hip prostheses.

Given the variability of the data used in this analysis, the only substitute for simultaneous recordings of all data from a group of instrumented patients appears to be the use of average values from large groups of different, though comparable individuals. Certainly, this approach is by no means perfect, however, the use of the optimization technique is an innovative way to determine whether solutions exist which can reconcile differences between different sets of data to produce muscle force values which are both reasonable and internally consistent.

5.3 ALTERNATIVE APPROACHES TO PREDICTING MUSCLE FORCES

5.3.1 Methodology

As the use of several sets of pooled or "consensus" data (e.g. EMG, kinematics, intravital hip forces), can compound the uncertainty associated with any one data set, it is useful to explore other approaches to partitioning the total muscle force between individual muscles. Three additional methods were explored:

Method 1. It was assumed that the force of contraction of each muscle was proportional to its physiologic cross-sectional area. This was equivalent to assuming that all active muscles had the same activation coefficient. The corresponding, `effective' value of the activation coefficient was calculated by solving each of the six equations of force and moment (i.e. equation 4.8), assuming that all values of α_j were equal. This led to six solutions for α_j ranging from 10.99 N/cm^2 (F_Y) to 35.95 N/cm^2 (M_X). The value of α_j derived from the transverse moment equation (M_Z) was ignored in calculation of an average value for α because the sum of the coefficients in equation 3.8 (i.e. $\Sigma\, \alpha_{ij}PCSAj$) were very close to zero and so the solution for α_j was artificially large (1143 N/cm^2). The average value of α derived from the five remaining

equations, was 20.22 N/cm^2. Thus, the force developed by each muscle was calculated as 20.22 PCSAj.

Method 2. It was assumed that the muscle forces were distributed according to the product of the physiologic cross-sectional area and the magnitude of the EMG signal of each muscle. The value of the activation coefficient for each individual muscle was calculated from the quantitative EMG data of Basmajian (1976). The force developed by each muscle was then calculated using the following expression:

$$\alpha_j = N\,\alpha_{av}\left(\frac{EMG_j}{\sum_j EMG_j}\right) \qquad (5.1)$$

where N = Number of muscles

$\alpha_{av} = 20.22\ N/cm^2$

EMG_j = integrated EMG signal of jth muscle, expressed as a percentage of the signal recorded during maximum voluntary contraction of the muscles, (all data derived from Basmajian)

α_j = activation coefficient (N/cm^2) of jth muscle

This expression weights the values of the activation coefficient of each muscle in direct proportion to the relative magnitude of its EMG signal compared to the sum of the EMG signals of all muscles combined.

Method 3. It was assumed that muscle forces were distributed according to the product of the physiologic cross-sectional area and the moment arm of each muscle with respect to the hip joint center. The activation coefficients of individual muscles were calculated by weighting α_{av} according to the moment arm of each muscle:

$$\alpha_j = N\alpha_{av}\left(\frac{ma_j}{\sum_j ma_j}\right) \qquad (5.2)$$

Muscle	Method of Solution			
	1	2	3	4
Gluteus Maximus	20.2	7.9	10.7	11
Gluteus Medius				
Anterior	20.2	39.7	31.3	30
Middle	20.2	39.2	27.9	30
Posterior	20.2	38.5	19.0	30
Gluteus Minimus	20.2	28.7	15.6	30
Tensor Fascia Lata	20.2	11.8	37.4	17
Semitendinosus	20.2	15.7	17.0	17
Semimembranosus	20.2	7.9	14.6	5
Biceps Femoris	20.2	4.3	13.3	5
Rectus Femoris	20.2	8.6	15.4	5

Table 5.1: Predicted values of the activation coefficient (N/cm^2) of each muscle active during early stance, based upon four different methods of calculation.

1: Assumption that all muscles are equally activated
2: Activation coefficients weighted according to the quantitative EMG data of Basmajian
3: Activation coefficients weighted according to the magnitude of the moment arm of each muscle
4: Activation coefficients predicted in this study

Where ma_j = moment arm of jth muscle (length of the component of the vector extending form the joint center to the line of action of each muscle which is perpendicular to the line of action of the muscle).

5.3.2 Results

The results of this analysis appear in Tables 5.1 and 5.2. In Table 5.1 , the predicted values of the activation coefficients are reported for each method of calculation in comparison with the four values derived earlier in this study by pooling muscles with similar levels of activation and optimizing the result.

The use of a single, average value for the activation coefficient (Method 1) led to values that were completely at variance with qualitative EMG recordings of the activity of the hip muscles during gait. In Table 5.2 it is shown that this assumption leads to large discrepancies between the predicted and 'consensus' values of the components of hip joint force and moment. The predicted values of the total muscle force was 26% larger than the consensus value (1752 N) while the resultant joint moment was almost identical to the consensus value (65.7 Nm). The discrepancies in each of the force and moment components were as follows: Fx (+9%), Fy (+75%), Fz (+23%), Mx (-44%), My (+66%) and Mz (-99%), where the number in parentheses corresponds to the difference between predicted values expressed as a percentage of the original value. This method of muscle force calculation ignores the fact that: (i) some muscles are much better positioned to generate motion due to their moment arm with respect to the joint center, and (ii) the level of activation of different muscles is distinctly non-uniform. It should be noted that most of the components predicted by this simple method lie outside the range of values reported within the literature.

Utilization of the EMG data to calculate muscle forces (Method 2) would seem certain to provide the most realistic and accurate estimates of hip muscle forces. However, EMG data are inherently more variable than kinematic and biomechanical data and their direct conversion to muscle forces is based upon several questionable assumptions. This method of calculation assumes that muscle force is linearly related to the magnitude of the integrated EMG signal and that the proportionality constant is the

Component	Method of Solution				Consensus Values*
	1*	2	3	4	5
Fx (N)	517	398	412	507	476
Fy (N)	746	435	457	427	427
Fz (N)	2013	1788	1804	1631	1631
Mx (Nm)	31	53.4	66.5	54.9	55
My (Nm)	58	40.5	39.6	38.3	35
Mz (Nm)	0.1	0.3	5	5.6	8

Table 5.2: Values of the component of force (N) and moment (Nm) acting at the hip joint, calculated using the six equations defined in 4.8 using the values of the activation coefficients presented in Table 5.1

* Values assumed in this study, based upon the analysis presented in Chapter 4.

same for each muscle (Hof & Van den Berg, 1981b). The fallacy of this assumption is suggested by the data in Table 5.1 which indicate that the three parts of gluteus medius are stimulated to levels around maximum voluntary contraction (40 N/cm^2) during normal walking, while the EMG data indicate that this muscle is developing only 60% of its maximum voluntary contraction.

This contradiction may arise if the true physiologic cross-sectional area of each muscle is underestimated, or if cross-talk is present between EMG electrodes, increasing the signal received from only one electrode during activities in which more than one muscle is activated. However, the most likely cause of this discrepancy is the assumption the force of contraction and the EMG signal are directly proportional. Nonetheless, use of quantitative EMG data led to relatively close agreement between the predicted and 'consensus' values of the components of force and moment. The predicted value of the total muscle force was only 8% larger than the consensus value of 1752N while the resultant joint moment was only 2% larger. Interestingly, this method of muscle force calculation provided the estimate of the transverse component of joint moment (5.0 Nm) closest to the consensus value (8 Nm). However, this approach also led to significant overestimation of F_Z (+11%), M_X (+21%) and M_Y (+13%) and underestimation of F_X (-16%), though all predicted values were within the range of published data.

The total muscle force predicted using the relative magnitude of the moment arm of each muscle (Method 3) was 9% larger than the consensus value while the resultant moment was 18% larger. The individual muscle forces were physiologically reasonable, with activation coefficients ranging from 10.7 N/cm^2 (gluteus maximus) to 37.4 N/cm^2 (tensor fascia lata). This method side-steps the issue of the difference in the level of activation of each muscle and assumes that the neuromuscular patterns of muscle activation have evolved so that those muscles with the greatest mechanical advantage will be recruited in order to perform activities with the greatest mechanical efficiency. However, this approach ignores the fact that both the magnitude of the moment arm and the orientation of each muscle determines its ability to resist externally applied forces and moments.

The activation coefficients predicted by this approach were not

wholly consistent with the EMG data of Basmajian (1976). Due to their relative position with respect to the joint center, it was predicted that gluteus minimus would not be very active (α = 15.6 N/cm^2) and that tensor fascia lata would act near its maximum voluntary contraction (α = 37.4 N/cm^2) in the early stance phase of the gait cycle. It was also predicted that the other two-joint muscles of the hip (semi-membranosus, rectus femoris and biceps femoris) would be more active in early stance than EMG studies demonstrate.

This approach to the calculation of muscle forces does not allow mechanical redundancy of any available muscles as all are assumed to be as active as demanded by their anatomic position. However, in practice, it is not possible for every muscle to have optimal anatomic placement for every functional activity. Thus, even if all muscles were activated in relation to their moment-arms in one phase of gait, this pattern of activation would not be maximally efficient in other phases where the hip joint is in a different position, or in other activities at the same joint position (e.g. in running or jogging compared to walking).

This suggests that some muscles may have developed lines of action relatively close to the hip joint in response to constraints other than optimization of mechanical efficiency. Factors such as the need to minimize inertial forces or retention of body heat through reduction of the surface area of the extremity may have been a predominant factor in driving the evolution of musculo-skeletal organization. Alternatively, some muscles may have acquired a specialized role in performing specific functional activities. This may have occurred even though it may have resulted in muscles that are minimally activated in many activities.

Weighting of the activation coefficients by moment-arm led to reasonable predictions of the six components of force and moment with overestimation of the values of F_Z (+10%) and M_Y (+16%), and under-estimation of F_X (-16%) and M_Z (-96%). However, with the exception of the transverse component of moment (M_Z), all predictions were within the normal variability of literature data.

5.3.3. Conclusion

The estimates of the components of force and moment that were closest to the 'consensus' values were produced by the method developed in this thesis. With the exception of the component of moment within

the transverse plane (M_Z), the discrepancy between the values predicted using this method and the initial consensus values derived from the literature ranged from 0 to 7%. Although this method of calculating muscle forces is clearly superior to the others studied in this work, it depends upon intravital force data which is only available for the hip joint. In cases where these data are unavailable or where use of this method is unwieldy, quantitative EMG or anatomic data describing the moment arm of each muscle could be employed to provide a reasonable estimate of the forces developed by individual muscles.

CHAPTER 6: DEFORMATION OF THE ACETABULUM DURING LOADING: EXPERIMENTAL STUDIES

6.1 INTRODUCTION

Based upon the previous investigation of the position of the pelvis and the femur during gait, the forces acting at the joint center and the forces developed by muscle contraction, an experimental model was developed using fresh cadaveric specimens. Using this model, the deformation of the acetabulum was measured during weight-bearing. To facilitate the interpretation of this data and to identify patterns of deformation consistent with uniaxial and biaxial bending, a mechanical facsimile of the bone around the acetabulum was developed, and instrumented in the same manner as the cadaveric specimens.

6.2 ANALOGUE STUDIES

6.2.1 Introduction

The distribution of deformation over the surface of the pelvis is highly complex and defies simple description. However, in order to conceptualize the loading response of this structure it is useful to talk in terms of deformation pattern arising from simple load conditions, including uniaxial and biaxial bending. An additional consideration, which becomes relevant in explaining differences between the deformation patterns of different specimens, is the effect of pelvic morphology on the distribution of cortical strain. In order to describe the predominant pattern of deformation of the pelvis while eliminating the confounding effects of specimen deterioration and morphologic variability, a mechanical analogue of the periacetabular region was developed and fabricated from reinforced polyester. This allowed highly reproducible measurement of surface deformation to be performed in 3-point bending, a load condition that previous authors have claimed as representative of physiologic loading.

6.2.2 Materials and Methods

A simple model was developed to represent the essential morphologic features of the pelvis in the vicinity of the acetabulum.

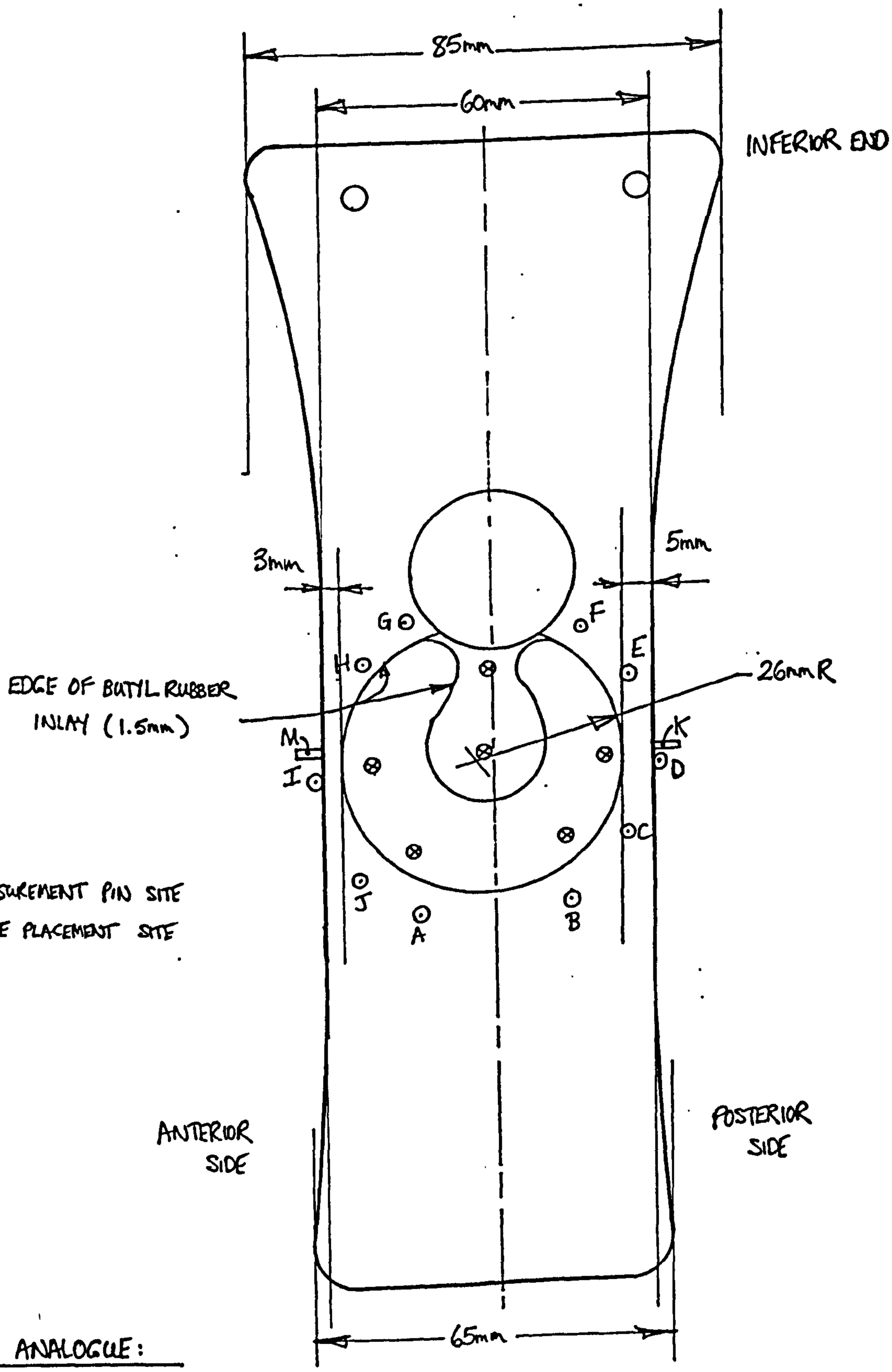

Figure 6.1a Layout of the acetabular analogue showing the top (lateral) view.

These features included the acetabular socket, the obturator foramen, the acetabular notch and the ischium and ilium (Fig. 61.a, b, c). The ischium and ilium were represented by solid plates, tapered in thickness to reduce their stiffness with respect to the acetabulum. Within the model, a central, hemispherical socket was eccentrically placed to simulate the normal pelvis, in which the anterior wall of the acetabulum is thinner than the posterior wall. The analogue was molded from polyester resin and fiberglass matting using a wooden mold with aluminum strips which were contoured to form its sides. The hemispherical socket was formed in situ using a Wood's metal hemisphere which could be melted to facilitate its removal from the cast component. Preliminary attempts to cast the analogue from unreinforced polyester resin resulted in parts which fractured through the walls of the hemispherical socket. To overcome this difficulty, three layers of glass mat were incorporated in the walls of the molded socket. Once the analogue was molded and sanded, a horseshoe of butyl rubber sheet, 1.5 mm in thickness, was glued to the base of the fiberglass socket to simulate the lunate surface of the normal acetabulum.

To simplify loading conditions, it was assumed that the most significant mode of deformation of the acetabulum was bending of the ilio-ischial column over a fulcrum formed by the femoral head. The loading of the pelvis was represented by a force applied to the acetabulum, balanced in turn by reaction forces developed in:

(i) the ilium, through the contraction of muscles, mainly the glutei and the action of the body forces transmitted across the ipsilateral sacroiliac joint, and

(ii) the ischium and pubis, through the contraction of muscles, mainly the hamstrings and forces transmitted across the contralateral sacroiliac joint and the pubic symphysis.

This was realized in a physical model by orienting the mechanical analogue anatomically with respect to the direction of the joint force. The iliac and the ischial/pubic reaction forces were generated by simply supporting the analogue in a mounting frame (Figs. 6.2, 6.3). The hemispherical socket within the analogue was loaded via a molded polyester hemisphere with a force directed at 40 degrees superior and 10 degrees posterior to the plane of the analogue. Eighteen stainless steel pins were implanted into the analogue to a depth of 4 mm at key points

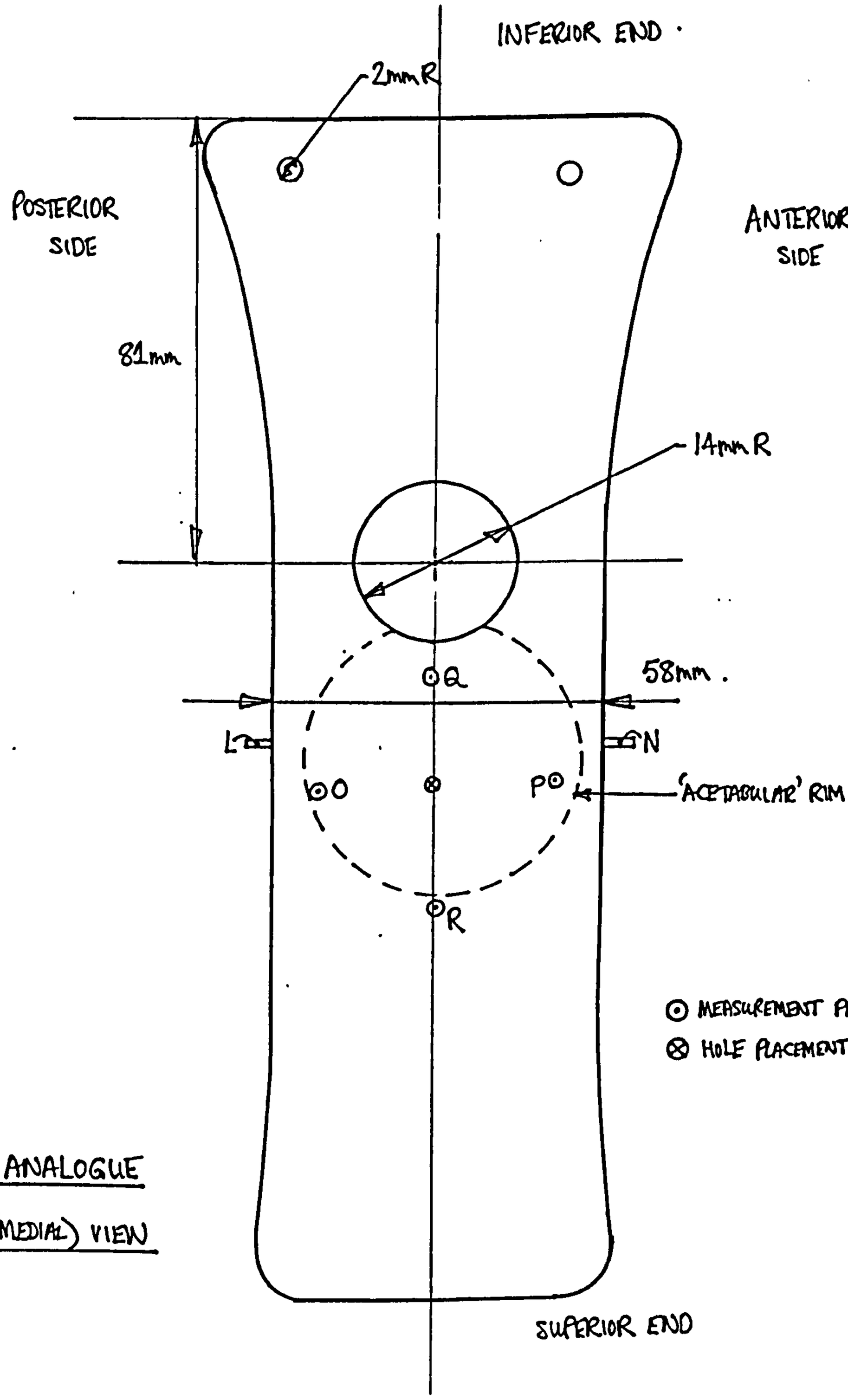

Figure 6.1b Layout of the acetabular analogue showing the bottom (medial) view.

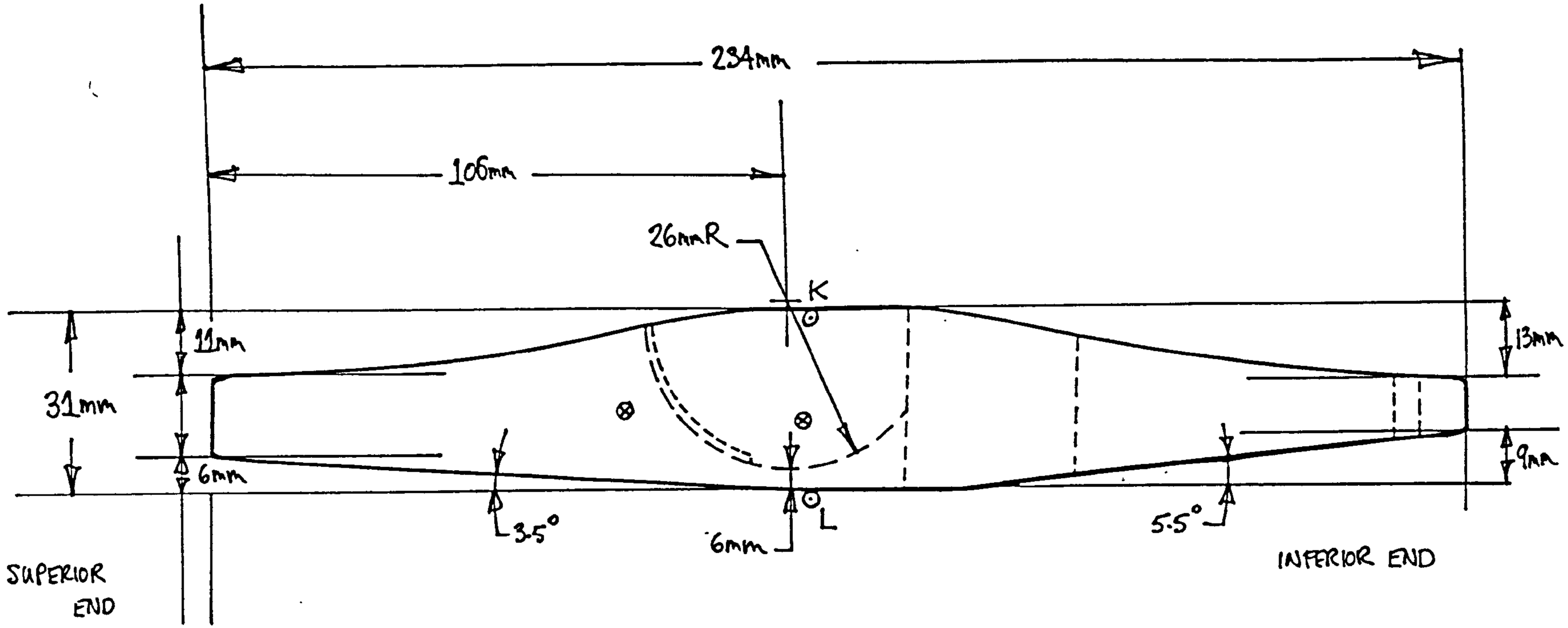

PELVIC ANALOGUE : SIDE VIEW

⊙ SITE OF MEASUREMENT PIN

⊗ SITE FOR HOLE PLACEMENT

Figure 6.1c Layout of the acetabular analogue showing the side views.

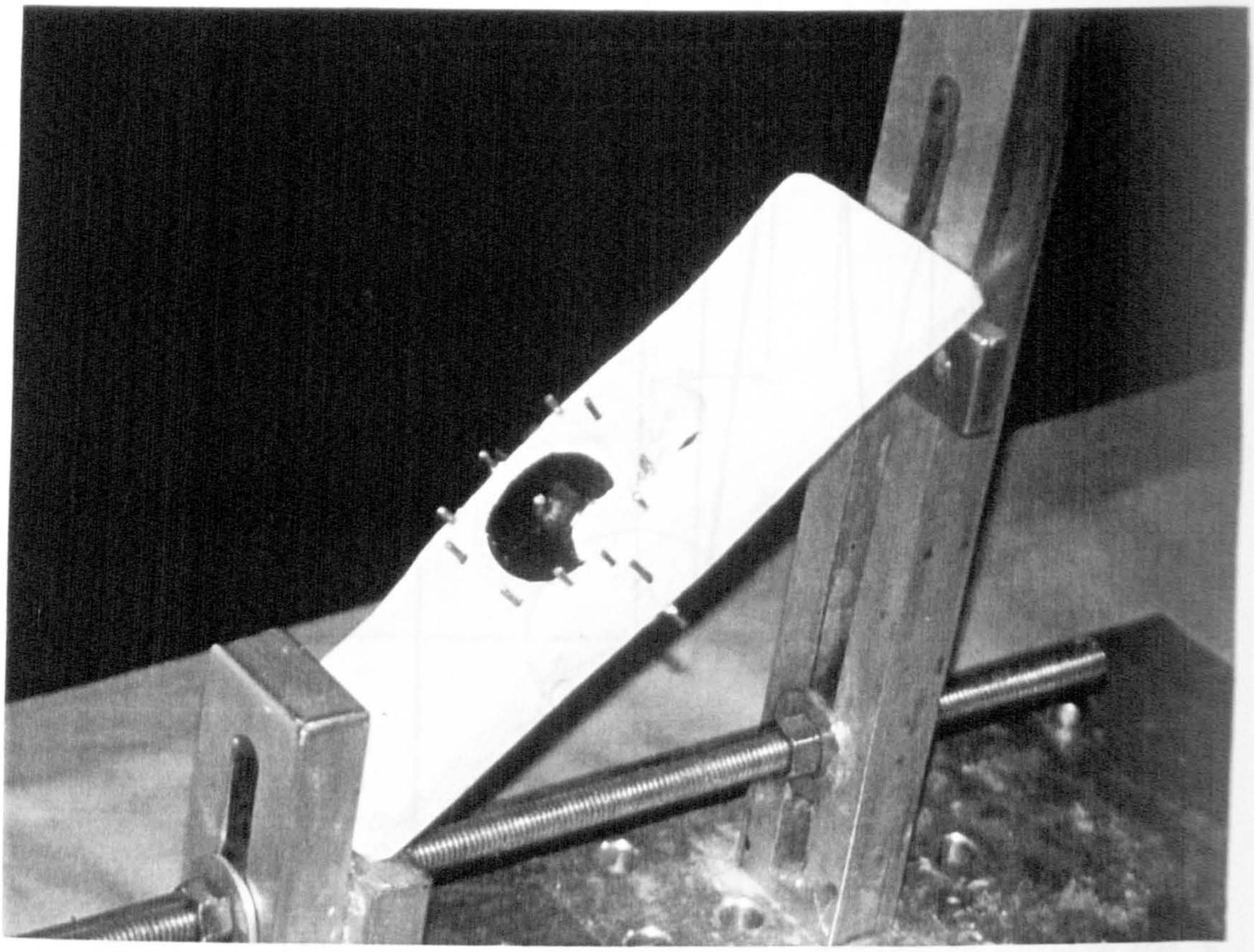

Figure 6.2 The acetabular analogue prior to attachment of the transducers. A metal supporting fixture maintains the alignment of the analogue with respect to a vertically directed load.

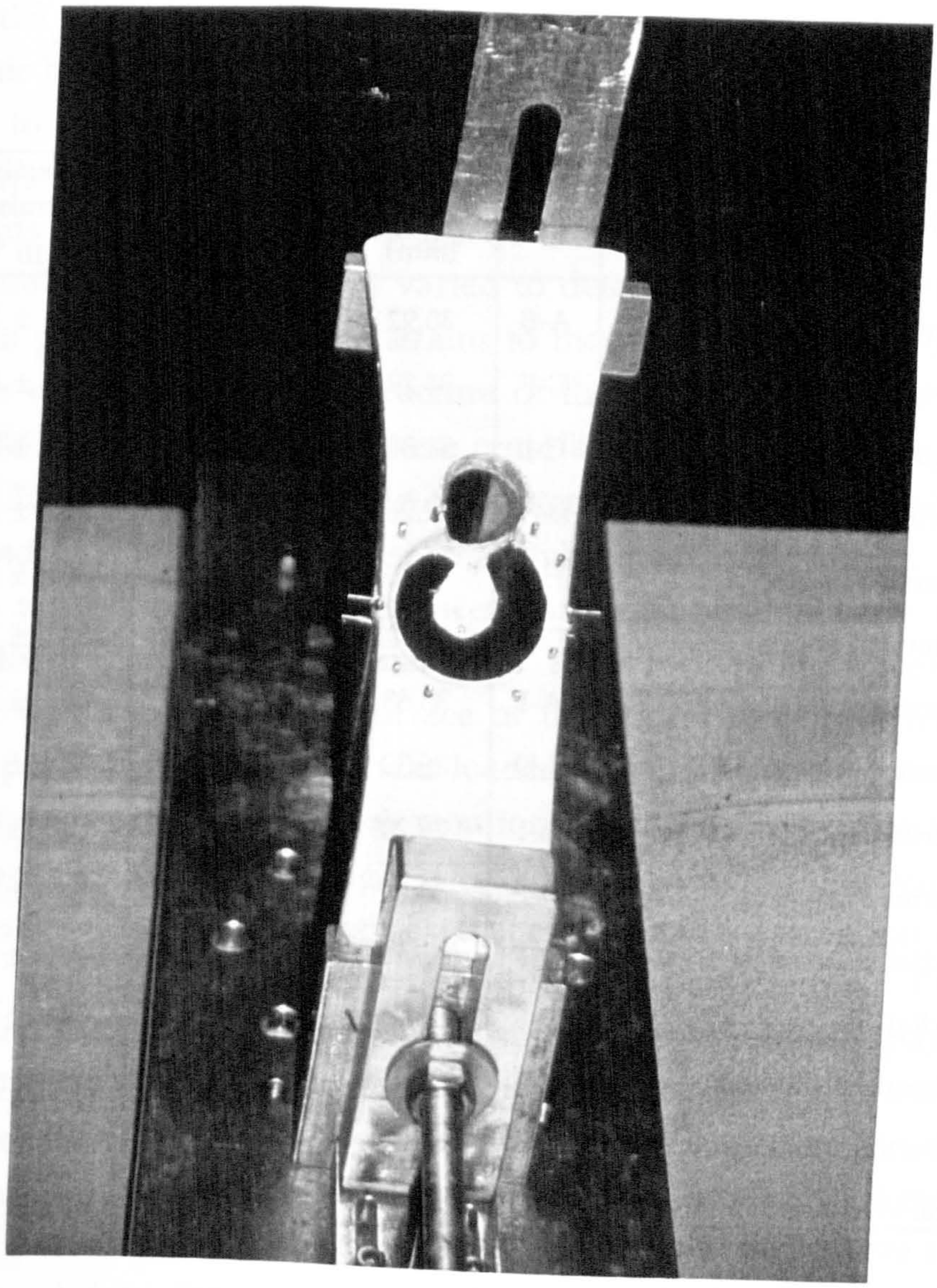

Figure 6.3 A top view of the acetabular analogue in the mounting fixture.

Measurement Site	Pins*	Gage Length (mm)	Deformation (μm)	Effective Strain ($\times 10^{-6}$)	n
1. Dome (beneath Illium)	A-B	30.92	10.4 ± 0.5	336 ± 15	8
2. Facets	G-F	34.29	34.7 ± 2.3	1013 ± 66	9
3. Superior Width	C-J	51.34	43.5 ± 1.4	849 ± 27	12
4. Inferior Width	E-H	52.26	37.8 ± 2.6	724 ± 50	11
5. Anterior Length	H-J	43.40	-121.7 ± 2.7	-2804 ± 61	8
6. Posterior Length	C-E	32.72	-76.7 ± 3.4	-2343 ± 104	8
7. Superior-Anterior	A-I	33.63	-30.2 ± 1.7	-899 ± 51	12
8. Superior-Posterior	B-D	36.30	-31.1 ± 2.2	-858 ± 60	11
9. Inferior-Anterior	G-I	29.20	-17.9 ± 1.0	-612 ± 35	10
10. Inferior-Posterior	D-F	33.05	-35.8 ± 2.5	-1083 ± 74	13
11. Medial Horizontal	O-P	45.99	-17.4 ± 0.9	-378 ± 19	8
12. Medial-Vertical	Q-R	46.02	42.8 ± 0.3	929 ± 7	6
13. Anterior Wall Depth	M-N	27.90	-9.6 ± 0.3	-344 ± 11	8
14. Posterior Wall Depth	K-L	31.47	-8.3 ± 0.7	-264 ± 22	6
15. Total Width	D-I	63.72	244.4 ± 5.3	3836 ± 83	10

Table 6.1 Measurements performed with the Acetabular Analogue. (mean± se)

* Refers to measurement sites depicted in Figure 6.1 a, b, c.

"Effective Strain" is defined by the change in length measured divided by the unloaded gage length (i.e.. distance separating pins)

around the acetabular socket (Fig. 6.1a, b, c) to allow measurement of deformation during loading.

Extensometers (MTS Corp., Minneapolis, USA) were attached to pairs of the steel pins using extension arms, custom fabricated knife edges and elastic bands. The body of each extensometer was supported by straps attached to a frame which was mounted on the analogue. The separation of 15 pairs of the pins was measured before and after the application of joint loads of up to 880N (200 lb) (table 6.1). In an initial series of experiments, the joint load was varied to determine how much load was needed to produce comparable strains to those observed in the biological specimen without yielding or fracture of the analogue. A joint reaction force of 880N (200 lb.) fulfilled these criteria and generated a longitudinal strain of 2000-3000 microstrain in the anterior and posterior walls of the socket, and so was selected for use in all subsequent experiments.

In a typical experiment, displacement measurements were recorded for 6-10 loading cycles of the analogue. Prior to loading, a water-based lubricant was applied to the surface of the socket to reduce friction as much as possible; the analogue was loaded and unloaded 6-10 times. The output of each extensometer was monitored using a strain gage amplifier (Measurements Group, Raleigh, USA) with an activation voltage of 10.00V and a gain of 2000. Both extensometers had a resolution of better than 0.4 mm and a sensitivity of around 2-6 mV/mm. Extensive precautions were taken to overcome artifacts due to microslippage at the knife edge/pin interface, bulk motion of the body of the transducer, misalignment of the knife-edges, and motion of the pins within the body of the analogue. If any set of readings exhibited variations of more than 20% or appeared not to be reproducible, the extensometers were removed and reattached to the specimen and a new set of measurements was taken. However, these measures were not necessary in the vast majority of the experiments performed.

6.2.3 Results*

The observed pattern of deformation was consistent with uniaxial bending (table 6.1), with compressive strains of 2000-3000 microstrain over the lateral surface of the analogue in combination with tensile strains over the medial surface (929 ± 7 microstrain). The longitudinal strains measured on the lateral surface were larger along the anterior edge of the socket (-2804 ± 61 microstrain), than the posterior edge (-2343 ± 104 microstrain). This was partly due to the fact that the applied load was oriented at 10 degrees posteriorly and the fact that the anterior wall was thinner than the posterior wall, as in the native acetabulum.

In the transverse direction, tensile stresses were present on the lateral surface of the analogue, corresponding to 724 ± 50 microstrain below the socket and 849 ± 27 microstrain above the socket. This is 0.28 - 0.33 of the average longitudinal strain of the anterior and posterior walls (-2574 microstrain), consistent with the expected Poisson effect. Over the medial surface of the analogue, the deformation pattern was also consistent with uniaxial bending, with elongation in the longitudinal direction (929 ± 7 microstrain) and contraction in the transverse direction (-378 ± 11). The ratio of these strains (0.41), was only slightly larger than the value of Poisson's ratio for rigid polymers (0.35). This suggests that the lateral bending of the walls of the socket was localized and only generated a minor component of transverse bending in the floor of the socket.

At specific sites, local deformation was influenced by the geometric features of the model. While the average value of the transverse strain measured above and below the socket was 787 microstrain on the lateral surface, the socket itself widened by approximately 240 μm with loading, corresponding to an effective strain of 3836 ± 79 microstrain. This increase in width was less pronounced above the edge of the socket, (336 ± 15 microstrain), than at the inferior measurement site between the lower edge of the socket and the through-hole simulating the obturator foramen (1013 ± 66 microstrain). This effect was presumably due to the stress concentrating effect of the through-hole. The localized widening of

---

* **Note:** To facilitate discussion of the results in comparison with analogous sites on the acetabulum, the surfaces of the analogue will be referred to using anatomic terminology (fig 6.1a,b,c). Thus, the upper surface of the analogue will be referred to as the lateral surface; the undersurface as the medial surface. Similarly, the side walls will be referred to as the anterior and posterior surfaces.

the socket also generated a large deformation gradient between the width of the analogue laterally and medially corresponding to bending of the anterior and posterior walls in an outward direction about the floor of the acetabulum. While the socket expanded by 3836 ± 83 microstrain at the rim, the floor of the socket contracted by 344 ± 11 microstrain with loading.

These data support the interpretation that the spherical ball simulating the femoral head acts as a wedge in both the medial and superior directions, causing the anterior and posterior columns of the acetabulum to spread apart and bend with respect to the acetabular floor and the medial wall. An effect of this spreading action is increased separation of the 'facets' inferiorly where the transverse reinforcement of the acetabular margin is interrupted by the `obturator foramen'.

6.3 CADAVERIC STUDIES

In this part of the study, deformation of the normal acetabulum was measured under conditions simulating loading of the pelvis during the early stance phase of gait. The muscle forces predicted by the previous analysis were applied to fresh cadaveric specimens which were instrumented to allow measurement of bony deformation.

6.3.1 Materials and Methods

6.3.1.1 Specimen selection

Ten anatomic specimens, each consisting of two femora and a pelvis with the spinal column transected at the L3/4 interspace were harvested from fresh cadavers donated to the Department of Cell Biology at Baylor College of Medicine in Houston. Each specimen was obtained at 2-5 days following the time of death, once serum cultures were processed to detect exposure to HIV and Hepatitis B viruses. Cadavers were excluded from use in this study if the donor:

(i) displayed evidence of osteoporosis or emaciation secondary to bed rest,

(ii) was a post-menopausal female, or

(iii) had a positive serum culture for HIV or HBV.

During removal of the pelvis from each cadaver, care was taken to maintain each hip joint and its attached capsule intact and to avoid division of any of the sacroiliac ligaments because of their role in

SAB#*	Age	Sex	Race**	Cause of Death
23470	52	M	W	Coronary Heart Disease
26679	51	M	W	Coronary Heart Disease
26662	53	F	W	Pneumonia, Lung Cancer
26687	65	M	W	Sudden Death, Cardiac Arrest
25293	65	M	W	Coronary Heart Disease, Emphysema

Table 6.2 Details of the donors of the 5 pelvises used in this study.

* Identification number of the State Anatomic Board of Texas.
** Reported as White/Black/Hispanic/Other

stabilizing the sacroiliac joint (Tile, 1984). Once each specimen was cleaned of all muscle and soft tissues, standard AP and lateral radiographs were prepared at a standard tube setting of 80 kV exposed for 1/30 second. Each radiograph was taken at a tube to cassette distance of 72 inches (1.83 m) to minimize distortion.

Each radiograph was examined for evidence of osseous pathology including previous trauma or metastatic disease. Based upon the density of each radiographic image, a subjective assessment was made of bone density and any specimen showing evidence of advanced osteopenia was excluded from this study. Through application of these exclusion criteria, five of the original specimens were considered suitable for further use. Details of the donors of these specimens appear in Table 6.2.

6.3.1.2 Specimen preparation

Both femora were sectioned transversely, 100 mm above the distal articular surface. The distal 100 mm of the right femur was potted in dental plaster in a cylindrical mold, (diameter: 79 mm) in a nominal position of 15 degrees of flexion and 9 degrees of adduction. All soft tissue was removed from each specimen. As subsequent measurements were performed on the right hip joint of each pelvis, the right hip was disarticulated to allow resection of the capsule from the rim of the acetabulum; the ligamentum teres and the transacetabular ligament. The inner and outer tables of the ilium were stripped of all periosteum and the fat pad was scraped out of the fovea of the acetabulum to reveal the medial wall. Each specimen was kept moist throughout this procedure.

The iliac crest was cleaned of adherent tissues along the line of insertion of the glutei and 10 to 15 holes of 1/8" (3.2 mm) diameter were drilled vertically into the top of the crest from the anterior superior to the posterior inferior iliac spines (figs 6.4a,6.4b, 6.5a, 6.5b, 6.6). All holes were irrigated with pulsatile lavage and compressed air to remove entrained fat, blood and bony debris. The crest was finally degreased with acetone and allowed to dry. Two units of acrylic bone cement (Surgical Simplex) were prepared and molded over the surface of the iliac crest. Manual pressure was applied to ensure maximum penetration into the drill holes and the exposed cancellous interstices of the anterior, superior and posterior surfaces of the crest. Once the acrylic bone cement had set, three holes (diameter: 6.9 mm) were drilled through the composite layer of

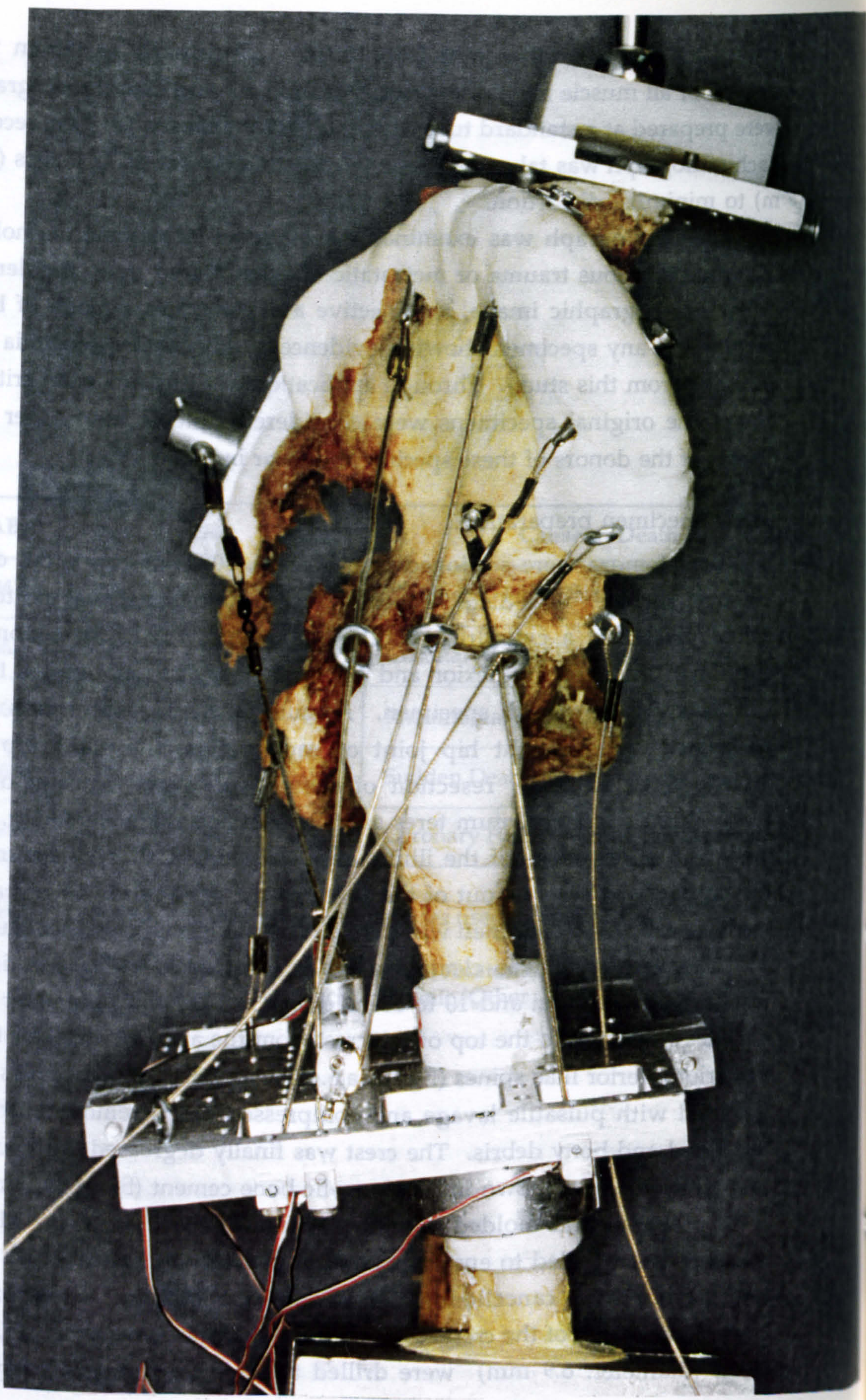

Figure 6.4a Lateral view of a pelvic specimen prior to attachment of the transducers. The loading cables and the most recent version of the instrumented base are clearly visible. Relevant features of the specimen are labeled in the drawing presented in figure 6.4b.

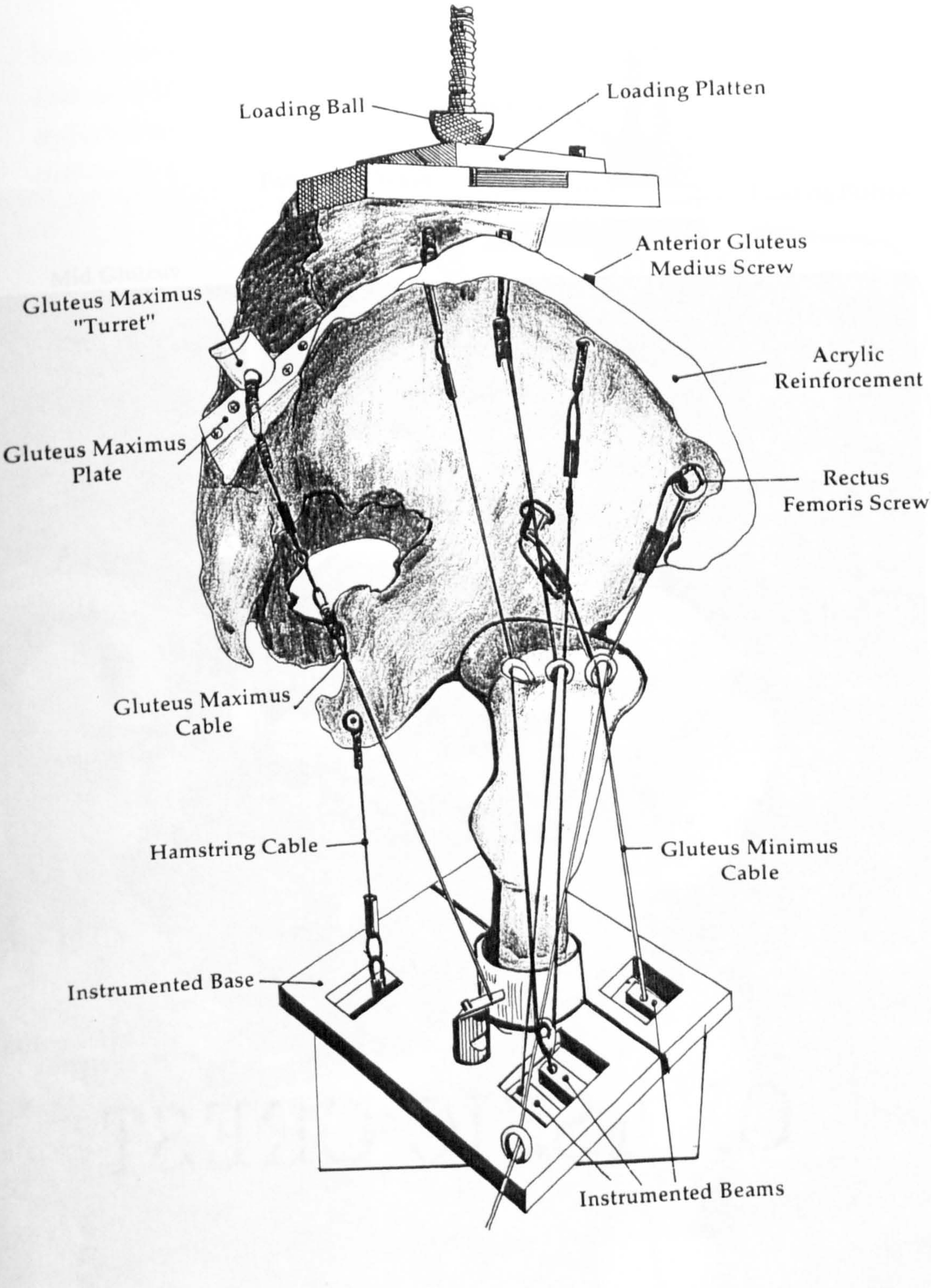
Loading Ball
Loading Platten
Anterior Gluteus Medius Screw
Gluteus Maximus "Turret"
Acrylic Reinforcement
Gluteus Maximus Plate
Rectus Femoris Screw
Gluteus Maximus Cable
Hamstring Cable
Gluteus Minimus Cable
Instrumented Base
Instrumented Beams

Figure 6.4b

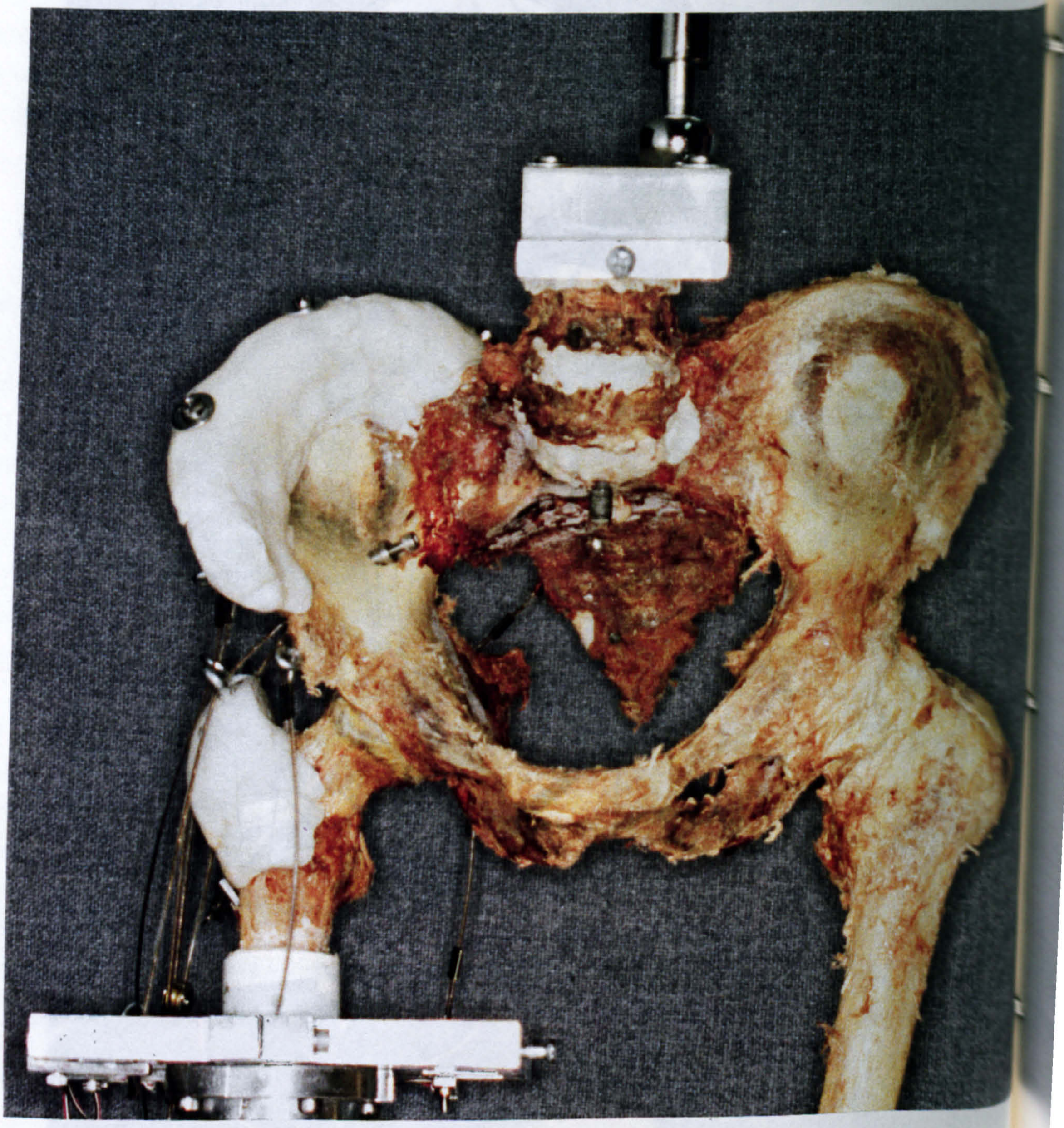

Figure 6.5a AP view of a pelvic specimen prior to attachment of the transducers. Key features are noted in the drawing in figure 6.5b.

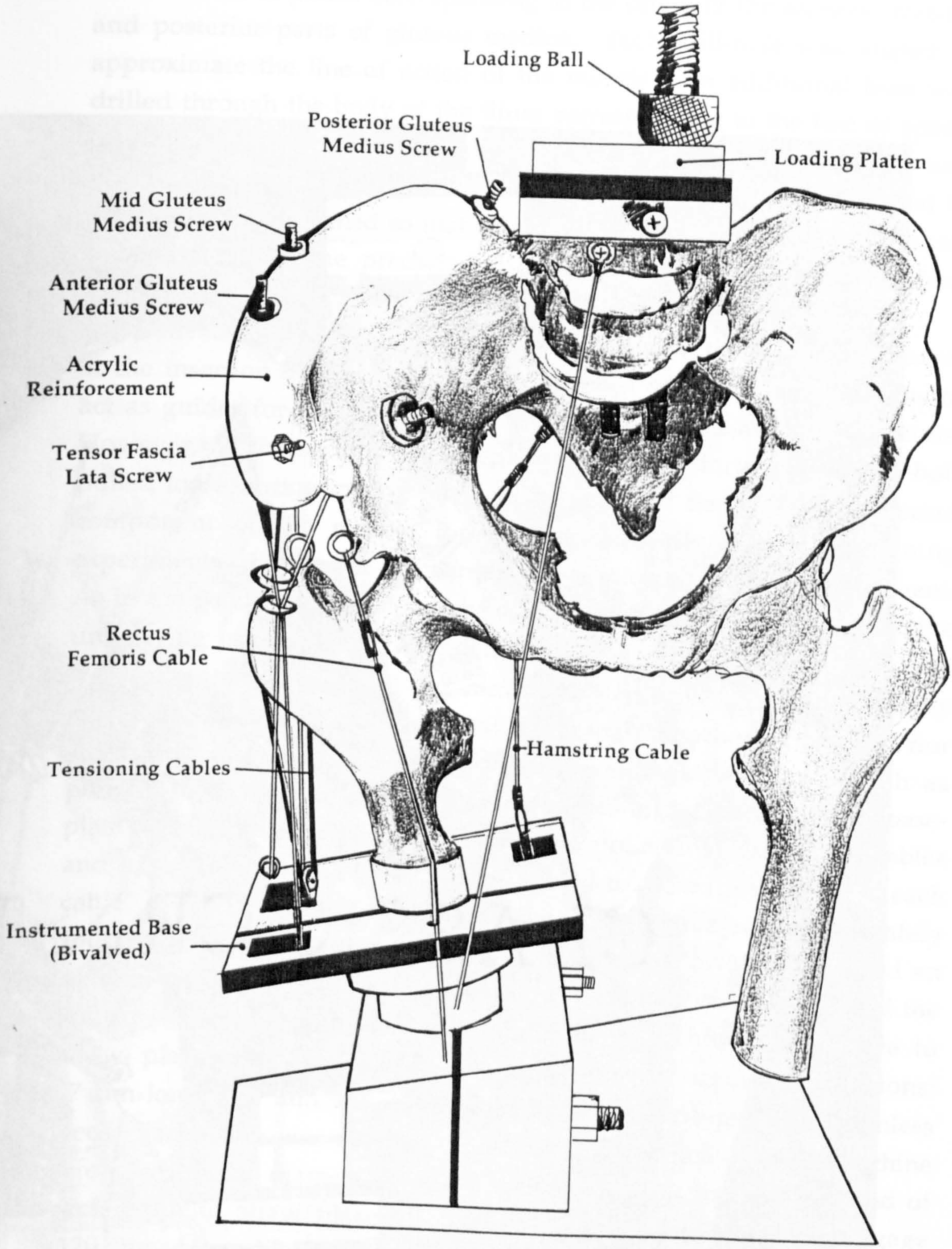
Loading Ball
Posterior Gluteus Medius Screw
Loading Platten
Mid Gluteus Medius Screw
Anterior Gluteus Medius Screw
Acrylic Reinforcement
Tensor Fascia Lata Screw
Rectus Femoris Cable
Hamstring Cable
Tensioning Cables
Instrumented Base (Bivalved)

Figure 6.5b

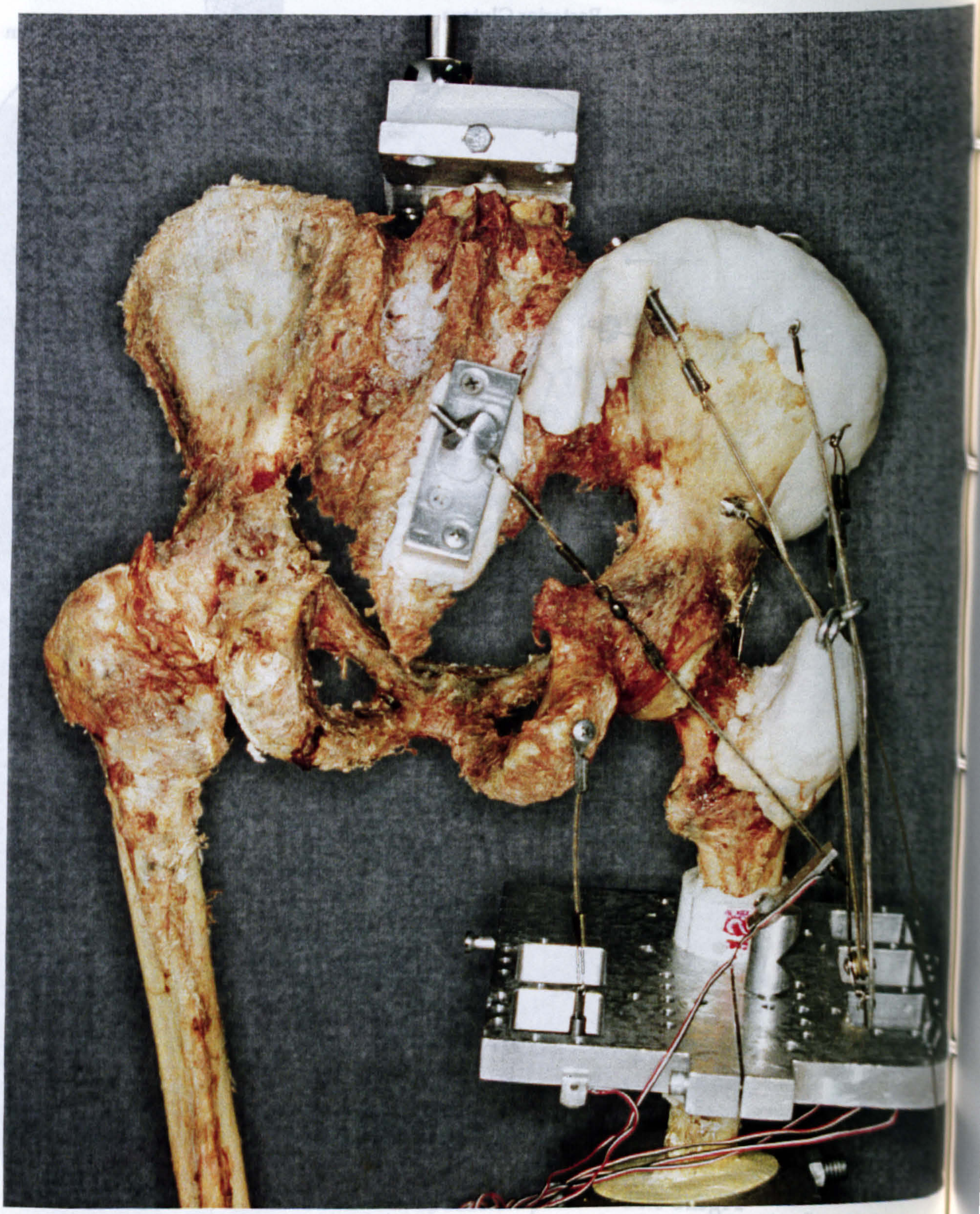

Figure 6.6 Posterior view of a pelvic specimen prior to attachment of the displacement transducers.

bone cement at points corresponding to the origin of the anterior, middle and posterior parts of gluteus medius. Each drill-hole was angled to approximate the line of action of the muscle. An additional hole was drilled through the body of the ilium corresponding to the line of action of gluteus minimus. A specially contoured aluminum bone plate was attached to the sacrum with four screws. A swiveling turret attached to the plate was positioned so that an oblique hole drilled through the turret corresponded to the predicted direction of the mid-third of gluteus maximus.

Threaded eye-bolts were screwed directly into the greater trochanter at the insertion of gluteus minimus and each part of gluteus medius to act as guides for cables that were subsequently used to load the pelvis. However, in the second specimen the most anteriorly placed eye-bolt pulled loose during testing through the action of the anteriorly directed component of the muscle force. Consequently, in the remaining experiments, the greater trochanter was reinforced with acrylic cement. As in the pelvis, the lateral surface of the bone was abraded to expose the underlying cancellous bone and multiple perforations were made into the trochanter with a 1/8" (3.2 mm) diameter drill. A unit of doughy acrylic cement was then forced into the prepared anchoring holes. Prior to setting, the surface of the acrylic cement was made as smooth as possible to minimize friction against the cables under load. A metal base-plate was fabricated to control the orientation of each of the loading cables and to support a series of load cells utilized to measure the load in each cable. The base-plate was clamped onto the femur at approximately 160 mm below the lesser trochanter. The plate was bivalved and had an internal hole of 50 mm diameter to allow it to be positioned around the femur. Three rectangular holes were machined through the plate to allow placement of 5 instrumented, cantilever beams (dimensions: 47 mm long x 10 mm wide x 3 - 5 mm thick), fabricated from stainless steel. Each beam was attached to the rectangular holes with a machine screw. A 3.2mm diameter hole was drilled through the opposite end of each beam to allow placement of a cable. A single, foil strain-gage (120 ohm, Micro-Measurements) was glued to the upper surface of each beam, close to its base and wired to an external strain gage amplifier in a quarter bridge configuration. An activation voltage of 3.00 V was employed in all experiments.

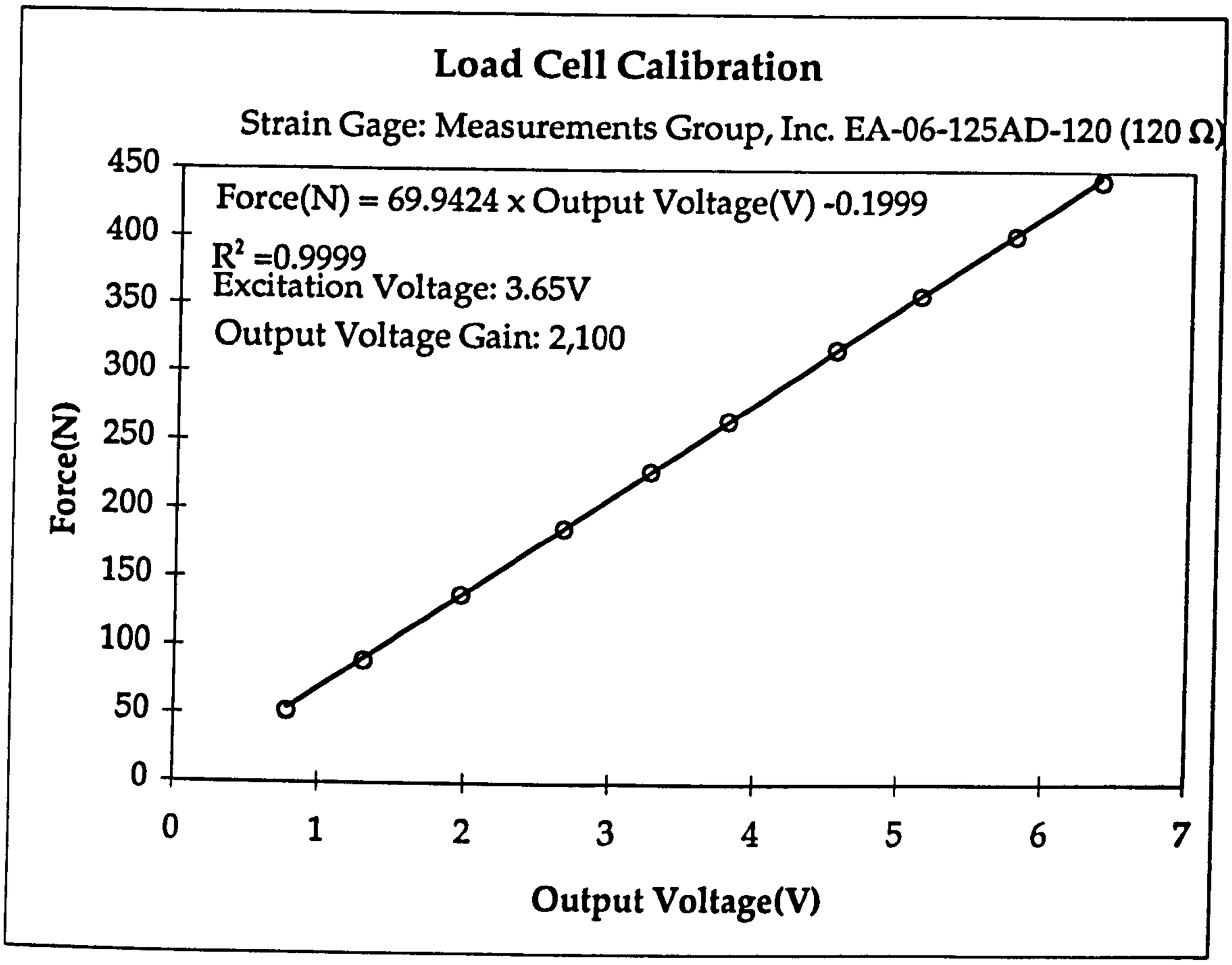

Figure 6.7 Typical load/voltage characteristics curve of one of the instrumented beams during loading and unloading.

All beam transducers were calibrated prior to use and at regular intervals during the course of the experimental studies (fig 6.7). During calibration, each beam transducer was loaded to 125% of its normal operating load. Each strain gage was protected from contamination with blood, fat and other body fluids through application of a layer of silicone rubber or an acrylic based insulating compound. In practice there was minimal change in the output or zero setting of each gage between experiments indicating that these measures were successful.

The vertebral column was transected through the body of L5 at an angle of approximately 40 degrees to ensure that the exposed surface of the vertebra was roughly horizontal once the pelvis was loaded. In the fourth and fifth pelvises, the L5/S1 disc was curetted and replaced with acrylic cement to prevent late collapse of the lumbar spine after repeated loading. An aluminum base-plate was cemented to the upper surface of the transected body of L5 and reinforced with three long bolts which were passed vertically through the body of L5 and the sacrum. Nuts and washers were attached to the end of each bolt and tightened before the acrylic cement polymerized. A nylon block was mounted on the surface of the aluminum plate using two machine screws which were placed medial and lateral to the mid-line of the plate. Longitudinal slots machined into the block allowed it to be moved anteriorly and posteriorly. A spherical depression machined into the block allowed the spinal load to be applied to the specimen in a fixed position using the modular head of a femoral prosthesis (diameter: 32 mm).

The point of application of the vertical load was approximately 200 mm superior to the hip joint center and 20 mm contralateral to the midline, close to the calculated position of the center of the gravity of the supported body as calculated by Maquet (1985) using the data of Braune and Fischer. The anterior/posterior location of the applied spinal load was close to the anterior border of the L4/5 disc space approximately 50 mm in front of the hip joint center. The exact position of anterior-posterior load application varied slightly with the geometry of each pelvis and was fine-tuned according to the degree of pelvic flexion obtained once the spinal load and all predicted muscle loads were applied.

6.3.1.3 Simulation of muscle forces

Muscle loading was simulated with braided, nylon-coated cables

Muscle Cable	Force
Gluteus Maximus	244 N (55 lb)
Gluteus Medius	
Anterior Third	312 N (71 lb)
Middle Third	156 N (35 lb)
Posterior Third	312 N (71 lb)
Gluteus Minimus	390 N (88 lb)
Hamstrings	225 N (51 lb)
Rectus Femoris	70 N (16 lb)
Tensor Fascia Lata	136 N (31 lb)

Table 6.3 Forces developed by tensioning each of the muscle cables.

(Sevenstrand Tackle Corp., Long Beach, CA, USA) attached to the pelvis. Separate cables were used to represent the anterior, middle and posterior parts of gluteus medius, gluteus minimus and gluteus maximus. A single cable was attached to the ischium to simulate the combined action of the hamstrings (semitendinosus, semimembranosus and biceps femoris). The target loads for each muscle are presented in Table 6.3. As the anterior and posterior parts of gluteus medius were assumed to develop equal forces, and share a similar insertion on the greater trochanter, the origins of both parts of the muscle on the ilium were joined with a single cable which passed through a pulley attached to a single load cell. Each cable was attached to its respective load cell with commercial cable crimps. Whenever possible, swivels were attached to each cable immediately above its connection with the load cell to allow the cable to be tensioned without twisting. The bending of each cable at its point of insertion on the femur was minimized through appropriate placement of the load cell within the base-plate. However, in order to keep the size of the base-plate within reasonable limits, it was necessary for the cable simulating gluteus minimus to bend sharply over the greater trochanter. To minimize any loss of tension due to friction, the change in direction of the cable was distributed over a large arc with a contoured, stainless-steel tube (external diameter: 6 mm) which served as a conduit. The cable was sheathed in teflon shrink-fit tubing to facilitate sliding.

Special devices were fabricated to allow each muscle cable to be tensioned to a predetermined load (Fig. 6.8). Stainless steel bolts (10-32UNF) were machined to a length of 50 mm. A cross slot was cut into one end of the bolt so that it could be turned with a screw driver. At the opposite end, a small hole (diameter: 1/16" (1.6 mm)) was drilled through the bolt to allow the braided cables to be looped through and fixed with a steel crimp. The threaded bolt was then screwed into a stainless steel sleeve with an external flange at its upper end. Steel washers (1" (25 mm) x 1/4" (6.4 mm)) cemented over the top of each through-hole within the iliac crest allowed the sleeve to be placed in each hole without damage to the bone during loading. Two parallel flats machined into the flange of the sleeve allowed it to be rotated with respect to the threaded bolt using a wrench and a screw driver. This shortened the cable thereby increasing its tension. During each experiment, this method of tensioning the cables worked adequately once each new cable and its crimps had been loaded

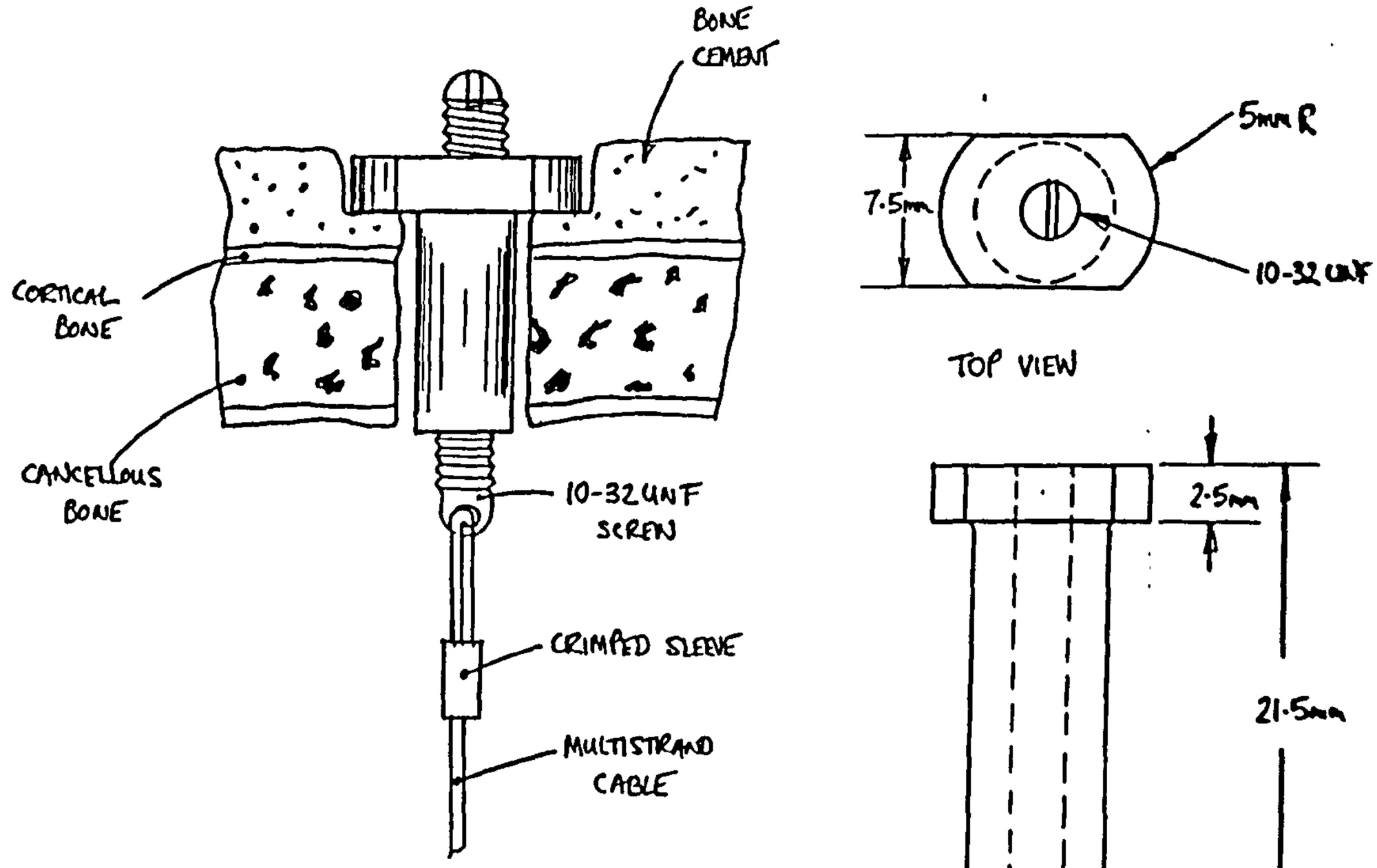

CUT-AWAY VIEW IN ILIUM

Figure 6.8 Diagrammatic representation of the cable tensioning screw and sleeve.

several times to remove the effects of permanent stretching and some slippage. However failure of the crimps was relatively common and was manifested by a long-term drift in the preset load. Most of the time, the preset load in each cable could be maintained for 10 to 15 minutes without more than a 10% loss of tension. However, this method of loading had several inherent deficiencies:

(i) the load present in each cable was directly related to the elongation of the cable under load. As the cables were relatively stiff, small changes in the length of any cable due to creep of the bone, slip of a crimp or some minor variation in the position of the pelvis would lead to significant loss of tension and disruption of all preset muscle forces.

(ii) As the cables ran in relatively similar directions, especially in the coronal plane, the tension within all cables was interdependent. This was particularly true of the hamstrings, gluteus maximus and gluteus minimus. It was also true of all of the cables simulating the glutei. Thus, alteration of the tension in each cable to reach five preset loads was a timeconsuming, iterative process which had to be performed each time the pelvis was unloaded and then reloaded.

(iii) As all significant cables were terminated in load cells mounted on to the bivalved base-plate, the forces and bending moments sustained by the base- plate were quite considerable. In the second experiment (SAB# 26679), this caused the two segments of the base-plate to angulate under load. This led to loss of tension within the cables and ultimately made it impossible to apply the target muscle loads to the pelvis. This problem was overcome by applying a heavy-duty stainless steel hose clamp to the cylindrical tube attached to the bottom of the base-plate and by joining the base-plate to the large base of the mounting fixture with a cable which was tensioned before loading the pelvis.

Because of these difficulties, a new loading apparatus was developed consisting of a bank of five pneumatic cylinders, each with a pressure regulator which allowed a constant load to be developed by each cylinder, ranging from 156 to 632 N (35 to 142 lbf) over a stroke length of up to 6 inches (152 mm). This method of loading will be utilized in future experiments performed to study the effect of femoral rotation and hip

joint anteversion on acetabular deformation.

Each cable was tensioned to the loads calculated in the earlier analysis of the muscle forces acting in early stance phase (Table 6.3). The forces developed by rectus femoris and tensor fascia lata were applied with cables attached to fixed weights of 84 N (19 lb) in view of their relatively small magnitude. The muscle forces were balanced with a spinal load of 770 N (175 lb), applied via a ball plunger to the sliding plate attached to the vertebral column. This load was selected to simulate the sum of the weight of the body supported by the weight-bearing hip (0.83 BW) and the inertial force generated by its acceleration (0.20 BW).

Muscle forces stabilizing the trunk were not included in the model as preliminary experiments showed that the position of the pelvis could be maintained without application of additional forces provided that the femur was prevented from rotating upon application of the spinal load. All experiments were performed within a dead-weight loading frame consisting of four upright supports, spaced so that an anatomic specimen could be placed within the frame with ease. Sufficient room was also allowed to enable a specialized radiographic box to be placed within the frame without contact between the box and either the specimen or the upright supports. This box had been previously developed in our laboratory to allow radiographic cassettes to be mounted orthogonally for measurement of displacement of biologic specimens using biplanar radiography (Kamaric et al, 1991).

A central threaded rod was mounted in an axial position within the center of the loading frame to provide axial loading of the pelvic specimen. Dead weights (25 lb (110 N)) were placed on a mounting bracket attached to the rod which was suspended, in turn, from a bar which traversed the top of the frame. By turning a threaded sleeve on the upper surface of the bar the weights were raised or lowered thereby loading the specimen within the space below. By using this method of loading, the maximum deformation of the specimen was limited, should a sudden loss of resistance occur due to fracture of the specimen or slippage of a muscle cable. The modular head of a femoral prosthesis (32 mm diameter) was attached to the lower end of the threaded rod to allow loading of each specimen via the nylon loading block mounted on the vertebral column. All experiments were performed with the hip joint maintained in 25 degrees of flexion, 9 degrees of adduction and 2 degrees

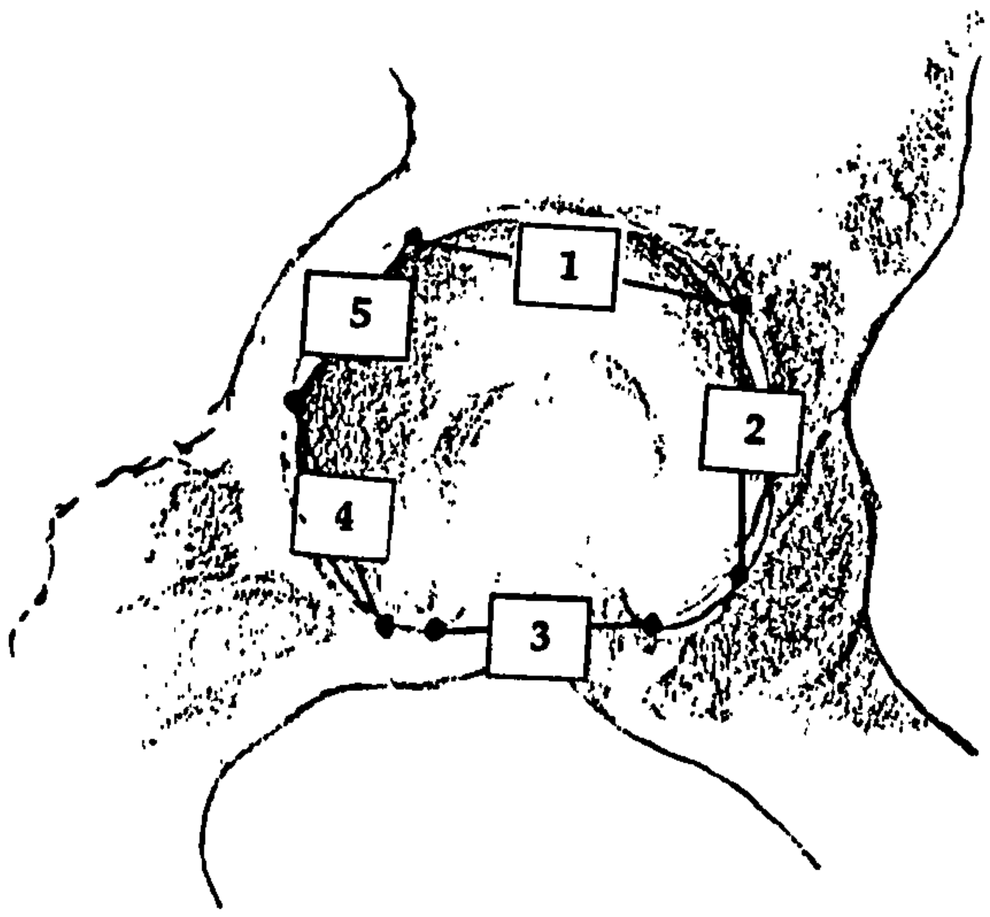

Lateral

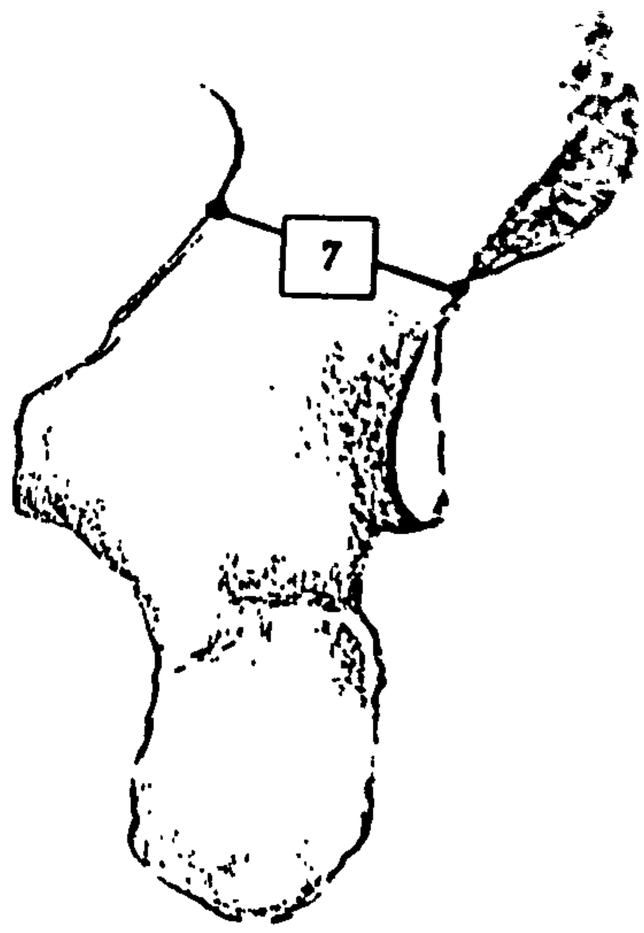

Posterior

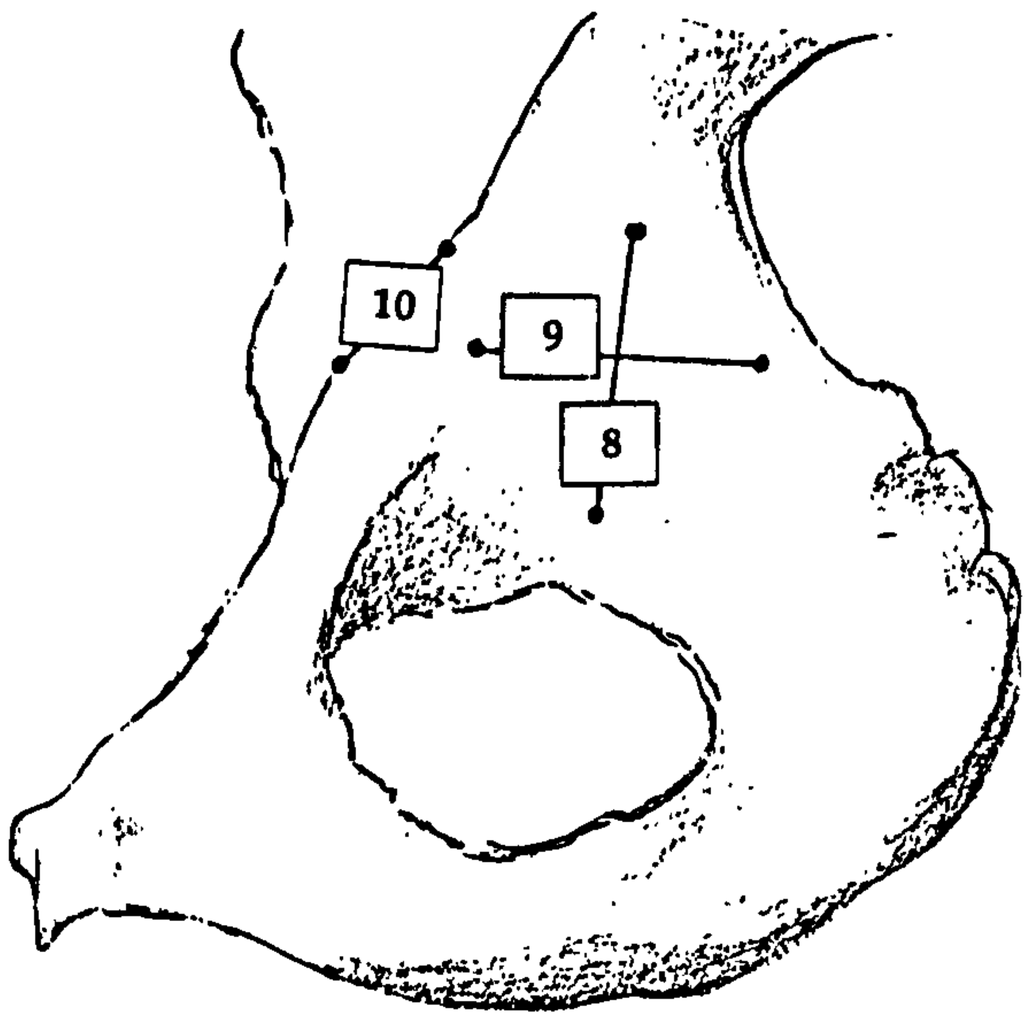

Medial

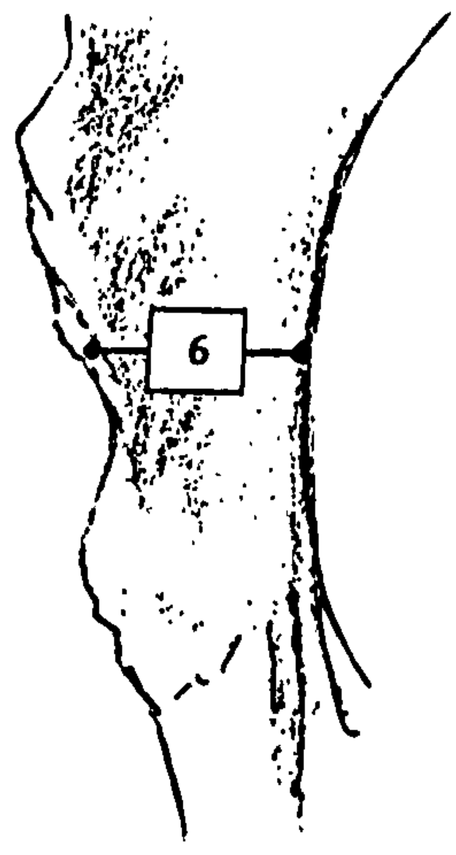

Anterior

Figure 6.9 Anatomic sites for placement of pins in the pelvis to allow measurement of bony deformation.

of internal rotation. Within the loading frame, the specimen was positioned in 10 degrees of forward flexion to allow the vertical load to act in the predicted direction of the resultant of the static and inertial components of body weight. As a result, the femur was inclined at 15 degrees with respect to the vertical, leading to a hip flexion angle of 25 degrees.

Early experiments demonstrated that the simplest way to achieve the desired combination of muscle forces and hip joint position simultaneously was to hold the pelvis and femur in their ultimate position prior to application of the spinal load. For this purpose, secondary cables were passed from the pelvis to the loading frame. Turnbuckles attached to these cables allowed the orientation of each specimen to be fine-tuned prior to loading. The spinal load was gradually applied in increments and each cable was tensioned to a corresponding proportion of its ultimate load. Once the full spinal load was applied and each of the primary muscle cables had been fully tensioned, the secondary cables were removed and the primary cables were adjusted.

6.3.1.4 Measurement of specimen deformation

The deformation of the acetabulum was measured with displacement transducers which monitored the distance between the pairs of steel pins (diameter: 1.9 mm) attached to the pelvis at key locations (Fig. 6.9). In order to measure acetabular deformation to an accuracy of 2μm or less it was imperative that there be no relative motion between the pin and the bone. Preliminary experiments with smooth pins of smaller diameter and with methods of directly bonding brackets and fixtures to the outer surface of the pelvis were unsuccessful, primarily because the bond of commercial adhesive to the bone was unreliable. Frequently, bonds formed between a layer of adhesive and the cortical shell would separate after the pelvis had been repetitively loaded as blood and fat oozed from the specimen.

The most reliable results were obtained using custom-made pins, fabricated from steel pop-rivets consisting of a central pin (1.9 x 40 mm) and a flanged sleeve (7 x 3.2 mm, flange diameter: 6.3 mm). As a first step, the sleeve was removed from the pin and the two components were degreased with acetone and coated with a cyanoacrylate catalyst (Micro-Measurements, Inc.). After air drying, the rivet was reassembled and the

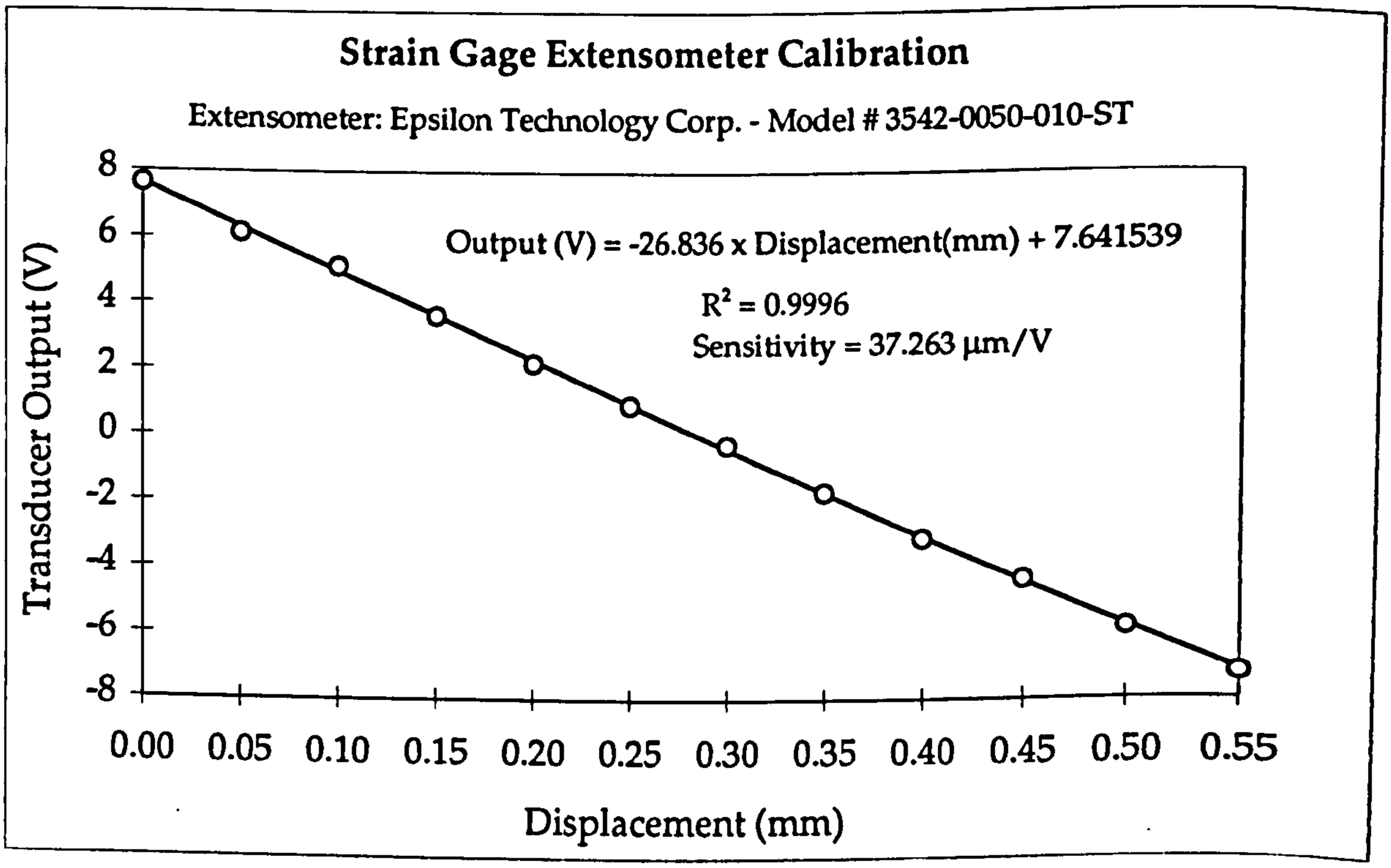

Figure 6.10 Typical calibration curve of one of the strain gauge extensometers used in this experiment.

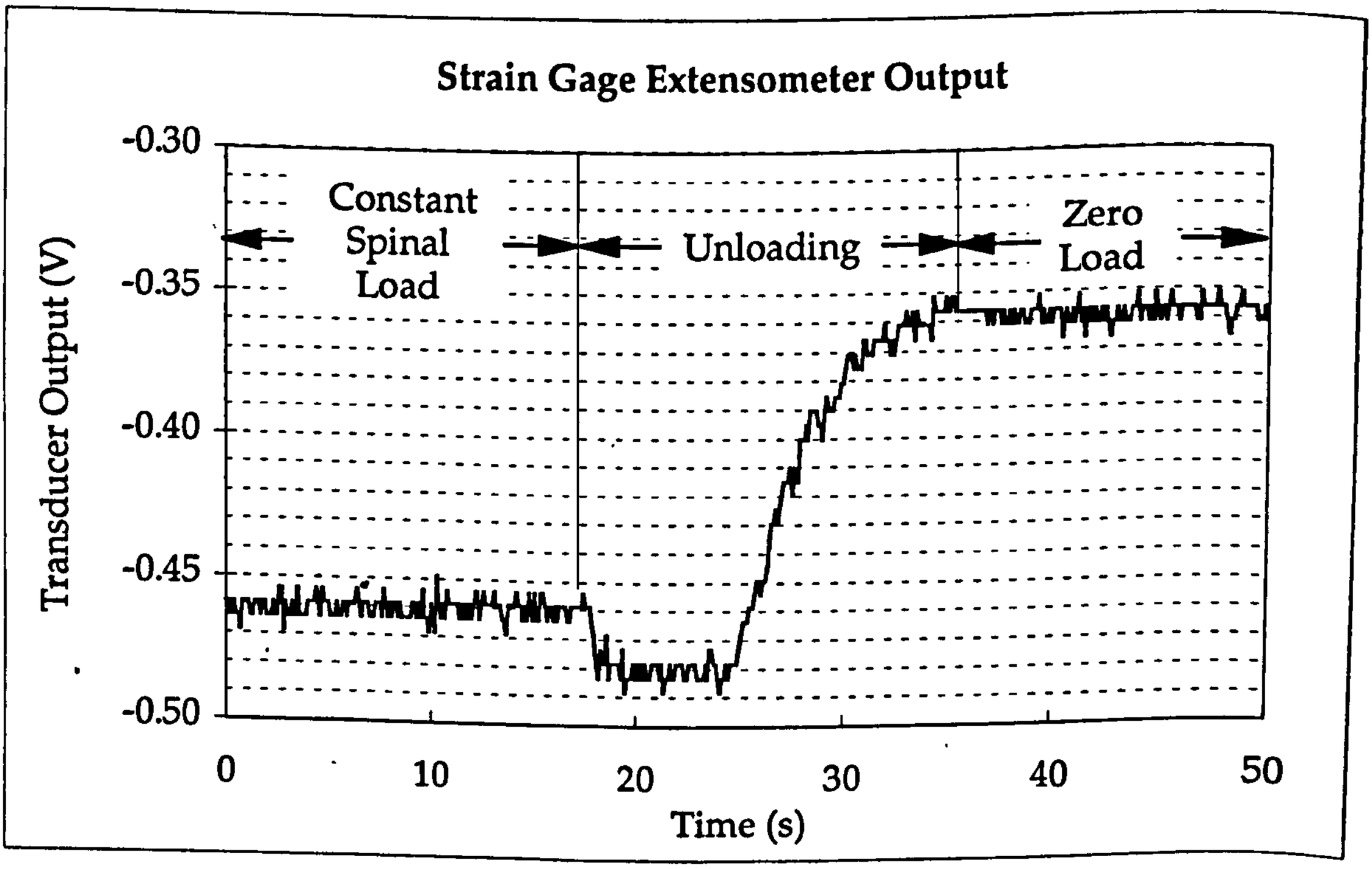

Figure 6.11 Typical output of a strain gauge extensometer under load and after removal of the spinal load. All data collected during this periods were average to allow the change in output to be calculated and converted into the change in pin separation.

sleeve was crimped onto the pin with a commercial crimping tool. Cyanoacrylate adhesive was infused into the junction between the sleeve and the pin and left to polymerize. This step was necessary as often the crimped sleeves could be rotated slightly around the central pin, although gross motion was eliminated. Once the adhesive had polymerized, four longitudinal flats were ground at 90 degree intervals on the surface of the sleeve to prevent loosening in rotation during manipulation of the displacement transducers.

The attachment of each pin to the pelvis proved challenging due to the presence of blood and fat and cancellous bone of variable quality beneath the thin cortical shell of the pelvis. Holes of approximately 4mm diameter and 7mm in depth were drilled through the outer cortex using a high speed motorized drill. Standard anatomic sites were selected for pin placement, including locations around the acetabular margin, at the anterior and posterior facets, along the pectineal line, at the medial and lateral borders of the outer walls of the acetabulum and at four sites on the dorsal surface of the ischium, immediately behind the acetabulum. Each hole was irrigated with pulsatile lavage and dried with compressed air prior to cementing. Further cleaning was performed with cotton-tipped rods soaked with acetone. The cortical surface surrounding each hole was abraded and coated with cyanoacrylate catalyst and adhesive which was left to polymerize. A small quantity of low viscosity acrylic cement was prepared and injected into each hole. Additional cement was applied to the sleeve on the pin which was then inserted into the hole and held in place until the cement had set. The pin was carefully loaded to ensure that there was no relative motion with respect to the bone or the acrylic cement.

Two types of transducers were used to monitor the separation of each pair of pins during loading. Initially, all measurements were performed with high accuracy strain gage extensometers (MTS Corp., Minneapolis, Minnesota) with a resolution of approximately 0.2 μm and an accuracy of better than 1 μm. Each extensometer was calibrated at regular intervals using a special fixture mounted on a mechanical testing machine (MTS) (figs 6.10, 6.11). Each extensometer was attached to the metal pins with special extension arms, fabricated to allow each leg of the extensometer to reach a pin without interference from the loading cables. Initial trials were performed with each leg of the extensometer rigidly

attached to a steel pin to minimize artifacts caused by relative motion between the pin and the knife edges attached to each arm. However, this led to errors in the readings because of the constraints placed upon the normal motion of the extensometer. Moreover, using this configuration, the response of the extensometer varied according to the relative orientation of the fixed and free legs with respect to both pins.

In view of these difficulties, all subsequent experiments were performed with knife edges fabricated from high strength blue steel shim stock and fixed to brass mounting brackets. Each knife edge was loaded against the surface with elastic bands. The body of each extensometer was supported using an external frame to avoid artifacts caused by moments generated about each measurement pin by the weight of the extensometer. Though this proved to be a workable solution, the following problems arose:

(i) It was impossible to avoid some motion of the body of the extensometer during loading of the specimen due to the deflection of the pelvis under load. At some sites this caused slippage between the knife edges and the pins.

(ii) The size of the extensometers limited their placement on the pelvis. This meant that no more than three measurement sites could be monitored simultaneously. Moreover, it was extremely difficult to attach the extensometers to some pins due to the close proximity of some of the loading cables or the presence of the femur.

(iii) To perform satisfactorily, the knife edges had to be placed perpendicular to the axis of the pin. Consequently for the extensometer to measure the relative movement of any two pins, the pins had to be as close to parallel as possible. At measurement sites located around the rim of the acetabulum this meant that each pin had to be bent into an 'L' shape to avoid impingement with the femoral head. Consequently, two separate pins had to be placed at some measurement sites, one parallel to a pin on each side (ie. one pin could not be used for two different measurements). This made pin placement and alignment increasingly complicated and prolonged the preparation time of each pelvis, which, in turn, limited the number of measurements that could be taken before biological

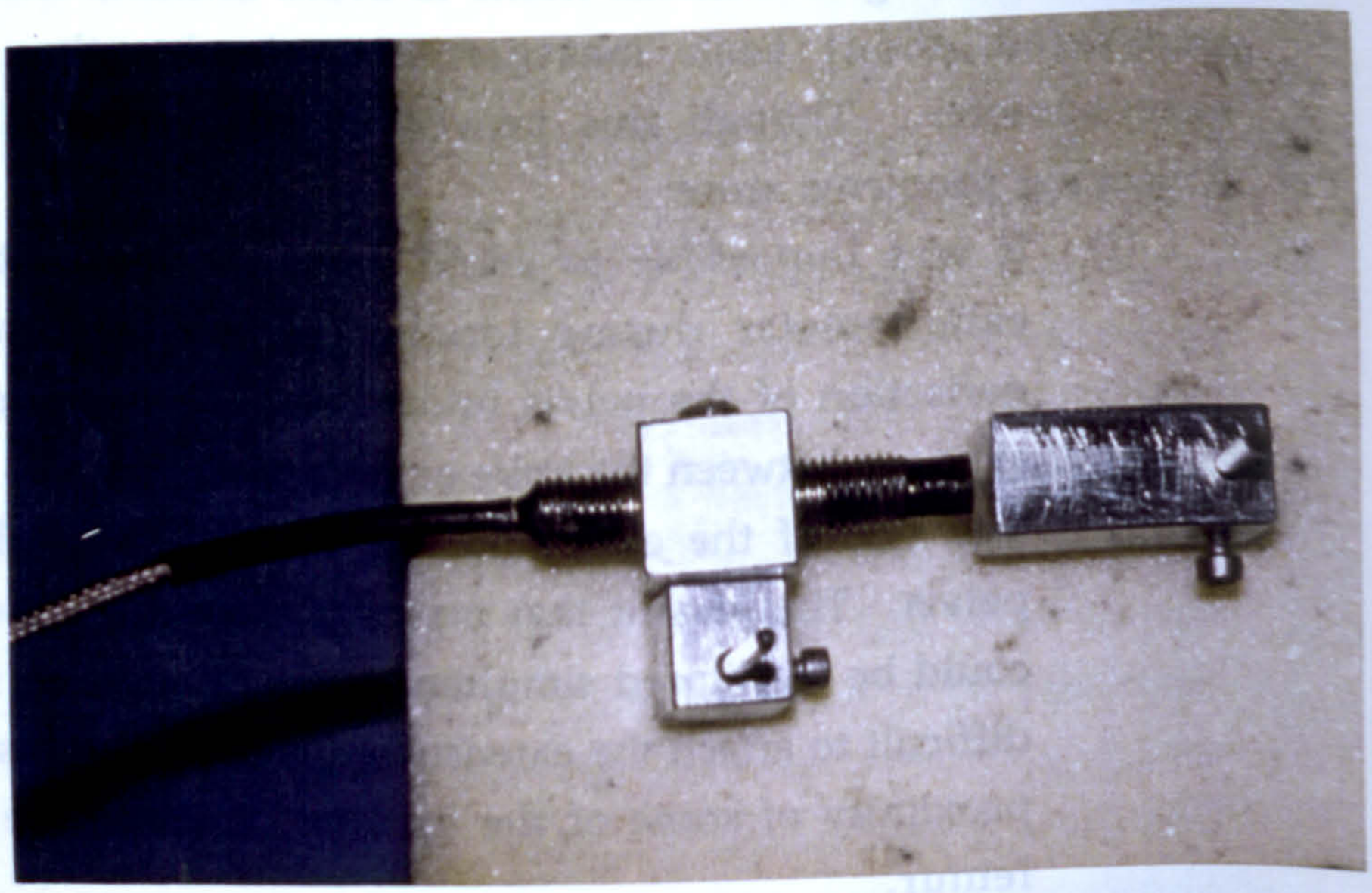

Figure 6.12 Typical mounting configuration of an eddy probe transducer and an inductive metal target.

deterioration of the fresh specimen rendered it unusable.

Initially, these obstacles were partly surmounted by rigidly attaching the fixed leg of the extensometer to one pin and allowing one knife edge to be positioned against the second pin. While this made the measurement easier to perform and more reproducible, it also introduced low frequency noise into the output of the extensometer which meant that the signal from the transducer could not be read directly from the digital voltmeter connected to the strain gage amplifier. To allow the signal to be averaged, it was stored in digital form using a data acquisition system (Data Translation) with 12 bit resolution equivalent to ± 5mV. All data were sampled at a frequency of 100 Hz for 70 seconds and averaged using spreadsheet software (Microsoft Excel).

Because of difficulties in the measurement of pin displacement around the mouth of the acetabulum, the strain gage extensometers were replaced with eddy current transducers which were selected because of their size (typically 5 mm diameter x 15 to 20 mm length) and their ability to measure the proximity of metal surface without contact (fig 6.12). Eddy current transducers consist of a miniature coil encapsulated in a polymer within a threaded stainless steel bearing. Wires attached to the coil deliver a constant current at a frequency of approximately 1.6 MHz. If a metal target is brought into the vicinity of the coil, the disturbance to the electric field causes the voltage needed to maintain a constant current to drop. The change in voltage is a function of the electrical properties of the target and its distance from the tip of the probe. Generally, the closer the target to the probe, the greater the sensitivity of the output to the proximity of the target. Typically, the oscillator/demodulator circuit driving the probes is connected to a linearizing circuit which produces a linear voltage response to changes in the separation of the probe and the target typically with a sensitivity with approximately 10 mV/mm at a supply voltage of 24 V (figs 6.13, 6.14).

Special brackets were fabricated to attach the eddy probes to the measurement pins. Each bracket consisted of two aluminum cubes measuring 10 mm per side. A 5 mm diameter hole was drilled through one cube for attachment of the eddy probe with a set screw. Similarly, a 2 mm diameter hole was drilled through the second cube to allow it to be attached to the pin with another set screw. Both cubes were connected with a machine screw which allowed the orientation of the probe to be

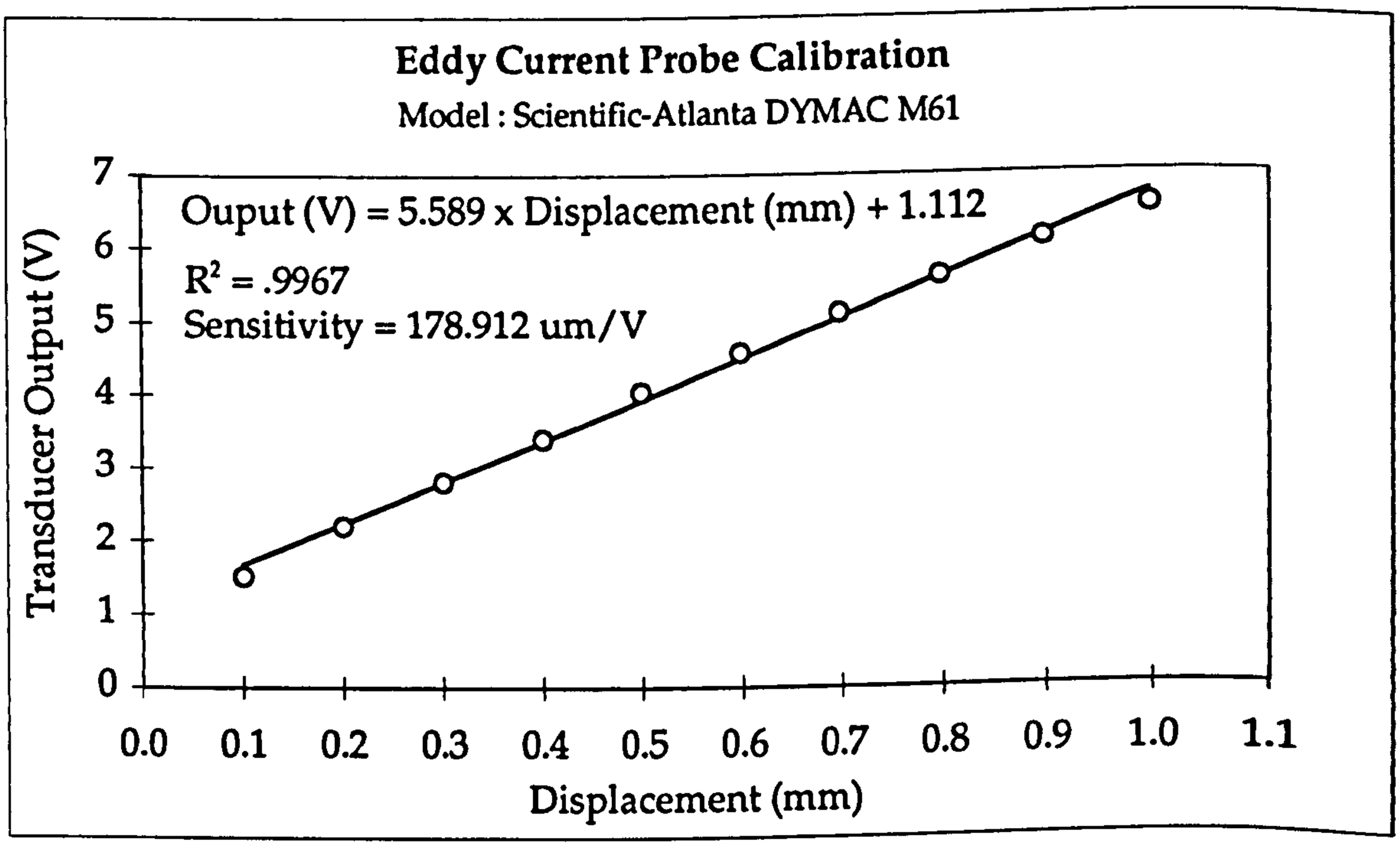

Figure 6.13 Typical calibration curve of one of the eddy probe transducers used in this experiment.

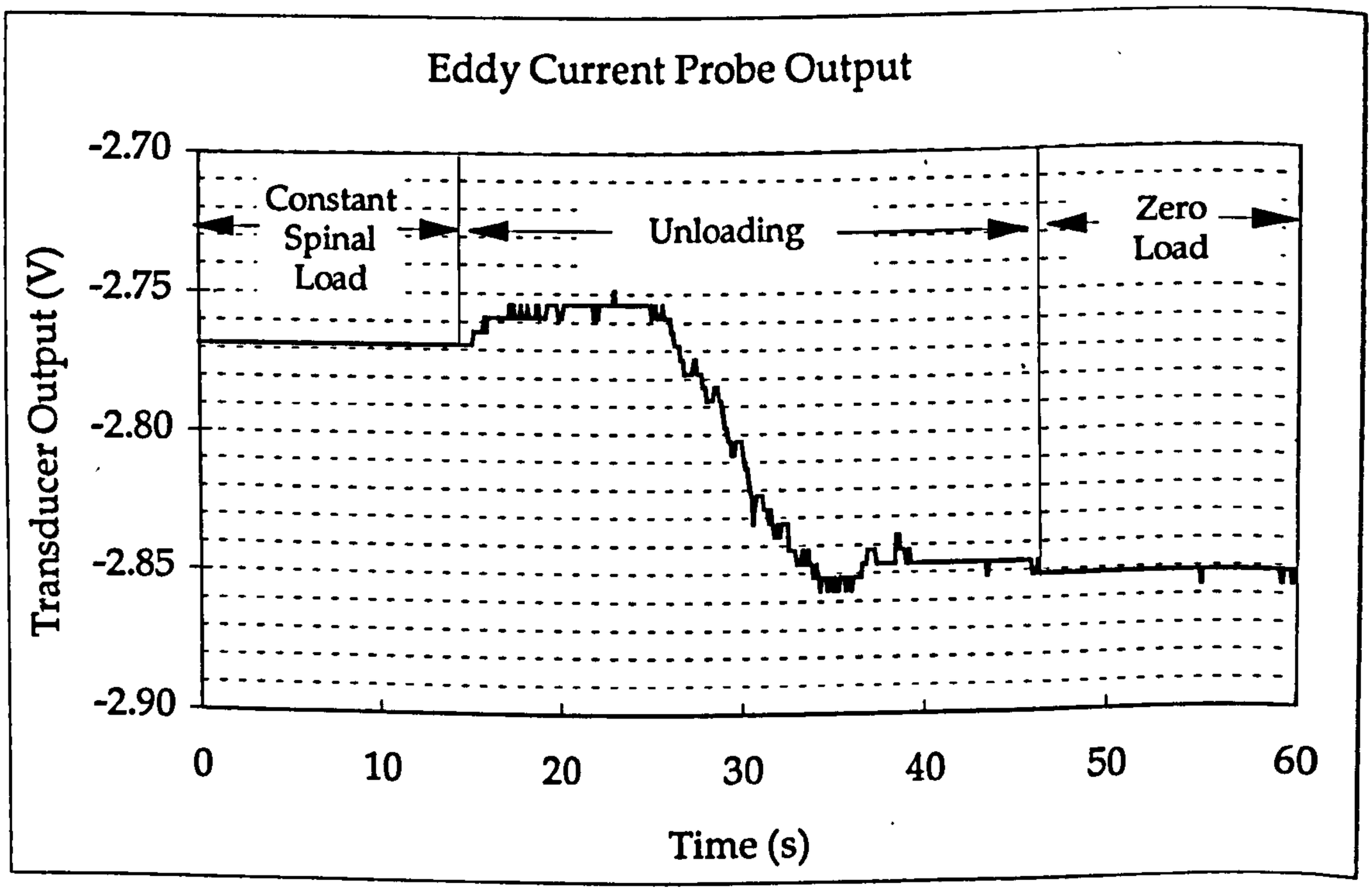

Figure 6.14 Typical output of an eddy probe transducer under load and after removal of the spinal load.

altered with respect to the pins. A similar configuration of aluminum cubes was used to make a target that could be rigidly attached to a second pin. The articulation of both the probe holding bracket and the target allowed the probe to be aligned perpendicular to the surface of the target, regardless of the relative orientation of any two pins.

Each probe was calibrated using an electronic caliper with a special attachment fixture to hold the probe and the target. The calibration procedure was performed prior to testing each new specimen. The deformation of the second and third pelvises was measured using both extensometers and eddy current transducers which allowed up to five measurement sites to be instrumented simultaneously. With the fourth pelvis, only one extensometer was used because of the greater convenience of the eddy probe devices.

6.3.2 Results

Average values for the deformation of four fresh pelvic specimens ranged from 3.1 ± 11.7 μm across the cotyloid facets to -58.1 ± 13.2 μm across the mouth of the acetabulum. The length of the acetabulum also decreased with loading by -24.6 ± 7.6 μm on the posterior side and 53.1 ± 18.7μm on the anterior side. Values for the average deformation of each pelvis measured at each of the recording sites are reported in Table 6.4. The actual values for the change in transducer output and the corresponding deformation recorded from each cycle of loading and unloading have been included on the computer disc in Appendix 6.1. To aid in comparison of values recorded in different specimens with different acetabular dimensions, the experimental data describing the change in separation of the pins spanning the measurement site were normalized with respect to the initial separation of the pins (typically 30-60 mm). For convenience, these data are referred to as "equivalent strains", expressed in units of microstrain (Table 6.5).

6.4 DISCUSSION

Under the loads simulating the early stance phase of walking, the pelvis and acetabulum underwent a complex pattern of deformation due to the interaction of (i) the direction of loading with respect to the principal planes of stiffness of the pelvis, (ii) the local effects of conformity between the femoral head and the socket, and (iii) the irregular, discontinuous geometry of the pelvis in the vicinity of the

Deformation (μm)									
Transducer Site	Specimen								
	23470		26679		26662		26687		Average
1. Ilium	-3.9 ± 1.1	(5)	-12.5 ± 0.6	(8)	-51.5 ± 1.1	(6)	-37.5 ± 0.4	(8)	-26.4 ± 11.0
2. Anterior Wall Length	-52.5 ± 1.4	(10)	-52.0 ± 4.0	(11)	-83.3 ± 1.4	(6)	-41.0 ± 1.0	(12)	-57.2 ± 9.1
3. Trans Facets	-1.7 ± 1.0	(17)	-7.5 ± 1.0	(10)	-36.4 ± 1.6	(9)	-18.2 ± 0.5	(9)	-16.0 ± 7.6
4. Posterior Wall Length	-22.3 ± 0.4	(9)	-17.9 ± 1.2	(5)	-46.6 ± 1.4	(6)	-14.3 ± 0.5	(6)	-25.3 ± 7.3
5. Roof	-22.3 ± 1.2	(8)	-56.4 ± 1.9	(8)	-29.1 ± 0.4	(7)	-22.9 ± 0.4	(8)	-32.7 ± 8.1
6. Anterior Wall Depth	17.6 ± 1.6	(5)	5.6 ± 0.2	(10)	12.8 ± 0.6	(9)	11.7 ± 0.3	(10)	11.9 ± 2.5
7. Posterior Wall Depth	4.8 ± 0.2	(7)	4.0 ± 0.3	(8)	4.1 ± 0.4	(9)	4.8 ± 0.2	(7)	4.4 ± 0.2
8. Medial Wall (Vertical)	16.5 ± 0.7	(6)	20.0 ± 0.5	(4)	1.1 ± 0.7	(9)	32.2 ± 0.3	(6)	17.5 ± 6.4
9. Medial Wall (Horizontal)	10.1 ± 1.5	(10)	13.2 ± 0.5	(6)	10.2 ± 0.4	(9)	15.1 ± 0.7	(8)	12.2 ± 1.2
10. Pectineal Line	34.6 ± 1.7	(3)	21.8 ± 0.6	(8)	46.2 ± 0.7	(9)	28.2 ± 0.5	(8)	32.7 ± 5.2
11. Width of acetabulum	N/A		-30.1 ± 1.9	(10)	-113.1 ± 1.4	(7)	-61.3 ± 1.1	(6)	-68.2 ± 24.2

Table 6.4 The deformation of the pelvis measured at 11 anatomic sites in the four cadaveric specimens. All values are reported in μm as the mean ± standard error. The number of individual measurements at each site is indicated in parentheses.

Site	Specimen				
	23470	26679	26662	26687	Average
1. Illium (A - B)*	-99 ± 27	-332 ± 16	-1409 ± 30	-1063 ± 10	-726 ± 307
2. Anterior Wall Length (A-I)	-1406 ± 38	-1708 ± 131	-2302 ± 40	-1127 ± 27	-1636 ± 252
3. Facets (F - G)	-40 ± 23	-150 ± 20	-797 ± 34	-395 ± 10	-345 ± 168
4. Posterior Wall Length (C - D)	-714 ± 12	-611 ± 40	-1282 ± 38	-368 ± 14	-744 ± 194
5. Roof (B - C)	-618 ± 32	-1247 ± 43	-799 ± 11	-580 ± 11	-811 ± 153
6. Anterior Wall Depth (P - Q)	440 ± 37	168 ± 6	541 ± 24	519 ± 14	417 ± 86
7. Posterior Wall Depth (N - O)	100 ± 4	111 ± 8	106 ± 10	124 ± 5	110 ± 5
8. Medial Wall (Vertical) (L - M)	421 ± 17	457 ± 11	571 ± 18	740 ± 8	547 ± 72
9. Medial Wall (Horizontal) (J- K)	225 ± 32	276 ± 11	266 ± 10	308 ± 14	269 ± 17
10. Pectineal Line (E - F)	1237 ± 62	1102 ± 32	2248 ± 33	1621 ± 26	1552 ± 257
11. Width of Acetabulum (A - C)	N/A	-436 ± 27	-1978 ± 24	-1048 ± 18	-1154 ± 448

Table 6.5 Average deformation of four fresh pelvic specimens, normalized with respect to the gage length utilized at each of the measurement sites. All data are reported ± standard error, in units of strain ($\times 10^{-6}$).

* Letters in parenthesis correspond to the measurement sites in figure 6.8.

acetabulum.

The surface displacement data indicate that the predominant pattern of deformation was the same in each of the four specimens and consisted of longitudinal bending (i.e. bending about a posterior-anterior axis) of the pelvis over a fulcrum formed by the femoral head. This conclusion is supported by the deformation measurements performed at sites along the anterior and posterior rim of the acetabulum and the dorsal surface of the ischium (ie. the inner wall of the pelvis behind the acetabulum). Loading caused longitudinal shortening of the anterior and posterior walls of the acetabulum by an average of -636 ± 252 and -744 ± 194 microstrain respectively. This was accompanied by elongation of the dorsal surface of the ischium by 547 ± 72 microstrain.

Because of the direction of the muscle forces and the relative narrowness of the anterior rim of the acetabulum in comparison with the posterior rim, the plane of bending appears to have been positioned posteriorly, hence the large value of compressive strain measured along the anterior wall. With loading, the longitudinal shortening of the anterior and posterior walls of the acetabulum was accompanied by elongation in the medial-lateral direction, as expected from simple strain theory. The ratio of the mediolateral and longitudinal measurements was 0.148 for the posterior wall and 0.255 for the anterior wall. The increase in depth of the acetabulum was 4 times larger on the anterior wall than on the posterior wall (417 ± 86 microstrain vs. 110 ± 5 microstrain).

Significant bending of the acetabulum also occurred in the transverse plane, with the anterior and posterior walls gripping the head of the femur and the acetabulum becoming slightly deeper with loading. There was also significant reduction in the width of the acetabulum at the level of the joint center (-1154 ± 448 microstrain), superiorly, over the roof of the acetabulum (-811 ± 153 microstrain), and inferiorly, at the cotyloid notch (-345 ± 168 microstrain). Conversely, the dorsal surface of the ischium behind the acetabulum lengthened in the transverse direction (269 ± 17 microstrain). This demonstrates that the predominant mode of loading was biaxial and not uniaxial bending. If the pelvis were subjected to uniaxial bending, as previous investigators have suggested, the Poisson effect would lead to transverse contraction of approximately 150 microstrain over the inner table, in response to the tensile strains

generated by bending in the coronal plane. In practice, tensile strains (269 ± 17 microstrain) were recorded due to the bending moments generated about the joint center by the components of each of the muscle forces in the transverse plane.

The overall effect of this biaxial deformation mode was circumferential constriction of the rim of the acetabulum (i.e. negative hoop strain). Thus compressive strains, ranging form -320 to -1636 microstrain were recorded at each one of the measurement sites around the peripheral rim, regardless of the orientation of each site with respect to the longitudinal and transverse axes of the pelvis. The largest tensile strains were recorded along the pectineal line, situated in a superomedial direction form the joint center. This was not surprising as the orientation of the pectineal line is fairly close to that of the joint reaction force and hence the principal plane of bending of the pelvis. Moreover, the cortical surface along the pectineal line is the most medially situated with respect to the neutral axis and so is expected to experience the highest fiber stress.

The variability of the deformation measurements may be attributed to two basic factors: differences in consecutive variations in measurements performed at the same site in each specimen and variations between the average values of deformation recorded at the same site for different specimens. In terms of the first source of variation, much of the time devoted to the development of the experimental methods described in this chapter was spent in devising methods of obtaining meaningful reproducible displacement measurements. A perplexing observation of these experiments, was that once a pelvis was mounted in the loading frame and the spinal and muscle loads were applied with the hip joint in the predetermined position, numerous measurements of the displacement of any two implanted pins could be made with very little variation from run to run. However, if a specimen was removed from the loading frame and the transducer assembly was detached from the specimen, changes of up to 50% in the initial values of pin displacement were often observed if the transducer was reattached and the specimen was reloaded at some later time. Despite the change in recorded pin displacement, all sets of measurements were very reproducible within any given series of experiments.

The changes in pin displacement between runs may be ascribed to the following factors:

(i) Loosening of the pins within the bone

(ii) Variations in the distance between the point of attachment of the transducers to the pins and the surface of the bone

(iii) Deterioration of specimens between runs

(iv) Variation in the exact flexion, adduction and internal rotation of the hip joint

(v) The presence of transverse forces and moments due to mechanical constraint between the loading ball and the loading platen mounted on the spine

(vi) Variations in the exact position of the femur and pelvis under zero load

(vii) Hysteresis during unloading of the specimen (i.e. insufficient time to establish a true unloaded datum for the undeformed acetabulum)

(viii) Viscoelastic creep of the specimen under load (ie. insufficient time to establish the terminal deformation of the acetabulum)

Measures were introduced to minimize the effects of each of these sources of error. In practice, each of these factors was found to be important at some stage of testing of the four pelves. However, the most significant causes of variation between runs were deterioration of the specimen over the duration of each experiment and the presence of constraint moments between the specimen and the loading apparatus.

Several measures were adopted to counteract the normal autolytic decay of the fresh specimens. Care was taken to remove all traces of soft tissue, especially muscle, from each pelvis and both femora; after dissection, specimens were soaked in phenol based embalming fluid for 10-15 minutes to kill all surface bacteria. This process was repeated at regular intervals during testing by spraying the pelvis with commercial disinfecting solution.

The deterioration of each pelvis affected the results primarily through progressive subluxation of the sacroiliac joint. With the first two specimens this caused the flexing moment generated by the spinal load to increase during the course of the experiment; this made it impossible to achieve the desired degree of flexion of the hip joint without adjusting the point of application of the spinal load. Earlier attempts to directly immobilize the sacroiliac joint with large lag screws placed in situ proved unsuccessful and were difficult to perform as the lag screws interfered

with the vertical bolts passed down through the spinal column. The sacroiliac joint was also protected against subluxing moment by attaching tensioning cables to the posterior edge of the loading plate attached to the vertebral column. By tightening the cables an extending moment was developed across the sacroiliac joint to counteract the effects of the spinal load.

Constraint forces may have developed during loading of the pelvic specimen because of deformation occurring with reduction of the femoral head within the acetabulum. Thus any small misalignments between the femur, the pelvis and the loading apparatus could cause constraining forces to develop in the transverse plane through the center of the hip joint without causing a change in the angular position of the pelvis with respect to the femur. Theoretically, these effects could be overcome through the use of two sets of two-degree of freedom mountings attached to the base of the specimen and the loading platen on the vertebral column. However, it was expected that this would make the specimen very difficult to balance in order to achieve the same three-dimensional position of the loaded hip joint on a reproducible basis.

One measure which greatly improved the reliability of the experimental measurements was the use of accurate indexing of the position of the mounting platform and the applied load with respect to the specimen. This ensured that precisely the same loading conditions were developed in each experiment. It was interesting to note that as the constraining forces acted in the transverse plane, the deformation measurements that displayed the greatest variability occurred at sites that were very sensitive to the rotational position of the pelvis. These were primarily the separation of the facets and the length of the anterior wall. Conversely, the deformation of the medial wall and the acetabular walls seemed to be relatively immune to the rotational position of the joint and so the deformation measurements were extremely reproducible. Once measures were introduced to counteract each of the sources of variation, the reproducibility of sets of measurements was typically better than 10-20%.

The average deformation of the four specimens was presented in tables 6.4 and 6.5 with the standard error of estimation of each mean. As the variability of the pooled data is up to an order of magnitude larger than the variability of the measurements in each individual specimen, it

is evident that the principal source of variation is related to differences between pelves. Sources of interspecimen variation include:

(i) differences in the morphology of each specimen, and

(ii) variations in the density of the cancellous and cortical bone of each pelvis.

Morphologic variations affect the deformation of the pelvis in several ways. The muscle force calculations of Chapter 4 were based on typical values for the moment arm and line of action of each active muscle. In practice, the same muscle forces were applied at the origin and insertion of each muscle as indicated by bony landmarks identified on each pelvis and femur. Consequently, the moment arm and inclination of each muscle would be different for each specimen, based upon its individual morphology and as a result, the moments generated by each muscle would vary slightly from specimen to specimen. The most significant effect of differences in the dimensions of each specimen would be its effect on the bending stiffness of the acetabulum in the transverse and coronal planes. The applied forces and moments were not scaled according to the dimensions of each pelvis, and yet measurements of the most basic dimensions of each specimen revealed variations of ± 20% which would also translate to differences in bending stiffness.

A further anatomic consideration is the effect of the orientation of the acetabulum with respect to the applied muscle and spinal loads. Radiographic measurements of each pelvis showed that the inclination of the acetabular rim varied in both abduction and anteversion. Although the vertical inclination (abduction of the socket) is expected to have a slight effect on the longitudinal strain values, variations in anteversion are expected to radically alter transverse strains at superior (e.g. ilium and roof) and inferior sites (ie. the facets) as well as the relative deformation of the anterior and posterior walls. This conclusion is supported by the results of Tienturier et al (1983) who reported large changes in the displacement of the acetabular facets with varying degrees of internal and external rotation of the pelvis. These variations are partly mimicked by differences in the inherent anteversion of the acetabulum, despite the constancy of the rotational alignment of the ilium and the ischium with respect to the femur.

The deformation of the pelvis would also vary with the inherent density of the bone as the elastic moduli of cortical and cancellous bone

Site	Deformation (μstrain)		Normalized Deformation*	
	Pelvi	Analogue	Pelvi	Analogue
Anterior Wall Length	-1636 ± 252	-2804 ± 61	-2.42 ± 0.37	-2.14 ± 0.05
Posterior Wall Length	-744 ± 194	-2343 ± 104	-1.10 ± 0.29	-1.79 ± 0.08
Ilium	-726 ± 307	336 ± 15	-1.07 ± 0.45	0.26 ± 0.01
Roof	-811 ± 153	-858 ± 60	-1.20 ± 0.23	-0.65 ± 0.05
Facets	-345 ± 168	1013 ± 66	-0.51 ± 0.25	0.77 ± 0.05
Width of Acetabulum	-1154 ± 448	3836 ± 83	-1.71 ± 0.66	2.93 ± 0.06
Anterior Wall Depth	417 ± 86	-344 ± 11	0.62 ± 0.13	-0.26 ± 0.01
Posterior Wall Depth	110 ± 5	-264 ± 22	0.16 ± 0.01	-0.20 ± 0.02
Medial Wall (Vertical)	547 ± 72	929 ± 7	0.81 ± 0.11	0.71 ± 0.01
Medial Wall (Horizontal)	269 ± 17	-378 ± 19	0.40 ± 0.03	-0.29 ± 0.01
Average**	676 ± 170	1311 ± 45	1.00	1.00

Table 6.6. Average values of deformation recorded at comparable measurement sites in loading experiments involving the fresh cadaveric pelvi and the mechanical analogue.

* Calculated as a multiple of the average deformation recorded at all sites.
** Average of the absolute values of the deformation measurements recorded at all 10 sites.

varies with the second power of their density (Zysset et al, 1994). This is particularly significant in interpreting the results of this study as the age of the donors ranged from 51 to 65 years. Standard radiographs prepared of all four specimens using identical radiographic technique with a set of bone standards of known density demonstrated substantial differences in apparent density due to varying degrees of osteopenia.

Some interesting observations may be made by comparing the deformation data derived from the cadaveric specimens and the mechanical analogue. In terms of the patterns of deformation, this comparison is best performed once the experimental data have been normalized to allow for the inherent differences in the applied load and the stiffness of the natural and polymeric specimens (Table 6.6). Once this is done, some distinct similarities are evident. Both underwent bending in the longitudinal direction over a fulcrum formed by the femoral head. This led to large compressive strains along the anterior and posterior walls of the acetabulum that were of greater magnitude anteriorly then posteriorly. In both cases, compressive stresses were generated in the roof of the acetabulum in the predominant direction of weight-bearing. The bending of the socket also generated tensile strains in a longitudinal direction along the medial wall of the socket that were almost identical in magnitude in both the cadaveric and analogue specimens, once all data were normalized for the average deformation of the specimen.

In contrast to the observations in the longitudinal direction, in the transverse direction the deformation pattern of the analogue was almost exactly opposite that of the cadaveric pelves. At each transverse measurement site, the acetabular analogue widened with loading, especially adjacent to the center of the socket (3836 ± 83 microstrain) and the 'obturator foramen' (1013 ± 66 microstrain). Conversely, cadaveric specimens became narrower with loading due to biaxial bending of the socket. This caused the edges of the acetabulum to draw closer together superior-inferiorly as well as anterior-posteriorly. This pattern of deformation was also reflected in the deformation of the medial wall which elongated longitudinally and transversely in the cadaveric pelves through biaxial stretching over the head of the femur. In the analogue, uniaxial stretching occurred and so the medial wall contracted transversely and elongated longitudinally. The Poisson effect was also in evidence along the anterior and posterior walls which shortened with

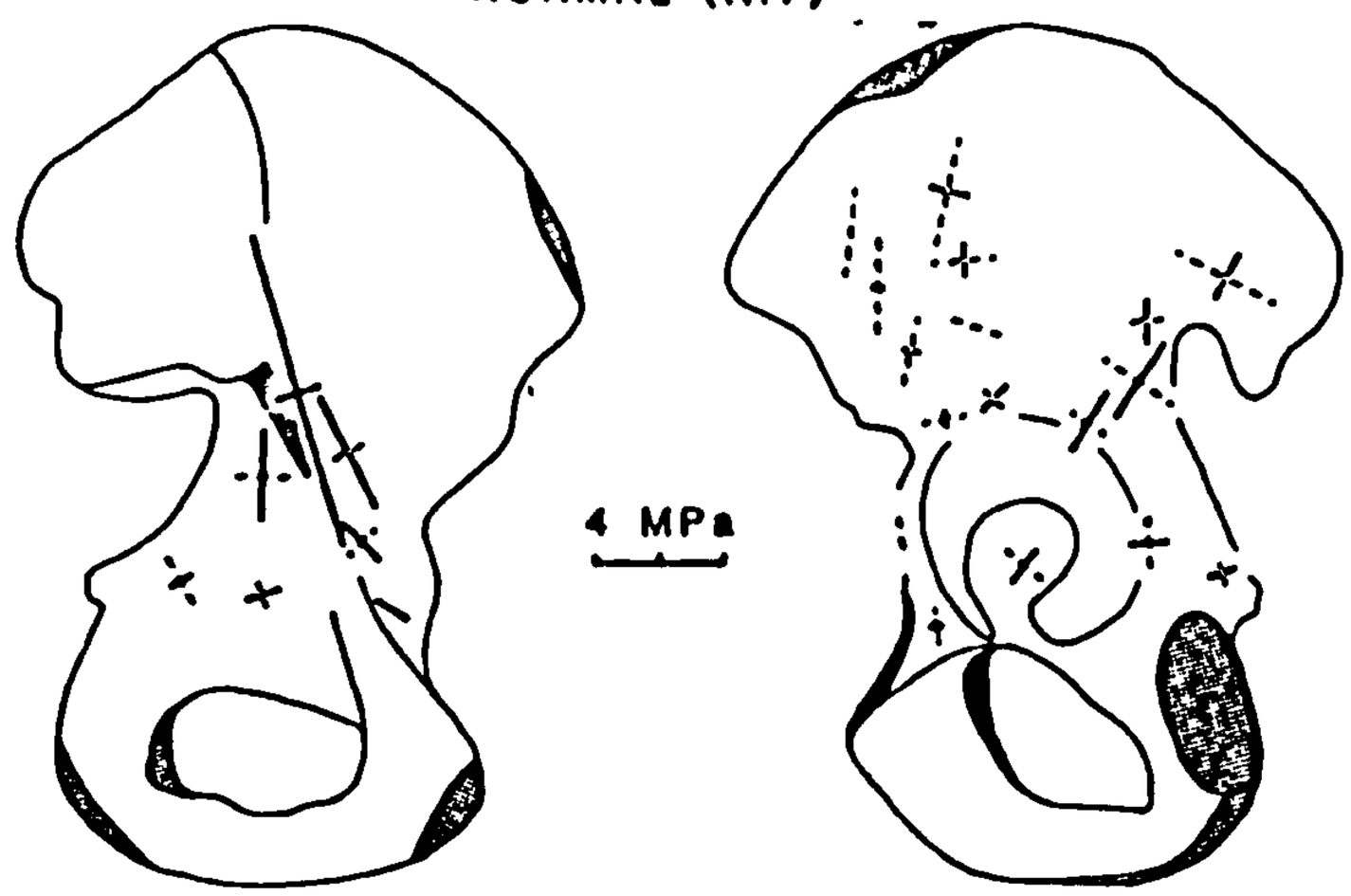

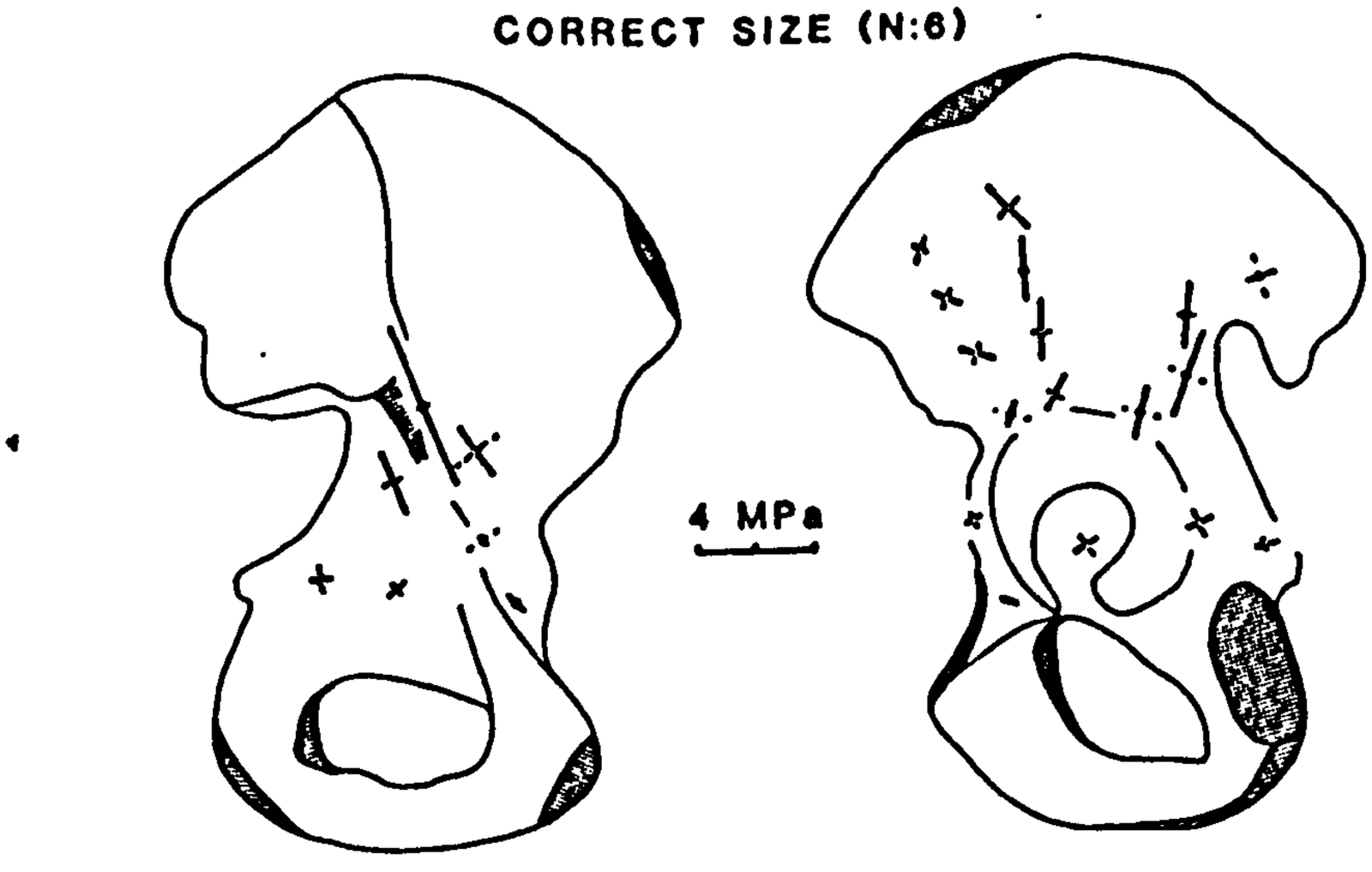

Figure 6.15 Diagrammatic representation of the strain gauge data of Finlay et al (1986a) derived from pelves loaded in contact with their matching femoral heads (upper diagram) and with a metal endoprosthesis with a head diameter matching the size of the acetabulum.

uniaxial bending in the analogue but elongated with bending in the transverse plane in the cadaveric specimens.

A logical explanation for these differences is that they are due to significant sagittal plane bending of the cadaveric pelvis by muscle forces acting posterior to the joint center. This is not surprising as the cables simulating gluteus maximus and the posterior part of gluteus medius transferred large forces to the cadaveric pelves, generating considerable bending moments in the transverse plane. A secondary effect, first proposed by Walmsley (1928) and later disputed by Hammond and Charnley (1967), may be the lack of congruity of the femoral head with the acetabulum leading to deformation of the socket with loading due to localized contact. Previous studies have shown that the femoral head makes initial contact within the dome of the acetabulum. This may cause the socket to elongate slightly with elastic contraction of the rim, in a pattern similar to that observed in this experiment. This stands in contrast to the mechanical analogue in which contact between the artificial femoral head and the artificial socket was more uniformly distributed due to the presence of closely fitting hemispherical surfaces.

The possible role of congruity in affecting the deformation of the acetabulum is supported by the work of Finlay et al (1986a) who examined the cortical strain distribution of the pelvis with varying degrees of undersizing and oversizing of the prosthetic femoral heads, selected to articulate with the natural acetabulum (Fig. 6.15). They found that when a metal hemisphere with a diameter matching the largest equatorial diameter of the original femoral head was loaded in the acetabulum, the strain distribution of the ilium was radically altered. Periacetabular strains were also affected and tended to be lower with the metal head, both medially and round the acetabular rim. Increases of only 1 mm in the diameter of the metal head caused dramatic increases, in cortical strains at all sites around the rim, in the floor of the acetabulum and over the medial wall (fig 6.16). Smaller, though statistically significant increases were measured along the pectineal line and the ilium. Conversely, undersizing the head diameter by 1mm had almost no effect on cortical strains over the medial wall of the pelvis. However, all tensile loading of the acetabular rim was replaced by compressive stresses which increased slightly over the weight-bearing dome.

Although Finlay et al did not simulate muscle loads in their

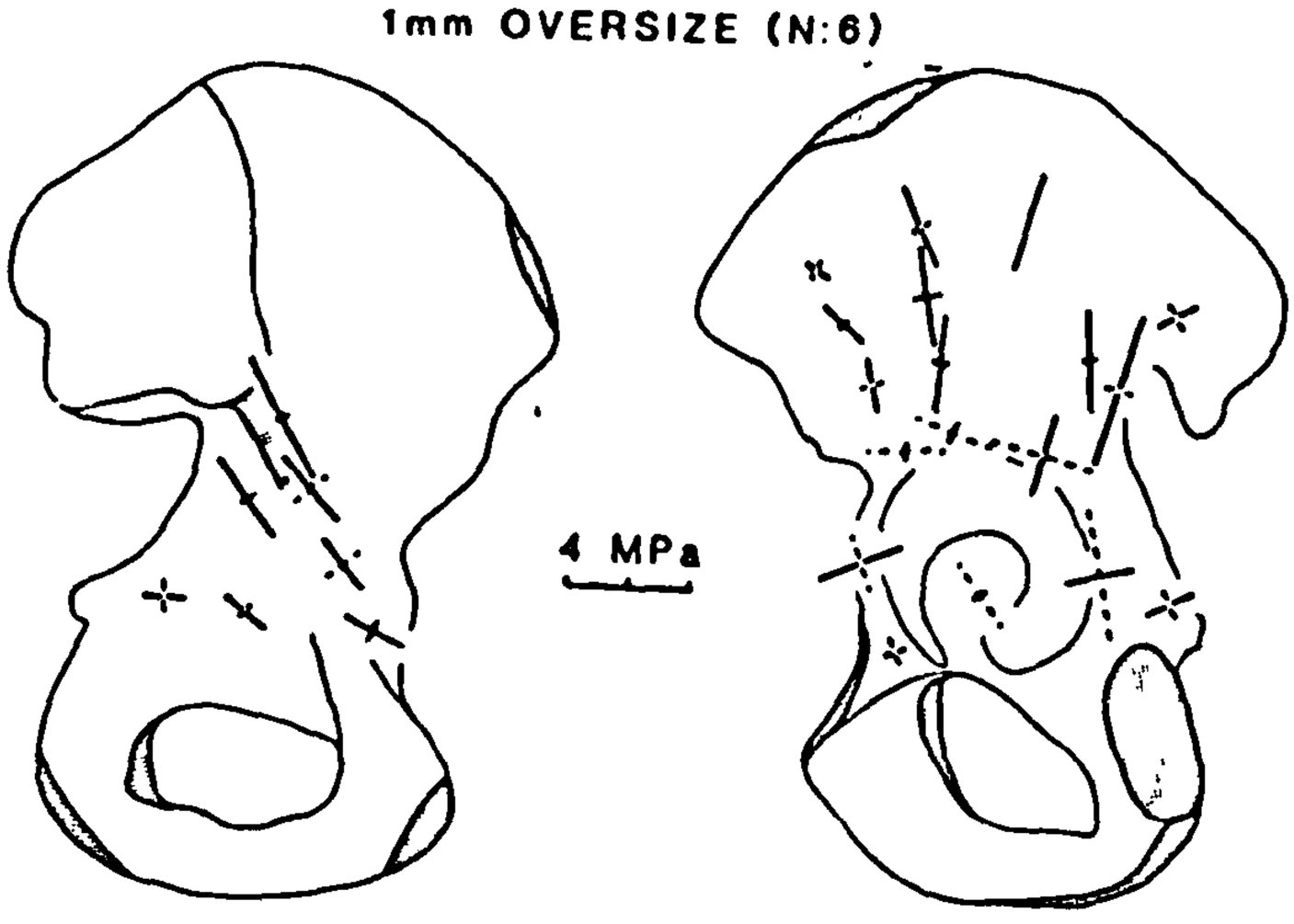

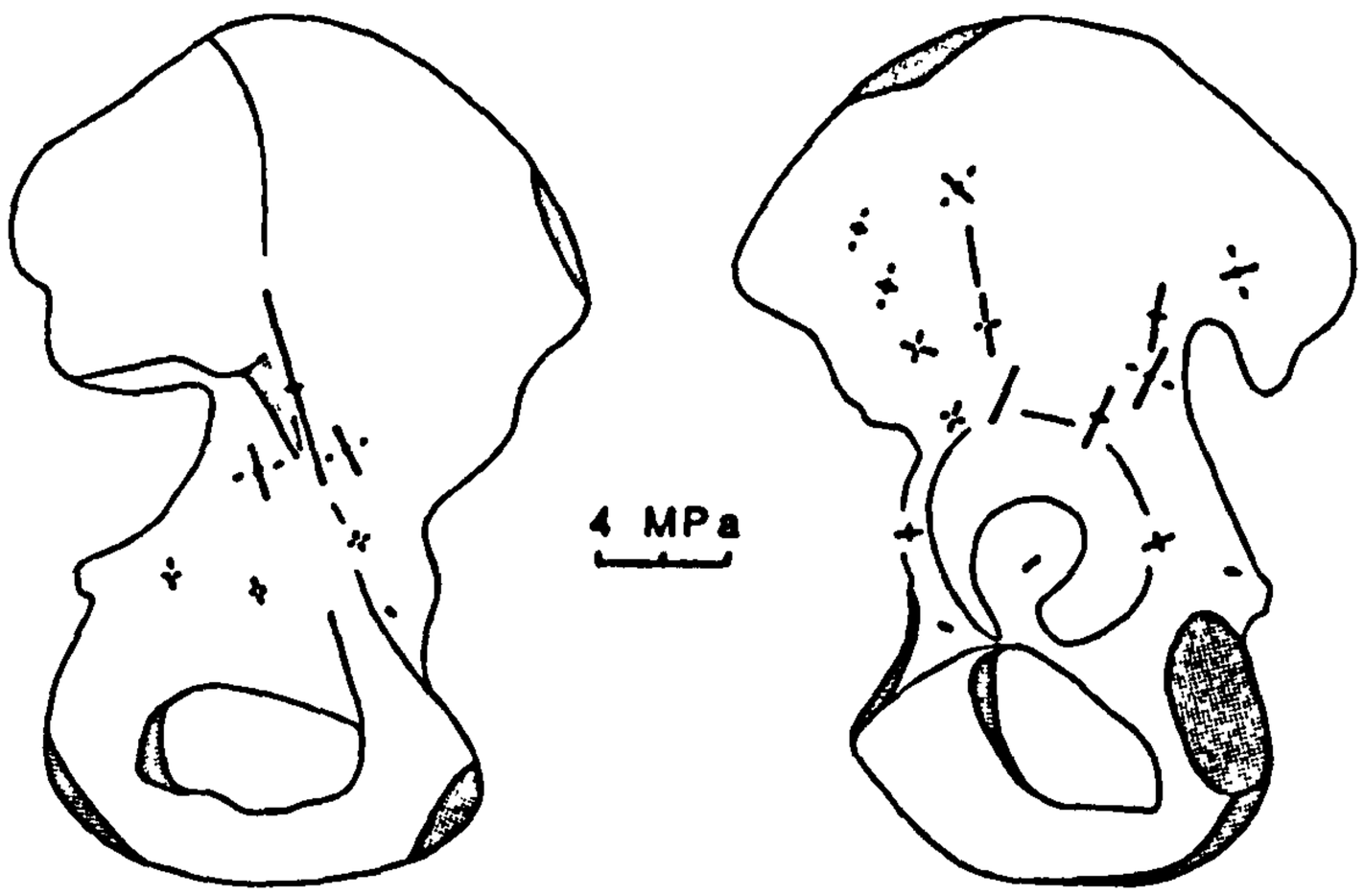

Figure 6.16 Strain gauge data of Finlay et al (1986a) measured during loading of pelves in contact with endoprostheses with heads 1 mm larger (upper diagram) and 1 mm smaller (lower diagram) than the diameter of the acetabulum.

experiment, their work demonstrated that relatively small changes in the congruity of the femoral head and the acetabulum can dramatically affect acetabular deformation. This may explain some of the differences between the cadaveric and analogue experiments. It most certainly would account for differences between cadaveric specimens if differences were also present in congruity of the hip joints.

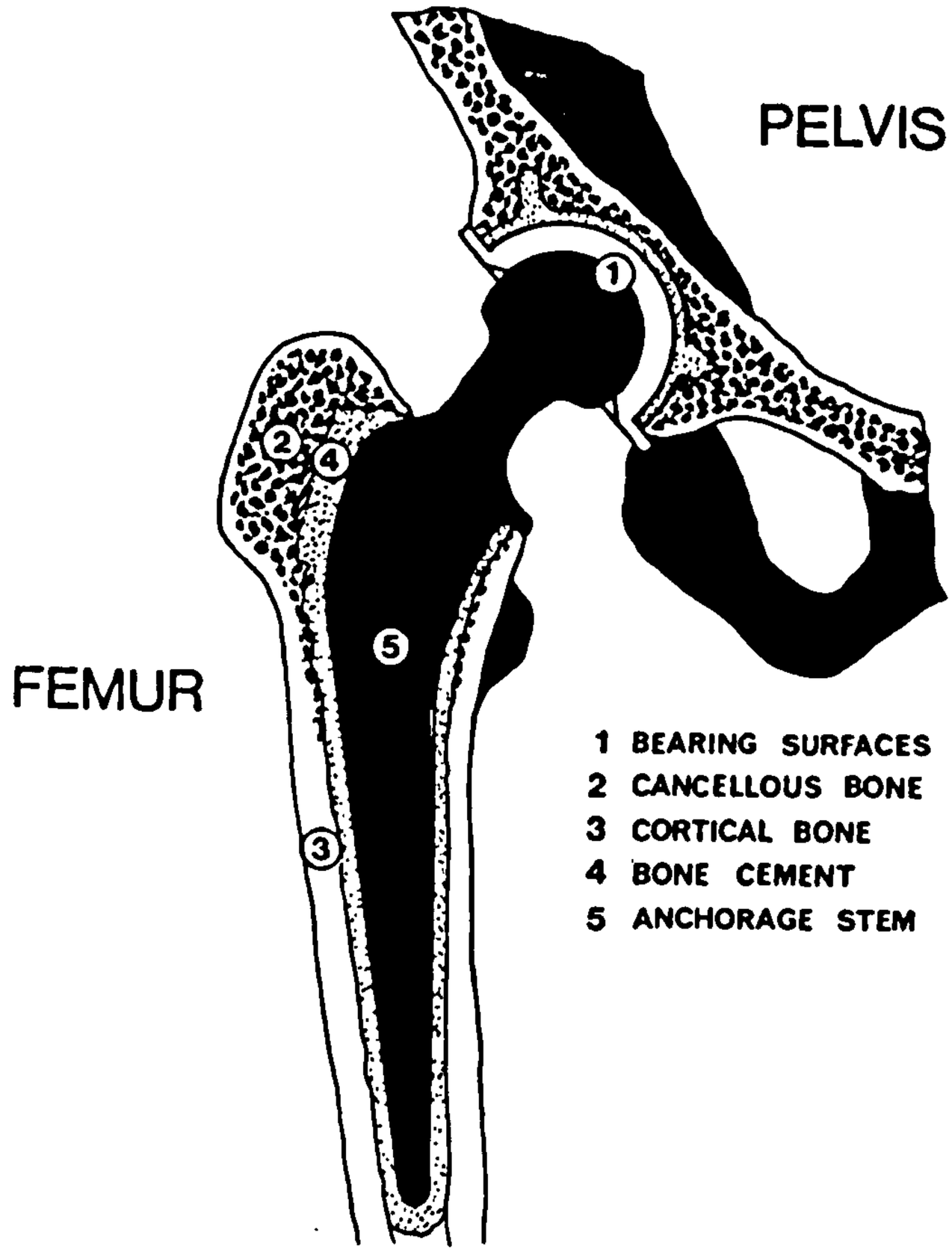

Figure 7.1 Schematic representation of a total hip replacement showing the femoral and acetabular components. In this example, both components have been fixed in the bone with an intermediate layer of bone cement (from Noble, 1983).

7.1 INTRODUCTION

The function of joints is compromised by numerous factors, including trauma, disease processes and abnormal load bearing. Degeneration of the joint or osteoarthrosis is associated with progressive restriction of joint movement, stiffness and severe pain on movement. Numerous palliative methods have been developed to treat the symptoms of arthritis, but once this condition fails to respond to conservative, non-operative measures, total joint replacement is often the only definitive treatment.

The design of joint replacements necessitates consideration of the composite mechanics of the artificial component, the host bone and the normal function of the healthy joint. In the first instance, the artificial component must fulfill a number of basic criteria, notably:

(a) compatibility with the host tissue and physiological processes within the body,

(b) extreme resistance to environmental degradation (e.g. corrosion) in conditions that include acidic crevice exposure and mild fretting at interfaces between dissimilar materials, and

(c) resistance to abrasion in combination with low sliding friction in the case of bearing surfaces.

The normal, articulating function of the diseased joint is restored by relining the acetabulum with a prosthetic socket, typically fabricated from ultra-high molecular weight polyethylene (fig 7.1). The polymeric liner is often reinforced with a metal shell of high strength cobalt-chromium or titanium alloy. The metal shell is generally designed so that the polymeric liner may be mechanically engaged intraoperatively in order to allow optimum positioning of the liner with respect to the pelvis. This form of modularity also allows a single shell to be used with a variety of liners of different inner diameters, designed to articulate with femoral heads of a variety of sizes. The diseased femoral head is typically replaced with a highly polished metal ball of 22, 28, or 32 mm in diameter, attached to a metal stem which is implanted within the intramedullary cavity of the femur. During a total hip replacement procedure, the cup is

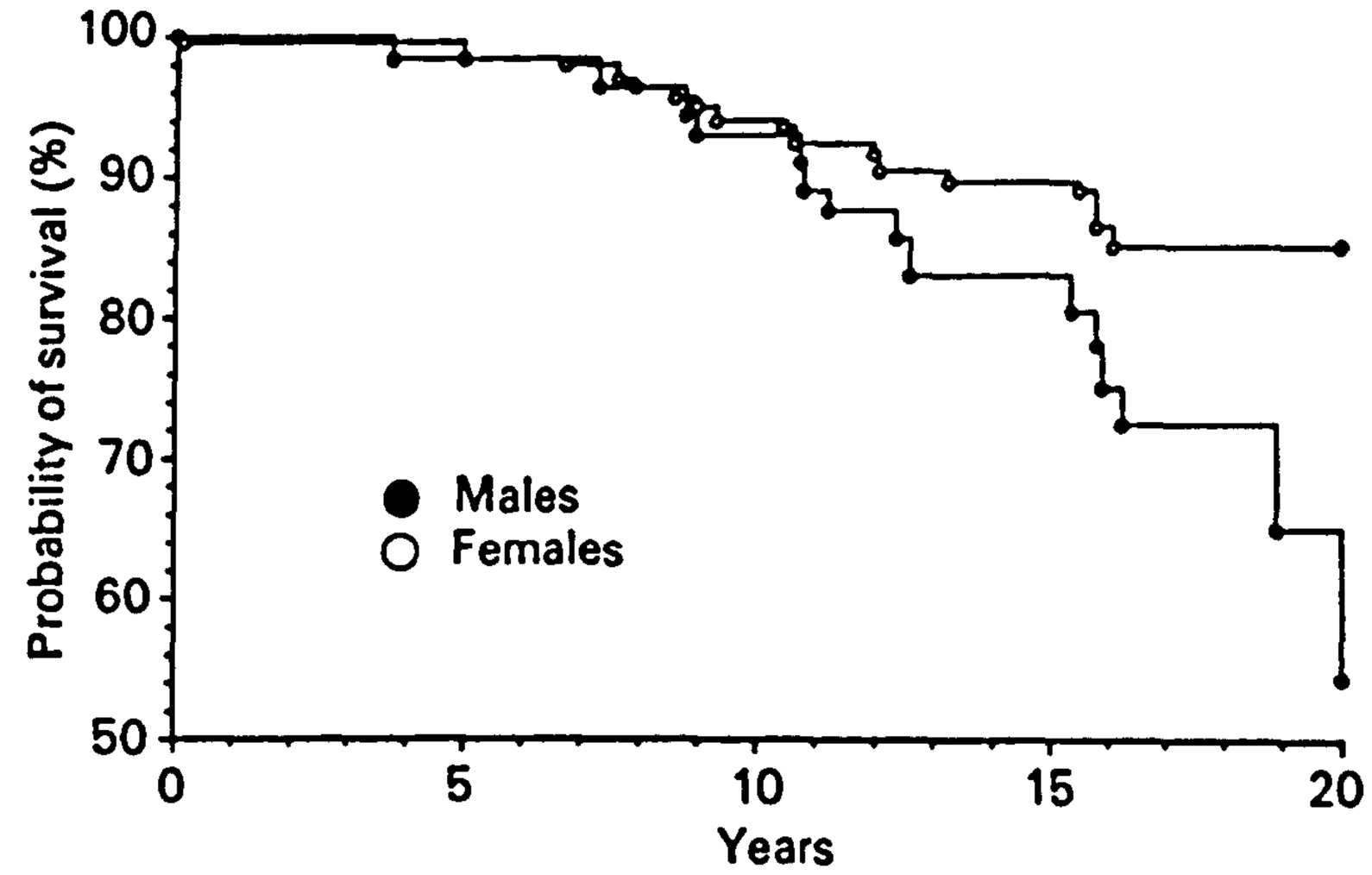

Figure 7.2 Survivorship of cemented Charnley hip replacements in males and females with failure defined as revision operation performed for any reason (from Joshi et al, 1993).

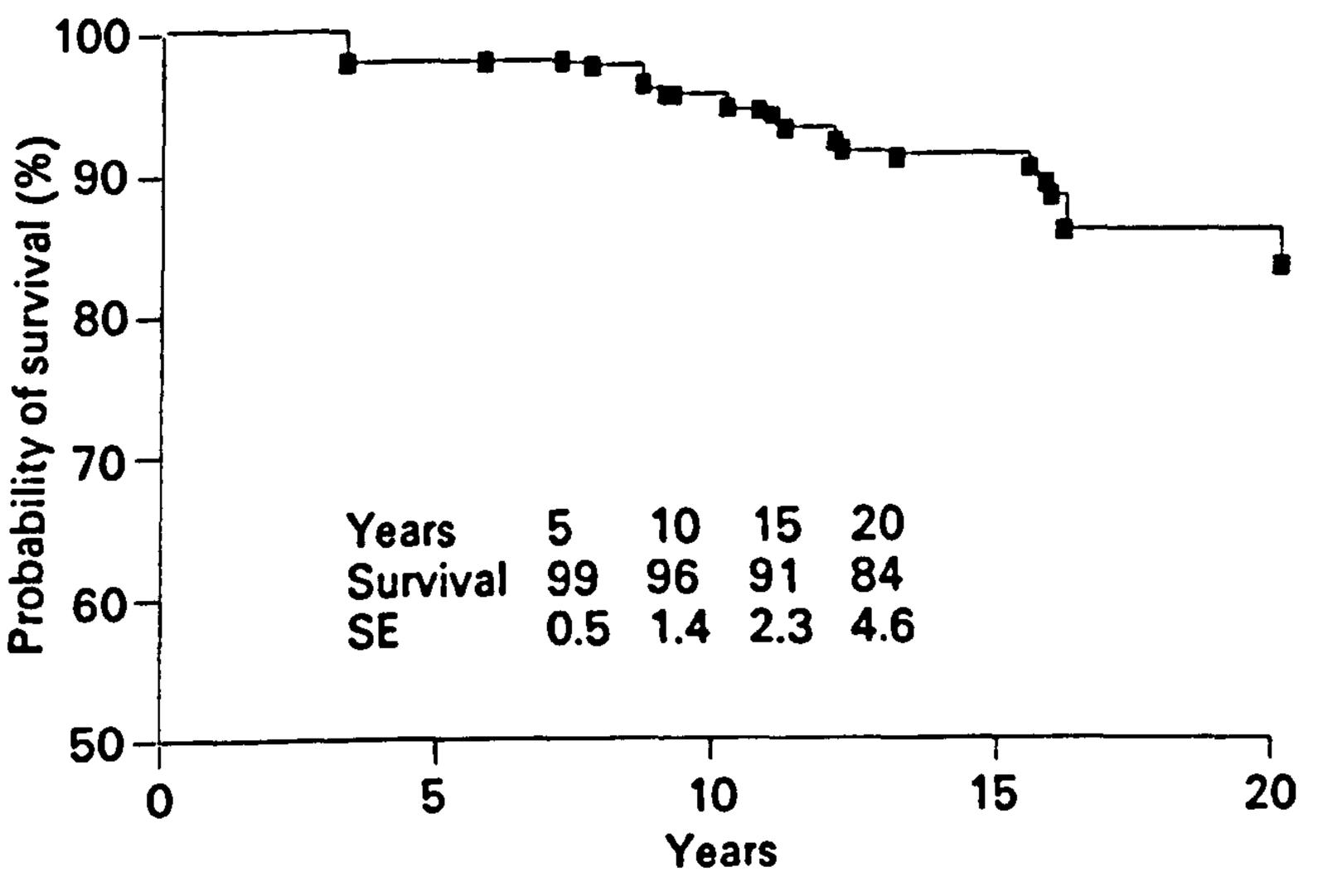

Figure 7.3 Survivorship of cemented acetabular cups of the Charnley design in patients who were 40 years or younger at the time of surgery. In this case, failure is defined as revision of a loose acetabular cup (from Joshi et al, 1993).

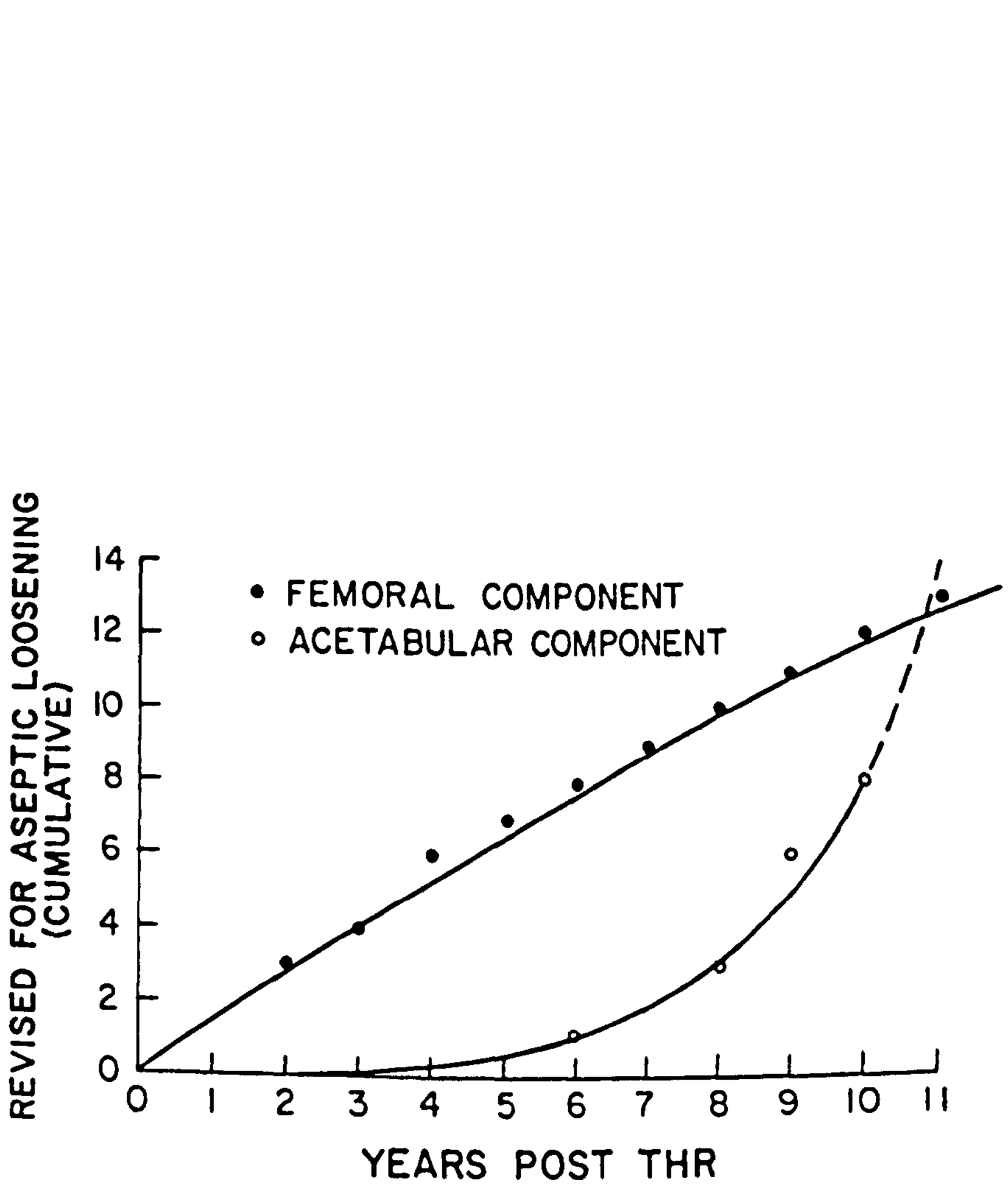

Figure 7.4 The cumulative incidence of revision of cemented femoral (dots) and acetabular components (circles) secondary to aseptic loosening, as reported by Sutherland et al (1982).

implanted in a hemispherical cavity reamed from the acetabulum of the pelvis; the femoral component is inserted once the head has been cut from the femur and the internal space within the medullary canal has been enlarged to accommodate the prosthesis. Once both components have been fixed in place, the prosthetic femoral head is mated with the socket, thus forming a new articulating joint.

A key consideration in the elimination of all pain with use of the artificial joint is rigid fixation of the femoral and acetabular components to the skeleton. This may be achieved in two ways, either through use of an acrylic grout ('bone cement') which cures within the bone, thereby fixing the prosthetic component in place, or through use of implants with porous outer surfaces which are implanted into the skeleton without an intermediate cementing agent. Under the correct conditions, bone cells grow into the porous surfaces of these 'cementless' prostheses, thereby providing rigid fixation and partial incorporation of the prosthetic component into the host skeleton.

7.2. CEMENTED ACETABULAR COMPONENTS: CLINICAL EXPERIENCE

The great success now enjoyed by joint replacement has come about only through extensive trial and error, marked in the past by numerous failures because of inadequacies in our understanding of the biomechanics of the musculoskeletal system and the demands placed upon materials implanted within the body. Cemented hip replacement has been shown to be one of the most successful surgical procedures performed to relieve pain and disability (Levy et al, 1985; Levy et al, 1988). In many series, this procedure provides complete relief of pain and a substantial improvement in quality of life to more than 90% of patients for up to ten years post-surgery (Kay et al, 1983; Nevitt et al, 1984). The popularity of this procedure has in fact been such that approximately 400,000 total joint arthroplasties are now performed annually worldwide.

Despite the overall success of cemented arthroplasties, the outcome of this procedure varies with many factors, including the age sex, weight and activity level of the patient (fig 7.2). In contrast to cemented fixation of the femoral stem, the clinical results of cemented acetabular replacement have been highly variable (Joshi et al, 1993; Onsten et al, 1994; Ritter & Campbell, 1987) (figs 7.3 and 7.4). Though cemented

acetabular replacements have performed well in older patients where the demands placed upon fixation are relatively low, the results have been less sanguine in younger and more active individuals (Ballard et al, 1994; Garcia-Cimbrelo & Munuera, 1992; Frankel et al, 1990). In many cases, although patients have no symptoms attributable to a loose prosthesis, radiographic changes at the interface between the cement and the acetabulum suggest the presence of unstable fixation (Hodgkinson et al, 1988). Quite frequently, radiolucent lines are visible on the radiograph corresponding to the presence of a fibrous membrane at the cement/bone interface (Cornell & Ranawat, 1986; DeLee & Charnley, 1976). In some cases, enlargement of the radiolucent lines is observed with time, corresponding to progressive loss of mechanical continuity between the cement mantle and the bone (Schmalzried et al, 1992). These radiographic findings are associated with enlargement of the implantation site with frank migration and rotation of the implant, ultimately leading to the development of a painful hip joint.

The first long-term studies of cemented acetabular replacement demonstrated an exponential rise in the incidence of failure and revision of these components after 8 to 10 years of implantation (Sutherland et al, 1982; Stauffer, 1982) (fig 7.4). It has often been claimed that this indicated that all attempts at cement fixation within the pelvis were fundamentally misguided and that loosening was inevitable. However, in more recent reviews of acetabular cups implanted with modern cementing techniques, considerably lower rates of loosening have been reported, though the incidence of long-term success varies with both the surgeon and the design of the prosthesis (Kobayashi & Terayama, 1990; Hodgkinson et al, 1993; Mulroy & Harris, 1990; Onsten et al, 1994).

Garcia-Cimbrelo & Munuera (1992) reviewed 680 cemented hip arthroplasties of the Charnley design, performed using an all-polyethylene cup of 22 mm internal diameter. All cases were performed between 1971 and 1979 and reviewed after an average period of twelve years and eight months (range: 1-19 years). Sixty-one cups showed radiographic evidence of loosening, corresponding to a predicted loosening rate of 19% at eighteen years post-operation, though only 9% of cases were considered to be clinical failures at the time of follow-up. Two temporal patterns of acetabular failure were observed: short-term or early loosening, which occurred within ten years of implantation, and late

loosening noted at ten years or more post-operatively. Forty-eight percent of loose cups loosened early; all showed evidence of compromised mechanical support due to such factors as bone deficiencies, previous congenital dislocation, acetabular fracture or protrusion. In the cases that loosened late, linear wear of the polymeric bearing surface in excess of 2mm was a common finding with progressive development of a complete circumferential radiolucency of the cement/bone interface, presumably in response to particulate debris, as demonstrated by the post-mortem specimens of Schmalzried et al (1992).

A number of technical factors appear to be associated with loosening and migration of cemented cups, including the use of larger diameter femoral heads (i.e. 32 mm), the use of cups with reduced clearance between the cup and the head and placement of the cup in excessive abduction. Other factors pertaining to surgical technique include the presence of incomplete containment of the cup within the acetabulum (Sarmiento et al, 1990), the use of three large anchorage holes for cement fixation after removal of the subchondral plate (Kobayashi & Terayama, 1990), and failure of pressurization of the cement into the acetabular bed (Hodgkinson et al, 1993; Cornell & Ranawat, 1986; Onsten et al, 1994).

Cemented fixation has been even less successful in revision arthroplasty. In a recent study of cemented revision cases, Snorrason and Karrholm (1990) utilized roentgen stereophotogrammatic analysis to measure prosthetic migration and found that all but one of fifteen acetabular components had migrated by 0.5 - 2.0 mm at only two years post implantation. However, sequential studies showed that cup migration was progressive in only about half of the cases studied. In other series of cemented revision arthroplasty the clinical outcome has been variable, with the incidence of re-revision of cemented cups ranging from 2 to 31% at 4-6 years (Hozack et al, 1990; Kershaw et al, 1991; Stromberg et al, 1988). Nonetheless, in every series, a substantial proportion of cases has shown evidence of radiographic failure at follow-up, especially in young patients with high activity levels (Stromberg et al, 1988). Given that the failure of cemented cups occurs early after revision arthroplasty, the underlying cause, in most instances, is probably mechanical in nature. Likely factors include the loss of subchondral bone and the presence of bony defects, both of which compromise the structural support of the prosthetic component and reduce the area

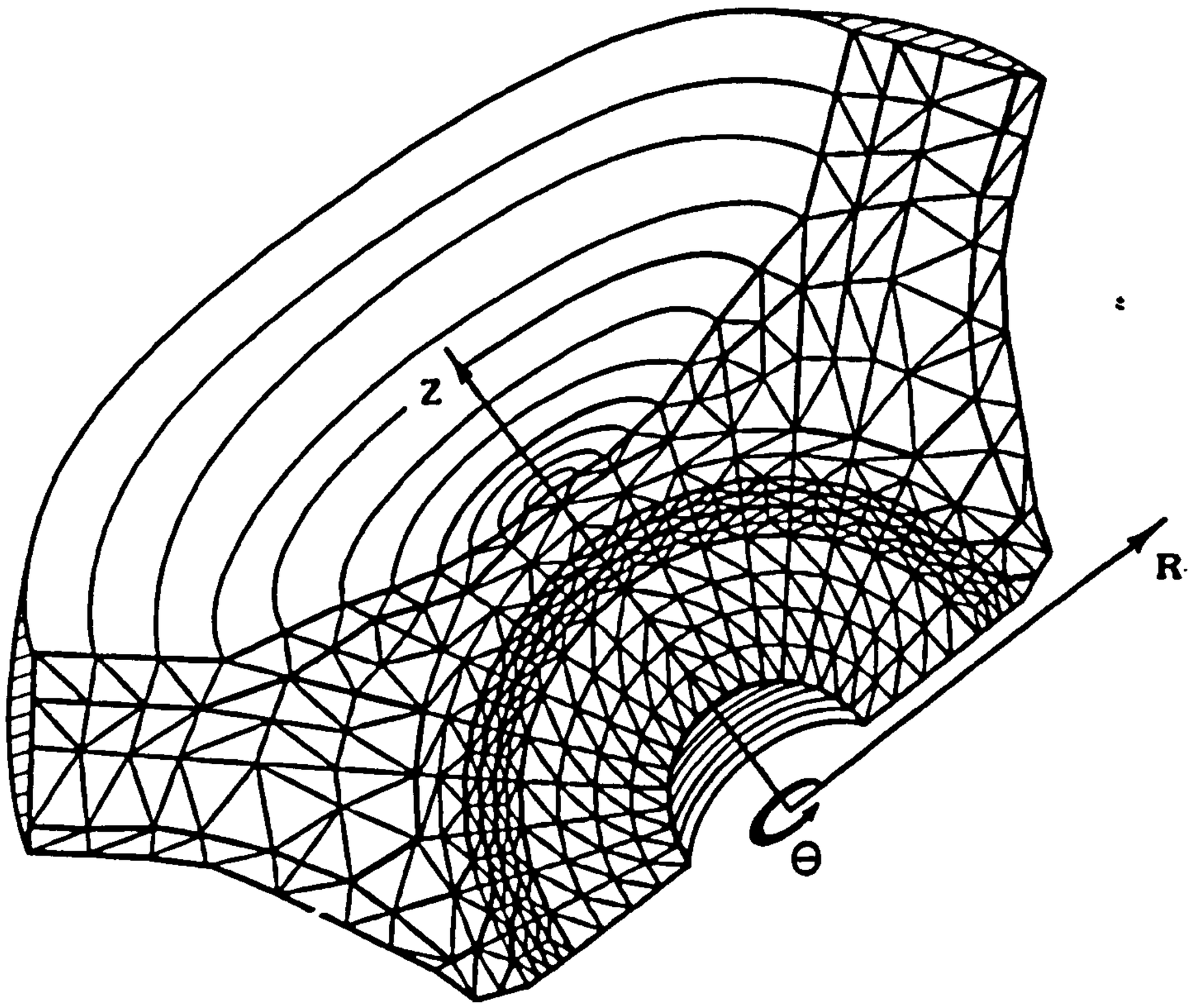

Figure 7.5 The axisymmetric finite-element model of the prosthetic hip joint developed by Pedersen et al (1982).

available for attachment of cement to bone. These conclusions have been borne out by the experiments of Markolf and Amstutz (1983) in which the presence of poor quality acetabular bone stock led to large values of cement/bone micromotion under load-bearing conditions, regardless of the cement technique employed.

7.3. STRATEGIES TO IMPROVE THE DURABILITY OF CEMENTED ACETABULAR CUPS: METAL BACKING

7.3.1 Introduction

The initial hypothesis for the etiology of aseptic loosening of cemented acetabular cups was mechanical failure of the cement/bone interface. This was attributed to deficiencies in cementing technique, manifested by inadequate preparation of the bony acetabulum, combined with poor pressurization of cement. This led to several innovations, including new methods of cement delivery and changes in implant design which subsequently led to a reduction in the incidence of late acetabular loosening. Other attempts to improve the longevity of fixation focused on ways of reducing the stresses developed within the cement mantle and the acetabular bone stock. They assumed that if the safety-margin of the cement mantle and its bony foundation were increased, the incidence of loosening would be significantly reduced. One of the design modifications considered to reduce cement stresses was the use of a metal shell to reinforce the polyethylene bearing surface.

7.3.2 Finite Element Studies

Several finite element studies have been performed to examine the effect of metal-backing on periacetabular stresses. Pedersen et al (1982) developed an axisymmetric finite element model of a cemented acetabular cup implanted in the acetabulum with a short segment of the pubis and the ilium in continuity (fig 7.5). The model was based upon a uniplanar section through the pelvis, posteriorly oriented at 15 degrees to the midcoronal plane. This section was chosen in order to obtain maximum symmetry of the bony pelvis. Acetabular components with an outer diameter of 51 mm and inner diameters of 22, 28, 35 and 44 mm were modeled with axisymmetric triangular elements. This corresponded to acetabular shells with total wall thicknesses of 14.5, 11.5, 8 and 3.5 mm.

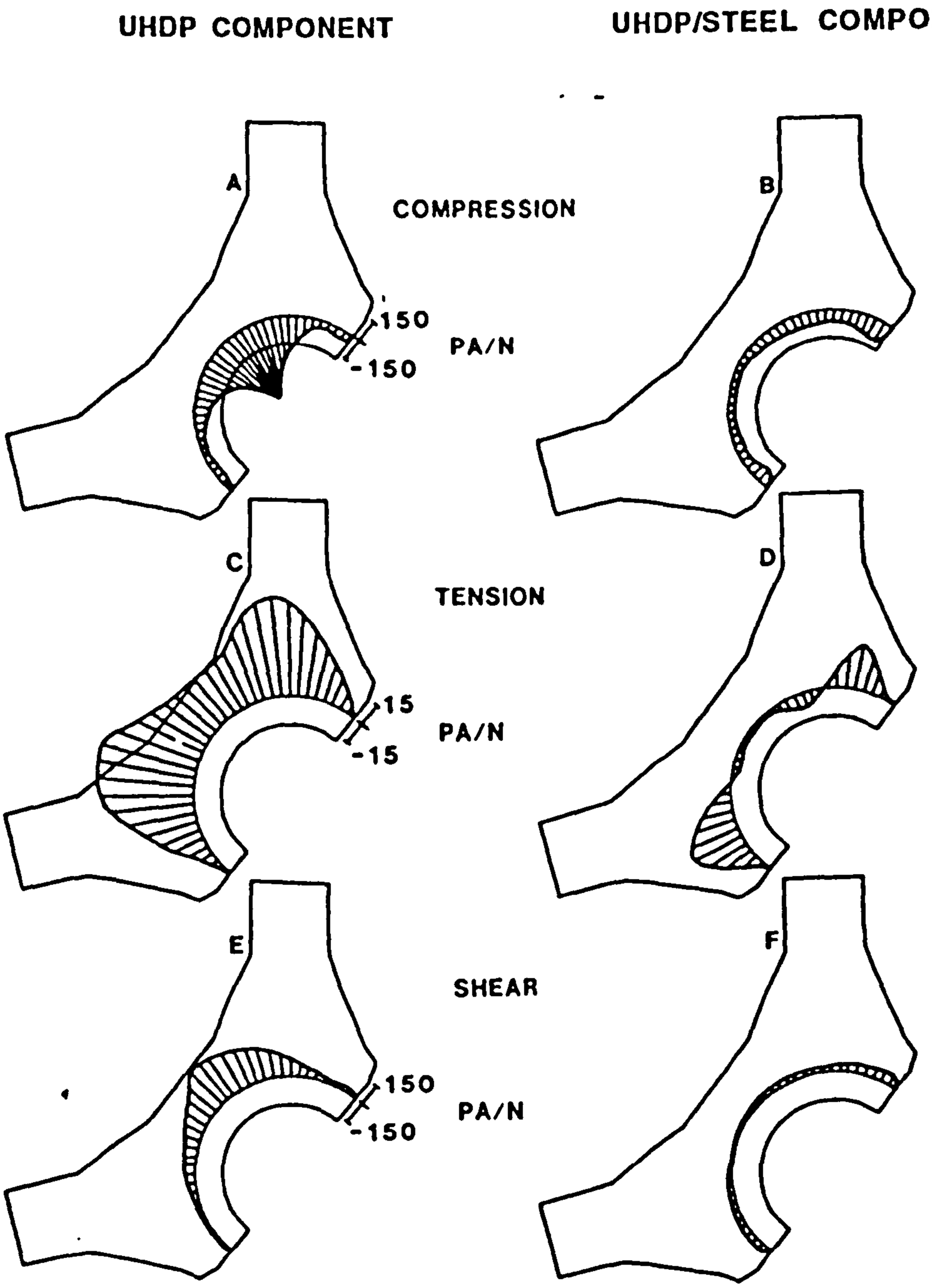

Figure 7.6 Predicted values of mantle stresses after implantation of metal-backed and all-polyethylene acetabular components from Pedersen et al (1982). The stresses associated with the polyethylene (UHDP) component are shown on the left (A, C, E). Note the scale of the tensile stresses is 1/10th that of the compressive and shear stresses.

The trabecular bone of the pelvis was represented by three zones of different elastic moduli ranging from 1.0 to 3.0 GPa. Different models were constructed of acetabuli with and without an intact subchondral plate, implanted with polyethylene cups of all four wall thicknesses. The effect of adding a 3 mm metal backing shell to each cup was also evaluated. A non-axisymmetric, conically distributed load was applied to the inner surface of each socket at 20 degrees to the vertical in the coronal plane. The external boundaries of the model were constrained along the cutting plane through the ilium and the pubis, however no constraint was placed over the bearing surface of the acetabular cup. The prosthetic femoral head was not included in the model.

Using the finite element method, stresses were calculated within the cement mantle and the underlying bone. It was predicted that the maximum tensile stress within the acetabular cement mantle would increase by approximately 300% if the wall thickness of the polyethylene liner were reduced from 14.5 to 3.5 mm. This would be accompanied by a 100% increase in the maximum compressive stress. Similar, though less dramatic, changes were predicted in the stresses within the subchondral bone surrounding the acetabular cup. Not surprisingly, removal of the subchondral plate also caused these stresses to increase by about 20% for each of the situations modeled.

The most dramatic changes were observed once a metal shell was incorporated in the model of the acetabular component (fig 7.6). In this case, the compressive and shear stresses within the cement became extremely uniform; tensile stresses were also significantly reduced. It was also predicted that metal-backing would shift the position of maximum tensile stress within the cement from the dome of the shell to areas located approximately 30 degrees from the superior and inferior edges of the metal shell. An interesting effect of the metal reinforcement was that the thickness of the polyethylene had virtually no effect on stresses within cement or bone as so much of the stiffness of the implant was derived form the shell and not the polymeric liner. In quantitative terms, it was predicted that the metal backing would reduce the maximum tensile stresses by approximately 85% and compressive stress by 75% compared to an all-polyethylene cup of minimum wall thickness (3.5 mm). With the thickest acetabular wall (14.5 mm), the reduction in stress was not as dramatic but even in this case, peak tensile and

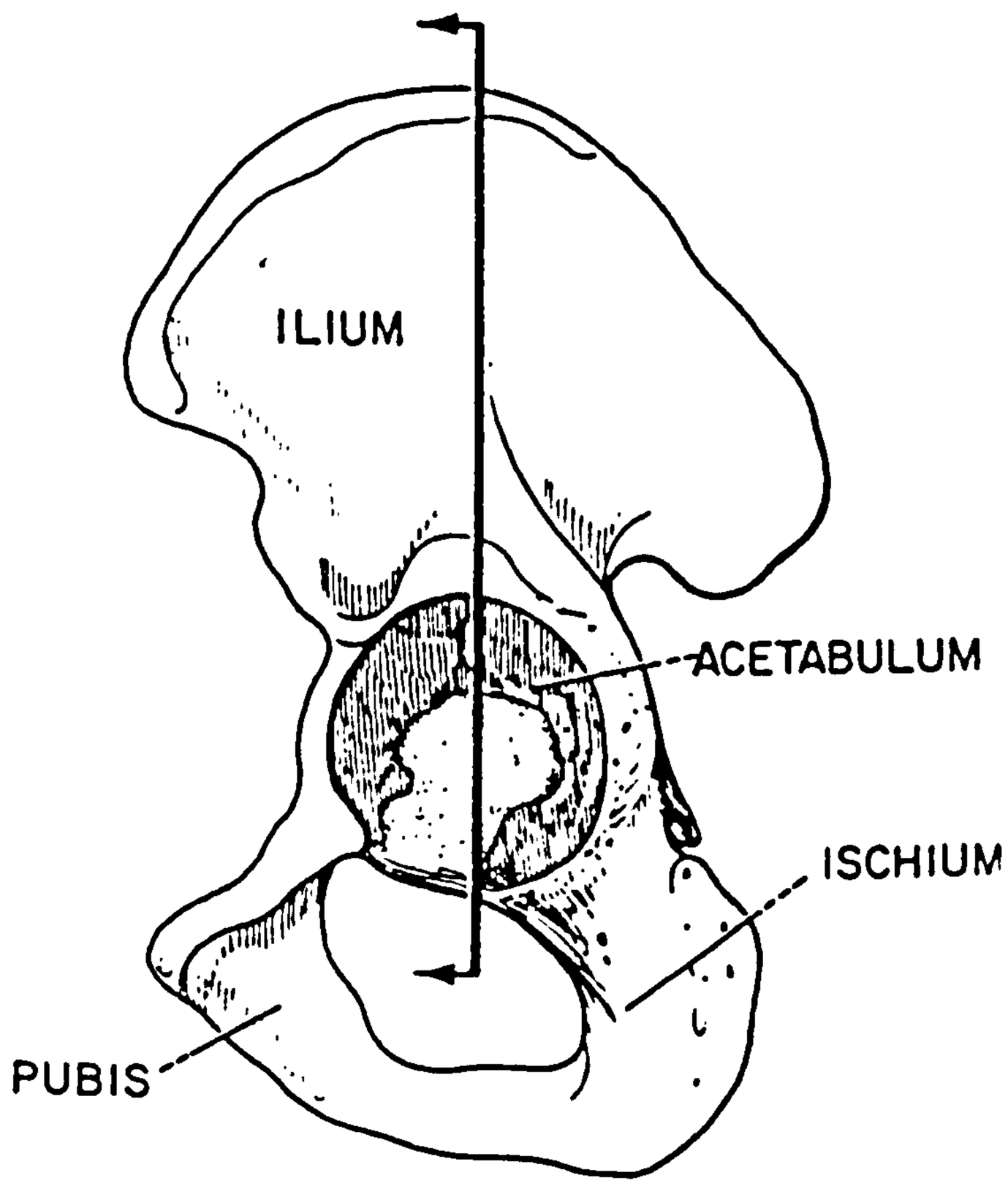

Figure 7.7 A lateral view of the pelvis showing the orientation of the section utilized by Vasu et al (1982) for the development of their uniplanar finite-element model.

compression stresses decreased by 30-50%. Even greater changes were predicted in subchondral bone where the peak tensile stress was increased 3-5 times in the absence of metal-backing.

A number of simplifications present within this model may have affected the accuracy of its predictions. The most critical assumption was the absence of constraint over the bearing surface of the acetabular cup. This allows the cup to deflect under load, even though, in practice, there is relatively little clearance between the bearing surface and the spherical femoral head. In practice this would markedly increase the stiffness of the acetabular component which would act as a thick, unbonded coating layer on the surface of the metal ball with constraint perpendicular to the bearing surface. Other limitations of the model include the use of an axisymmetric representation of acetabular geometry which is expected to increase the apparent stiffness of the bony pelvis with respect to the relatively flexible acetabular cup. This would exaggerate the effect of metal-backing on the stresses generated within the cement and subchondral bone. The subchondral plate represented within the model also appears to be unrealistically thick (1.5 - 2.0 mm), due to the relative coarseness of the finite elements. This would again overestimate the contribution of metal-backing to stress reduction.

Another finite-element model of cemented acetabular cup was developed by Vasu et al (1982), based upon a vertical slice of the pelvis taken through the center of the acetabulum before and after implantation of a cemented acetabular cup (fig 7.7 - 7.9). These plane strain models consisted of between 300 and 600 isoparametric quadrilateral elements with non-homogeneous representation of the elastic properties of cancellous bone, based upon inspection of the trabeculae in a section of one cadaveric specimen. The model also included a segment of the weight-bearing surface and the floor of the acetabulum extending to the acetabular notch (fig 7.8). It was assumed that the acetabular notch and the iliac wing could be represented as fixed boundaries to support the two-dimensional model. Using this representation, five models were prepared: three consisted of an acetabular cup without metal backing, implanted in cement of 1, 3 and 5 mm in thickness and two of a cup consisting of a Co-Cr metal shell of 2 mm in thickness with a 3 mm cement mantle. The bearing surface of the metal-backed implants was loaded using diffuse and concentrated distributions of contact forces,

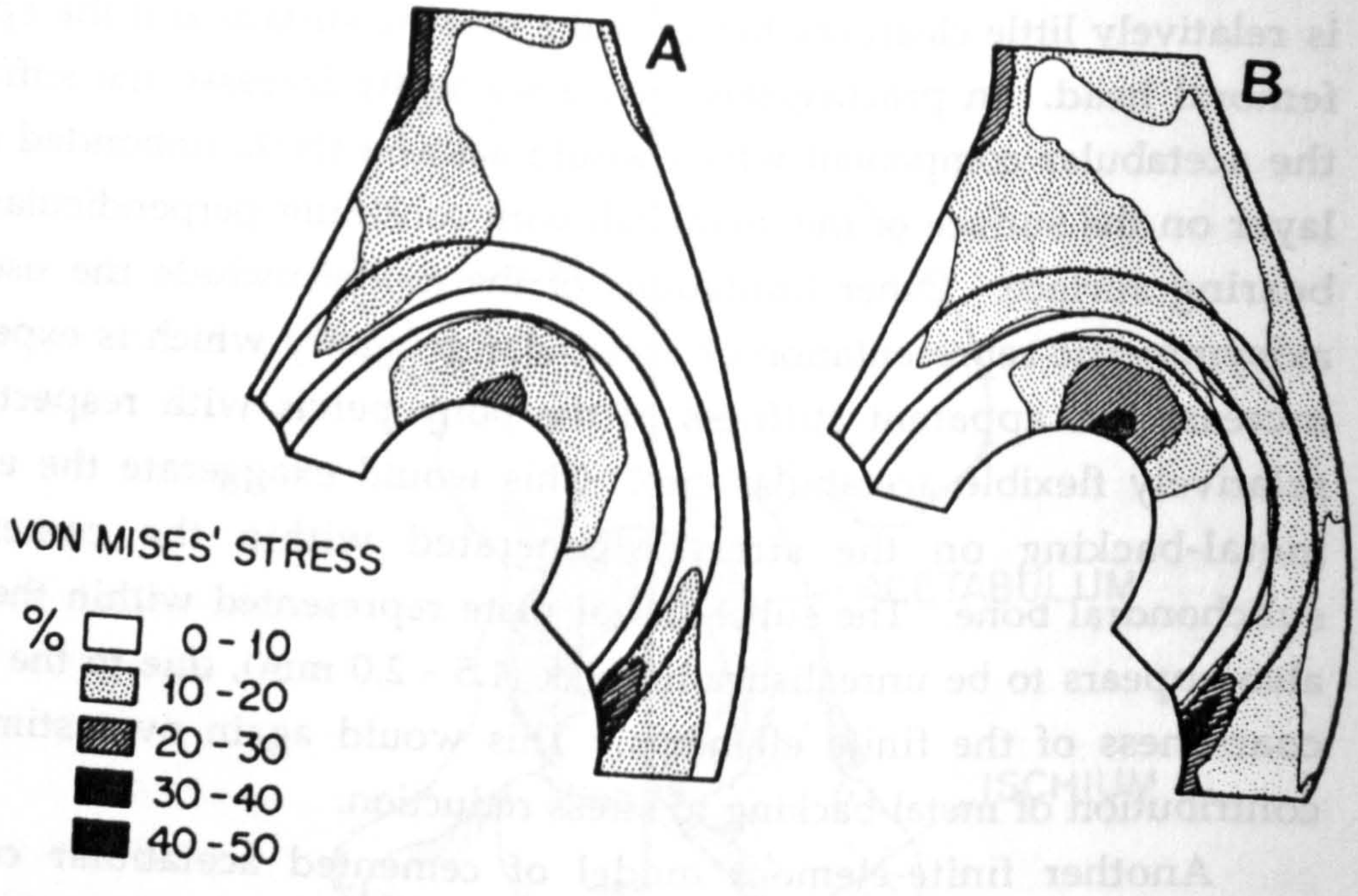

Figure 7.10 Von Mises' yield contours predicted by Vasu et al (1982) following implantation of metal-backed acetabular components, assuming diffuse (a) and concentrated (b) distributions of the joint reaction force.

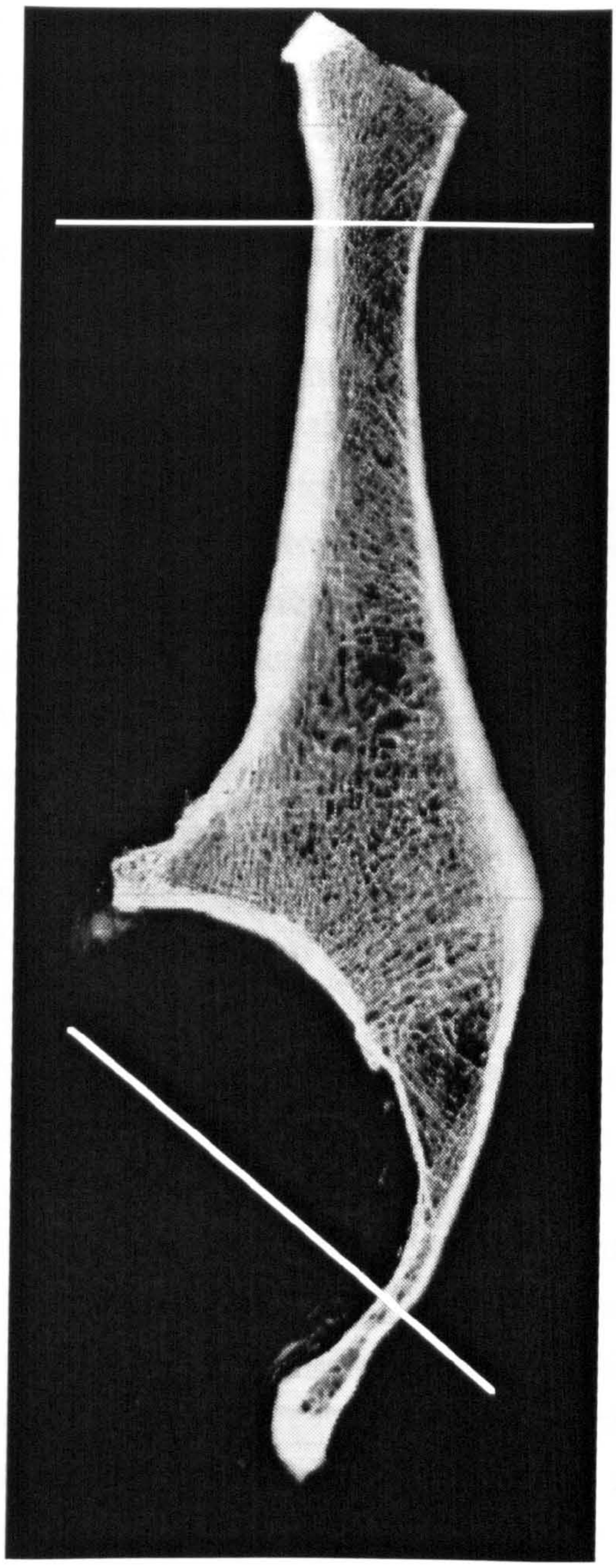

Figure 7.8 Roentgenogram of the model slice of Vasu et al (1982), showing trabecular orientation.

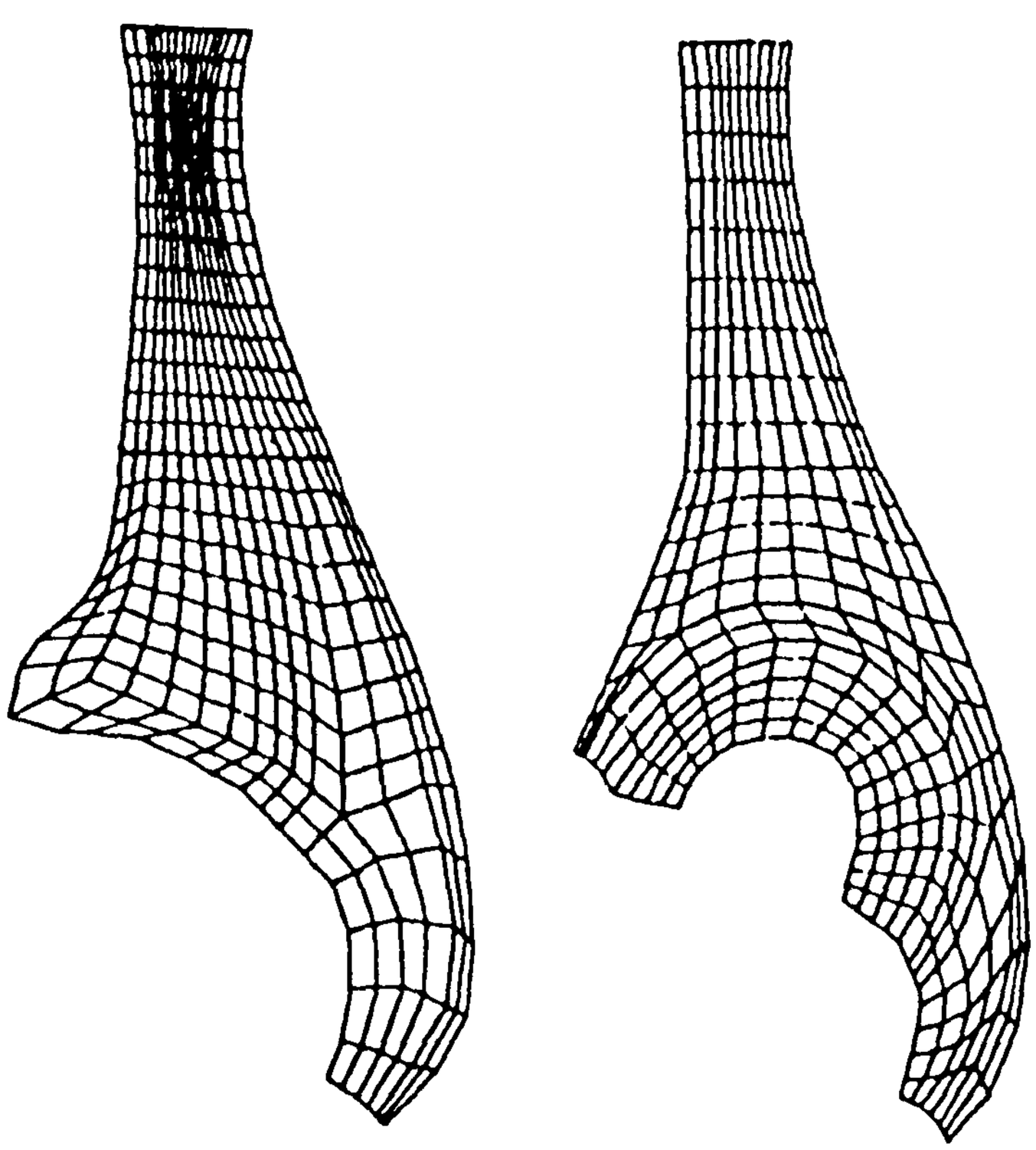

Figure 7.9 Finite element meshes developed by Vasu et al (1982) to represent the acetabulum before and after joint replacement.

though in each case it was assumed that the resultant contact force would be directed supero-medially at 21 degrees to the vertical. The subchondral plate was not explicitly represented in any of the models.

In the models of a non-metal backed prosthesis, increasing cement thickness reduced the maximum stress within the cancellous bone of the pelvis, the medial wall of the ilium, the cement and the cup. The addition of metal-backing dramatically reduced stresses in almost all areas of the implant, the cement mantle and adjacent bone (fig 7.10). This was associated with a reduction in the bending of the shell and increased load transfer from the acetabulum to the medial and lateral walls of the pelvis which have a higher yield stress than the cancellous areas beneath the subchondral plate. This same pattern of load transfer was present with both a diffuse and a concentrated distribution of contact pressure although both models predicted that an area of high stress concentration would be present within the cement mantle adjacent to the inferior rim of the cup. Although the authors recognized the presence of this area of increased stress, they suggested that it might have been an artifact caused by the simplistic representation of the boundary conditions stabilizing the inferior half of the acetabulum.

This finite-element model has several fundamental deficiencies. Firstly, in the real pelvis, the vertical slice taken through the center of the acetabulum is constrained by out-of-plane structures including the sacro-iliac joint superiorly, and the pubis and ischium, inferiorly. It may be assumed that the superior boundary can be represented by rigidly fixing the ilium without significantly altering periacetabular stresses, in view of the relative distance of the acetabulum from the ilium. However, the out-of-plane support provided by the pubic and ischial rami occurs directly adjacent to the edge of the acetabular cup. Consequently, the stresses predicted within at least the lower half of the cup and adjacent cement and bone are expected to be erroneous.

Secondly, the model constructed by Vasu et al does not depict a cup of appropriate size or orientation for the acetabulum depicted in their model. Although the model of Vasu et al has a strong physical resemblance to a section taken through the ilium and ischium, the plane of section was taken through the floor of the acetabulum and not the ischium. At surgery, a cup would be implanted so that it filled the entire space extending from the superior rim of the acetabulum to the lower

boundary of the model, if not slightly below. Vasu et al (1982) have erroneously modeled a cup of almost half the diameter of their acetabulum placed high up within the ilium, leaving most of the floor of the acetabulum uncovered. This bears little resemblance to the morphology of the pelvis following total hip arthroplasty and is expected to over-estimate the reduction in stresses produced by the metal-backed component. This conclusion is based on the observation that, within the model, the acetabular cup is supported by cancellous bone of minimal stiffness which would not be capable of supporting the prosthesis without generation of large bone and cement stresses.

Thirdly, the plane strain model appears to have little real resemblance to the mechanical characteristics of both the prosthesis and the pelvis, given the profound effect of out-of-plane contributions to the stiffness of these components. This is especially critical in the context of stresses within periacetabular bone which are strongly influenced by the relative stiffness of the bone and the implant. In this model the metal-backing of the acetabular cup is represented by a semi-annular ring which will be far more flexible than a complete hemispherical shell. This leads to an underestimation of the effect of metal-backing in comparison with the predictions of the axisymmetric model. As in the model of Pedersen et al, the bearing surface was represented by an unconstrained boundary with a distributed load corresponding to the joint reaction force. This is expected to greatly underrepresent the effective stiffness of non-metal backed cups, which derive substantial reinforcement from the presence of a metal femoral head. As previously, this assumption is expected to lead to erroneous predictions of stresses within the cement and periacetabular bone.

Two more recent studies (Rapperport et al, 1987; Dalstra & Huiskes, 1991) have attempted to address many of the deficiencies of the previous finite element models. Rapperport et al developed an improved version of the two dimensional model of Vasu et al and predicted the stress distribution generated after implantation of a cementless, porous-coated cup. The pelvis was represented by a slice taken through the acetabulum, the pubis and the ischium in the same inclined plane as the model of Crowninshield et al (1983). The model included a metal femoral ball loaded in contact with the socket. To compensate for the lack of the inherent out-of-plane stiffness of a hemispherical prosthesis, the elastic

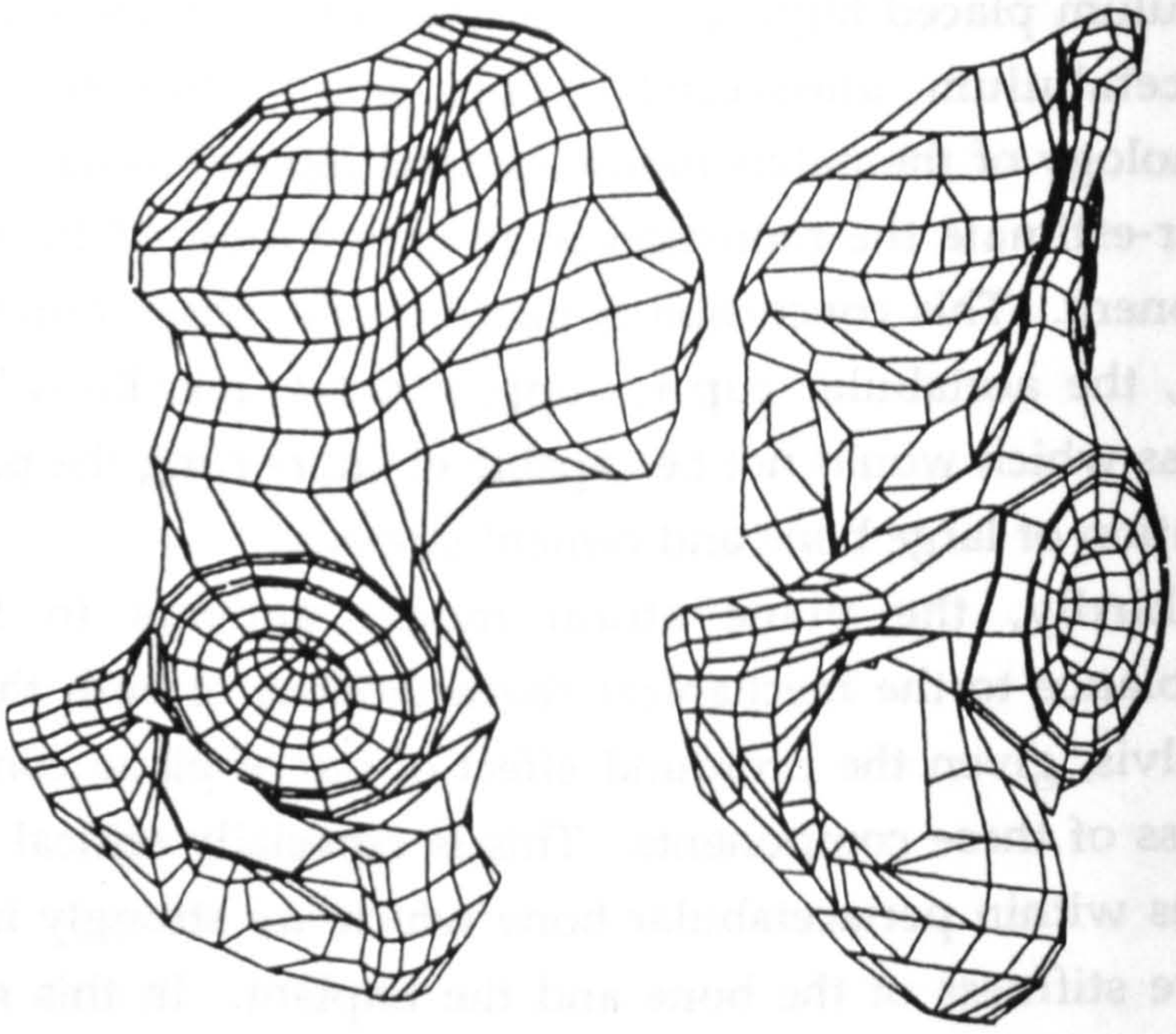

Figure 7.11 Lateral (left) and frontal (right) views of the finite element model of Dalstra and Huiskes (1991).

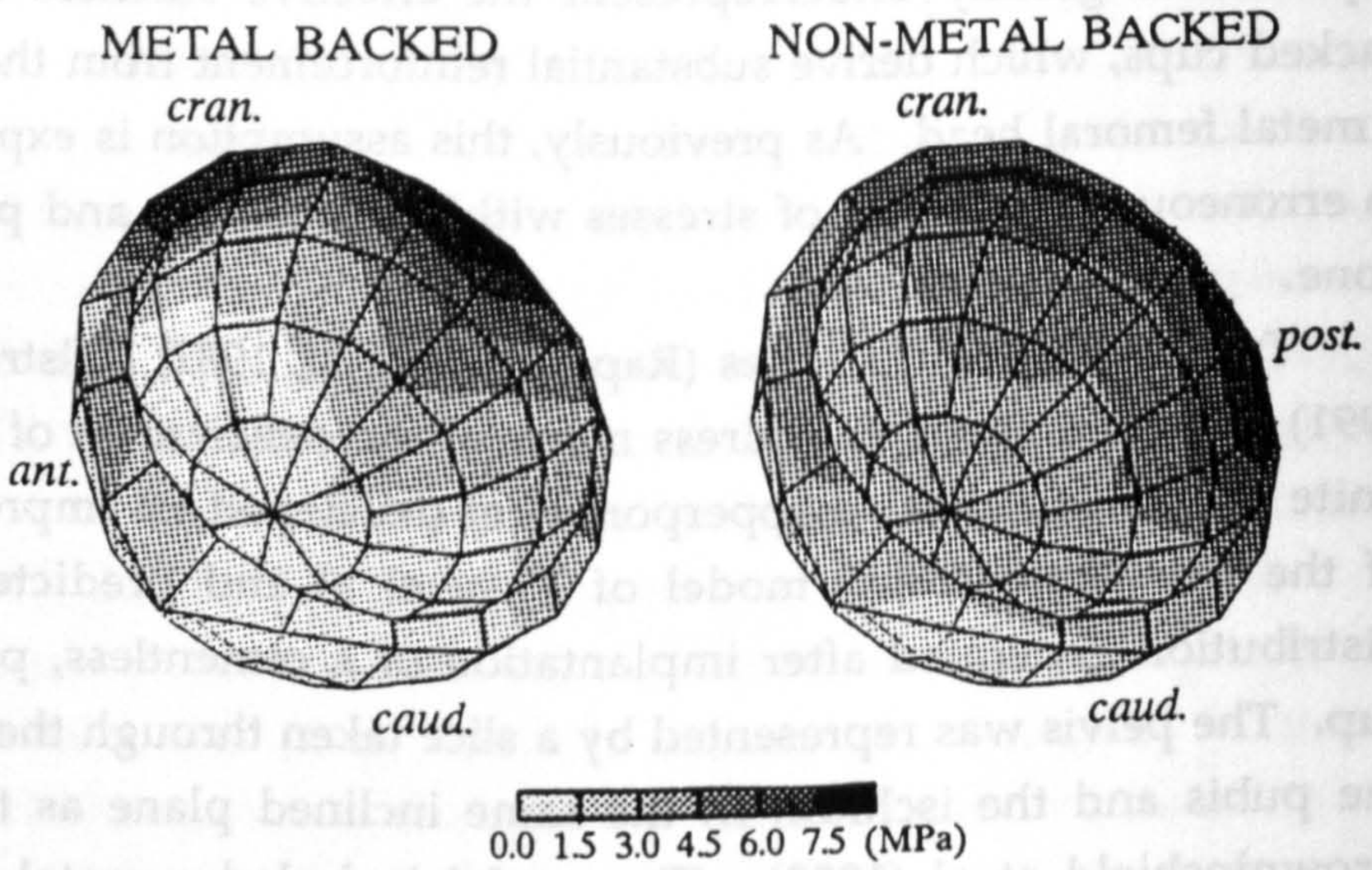

Figure 7.12 Von Mises' stress patterns in the cement mantle at the beginning of stance phase, as predicted by Dalstra and Huiskes (1991).

modulus of the liner was assumed to be the same as the shell (ie. 208 GPa).

Dalstra and Huiskes (1991) developed a three-dimensional finite element model of an entire hemipelvis implanted with a cemented cup with the femoral head in place (fig 7.11). Two models were studied, one of an all-polyethylene prosthesis and another in which the elements representing the outer layer of the cup were assumed to have the elastic modulus of titanium, to simulate a 2 mm metal backing. A variety of loading conditions was examined, including muscle and joint reaction forces present at three different stages during the normal gait cycle. The results of this study show that the predicted stresses within the cement and periacetabular bone are strongly influenced by the loading condition and the three-dimensional distribution of stiffness within the pelvis.

When a simple uniaxial joint force was imposed on the model, the stress distribution within the cement was dominated by the transverse contraction ('pinching') of the pelvis between the pubic and ischial columns. This led to localized areas of high stress that were alleviated by the presence of a metal-backing. With the simple loading, the metal backing shell reduced peak cement stresses by approximately 20% for a joint reaction force directed perpendicular to the rim of the cup, but less than 10% for the same force directed 30 degrees more superiorly. However, once physiologic loading was assumed, the presence of muscle forces changed the deformation pattern of the pelvis; bending was increased with less pinching of the cup between pubic and ischial columns. This caused an elevation of edge effects due to the discontinuity in bending stiffness associated with the rim of the shell. As a result, metal-backing caused the peak stresses in the cement to increase by 8 to 18% in the presence of physiologic loading. Under these conditions, the maximum stresses were observed around the peripheral rim of the mantle, both cranially and posteriorly (fig 7.12). These areas are almost exactly opposite the regions of maximum stress predicted by the earlier two-dimensional models.

7.3.3 Clinical Results of Metal-Backed Cups

Several clinical studies have examined the performance of metal-backed acetabular cups in cemented hip replacement. Harris from Boston developed the first metal-backed cemented cup in 1970, primarily for use

in younger patients. The original rationale for this design was that it modularity would allow the polyethylene insert to be replaced if it became excessively worn or deformed. Harris and White (1982) reviewed the results of fifty-three total hip replacements performed using this acetabular component. Only nine cases were personally seen by the authors, through pre-operative, post-operative and follow-up radiographs were available for all patients. At an average follow-up of 6.5 years (range: 5-9 years), two (6%) implants had been revised for aseptic loosening, and one additional implant was loose and had been scheduled for revision, making an overall incidence of loosening of 9%.

The authors attempted to prove that their study confirmed the superiority of metal-backing by comparing their results to those of another series performed by Dorr et al (1983) who reported a 30% incidence of failure in a small series of 43 cemented, non-metal backed components after the same post-operative period. This comparison is of doubtful validity given that the results of all cemented joint replacements depend to a large degree on several factors which went uncontrolled in this study, including the individual techniques of the surgeon (Cornell & Ranawat, 1986; Kobayashi & Terayama, 1990), the preoperative diagnosis (Snorrason et al, 1993) and the lateral tilt and bony coverage of the prosthesis (Sarmiento et al, 1990; Ritter et al, 1992). Furthermore, the authors did not perform a statistical analysis of their data, although it appears that the difference in their incidence of loosening (9%) and that of Dorr et al is large enough to be statistically significant. Nonetheless, experience with larger term studies since the work of Harris and White has shown that few cups generally fail within the first 8 years of surgery (Petrera & Rubash, 1994). This suggests that in series that have unusually high failure rates, the number of patients studied was relatively small (i.e. consisting of less than 100 subjects). This allows several exceptional cases to have a large impact on the apparent success of the procedure. Thus, the small series of Dorr et al has not proved to be representative of the true performance of cemented, non-metal backed cups, even in younger patients.

Ironically, Harris and Penenberg (1987) reviewed the same group of patients at an average of 11.3 years (range: 10 to 13.5 years) after their original operation and found that the total incidence of cups that had been revised or were radiographically loose had increased to 41%. Almost

all cemented cups implanted into patients of thirty years of age or younger had become loose, despite the presence of metal backing. The authors explained that the hazard function for loosening 'seemed to accelerate after five years'. Despite this high failure rate, the authors still contended that metal-backed cups were more durable than all-polyethylene components though they cautioned against the use of total hip replacement in the younger patient (thirty years or younger). This position was supported by the observation that only 15% of cups in patients older than thirty had been revised or were radiographically loose at ten year minimum follow-up. Again, as the authors reported no contemporaneous data from their own patients with non-metal backed prostheses, a meaningful assessment of the true impact of metal-backing is not feasible.

A study which attempted to compare the durability of all-polyethylene metal-backed components was performed by Ritter et al (1990) who implanted 238 cups between 1980 and 1983, 138 of which were metal-backed and 100 all-polyethylene. All procedures were performed by the same orthopedic surgeon using the same operative approach and cementing technique. The metal-backed component consisted of a titanium metal shell of 1.4 mm in thickness with a series of holes which allowed polyethylene stubs to protrude through the shell to a height of 2.6 mm to act as cement spacers. All cups were implanted with titanium alloy femoral stems with 28 mm femoral heads, also manufactured from titanium alloy. The authors followed all of their patients clinically and radiographically for an average of 5.2 years (range: 1 - 8 years). Each follow-up radiograph was evaluated for the presence of radiolucent lines at the bone-cement interface and for prosthetic migration of more than five millimeters.

There was no difference between the pain or function of patients with metal-backed and non-metal backed cups at follow-up. However, significant differences were present in terms of the incidence of complete radiolucencies (non-metal backed cups: 23%, metal-backed: 39%, $p = 0.0001$), migration of more than 5mm (non metal-backed: 2%, metal-backed: 4.4%, $p = 0.0001$) and revision (non-metal backed: 2%, metal-backed: 5.8%, $p = 0.0034$). These differences remained highly significant ($p = 0.001$) even when the data were corrected for the effects of the age of each patient, the thickness of cement and polyethylene and the lateral tilt

of the acetabular cup.

While it cannot be disputed that the metal-backed cups implanted by Ritter et al (1990) did have an increased incidence of aseptic loosening and failure, the relevance of these observations to contemporary designs of cemented hip prostheses is debatable. Firstly, titanium femoral stems are rarely used in cemented hip replacement because of release of metal oxide particles at the stem/cement interface secondary to micromotion of the implant within the cement mantle. This has been shown to lead to increased rates of loosening and wear (Lombardi et al, 1993). Similarly, titanium alloy heads are rarely used in any designs of hip replacement due to their poor performance in the presence of third body particles, particularly bone cement. While it may be argued that this factor is not relevant because all of the cases in this series had the same design of femoral prosthesis, it is possible that loosening of the metal-backed components was accelerated in the presence of metal and oxide debris due to accelerated abrasion of polyethylene at its interfaces with both the femoral head and the metal backing shell. This phenomenon has been observed in acetabular cups of similar construction implanted without cement (Huk et al, 1994).

Secondly, many of the metal-backed cups of Ritter et al showed evidence that loosening originated at the junction of the polyethylene spacers with the metal shell, presumably due to micromotion and generation of polymeric debris. This mode of failure is comparable to the loosening of all polyethylene acetabular cups of the RM design which were implanted without cement (Wilson-MacDonald et al, 1990). These implants performed well for the first six years post-operatively but then failed rapidly at six to nine years due to abrasion of the outer surface of the cup at points in direct contact with bone. At nine years, the survivorship of these components was only 71% (Wilson-MacDonald et al, 1990).

Thirdly, since the publication of the reports of metal-backed cups by Harris and Penenberg (1987) and Ritter et al (1990), much has been learned about the etiology of aseptic loosening of cemented acetabular prostheses that was not appreciated by the advocates of metal-backed components. Studies performed by Schmalzried et al (1992) have shown that loosening of cemented cups occurs secondary to the biological response of the cement/bone interface to wear debris and is not primarily mechanical in

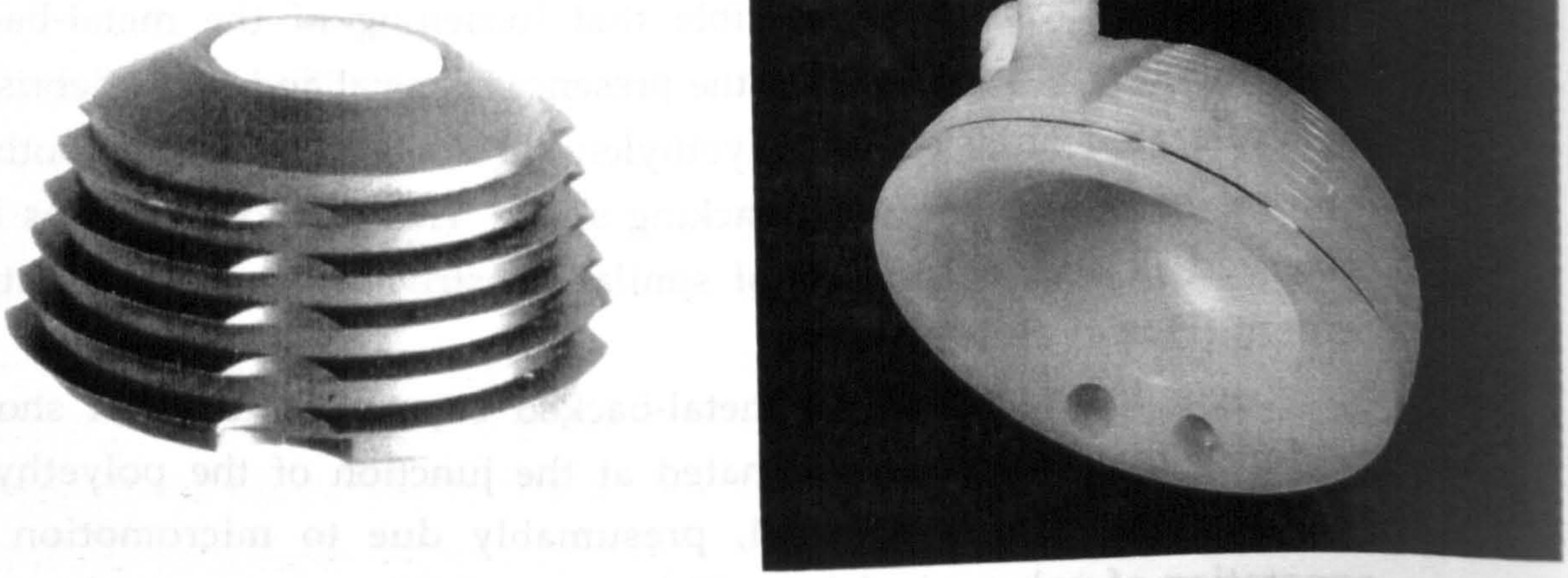

Figure 7.13 Early designs of cementless acetabular cups. The truncated threaded design (left) consisted of a threaded metal shell with a polyethylene insert. The RM prosthesis (right) consisted of a single piece polyethylene component with two parallel pegs to enhance stability.

origin. For this reason, it is unlikely that differences in the durability of metal-backed and all-polyethylene components can be explained in mechanical terms; it is far more likely that design features of the metal-backed components led to increased production of polyethylene debris with accelerated loosening of the cement/bone interface as the result. It remains to be seen whether the most recent designs of metal-backed acetabular cups, if fixed within the acetabulum with cement, would loosen at a greater rate than non-metal backed components of the same design.

7.4 CEMENTLESS FIXATION OF ACETABULAR PROSTHESES

7.4.1. Introduction

Due to the variable outcome of cemented acetabular fixation and the massive loss of bone often associated with loose cemented cups, there have been numerous attempts to develop methods of direct attachment of acetabular shells to the skeleton without an intervening layer of acrylic cement. This has led to a variety of implant designs, including: (i) polymeric shells with integral anchoring posts, (ii) metal shells with a conical or cylindrical outer profile, and (iii) metal shells with peripheral screw threads for immediate fixation within the acetabulum (fig 7.13). Although authors have claimed excellent short-term results for all these designs, few have performed acceptably at 5-10 years post-operatively. In many cases, observations showed excessive, progressive migration and tilting which was not always associated with clinical failure until migration became extreme and reoperation imminent. Histologic examination of tissues obtained at reoperation confirmed the presence of a thick fibrous membrane at the implant/bone interface indicative of unstable fixation (Schmalzried et al, 1994; Bono et al, 1994; Tallroth et al, 1993; Bobyn et al, 1988; Fox et al, 1994).

These experiences have led to the emergence of hemispherical, porous-coated prostheses as the most reliable solution to cementless acetabular replacement available for general use. In the United States the use of these components has become widespread within the last decade, to the point that implants of this type are now used more commonly than any other design, out-numbering cemented acetabular cups by a factor of ten. Up until the present day, the clinical performance of hemispherical

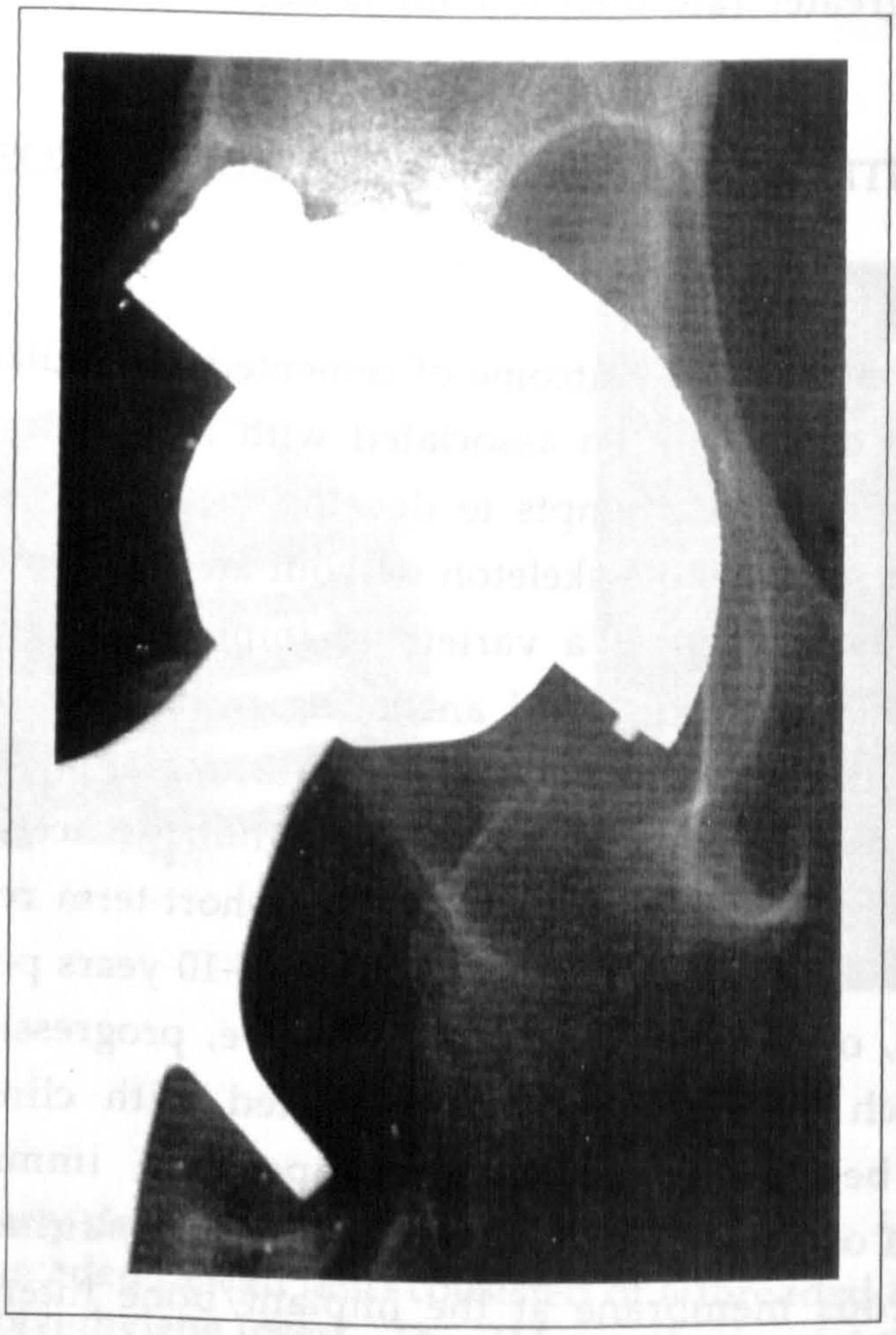

Figure 7.14 An AP radiograph taken only 3 years after placement of a cementless acetabular cup. A large osteolytic defect is present in the ilium, superior to the acetabular dome. The femoral head is eccentrically located, suggested considerable wear of the UHMWPE.

cementless prostheses has been most encouraging, based upon reviews performed at up to eight years postoperatively. In most series, the incidence of groin pain, a symptom traditionally related to cup instability, has been very low; the radiographic appearance of most components at follow-up has also been suggestive of stable bony fixation. However, several authors have shown that the radiologic appearance of the cementless implant/bone interface can be extremely misleading as only a 'sky-line' view of the interface is visible on any one radiograph (fig 7.13). Moreover, the presence of a significant thickness of bone both in front and behind the prosthesis obscures visualization of fibrous ingrowth which appears superimposed on normal cancellous bone. Consequently, fibrous membranes can be masked by superimposed bony images which may mimic bony attachment to the surface of the prosthetic component.

Another peculiarity of acetabular radiographs is that most cementless components migrate slightly during the first 12 months of implantation before a stable position is established within the acetabulum. Thus, the distinction between a stable and unstable prosthesis is a question of the magnitude and the time-course of component migration rather than its presence. However, even when acetabular shells migrate, they generally move into gaps formed at the interface, and so an unstable cup may migrate for several millimeters before a fibrous zone becomes radiographically visible.

Another consideration is the response of the bone/cup interface to wear debris (fig 7.14). Histologic evidence derived from implant retrieval studies of cemented acetabular cups suggests that aseptic loosening may occur in response to polyethylene wear debris and not to acrylic cement. It has been postulated that when a fibrous membrane is present at the cement/bone interface, polyethylene particles accumulate and are ingested by macrophages. After ingesting foreign body particles, these cells excrete activating agents that can trigger rapid osteoclastic activity at the interface with progressive loss of bone from around the prosthesis. If this process is an inevitable response to polyethylene wear debris, osteolysis of the implant/bone interface may become a common complication of all arthroplasties performed in young and active individuals, regardless of whether the acetabular cup is implanted with or without acrylic cement. Moreover, as the fibrous membrane appears to facilitate transport of particles around the cementless interface, efforts to

maximize bony attachment may lead to greater biologic durability of cementless components.

7.4.2 Bony Fixation of Cementless Prostheses: The Effect of Interface Motion

Cementless prostheses develop durable fixation within the bony acetabulum through two basic mechanisms:

(a) Initially, almost all stability of the cup/bone interface is gained from the mechanical interlock of the acetabular shell within the implantation site. The outer surface of most prostheses is mechanically augmented with threads, fins, or rough surface coatings to increase the mechanical stability at the interface. The presence of these features is thought to reduce the motion occurring between the shell and the acetabulum sufficiently to allow attachment of biological tissues to the prosthesis.

(b) After several months within the body, tissue grows into gaps between the reamed acetabulum and the metal shell and into the surface of the shell itself if a porous coating is present. Initially, fibrous tissue is present which then forms immature bone. If the motion of the interface is small enough, the bone matures and becomes more mineralized. With this process, the stiffness of the interface progressively increases, thereby reducing the motion of the implant and increasing its resistance to mechanical disruption

Little is known about the interaction between osseo-integration of the cup/bone interface and its susceptibility to osteolysis. It is widely believed that implants fixed by bony ingrowth will be the most stable in the long-term and that, within the pelvis, ingrowth will not cause adverse remodeling due to changes in the pattern of loading of periacetabular bone. However, the interplay between mechanical and biologic factors within the acetabulum has not been studied in detail. Much remains to be discovered about the factors mediating stable tissue attachment to porous surfaces and to the mineralization of the prosthetic interface.

The major factor determining the type of tissue present at the bone/implant interface appears to be the magnitude of interfacial

movement during the immediate post-operative period. Pilliar et al (1986) reported the results of experiments performed with porous coated segmental replacements implanted in the femora of adult beagle dogs. Each implant consisted of a porous coated intramedullary rod of 5 mm in diameter and approximately 3.5 cm in length. These implants were undersized with respect to the intramedullary canal, so that gaps were present between the implant surface and the cortical walls of the femur. One year after the rods were implanted, the animals were sacrificed and their femora were harvested for mechanical testing of the implant/bone interface. The displacement of each rod was measured under axial loads ranging from 20 N tension to 20 N compression at 37°C in physiologic saline. After testing, histologic sections were prepared of each specimen and examined to determine the type of tissue present at the implant interface.

With the application of 20 N of compression and tension, the apparent displacement of the specimens with direct bony attachment did not exceed 28 μm. In comparison, specimens fixed with fibrous tissue underwent deflections of 100-220 μm in compression and 50-310 μm in tension, depending upon the density of the tissue and the alignment of its fibers with the surface of the implanted rod. However, even in the case of the stiffest fibrous interface, the total displacement of the interface was 150 μm under less demanding mechanical conditions than those generated by normal weight-bearing.

In a second series of experiments described in the same publication, Pilliar et al placed porous-coated endodontic implants through the root canals of mandibular teeth of five adult dogs. In each animal the implant was rigidly fixed within the tooth and was free to move within the underlying alveolar bone during normal loading of the tooth, which previous studies had shown to be approximately 22 μm (range: 11 - 90 μm). Despite the presence of initial motion of the implant/bone interface, bony ingrowth occurred into the surface of each porous implant, again suggesting that small degrees of micromotion may be tolerated without loss of bony fixation. These experiments support the conclusion that motion at the interface determines the type of tissue growing into a porous surface and suggest that while displacements of around 20 μm, and possibly as large of 90 μm, will not hinder bony ingrowth, larger displacements of 150 μm or greater will lead to attachment of the porous

surface by a layer of well-organized, fibrous connective tissue.

Burke et al (1993) developed a method to apply controlled amounts of micromotion to the porous-coated implants in vivo using a motorized platform which produced cyclic displacements equivalent to 0 - 350 μm of interface motion at 0.5 Hz. Pins of 7 mm in diameter were fabricated with a coating of titanium fiber-mesh and implanted in the distal femora of 20 dogs. The animals were divided into four groups which received 0, 20, 40 and 150 μm of cyclic micromotion delivered by a motorized device for 8 hours per day for a period of 6 weeks. The torque required to rotate each pin was continuously monitored and after six weeks all dogs were sacrificed.

Histological examination of the pin/bone interface showed that in the groups with 0 and 20 μm of interfacial motion, mature trabecular bone and normal marrow products were present throughout the fiber mesh coating. In the 40 μm group the porous mesh was occupied by trabecular bone in continuity with the surrounding bone with patchy areas of fibrocartilage and fibrous tissue which bridged the interface. Trabecular microfractures were present in some areas with bridging fibro-callus. In the 150 μm group, a dense layer of fibrous tissue surrounded each of the coated implants and while bone was present within the mesh coating, it had no continuity with surrounding bone. Interestingly, there was no difference between the amount of bone present within the mesh coatings of all four groups of implants. This study suggests that immature bone is able to grow across moving interfaces which undergo displacements as large as 150 μm, but that as the bone matures, calcification causes the trabeculae to fracture, leading to formation of a fibrous membrane which is better adapted to the dynamic environment present at the interface.

One of the most interesting facets of this study was that it was possible to directly observe the motion of the pin/bone interface by attaching the motorized platform to each specimen at necropsy. Using a high resolution dissecting microscope, the investigators confirmed that in the 20 μm specimens there was minimal slippage at the interface under load and that elastic deformation of trabeculae was visible for a distance of up to 5 mm from the surface of the implant. In contrast, at 40 μm of micromotion, areas of slippage were present between the implant and the bone, interspersed with regions of continuity within the trabecular

structure which acted in the same manner as the 20 μm group. In the 150μm specimens, most of the applied motion translated to slippage between the porous coating and the bony matrix within the encapsulating fibrous membrane.

Some preliminary observations were reported by Hollis et al (1993) who developed an animal model for studying the effects of micromotion consisting of a cylindrical porous-coated (beaded) titanium plug implanted transcortically into the femur of a dog. The size of the beads was not reported. In their initial study, four plugs were implanted in the right and left femora of four animals. Each plug was rotated by 25, 50, 100 and 200 μm (total excursion) for 10 minutes, twice a day for four weeks using a D.C. motor. The plugs in the contralateral limb were not rotated and were treated as controls on the assumption that (i) the animals would not have preferred one limb over the other and (ii) differences between the ipsilateral and contralateral response could be attributed to different levels of interface motion and not differences in a generalized response to implantation. After the 4-week period all animals were sacrificed. Curiously, the plugs that were not displaced showed the least amount of bony ingrowth (<50%), while all specimens that underwent 25 - 100 μm of motion displayed 85-90% of ingrowth (fig 7.15). The implants with 200 μm of micromotion had significantly less ingrowth than all but the control group. Interfacial motion also influenced the ingrowth of bone into smallest pores within the beaded coatings. At 100 and 200 μm of motion, bone was present within the larger pores but did not extend to the surface of the substrate. Similar observations were made at 50 μm although bony ingrowth occurred in large and small pores within the ingrowth surface. Complete incorpora-tion of bone within the porous layer was only observed within the 25 μm group in which bone invaded the entire depth of the ingrowth coating.

Although in this study, application of 200 μm of motion for 20 minutes each day caused disruption of bony ingrowth, this observation provides little insight into the effect of a given level of micromotion for a prolonged period e.g. 12 hours/day. Given the limited duration of motion in this study, it is probable that much of the disruption caused by movement of the interface was repaired during the stationary periods between applications of surface displacement.

On the basis of these studies, it appears that, within the dog, the optimal mechanical conditions for bony ingrowth into porous coatings

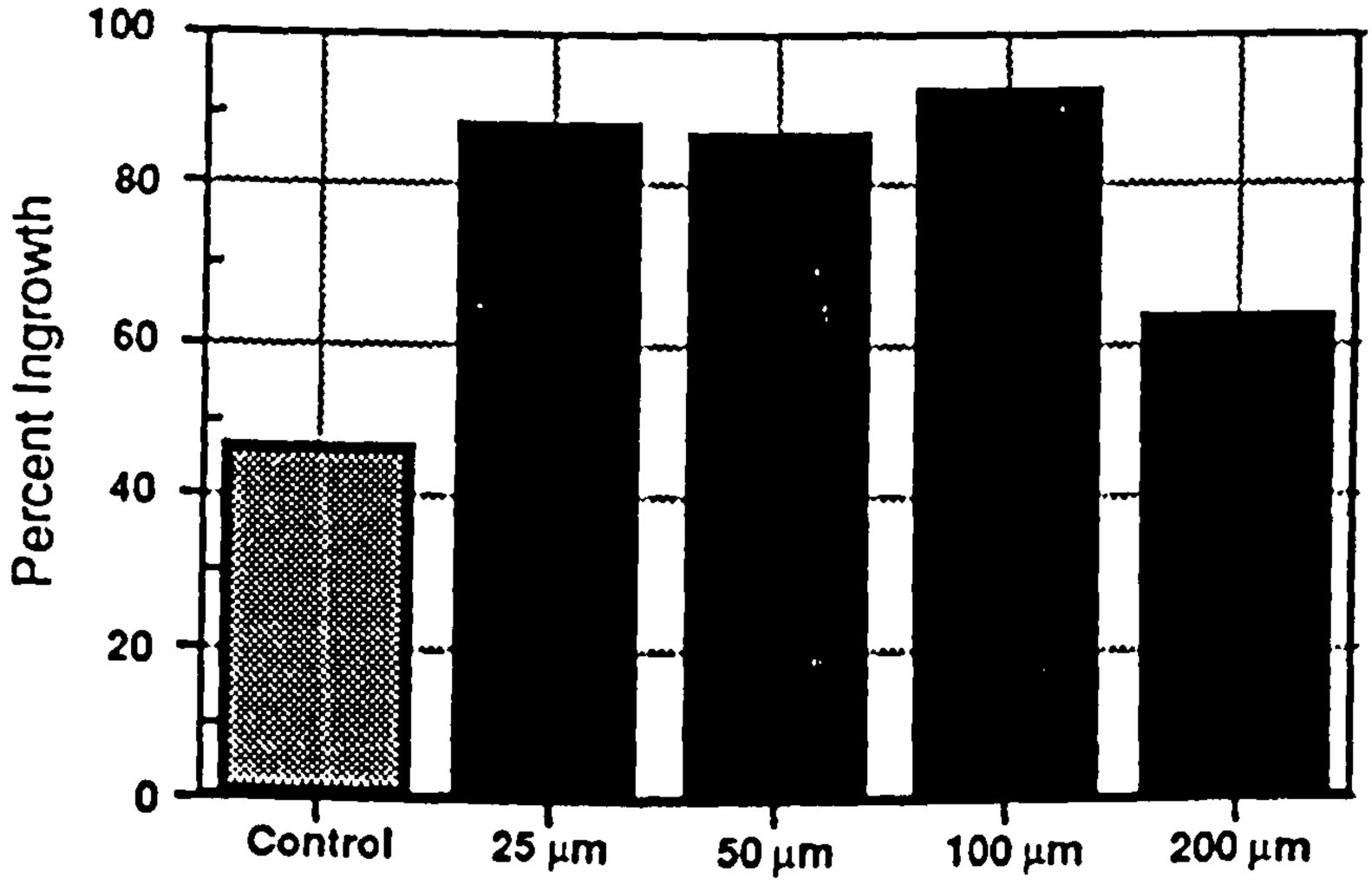

Figure 7.15 The extent of bony ingrowth into cylindrical porous-coated plugs implanted into canine femora and subjected to different amplitudes of interface displacement (from Hollis et al, 1993).

include relative motion at the implant/bone interface of 40 μm or less. This is considerably lower than the value of 100 μm which has been widely quoted without any real clinical or experimental basis. Although this value cannot be extended to humans without qualification; it is unlikely that the threshold for micromotion is any higher in human bone, especially in the older patient, as previous experimental studies have demonstrated that bony ingrowth is generally far more extensive and consistent in the canine than in the human. While previous studies have reported bony ingrowth into 30-60% of the available porous surface (Harris et al, 1983; Spector et al; 1978) of canine prostheses, values of 5-15% appear typical of human retrievals. Moreover, additional factors including age, pathologic conditions and the use of anti-inflammatory medications may also profoundly diminish the rate and extent of bony attachment to cementless prostheses (Rivero et al, 1987; Spector, 1987).

7.4.3 Retrieval Analysis of Cementless Prostheses

In several studies, the tissue present at the implant/bone interface has been characterized through examination of prostheses retrieved at revision or following the demise of the patient (Cook et al, 1988; Collier et al, 1988; Pidhorz et al, 1993; Engh et al, 1993). Cook et al (1988) studied 36 total hip components, including 14 acetabular prostheses of four different designs (AML, PCA, LSF, Harris-Galante) retrieved after an average of 5.5 months (range 1-18 months) in situ. Histological analysis and microradiography showed that most of the porous interface was filled with adherent fibrous tissue. In eight of these components there was no bony ingrowth, while in one additional instance bone was present in less than 5% of the porous-coated surface. More bony attachment was seen in the femoral components, although this never exceeded 10% of the surface available for ingrowth. Most of the bone which grew into the surface of the acetabular shells was seen in the vicinity of screw holes in which screws had been present to augment fixation. In some cups, ingrowth was observed around other adjunctive features, including pegs or spikes which were an integral part of some shell designs. In all cases, the most common location of bony attachment was in the superior-lateral quadrant of the acetabulum.

In a similar study, Collier and coworkers (1988), presented the results of histological analyses performed on 162 cementless components (104

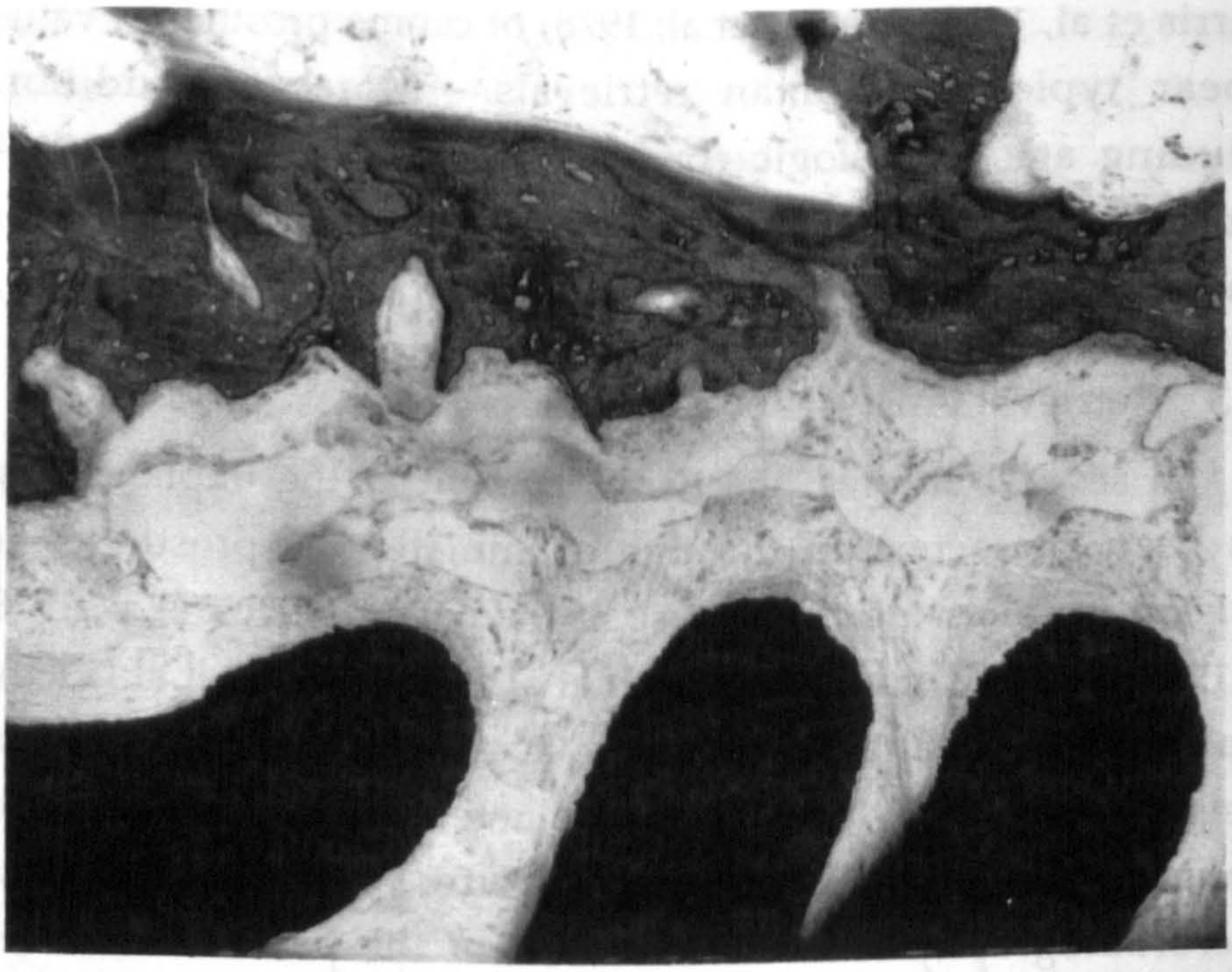

Figure 7.16 Histologic section of an acetabular component retrieved 54 months after implantation demonstrating fibrous attachment. The interfacial membrane contained moderately dense connective tissue without histiocytes, plasma cells, or lymphocytes. Note the vascularity of this tissue and the reactive bone front (original magnification X 120) (from Pidhorz et al, 1993).

femoral stems and 58 acetabular cups) which had been explanted for pain, loosening, infection or malposition. Although the authors did not present their histological observations as a function of the cause of implant retrieval, only 16% of the acetabular prostheses showed any evidence of bony ingrowth. However, the thickness and morphology of the adherent fibrous tissue varied considerably between specimens. In many cases which were revised because of pain or loosening, the prosthesis was covered with a thick layer of highly organized fibrous tissue with evidence of osteoclastic activity. The studies of both Cook et al and Collier et al demonstrate that:

(i) the presence of bony ingrowth does not guarantee a painless prosthesis,

(ii) fibrous attachment is a universal observation in cementless prostheses, and

(iii) in many cases, fibrous tissue provides the only form of fixation of the shell to the acetabulum.

Recently, Pidhorz et al (1993) studied eleven cementless acetabular components retrieved at autopsy, all of the Harris-Galante design (Zimmer, Warsaw, Indiana, USA). They determined the degree of tissue ingrowth into the porous fiber-mesh surface of the implant and assessed the reaction of the implantation site to metal and polymeric debris generated at interfaces between the shell, the screws and the liner. All components were implanted using adjunctive screw fixation; the period of implantation ranged from 5 weeks to 75 months (average: 41 months). The authors prepared five cross-sections of each component after embedding in polymethylmethacrylate and examined the tissue within the porous surface. Adherent and ingrown tissue was classified as either bone, marrow, cartilage, fibrous tissue or necrosis at four different levels within the depth of the coating. Bony ingrowth was quantified using two measures: the volume fraction of void space occupied by mineralized bone and the extent of ingrowth, defined as the percentage of all micrographic fields containing some bone.

Of the eleven cups examined, ten had some bone grown into the coating; however, the volume fraction of bone varied widely between specimens from 0.8 to 27.6% with a mean value of 12.1 ± 8.2% (fig 7.16). The extent of bony ingrowth averaged 29.7 ± 20.1% (range 0 to 55.0%) at the interface but decreased dramatically throughout the depth of the

coating to only 5.4 ± 8.2% at the surface of the substrate. Curiously, there was no correlation between the amount of ingrowth and the period of implantation. Moreover, variations in the degree of ingrowth from point to point over the surface of the implant were not found to be statistically significant (periphery: 29.1 ± 26.7%, remainder of the surface: 19.0 ± 15.2% $p > 0.05$). This is not entirely surprising as the diameter of each of the shells was matched to the size of the last acetabular reamer with the addition of screws to augment the initial stability of the shell/bone interface. Consequently, one would not expect preferential contact between the acetabulum and the periphery or the dome of the implant.

The one factor that had a significant effect on the extent of bony ingrowth was the use of screw fixation; there was approximately 50% more ingrowth adjacent to holes which had been used for screw placement than holes which had been left empty (extent of ingrowth within coating: 34.7 ± 34.0% (screws) vs. 19.5 ± 16.0% (no screws), $p < 0.05$). Moreover, histological examination of the tissue surrounding the retrieved components showed that foci of fibrocartilage were present at points over the interfaces of ten of the eleven specimens examined, but never adjacent to fixation screws. These findings speak to the important influence of screws in stabilizing the interface by reducing micromotion and, possibly, in reducing the width of any gaps between the shell and the reamed bony surface.

In another retrieval study, Engh et al (1993) examined nine porous-coated acetabular components retrieved at autopsy after an average period of implantation of 50 months (range: 17 to 87 months). All prostheses were obtained from patients whose prosthetic hips were functioning well at the time of their death. Three different designs of prostheses had been implanted at a single institution with extensive experience in cementless hip arthroplasty. Six prostheses consisted of a porous coated titanium shell with rim holes for peripheral screw fixation, and a modular polyethylene liner (Arthropor design (Joint Medical Products, Stanford, Connecticut, USA: 3 implants); Trilock design (DePuy, Warsaw, Indiana, USA: 3 implants)). A further 3 implants were of the AML design (DePuy, Warsaw, Indiana, USA) consisting of a porous coated cobalt-chromium shell with three integral porous-coated spikes and a fixed polyethylene liner. In this design the liner was pre-attached to the shell by the manufacturer.

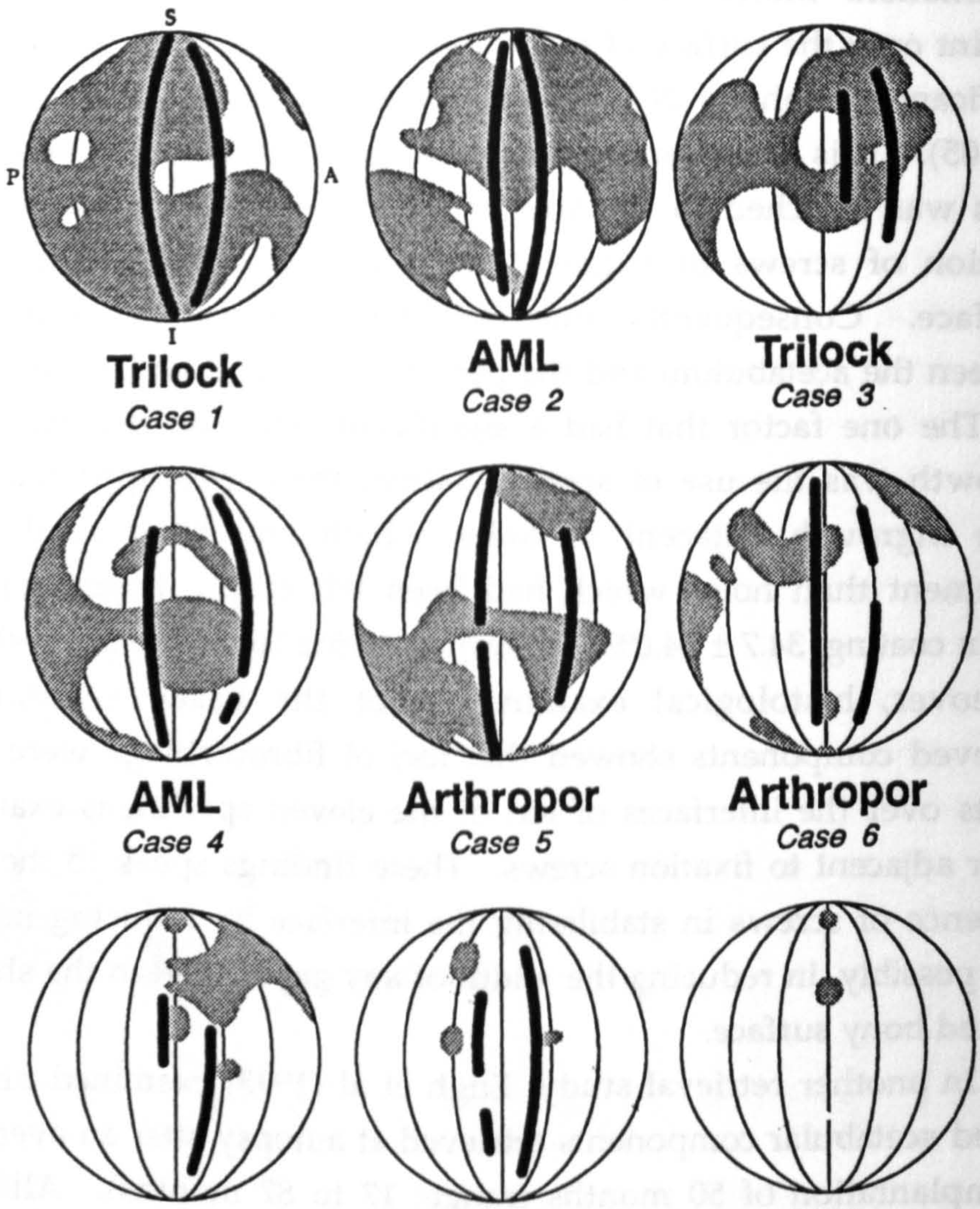

Figure 7.17 Distribution of bony ingrowth over the surface of nine cementless cups examined by Engh et al (1993). Areas of bony contact or bony ingrowth have been combined and are represented by the shaded regions, while areas in which neither bone contact nor ingrowth was seen histologically are represented by white spaces. The solid black lines represent areas where a shell/bone radiolucency was not visible on radiographs. S = superior, A = anterior, and P = posterior.

Each of these implanted specimens was fixed, embedded in ethylmethacrylate and cut into six, wedge-shaped sections. Thin sections, cut from the surface of each wedge were examined using back scattered scanning electron microscopy to determine the extent of bony ingrowth into the porous coating of each prosthesis. These measurements showed that most of the interface was ingrown with dense fibrous tissue, and an average of only 13% (range: 1-36%) of the porous surface was ingrown with bone (fig 7.17). Curiously, there was no demonstrable relationship between the duration of implantation and the amount of bony ingrowth. Moreover, the extent of ingrowth did not vary as a function of position on the surface of the acetabular shell. Though there was no difference between the ingrowth in the weight-bearing and non-weight-bearing areas of the interface, a peripheral zone of fibrous fixation was most common when the subchondral plate had been retained during reaming. In these cases, remnants of articular cartilage were often observed between the shell and the acetabular margin, suggesting that reaming of the original acetabulum had been inadequate. A surprising observation was that even in the prosthesis with the most bone ingrowth, direct fibrous communication was present between the rim and the floor of the acetabulum.

None of the specimens showed evidence of granulomatous tissue or the presence of foreign bodies, including polyethylene debris. This is not surprising, given that the duration of implantation of these prostheses averaged only 50 months and that osteolytic lesions have been reported in only about 5% of cementless acetabuli at 5 years in comparison with 20% at eight years postoperatively (Beauchesne et al, 1992; Schmalzried et al, 1994).

7.4.4. Clinical Results of Cementless Acetabular Cups

In the United States, hemispherical, porous-coated acetabular cups have been in widespread clinical use for approximately eight years and so meaningful clinical reports documenting the performance of these devices are now starting to appear. Recently, Engh and co-workers reported on the radiographic results of 115 porous-coated acetabular cups of the AML design implanted for an average follow-up of 7.5 years. Radiolucent gaps at the cup/bone interface were observed on the first post-operative radiographs of 63% of cases, though these gaps only

progressed in 11% of cases. Only two implants (1.7%) had circumferential radiolucencies indicative of mechanically unstable fixation.

The major observation of this study was that osteolysis occurred relatively frequently within the acetabulum (15%) and the proximal femur (23%). Though revision was uncommon, the progressive nature of the osteolytic changes suggests that a significant proportion of these implants may fail in the future. This conclusion is consistent with the clinical performance of the early generations of cemented acetabular components in which failure increased exponentially after about the eighth year of implantation. A statistically significant finding of the study of Engh et al was an association between the occurrence of osteolytic lesions and the change in position of the femoral head within the acetabulum, primarily due to wear of the polyethylene liner. This is consistent with the assumption that polyethylene wear debris provokes resorption of bone through stimulation of macrophages and osteoclasts.

Several authors have presented results from the acetabular cups of the Porous Coated Anatomic (PCA) design. In 1988, Callaghan et al reported a consecutive series of 47 patients in whom 50 PCA prosthesis were implanted and reviewed after a minimum follow-up of two years. Through analysis of sequential radiographs, the authors attempted to measure migration of the acetabular components within the pelvis. Changes in the vertical position of the prosthesis were measured with reference to a line connecting the inferior aspects of the contralateral and ipsilateral teardrops (the radiographic image of the floor of the acetabulum in the vicinity of the cotyloid notch). Horizontal migration was defined as the change in the distance between the center of the cup and a vertical line drawn through the center of the ipsilateral teardrop. The inclination of the cup from the horizontal was also measured and all radiodense lines surrounding the acetabular shell were noted.

At follow-up, radiolucent lines were present over the central third of the acetabular surface in 20% of cases, although progression of radiolucencies was observed in only one case. No lines were present over the superior third of the cups, though lines were visible in the inferior third in 52% of cases suggesting vertical cup migration. In 12% of prostheses, the width of these radiolucent lines increased on successive radiographs, though a change in the migration of the cup was detected in only one case (2%). Eighteen percent of acetabular components also

showed evidence of loss of beads from the porous coating. These observations indicate that fixation of many of these components was not stable, leading to settling of the implant within the implantation site. This conclusion is confirmed by the studies of Karrholm and Snorrason (1992) using roentgen stereophotogrammetry. They followed the motion of 22 implanted cups for a period of two years postoperatively and found that all components migrated by approximately 500 μm in a superolateral direction after implantation. In over half of the cases studied, these motions were associated with the development of progressive radiolucencies.

Heekin and colleagues (1993) extended the original study of Callaghan et al by reviewing 100 cases of PCA hip prostheses at five to seven years postoperatively. At follow-up, two of the acetabular components had been revised. Both were loose and had excessive wear of the polyethylene liner and, in one case, substantial loss of acetabular bone secondary to osteolysis. A disturbing finding was that in 6% of cases, acetabular migration exceeded 5 mm horizontally or vertically. In addition to the two cases revised for frank failure, a further fifteen percent of implants had progressive radiolucencies of the implant/bone interface suggestive of loosening some time in the future.

In a similar series Kim and Kim (1993) followed 116 consecutive PCA prostheses for a minimum of 6 years (range: 6 to 7.5 years). Aseptic loosening of the acetabular cup was observed in three patients. Moreover, in 20 cases excessive polyethylene wear was noted, ranging from 5 to 11 mm. This corresponded to an average wear rate of 1.3 mm/year (range: 0.88-1.93), approximately ten times that of other series (Pedersen et al, 1995; Joshi et al, 1995). In ten patients (9%) osteolytic lesions of the acetabulum were identified on follow-up radiographs. The area of bone affected by osteolysis varied from 10 to 75 mm in diameter and in one case involved the entire superior pubic ramus. These observations are disturbing, given that plain radiographs significantly underestimate the severity of osteolytic lesions within the acetabulum (Maloney et al, 1993)

Schmalzried and Harris (1992) reviewed the clinical and radiographic results of the Harris-Galante porous coated acetabular component. This implant consisted of a modular polyethylene liner and a titanium-alloy hemispherical shell. The external coating of the shell consisted of

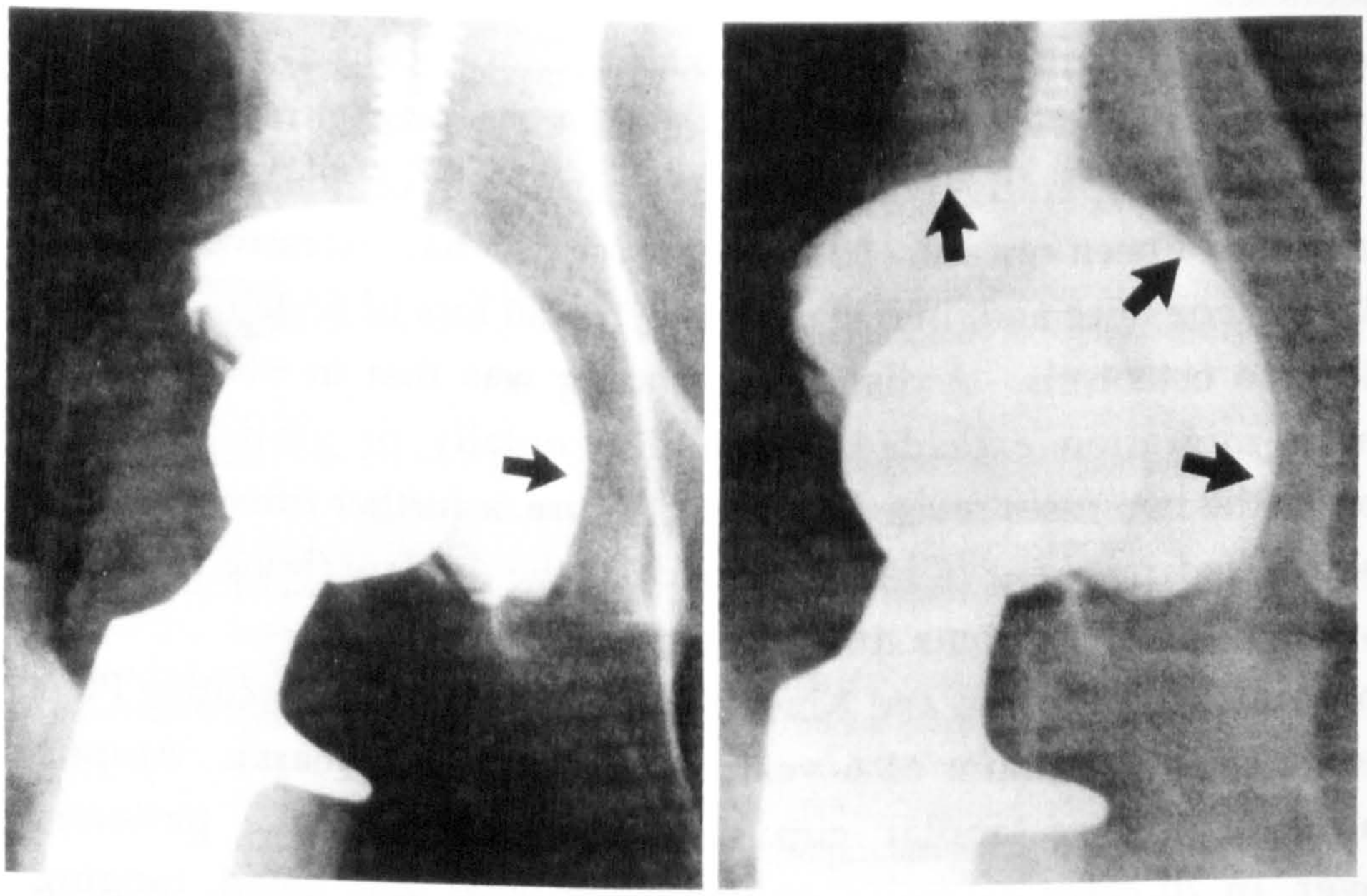

Figure 7.18 A case reported by Schmalzried et al (1992) in which a porous coated titanium cup demonstrated evidence of excellent circumferential contact with bone on the early postoperative radiograph (left). However, after 67 months, bony contact was absent in all zones of the interface (arrows), with the appearance of a thin, continuous radiolucent line.

sintered titanium fibers compressed to form a mesh with a random fiber orientation and interstices of suitable dimensions to support bony ingrowth. Multiple holes were present within the shell to allow initial fixation using cancellous bone screws. Eighty cases (eighty-three hips) were reviewed with a follow-up of 68 months (range: 5 to 7 years). In all cases, the shell was implanted "line-to-line" with the reamed acetabulum, in the sense that the outer diameter of the acetabular shell matched the nominal diameter of the reamer used to prepare the acetabulum, with no preset level of interference between the shell and the implantation site. In each case, two to five screws were used to fix the shell within the acetabulum.

Four of the acetabular components (5%) were revised prior to follow-up; two due to disassembly of the polyethylene liner from the shell, one due to metallosis secondary to contact between one of the titanium screws and a stainless steel fracture fixation device, and another due to osteolysis around one of the acetabular screws and loosening of the femoral stem. At follow-up, none of the components demonstrated migration which could be detected by plain radiography, and radiographic evidence of osteolysis was only present in one case. However, progressive development of radiolucent zones occurred in a significant number of components (fig 7.18). On the immediate postoperative films, gaps were visible at the bone interface of 41 cups (49%), almost always at the perimeter of the component. At two years post-operation, one quarter of these gaps were no longer visible, due to settling of the component or formation of bone at the original interface, and in the remaining cases, the gaps were unchanged (fig 7.19). However 49 cups (58%) had new radiolucencies, predominantly distributed in peripheral zones. In approximately half of these cases (22 hips, 27%), the radiolucencies were progressive and were larger on the five year follow-up radiograph, although no component had a continuous radiolucent line.

There was an interesting correlation between the presence of initial gaps at the cup/bone interface and the development of progressive radiolucencies. In this series, of the 42 components without peripheral gaps, only six (14%) went on to develop progressive radiolucent lines, whereas progressive radiolucencies were noted in 39% of components with a peripheral gap on the first post-operative radiograph ($p < 0.025$). This suggests that the gaps themselves may dispose acetabular cups to

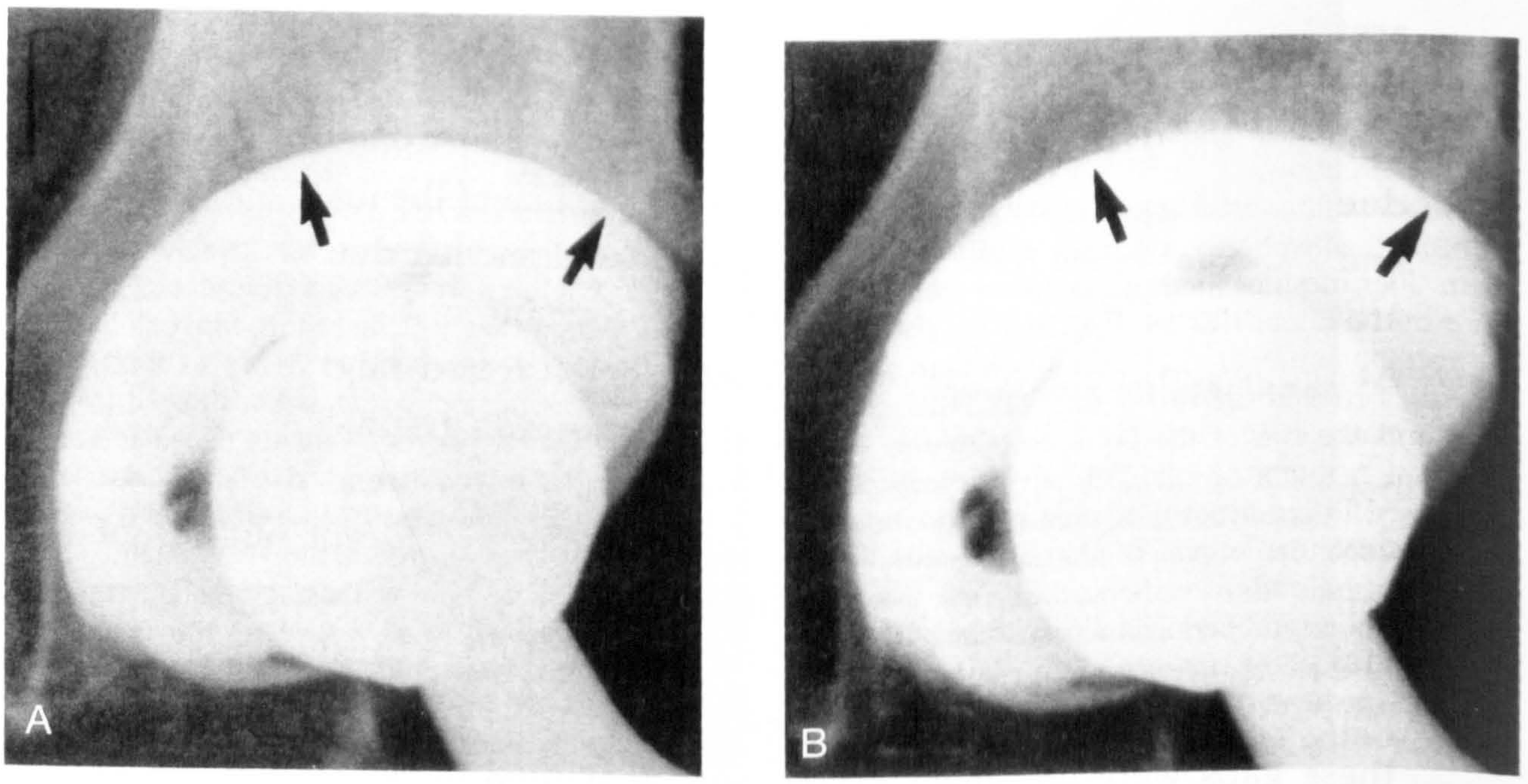

Figure 7.19 Typical radiographic appearance of a cementless acetabular cup, postoperatively (A) and at follow-up (B) as reported by Schmalzried et al (1994). Initially (A), small gaps between the porous mesh and bone are indicated by radiolucent lines (arrows). At two years post-implantation, complete resolution of the gap in zone 2 has occurred with partial resolution of the gap in zone 1. The appearance of this interface on the 5-year follow-up radiograph was unchanged.

formation of radiolucent lines, either by increasing the micromotion of the shell within the bone or by acting as a pathway for entry of polyethylene debris. Alternately, the gaps, per se, may not directly cause instability but may indicate that a component was implanted using sub-optimal surgical technique, possibly including enlargement of the implantation site during reaming or displacement of the implant during tightening of the cancellous screws.

CHAPTER 8 THE BIOMECHANICS OF CEMENTLESS CUP FIXATION

8.1 THE OPTIMUM METHOD OF INITIAL FIXATION OF CEMENTLESS ACETABULAR CUPS

The fundamental design objective of contemporary cementless acetabular components is to achieve the maximum area of bony attachment to the surface of the shell in the shortest possible time post-operatively. This is only possible if the displacement of the cementless interface that occurs with weight-bearing is limited to approximately 40 μm. Previous clinical experience suggests that this degree of immobility can be achieved at some points over the cementless acetabular interface if the acetabulum is reamed to a hemispherical shape and the matching prosthetic component is mechanically fixed to the acetabular bed with lag screws. Some have advocated implantation of acetabular shells 1 to 4mm larger than the reamed acetabulum in order to avoid the use of screws. As the oversized shell is driven into the socket the acetabulum is deformed, primarily through separation of the anterior and posterior walls. This deformation generates a compressive reaction force at the bone/metal interface, thus providing resistance to motion.

Although this mode of implantation is appealing to the surgeon and minimizes the duration of the operative procedure, it has a number of disadvantages. Firstly, fitting of oversized cups causes large, localized stresses within the acetabular rim which could result in a fracture, especially in the presence of mechanically compromised or osteoporotic bone (Curtis et al, 1992). In practice, bony defects may be present if the socket has been over-reamed or if cement has been removed in preparation for revision arthroplasty. In these situations, stable fixation is unlikely if an oversized prosthesis is impacted into the acetabulum. Secondly, bone responds visco-elastically to loading. Thus, with time, the expanded acetabulum will relax, causing a gradual decline in the compressive forces developed between the shell and the bone. This will lead to a reduction in the resistance of the interface to micro-motion and may also compromise the fixation of the prosthesis. At present it is not known how rapidly the reaction forces generated by mechanical interference are dissipated, however, if biological fixation of the prosthesis is impaired, micromotion of the implant may increase to the

point that activity provokes pain and the clinical success of the replacement is compromised.

A third factor influencing the selection of the optimum method of acetabular fixation is the practical difficulty of obtaining a close fit between the shell and the bony socket. In practice, although the surgeon attempts to create a hemispherical cavity to match the profile of the prosthetic component, the interface between the cup and the acetabulum consists predominantly of gaps with interspersed regions of localized contact. This appearance is due to the fact that the acetabulum is ellipsoidal and is composed of non-homogeneous bone; this makes it extremely difficult to machine the acetabulum to a perfect hemisphere as the reaming instrument tends to cut preferentially into softer areas of bone, leaving an enlarged cavity (Engh et al, 1992).

An additional factor is the elastic anisotropy of the socket itself. During implantation of the acetabular shell, the acetabulum deforms non-uniformly as areas of soft bone are plastically deformed leaving any remnants of the subchondral plate to resist compression. This is expected to lead to non-uniformity in the deformation of the acetabulum and the distribution of contact stress at the shell/bone interface. There are two possible consequences. The shell may be held predominantly at only two points on opposite sides of the acetabular rim leading to instability with loading. This will prevent stable implant fixation from developing under repetitive, weight-bearing conditions. Alternatively, excessive interfacial stresses may be generated by highly localized shell/bone contact leading to osseous remodeling and dissipation of the compressive forces necessary to stabilize the interface. This phenomenon was observed in earlier designs of cementless acetabular prostheses with large circumferential threads which were screwed into the acetabular bed. The torques employed during implantation of these devices often caused development of large, localized stress at the tips of the first and last threads embedded within the bone. Although these components demonstrated substantial intraoperative rigidity, post-operative loosening was common with the formation of an extensive fibrous membrane between the threaded periphery of each implant and the bony acetabulum. Analytical studies have suggested that in these cases, bone resorption was initiated by the stresses developed at the thread/bone interface.

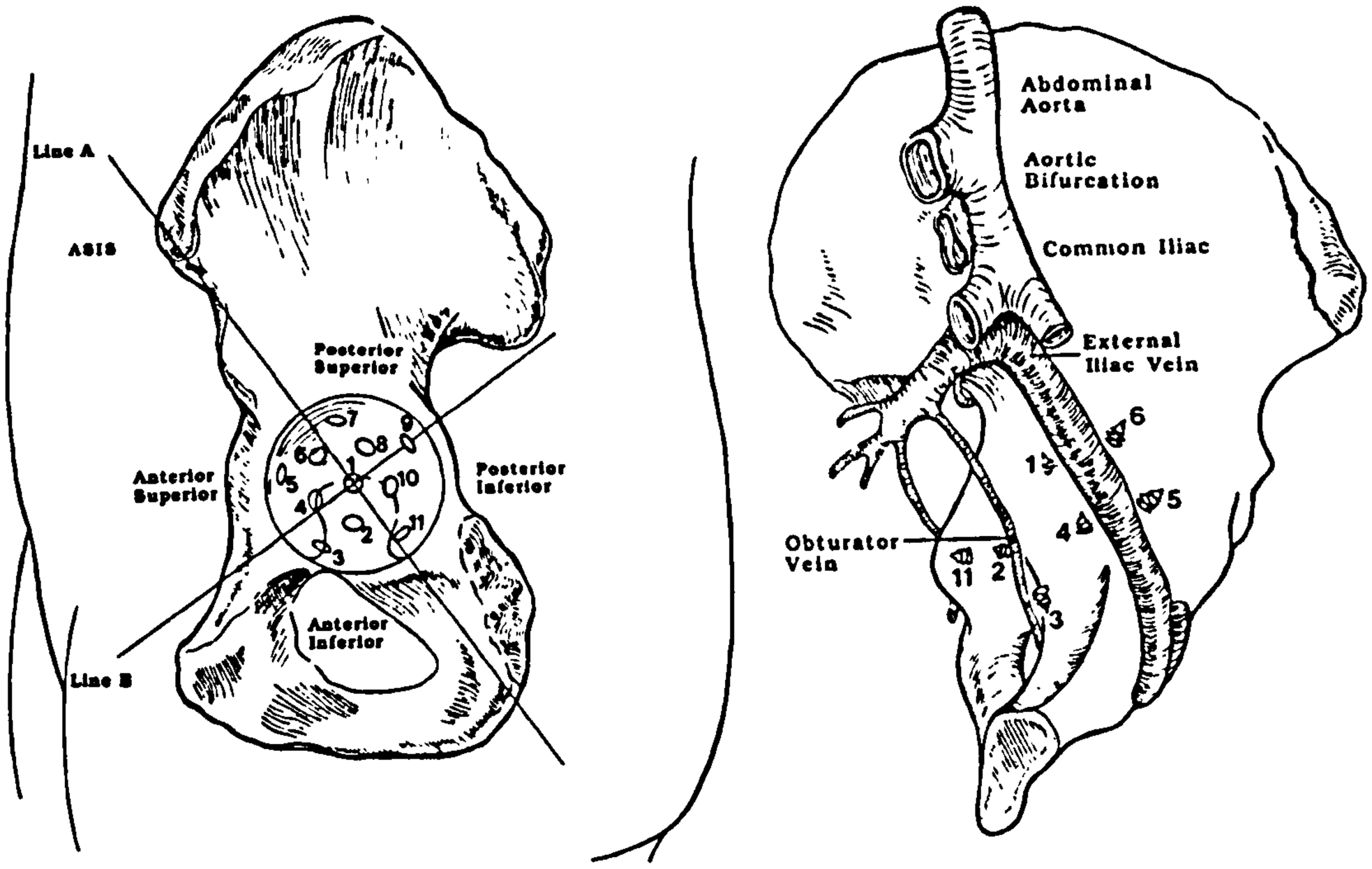

Figure 8.1 Diagrammatic summary of the anatomic studies of Wasielewski et al (1990). Long screws were placed through an acetabular cup at eleven locations (left). The location of each screw was identified on the quadrilateral intrapelvic surface, relative to the iliac venous system. Screws 1, 4, 5, and 6 emerged near the external iliac vein after being inserted in the anterior superior quadrant of the pelvis (left). Screws 2 and 3 emerged near the obturator vein and originated from the anterior inferior quadrant (ASIS = anterior superior iliac spine).

The need for augmentation of interference fixation using screws passed through the acetabular shell and into the underlying bone is supported by biomechanical studies in which the acute stability of cementless acetabular prostheses has been measured in the laboratory. These studies have demonstrated that the use of screws significantly increases the stability of the cementless interface, especially under large torsional loads. This is consistent with the hypothesis that screws pull the relatively elastic acetabulum onto the surface of the relatively rigid prosthesis, thereby increasing the area of localized contact and the resistance of the interface to motion under load. Thus, adjunctive screw fixation can increase the area of direct bony ingrowth and thus reduce the likelihood of implant loosening and symptomatic implant/bone motion.

The efficacy of screw fixation is also demonstrated by acetabular shells retrieved at post-mortem or at revision procedures performed for reasons other than prosthetic loosening. In several studies, the extent of bony ingrowth into the porous surfaces of acetabular component has been found to be highly variable and unpredictable, although implants fixed with screws have consistently demonstrated ingrowth in the vicinity of screws used to anchor the shell to the bone. This presumably occurs because at points of anchorage, the relative micromotion between the implant and the relatively flexible acetabulum is sufficiently low to support osseous attachment.

Despite the popularity of screw fixation, there has been a small, but serious incidence of intraoperative fatalities associated with screw placement in the acetabulum. These complications have arisen from intrapelvic penetration of screws or drills leading to laceration of neurovascular structures, principally the external iliac artery or vein. Although most cases of death related to screw fixation have occurred intraoperatively or at least in the immediate postoperative period, in several instances deaths have been reported some years postoperatively due to progressive erosion of vital structures by screws protruding through the inner wall of the pelvis. Because of these alarming complications, some authors have advocated abandonment of screw fixation entirely while others have claimed, on the basis of cadaveric studies, that significant risks are only associated with screw placement in a "danger zone" situated over approximately one quarter of the anterior surface of the acetabulum (figs. 8.1, 8.2).

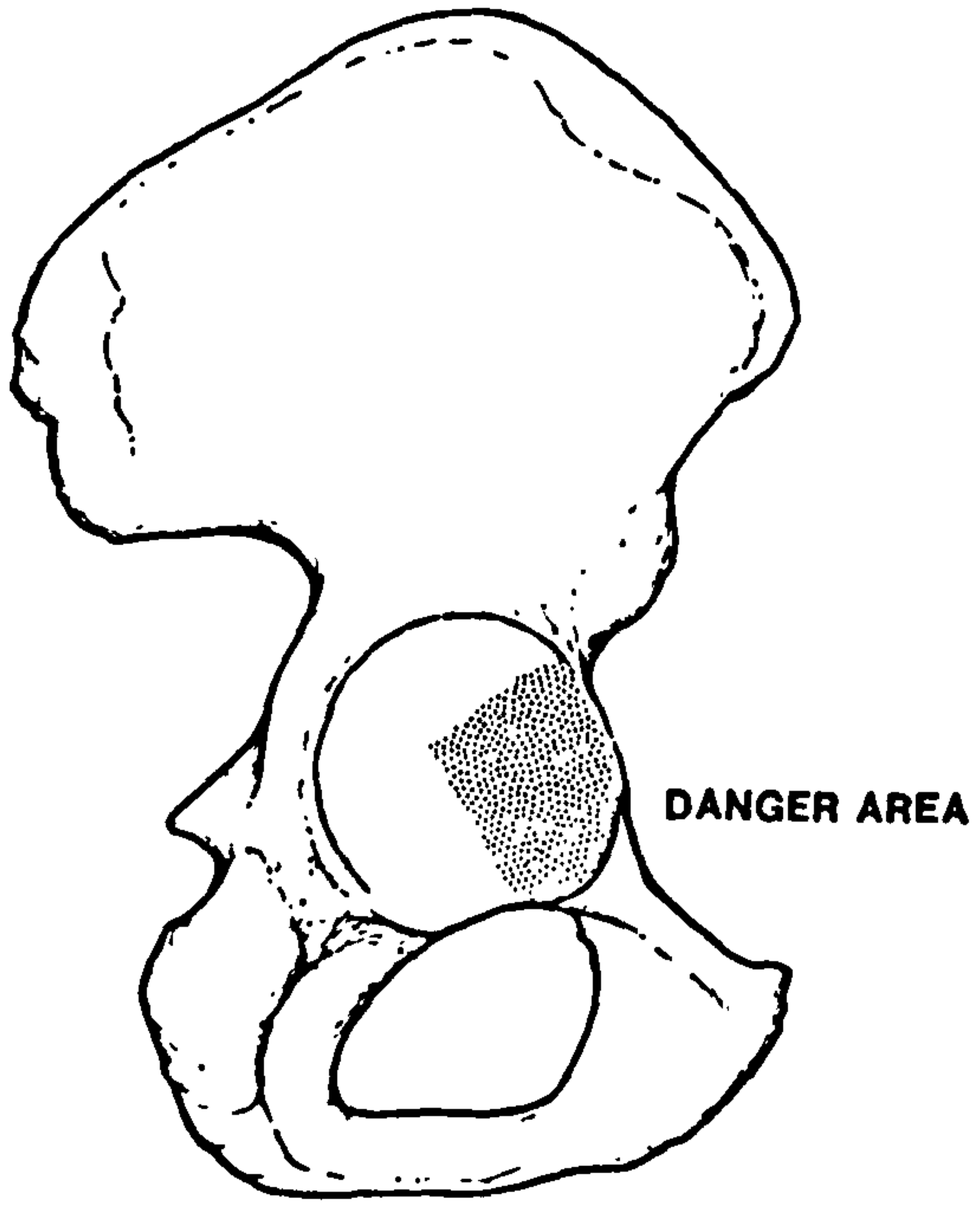

Figure 8.2 Drawing of the right acetabulum. The shaded area represents the danger zone for the penetration of intrapelvic structures by a screw or drill-bit as postulated by Keating et al (1990).

Despite this advice, anatomic texts which illustrate the neurovascular structures within the pelvis show an abundance of veins, arteries and nerves within the intrapelvic cavity, medial to virtually all of the acetabular surface (fig 8.3). Structures which are especially prominent include the external iliac artery and vein, the obturator artery, vein and nerve and the femoral nerve. An additional consideration is the occurrence of anatomic variations of these structures, particularly of the external iliac vessels and the obturator nerve which can make prediction of the course of these structures particularly hazardous. This suggests that the reliance upon a dependable "safety zone" for bicortical screw placement is ill advised and that a more prudent course of action is to completely avoid placement of drills and screws which penetrate the inner wall of the pelvis. An alternative course is unicortical fixation using screws which gain purchase in cancellous bone. It is theoretically possible to fix a prosthetic shell to the pelvis using screws placed only in the areas of greatest intracortical thickness of the pelvis. Moreover, if the geometry of the pelvis is relatively predictable, it may be possible to select the length of each screw based upon its position within the acetabulum to maximize its strength of purchase while still avoiding intrapelvic penetration.

8.2 THE EFFECT OF PROSTHETIC COMPONENTS ON THE STRAIN DISTRIBUTION WITHIN THE PELVIS

In general, prosthetic devices radically alter load transmission within bone due to reinforcement effects at the implantation site. This can lead to dramatic changes in the structure of the skeleton as bone responds dynamically to the local stress level. Within the pelvis, a fundamental concern is that the use of shells that are large, oversized, and have a potential for rigid bony attachment may lead to catastrophic peri-acetabular bone loss, ultimately leading to prosthetic failure. While the effect of prosthetic design on acetabular osteopenia has yet to be studied in any detail, several biomechanical experiments have been reported in which strain changes have been measured following acetabular replacement.

Several authors studied the effect of cemented acetabular cups on strains within the pelvis. One of the most comprehensive studies of the distribution of cortical strains over the surface of the pelvis was

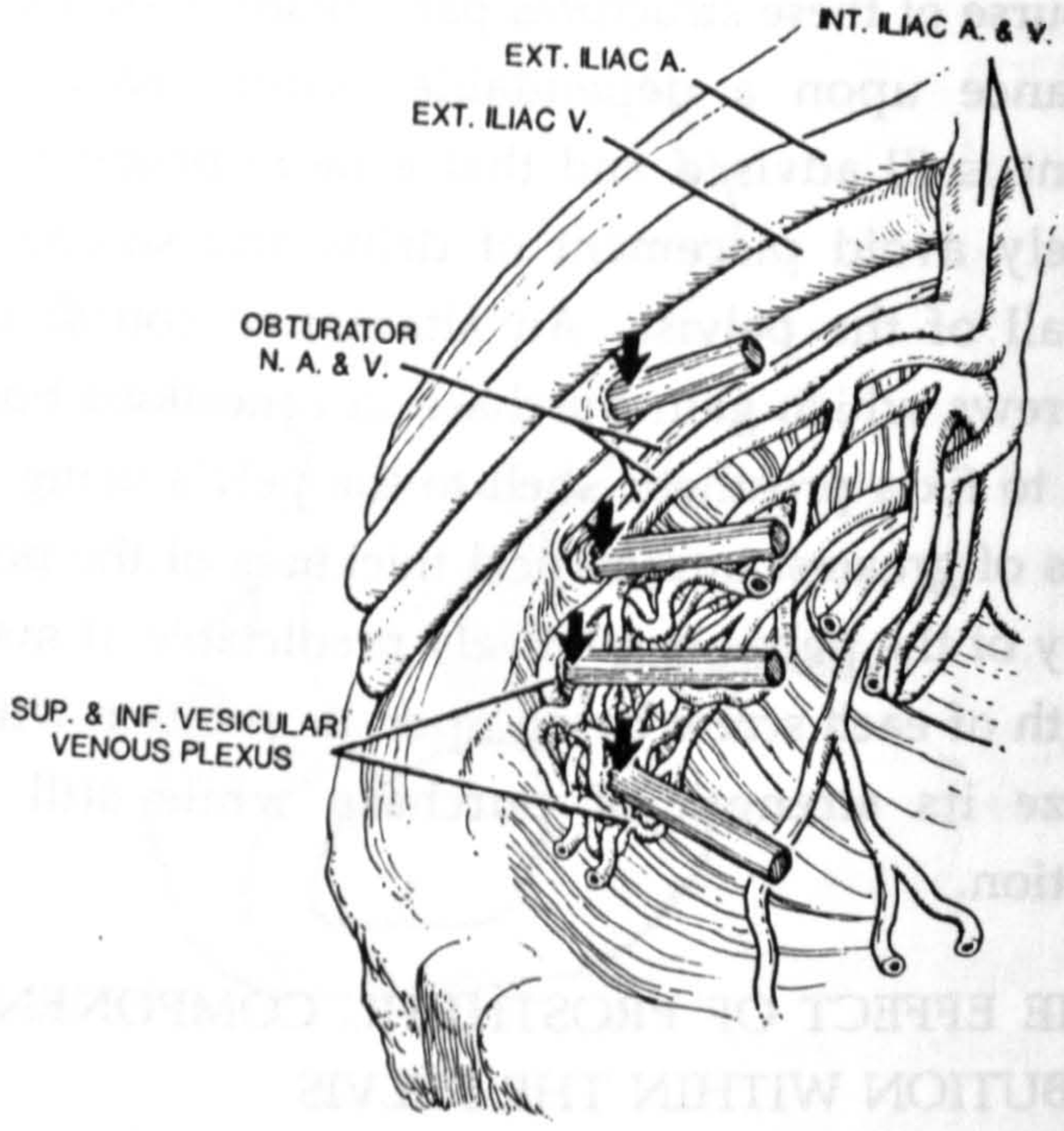

Figure 8.3 Schematic illustration of experiments reported by Keating et al (1990) showing the right pelvic brim. The arrows indicate penetration of the external iliac vein, obturator vein, and tributaries of the internal iliac vein by fixation pins drilled into the anterosuperior quadrant of the acetabulum.

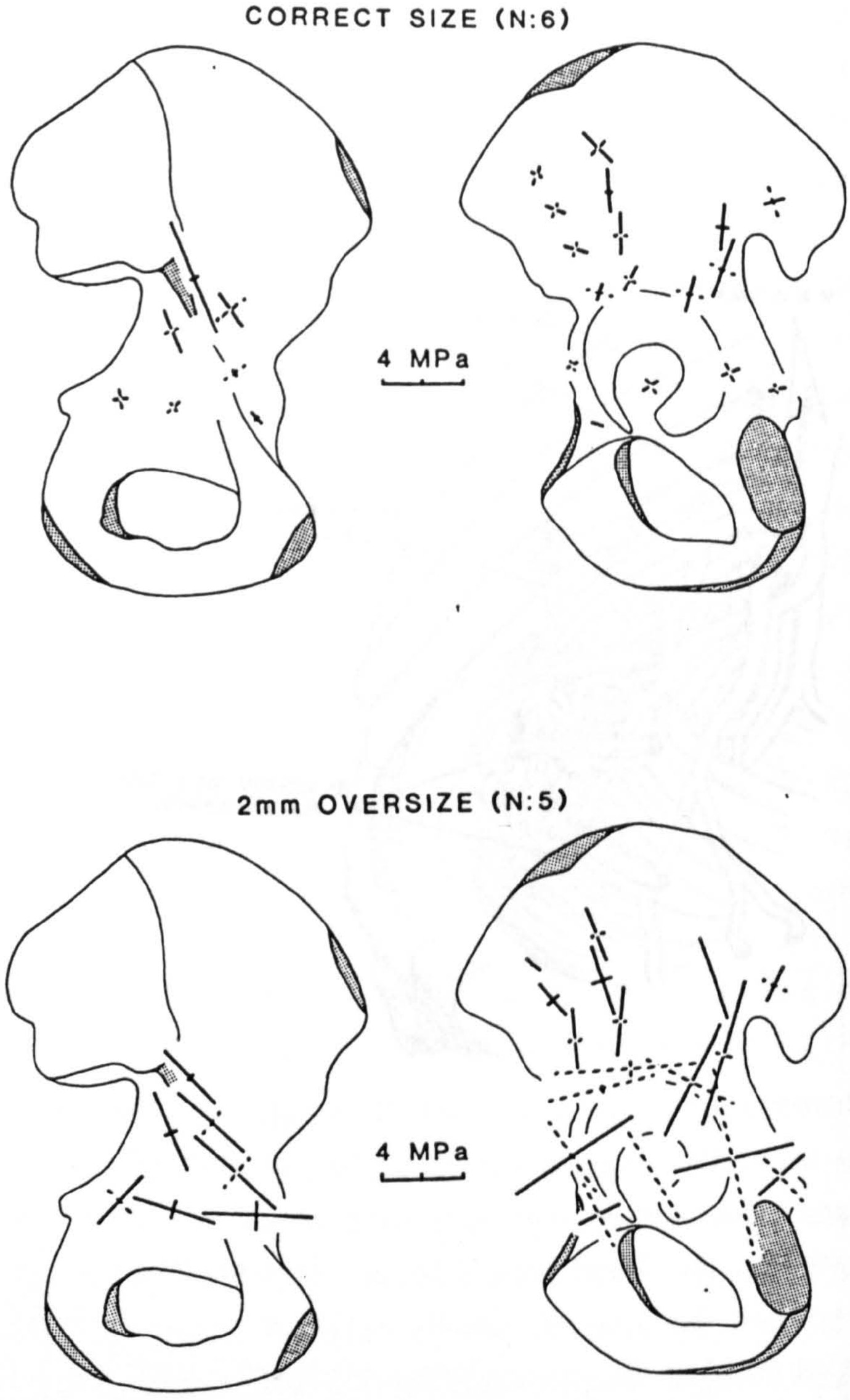

Figure 8.4 Summary of the strain gauge data of Finlay et al (1986) derived from pelves loaded to 2.5 kN with endoprostheses correctly sized to match the acetabulum and 2 mm oversize. Tensile stresses are denoted by the broken lines.

performed by Finlay et al (1986a, 1986b) who studied the effect of the fit between metal prosthetic heads and the natural acetabulum on strains developed with weight-bearing. The medial and lateral surfaces of seven embalmed hemipelvi were instrumented with 25 strain gage rosettes and the ilium of each specimen was embedded in a holding fixture. Physiologic loading was simulated with a singe force of up to 2,500 N, oriented in the direction of the joint reaction force in single legged stance. Muscle forces were not simulated.

Loading of the acetabulum was performed on the normal femoral head and metal spheres of diameters matching the acetabulum and 1 and 2 mm larger and 1 and 2 mm smaller. This situation is very analogous to implantation of a cementless acetabular cup which is deliberately oversized in order to develop increased stability within the reamed acetabular socket. In the presence of oversized femoral heads, Finlay et al measured very large increases in circumferential tensile strains around both the rim of the acetabulum, the base of the posterior wall and within the floor of the socket itself. The largest tensile strains were observed within the posterior and superior rim where implantation of the 2 mm oversized femoral head caused increases in strain of 530 and 885% respectively (Fig. 8.4).

Changes in the strain distribution of the pelvis generated by different designs of cemented acetabular cups were reported by Lionberger et al (1985) who measured cortical stresses at five sites on the medial and lateral surfaces of five fresh adult pelves. The iliac wings of each specimen were encased in plaster down to the inferior borders of the sacro-iliac joints. A static load of 1,336 N (300 lbs.) was applied to the acetabulum via the normal femoral head and then through solid stainless steel hemispheres with the following modifications: (i) a plain hemisphere, (ii) a hemisphere with a peripheral flanges for superior, anterior and posterior rim contact, (iii) a hemisphere with a single tapered iliac peg, and (iv) a combination of the iliac peg with a continuous peripheral flange. Loads were applied to the pelvis in 20° of extension, neutral and 30° of flexion at 16° to the vertical in the frontal plane.

There was relatively little difference between the strains observed with the original femoral head and the plain hemisphere cemented into the acetabulum. In both cases, strains were significantly higher in flexion than in neutral or extension, especially over the posterosuperior quadrant

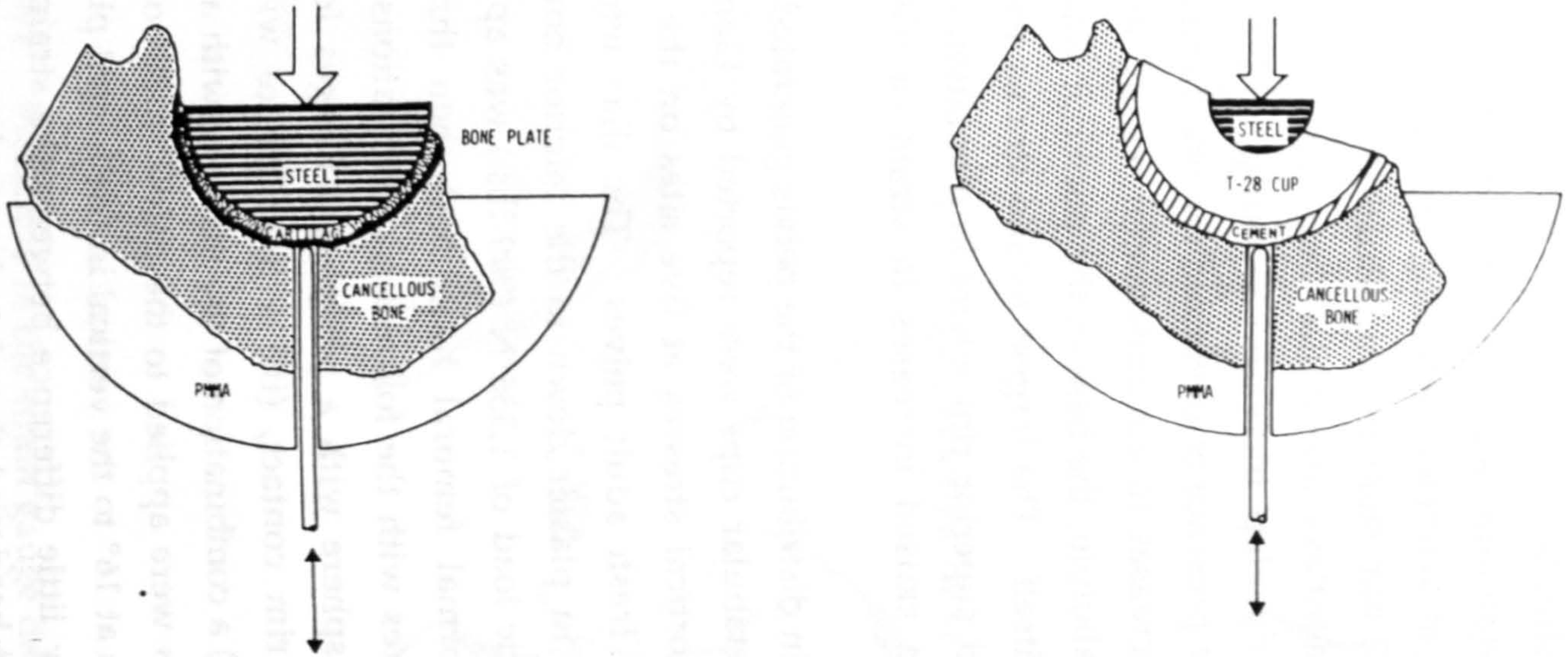

Figure 8.5 Configuration of experiments performed by Markolf and Amstutz (1983) in which the motion of a hemiarthroplasty (left) and a cemented acetabular cup (right) were measured during loading. The displacements of the subchondral plate and the cement/bone interface were measured with an extensometer attached to the plunger and to the acrylic potting compound.

of the acetabular rim. The effect of the acetabular components on the strain distribution was found to be similar despite variations in design which included the presence of a peripheral flange and a single tapered peg extending from the surface of the prosthesis up into the ilium. When each prosthesis was cemented into the acetabulum with minimal resection of the subchondral plate, the change in the stress distribution was most pronounced antero-medially, over the quadrilateral surface, where tensile strains decreased by 65% and compressive strains increased by 48% due to the stiffening effect of the rigid prosthesis. Within the acetabular rim, tensile strains decreased by 22-54% while compressive strains were elevated by 0-25%. These observations support the conclusion that prosthetic components will substantially reduce the bending of the normal acetabulum at least when fixed with acrylic cement.

8.3 EXPERIMENTAL MEASUREMENTS OF IMPLANT STABILITY

Within the literature, there are several reports of experiments in which attempts have been made to measure the interface motion between the acetabulum and implanted prostheses. Markolf and Amstutz (1983) measured the motion of the cartilage/sub-chondral junction during loading in contact with a hetal hemisphere. Additional measurements were performed in the same specimen implanted with cemented, all-polyethylene acetabular cups. Eleven periacetabular bone specimens were resected from human pelves and cast into plaster hemispheres to facilitate positioning during the subsequent loading experiments. A hole was drilled through the mounting block, the inner table of the pelvis and the subchondral plate to allow a spring-loaded plunger to be placed in contact with the cartilage layer lining the acetabulum (Fig. 8.5). A load of 2,000 N was applied in the estimated direction of the joint reaction force and the displacement of the plunger was measured.

Once the measurements with the hemiarthroplasty were completed, the acetabulum was reamed and the acetabular cup was cemented in place. Loading was then performed with the spring-loaded plunger abutting the outer surface of the cement mantle so that the measured displacement included the deformation of cancellous bone, cartilage or acrylic cement, and not solely the motion of the metal/bone interface.

Configuration	Gross Displacement		Relative Displacement	
	Bone Quality		Bone Quality	
	Good (n=8)	Poor (n=3)	Good (n=8)	Poor (n=3)
Hemiarthroplasty	253 ± 51 μm	366 ± 20 μm	82 ± 21 μm	224 ± 64 μm
Prosthesis with plate intact	299 ± 46 μm	427 ± 52 μm	50 ± 20 μm	192 ± 61 μm
Prosthesis with plate resected	314 ± 31 μm	424 ± 60 μm	84 ± 31 μm	227 ± 80 μm
Surface replacement with plate resected	243 ± 12 μm	468 ± 29 μm	80 ± 35 μm	223 ± 75 μm

Table 8.1 Results reported by Markolf and Amstutz (1983) for interface motion at the acetabular dome during loading to 2000N. (all values mean ± standard deviation)

The deformation of the acetabulum was quite variable and was strongly influenced by the quality of the cancellous bone and the thickness of the subchondral plate (Table 8.1). In any given specimen, the gross motion varied little with the different prosthetic configurations, and ranged from 243-314 μm in specimens with good bone to 366-468 μm in specimens with bone of poor quality. However, the relative motion of the implant/bone interface contributed only 17-33% to the gross motion of the specimen and was strongly influenced by the quality of the peri-acetabular cancellous bone. In bone classified as 'good', cemented cups implanted with the subchondral plate intact displayed relative motions of 50 ± 20 μm. When the same components were implanted without cement or following removal of the subchondral plate, the relative motion of the interface increased to 80-84 μm. In cases where the bone quality was poor, these values tripled and ranged from 192-224 μm, regardless of the experimental conditions.

It must be emphasized that in all the experiments reported by Markolf and Amstutz using cemented components, the cement was not pressurized into the cancellous bone bed and anchorage holes were not drilled through the subchondral plate or into reamed cancellous bone. In clinical practice using contemporary cementing techniques, the subchondral plate is expected to have much less effect than this study would suggest due to several factors. These include the reinforcing effect of the interdigitated cement layer and the reduction in stiffness of the subchondral plate caused by the effects of acetabular reaming and the use of drill holes to enhance cement penetration.

The displacement of the implant/bone interface of cementless acetabular cups has been measured by several investigators in bench top experiments (Table 8.2). Tooke et al (1988) implanted two designs of cementless cups in twelve mongrel dogs: one with circumferential threads and the other with a circumferential porous coating. At 2 and 6 months postoperatively, three animals from each group were sacrificed and the acetabular prostheses were excised with contiguous regions of the ilium, pubis and ischium. Each specimen was potted in acrylic cement and loaded to 250 N in a mechanical testing machine. During loading, a differential strain-gage transducer was used to measure the relative displacement of the rim of each cup and the adjacent bony margin at sites adjacent to the pubis, the ilium and the ischium (Fig. 8.6). Overall, there

Study	Method of Loading	Load Applied	Number of Specimens	Number of Implant Configurations Tested	Transducer Design
Lachiewicz et al (1989)	Oblique; embedded Specimens	1000N	20 human pelves	3	Strain gaged brass strip, rigidly fixed to liner and bone
Tooke et al (1988)	Axial; embedded Specimens	250N	12 canine pelves	2	Strain gage Extensometer; Axial displacement at rim
Litsky et al (1990)	Axial Compression on rim of cup; Foam blocks	0-5000N	polyurethane foam blocks	6	Two transducers measured motion of rim at point of loading and contralaterally.
Clarke et al (1991)	Axial Compression (686N) with torsion; embedded specimens	100Nm Torque	10 human pelves	2	Cross-head of testing machine. Failure defined as 20° rotation
Stiehl et al (1991)	Axial; embedded specimens	Preconditioning: 100,000 cycles 100-1000N Measurements: 5 cycles to 1500, 2000, 2500, 3000N	33 human hemi pelves	5	6 LVDTs, located at 2 rim sites
Takedani et al (1991)	Axial Compression (750N) with cyclic torsion; Embedded specimens	Loaded from ±5Nm to failure in 2.5Nm increments	45 embalmed human acetabuli	8	One LVDT measured axial rotation. Three LVDTs measured cup motion at 3 sites around rim.
Curtis et al (1992)	Axial Compression (686N) with torsion; embedded specimens	±6.8Nm followed by 100Nm	40 fresh human acetabuli	4	Cross-head of testing machine Angular displacement under 6.8Nm measured in addition torque required to produce 1° and 2° rotation
Perona et al (1992)	Axial Compression; Embedded Specimens	2354N	11 fresh human pelvi	5	3 Eddy probe transducers monitored rim motion at 3 sites

Table 8.2 Summary of published studies that attempted to measure the stability of cementless acetabular cups.

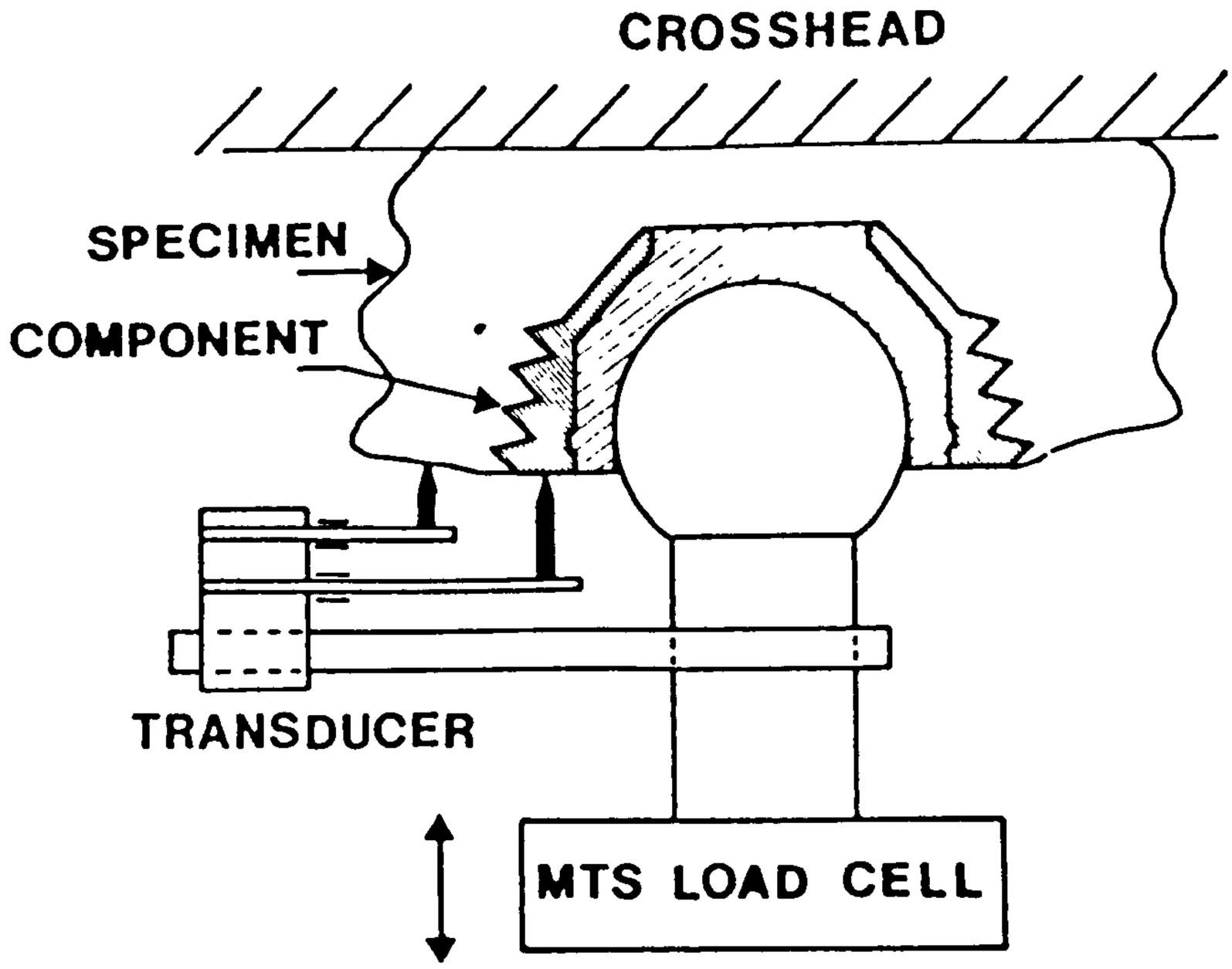

Figure 8.6 Experimental configuration reported by Tooke et al (1988) to measure the displacement of a threaded cup within the acetabulum.

was little variation in the magnitude of shell/bone motion measured at the three locations in each specimen. At two months, the porous-coated cups moved an average of only 9 μm with 250 N of load (range of micromotion values: 0 - 18 μm), while the motion of the threaded components averaged 39 μm (range: 0 - 62 μm). At six months, these values increased to 19 μm (range: 0 - 33 μm) and 52 μm (range: 5-125 μm) respectively. The porous-coated specimens displayed significantly less motion than the threaded components at both time intervals ($p = 0.0006$).

Many bench-top studies have been reported using cadaveric specimens, however, in all of these experiments, the loading of the pelvis and acetabulum has been either non-physiologic or grossly over-simplified. Litsky et al (1990) implanted six designs of metal-backed acetabular shells into reamed blocks of closed-cell polyethylene foam and applied compressive loads of up to 5,000 N at one point on the peripheral rim of each device. The motion of each cup was measured at the point of load application and at a second point directly opposite on the rim of the shell. They found that displacement of the shells was linear between loads of 250 and 1000N and so reported the change in cup position over this loading range. The magnitude of the observed displacement ranged from 132 ± 47 μm for cemented prostheses to 168 ± 34 μm for shells with peripheral threads to 194 ± 43 μm for shells fixed with dome or rim screws. The lowest initial stability (239 ± 54 μm) was achieved with porous coated shells implanted without screw fixation in a press fit (interference) mode. While this model in no way simulates the loading or interface conditions present within the acetabulum, it nonetheless provides some insight into the relative stability of alternative methods of mechanical stabilization of implanted shells and the approximate magnitude of the gross deformation of the interface.

Most studies have been performed in the laboratory using embalmed specimens obtained from cadaveric donors. Typically, hemipelvi have been embedded in blocks of plaster and implanted with acetabular prostheses. The motion of the acetabular cup has then been measured at the peripheral rim under simple loading conditions (Table 8.2). Tooke et al, 1988; Lachiewicz et al, 1989; Clarke et al, 1991; Stiehl et al, 1991; Perona et al, 1992). Lachiewicz et al (1989) implanted porous-coated acetabular cups of three different designs in 20 human acetabuli (12 embalmed and 8 fresh): These implants included a hemispherical cup with three trans-

acetabular screws (Harris-Galante, Zimmer), a cup with three integral, parallel spikes (AML, DePuy) and a hemispherical cup with two superiorly placed pegs (PCA, Howmedica). Each acetabular specimen was embedded in a block of acrylic cement and loaded in a direction which was said to simulate 'partial weight-bearing with ambulatory supports'. The relative displacement of the polyethylene liner with respect to the underlying bone was monitored during application of a load of 1,000 N. The average displacement in the direction of loading was 570 ± 310 μm with the shell fixed with screws, 690 ± 550 μm with the component with 3 spikes and 970 ± 940 μm with the two-pegged design. Due to the broad scatter of the data, no statistically significant inferences could be drawn from these data. Moreover, it was not determined how much of the observed displacement occurred at the shell-liner interface rather than the shell-bone interface. The variability of the experimental results also suggests that the technical quality of the implantation procedure and/or the mechanical properties of the specimens themselves may have been poorly controlled.

The authors of this study also measured the torsional capacity of the three designs of acetabular cups implanted in the same specimens. The strength of fixation of each implant was assessed by the maximum torque required to generate 25 degrees of rotation without application of axial load. Under these conditions, the average maximum torque was 46 N-m for the shell fixed with screws and 32 Nm for both the two-pegged and three-spiked components ($p < 0.05$). The greatest variation in fixation strength was observed with the three-spiked design.

A similar torque test was performed by Clarke et al (1991), using two of the designs evaluated by Lachiewitcz et al: the Harris-Galante Cup (Zimmer) implanted with three cancellous screws and the PCA Cup (Howmedica) with two integral fixation pegs. Both components were implanted line-to-line after the acetabulum has been machined with a reamer of matching diameter. Slots were machined into the rim of each acetabular shell to enable torque to be applied to each implant. Two sets of experiments were performed: in the first experiment, the shell was loaded biaxially with a compressive force of 686N and a fully reversed cyclic torque of 6.8Nm in order to measure the 'initial looseness' of the prosthesis. In the second experiment, the torque required to produce 2 degrees and 20 degrees of rotation was determined.

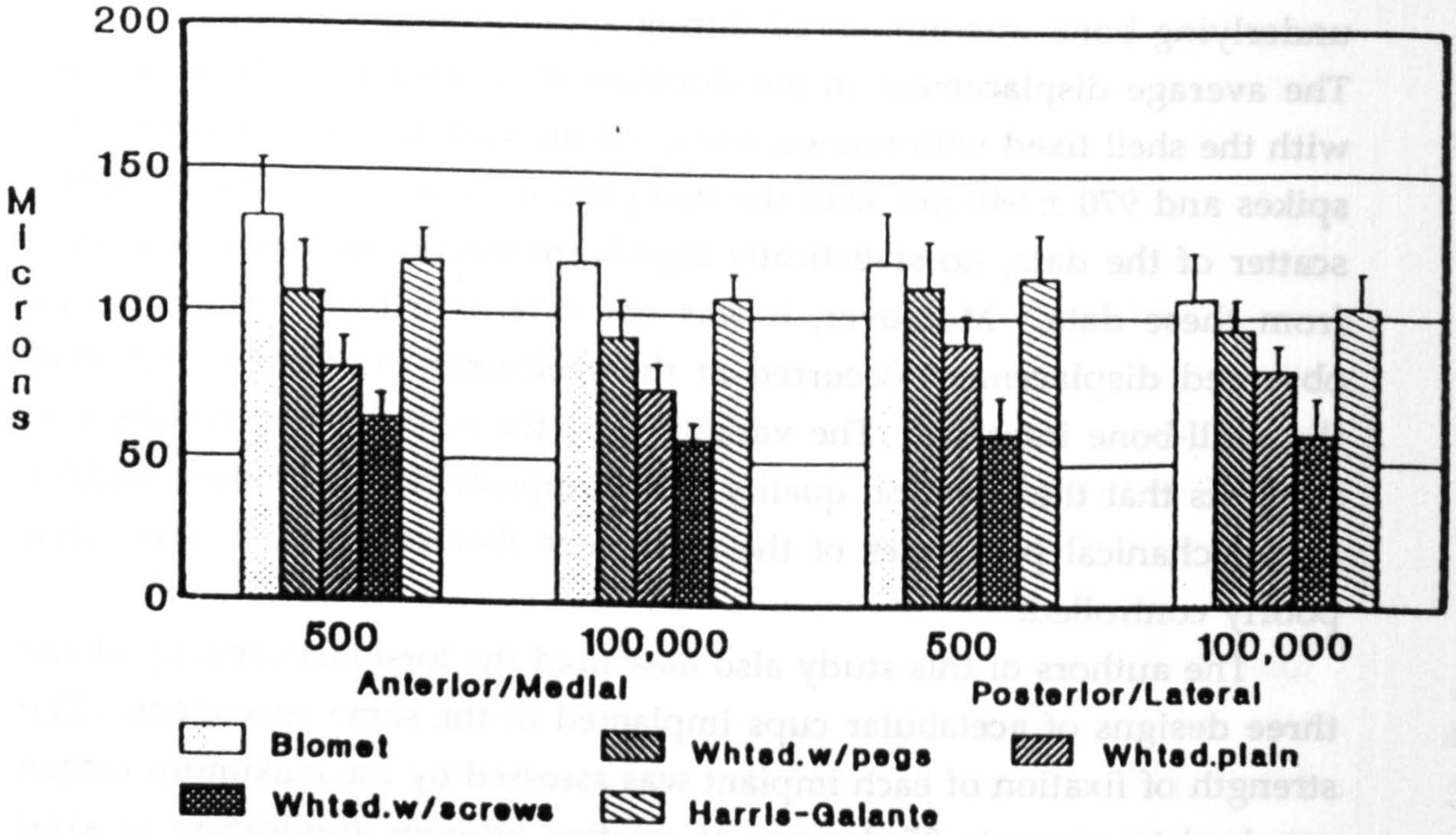

Figure 8.7 Relative axial motion of the acetabular rim and cups of five different designs during loading from 100 to 1000 N. Measurements are reported at two positions around the rim after loading for 500 and 1,000,000 cycles at 5 Hz (from Stiehl et al, 1991).

The results indicated that in both the initial cyclic loading test and in the torque to failure experiments, the shell fixed with pegs was more stable than the shell fixed with screws. In the cyclic torsion test, the mean rotational motion of the actuator of the testing machine was 0.16 degrees with peg fixation and 0.26 degrees with screw fixation. As tranducers were not applied to the shell and the acetabulum it was not possible to assess how much of this rotational movement occurred at sites other than the cup/bone interface. Similarly, the reaction torque at 2 degrees of cross head rotation was 44 ± 20 Nm for peg fixation and 23 ± 14 Nm for screw fixation ($p < 0.03$). However, as acetabular cups are not exposed to large repetitive torques within the body and as 2 degrees of true shell/bone rotation is equivalent to 1000 μm of interface motion, it is unclear how the results of this experiment relate to the performance of the two implant designs in service.

One potential deficiency of acetabular micromotion studies published in the literature is the lack of preconditioning of the shell/bone interface through repetitive loading to simulate 'settling in' of the joint components. This phenomenon was investigated by Stiehl et al (1991) who tested five different configurations of porous-coated cups in 33 embalmed acetabuli. As in previous studies, each specimen consisted of a hemipelvis embedded in dental stone. In this case, interface motion was measured with two sets of three orthogonally placed linear variable differential transformers (LVDTs) rigidly attached to the plaster block. These transducers were used to follow the three-dimensional motion of two metal blocks attached to antero-medial and postero-lateral sites on the peripheral rim of each shell. A sinusoidal loading cycle was applied via a metal head in a loading direction that simulated the position of the hip in full extension. Loads from 100 - 1,000 N were applied at a frequency of 5 cycles/second for 500 and 100,000 cycles. After both of these periods of cyclic loading, the permanent change in position (subsidence) of the cup and its dynamic motion (micromotion) was measured in loading to 1000 N.

This experiment demonstrated large variations between specimens in terms of subsidence and micromotion; this prevented statistically significant differences being demonstrated between the five cup designs evaluated in the study (Fig. 8.7). Nonetheless, the micromotion of the five designs ranged by a factor of approximately 2, from 60 to 130 μm. The

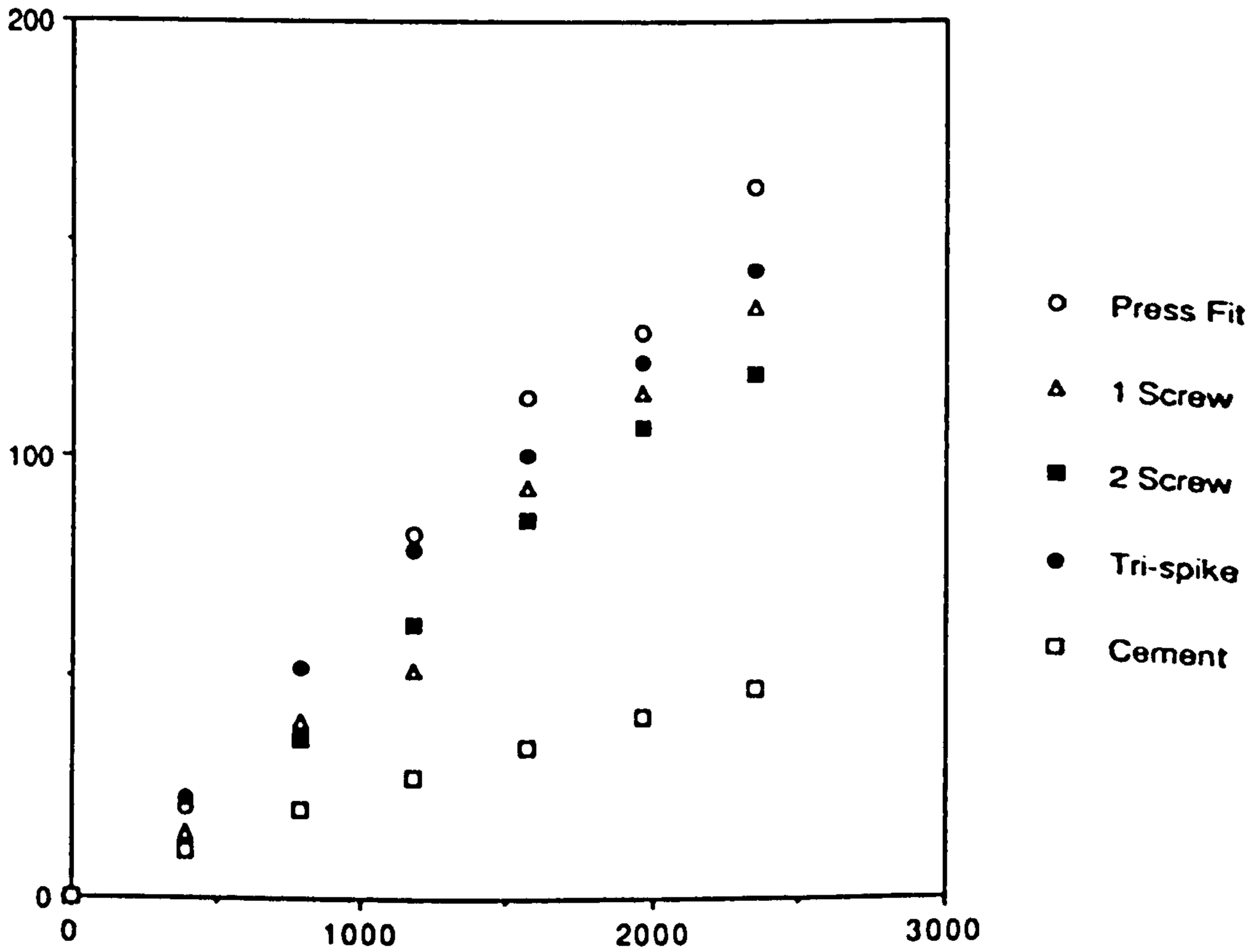

Figure 8.8 Typical load/displacement behavior of the different acetabular components as measured at the ilium (from Perona et al, 1992).

most stable component was a hemispherical porous-coated shell (Whiteside cup, Dow Corning Wright Inc.), implanted with a 1mm interference fit and augmented with two 6.5 mm bone screws; the least stable was a porous-coated shell of hemispherical configuration with the addition of 1.5 mm of radial expansion to the peripheral rim to enhance interference fixation upon implantation.

Perona and co-workers (1992) also attempted to address the deficiencies of early micromotion studies; they performed experiments using more realistic loads than previous studies (up to 2350 N) applied in an anatomic direction to cups implanted in fresh pelvic specimens. Shell/bone motion was measured at the rim of each cup in the vicinity of the ilium, pubis and ischium. In this study, the pelvis was not bisected, but both ilia were embedded in a block of dental stone, thereby eliminating most of the flexibility of the pelvic ring. Several types of implant fixation were evaluated in this study: initially, a hemi-spherical, porous-coated titanium shell was implanted with 2 mm of interference without adjunctive fixation. After testing, the experiment was repeated with one and then two 4.5 mm screws inserted into the dome of the acetabulum. Experiments were also performed using a cup of similar design with the addition of three integral spikes located at equally spaced points around the outer surface, immediately below the peripheral rim. After these runs were completed, a hemispherical shell was cemented into each specimen and the experimental measurements were repeated.

An interesting result of this study was that there were no statistically significant differences between the stability of the cementless devices. However, large differences were present between the average micromotion recorded at the three measurement sites. At the ischium, average micromotion ranged from only 39 ± 23 μm for the tri-spike shell to 51 ± 19 μm for a cup fixed with one cancellous screw ($p > 0.05$), while motion within the ilium was 143 ± 88 μm and 134 ± 82 μm for the same components (Fig. 8.8). At the pubic measurement site, intermediate values were recorded, ranging from 67 ± 44 μm for the tri-spike cup to 98 ± 49 μm for the hemispherical shell augmented with one bone screw. Large variations in interface motion were recorded with all devices, typically ranging by a factor of 5 to 10. For example, although the average micromotion at the pubic measurement site was 80 ± 40 μm for the cup fixed with two screws, individual values varied from 40 to 175 μm. This

supports the conclusion that surgical technique and variations in the characteristics of individual pelves may have more influence over interface micromotion than the specific design features of different implants. It is also possible that the experimental set-up exaggerated the effect of differences in the stiffness and morphology of the periacetabular bone of each specimen due to the constraint imposed by the embedding procedure.

Takedani et al (1991) examined the influence of three variables on the motion of acetabular prostheses: screw fixation, peg fixation and the degree of reaming of the acetabulum. Acetabular cups were loaded in cyclic torsion under a constant axial load of 750 N. Torque was applied about the axis normal to the mouth of the acetabulum for 30 cycles at 0.5 Hz and was increased from 5 Nm by 2.5 Nm per cycle until failure of fixation. As in previous studies, acetabuli were resected from embalmed pelves and potted in a holding fixture. The rotational and axial migration of the shell were measured at anterior, posterior and superior sites around the acetabular margin with an array of four LVDTs supported by a holding fixture. The relative stability of different implant configurations was assessed from the torque required to cause 2 mm of rotational displacement of the rim of the shell or fracture of the specimen. The results from four specimens were reported for each of eight different combinations of implant design and the degree of reaming of the implantation site.

The highest mean failure torque (60 ± 28 Nm) was observed in cups implanted with adjunctive fixation with pegs and screws when one millimeter of interference was present between the shell and the reamed acetabulum when the subchondral plate remained intact. These components had significantly greater torsional resistance ($p < 0.05$) than components implanted in sockets which were over-reamed by 1 mm without adjunctive fixation. At low torsional loads (less than 15 Nm), there was no significant difference between the rotational resistance of cups implanted with over- and under-reaming of the socket. In terms of axial migration, the least motion was observed in cups which were fixed using bone screws in both under- and over-reamed specimens.

Although the conclusions of this study are interesting, it is not possible to directly relate them to the performance of acetabular cups within the body as the authors applied a fixed axial load and cyclic axial

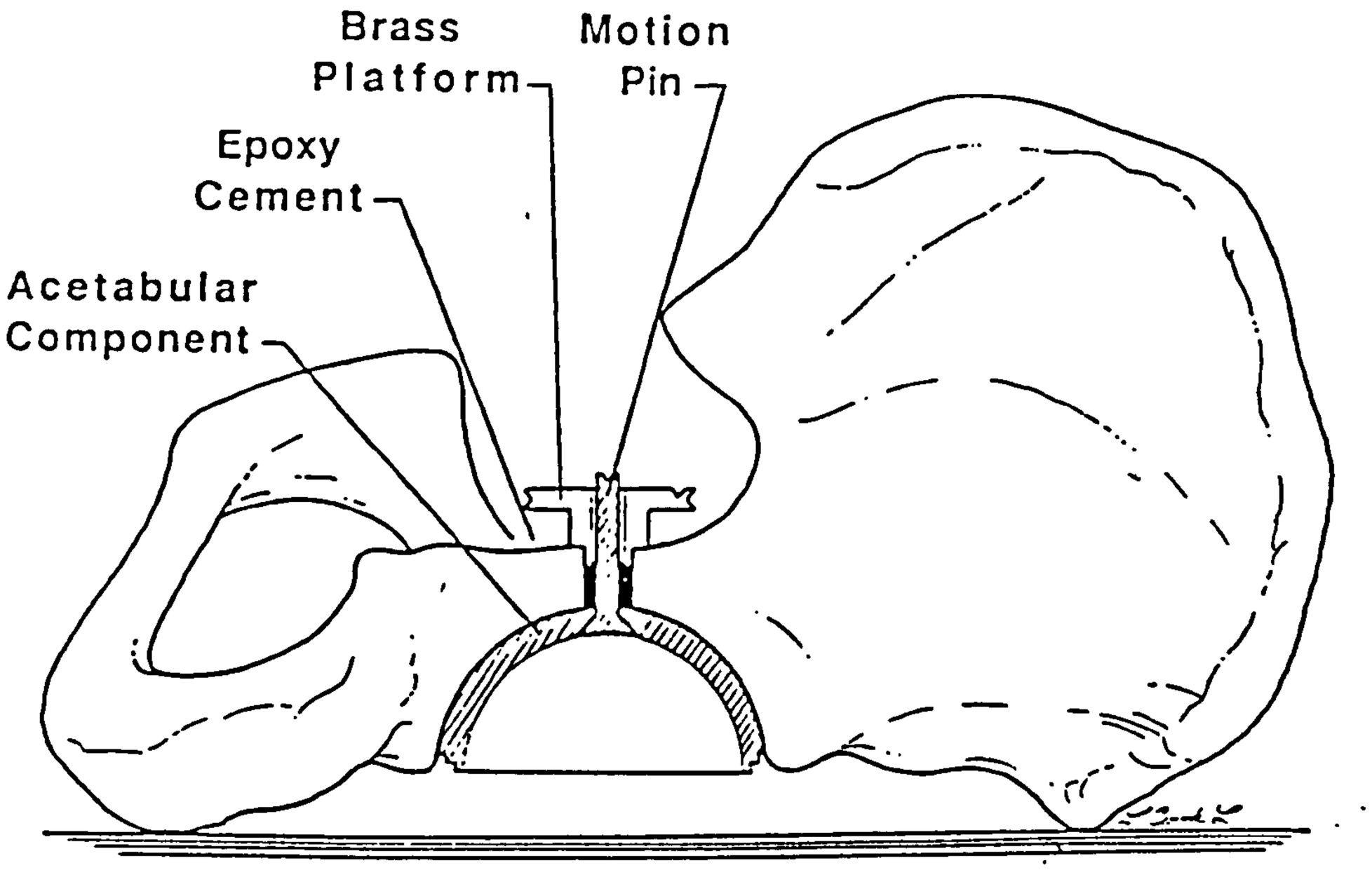

Figure 8.9 Diagrammatic representation of the measurement technique of Maloney et al (1990) and Kwong et al (1994). A motion pin is passed through a hole in the pelvis and attached to the implanted acetabular cup. A surrounding brass platform is attached to the pelvis to allow the motion of the pin to be measured relative to the surrounding bone.

rotation. During normal activities, the physiologic loads on the cup/bone interface do not act normal to the mouth of the acetabulum. Moreover, the torque developed around the acetabular rim is very small due to the low coefficient of friction of the bearing surface. As this relationship between the response of cementless cups to these non-physiologic conditions and more physiologic modes of loading is unknown, it cannot be assumed that the authors' conclusions are pertinent to the clinical performance of joint replacements.

A more valid model of the loaded acetabulum was described by Maloney et al (1990) in a study of the influence of screws on the stability of hemispherical acetabular cups. Six cadaveric hemipelves were mounted in a mechanical testing machine, in two orientations: (i) 'anatomically' with a direct vertical load and (ii) with ten degrees of flexion and fifteen degrees of adduction in an attempt to simulate loading during the stance phase of gait. An abductor strap was attached to the greater trochanter and the iliac crest to simulate the loading of the abductors and an axial load of 880 N (200 lb.) was applied to the spine resulting in a joint reaction force of 1,100 N (250 lb.). Each specimen was implanted with a hemispherical cementless acetabular shell, modified to allow attachment of two pins, one within the dome and another within a peripheral screw hole. After implantation of each cup, both pins were placed through holes in the acetabulum and threaded into the cup. A sleeve was then placed over each pin and rigidly fixed to the pelvis to allow measurement of relative motion with a strain-gage extensometer (Fig. 8.9). Four screws were threaded through each cup at the start of each experiment: two were placed vertically into the ilium; one was placed supero-medially into the dome of the acetabulum and one was placed anterolaterally. After each loading sequence, one of the screws was removed and the experiment was repeated until no screws remained to augment shell fixation.

The motion of the cup was greater in the loading configuration simulating stance than with a simple vertical load, especially within the acetabular dome. The magnitude of the micromotion between the shell and the acetabulum increased dramatically as screws were removed. With three and four screws present, micro-motion ranged from only 6 to 29 μm at both measurement sites. However, motion at the acetabular dome rose to 48-62 μm with only two screws and 28-128 μm when one screw remained in place. In this study, the authors only reported average

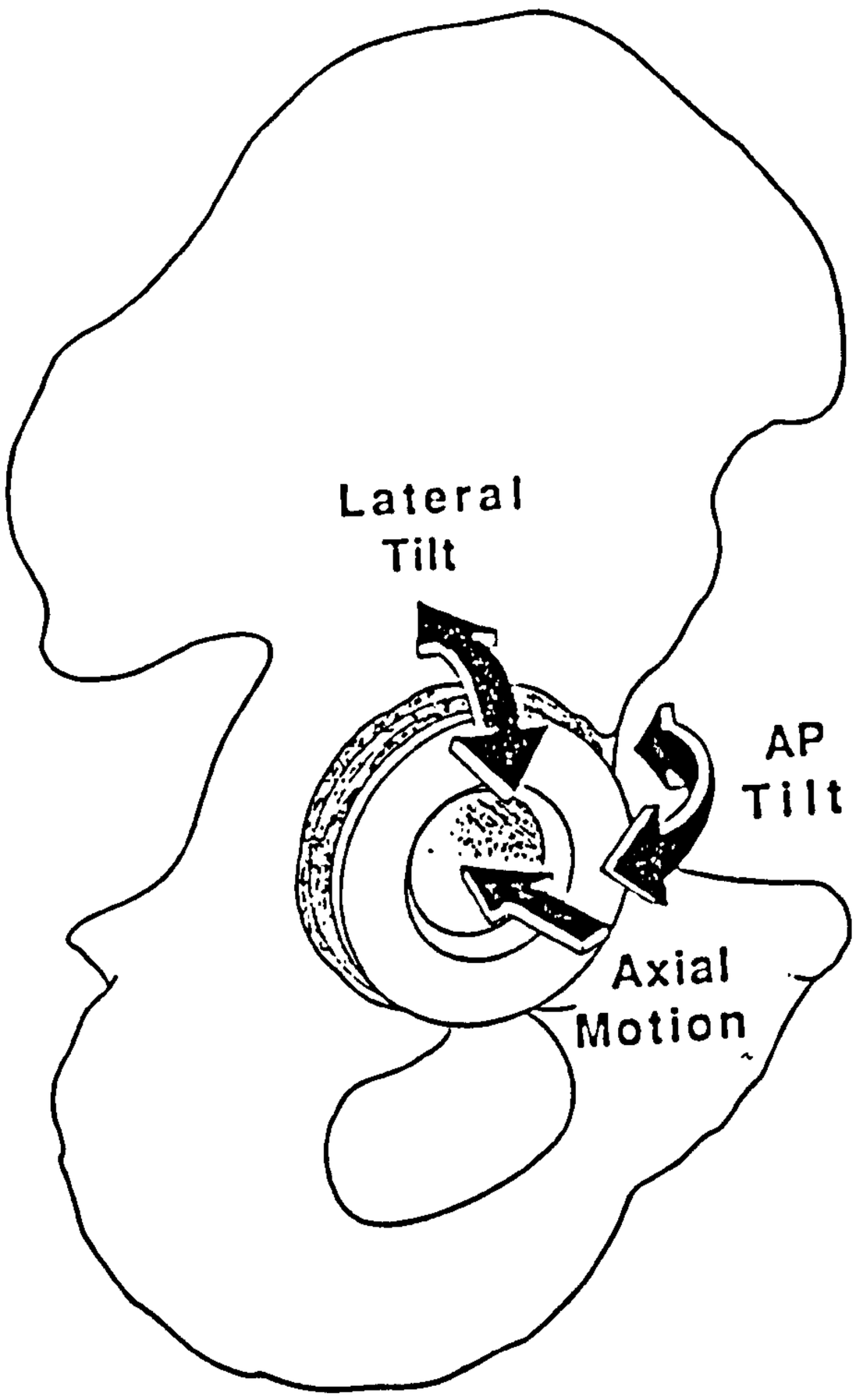

Figure 8.10 Schematic illustration of the terminology adopted by Maloney et al (1990) and Kwong et al (1994) to describe implant motion.

values of shell/bone micromotion without standard deviations, although it was noted that micromotion in excess of 200 μm was observed in some specimens with single screw fixation.

While the work of Maloney et al appears to answer many questions regarding the magnitude and distribution of micromotion at the cementless acetabular interface, a number of issues affects the interpretation of data and their translation into clinical practice. Firstly, the methods used to simulate muscle loading are oversimplified as attachment of an abductor strap to the iliac crest leads to what is essentially a frontal plane simulation of hip joint loading as the moment arm of the abductor strap in the sagittal plane is too small to produce significant bending of the pelvis in the transverse plane. This may explain the relatively large magnitude of micromotion attributed by the authors to "AP tilting" of the prosthesis (Fig. 8.10). In the coronal plane, the joint reaction force was oriented more vertically than the resultant forces recorded in previous studies using instrumeted prostheses. Nonetheless, the loading configuration of Maloney et al may simulate the position of the hip joint in patients who lean over the prosthetic joint during gait.

Secondly, the most significant loading of the hip joint occurs during early stance and terminal stance where the muscle and inertial loads are greatest. Maloney et al, attempted to model the hip joint in mid-stance where lower joint reaction loads are present and where acetabular deformation is expected to be less. Moreover, at this stage in the gait cycle, the hip is adducted by an average of 5 degrees and flexed to only 10 degrees. It appears that the selection of 15 degrees of adduction was made to achieve static equilibrium of the experimental model and not to simulate physiologic loading. However, this modification is expected to affect the pattern of micromotion at the cup/bone interface because of changes in the magnitude and direction of the abductor force caused by the use of an abnormally directed joint reaction force.

A similar study was performed in the same laboratory by Kwong et al (1994) to examine the effect of adjunctive screw fixation and oversizing of the acetabular shell on the micromotion of porous-coated acetabular components. Three fresh pelves were stripped of soft tissue, divided into hemipelvi, and embedded in blocks of plaster. Fiber-mesh coated, titanium alloy shells (Harris-Galante acetabular cup system, Zimmer, Inc.)

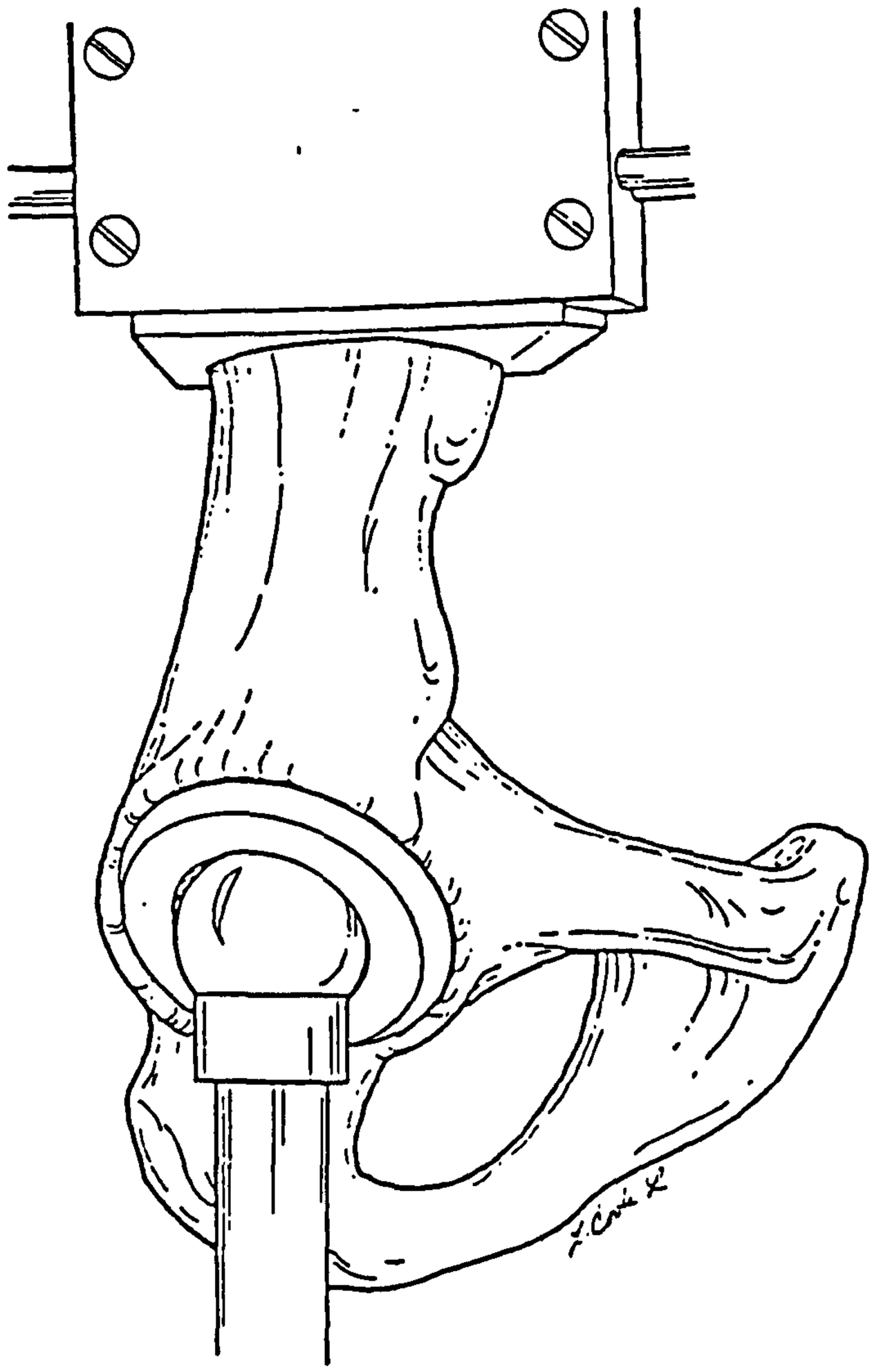

Figure 8.11 The loading conditions reported by Kwong et al (1994) to simulate single-legged stance in a servo-hydraulic testing machine. No abductor simulation was utilized.

were implanted in each specimen with 2 mm of interference between the diameter of the shell and the socket. To measure the extent of direct shell-bone contact, discs of pressure sensitive film of 5 mm in diameter were placed at multiple sites between the shell and the reamed surface of the acetabulum. A polyethylene liner was then inserted into each shell and a load of 200 lb. was applied axially at 15 degrees of abduction and 20 degrees of forward flexion to "simulate the resultant force during weight-bearing"; no attempt was made to reproduce muscle loads (Fig. 8.11). The method for measuring cup/bone motion was identical to that of Maloney et al (1990): a brass platform was cemented to the inner wall of the pelvis and two pins were attached to the acetabular shell and passed through a central hole in the platform. Relative motion between the pin and the platform was measured at two sites with electrical extensometers: at the dome of the shell overlying the medial wall of the acetabulum and at the peripheral rim of the shell against the posterior wall.

The authors did not report whether their specimens were cyclically loaded before displacement measurements were taken, or whether they only measured the movement of the implant during the first loading cycle. Nonetheless, after measurement of shell/bone micromotion, four 6.5 mm cancellous crews were inserted through holes within the shell and tightened to a torque of 12 in-lb (1.4 Nm). The micromotion experiments were then repeated. As in the previous experiments, the loading procedure was repeated with successive removal of screws; thus, cup/bone motion was measured with three, two, one and no screws supplementing initial fixation. After each screw was removed from the pelvis, the remaining screws were not retightened prior to reloading. The entire experimental procedure was repeated after the acetabulum was reamed to increase its diameter by 1mm and then 2mm, leading to shell/bone interferences of 1 and 0 mm respectively.

The micromotion data were highly variable, ranging between 7.8 to 148.0 μm in the direction of loading and 0.5 to 139.2 μm in lateral displacement corresponding to superoinferior rotation of the shell. When some degree of interference was present between the shell and the acetabulum, the number of screws had little effect on micromotion. However, in the exact-fit (zero interference) condition, the use of screws reduced axial motion of the implant from 82.8 ± 44.8 μm with one screw to 32.9 ± 9.4 μm with two screws (Fig. 8.12). The authors did not present a

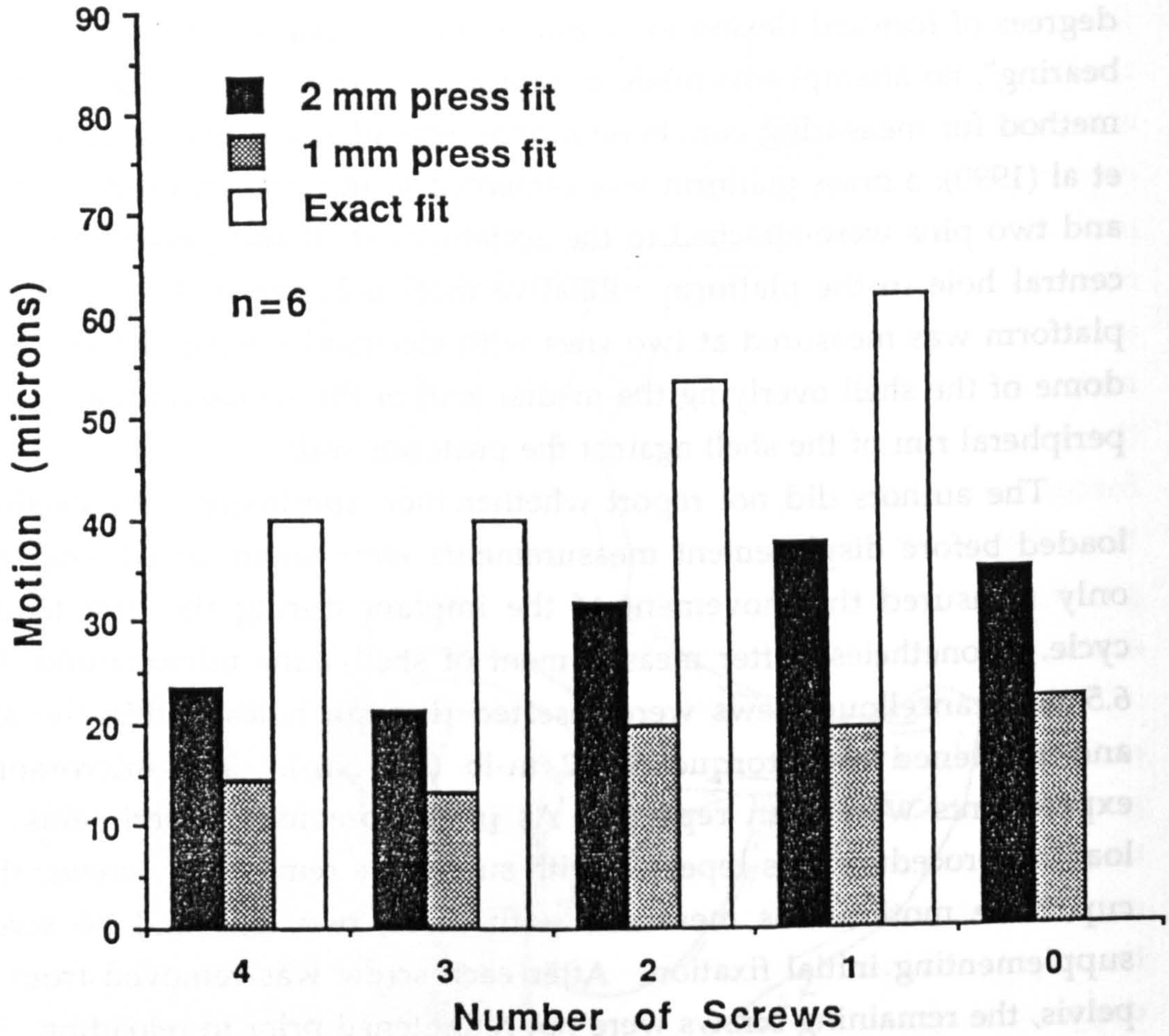

Figure 8.12 Data reported by Kwong et al (1994) for the lateral tilt of acetabular cups implanted with 2 mm, 1 mm and no interference between the shell and the reamed acetabulum. All displacements were measured at a peripheral pin site.

statistical analysis of their results and so it is often difficult to tell which variables had a statistically significant effect upon implant stability. The most important variable in this study appeared to be the degree of interference between the implant and the implantation site, although there was a great deal of variation between specimens. In cups fixed with two screws, axial motion was 25.1 ± 8.0 μm with 2 μm of interference, 32.3 ± 12.1 μm with 1mm of interference, and 32.9 ± 9.4 μm with no interference. Lateral motion averaged 32.0 ± 24.1 μm (2mm), 19.9 ± 22.3 μm (1mm) and 53.6 ± 52.2 μm (0 mm) respectively. The authors concluded that the optimum conditions for implantation of cementless cups was 1mm of shell/socket interference independent of the presence of screws, although they went on to recommend the use 3 - 4 mm of interference in clinical practice!

This study has several fundamental deficiencies. The loads applied to the acetabulum were too low to simulate normal walking where joint reactive forces of 600 lb. (2,600 N), three times larger than the loads applied in this study, are not uncommon. Moreover, the direction of loading is non-physiologic as the joint reaction force typically passes at 50 - 60 degrees to the rim of the acetabulum and not 15 degrees as modeled in this work. As no muscle forces were simulated, the deformation in this experiment of the pelvis is expected to be entirely different from that observed in vivo. This conclusion was demonstrated by the previous experiments of Lionberger et al (1985) and Finlay et al (1986a, 1986b) in comparison with the strain gage studies of Jacob et al (1976) and the measurements performed in Chapter 6 of this work. Consequently, the magnitude and direction of cup/bone motions reported by Kwong et al are not expected to bear much resemblance to these occurring in the body.

It is not possible to accurately assess the meaning of the results presented by Kwong et al without an appropriate statistical analysis. This is difficult in this case because of the relatively small number of specimens, combined with the variability of the data, and the lack of normality of their distribution. Several factors inherent in the design of this experiment probably contributed to the variability of the micromotion measurements. A major criticism of this work is that the investigators did not use different shells to generate 2 mm, 1 mm and 0 mm of interference with the socket. Rather, they reamed the

acetabulum between runs and implanted the same oversized shell. This raises the very real possibility that the shape and the size of the socket changed with each experiment, so that differences in the data may be attributable to variations in the shape of the acetabulum as much as the interference it developed with the implanted component. This stands in contrast to the exacting precautions that the authors took to maximize the area of contact between the acetabulum and each implant; these precautions included control of the depth and orientation of the reamers, selection of reamers that closely matched the size of the shells implanted in the acetabulum and reaming of the socket until contact was achieved between the hemispherical reamer and the floor of the acetabulum.

The authors stated that approximately 50% of the subchondral cortex was sacrificed during preparation of each of their specimens, however, in the course of each experiment the acetabulum was reamed by an additional 2mm to eliminate the interference between the shell and the socket. On this basis of his experience in performing similar experiments, the author expects that this additional reaming would significantly increase the flexibility of the acetabulum, leading to changes in the micromotion of implanted components. This concern could have been checked by implanting a larger shell at the end of each experiment to re-simulate a condition of 2mm of interference. Differences in micromotion between this configuration and the initial runs in which 2 mm of interference was present would have pointed to effects attributable to changes in the flexibility of the pelvis secondary to reaming.

Another deficiency of this study was the method of measuring of micromotion. In both the studies of Maloney et al and Kwong et al, cup motion was described in terms of axial displacement, i.e. motion in a direction along the axis of a radially directed pin, and "AP tilting" and "lateral tilting", i.e. motion in two orthogonal directions normal to the axis of the pin. A tacit assumption of this methodology is that the shell and acetabulum act as rigid bodies. Thus, the authors have assumed that interface motion can be defined by measuring orthogonal components of the displacement of the shell and the pelvis at different sites. This approach ignores the normal elastic deformation of the acetabulum which causes all components of interface motion to be 'site specific'. An additional concern is that the measurements of "interface" motion were taken at some distance from the interface, typically near the medial

surface of the pelvis. For this reason, the data reported in this study correspond to the sum of the displacement of the interface and the elastic deformation of the medial wall of the pelvis.

The experimental design of Maloney et al and Kwong et al was also based upon the assumption that the insertion and subsequent removal of bone screws from an acetabular shell would not influence the fixation generated by the screws that remained. Thus, if a cup was fixed with four bone screws and then two were subsequently removed, it was assumed that the residual fixation provided by the two remaining screws would match the fixation generated by two screws inserted at the start of the experiment. However, during placement of successive screws that are not coaxially oriented, there will be, of necessity, some lateral displacement of the shell within the acetabulum as the balance of lateral forces at each screw/shell interface is disturbed. As screws are removed, it is expected that the shell will move into a slightly deeper position within the acetabulum with some loss of the compressive force originally present between each of the remaining screws and the acetabular shell. Thus, an experiment in which four screws are placed into the acetabulum and are then sequentially removed is expected to be biased towards the original state of fixation (i.e. four screws), and would not fairly represent the placement of one, two or three screws de novo. This bias would have been reduced if each screw had been retightened to a set torque prior to each loading sequence and if new screws had been added rather than removed after each experiment.

CHAPTER 9. DEVELOPMENT OF AN EXPERIMENTAL MODEL TO MEASURE IMPLANT MOTION IN THE ACETABULUM

9.1 INTRODUCTION

As described in Chapter 8, many authors have attempted to simulate the mechanical environment of cementless acetabular cups in biomechanical experiments aimed at evaluating the relative motion between the implant surface and the acetabulum. In the majority of studies, commercial implants of different designs have been evaluated in an attempt to identify the most stable product with little attention to rigorous scientific analysis of the relationship between design features and implant performance, per se. It is certainly true that, in some studies, observed differences between different implants have been attributed to specific design features, through on a post-hoc basis. However, in almost all experimental studies, implants were evaluated that differed in more than one design parameter making it difficult to separate the role of potentially conflicting variables.

Many factors may contribute to the stability of acetabular cups. Previous studies have consistently demonstrated that hemispherical cups implanted without interference with the reamed acetabulum are susceptible to excessive motion under load, especially in the absence of adjunctive screw fixation. Conversely, shells implanted into acetabuli under-reamed by 1 - 3 mm appear to be stable, especially if this mode of fixation is augmented with transacetabular screws. However, the use of interference fixation carries with it several potential risks. In the under-reamed socket, fixation is localized and is confined to the peripheral rim of the acetabulum. Attempts to increase the depth of placement of a cup and hence the area of shell/bone contact can lead to fractures of the anterior or posterior wall. Conversely, if a cup is not seated properly, fixation may diminish with time as the bony acetabulum relaxes; this may allow the cup to toggle because of preferential contact with the anterior and posterior sides of the socket. The implant also may be susceptible to traumatic dislodgment through accidental contact with the femur or the neck of the femoral component. All of these considerations point to a need to define the optimum conditions for stable fixation of

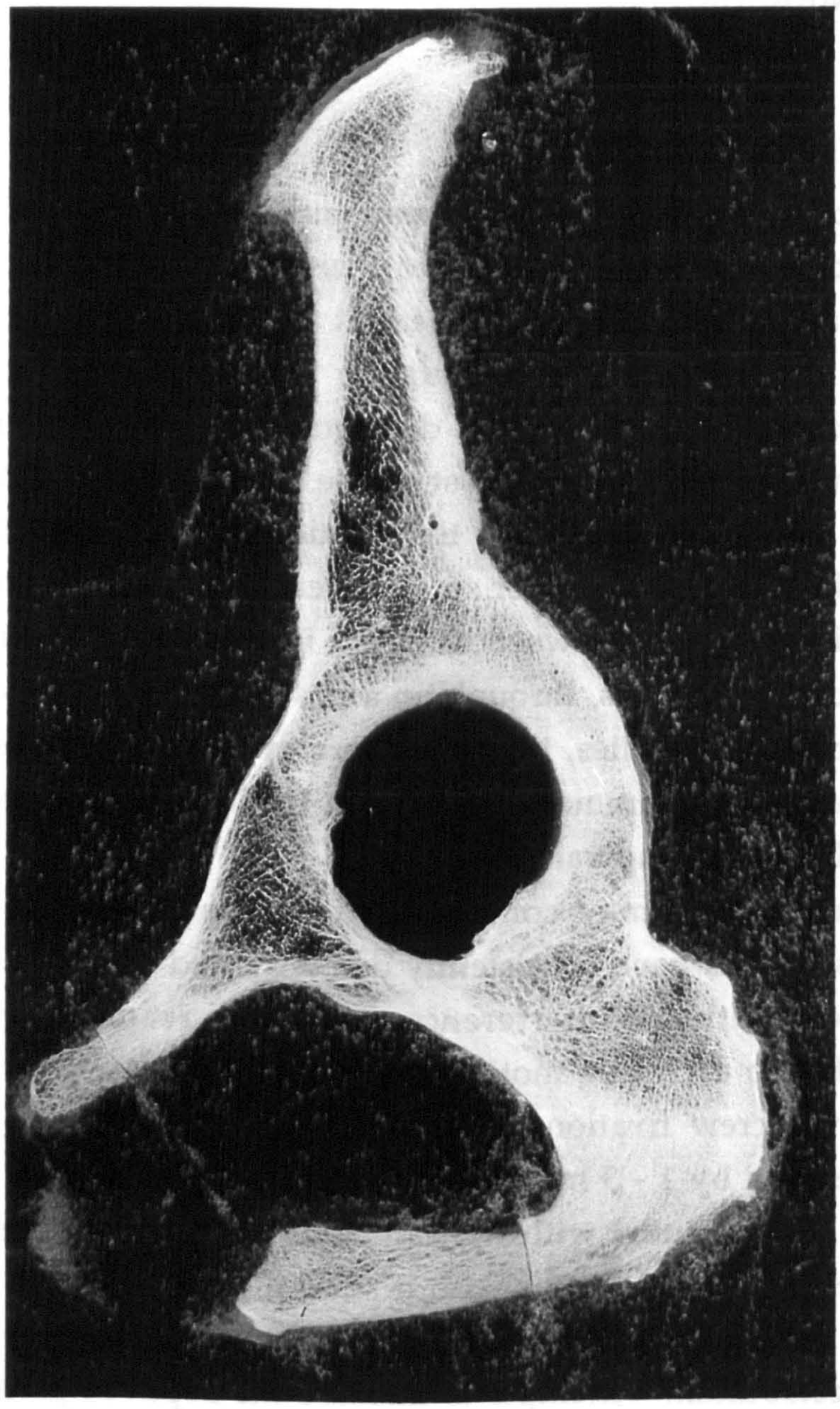

Figure 9.1 Contact radiograph of a 5 mm slice taken through the pelvis, parallel to, and approximately 10 mm medial to the mouth of the acetabulum.

acetabular cups with and without the use of adjunctive transacetabular screws.

9.2 ACETABULAR IMPLANT DEVELOPMENT

In order to experimentally evaluate the role of several design features on the stability of fixation of cementless acetabular cups, a basic implant design was developed which could be used with a variety of surface coatings, with and without screw fixation. The first stage in the design process was to determine the optimum placement of bone screws in the acetabulum to provide fixation of the acetabular shell.

Several criteria were established for placement of screws within the acetabulum:

(i) the screws had to engage the densest bone accessible from the joint,

(ii) it was assumed that each screw would be oriented perpendicular to the surface of the cup, to minimize screw/liner impingement,

(iii) screws would not be placed in any position where there was a reasonable chance of neurovascular injury.

9.2.2 The Distribution of Bone Density

The distribution of pelvic bone density was assessed through inspection of a series of sections taken through the pelvis parallel with the mouth of the acetabulum (Fig. 9.1). Contact radiographs were prepared of three specimens and subsequently digitized and computer enhanced to indicate areas of varying bone density. Examination of bone slices from the mouth of the acetabulum through to the sacroiliac joint revealed that the strongest bone stock was present beneath the acetabular rim and within the body of the ischium. Conversely, the cancellous bone within the ilium, immediately superior to the acetabulum, was observed to be of relatively low density and was therefore considered less suitable for screw fixation. Similarly, the bone within the pubic ramus was generally of low density, leading to inferior pull-out strengths of cancellous screws in previous biomechanical studies.

Vertical slices taken through the ilium indicated the presence of strong cancellous bone superior and medial to the acetabular dome corresponding to the coalescence of the principal bony arcades of the

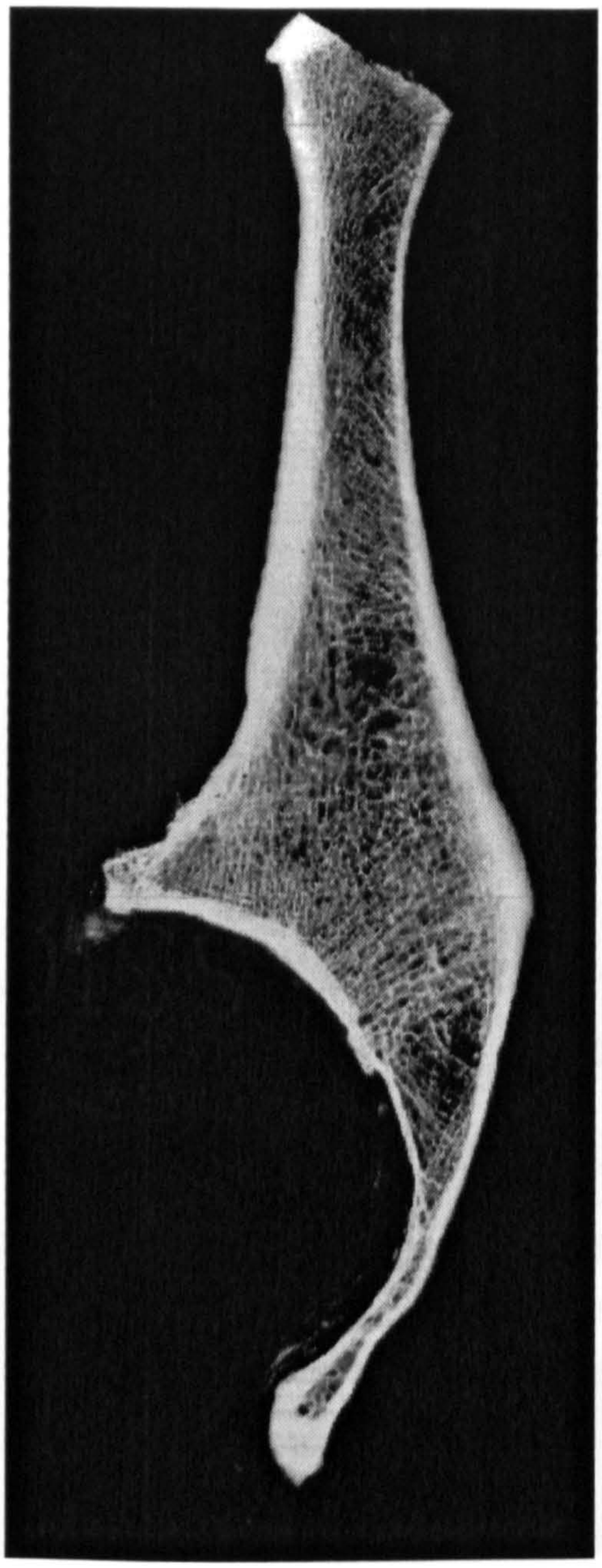

Figure 9.2 Contact radiograph of a vertical slice through the acetabulum and the ilium, showing the weight-bearing dome, the subchondral plate and the medial wall extending down to the acetabular notch.

pelvis. This is an ideal place for screw placement, given its orientation with respect to the joint reaction force. However, the projected area of this zone was found to be relatively small in comparison with the area of the acetabulum itself and so might be difficult to engage on a reliable basis. Fixation in this area would also require longer screws which are more susceptible to significant bending leading to mechanical failure. These studies indicate that a relatively small area of the acetabular surface provides access to regions of the pelvis suitable for screw placement. These areas of bone are situated:

(i) immediately medial to the acetabular rim,
(ii) within the body of the ischium, and
(iii) within the dome of the acetabulum, medial to the ilio-pectineal line

9.2.3 The Intracortical Thickness of the Pelvis

In view of the ubiquitous distribution of veins, arteries and nerves over the dorsal surface of the pelvis, it was decided that the best strategy to minimize the risk of neuorvascular injury would be to restrict screw placement to the interior of the pelvis. This form of screw fixation is generally termed 'unicortical' in contrast to 'bicortical' fixation in which the screw engages both the inner and outer cortices. Although it would appear logical that the longest possible screw would provide the greatest purchase in cancellous bone, longer screws (e.g. 35 mm) provide little advantage over shorter screws (e.g. 25 mm) within the pelvis due to the nonuniform distribution of cancellous density. Beneath the subchondral surface of the acetabulum there is a dense layer of cancellous bone of 5-10mm in thickness that supports the weight-bearing surface (Fig. 9.2). At deeper levels, the bone is of lower density, and in older individuals may be virtually non-existent, especially within the anterior and posterior columns (Fig. 9.3). This suggests that the length of unicortical screws may not critically affect the strength of fixation of acetabular cups provided that the strong subchondral bone is engaged within the coarsest available screw threads.

To guide the placement of screw holes within the acetabular shell, nine pelves were obtained from the dissecting room for detailed analysis (Table 9.1). Standard radiographs were prepared of each specimen to confirm the absence of prior pelvic trauma, malignancy or bony

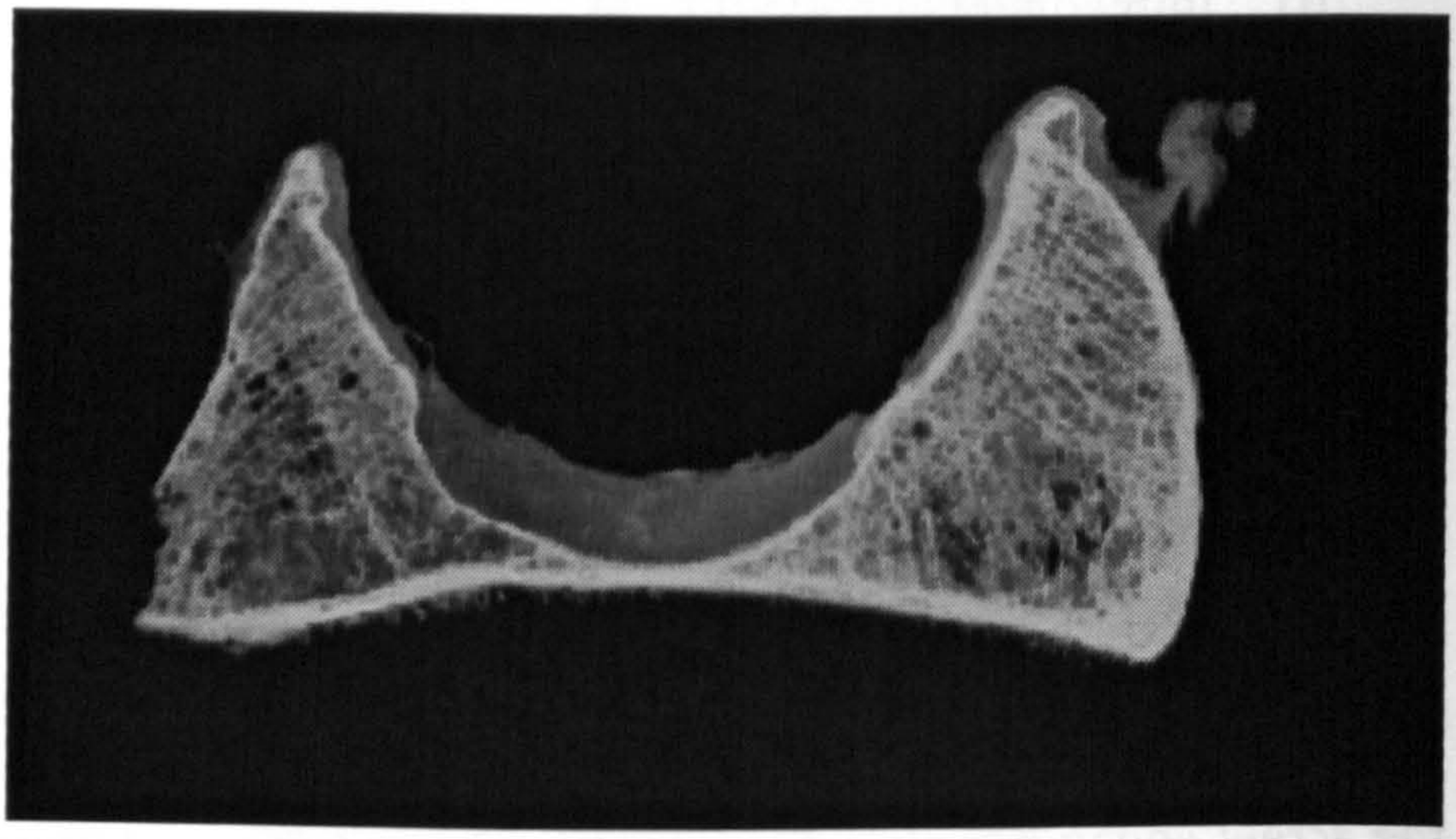

Figure 9.3 Contact radiograph of a 5 mm transverse slice taken through the center of the acetabulum of an osteoporotic specimen. Low cancellous bone density is visible in the anterior wall (left) compared to the posterior wall (right). The weight-bearing lunate surface is seen to occupy only half of the boundary of the socket.

Specimen No.	Age	Sex	Side	Cause of Death	Acetabular Diameter * (mm)
1	84	Female	Right	Chronic hear failure	40
2	Unknown	Female	Left	Unknown	44
3	64	Female	Left	Pulmonary embolism	45
4	Unknown	Female	Left	Unknown	49
5	58	Female	Right	Carcinoma	50
6	66	Male	Left	Pneumonia	52
7	Unknown	Male	Right	Unknown	54
8	67	Male	Left	Metastatic carcinoma	56
9	Unknown	Male	Left	Unknown	57

Table 9.1 Descriptive data pertaining to the acetabular specimens

* Measured anterior to posterior

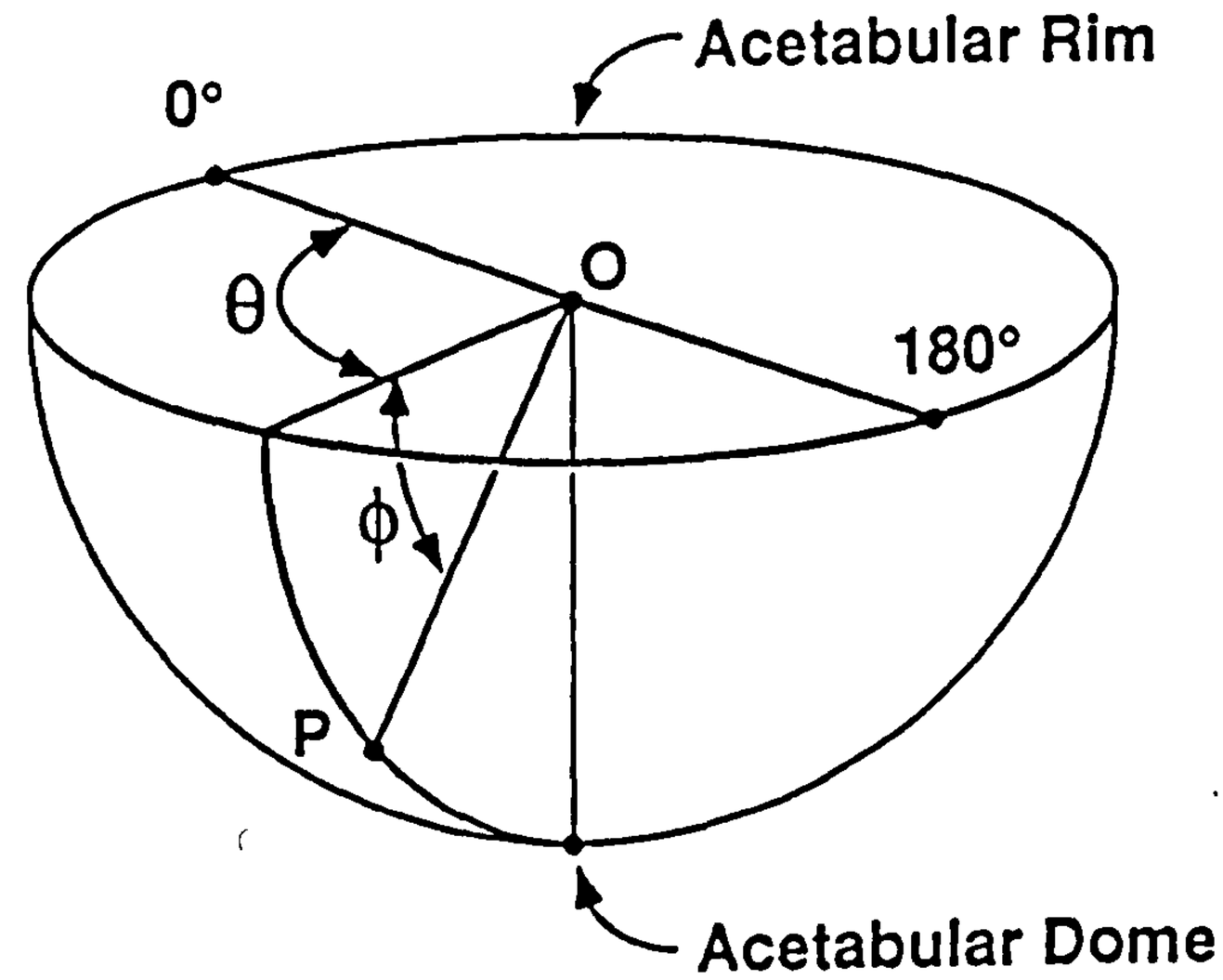

Figure 9.4 A point (P) on the surface of the reamed acetabulum can be described with respect to the fixed anatomic landmarks using angles of latitude and longitude.

abnormality, including degenerative arthritis of the hip. Wood's metal hemispheres were prepared to match the diameter of each acetabulum and cemented in place with the flat surface of the implant lying parallel to the acetabular margin. These implants served to define the center of the acetabular margin on slices of each specimen generated by subsequent sectioning.

Each specimen was embedded in a block of rigid polyurethane foam, and sectioned into 16 wedge shaped slices which joined at the center of the acetabulum. Photographic replicas were prepared of each slice for later analysis. On each slice, the distance from the center of the acetabular implant to the inner wall of the pelvis was measured as a function of the angle of latitude from the face of the implant (Figs. 9.4, 9.5). The distance from the center to the surface of the hemisphere plus an allowance for the thickness of the cement layer (typically 1 - 2 mm) was subtracted from each measurement to allow calculation of the intracortical thickness of the pelvis.

Based on an initial pilot study of four specimens of 44, 49, 54, and 57 mm (specimens 2, 4, 7, and 9), it was established that the cortical contours of each slice of the acetabulum were scaled in relatively close proportions to the diameter of the acetabulum itself. In figure 9.6. , the distribution of intracortical thickness is depicted for each normalized acetabular diameter and for a fixed thickness of 20 mm. It can be seen that the contours of the normalized values are relatively consistent, despite the broad range of sizes of specimens covered by the sample. For this reason, all measurements of intracortical thickness were normalized and then represented on standard plots at intervals of 30%, 40%, 50% and 60% of the acetabular diameter (fig 9.7).

In order to measure the area within each contour on the surface of the acetabulum the data were also plotted using a projection in which the spacing of lines of constant latitude was varied in proportion to the area between each line on the surface of a hemisphere. Thus the area of any zone on this two-dimensional projection corresponds directly to its true surface area on the curved hemispherical surface of the reamed acetabulum. Using this projection, the area of each zone corresponding to the 30%, 40%, 50%, and 60% boundaries was calculated for each acetabulum and averaged.

For an intracortical thickness of only 30% of acetabular diameter

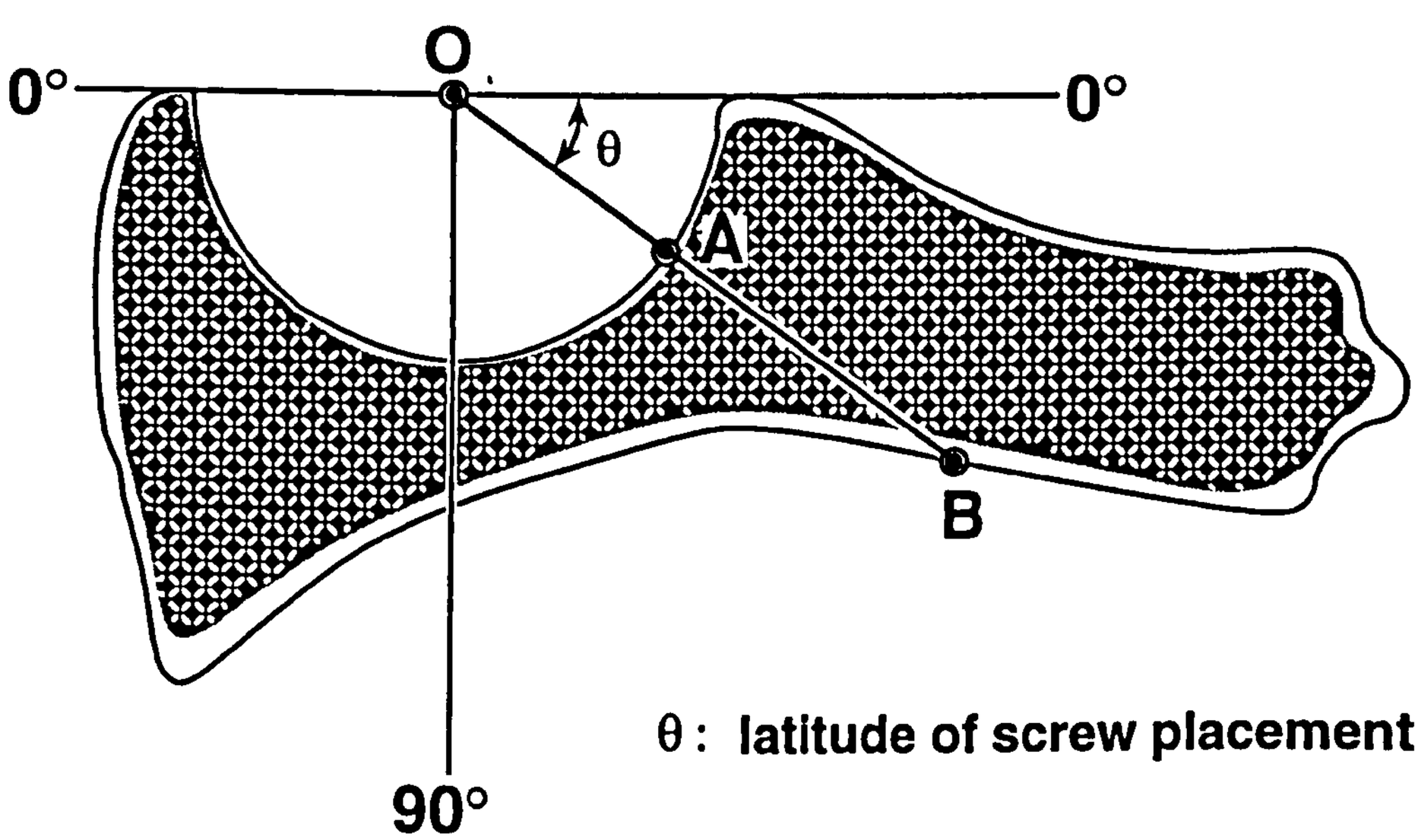

Figure 9.5 Slices taken through the acetabulum may be analyzed to determine the maximum length of bone (AB) available for placement of a screw perpendicular to the surface of the shell. The position of the screw within the shell (A) may be described by the location of the slice and the angle (J) between the axis of the screw and the mouth of the acetabulum.

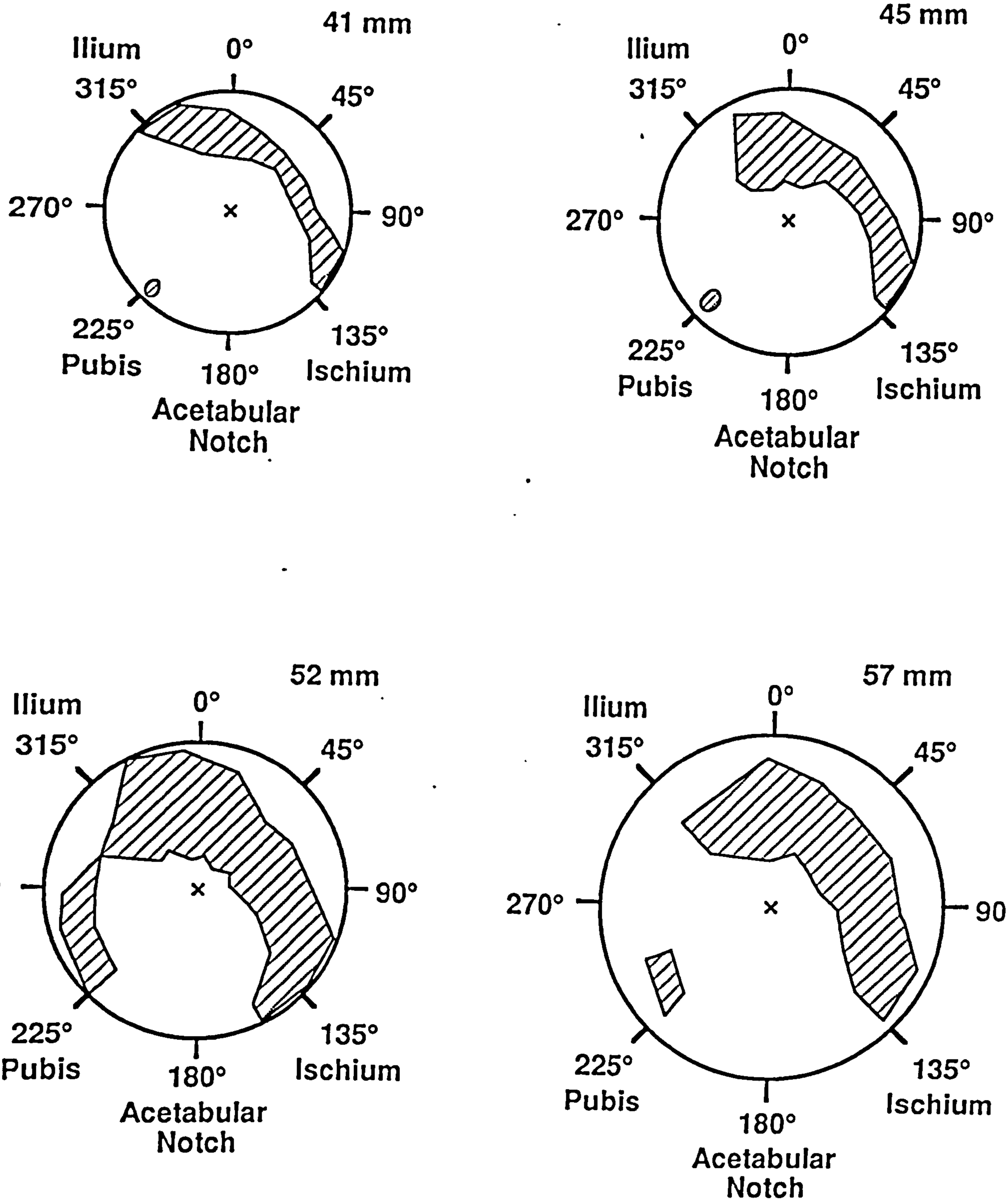

Figure 9.6 Positions within the acetabulum where screws of 20 mm or larger may be placed perpendicular to the reamed surface without penetration of the inner cortex of the pelvis. These diagrams summarize observations performed on acetabular specimens of 41, 45, 52, and 57 mm in diameter.

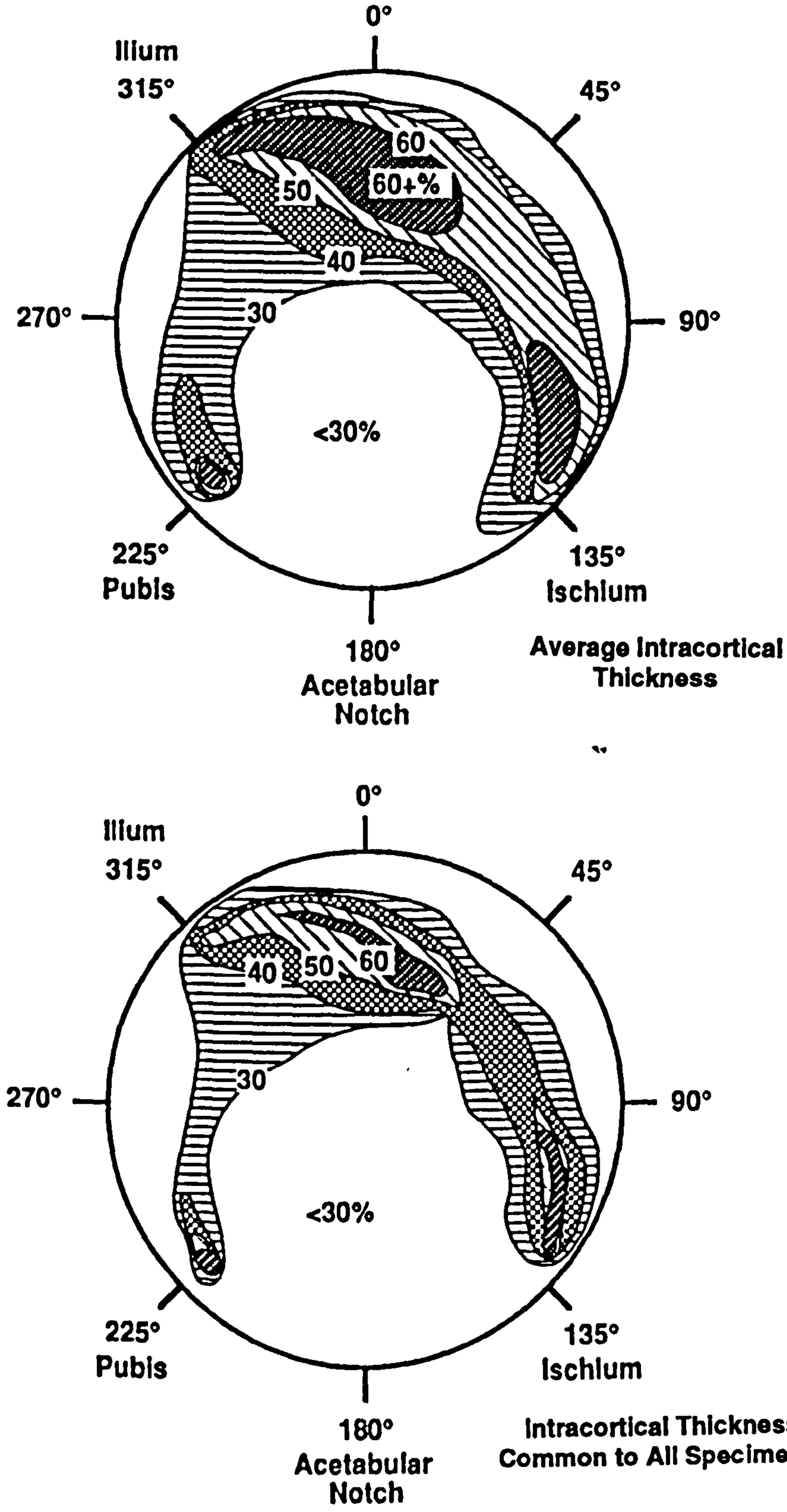

Figure 9.7 The intracortical thickness of the pelvis, measured perpendicular to the acetabular surface. All values are expressed as a percentage of the acetabular diameter. The upper diagram, was constructed using the average thickness of all nine specimens, while the lower diagram depicts the minimum thickness available at each point over the acetabular surface.

(approximately 15 mm in the average acetabulum), the distribution of sites for unicortical screw placement resembled the original lunate surface with the exception of peripheral zone present both anteriorly and posteriorly and extending for 30 to 50° from the face of the acetabulum. The total surface area present posteriorly was found to be significantly larger and certainly less variable than that present anteriorly.

At 40% of the acetabular diameter, the available area for screw placement was restricted almost entirely to an arc extending from the ilium to the ischium around the posterior half of the acetabulum. The anterior boundary of this zone was found to extend from 70-80° superiorly to approximately 30° adjacent to the ischial facet. Its posterior border reached a latitude of only 45° midway between the ilium and the ischium. Over the anterior half of the acetabulum only a small area was present in which the intracortical thickness exceeded 40% of the acetabular diameter. This area was in the vicinity of the anterior facet over the body of the pubis. In all but one specimen, all of the remaining anterior half of the acetabulum would not support unicortical fixation with screws whose length exceeded 40% of the acetabular diameter.

With the exception of a small area immediately over the pubis, unicortical fixation could not be obtained in the anterior half of the acetabulum using screws of a length equal to 50% of the acetabular diameter. Within the posteroinferior quadrant the size and location of areas available for replacement of screws this length varied to such an extent that unicortival fixation was still available in a of the pelvis in some of the specimens sampled. Superiorly, the zone still extended from 35 to 75° of latitude.

At 60% of the acetabular diameter, two small zones were found, corresponding to the superior and inferior limbs of the posterior column of the pelvis. Superiorly, this zone extended from the direction of the sciatic buttress posteriorly to the iliac wing anteriorly, however, the exact position of the region varied significantly between specimens, especially on the anterior side of the pelvis. A common zone was found which extended from 25° posteriorly from the superior reference point and was located at a latitude of 50 to 60° from the rim of the acetabulum. Inferiorly, a second zone was present over the body of the ischium, however, its latitude varied between specimens so that only a narrow band was common to every pelvis.

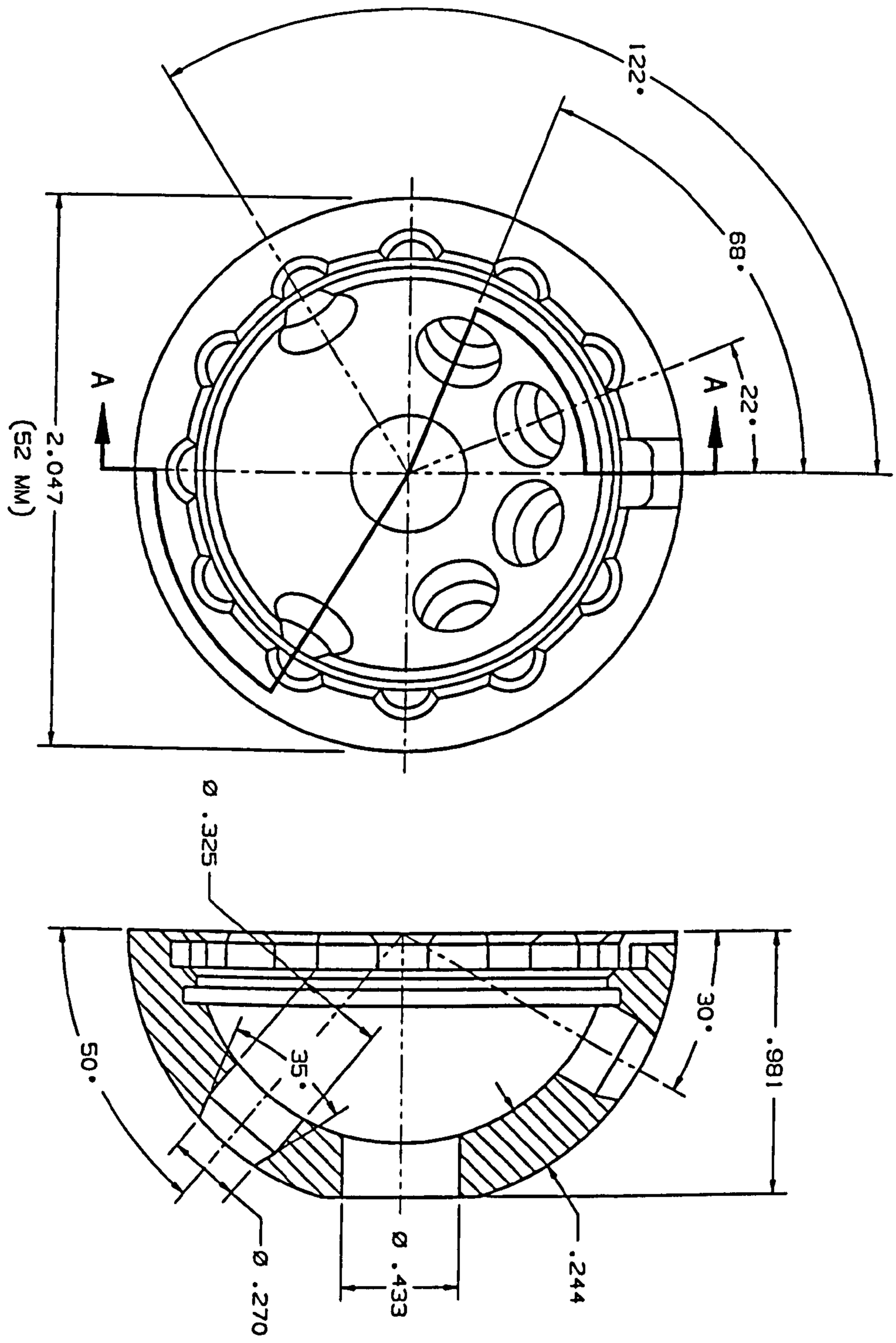

Figure 9.8 Diagrammatic representation of the acetabular shell utilized in the measurement of implant/bone micromotion.

This information was utilized to determine the best placement of screw holes within an acetabular shell, on the assumption that the axis of the screw would be perpendicular to the surface of the shell and the length of each screw would have to exceed 10 mm for adequate purchase in the average acetabulum (diameter: 52 mm). On the basis of these assumptions, an implant was designed with six holes to accommodate 6.5mm bone screws (Figs 9.8). The holes were located within the zone corresponding to an intracortical thickness exceeding 40% of the acetabular diameter. Four holes were situated in the superior half of the shell spaced at 44 degree intervals at a fixed angle of 50 degrees from the rim. Two further holes were located inferiorly for ischial fixation (the same cup was intended for use in both the right and left acetabulum). Both of the ischial holes were located at 58 degrees anterior and posterior to the inferior axis of the component at 30 degrees to the rim.

9.3 SELECTION OF A TECHNIQUE TO MEASURE SHELL/BONE MICROMOTION

9.3.1 INTRODUCTION

Several criteria may be postulated to describe an ideal method for measuring the relative motion of the acetabulum and an acetabular shell. For application to the experiments in this study, the measurement method must:

(i) be capable of measuring motion of up to 200 μm in three orthogonal directions with an accuracy of better than 5 μm,
(ii) not alter the relative motion of the bone-implant interface,
(iii) not affect the stiffness of the bone or the implant,
(iv) allow measurement of interfacial motion at five or six discrete points over the surface of the acetabulum which are not directly accessible from the external surfaces of the pelvis or the acetabular shell, and
(v) be relatively inexpensive.

In reality, no single method appears to satisfy all of these criteria, principally because, once the acetabular cup is implanted, the interface is only directly accessible around the rim of the acetabulum where relative motion is expected to be least. Another prohibitive factor is the magnitude of the relative motions which are expected to be small,

ranging form 20-50 μm at most measurement sites.

9.3.2 BIPLANAR RADIOGRAPHY

One potentially useful method is based upon biplanar radiography, which can be used to measure the three-dimensional position of spherical markers implanted into the bone and the implant. Two radiographs are prepared of each specimen using different sources of x-rays. Through the known geometric relationship between the x-ray sources it is then possible to calculate the position of the radiographic markers. The motion at the implant/bone interface is calculated as the difference between the relative positions of the radiographic markers before and after loading. This technique has been utilized in many previous studies to follow the complex, three-dimensional movement of human and artificial joints and the motion of the implant/bone interface. Biplanar radiography has the enormous advantage that it can be used to measure the internal motion of structures which are not accessible during loading. This has led us to use this technique in a number of previous studies of which we have successfully measured such things as the deformation patterns of intervertebral discs, the motion of the subtalar joint and patterns of radio-ulnar instability after severe injuries of the forearm (Kamaric et al, 1991).

To investigate the applicability of this method to the measurement of motion at the acetabular interface, radiolucent acetabular cups were fabricated from aluminum and an array of spherical chrome-steel balls of 1.6mm diameter (Small-parts Inc., Miami, Florida) were embedded at four sites within each shell. Another set of six balls was embedded in the reamed subchondral surface of a cadaveric acetabulum. After impacting the shell into the acetabulum, the specimen was suspended within a metal frame which had been fabricated to allow two radiographic cassettes to be supported orthogonally. All four sides of the frame were reinforced with translucent sheets of plexiglas. Calibration markers were embedded in each of the plexiglas sheets to allow the position of the radiographic sources to be determined prior to measurement of the position of the radiographic markers within the shell and the acetabular specimen.

Three identical pairs of biplanar radiographs were prepared of the specimen without altering its position between exposures. The separation of two of the balls within the pelvis was measured using each

pair of radiographs to assess the inherent reproducibility of the method. The variability of these measurements was ± 87.3 μm at the 95% confidence level which exceeded the acceptable level of error for measurement of interfacial motion by more than one order of magnitude! This inaccuracy is attributable to several sources, including:

(i) errors in the calculated position of the radiographic source, the specimen and the film,

(ii) the fact that x-rays are generated by a source of finite size and not at a single point in space,

(iii) the presence of motion or vibration of the specimen or the radiographic box during exposures,

(iv) the inherent resolution of the electronic digitizing table which is used to measure the position of each of the implanted markers on each of the radiographs, and

(v) the assumption that both films are orthogonal and that the x-ray film and the calibration markers embedded in the radiolucent sides of the box lie in planes which are parallel.

Since these experiments, we have developed new techniques to reduce some of these sources of error, however, even under the best of circumstances the reproducibility of the measurements still exceeds 50 μm (95% confidence).

9.3.3 ELECTRO-MECHANICAL TRANSDUCERS

Many of these problems could be overcome using a second method of measuring interfacial motion in which the body of a displacement transducer is placed within holes drilled into the acetabular bed and attached to the subchondral bone. A suitable device would be a miniature linear variable displacement transformer (LVDT) consisting of an external sleeve and a central core. As micromotion at the shell/bone interface is expected to occur simultaneously in three orthogonal directions, the central core must be able to move within the sleeve or bend laterally without affecting its electrical output or axial displacement. Alternatively, the junction between the transducer and the shell may be designed so that the core is able to slide on the surface of the shell without loss of contact during loading.

This approach has the following potential shortcomings:

(i) Most displacement transducers, including LVDTs are relatively

large compared to the dimensions of the pelvis. The minimum external diameter of commercially available devices is 8-10 mm. Holes of this size are expected to significantly alter the deformation of the acetabulum itself and thus the micromotion of the shell/bone interface.

(ii) Even if this method were feasible for measurement of displacements normal to the surface of the shell, another transducer or set of transducers would have to be used to measure the sliding components of motion at the interface.

Another method for measuring shell/bone motion is to attach strain gage extensometers to the shell and the acetabulum. These instruments have the advantage that displacements can be measured with an accuracy of around 1 - 2 μm and a resolution of 0.2 - 0.5 μm. Previous investigators have used strain gage extensometers to measure motion between bone and a variety of prosthetic devices including femoral stems and acetabular shells. However, as most strain gage extensometers have typical dimensions of at least 20 mm x 10 mm, there is insufficient room for these devices to be embedded within the body of the acetabular shell or the acetabulum. Consequently, extensometers must be placed on the external surface of the pelvis and mechanically connected to the implanted prosthesis. This may be achieved by passing steel pins through holes drilled through the pelvis to the acetabulum and rigidly attaching them to the acetabular shell. One leg of the extensometer is then attached to one of the pins while the other leg is attached to the surface of the acetabulum or the medial wall of the pelvis. If the extensometer is not directly attached to the bone immediately adjacent to the shell, the displacement measured by the device will correspond to the sum of motion occurring at the cup/bone interface and the elastic deformation of the pelvis between the acetabulum and the measurement site. To isolate the motion of the interface, the extensometer can be mounted on a rigid sleeve passed through the wall of the pelvis and fixed to the acetabulum within the subchondral bone. These readings will be valid measures of interfacial motion provided that the pin is free to move without contacting the sleeve.

Although, in theory, this method appears relatively straight-forward, in practice it presents several difficulties:

(i) Over approximately one quarter of the acetabular surface, the

intracortical thickness of the pelvis exceeds 20 mm, and in some places is greater than 40 μm. This can make placement of the transacetabular holes difficult, moreover, errors may be introduced into measurements of micromotion due to bending of the subchondral bone causing lateral motion of the end of the sleeve.

(ii) Extensometers are relatively bulky and require a space of approximately 10 mm in radius around the exit site of the pin without encumbrance from bony structures or external cables. This consideration would not limit the selection of a transducer if experiments were to be performed with simple loading configurations, i.e. without the addition of cables. However, the ideal measurement technique would be applicable to simple loading experiments and, ultimately, to more physiologic models of the pelvis, complete with cables simulating muscle action. As these cables must pass over the posterior surface of the ilium to simulate the action of gluteus minimus, medius and maximus, space is extremely limited for placement of extensometers.

(iii) During implantation of acetabular shells it is not possible to exactly predict the three-dimensional position of the shell within the bone. Small variations in the orientation of the prosthesis can change the relative position of fixed points on the shell and the implantation site by up to 5 mm. It is therefore impractical to drill holes in the anatomic specimen prior to seating the shell, on the assumption that the holes within the shell and the acetabulum can be aligned after implantation of the prosthesis.

(iv) A fundamental assumption of any experiment in which holes are drilled through the pelvis to provide access to the shell/bone interface is that the holes themselves will not affect interface motion. However, quite large holes of up to 7 mm diameter are needed if rigid sleeves are to be placed within each hole to allow direct measurement of interface motion. This could cause a significant reduction of the structural stiffness of the pelvis, leading to artificially larger values of micromotion.

A series of experiments was performed to assess the significance of

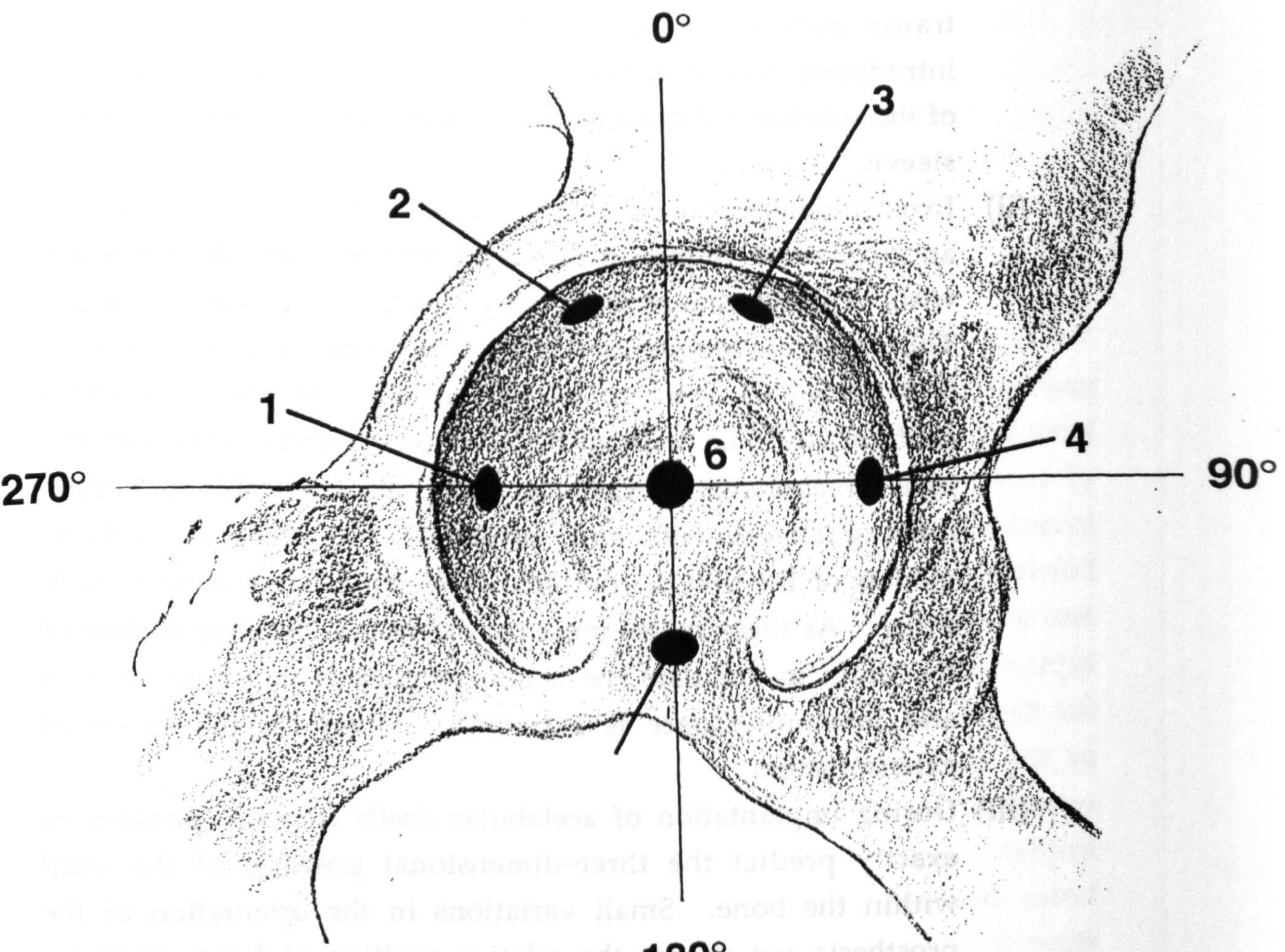

Hole No.	Longitude	Latitude
1	270 °	30 °
2	335 °	25 °
3	25 °	25 °
4	90 °	30 °
5	180 °	45 °
6	--	90 °

Figure 9.9 Anatomic sites for placement of drill holes in the acetabulum.

each of these potential difficulties and to investigate if they could be overcome. Three embalmed pelves were obtained to determine if holes of less than 30 mm in length could be placed within the acetabulum while still providing access to each quadrant of the acetabular interface. The proximity of each potential exit site to cables used to simulate muscle loading was also studied. Based upon both of these considerations, six anatomic sites were identified for placement of holes passing perpendicular to the acetabular surface (Fig. 9.9).

To allow each measurement hole to be drilled after placement of the prosthetic shell, a technique was developed in which the shell was implanted in the acetabulum and then a drill was passed through each hole within the shell and then through the underlying pelvis and its cortical wall. The drill was replaced with a smooth pin of the same diameter which was rigidly attached to the shell. This pin then served as a guide for a cannulated drill which could be passed from the medial surface of the pelvis to the subchondral surface to make a hole of correct size and placement.

9.4 THE EFFECT OF TRANSACETABULAR HOLES ON IMPLANT-BONE MICROMOTION

The effect of drill holes on interface displacement was studied using a variety of methods. As no reliable method exists to allow measurement of the internal motion of the interface to accuracies approaching 5-10 μm it was assumed that if drill holes had a significant effect on motion of the interface it would be reflected in changes in the deformation of the acetabulum under load. This would be true, especially in the presence of a low friction interface between femoral head and the acetabular surface which would allow the acetabulum to deform without significant restraint in terms of bending about the hip joint.

9.4.1 Materials and Methods

To test the hypothesis that transacetabular holes would significantly affect acetabular deformation, six holes of 5 mm diameter were drilled in the fresh cadaveric specimens used in the earlier loading experiments. The holes were placed at the six sites previously determined to be suitable for placement of transducers on the external surface of the pelvis (Fig. 9.9). The specimen was then returned to the loading frame and tested

Measurement Site	Gauge Length (mm)	No Holes		5 mm Holes	
		Deformation (μm)	n	Deformation (μm)	n
1. Beneath Ilium	39.60	4.2 ± 1.1	5	4.6 ± 2.3	5
2. Anterior Rim	37.36	54.2 ± 1.5	11	57.9 ± 5.9	6
3. Facets	43.84	1.7 ± 1.0	17	35.3 ± 5.7	5
4. Ischium - Posterior Rim	31.30	19.2 ± 0.3	9	16.7 ± 0.2	6
5. Ilium - Posterior Rim	36.11	22.1 ± 1.2	8	N/A	-
6. Depth of Anterior Wall	40.12	30.0 ± 2.8	5	58.8 ± 15.3	4
7. Depth of Posterior Wall	48.28	6.0 ± 0.2	7	2.2 ± 0.2	5
8. Medial Wall (Vertical)	39.21	17.5 ± 0.7	6	22.3 ± 2.9	5
9. Medial Wall (Horizontal)	45.16	11.9 ± 1.7	10	45.3 ± 4.1	8
10. Pectineal Line	28.01	47.3 ± 2.4	3	18.0 ± 3.4	7

Table 9.2 Measurements of deformation of the fresh acetabular specimen with and without 5 mm holes.

* These measurement sites are graphically depicted in Figure 6.9.

under identical conditions to the original experiments performed without transacetabular holes using a spinal load of 175 lb (778 N) and the muscle forces set forth previously.

9.4.2 Results

The average values for the deformation of the pelvis, recorded at each of the 10 sites are presented in Tables 9.2 and 9.3. Although the general pattern of deformation was similar to that seen in the same specimen without transacetabular holes, there are some striking differences. Small changes in deformation (<20%) were measured at three sites (beneath the ilium, along the anterior rim and along the posterior wall inferiorly down to the ischium). A peculiar observation was the development of a significant compressive strain between the acetabular facets (-804 vs. -38 microstrain). An increase in the magnitude of the recorded strain might be explained by a reduction in the stiffness of the specimen, especially within the acetabular notch where one of the 5mm holes was located. However, the change from virtually no strain to a compressive strain suggests that there was some alteration in the loading of the specimen after hole placement. This is further suggested by the dramatic reduction in tension along the pectineal line (644 vs. 1687 microstrain). Placement of the 5mm holes also appeared to radically alter the balance of load transmission between the anterior and posterior walls of the pelvis with the mediolateral strain increasing by 96% in the anterior wall and decreasing by 74% in the posterior wall. There was also an inexplicable increase in the transverse strain over the dorsal surface of the ischium (+280%) despite the relative modest increase in the longitudinal component (+27%).

These results are considered to be more a reflection of the mechanical deterioration and progressive deformation of the biological specimen than the effect of the transacetabular holes. This was reflected in changes in the geometry of the specimen and the position of the spinal load with respect to the hip joint. Substantial changes were also noted in the condition of the cancellous bone and the sacro-iliac ligaments which became necrotic and stretched out with repetitive loading. In addition, while measurements were being made on the specimen after 5 mm holes had been drilled in the acetabulum, the flexion moment generated by the spinal load caused subluxation of the sacro-iliac joints. The joints were

Site	No Holes		5 mm Holes		Change in Strain
	Effective Strain ($\times 10^{-6}$)	n	Effective Strain ($\times 10^{-6}$)	n	
1. Beneath Ilium	-107 ± 29	5	-115 ± 57	5	+7%
2. Anterior Rim	-1451 ± 39	11	-1551 ± 158	7	+7%
3. Facets	-38 ± 22	17	-804 ± 131	5	+2015%
4. Ischium - Post. Rim	-614 ± 10	9	-532 ± 49	6	-13%
5. Ilium - Post. Rim	-611 ± 32	8	N/A	N/A	N/A
6. Anterior Depth	747 ± 70	5	1465 ± 381	4	+96%
7. Posterior Depth	124 ± 5	7	45 ± 4	5	-14%
8. Medial - Vertical	446 ± 18	6	568 ± 74	5	+27%
9. Medial - Horizontal	264 ± 38	10	1002 ± 91	6	+280%
10. Pectineal Line	1687 ± 84	3	644 ± 123	7	-72%

Table 9.3 The effective strain measured at each anatomic location using the fresh acetabular specimen with and without transacetabular holes.

"Effective Strain" is defined by the change in length that occured with loading divided by the unloaded gauge length (i.e. distance separating the measurement pins).

reduced back to their original position and fixed with cancellous bone screws to prevent further subluxation. However, this method of fixation gradually failed once the spinal load was restored due to inadequate screw purchase in the necrotic cancellous bone. Subsequently, the sacroiliac joints were stabilized using a circumferential cable and turnbuckle which was attached to the loading fixture, however this could not prevent some subluxation of the sacrum from its original anatomic position. For this reason, it is likely that much of the change observed in pelvic deformation between experiments was due to irreversible deterioration of the specimen itself and not the presence of screw holes within the specimen.

Additional factors suggested that the readings obtained in the specimen after drilling the 5mm holes were of questionable validity:

(i) At a number of measurement sites the arms of the extensometers and the cables used to simulate muscle forces were in very close proximity during loading due to the bulk deformation of the pelvis. This made accurate measurement of acetabular deformation extremely difficult without artifacts caused by contact between the transducer and a cable during loading.

(ii) As the specimen aged, the cartilage on both the femoral and acetabular surfaces dried out and shrunk despite efforts to keep it rehydrated. This caused the femoral head to become loose within the socket and dramatically altered the contact area of the articulation and, presumably, the distribution of contact stress. This factor may have also had a significant effect on acetabular deformation.

9.5 STUDIES PERFORMED WITH THE ACETABULAR ANALOGUE

9.5.1 INTRODUCTION

In view of the complications experienced with the fresh acetabular specimen, it was thought advisable to restrict the use of cadaveric material to experiments where fewer measurements were being performed for each loading condition or specimen configuration. For the purpose of the present study of the effect of transacetabular screw holes on acetabular deformation, it was decided that a more satisfactory approach

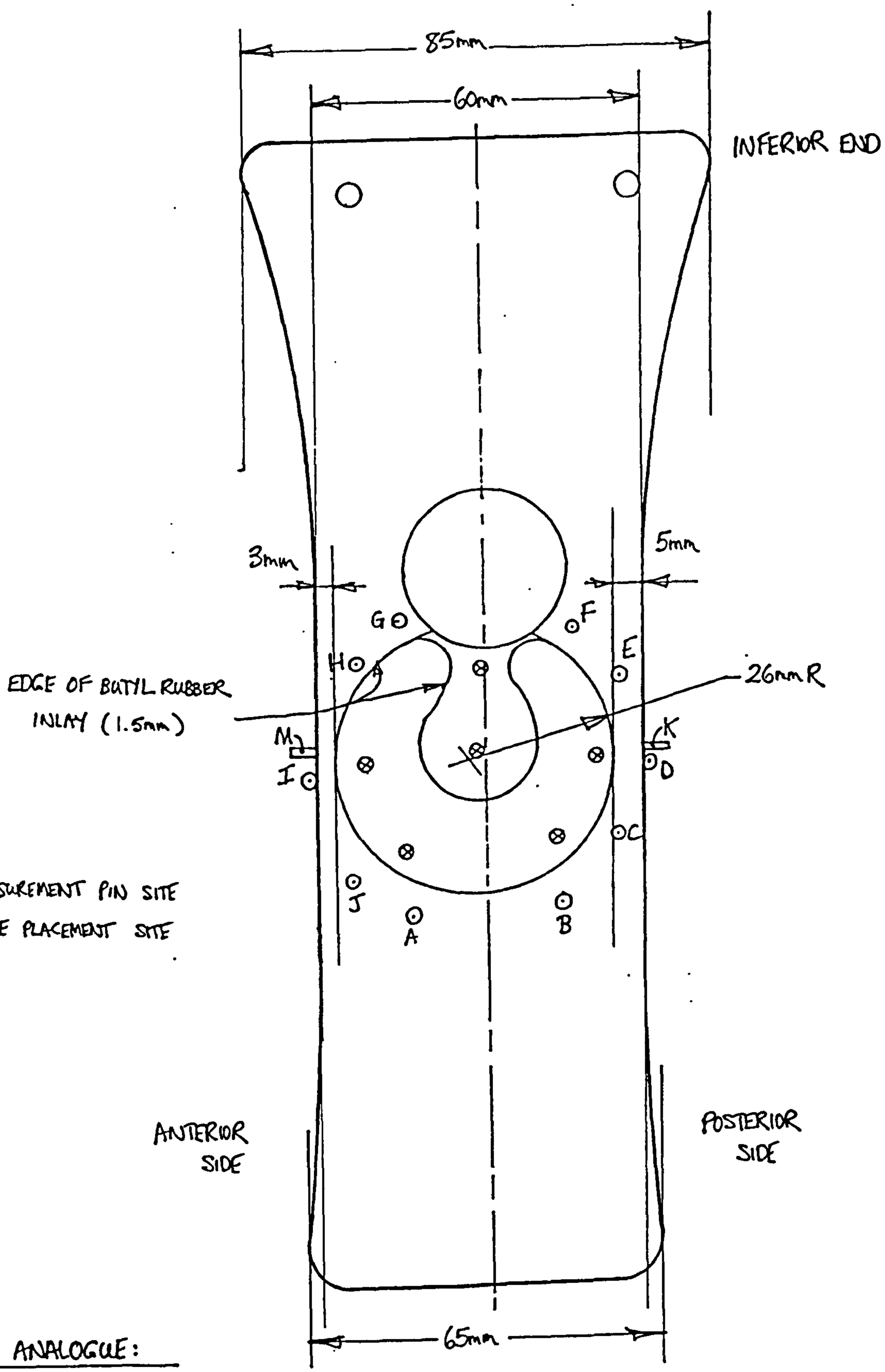

PELVIC ANALOGUE:

TOP (LATERAL) VIEW

Figure 9.10a Layout of the acetabular analogue showing the top (lateral) view.

would be to utilize the mechanical analogue of the pelvis developed in Chapter 6.

9.5.2 MATERIALS AND METHODS

As previously discussed, this simple analogue consists of a fiberglass plate with integral features designed to simulate the acetabular socket, the obturator foramen, the acetabular notch and the ischium and ilium (Fig 9.10a, b, c). The geometry of the ischium and ilium was represented by solid plates which were tapered in thickness to reduce their stiffness with respect to the acetabulum. Within the model, a central, hemispherical socket was eccentrically placed to simulate the normal pelves, in which the anterior, wall of the acetabulum is thinner than the posterior wall. The analogue was molded from polyester resin and fiberglass matting using a wooden mold with aluminum strips which were contoured to form its sides. The normal layer of cartilage lining the lunate surface was simulated with a horseshoe of butyl rubber sheet, 1.5 mm in thickness, glued to the base of the fiberglass socket. The mechanical analogue was simply supported in a mounting frame and loaded with 200 lb. via a molded polyester hemisphere acting at 40 degrees superiorly and 10 degrees posteriorly to the plane of the analogue. Eighteen stainless steel pins were implanted around the socket of the analogue to a depth of 4 mm to allow measurement of deformation during loading.

Extensometers (MTS Corp., Minneapolis, USA) were attached to pairs of the steel pins using extension arms, custom-fabricated knife-edges and elastic bands as previously described. The body of each extensometer was supported by straps attached to a frame which was mounted on the analogue. Measurements were taken at a total of 15 sites before and after loading. In a typical experiment, displacement measurements were recorded for 6-10 loading cycles of the analogue. Prior to loading, a water-based lubricant was applied to the surface of the socket to reduce friction as much as possible, the analogue was loaded and unloaded 6-10 times. The output of each extensometer was monitored using a strain gage amplifier (Measurements Group, Raleigh, USA) with an activation voltage of 10.00V and a gain of 2000. Both extensometers had a resolution of better than 0.4 μm and a sensitivity ranging from 2 - 6 mV/μm. Extensive precautions were taken to overcome artifacts due to microslippage at the knife-edge/pin interface, bulk motion of the body of

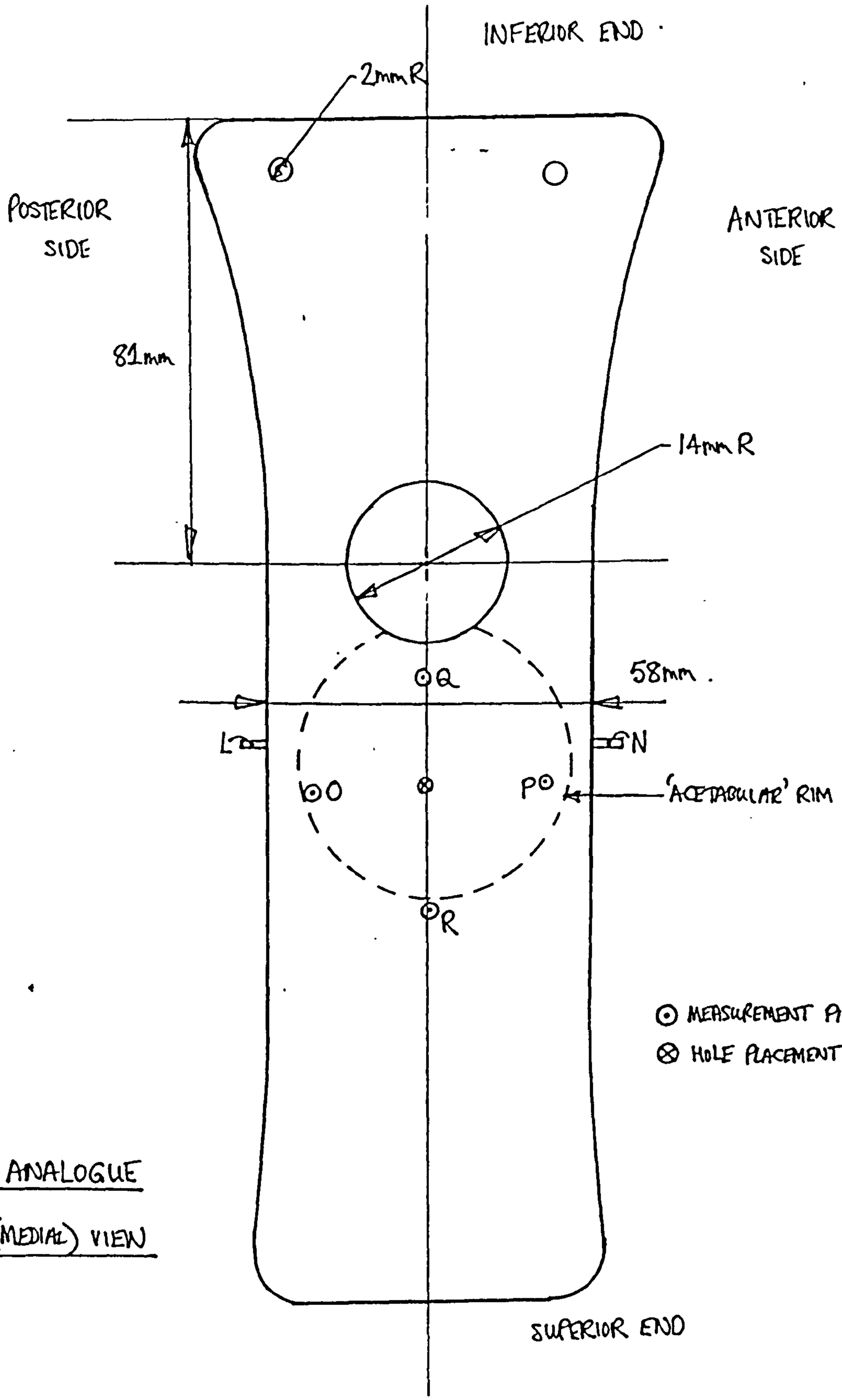

Figure 9.10b Layout of the acetabular analogue showing the bottom (medial) view.

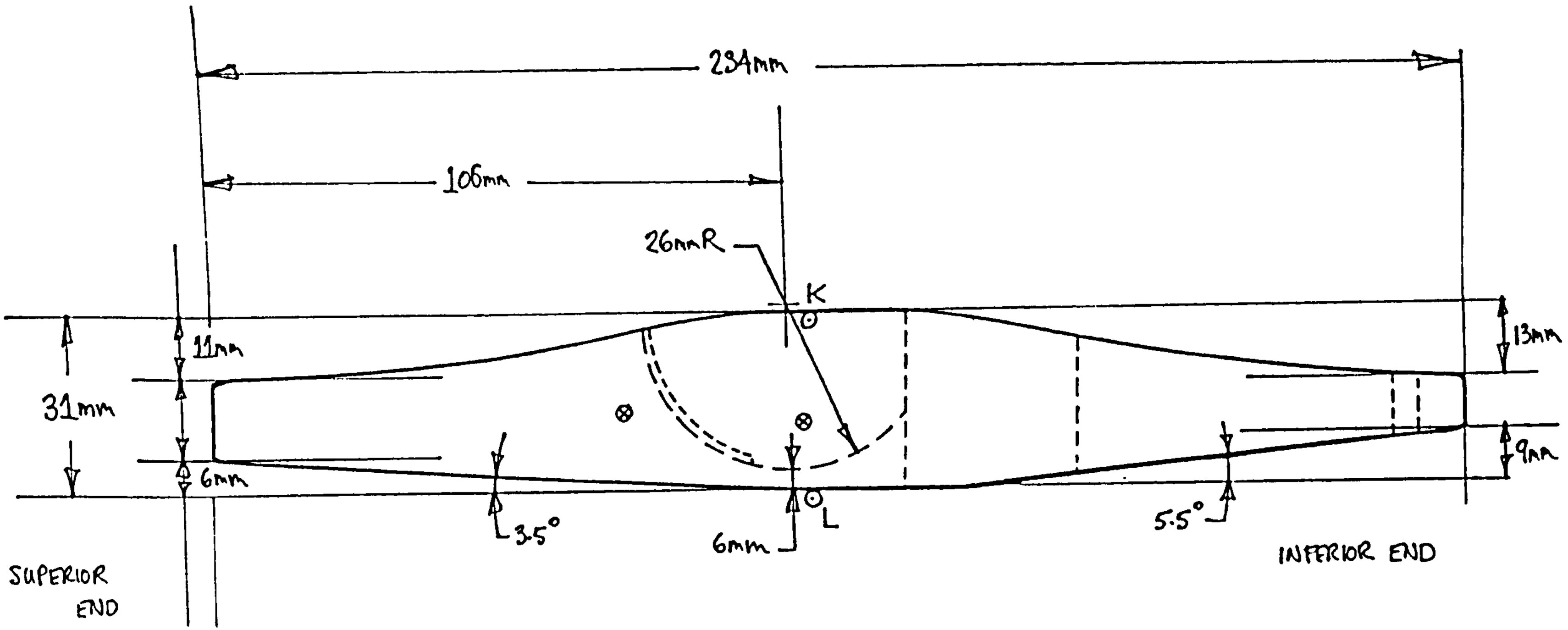

Figure 9.10c Layout of the acetabular analogue showing the side views.

Measurement Site	Initial Strain (10^{-6})	Change (0 to 7mm)		Maximum Change		
		(%)	p	(%)	p	Hole Size (mm)
Dome	336	+ 7%	NS	+ 16%	< 0.001	3 mm
Facets	1013	- 47%	< 0.001	- 47%	< 0.001	7 mm
Sup. Width	848	+ 11%	< 0.001	+ 15%	< 0.001	5 mm
Inf. width	724	- 4%	NS	- 4%	NS	7 mm
Ant. Length	-2804	- 7%	< 0.001	- 7%	< 0.001	7 mm
Post Length.	-2343	+ 20%	< 0.001	+ 20%	< 0.001	7 mm
Sup. Ant.	-899	+ 12%	< 0.001	+ 12%	< 0.001	7 mm
Inf. Ant	-858	+ 1%	NS	+ 9%	NS	3 mm
Inf. Post	-1083	- 9%	< 0.01	- 12%	< 0.001	3 mm
Sup. Post.	-612	+ 28%	< 0.001	+ 36%	< 0.001	3 mm
Med. Hor.	-378	+ 15%	NS	+ 1%	< 0.001	5 mm
Med. Vert,	930	+ 1%	NS	- 17%	< 0.001	5 mm
Ant. Depth	-344	- 19%	< 0.01	- 26%	< 0.001	5 mm
Post. Depth	-264	- 50%	< 0.001	- 50%	< 0.001	7 mm
Total Width	3836	+ 11%	< 0.001	+ 11%	< 0.001	7 mm

Table 9.4 Summary of strain measurements performed using Analogue of Pelvis with transacetabular holes of 0 to 7mm diameter.

Initial strain: Average strain measured without holes
Change (0 to 7mm): Change in strain between average values measured with 7mm holes and without holes.
Maximum change: Maximum change in average strain observed with 3, 5 or 7 mm holes compared to initial values without holes.
Hole size at max change (mm): Hole diameter (3, 5 or 7mm) at which the maximum change was observed from the initial conditions.

the transducer, misalignment of the knife-edges, and motion of the pins within the body of the analogue. If any set of readings exhibited variations of more than 20% or appeared not to be reproducible, the extensometer was removed and reattached to the specimen and a new set of measurements was taken. However, these measures were not necessary in the vast majority of the experiments performed.

Once all data were collected, the acetabular analogue was removed from its mounting frame and six holes of 3.4 mm diameter were carefully drilled through the entire specimen using the positions previously selected for monitoring motion at the shell/bone interface. The analogue was remounted, the articular surface was lubricated and the deformation of the acetabulum was again measured under a joint load of 880 N (200 lb). This procedure was repeated after the drill holes were successively enlarged to 5.0 and 7.1 mm.

9.5.3 RESULTS

The measurements performed using the acetabular analogue are summarized in table 9.4 and listed in their entirety in Appendix A.2. The variation in effective strain function of the diameter of the holes drilled in the acetabulum have also been presented graphically in Figs. 9.11 to 9.17. The presence of holes within the walls of the acetabular analogue led to general and local changes in the deformation patterns, as reflected by the strain measurements. Holes of 7 mm in diameter caused the overall deformation of the model to increase by 10 - 20%. The total width of the analogue increased by 11% in the presence of 7 mm holes, while similar changes were observed in the longitudinal strain measured along the posterior (+20%) and anterior (-7%) walls.

The presence of holes appeared to cause a shift in the neutral axis in bending, both in the coronal and sagittal planes. Along the anterior side of the lateral surface, the longitudinal strain increased slightly after creation of 3 mm holes an then decreased with enlargement of the holes to 5 and then 7 mm. An overall reduction of strain by 12% was observed between the 3 and 7 mm measurements. Conversely, along the posterior side, the compressive strain increased continuously with hole size, the analogue with 7 mm holes having 20% greater longitudinal strain than the unperforated specimen. Similarly, while the longitudional strain beneath the socket decreased by 17% with 7 mm holes, the elongation of

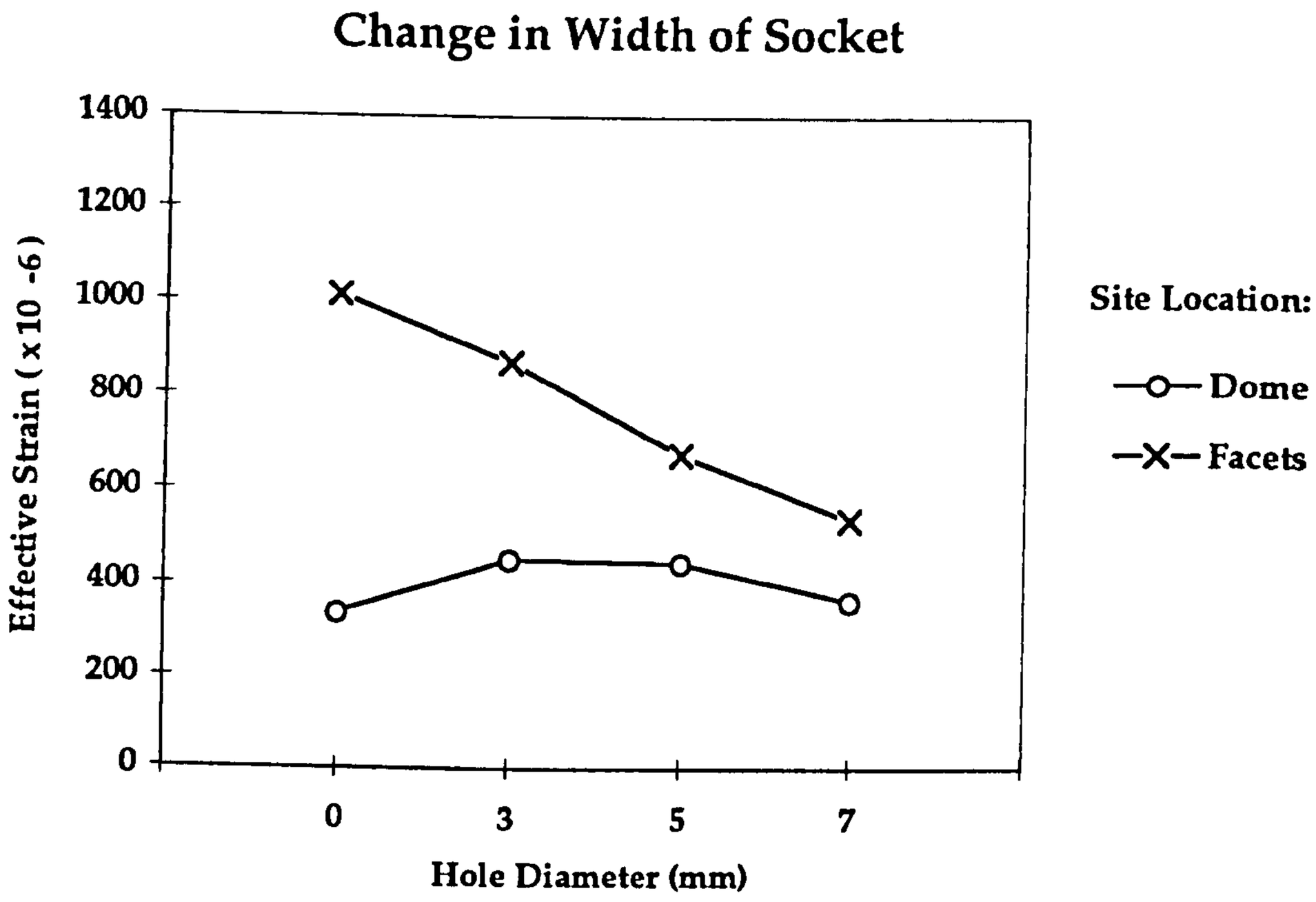

Figure 9.11 The variation in transverse strains with transacetabular hole diameter at the dome and between the facets of the acetabular analogue.

Dome: Immediately above socket (50% width of analogue)

Facets: Across junction of socket and through-hole.

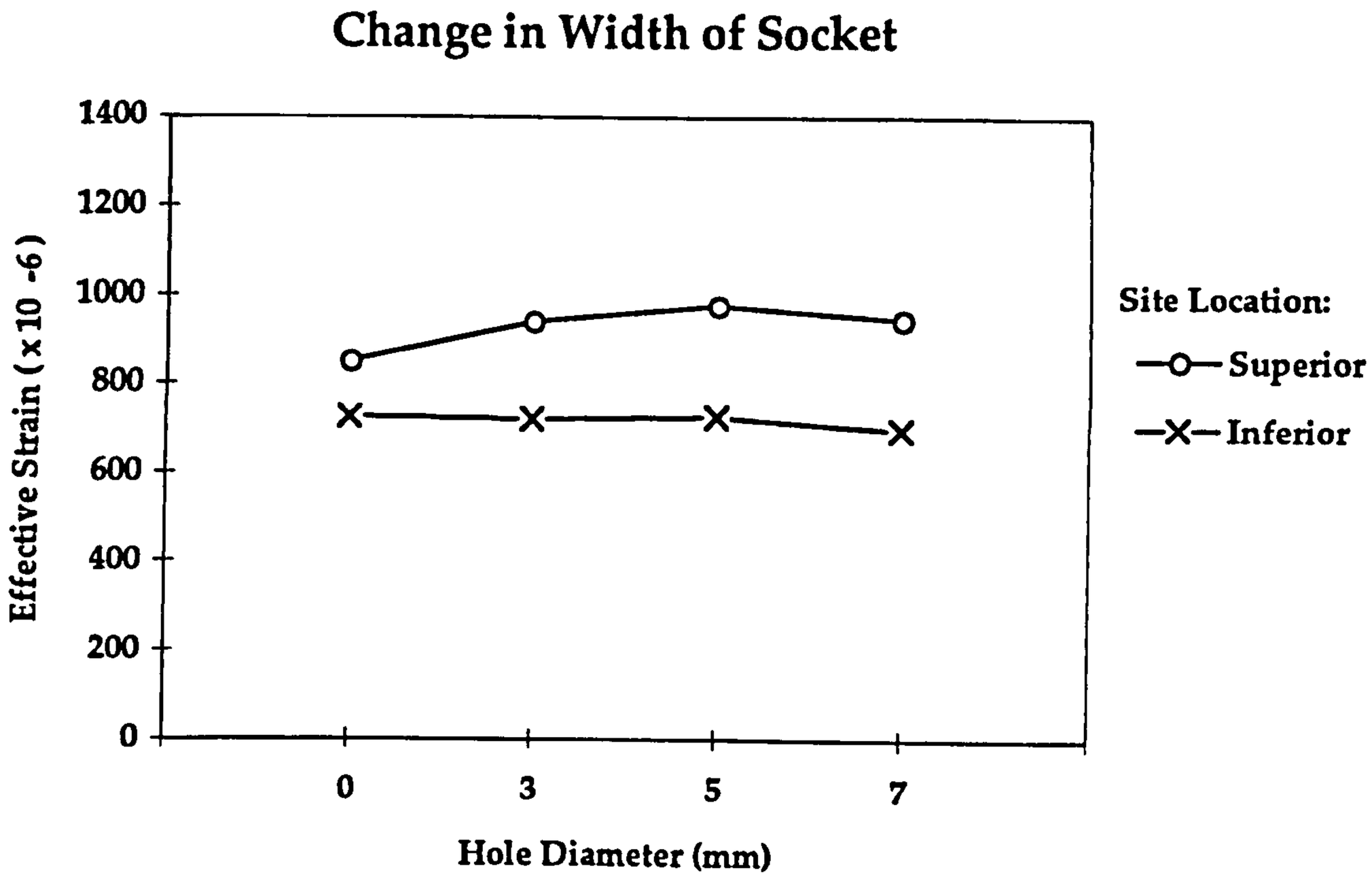

Figure 9.12 The variation in transverse strains with transacetabular hole diameter at superior and inferior measurement sites on the lateral surface of the acetabular analogue.
Superior: Immediately above socket (85% width of analogue)
Inferior: Immediately beneath socket (85% width of analogue)

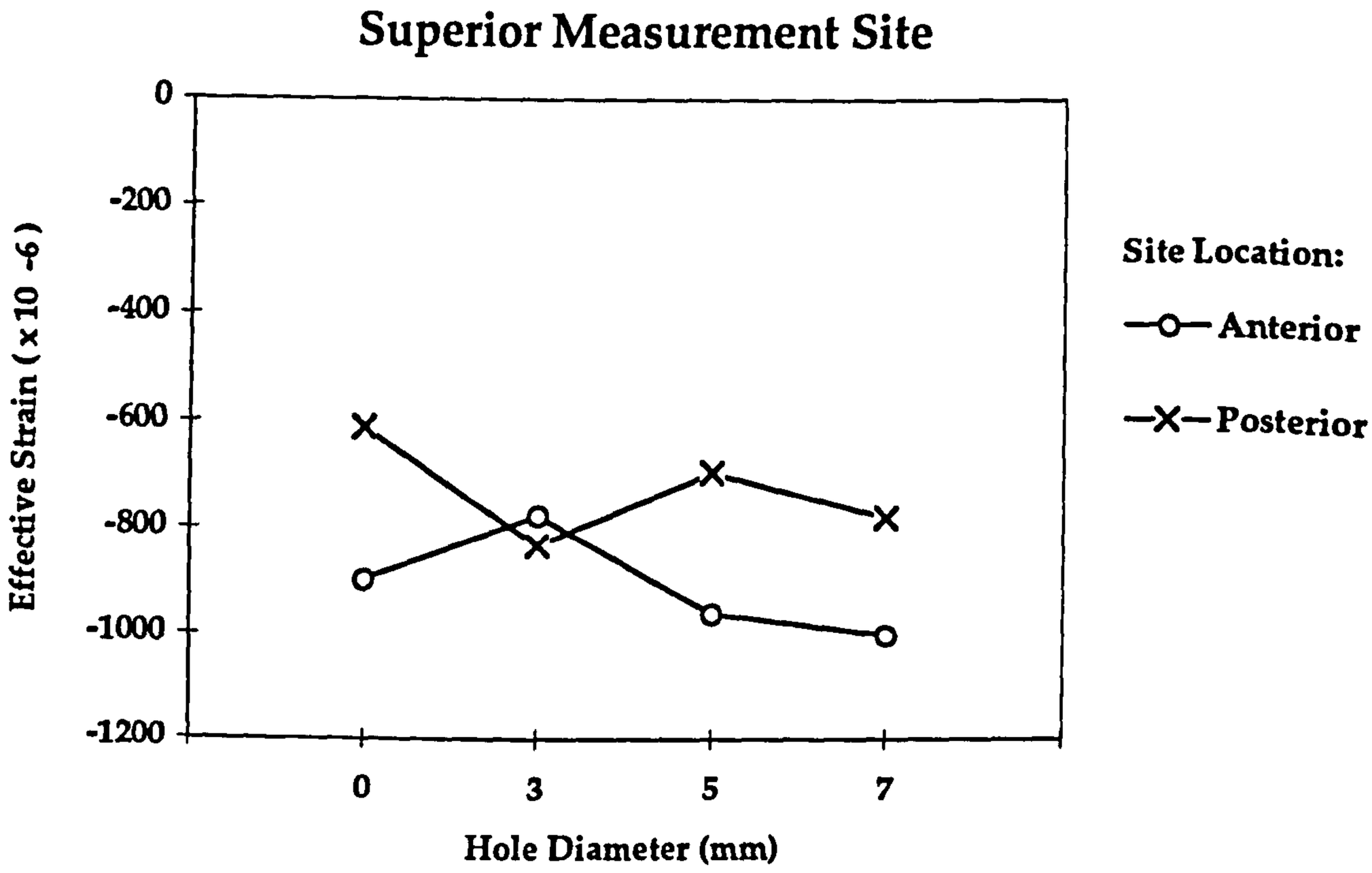

Figure 9.13 The effective strain measured within the antero-superior and postero-superior quadrants of the acetabular analogue for a range of transacetabular hole diameters.

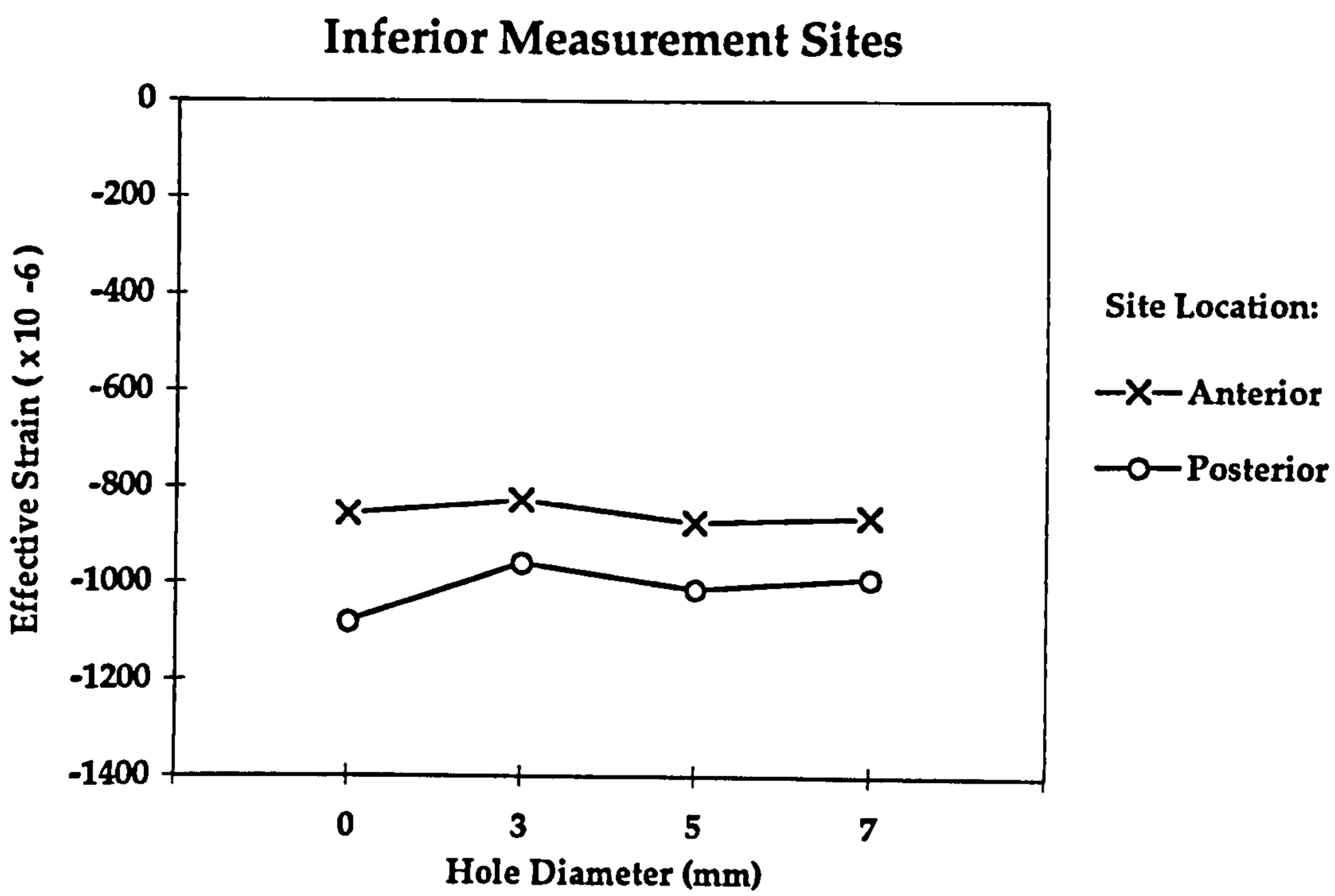

Figure 9.14 The effective strain measured within the antero-inferior and postero-inferior quadrants of the acetabular analogue for a range of transacetabular hole diameters.

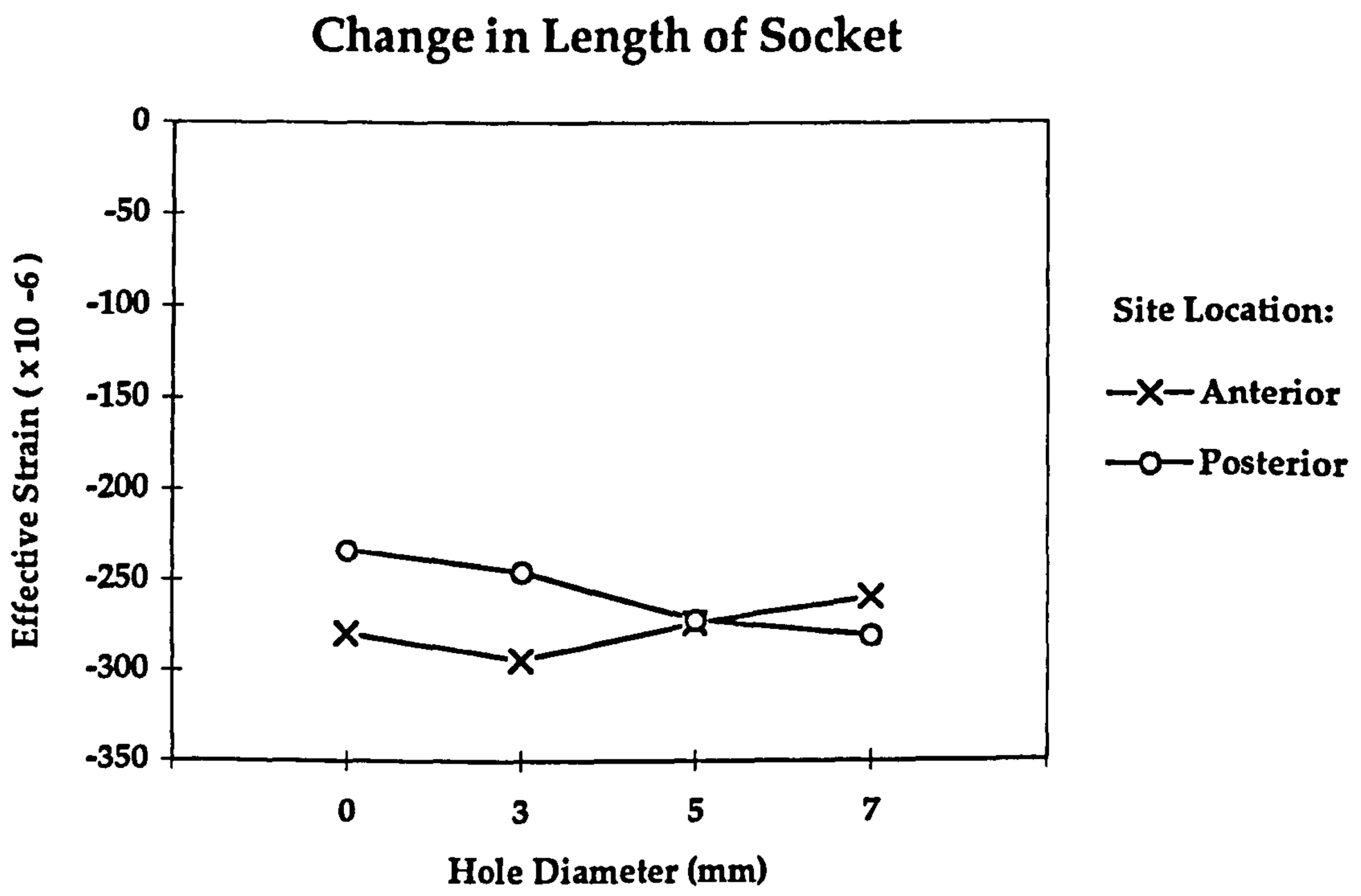

Figure 9.15 Variation of longitudinal strains measured along the anterior and posterior surfaces of the acetabular analogue as a function of transacetabular hole diameter.

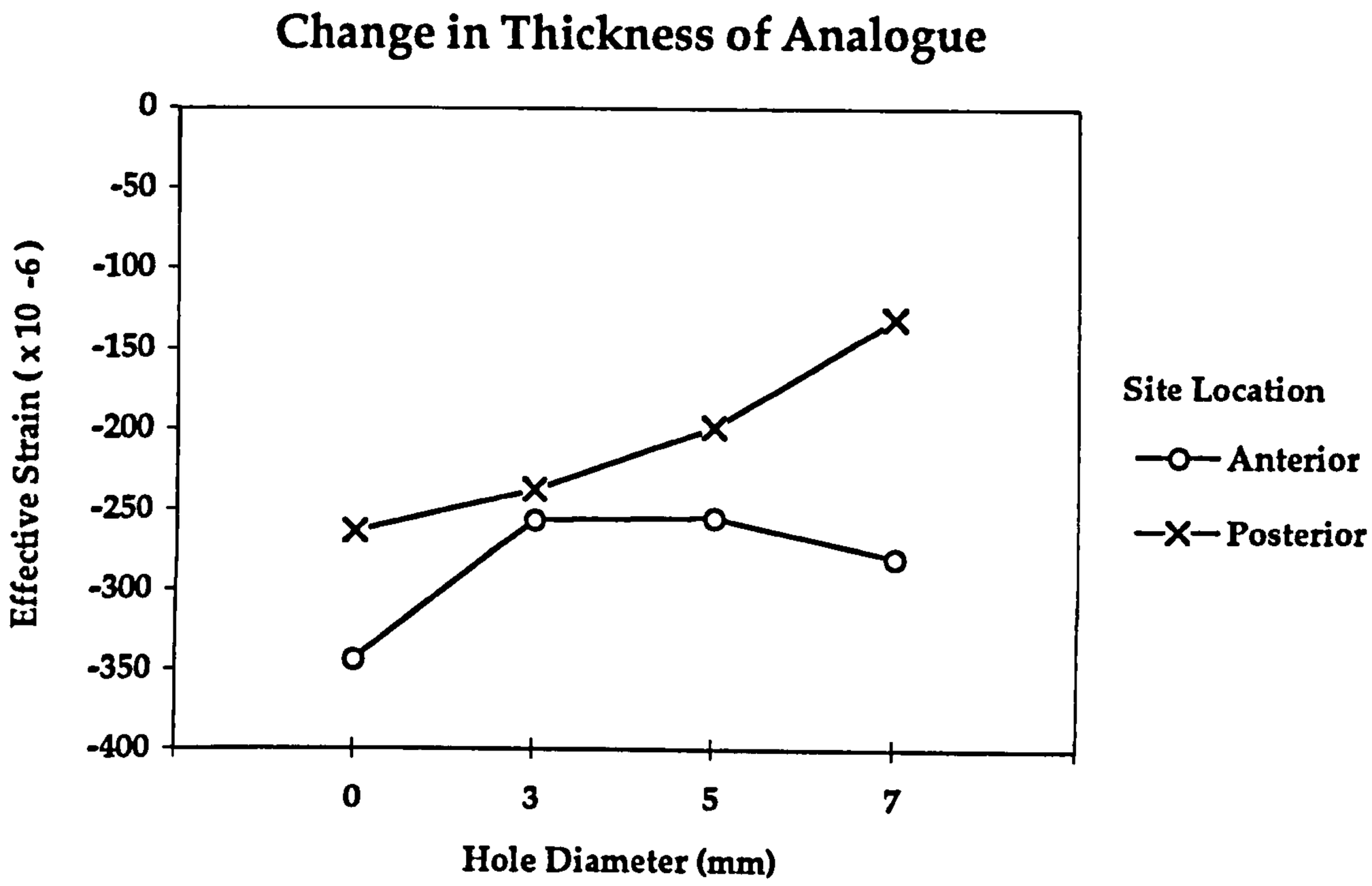

Figure 9.16 Variation in the thickness of the analogue with transacetabular hole diameter. All measurements were made in a mediolateral direction on the anterior and posterior walls of the acetabular analogue in the vicinity of the hemispherical socket.

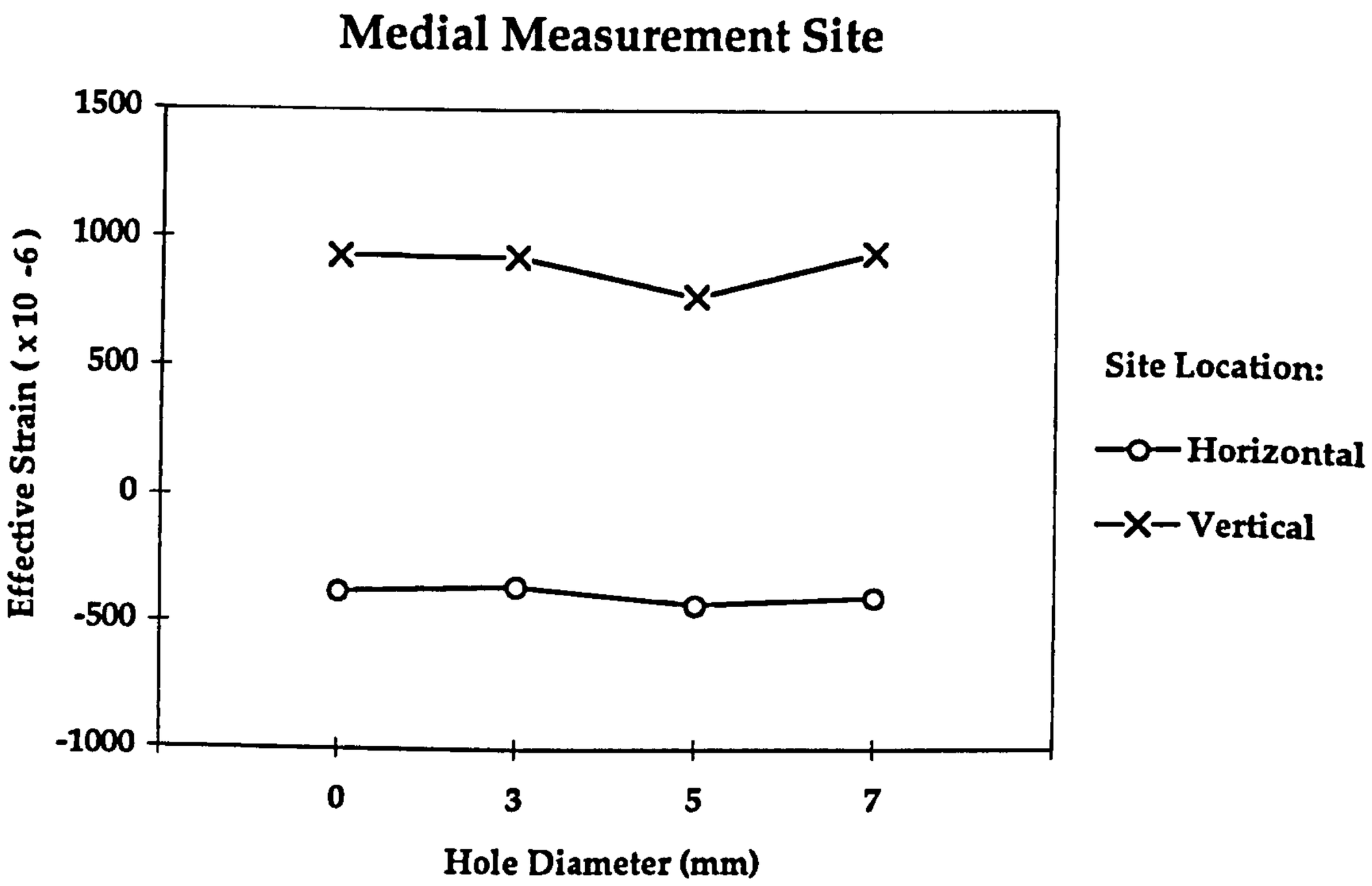

Figure 9.17 The effect of transacetabular hole diameter on effective strains measured on the medial surface of the acetabular analogue directly behind the hemispherical socket.
Vertical = supero - inferior direction,
Horizontal = antero - posterior direction.

the lateral surface increased by an average of 7%, indicating a shift in the neutral axis toward the medial surface.

In contrast, no change was observed in the transverse deformation of the anterior and posterior edges of the inferior rim of the socket as a function of hole size. The deformation at the facets does however, mean that any measurements of transverse interfacial motion in the vicinity of the acetabular notch itself may underestimate the true values present in the native acetabulum.

9.5.4 CONCLUSIONS

On the basis of the measurements performed with the acetabular analogue, it is concluded that:

(i) The overall deformation of the acetabulum is relatively insensitive to the presence of transacetabular holes of up to 7 mm in diameter.

(ii) Hole placement through areas where the wall of the acetabulum is relatively thin (e.g. the anterior and posterior walls and the floor of the acetabulum) can lead to local changes in deformation of up to 50% for holes of 7 mm in diameter.

(iii) The effect of holes is likely to be much greater perpendicular to the mouth of the acetabulum than within the plane of the acetabular mouth itself.

CHAPTER 10 IMPLANT/BONE MOTION IN THE ACETABULUM: EXPERIMENTAL STUDIES*

10.1 INTRODUCTION

Numerous factors can be reasonably expected to influence the stability of the fixation of cementless acetabular cups. These include:

(i) the coefficient of friction of the interface between the cup and the reamed acetabulum,

(ii) the area and distribution of contact between the shell and the socket,

(iii) the degree of interference between the shell and the reamed acetabulum,

(iv) the method of loading employed to evaluate implant stability,

(v) the presence of remnants of cartilage and soft-tissue in the cup/bone interface,

(vi) the presence of integral design features, typically spikes and pegs, intended to help stabilize the shell during initial implantation,

(vii) the use of transacetabular bone screws, passed through the shell and into the bony acetabulum.

Within the femur, recent experimental and theoretical studies of the fixation of cementless prostheses have emphasized the importance of frictional conditions at the implant/bone interface in determining the response of the prosthesis to loading. It is also likely that interface friction will also have a significant effect on the stability of acetabular fixation. One of the factors that has the most influence over frictional conditions at the interface is the coating applied to the prosthesis to promote bony attachment. Acetabular components are now available with a wide variety of surface coatings, including spherical beads, wire mesh, plasma-sprayed metals and hydroxapatite.

*Note: All of the experiments described in this chapter were conceived of, planned and directly supervised by the author. However, most of the experimental measurements were performed by personnel under the direction of the author and not by the author himself.

SAB*	Age	Sex
20845R	62	M
25268R	60	M
23158L	78	F
23158R	78	F
20850L	79	F

Table 10.1 Details of body donors from whom pelvic specimens were derived for measurement of cup/bone micromotion.

***SAB** : Cadaver reference number issued by the State Anatomic Board of Texas.

In this study, three of these options were selected to compare the influence of the ingrowth surface on the micromotion of acetabular cups implanted in the same set of acetabular specimens.

10.2 MATERIALS AND METHODS

Nine fresh pelves with an acetabular diameter of 49-50 mm were selected from a collection of anatomic specimens. Each pelvis was disarticulated from both femora and had the sacrum and the body of L5 attached. The anteroposterior diameter of the acetabuli was measured directly on each specimen. Standard AP and lateral radiographs were prepared of each pelvis at a tube setting of 80 kV exposed for 1/30 second. Each radiograph was taken at a tube to cassette distance of 72 inches (1.83m) to minimize geometric distortion and was examined for evidence of osseous pathology including previous trauma or metastatic disease. Based upon the density of each radiographic image, a subjective assessment was made of bone density and any specimen showing evidence of advanced osteopenia was excluded from use in this study.

Based upon these criteria, five pelves were chosen from two male and three female donors with an average age of 71.4 years (range: 60-79 years) (Table 10.1). All specimens were divided longitudinally and stripped of all soft tissue including any remnants of the acetabular capsule. Each acetabulum was prepared for implantation using standard hemispherical reamers (Howmedica, Inc.). Initially, a standard 48 mm reamer was directed medially in the acetabulum until contact was achieved with the floor. Subsequent reaming was performed in 1 mm increments with each reamer directed along an axis approximating the direction of weight-bearing. Great care was taken to keep each reamer centrally placed within the bony socket to avoid excessive thinning of the anterior wall with enlargement of the implantation site. During reaming, the socket was also repetitively inspected to prevent reaming through the medial wall. An attempt was made to ream each specimen to the depth of a full hemisphere unless this was prevented by the shallowness of the original socket and the risk of excessive thinning of the medial wall. After reaming to 51 mm, a 52 mm cup was implanted into each acetabulum to provide a nominal interference of 1 mm. Repeated hammer blows were used to ensure that each implant reached a position of maximum stability.

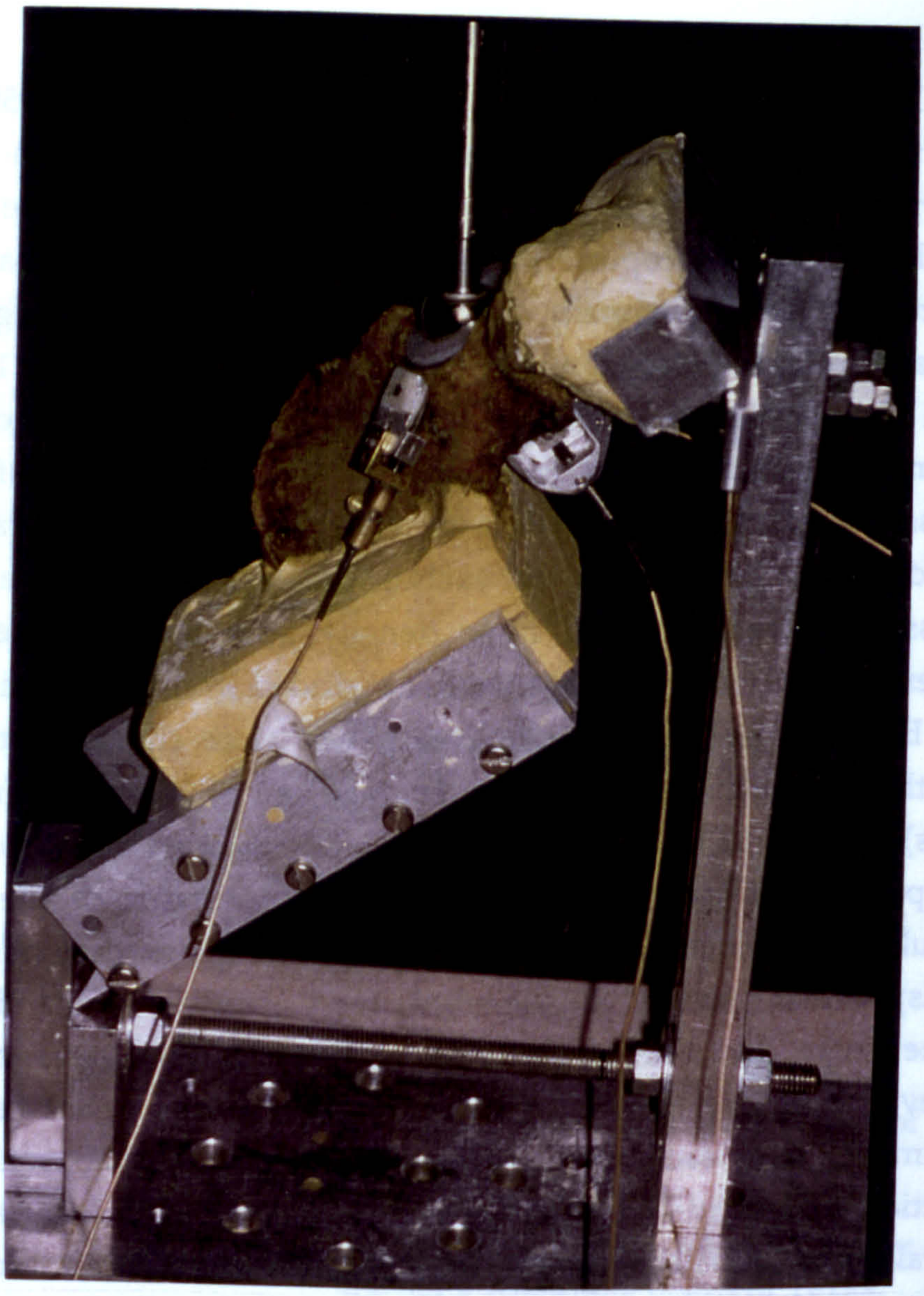

Figure 10.1 Oblique side view of a hemipelvis in the three-point loading frame. Transducers measuring cup/bone motion at the dome and the floor of the acetabulum are visible.

Six acetabular cups of the same basic hemispherical design developed in Chapter 9 were obtained from an implant manufacturer (Howmedica, Inc.). All cups were of the same size (52mm) but were manufactured from different alloys (CoCr or Ti6Al4V) to accommodate the following ingrowth coatings:

a) Spherical CoCr beads (pore size: 425 mm; porosity: 35%) sintered onto a forged CoCr shell;

b) Plasma-sprayed cp titanium deposited on a forged titanium alloy (Ti6Al4V) shell;

c) Hydroxapatite (25-50 mm thickness), vacuum sprayed onto a forged titanium alloy (Ti6Al4V) shell.

Four holes of 2.3 mm diameter were drilled and tapped in each of the shells at the positions listed in Table 10.2. The inferior pubic ramus and the wing of the ilium of each specimen were separately potted in blocks of dental plaster. This enabled the specimen to be supported at points located superior and inferior to the acetabulum with preservation of the normal flexibility of the pelvis. Each specimen was positioned in a loading fixture which supported the ischium and the ilium in an inclined position (Fig. 10.1, 10.2, 10.3).

The inclination of the specimen was fixed such that the joint reaction force could be applied in a vertical direction. In this position, the applied load was oriented at 65 degrees to the mouth of the acetabulum in the coronal plane and 10 degrees posterior in the transverse plane. These values were calculated by combining published data for the orientation of the acetabulum (Terver et al, 1982) with intra-vital data describing the direction of the joint reaction force in early stance. Through analysis of a series of CT scans, Terver et al found that the average anteversion of the male pelvis was 15 ± 4 degrees with an inclination to the vertical of 35 ±6 degrees. Typical values for the direction of the joint reaction force in early stance phase are 20 degrees medial to vertical in the coronal plane and 25 degrees posterior to lateral in the transverse plane. If it is assumed that an acetabular cup will be implanted in 45 degrees of abduction and 15 degrees of anteversion, the inclination of the joint reaction force will be 65 degrees (45 + 20 degrees) in the coronal plane and 10 degrees (25 - 15 degrees) in the transverse plane.

Each specimen was loaded in a mechanical testing machine (Bionix, MTS) using an indentor with a 32 mm femoral ball which mated with the

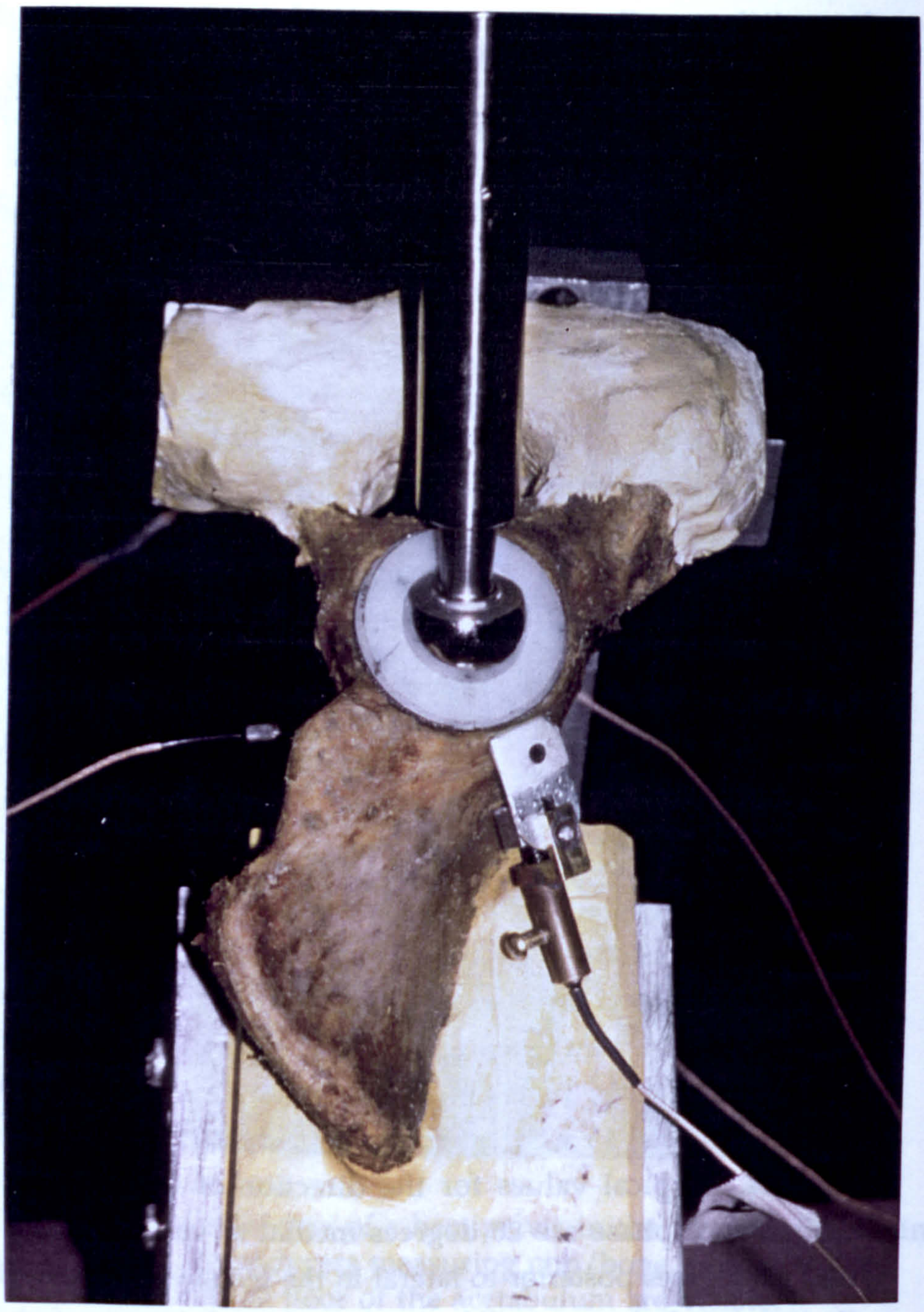

Figure 10.2 A hemipelvis mounted in the loading frame, as viewed from the front.

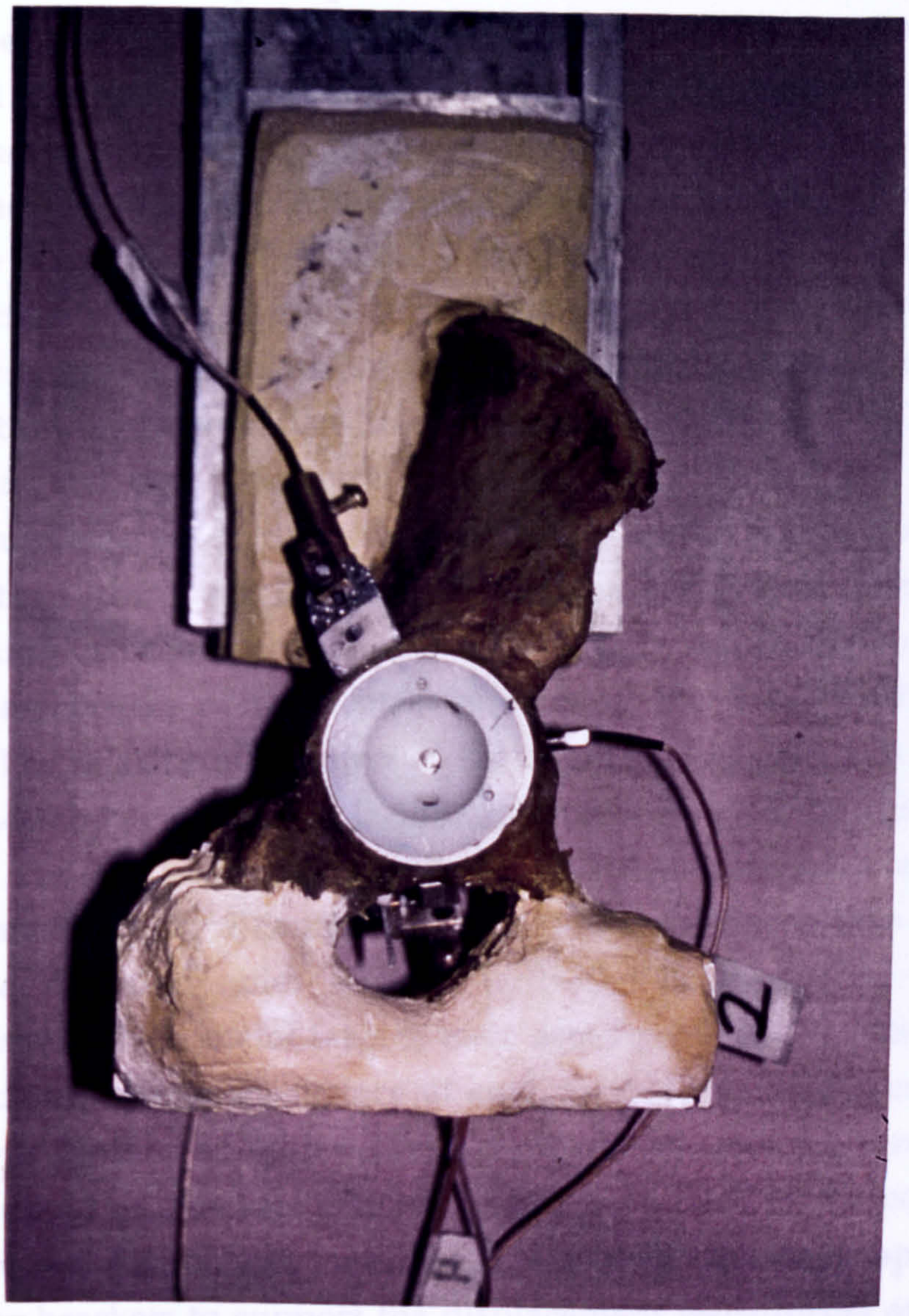

Figure 10.3 Top view of the potted hemi pelvis with the loading rod removed. The slotted head of the threaded motion pin located in the floor of the acetabulum is visible through a hole machined in the cup liner. Also, the transducer located within the cotyloid notch can be seen through the obturator foramen.

acetabular liner. During loading, the pelvis was supported by the plaster blocks which rested on the base of the testing machine. Lateral motion of the blocks was not constrained during loading. The hydroxyapatite (HA) coated shell was always implanted in each acetabulum first, followed by the beaded and the plasma-sprayed components. This sequence of testing reflected the apparent order of roughness of the surfaces of the three shells and was adopted to minimize the effects of mechanical erosion of the reamed surface during implantation and loading of each component.

The components of cup/bone motion perpendicular and parallel to the interface were measured during loading from 20 to 2000 N (5 to 454 lb). These measurements were performed at three sites corresponding to the position of the threaded holes in each acetabular cup. On the pelvic specimen, the three measurement sites were: (i) on the floor of the acetabulum adjacent to the pole the cup, (ii) within the cotyloid notch and (iii) within the 'weight-bearing' surface (superior dome). During preparation of each specimen, pilot holes were drilled through the inner and outer cortices of the acetabulum using the holes in the shell as a guide. The relative orientation of the cup and the specimen was marked on the acetabular margin to facilitate repositioning of the shell within the socket. The shell was then removed, and the holes were enlarged to 5 mm diameter using a cannulated drill. The shell was then reimplanted with the threaded holes aligned with the holes drilled through the acetabulum. Three metal targets were attached to metal pins which were threaded into the outer surface of each shell. The displacement of each target was monitored with eddy-current transducers (Spectral Dynamics, Inc.) mounted on brackets attached to the inner wall of the pelvis.

Several difficulties were encountered in developing special mounting brackets to support the displacement transducers at each site on the surface of the pelvis. One characteristic of eddy probe transducers is a relatively short measuring range compared to the diameter of the probe itself. Typically, a suitable transducer with a diameter of 5 mm, has a measuring range of only 2-3 mm. The output of these transducers is also sensitive to the orientation of the probe with respect to the face of the inductive metal target. Consequently, the brackets supporting the probes must be accurately aligned with the face of the target during attachment to the pelvis, or must allow the orientation of the probe to be adjusted after attachment of the mounting bracket to the pelvis. This requirement

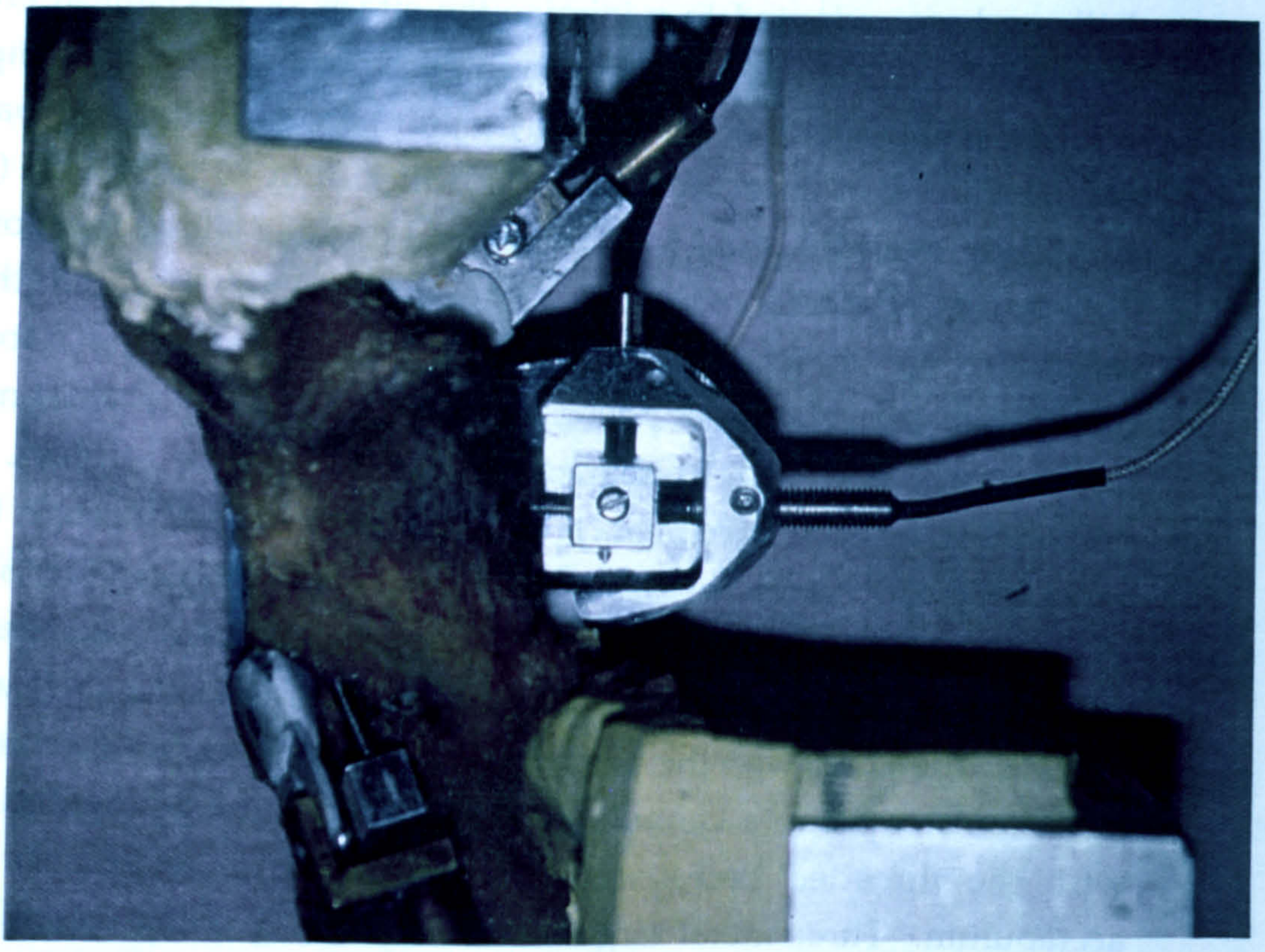

Figure 10.4a Side view of the orthogonal mounting bracket designed to support the three transducers measuring implant motion over the floor of the acetabulum. The metal target can be seen attached to the threaded motion pin with two probes positioned to measure the superior-inferior and medial-lateral component of cup/bone motion.

proved challenging when a single transducer was used to measure uniaxial displacement, and became virtually impossible when three orthogonal transducers were to be attached to the uneven, inclined surface of the cortical wall of the pelvis. This problem proved especially difficult in the cotyloid notch where space was limited due to the presence of the inferior mounting block that encapsulated the inferior pubic ramus and the ischial tuberosity.

This problem was initially solved using aluminum 'L' sections which were slotted to allow attachment of the transducer. A through-pin was screwed into the acetabular cup to facilitate alignment of each mounting bracket . A brass tube with a large flange at one end was then passed over the pin until it came into contact with the cortical surface. A small quantity of premixed acrylic cement was packed between the cortex and the brass flange and allowed to set. The brass tube was then removed and the 'L' shaped bracket was attached to the acrylic mounting surface with cyanoacrylate adhesive. Once the target was attached to the pin and the alignment of the eddy probes was checked, it was found that small adjustments were often required to ensure that the probe was correctly oriented with respect to the target. Initially this was done by bending and twisting each bracket, although this proved extremely time-consuming. A faster method, adopted in later runs, was to use hot-melt adhesive which was delivered to the mounting surface using a glue-gun. This allowed the probe-holding bracket to be positioned so that the probe was perpendicular to the target, before the adhesive became rigid. This solution proved extremely effective and did not lead to loosening, motion or premature separation during any of the micromotion experiments.

A different solution was needed in the case of the measurement site directly medial to the shell on the floor of the acetabulum to allow three orthogonal measurements of target displacement. To solve this problem, a solid aluminum mounting block (approximate dimensions: 40 mm x 40 mm x 35 mm) was fabricated with a central cube-shaped cavity, designed to fit over the target to facilitate alignment (Figure 10.4a, b). Three orthogonal holes (diameter: 6.25 mm) were drilled from the outer surface of the cube to the inner cavity to allow placement of eddy probe transducers. Set screws were added to control the depth of the transducers within each hole. Assembly of the transducer holder on the pelvic

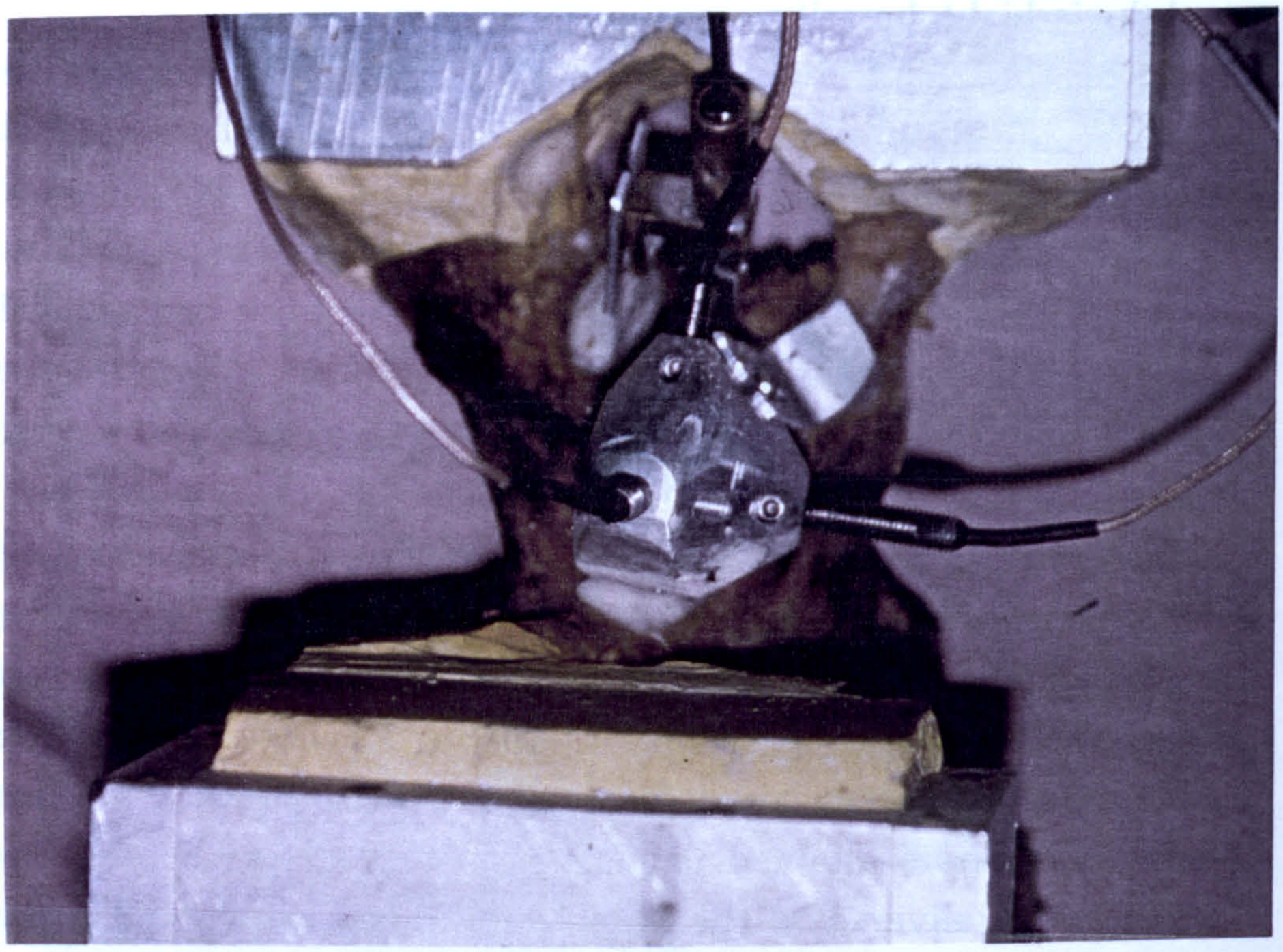

Figure 10.4b Back view of the orthogonal mounting bracket.

specimens started with placement of a thick walled aluminum box (wall thickness: 6.3 mm) over the stainless-steel target. This allowed the optimum gap to be maintained between the holder and the target during assembly. Once the holder was mounted over the cube and the target, the space between the base of the holder and the pelvis was filled with acrylic cement. After the cement had cured, the holder was glued to the acrylic surface with cyanoacrylate adhesive, the hollow cube was removed, and the transducers were positioned within the holder.

An initial pilot study was performed with an embalmed specimen with three transducers at each measurement site to determine the principal directions of micromotion (one component perpendicular to the interface and two components parallel to the interface). This experiment demonstrated that the transverse (shear) components of micromotion at the notch and the superior dome were negligible, presumably because of the peripheral interference fit present between the shell and the rim of the acetabulum. This observation allowed four of the transducers to be eliminated, leaving five remaining probes (three on the floor of the acetabulum, one in the cotyloid notch and one within the superior dome). This allowed measurement of the normal (perpendicular) component of micromotion at each site and the two shear components of micromotion (superior/inferior and medial/lateral) over the floor of the acetabulum.

Each cup was mounted in the testing machine and placed under a static load of 44N (10lb) to establish the baseline position of the implant with respect to each of the eddy probe transducers. The joint load was then increaased to 880N (200lb) and maintained for 20 seconds to allow aquisition of displacement data. This was followed by unloading to 44N and measurement of the transducer signals. This procedure was repeated three times; data collected the third cycle in unloading the cup were used to calculate the micromotion of the shell/bone interface.

To compensate for the large variation between specimens, all data were normalized prior to statistical analysis. For each measurement site, the average micromotion was calculated for all runs performed in each specimen, using all three cup designs. This value was then used to normalize all data recorded at that measurement site. Analysis of variance (ANOVA) was performed on the normalized data to ascertain whether there was a significant variation in the micromotion of cups with different surface coatings. If the variation was found to be

Measurement Site	* Average ± S.E.	Range
Cotyloid Notch (Normal Component)	57.7 ± 2.7	21.1 - 85.6
Superior Dome (Normal Component)	36.5 ± 7.3	9.2 - 108.6
Acetabular Floor		
Medial/Lateral (Normal Component)	16.6 ± 4.2	-3.1 - 61.9
Anterior/Posterior (Shear Component)	7.2 ± 1.1	-11.0 - 18.4
Superior/Inferior (Shear Component)	32.0 ± 5.0	-21.7 - 74.6
Total Shear	33.3 ± 5.0	14.7 - 74.7

Table 10.2 Micromotion data for all three acetabular cups combined according to measurement site.

* The average and standard error were calculated using the absolute values of the individual measurements (i.e. the direction of interface motion was ignored).

significant at the 5% level, t-tests were performed to compare the micromotion of groups of cups with different coatings on a pairwise basis (e.g. porous coated vs. HA coated). Conventional ad-hoc multiple-range comparisons were not performed on all three groups simultaneously because of large differences in the variance of the three groups caused primarily by the variability of the micromotion of the porous-coated components.

10.3 RESULTS

Upon loading, the predominant motion of the acetabular cups consisted of peripheral compression of the implant/bone interface, with reduction of the separation of the component and the superior, inferior and medial surfaces of the acetabulum (table 10.2). The separation of the cup and the inferior edge of the medial wall decreased by an average of 57.7 ± 2.7 μm (range: 21.1 to 85.6 μm) within the cotyloid notch, and 36.5 ± 7.3 μm (range 9.2 to 108.6 μm) within the superior dome. Significant sliding was observed between the pole of the implant and the floor of the acetabulum. This corresponded to displacement of the cup in a superior direction by an average of 32.0 ± 5.0 μm (range: 21.7 μm inferior to 74.6 μm superior). A small component of shear displacement also occurred in the anterior-posterior direction (average: 7.2 ± 1.1 μm posterior; range: 11.0 μm anterior to 18.4 μm posterior).

Large differences were found between the micromotion of shells with different surface coatings (table 10.3, fig 10.5). In general, the cup with the beaded coating exhibited the largest micromotion at all three measurement sites. The relative micromotion of the plasma spray coated and hydroxyapatite coated cups varied with the measurement site. Within the superior dome, the plasma-spray coated cups displayed relatively little micromotion (average: 18.7 ± 2.8 μm) which was 50% lower than the hydroxyapatite coated shell (37.3 ± 5.5 μm), and 65% less than the porous coated shell (53.3 ± 9.3 μm). Statistical analysis demonstrated that there was a significant variation in micromotion between the three designs (ANOVA, $p = 0.027$). Moreover, the differences between the plasma-spray coated and the HA coated shells ($p = 0.047$) and the plasma-spray coated and the porous-coated shells ($p = 0.027$) were statistically significant at the 5% level. The difference between the porous coated and HA coated shells was not found to be statistically significant

Surface	Component of Micromotion					
	Normal			Shear (floor)		
	Notch Area	Ace. Floor	Sup. Dome	Ant/Post	Sup/Inf	Total
Porous Coated (PC)	72.7 ± 2.9	28.5 ± 10.5	53.3 ± 9.3	6.7 ± 2.2	45.8 ± 11.6	46.3 ± 11.7
Hydroxyapatite (HA)	48.9 ± 4.3	11.6 ± 4.1	37.3 ± 5.5	9.4 ± 2.4	30.0 ± 6.6	32.5 ± 5.6
Plasma Spray (PS)	51.5 ± 4.0	9.6 ± 2.7	18.7 ± 2.8	5.4 ± 1.8	20.1 ± 5.1	21.0 ± 5.2
p-values						
PC vs HA	0.007	0.172	0.209	0.423	0.276	0.327
PC vs PS	0.008	0.694	0.027	0.653	0.092	0.098
HA vs PS	0.685	0.119	0.047	0.212	0.271	0.169

Table 10.3 Components of micromotion measured for the acetabular cups with three different surface coatings (all values average ± standard error).

Note: The average and standard error were calculated using the absolute values of the individual measurements (i.e. the direction of interface motion was ignored).

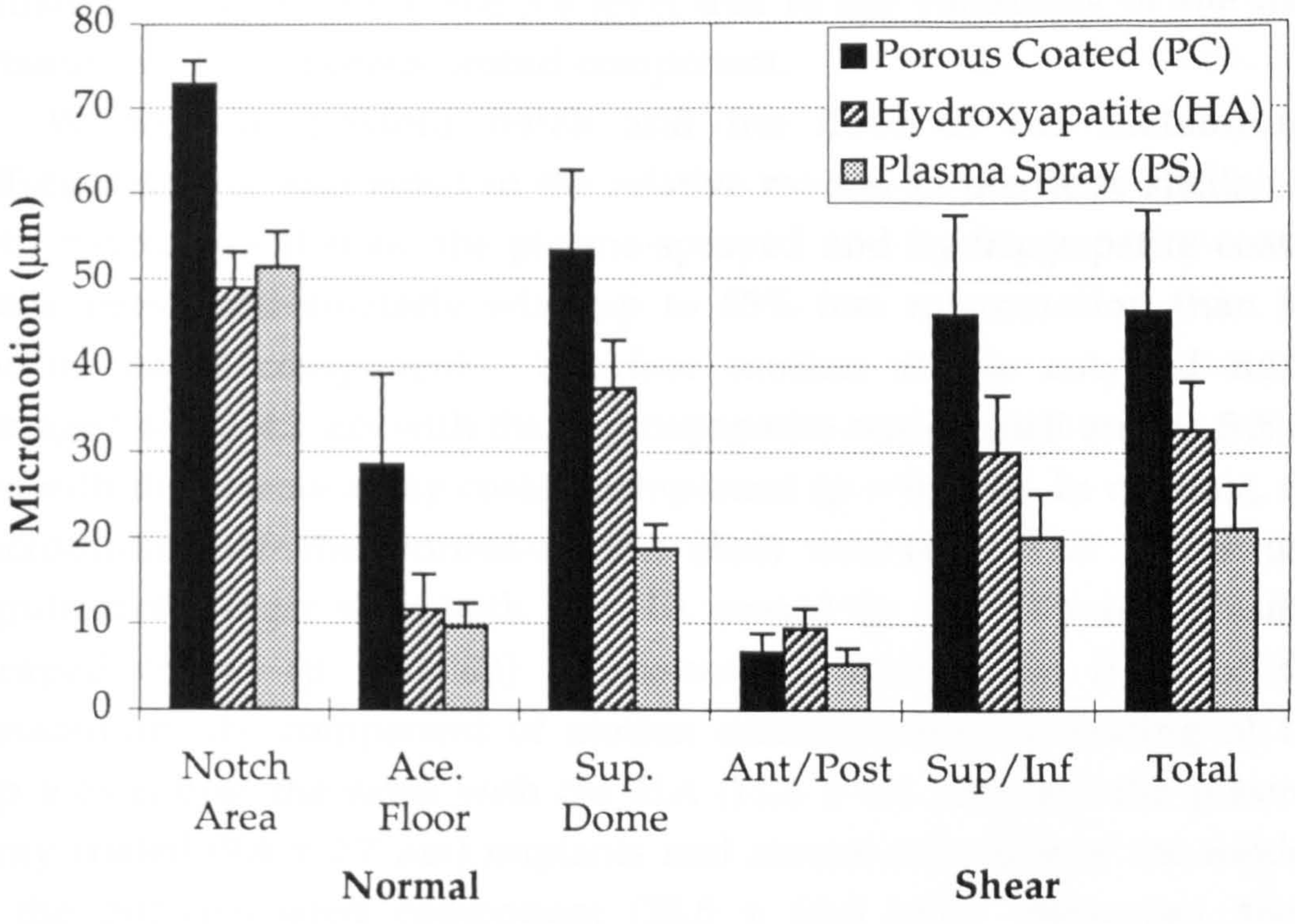

Figure 10.5 The average components of cup/bone micromotion for the three designs of acetabular cups implanted in this experiment.

($p = 0.209$) due to the scatter of the data.

A similar pattern was present in the superior-inferior component of motion parallel to the shell/bone interface. In each case loading caused the shell to more superiorly by an average of 20.1 ± 5.1 μm with the plasma-sprayed shell, 30.0 ± 6.6 μm with the HA coated shell and 45.8 ± 11.6 μm with the beaded design. However, these differences were not statistically significant at the 5% level due to the variability of the data obtained with the porous-coated component.

Within the cotyloid notch and the floor of the acetabulum, differences were also noted in the relative motion of the three shells. At both measurement sites, the plasma-sprayed and hydroxyapatite coated shells performed similarly with up to 65% less micromotion than the porous-coated component. Interface motion at the cotyloid notch averaged 48.9 ± 4.3 μm with the hydroxyapatite coated shell and 51.5 ± 4.0 μm with the plasma spray coated component ($p = 0.685$). In contrast, the micromotion of the porous-coated shell averaged 72.7 ± 2.9 μm, significantly larger than both the HA coated ($p = 0.007$) and plasma-sprayed coated ($p = 0.008$) components. Within the floor of the acetabulum, the component of motion corresponding to seating of the cup was almost the same with the HA (11.6 ± 4.1 μm) and the plasma-spray coated (9.6 ± 2.7 μm) implants and almost one-third of the motion of the porous-coated component (28.5 ± 10.5 μm). However, these differences were not statistically significant at the 5% level.

The transverse component of micromotion over the floor of the acetabulum was too small and too variable for the ingrowth surface to be a significant factor (ANOVA, $p=0.443$). In this case, the average micromotion only ranged from 5.4 ± 1.8 μm with the plasma-sprayed component to 9.4 ± 2.4 μm with the HA coating.

10.4 DISCUSSION

The experimental data support the conclusion that the ingrowth surface of the acetabular shell strongly influences the magnitude of cup/bone micromotion and hence the rigidity of cementless fixation of the implants examined. In this study, increases in micromotion of up to three-fold were observed with porous coated cups in comparison with plasma-spray coated hydroxyapatite-coated components. The major cause

of these differences is expected to be the frictional coefficient of the shell/bone interface which, on the basis of a manual inspection, appeared to be lowest with the beaded surface and greatest with the plasma-sprayed titanium coating.

These differences appear to arise from the size of the surface features and their minimum radius of curvature. On the microscopic level, the plasma-sprayed coating consists of relatively coarse asperities with sharp surface features; this is advantageous in increasing the mechanical traction between the cup and underlying bone because the sharp edges of the coating can easily engage the bony surface. The hydroxyapatite coating is expected to develop less friction in contact with cancellous bone because it has finer features than the plasma sprayed surface. However, the ceramic layer does have significant roughness on a microscopic scale, in part because of the presence of an undercoating of fine plasma-sprayed cp titanium which is added to increase the bond strength.

The relatively low coefficient of friction of the beaded coating is attributable to the size of the beads which typically ranges from 350 - 850 μm. Given their regular, spherical shape and smooth surface, the radius of curvature of the beads is probably one to two orders of magnitude larger than those of plasma-sprayed titanium. During implantation of a cup with a beaded surface, it is conceivable that the contact pressure developed between each bead and the reamed acetabulum may not be sufficient to generate effective penetration of the bony surface. As a consequence, traction would be compromised and the friction coefficient developed between the socket and the implant would be low, at least in comparison with a plasma-sprayed surface.

Another factor contributing to the stability of cups with different coatings may be variations in the degree of interference actually attained between the shell and the acetabulum at implantation. White et al (1994) have demonstrated that acetabular cups and reamers supplied by each of the orthopedic manufacturers vary from the nominal outer diameter by 0.5 - 0.75 mm. In this experiment, the same set of reamers was used to prepare every acetabulum so that instrument variations would not have been a factor, however, differences in the true diameter of the acetabular components could have contributed to variations in the true degree of mechanical interference generated by each shell. It is conceivable that the dimensional tolerances adopted for manufacture of cementless acetabular

cups may vary with the nature of the ingrowth coating, although each one of the prostheses used in this experiment was inspected by the manufacturer and found to conform with the normal tolerances for prostheses offered for clinical use.

The experimental data reveal for the first time that the micromotion at the shell/bone interface is non-uniform and site-specific. For each of the implants tested, the largest values of micromotion were recorded at the cotyloid notch at the inferior edge of the implantation site. Typically, the micromotion recorded at this site was almost double the motion measured at the superior dome, which has been a common location for measurements in previous studies. This suggests that little stock should be placed in the magnitude of the interface motions reported in previous studies, although the relative effect of changes in implant design or methods of fixation may be more valid. As most studies measured peripheral cup/bone motion, which was not measured in this experiment, it is not possible to tell whether the values reported reflect motion at other points over the surface of the shell which are not directly accessible to externally mounted transducers. Based upon the data of this study, it appears that the acetabular cup is pinned at discrete points over its surface and that under load, the implant toggles about those areas of support, leading to relative motion between the implant and the bone.

Superimposed upon this motion is the elastic deformation of the acetabulum itself which, in turn, will be influenced by the support provided by the implant. When an acetabular cup is implanted with peripheral interference, it is expected that the micromotion will be least at sites around the peripheral rim which is where the component gains its primary support. Conversely, interface motion over the floor of the acetabulum is expected to be greatest, especially in the superior-inferior direction as this location is furthest removed from the rim and is the area of least contact between the shell and an under-reamed socket. As the aim of acetabular fixation is to obtain intimate contact without relative motion over as much of the ingrowth surface as possible, peripheral measurements of implant stability can be extremely misleading. To fairly represent the stability of most of the acetabular interface, cup/bone micromotion must be measured at sites which are the most prone to gap formation and thus loss of reinforcement of the acetabulum through contact with the prosthesis. Based upon the work of Engh et al (1993) and

Callaghan et al (1988), these sites are the floor of the acetabulum, the cotyloid notch and the superior dome, the same areas that were selected for the measurements performed in this study.

This experiment suggests the distinct superiority of one ingrowth surface, the plasma-sprayed titanium, for immobilizing the cup/bone interface. This conclusion is not only borne out by the average values of interface micromotion at each of the measurement sites, but the unusual consistency of the values from site to site and between different specimens. This suggests that this particular coating may be less sensitive to variations in surgical technique and the precise distribution of shell/bone contact achieved intraoperatively.

It is tempting to make predictions about the likelihood of bony fixation of cups fabricated with the surface coatings evaluated in this study. In theory, this could be undertaken by comparing the measured values of interface motion with some threshold value, beyond which bony ingrowth would not be observed (e.g. 40 or 100 μm). On this basis, it would be possible to estimate how much of the interface of each specimen would be fixed by osseous rather than fibrous tissue. However, for a variety of reasons, such an exercise is expected to yield results with bearing little relationship to reality. Firstly, the loading conditions imposed on the pelvic specimen are highly simplified and only approximate, at best, the superior-inferior component of pelvic deformation in early stance phase. As the experiments of Chapter 6 demonstrated, the acetabulum is subjected to significant deformation in both the coronal and sagittal planes and so, in practice, the mediolateral component of interface shear is expected to be larger than measured in this experiment. In addition, the nominal load of 2,000 N, applied in a simple three-point bending configuration may not be mechanically equivalent to the normal loading of the pelvis in its anatomic orientation in which the reaction force balancing the joint load is distributed in a more complex manner. To confirm the equivalence of these loading modes, even in the superoinferior direction, a separate loading experiment would be necessary using both methods of loading of the same pelvic specimens.

Secondly, the threshold values of micromotion differentiating fibrous and bony ingrowth are poorly characterized, both in terms of the magnitude and direction of motion with respect to the interface. As

reported in Chapter 7, few animal studies have been conducted to examine the biologic response of ingrowth surfaces to variable amounts of interface displacement. In each of these studies, the displacement of the interface has occurred in shear or has not been characterized. No studies have elucidated the contribution of motion perpendicular to the implant surface, or the validity of extrapolating data derived from young animals to middle-aged humans. An additional consideration is the role of the ingrowth surface itself, as it is conceivable that different coatings may support bony ingrowth in the face of different levels of interface motion. This is clearly the case with hydroxyapatite which is osteo-conductive; it may also be a consideration in the biologic response of different metallic ingrowth surfaces.

Despite these concerns, the data derived from the present experiment do suggest that the normal pattern of biologic incorporation of the shell/bone interface would be distinctly non-uniform. If an acetabular cup is implanted with some degree of interference, bony attachment would be expected to occur around the rim of the prosthetic component and, in some instances, within the superior dome. Conversely, the floor of the acetabulum behind the shell is predicted to be an area in which bony ingrowth would be difficult to achieve and fibrous attachment would predominate. This may also be true in the cotyloid notch, especially with beaded components. It is interesting to note that these predictions correlate very closely with the observations made of Engh et al in reviewing patterns of tissue attachment to nine cementless acetabular cups retrieved at autopsy. This suggests that the site to site variation in micromotion may explain the patterns of ingrowth into acetabular prostheses and that new designs that immobilize more of the cementless interface could lead to more extensive bony attachment. Ultimately this could lead to improvements in the long-term performance of these devices and a reduction of the incidence of osteolysis.

CHAPTER 11 CONCLUSIONS AND SUGGESTIONS FOR FUTURE WORK

11.1 CONCLUSIONS AND SUMMARY OF RESULTS

(i) In early stance phase, at the first maximum of the hip joint reaction force:

(a) it is estimated that the joint reaction force is 3.4 times body weight at a walking speed of 1.1 m/s. Within a coordinate systems defined by the principal axes of the femur, it is estimated that this force is oriented such that 1.13 BW is directed laterally, 0.769 BW is directed posteriorly and 3.1 BW is directed inferiorly.

(b) the resultant muscle force acting on the femur is estimated to be 2.50 BW, oriented such that 0.68 BW is directed medially, 0.61 BW is directed posteriorly and 2.33 BW is directed superiorly.

(c) it is assumed that during this stage of the gait cycle, the following hip muscles are active: gluteus maximus; gluteus medius (all parts); gluteus minimus; tensor fascia lata; semitendinosus; semimembranosus; biceps femoris; rectus femoris.

(d) it is estimated that these muscles contract with the following activation coefficients, defined as the average force of contraction per unit cross-sectional area: gluteus maximus: 11 N/cm2; gluteus medius (all parts): 30 N/cm2; gluteus minimus: 30 N/cm2; tensor fascia lata: 17 N/cm2; semitendinosus: 17 N/cm2; semimembranosus: 5 N/cm2; biceps femoris: 5 N/cm2; rectus femoris: 5 N/cm2.

(e) it is estimated that the active hip muscles generate the following forces of contraction: gluteus maximus: 244N; gluteus medius (anterior part): 312N; gluteus medius (middle part): 156N; gluteus medius (posterior part): 312N; gluteus minimus: 390N; tensor fascia lata: 136N; semitendinous: 85N; semimembranosus: 70N, biceps femoris: 70N and rectus femoris: 70N.

(ii) The predominant pattern of pelvic deformation is biaxial bending. With load-bearing in early stance phase, muscle forces bend the pelvis over a fulcrum formed by the femoral head. This bending occurs in both the coronal and transverse planes, causing the femoral head to be 'pinched' circumferentially.

(iii) With loading, the acetabulum contracts in a longitudinal direction by an average of 57. 2 ± 9.1 μm anteriorly and 25.3 ± 7.3 μm posteriorly. This corresponds to equivalent strains of 1636 ± 252 and 744 ± 194 microstrain respectively.

(iv) In the transverse direction, loading caused a contraction of 68.2 ± 24.2 μm in the overall width of the acetabulum, corresponding to an effective strain of 1154 ± 448 microstrain. Less contraction was observed inferiorly, at the facets (16.0 ± 7.6 μm, 345 ± 16.8 microstrain) and superiorly, over the weight-bearing dome (32.7 ± 8.1 μm, 811 ± 153 microstrain).

(v) The acetabulum became slightly deeper under load with stretching of the anterior and posterior walls in a medial-lateral direction. Elongation of the anterior wall (11.9 ± 2.5 μm, 417 ± 86 microstrain) was greater than the posterior wall (4.4 ± 0.2 μm, 110 ± 5 microstrain).

(vi) The dorsal surface of the ilium and ischium, immediately behind the acetabulum, was subjected to biaxial stretching. Elongation was greater in a longitudinal (17.5 ± 6.4 μm, 547 ± 72 microstrain) than a transverse direction (12.2 ± 1.2 μm, 269 ± 17 microstrain). The pectineal line was a site of significant elongation under load (32.7 ± 5.2 μm, 1552 ± 257 microstrain).

(vii) Both the pattern and magnitude of deformation of the acetabulum varied considerably from specimen to specimen. This was primarily related to the degree of anteversion of the socket with respect to the remainder of the pelvis and was most apparent in transverse components of deformation (eg. the facets). Other sources of variability included the width and bone density of individual specimens.

(viii) Some components of bony deformation varied little between specimens. These included the depth of the socket and the elongation of the inner table of the pelvis.

(ix) Uniaxial bending did not reproduce the pattern of pelvic deformation generated by physiologic loading. Although the longitudinal components of strain were comparable, the transverse components were tensile with uniaxial bending rather than compressive as in the physiologic load configuration. This suggests that in experiments involving uniaxial (eg. three-point bending)

loading of the pelvis, deformation measurements should be restricted to a longitudinal direction to be relevant to the structural response in vivo.

(x) During three-point bending, cementless acetabular shells implanted in the reamed acetabulum are squeezed in a longitudinal direction (ie. superiorly and inferiorly) in a manner akin to the original femoral head.

(xi) Relative motion between the shell and the socket is non-uniform. Perpendicular to the interface, the greatest motion is observed inferiorly at the cotyloid notch where the distance between the shell and the bone was reduced by 57. 7 ± 4.6 μm with application of load. Similarly, at the superior dome, loading caused compression of 36.5 ± 7.3 μm. Behind the implant, the space between the cup and the floor of the acetabulum was reduced by an average of 15.6 ± 4.4 μm with loading.

(xii) A major component of cup/bone micromotion occurred parallel to the interface between the dome of the shell and the floor of the socket. In three-point bending, joint loading caused the shell to move in a superior direction by an average of 25.7 ± 7.1 μm. In this load configuration, anterior-posterior motion was negligible (0.6 ± 2 μm).

(xiii) The distribution and magnitude of motion of the acetabular interface varied significantly with the nature of the surface coating on the outer surface of the implant. The largest motions were consistently seen with beaded, Co-Cr implants which exhibited 50-200% more micromotion than the hydroxyapatite and plasma-spray coated components at all measurement sites. The perpendicular component of implant/bone motion of the hydroxyapatite and plasma-spray coated cups was similar within the acetabular notch and over the floor of the socket. However, within the weight-bearing dome, the HA coated component produced almost twice the motion of the plasma-spray coated implant. Similarly, behind the shell, motion parallel to the floor of the socket was 40% less with the plasma-sprayed surface.

(xiv) The effect of surface coatings on implant stability appears to be related to differences in the coefficient of friction of the shell/bone interface. Implant coatings that are relatively smooth (eg. beaded

surfaces) or that have fine surface features (eg. hydroxyapatite coatings) lead to greater relative motion than coatings that are coarse and sharp (eg. plasma-sprayed surfaces).

(xv) The use of plasma-spray coating on acetabular shells leads to very low levels of interfacial micromotion; four of the five components of motion were less than 20 μm under the conditions used in this study. Only motion at the cotyloid notch exceeded 40μm (average: 51.5 ± 4.0 μm).

(xvi) It is predicted that plasma-spray coated cups will have a greater area of bony ingrowth than those with beaded coatings. Plasma-sprayed coated components are also expected to be more tolerant of errors in preparation of the socket and implantation of the shell which can lead to fibrous encapsulation of the implant and excessive micromotion of the cementless interface.

11.2 SUGGESTIONS FOR FUTURE WORK

In consideration of the fields of investigation persued in this thesis, it is suggested that future studies could be perfromed in the following areas:

11.2.1 Prediction of Hip Muscle Forces

At present it is not possible to accurately predict muscle forces during gait because simultaneous measurements of intravital hip reaction forces, ground/foot reaction forces, joint kinematics and EMG of the hip muscles have not been obtained from the same subject. Even with these data, it is not possible to accurately distribute the net force of muscle contraction between individual muscles unless the physiologic cross-sectional area of each muscle of the test subject is known in addition to the relationship between the magnitude of the rectified EMG signal and the force of contraction of each individual muscle.

To further elucidate these questions, the following studies are proposed:

(a) Further study is needed of subjects implanted with instrumented prostheses. Simultaneous measurement of biomechanical, kinematic and EMG data would allow a more accurate prediction of muscle forces and critical assessment of alternate methods of

calculation of these forces. These data would also allow investigators to detect any abnormalities in the gait patterns of individuals with instrumented implants and to determine whether data derived from these prostheses should be regarded as indicators of normal joint physiology.

(b) Additional research is required to combine mathematical models of muscle contraction with functional models of gait and segmental loading. In separate studies, muscle physiologists have developed complex mathematical descriptions of individual muscles while bioengineers have developed biomechanical models of the musculoskeletal system during a variety of activities, most commonly walking. In the present thesis, muscle contraction was crudely described using fixed values of the 'activation coefficient' of each muscle and its physiologic cross-sectional area. This simplistic representation is adequate for approximation of forces for applications in which accurate predictions are not critical. However, adoption of a more detailed description of each muscle is expected to lead to much more realistic models of muscle activity and joint loading.

(c) Quantitative EMG data could be extremely valuable in predicting muscle forces if more accurate methods existed to relate electrical activity to the force of contraction of individual muscles. Previous studies have shown that while some muscles demonstrate a proportional relationship between the force of contraction and the integrated EMG signal, others respond non-linearly to activation, depending upon the distribution of fast and slow muscle fibers. Additional research is needed to more fully describe the force/EMG relationships of the muscles of the human body. A fruitful approach to this problem may be to utilize animals with similar muscles to the human. Muscle tissue harvested from an animal could be used to relate an electromechanical characterization of each muscle to the structure and fiber types present. If this were successful, it would then be possible to predict the response of human muscles to stimulation through microstructural similarities between human and animal tissue. It may also be possible to perform some electrophysiologic measurements on small samples of

human muscle obtained intraoperatively.

11.2.2 Deformation of the Acetabulum During Loading

The work described in this thesis could be expanded through the following studies:

(a) Pelvic deformation could be characterized in a broad range of functional activities. The cadaveric model developed in this study has been enhanced and simplified through the use of pneumatic actuators to generate muscle forces. This allows the force/displacement characteristics of individual muscles to be simulated through computer control of precision pneumatic valves. With this flexibility, it is possible to simulate the entire gait cycle with the addition of muscles not active in early stance (e.g. iliopsoas). Additionally, the response of the pelvis to high demand activities (e.g. stair-climbing, rising out of a chair) could be studied.

(b) The response of the pelvis to loading following injury and surgical reconstruction could be studied. Pelvic fractures are relatively common following motor vehicle and industrial accidents and some fracture patterns are difficult to stabilize. It would be useful to study the interfragmentary stability of alternative methods of repairing these fractures using the cadaveric model developed in this thesis. This could lead to improved methods of fracture fixation and rehabilitation in the face of these debilitating injuries.

(c) Three dimensional finite element models of the acetabulum and pelvis are evolving to the point that useful and realistic predictions can be made concerning the distribution of bony deformation and internal stresses. This approach is ideally suited to parametric analysis of variables affecting the mechanical response of the pelvis to external loading. While theoretical stress analysis provides much greater detail than experimental measurements with greater convenience and less overall expense, experimental validation of finite element models is critical to their use and acceptance. In future studies, a 3-D finite element model of the pelves loaded in this study could be developed in order to compare the predictions of these

models with the measurement performed in the loading experiments. It may then be possible to adjust the finite element models to enhance the accuracy of their predictions.

11.2.3 Motion of the Cup/Bone Interface

The experimental study of implant motion described in this thesis examined one of numerous factors that influence the mechanical stability of cementless prostheses within the acetabulum. Future research could pursue the following avenues:

(i) Experiments performed with the mechanical analogue of the acetabulum demonstrated that the loading of the pelvis cannot be accurately depicted by uniaxial bending as a significant bending also occurs in the transverse plane. For this reason, the micromotion measurements reported in Chapter 10 were only performed along the superoinferior axis of the acetabulum. The measurements of interface motion should be repeated using the same cadaveric model used for measurement of acetabular deformation. This would generate more realistic deformation of the pelvis and would allow the motion of the interface to be measured at sites along the anterior and posterior walls of the acetabulum. Meaningful data could also be collected describing transverse components of micromotion.

(ii) It would be extremely useful to relate the observed pattern and magnitude of shell/bone motion to simultaneous measurements of acetabular deformation. This would allow us to directly relate interface motion to the elastic deformation of the pelvis and would help elucidate the contribution of the fit of the shell within the acetabulum to implant stability.

(iii) Although it is possible to measure interface motion, the underlying role of structural and morphologic factors is unknown. Valuable information could be obtained by measuring the precise distribution of contact between the shell and the socket and relating this to the micromotion observed in different specimens. The bone density and bending stiffness of each pelvis could also be related to these stability measurements.

(iv) Further experimental investigations are needed to study the effect of the following variables on the stability of the cup/bone

interface:

(a) the true difference in diameter of the reamed socket and the acetabular shell,

(b) the flexibility of the acetabular cup,

(c) the contribution of adjunctive fixation, especially bone screws to implant stability, and

(d) the use of compacted graft to enhance implant fixation in osteoporotic bone.

(v) The fixation of cementless cups within the damaged acetabulum remains controversial. Several long term studies have discredited the use of allografts to reconstruct the acetabular socket. In many revision cases the only feasible alternatives are to implant large shells supported by small areas of residual bone or to fill osseous defects with elongated shells despite the cost of these components and difficulties in achieving an accurate fit to the damaged socket. The relative merits of each of these approaches could be quantified through experimental simulation of standardized bony defects in cadaveric pelves. Using these specimens, the stability of various fixation strategies could be determined utilizing the same experimental methods described in Chapter 10.

(vi) This study has focused upon interface stability as the critical parameter characterizing the mechanical performance of cementless acetabular prostheses. This is certainly warranted, as instability of the shell/bone interface will comprise asymptomatic function of the artificial hip and may lead to osteolysis if extensive areas of fibrous tissue are present between the implant and the acetabulum. However, an additional consideration is stress-shielding of periacetabular bone in the presence of rigid, ingrown acetabular shells. With the increasing use of oversized cups to achieve initial stability without adjunctive fixation, bony fixation is frequently restricted to the peripheral rim of the acetabulum. This distorts the normal physiologic transmission of load to the pelvis and may ultimately lead to the development of osteopenia of periacetabular bone, particularly medial to the cup. Whether the resulting increase in osseous porosity will lead to a greater

incidence of osteolysis and late implant failure has yet to be determined.

A potentially valuable field of study is the effect of acetabular replacement on the stress distribution within the pelvis. This subject should be explored through development of a three-dimensional finite element model of the pelvis with particular attention to periacetabular bone. Once such a model has been validated through experimental measurements of extracortical stresses, the effect of numerous variables describing the surgical preparation of the acetabulum and the design of the prosthesis could be explored to minimize stress-shielding of the pelvis. Armed with this knowledge and data describing the effect of the same variables on implant stability, more rational decisions could be made in the design and selection of prosthetic devices for replacement of the acetabulum.

REFERENCE LIST

1. Abbott BC and Wilkie DR (1953), The Relation Between Velocity of Shortening and the Tension Length Curve of Skeletal Muscle. J Physiol 120:214-223.

2. Amstutz HC, Kabo M, Hermens K, O'Carroll PF, Dorey F, & Kilgus D (1987), Porous Surface Replacement of the Hip with Chamfer Cylinder Design, Clinical Orthopedics and Related Research 222:140-60.

3. Amstutz HC, O'Carroll PF, Kabo JM and Kim WC (1985), Comparative Experience with Canine and Human Cementless Acetabular Components, Proceedings of Hip Society, 235-49.

4. Andriacchi TP and Strickland AB (1985), Gait Analysis as a Tool to Assess Joint Kinetics in "Biomechanics of Normal and Pathological Human Articulating Joints", ed N Berme, AE Engin and KM Correia da Silva, Martinus Nijhoff, Hingham, pp 83-102.

5. Apel DM, Smith DG, Schwartz CM and Paprosky WG (1989), Threaded Cup Acetabuloplasty: Early Clinical Experience. Clin Orthop 241:183-189.

6. Armbuster TG, Guerra J, Resnick D et al (1978), The Adult Hip: An Anatomic Study.I. The Bony Landmarks. Radiology 128:1-10.

7. Arsenault AB, Winter DA and Marteniuk RG (1986), Is There A "Normal" Profile of EMG Activity in Gait?, Med. & Biol. Eng. & Comput. 24:337-343.

8. Aust JC, Bredenberg CE and Murray DG (1981), Mechanisms of Arterial Injuries Associated with Total Hip Replacement. Arch Surg 116:345-349.

9. Ballard WT, Callaghan JJ, Sullivan PM and Johnston RC (1994), The Results of Improved Cementing Techniques for Total Hip Arthroplasty in Patients Less Than Fifty Years Old. J Bone Joint Surg 76A:959-964.

10. Barbenel JC (1983), The Application of Optimization Methods for the Calculation of Joint and Muscle Forces. Engineering in Medicine12:29-33.

11. Basmajian JV (1976), The Human Bicycle in "Biomechanics V-A", ed. PV Komi, University Park Press, Baltimore, 1A:297-302.

12. Basmajian JV and DeLuca CJ (1962), Lower Limb in "Muscles Alive: Their Functions Revealed by Electromyography", ed. JV Basmajian, Williams & Wilkins, Baltimore, pp. 125-152.

13. Basmajian JV and DeLuca CJ (1985), Human Locomotion in "Muscles Alive, Their Functions Revealed by Electromyography, 5th edition", Williams & Wilkins, Baltimore pp. 310-353.

14. Battye CK and Joseph J (1966), An Investigation by Telemetering of the Activity of Some Muscles in Walking. Med. & Biol. Eng. 4:125-135.

15. Bauer TW, Stulberg BN, Ming J, and Geesink RGT (1993), Uncemented Acetabular Components. J Arthroplasty 8:167-177.

16. Beauchesne RP, Engh CA and Suthers K (1992), Roentgenographic Evaluation of the AML Porous-Coated Acetabular Component: A Six-Year minimum Follow-up Study. Orthop Trans 16:834.

17. Bergmann G, Graichen F and Rohlmann A (1989), Load Directions at Hip Prostheses Measured in-vivo. J Biomechanics 22:986

18. Bergmann G, Graichen F, and Rohlmann A (1993), Hip Joint Loading During Walking and Running, Measured in Two Patients. J Biomechanics 26: 969-990.

19. Bertin KC, Freeman MAR, Morscher E, Oeri A, and Ring PA (1985), Cementless Acetabular Replacment Using a Pegged Polyethylene Prosthesis. Arch Orthop Trauma Surg 104:251-261.

20. Bigland-Ritchie B, Kukulka CG and Woods JJ (1980), Surface E.M.G./Force Relation in Human Muscles of Different Fibre Composition, J Physiology 308:103P-104P.

21. Bo WJ, Wolfman NT, Wayne AK and Mesechan I (1990), Basic Atlas of Sectional Anatomy with Correlated Imaging, W.B. Saunders Company, Philadelphia.

22. Bobyn JD, Engh CA and Glassman AH (1987), Histological Analysis of a Retrieved Microporous-Coated Femoral Prosthesis: A Seven-Year Case Report. Clin Orthop 224:303-10.

23. Bobyn JD, Engh CA and Glassman AH (1988), Radiography and Histology of a Threaded Acetabular Implant: One case studied at two years. J Bone Joint Surg 70B:302-304.

24. Bobyn JD, Pilliar RM, Cameron HU and Weatherly GC (1980), The Optimum Pore Size for the Fixation of Porous-Surfaced Metal Implants By the Ingrowth Of Bone. Clin Orthop 150:263-270.

25. Bono JV, Sanford L and Toussaint JT (1994), Severe Polyethylene Wear in Total Hip Arthroplasty: Observations From Retrieved AML PLUS Hip Implants with an ACS Polyethylene Liner. J Arthroplasty 9:119-125.

26. Bragdon CR, Jasty M, Lowenstein JD and Burke DW (1993), The Histology of Bone Ingrowth at the Implant/Bone Interface Under Known Amounts of Micromotion. Trans Orthopedic Research Society 17:468.

27. Brand RA, Crowninshield RD and Pedersen DR (1982), Architecture of the Periacetabular Trabecular Bone. J Orthop 5:299-304.

28. Brand RA, Crowninshield RD, Wittstock CE, Pedersen DR and Clark CR (1982), A Model of Lower Extremity Anatomy. J Biomech Eng 104:304-310.

29. Brand RA, Pedersen DR, Davy DT, Kotzar GM, Heiple KG and Goldberg VM (1994), Comparison of Hip Force Calculations and Measurements in the Same Patient. J Arthroplasty 9:45-51.

30. Bresler B and Frankel JP (1950), The Forces and Moments in the Leg During Level Walking. Transactions of the ASME pp. 27-36.

31. Brismar B, Veress B and Svensson O (1992), Injury of the Femoral Artery in Total Hip Replacement Causing Abdominal Pain and Hypovolemic Shock. J Bone Joint Surg 74A:1560-1562.

32. Brown RH, Davy DT, Heiple KG Sr, Kotzar GM, Heiple KG Jr, Berilla J, Goldberg VM and Burstein AH (1985), In-vivo Load Measurements on a Total Hip Prosthesis. Trans Orthopaedic Research Society 9:335.

33. Brown TRM, Nicol AC and Paul JP (1984), Comparison of Loads Transmitted by Chanley and CAD Muller Total Hip Arthroplasties. Proceedings IMech Eng pp. 63-68.

34. Bulcke JA, Termote JL, Palmers Y and Crolla D (1979), Computed Tomography of the Human Sekletal Muscular System. Neuroradiology 17:127-136.

35. Bullough P, Goodfellow J and O'Connor J (1973), The relationship between Degenerative Changes and Load-Bearing in the Human Hip. J Bone Joint Surg 55B:746-758

36. Bullough P, Goodfellow J, Greenwald AS, and O'Connor J (1968), Incongruent Surfaces in the Human Hip Joint, Nature 217:1290.

37. Burke DW, Bragdon JD and Lowenstein JD (1993), Mechanical Aspects of the Bone-Porous Surface Interface Under Known Amounts of Implant Motion: An in vivo Canine Study. Trans Orthopedic Research Society 17:470.

38. Byers PD, Contemponi CA and Farkas TA (1970), A Postmortem Study of the Hip Joint. Including the Prevalence of the Features of the Right Side. Ann Rheum Dis 29:15-31.

39. Cahill DR and Orland MJ (1984), Atlas of Human Cross-Sectional Anatomy, Lea & Febiger, Philadelphia.

40. Cahill DR, Orland MJ and Reading CC (1990), Atlas of Human Cross-Sectional Anatomy: Wtih CT and MR Images, Wiley-Liss, New York.

41. Callaghan JJ, Dysart SH and Savory CG (1988), The Uncemented Porous-Coated Anatomic Total Hip Prosthesis, J Bone Joint Surg, 70-A:337-346.

42. Campanacci (1967), as quoted by Tile M (1984).

43. Cappozzo A (1986), A. Human Skeletal System Loading Patterns Associated with Activities of Daily Living, in "Biological and Biomechanical Performance of Biomaterials" ed P Christel, A Meunier and AJC Lee, Elsevier Science Publishers B. V., Amsterdam pp 429-440.

44. Cappozzo A, Figura F, Marchetti M (1976), The Interplay of Muscular and External Forces in Human Ambulation. J Biomechanics 9:35-43.

45. Carter DR, Vasu R and Harris WH (1982), Stress Distributions in the Acetabular Region - II. Effects of Cement Thickness and Metal Backing of the Total Hip Acetabular Component. J Biomechanics 15:165-170.

46. Carter DR, Vasu R and Harris WH (1983), Periacetabular Stress Distributions after Joint Replacement with Subchrondral Bone Retention. Acta Orthop Scand 54:29-35.

47. Cathcart RF (1971), The Shape of the Femoral Head and Preliminary Results of Clinical Use of a Non-Spherical Hip Prosthesis. J Bone Joint Surg 53A:397.

48. Cathcart RF (1972), The Shape of the Normal Femoral head and Results from Clinical Use of More Normally Shaped Non-Spherical Hip-Replacement Prostheses. J Bone Joint Surg 54A:1559.

49. Challis JH and Kerwin DG (1993), An Analytical Examination of Muscle Force Estimations Using Optimization Techniques. J Engineering in Medicine 207:139-148.

50. Cimbrelo-Garcia E and Munuera L (1992), Early and Late Loosening of the Acetabular Cup After Low-Friction Arthroplasty. J Bone Joint Surg 74A:1119-1129.

51. Clark JM and Haynor DR (1987), Anatomy of the Abductor Muscles of the Hip as Studied by Computed Tomography, J Bone Joint Surg, 69-A:1021-1031.

52. Clarke HJ, Jinnah RH, Warden KE et al (1991), Evaluation of Acetabular Stability in Uncemented Prostheses. J Arthroplasty 6: 335-340.

53. Clarke IC and Amstutz HC (1975), Human Hip Joint Geometry and Hemiarthroplasty Selection in "The Hip", C.V. Mosby Company, pp.63-89.

54. Collier JP, Mayor MB, Chae JC, Surprenant VA, Surprenant HP and Dauphinais LA (1988), Macroscopic and Microscopic Evidence of Prosthetic Fixation with Porous-Coated Materials. Clin Orthop 235:173-180.

55. Cook SD and Thomas KA (1991), Fatigue Failure of Noncemented Porous-Coated Implants. A Retrieval Study. J Bone Joint Surg 73B:20-24.

56. Cook SD, Barrack RL, Thomas KA and Haddad RJ Jr. (1988), Quantitative Analysis of Tissue Growth into Human Porous Total Hip Components. J Arthroplasty 3:249-262.

57. Cook SD, McCluskey LC, Martin PC and Haddad RJ Jr(1991), Inflammatory Response in Retrieved Noncemented Porous-Coated Implants. Clin Orthop 264:209-222.

58. Cook SD, Thomas KA, Haddad RJ Jr. (1988), Histologic Analysis of Retrieved Human Porous-Coated Total Joint Components. Clin Orthop 234:90-101.

59. Cornell CN and Ranawat CS (1986), The Impact of Modern Cement Techniques on Acetabular Fixation in Cemented Total Hip Replacement. J Arthroplasty 1:197-202.

60. Crowninshield RD (1978), Use of Optimization Techniques to Predict Muscle Forces. Trans ASME, 11:88-92.

61. Crowninshield RD and Brand RA (1981), A Physiologically Based Criterion of Muscle Force Prediction in Locomotion. J Biomechanics 11:793-801.

62. Crowninshield RD, Johnston RC, Andrews JG and Brand RA (1978), A Biomechanical Investigation of the Human Hip. J Biomechanics 11:75-85.

63. Crowninshield RD, Pedersen DR, Brand RA and Johnston RC (1983), Analytical Support for Acetabular Component Metal Backing in "The Hip", ed. DS Hungerford, C.V. Mosby Company, pp. 207-215.

64. Curtis MJ, Jinnah RH, Wilson VD and Hungerford DS (1992), The Initial Stability of Uncemented Acetabular Components. J Bone Joint Surg 74B:372-376.

65. Dalstra M and Huiskes R (1990), The Pelvic Bone as a Sandwich Construction: A Three Dimensional Finite Element Study. Proceedings European Society of Biomechanics. University of Aarhus, B32.

66. Dalstra M and Huiskes R (1991), The Influence of Metal Backing in Cemented Cups. Trans Orthopedic Research Society 15: 272.

67. Davy DT, Kotzar GM, Brown RH, Heiple KG, Goldberg VM, Heiple KG Jr, Berilla J and Burstein AH (1988), Telemetric Force Measurements across the Hip after Total Arthroplasty. J Bone Joint Surg 70A:45-50.

68. De Lee JG and Charnley J (1976), Radiological Demarcation of Cemented Sockets in Total Hip Replacement. Clin Orthop 121:20-32.

69. Dorr LD, Takei GK and Conaty JP (1983), Total Hip Arthroplasties in Patients Less Than Forty-Five Years Old. J Bone Joint Surg 65A:474-479.

70. Dostal WF and AndrewsJG (1981), A Three Dimensional Biomechanical Model of Hip Musculature. J Biomechanics 14:803-812.

71. Eberhart HD, Inman VT and Bresler B (1954), The Principal Elements in Human Locomotion in "Human Limbs and Their Substitutes", eds. PE Klopsteg and PD Wilson, McGraw-Hill, New York.

72. Engh CA, Bobyn JD and Glassman AH (1987), Porous-Coated Hip Replacement. The Factors Governing Bone Ingrowth, Stress Shielding, and Clinical Results. J Bone Joint Surg 69B:45-55.

73. Engh CA, Griffin WL and Marx CL (1990), Cementless Acetabular Components. J Bone Joint Surg 72B:53-59.

74. Engh CA, Zettl-Schaffer KF and Kukita Y (1993), Histological and Radiographic Assesment of Well-Functioning Porous-Coated Acetabular Components: A Human Post-Mortem Retreival Study. J Bone Joint Surg 75A:814-824.

75. English TA and Kilvington M (1979), In Vivo Records of Hip Loads Using a Femoral Implant with Telemetric Output. J Biomed Eng 1:111-115.

76. Finlay JB, Bourne RB, Landsberg RPD and Andreae P (1986a), Pelvic Stresses in Vitro-I. Malsizing of Endoprotheses. J Biomechanics 19:703-714.

77. Finlay JB, Bourne RB, Landsberg RPD and Andreae P (1986b), Pelvis Stresses In vitro-II. A Study of the Efficacy of Metal-Backed Acetabular Prostheses. J Biomechanics 19:715-725.

78. Fox GM, McBeath AA and Heiner JP (1994), Hip Replacement with a Threaded Acetabular Cup. J Bone Joint Surg 76A:195-201.

79. Frankel A, Balderston RA, Booth RE, and Rothman RH (1990), Radiographic Demarcation of the Acetabular Bone-Cement Interface. J Arthroplasty 5:S1-S3.

80. Friedman RJ, Black J, Galante JO, Jacobs JJ and Skinner HB (1994), Current Concepts in Orthopaedic Biomaterials and Implant Fixation in "Instructional Course Lectures". ed M Schafer, American Academy of Orthopaedic Surgeons, Chicago, Illinois.

81. Fuchs MD, Salvati EA, Wilson PDJr, Sculco TP, and Pellicci PM (1988), Results of Acetabular Revisions with Newer Cement Techniques. Orthop Clinics of North America 19:649-655.

82. Galante J, Sumner DR, and Gachter A (1987), Surface Structures and Bone Ingrowth in Cement-Free Fixed Prosthesis. Orthopaedics 16:197-205.

83. Garcia-Cimbrelo E and Munuera L (1992), Early and Late Loosening of the Acetabular Cup After Low-Friction Arthroplasty. J Bone Joint Surg 74A:1119-1129.

84. Gerhardt, P and Frommhold, W (1988), Atlas of Anatomic Correlations in CT and MRI. Georg Thieme Verlag, Stuttgart, New York.

85. Ghelman B (1979), Radiographic Localization of the Acetabular Component of Hip Prosthesis. Radiology 130: 540-542.

86. Giacchetto J and Gallagher JJ (1988), False Aneurysm of the Common Femoral Artery Secondary to Migration of a Threaded Acetabular Component. Clin Orthop 231:91-96.

87. Goldberg VM, Davy DT, Kotzar GL, Heiple KG Sr, Brown RH, Heiple KG Jr., Berilla J and Burstein AH (1988), In Vivo Hip Forces in "Non-Cemented Total Hip Arthroplasty", ed R Fitzgerald Jr, Raven Press, Ltd., New York, pp. 251-256.

88. Gore TA, Higginson GR and Stevens J (1984), The Kinematics of Hip Joints: Normal Functioning. Clin Phys Physiol Meas 5:233-252.

89. Green DL, Morris JM (1970), Role of Adducutor Longus and Adductor Magnus in Postural Movements and in Ambulation. Am J Phys Med 49: 223-240.

90. Greenwald AS (1974), Joint Congruence Dynamic Concept, in "The Hip, Proceedings of the Second Scientific Meeting of the Hip Society" ed WH Harris, The C.V. Mosby Company, St. Louis.

91. Greenwald AS and Haynes DW (1972), Weight-Bearing Areas in the Human Hip Joint. J Bone Joint Surg 54B:157-163.

92. Greenwald AS and O'Connor JJ (1971), The Transmission of Load Through the Human Hip Joint. J Biomechanics 4:507-528.

93. Guerra J Jr, Armbuster TG, Resnick D, Goergen TG, Feingold ML, Niwayama G and Danzig LA (1978), The Adult Hip: An Anatomic Study. Diagnostic Radiology 128:11-20.

94. Hammond BT and Charnley J (1967), The Sphericity of the Femoral Head. Med Biol Eng 5:445-453.

95. Hansen TM and Koeneman JB (1989), 3-D FEA Analysis of the Human Pelvis. Proceedings 4th International Meeting of the ASME Finite Element Users Group, pp 1560-1578

96. Hardt DE (1978), Determining Muscle Forces in the Leg During Normal Human Walking - An Application and Evaluation of Optimization Methods. J Biomech Eng., 100:72-78.

97. Harris WH and Penenberg BL (1987), Further Follow-up on Socket Fixation Using a Metal-Backed Acetabular Component for Total Hip Replacement. J Bone Joint Surg 69A:1140-1143.

98. Harris WH and White RE (1982), Socket Fixation using a Metal-Backed Acetabular Componenet for Total Hip Replacement. J Bone Joint Surg 64A:745-748.

99. Harris WH, White RE Jr, McCarthy JC, Walker PS and Weinberg EH (1983), Bony Ingrowth Fixation of the Acetabular Component in Canine Hip Joint Arthroplasty. Clin Orthop 176:7-11.

100. Heekin RD, Callaghan JJ, Hopkinson WJ, Savory CG and Xenos JS (1993), The Porous-Coated Anatomic Total Hip Prosthesis Inserted without Cement. J Bone Joint Surg 75A:77-91.

101. Hill AV (1953), The Mechanisms of Active Muscle. Proc Roy Soc London 141:104-117.

102. Hodgkinson JP, Maskell AP, Paul A and Wroblewski BM (1993), Flanged Acetabular Components in Cemented Charnley Hip Arthroplasty, J Bone Joint Surg 75B:464-467.

103. Hodgkinson JP, Shelley P and Wroblewski BM (1988), The Correlation Between the Roentgenographic Appearance and Operative Findings at the Bone/Cement Junction of the Charnley Low Friction Arthroplasty. Clin Orthop 228:105-109.

104. Hof AL and Van den Berg JW (1981a), EMG to Force Processing I: An Electrical Analogue of the Hill Muscle Model. J Biomechanics 14:747-758.

105. Hof AL and Van den Berg JW (1981b), EMG to Force Processing III: Estimation of Model Parameters for the Human Triceps Surae Muscle and Assessment of the Accuracy by Means of a Torque Plate. J Biomechanics 14:771-785.

106. Hollinshead WH (1969), Textbook of Anatomy, 2nd Edition, Harper & Row, New York.

107. Hollinshead WH, and Rosse C (1985), Buttock, Thigh, and Hip Joint in "Textbook of Anatomy, Fourth Edition", Harper & Row, Philadelphia, pp.349-399.

108. Hollis JM, Stewart CL, Hofmann OE and Flahiff CM (1993), Effect of Micromotion on Ingrowth Into Porous Coated Implants. Trans of Orthopedic Research Society 17:472.

109. Howie JI (1985), Computed Tomography of the Bony Pelvis: A Protocol for Multiplanar Imaging. J. Canadian Assoc. of Radiologists. 36:278-286.

110. Hoy MG, Zajac FE and Gordon ME (1988), A Musculoskeletal Model of the Human Lower Extremity: The Effect of Muscle, Tendon, and Moment Arm on the Moment-Angle Relationship of Musculotendon Actuators at the Hip, Knee, and Ankle. J Biomechanics 23:157-169.

111. Hozack WJ, Rothman RH, Booth RE, Balderston RA, Cohn JC and Pickens GT (1990), Survivorship Analysis of 1,041 Charnley Total Hip Arthoplasties. J Arthroplasty 5:41-47.

112. Huk OL, Bansal M, Betts F, Rimnac CM, Lieberman JR, Huo MH and Salvati EA (1994), Polyethylene and Metal Debris Generated by Non-articulating Surfaces of Modular Acetabular Components. J Bone Joint Surg 76B:568-574.

113. Hungerford DS and Kenna RV (1983), Preliminary Experience with a Total Knee Prosthesis with Porous Coating Used without Cement. Clin Orthop 176:95-107.

114. Inman VT (1947), Functional Aspects of the Abductor Muscles of the Hip. J Bone Joint Surg 29: 607-619.

115. Inman VT, Ralston HJ, Saunder JB de CM, Feinstein B and Wright EW (1951), Relation of Electromyogram to Muscular Tension. Prosthetic Devices Research Project. University of California, Series II, Issue 18.

116. Jacob HAC, Huggler AH, Dietschi C and Schreiber A (1976), Mechanical Function of Subchondral Bone as Experimentally Determined on the Acetabulum of the Human Pelvis. J Biomechanics 9:625-627.

117. Janda V and Stara V (1965), The Role of Thigh Adductors in movement patterns of the hip and knee joint. Courrier (Centre Internat de l'Enfrance) 15:1-3.

118. Jensen RH and Davy DT (1975), An Investigation of Muscle Lines of Action about the Hip: A Centroid Line Approach vs. The Straight Line Approach. J Biomechanics 8:103-110

119. Johnston RC (1974), Detailed Analysis of Hip Joint during Gait in "Proceedings of the Second Meeting of the Hip Society" ed WH Harris, Mosby Company, St. Louis.

120. Jonsson B and Steen B (1966), Function of the Gracilis Muscle. An Electromyographic Study, Acta Morphol Neerl-Scan 4:325-341.

121. Joshi AB, Markovic L, Noble PC and Murphy JC (1995), Long Term Wear of the Acetabular Cup: Analysis of Risk Factors. Trans Orthopedic Research Society 18:243 - 40.

122. Joshi AB, Porter ML, Trail IA, Hunt LP, Murphy JC and Hardinge K (1993), Long-Term Results of Charnley Low-Friction Arthroplasty in Young Patients. J Bone Joint Surg 75B:616-623.

123. Kadaba MP, Ramakrishnan HK and Wooten ME (1990), Measurement of Lower Extremity Kinematics During Level Walking. J Orthopedic Research 8:383-392.

124. Kadaba MP, Ramakrishnan HK, Wooten ME, Gainey J, Gorton G and Cochran GVB (1989), Repeatability of Kinematic, Kinetic, and Electromyographic Data in Normal Adult Gait. J Orthopedic Research 7:849-860.

125. Kadaba MP, Wootten ME, Ramakrishnan HK, Hurwitz D and Cochran GVB (1987), Assessment of Human Motion with Vicon in "Proceedings of the ASME Biomechanics Symposium" ed DL Butler and PA Torzilli, AMD, 84:335-338.

126. Kamaric E, Noble PC, Reardon JP and Tullos HS (1991), Optimized Biplanar Radiography for Three-Dimensional Coordinate Measurement. Proceedings: Biomechanics Symposium AMSE 120:321.

127. Kang JD, McKernan DJ, Kruger M, Mutschler T, Thompson WH and Rubash HE (1991), Ingrowth and Formation of Bone in Defects in an Uncemented Fiber-Metal Total Hip-Replacement Model in Dogs. J Bone Joint Surg 73A:93-105.

128. Kapandji I (1987), "The Physiology of the Joints, Vol 2". Churchill Livingstone, Edinburgh.

129. Karlsson E and Jonsson B (1965) , Function of the Gluteus Maximus Muscle: An Electromyographic Study. Acta Morphol Neerl-Scan 6:161-169.

130. Karrholm J and Snorrason F (1992), Migration of Porous Coated Acetabular Prostheses Fixed with Screws: Roentgen Stereophotogrammetric Analysis. J Ortho Res 10:826-835.

131. Kay A, Davison B, Badley E, Wagstaff S (1983), Hip Arthroplasty: Patient Satisfaction. Br J Rheumatol 22:243-249.

132. Keating EM, Ritter MA and Faris PM (1990), Strutures at Risk from Medially Placed Acetabular Screws. J Bone Joint Surg 72A:509-511.

133. Kershaw CJ, Atkins RM, Dodd CAF and Bulstrode CJK (1991), Revision Total Hip Arthroplasty for Aseptic Failure. J Bone Joint Surg 73B:564-568.

134. Kim YH and Kim VEM (1993), Uncemented Porous-Coated Anatomic Total Hip Replacement: Results at Six Years in a Consecutive Series. J Bone Joint Surg 75B:6-14.

135. Kobayashi S and Terayama K (1990), Radiology of Low-Friction Arthroplasty of the Hip: A Comparison of Socket Fixation Techniques. J Bone Joint Surg 72B:439-443.

136. Koeneman JB, Hansen TM and Beres K (1989), Three Dimensional Finite Element Analysis of the Hip Joint. Trans Orthopedic Research Society 13:223.

137. Koh TJ and Grabiner MD (1992), Cross Talk in Surface Electromyograms of Human Hamstring Muscles. J Orthopedic Research 10:701-709.

138. Kortike JG and Sick H (1983), Atlas of Sectional Human Anatomy Volume 2, Urban and Schwarzenberg, Baltimore - Munich.

139. Kwong LM, O'Connor DO, Sedlacek RC, Krushell RJ, Maloney WJ and Harris WH (1994), A Quantative In Vitro Assessment of Fit and Screw Fixation on the Stability of Cementless Hemispherical Acetabular Components. J Arthroplasty 9:163-170.

140. Lachiewicz PF, Suh PB and Gilbert JA (1989), In Vitro Initial Fixation of Porous-coated Acetabular Total Hip Components: A Biomechanical Comparative Study. J Arthroplasty 4:201-205.

141. Lamoreux LW (1971), Kinematic Measurements in the Study of Human Walking. Bull Prosthet Research 10-15:3-84.

142. Laurence M, Freeman MAR and Swanson SAV (1966), Biomechanics, Section of Orthopaedics. Proceedings of the Royal Society of Medicine 59:943-948.

143. Lehmkuhl LD and Smith LK (1983), Brunnstrom's Clinical Kinesiology, Fourth Edition, F.A. Davis Company, Philadelphia.

144. Letournel E and Judet R (1981), Fractures of the Acetabulum. Translated and edited by R. A. Elson, Chapter I, Surgical Anatomy, Publishers: Springer-Verlag, Berlin, Heidelberg, New York, pp 1-6.

145. Levens AS, Berkeley CE, Inman VT and Blosser JA (1948), Transverse Rotation of the Segments of the Lower Extremity in Locomotion. J Bone Joint Surg 30A:859-872.

146. Levy RN, Noble PC, Scheller A, Tullos H and Turner R (1988), Prolonged Fixation of Cemented Total Hip Replacement. Surgical Rounds for Orthopedics pp 15-22.

147. Levy RN, Volz RG, Kaufer H, Matthews LS, Capozzi J, Sturm P, Sherry H. (1985), Progress in Arthritis Surgery. With Special Reference to the Current Status of Total Hip Arthroplasty. Clin Orthop 200:299-321

148. Ling RS (1992), Clinical Experience with Primary Cemented Total Hip Arthroplasty. Chir Orgami Mov 77:373-381.

149. Lionberger D, Walker PS and Granholm J (1985), Effects of Prosthetic Acetabular Replacement on Strains in the Pelvis, J Orthopaedic Research, 3:372-379.

150. Litsky AS, Pophal SG and Noiles DG (1990), Initial Fixation of Uncemented Acetabular Prosthesis. Trans Society for Biomaterials 13:217.

151. Lombardi AV, Mallory TH and Vaughn BK (1993), The Performance of Cemented Femoral Components as a Function of their Metallic Composition. Orthopedic Trans 16:644.

152. Lord G, and Bancel P (1983), The Madreporic Cementless Total Hip Arthroplasty: New Experimental Data and a Seven-Year Follow-Up Study, Clin Orthop 176:67-76.

153. Lyons K, Perry J, Gronley JK, Barnes L and Antonelli D (1983), Timing and Relative Intensity of Hip Extensor and Abductor Muscle Action during Level and Stair Ambulation, Physical Therapy, 63:1597-1605.

154. Maloney WJ, O'Conner DO, Burke DW, Zalenski EB and Harris WH (1990), Micromotion of Cementless Hemispherical Acetabular Components Fixed with Screws: Quantification and the Effect of the Number of Screws on Stability. Transactions Society for Biomaterials p 173.

155. Maloney WJ, Peters P, Engh CA and Chandler H (1993), Severe Osteolysis of the Pelvis in Association with Acetabular Replacement without Cement. J Bone Joint Surg 75A:1627-1635.

156. Mankin JH (1974), Patterns of Cartilage Wear and Osteoarthritis of Hip, in "The Hip, Proceedings of the Second Scientific Meeting of The Hip Society" ed WH Harris, The C.V. Mosby Company.

157. Maquet PJ (1985), Biomechanics of the Hip As Applied to Osteoarthritis and Related Conditions. Springer-Verlag, New York.

158. Markolf KL and Amstutz HC (1983), Compressive Deformations of the Acetabulum During In Vitro Loading. Clin. Orthop. 173:284-292.

159. Matsusaka N (1986), Control of the Medial-lateral Balance in Walking. Acta Orthop Scand 57:555-559.

160. Mattingly DA, Hopson CN, Kahn A and Giannestras JJ (1985), Aspetic Loosening in Metal-Backed Acetabular Components for Total Hip Replacement. J Bone Joint Surg 67A: 387-391.

161. McKibbin B (1970), Anatomic Factors in the Stability of the Hip Joint in the New Born. J Bone Joint Surg 52B:148-159.

162. McLeish RD and Charnley J (1969), Abduction Forces in the One-Legged Stance. J Biomechanics 3:191-209.

163. Merchant AC (1965), Hip Abductor Muscle Force - An Experimental Study of the Influence of Hip Position with Particular Reference to Rotation. J Bone Joint Surg 47A:462-477.

164. Meryrueis JP, Camelo M, Masselot A, Cazenave A and Viandler JP (1986), La fixation du cotyle dans les prostheses totales cimentees de hanche Etude experimentale. Rev Chir Orthop 72:77-80.

165. Miller GJ, Petty W and Piotrowski G (1985), Strain Changes Due To Acetabular Cup Implantation. Trans Orthopedic Research Society 9:120.

166. Morscher EW, Dick W and Kernen V (1982), Cementless Fixation of Polyethylene Acetabular Component in Total Hip Arthroplasty. Arch Orthop Traumat Surg 99:223-230.

167. Mulroy RD and Harris WH (1990), The Effect of Improved Cementing Techniques on Component Loosening in Total Hip Replacement: A Minimum Five Year Follow-up. J Bone Joint Surg 72B:439-443.

168. Munuera L and Garcia-Cimbrelo E (1992), The Femoral Component In Low-Friction Arthroplasty After 10 Years. Clin Orthop 279:163-165.

169. Murray DW (1993), The Definition and Measurement of Acetabular Orientation. J Bone Joint Surg 75B:228-232.

170. Murray MP, Drought AB and Kory RC (1964), Walking Patterns of Normal Men. J Bone Joint Surg 46A:335-360.

171. Murray MP, Mollinger LA, Gardner GM and Sepic SB (1984), Kinematic and EMG Patterns during Slow, Free, and Fast Walking, J Orth. Research 2:272-280.

172. Nachbur B, Meyer RP, Verkkala K and Zurcher R (1979), The Mechanisms of Severe Arterial Injury in Surgery of the Hip Joint. Clin Orthop 141:122-133.

173. Nevitt MC, Epstein WV, Masen M and Murray WR (1984), Work Disability Before And After Total Hip Arthroplasty. Assesment of Effectiveness And Reducing Disability. Arthritis Rheum 4:410-421.

174. Noble PC (1983), Special Materials for the Replacement of Human Joints. Metals Forum 6:59-80.

175. Nunn D, Freeman MAR, Hill PF and Evans SJW (1989), The Measurement of Migration of the Acetabular Component of Hip Prostheses. J Bone Joint Surg 71B:629-631.

176. Oberlander W (1973), Die Beanspruchung des Menschlichen Huftgelenks, V. Die Verteilung der Knochendichte im Acetabulum. A. Anat Entwickl-Gesch 140:367-384.

177. Oberlander W, Kurrat HJ and Breul R (1978), Untersuchungen zur Ausdehnung der knöchernen Facies lunata. Z Orthop 116:675-682.

178. Onsten I, Besjakov J and Carlsson AS (1994), Improved Radiographic Survival of the Charnley Prosthesis in Rheumatoid Arthritis and Osteoarthritis. J Arthroplasty 9:3-8.

179. Oonishi H, Isha H and Hasegawa T (1983), Mechanical Analysis of the Human Pelvis and its Application to the Artificial Hip Joint By Means of the Three Dimensional Finite Element Method. J Biomechanics 16:427-444.

180. Oonishi H, Tatsumi M and Kawaguchi A (1986), Biomechanical Studies of Fixations of an Artificial Hip Joint Acetabular Socket by Means of 2D-FEM in "Biological and Biomechanical Performance of Biomaterials", ed P Christel, A Meunier and AJC Lee, Elsevier Science Publishers BV, Amsterdam, pp. 513-518

181. Patriarco AG, Mann RW, Simons SR and Mansour JM (1981), An Evaluation of the Approaches of Optimization Models in the Prediction of Muscle Forces During Human Gait. J Biomechanics 14:513-525.

182. Paul JP (1967), Forces at the Human Joint, PhD Thesis, University of Glasgow, Glasgow.

183. Paul JP (1971), Comparison of EMG Signals from Leg Muscles with the Corresponding Force Actions Calculated from Walkpath Measurements in "Proceedings of Conference on Human Locomotor Engineering", University of Sussex, London. pp. 13-28.

184. Paul JP (1976), Approaches to Design - Force actions transmitted by joints in the human body. Proc R Soc Lond B 192:163-172.

185. Paul JP (1976), Loading on Normal Hip and Knee Joints and on Joint Replacements, Advances in Artificial Hip and Knee Joint Technology, Eds., Schaldach, M., Hohmann, D., Thull, R., and Hein, F., Publishers: Springer-Verlag Berlin Heidelberg,

186. Paul JP (1993), Biomechanics of Joint Replacement Implants, Queen Margaret College, Edinburgh.

187. Paul JP, Radin EL and Rose RM (1972), Biomechanical Aspects of Orthopaedic Implants, Perspectives in "Biomedical Engineering" ed RM Kenedi, University Park Press, London, pp. 95-101.

188. Pedersen DR, Callaghan JJ, Olejniczak JP and Johnston RC (1995), Polyethylene Wear Rates for Five Different In-Vivo Acetabular Components Used Over a Five to Twenty-Two Year Period. Trans Orthopedic Research Society 18:115 - 20.

189. Pedersen DR, Crowninshield RD, Brand RA and Johnston RC (1982), An Axisymmetric Model of Acetabular Components in Total Hip Arthroplasty. J Biomechanics 15:305-315.

190. Pedotti A, Krishnan VV and Stark L (1978), Optimization of Muscle-Force Sequencing in Human Locomotion. Mathematical Biosciences 38: 57-76.

191. Penrod DD, Davy DT, Singh DP (1974), An Optimization Approach To Tendon Force Analysis. J Biomech 7:123-129.

192. Perona PG, Lawrence J, Paprosky WG, Patwardhan AG and Sattori AA (1992), Acetabular Micromotion as a Measure of Initial Implant Stability in Primary Hip Arthroplasty: An In Vitro Comparison of Different Methods of Initial Acetabular Component Fixation. J Arthroplasty 7:537-547.

193. Petrera P and Rubash HE (1994), Fixing the Cup. Instructional Course Lectures of the American Academy of Orthopedic Surgeons 43:393-407.

194. Petty W, Piotrowski G and Miller GJ (1981), In Vitro Evaluation of the Effect of Acetabular Prosthesis Implantation on Human Cadaver Pelves. Trans Orthopedic Research Society 5:73.

195. Pidhorz LE, Urban RM, Jacobs JJ, Sumner DR and Galante JO (1993), A Quantitative Study of Bone and Soft Tissues, in Cementless Porous-Coated Acetabular Components Retrieved at Autopsy. J Arthroplasty 8:213-225.

196. Pilliar RM, Lee JM and Maniatopoulos C (1986), Observations of the Effect of Movement on Bone Ingrowth into Porous-Surfaced Implants. Clin Orthop 208:108-113.

197. Rabischong P, Bonnel F, Oohishi H, Asaada P and Micaleff JP (1977), Comportement Biomecanique du Bassin a L'Etat Normal et Avec Prothese Total de Hanche. Rev Chir Orthop 63 (Suppl II):95-99

198. Ramakrishnan KK, Kadaba MP and Wootten ME (1990), Lower Extremity Joint Movements and Ground Reaction Torque in Adult Gait in "Biomechanics of Normal and Prosthetic Gait" ed JL Stein, ASME, BED-4:87-92.

199. Ramakrishnan KK, Kadaba MP, Wootten ME (1990), Lower Extremity Joint Movements and Ground Reaction Torque in Adult Gait. J Orthop Research 8:87-92

200. Rapperport DJ, Carter DR and Schurman DJ (1987), Contact Finite Element Stress Analysis of Porous Ingrowth Acetabular Cup Implantation, Ingrowth and Loosening. J Ortho. Res. 5:548-561.

201. Reiley MA, Bond D, Branick RI and Wilson EH (1984), Vascular Complications Following Total Hip Arthroplasty. Clin Orthop 186:23-28.

202. Resnick D and Niwayama G (1988), Anatomy of Individual Joints, in "Diagnosis of Bone and Joint Disorders, Second Edition, Vol. 2" W.B. Saunders Company, Philadelphia pp. 700-707.

203. Ring PA (1978), Five to Fourteen Year Interim Results of Uncemented Total Hip Arthroplasty, Clin Orthop 137:87-95.

204. Ring PA (l983), Uncemented Acetabular Replacement. Arch Orthop Trauma Surg 101:225-229.

205. Ritter MA and Campbell ED (1987), Long-term Comparision of the Charnley, Muller and Trapezoidal 28 Total Hip Prosthesis. J Arthroplasty 2:299-308.

206. Ritter MA, Faris PM, Keating EM and Brugo G (1992), Influential Factors in Cemented Acetabular Cup Loosening. J Arthroplasty 7:365-7.

207. Ritter MA, Keating EM, Faris PM and Brugs G (1990), Metal-Backed Acetabular Cups in Total Hip Arthroplasty. J Bone Joint Surg 72A:672-677.

208. Rivero DP, Skipro AK, Singh M, Urban RM and Galante JO (1987), Effect of Disodium Etidronate (EHDP) on Bone Ingrowth in a Porous Material. Clin Orthop 215:279-286.

209. Rohrle H, Scholten R, Sigolotto C and Sollbach W (1984), Joint Forces in the Human Pelvis-Leg Skeleton During Walking. J Biomechanics 17:409-424.

210. Rozin R, Robin GC, Magora A, Simkin A and Gonen B. (1971), Gait Analysis in Normal Individuals. Electromyography 2:183-190.

211. Rubenstein HJ, Manley MT, Badalamente and Stern L (1981), Trabecular Morphology and Biomechanics of the Human Pelvis. Proceedings: ASME Biomechanics Symposium, ed WC Van Buskirk and SLY Woo, 43:205-207.

212. Rubenstein J, Kellam J and McGonigal D (1982), Acetabular Fracture Assessment with Computerized Tomography. J Canadian Assoc of Radiologists 33:139-140.

213. Rubenstein J, Kellam J and McGonigal D (1982), Cross-Sectional Anatomy of the Adult Bony Acetabulum. J Canadian Assoc of Radiologists 33:137-138.

214. Rydell NW (1964), Forces in the Hip-Joint in "Biomechanics and Related Bio-engineering Topics" ed RM Kenedi, Pergamon Press, Oxford, London, Edinburgh, New York, Paris, Frankfurt, pp. 351-357.

215. Rydell NW (1966), Forces Acting on the Femoral Head-Prosthesis, Acta Orthopaedica Scandinavica Supplementum 88:16-20.

216. Saks BJ (1986), Normal Acetabular Anatomy for Acetabular Fracture Assessment: CT and Plain Film Correlation. Radiology 19:139-145.

217. Sarmiento A, Ebramzadeh E, Gogan WJ and McKellop HA (1990), Cup Containment and Orientation in Cemented Total Hip Arthroplasties. J Bone Joint Surg 72B:996-1002.

218. Schmalzried TP and Harris WH (1992), The Harris-Galante Porous-Coated Acetabular Component with Screw Fixation. J Bone Joint Surg 74A:1130-1139.

219. Schmalzried TP, Guttmann D, Grecula M and Amstutz HC (1994), The Relationship between the Design, Position, and Articular Wear of Acetabular Components Inserted without Cement and the Development of Pelvic Osteolysis. J Bone Joint Surg 76A:677-688.

220. Schmalzried TP, Jasty M and Harris WH (1992), Periprosthetic Bone Loss in Total Hip Arthroplasty: Polyethylene Wear Debris and the Concept of the Effective Joint Space. J Bone Joint Surg 74A:849-863.

221. Schmalzried TP, Wessinger SJ, Hill GE and Harris WH (1994), The Harris-Galante Porous Acetabular Component Press-Fit Without Screw Fixation. J Arthroplasty 9:235-242.

222. Schmidt F (1874) (as quoted by Clake and Amstutz (1975) who quote the reference: Uber Form und Mechanik des Multgelenkes. Dsch Z Chir Vol 3.

223. Schreiber A, Huggler AH, Dietschi C and Jacob H (1976), Complications after Joint Replacement - LongTerm Follow-up, Clinical Findings and Biomechanical Research in "Advances in Artificial Hip and Knee Joint Technology" ed M Schaldach and D. Hohmann, Springer-Verlag, New York.

224. Seireg A and Arvikar RJ (1973), A Mathematical Model for Evaluation of Forces in Lower Extremities of the Musculo-Skeletal System. J Biomechanics 6:313-326.

225. Seireg A and Arvikar RJ (1975), The Prediction of Muscular Load Sharing and Joint Forces in the Lower Extremities During Walking. J Biomechanics 8:89-102.

226. Shiavi R (1990), Electromyographic Patterns in Normal Adult Locomotion in "Gait in Rehabilitation", ed GL Smidt, Churchill Livingstone, New York, Edinburgh, London, Melbourne, pp.97-119.

227. Shiavi R, Champion S, Freeman F and Griffin P (1981), Variability of Electromyographic Patterns for Level-Surface Walking through a Range of Self-selected speeds. Bulletin of Prosthetic Research 18:5-14.

228. Shoenfeld NA, Stuchin SA, Pearl R, and Haveson S (1990), The Management of Vascular Injuries Assocaited with Total Hip Arthroplasty. J Vasc Surg 11:549-555.

229. Smidt GL (1971), Hip Motion and Related Factors in Walking. Physical Therapy 51:9-21.

230. Snorrason F and Karrholm J (1990), Primary Migration of Fully-Threaded Acetabular Prosthesis: A Roentgen Stereophotogrammetric Analysis. J Bone Joint Surg 72B:647-652.

231. Snorrason F and Karrholm, J (1990), Early Loosening of Revision Hip Arthroplasty. J Arthroplasty 5:217-229.

232. Snorrason F, Karrholm J and Holmgren C (1993), Fixation of Cemented Acetabular Prostheses: The Influence of Preoperative Diagnosis. J Arthroplasty 8:83-90.

233. Spector M (1987), Historical Review of Porous-Coated Implants. J Arthroplasty 2:163-177.

234. Stauffer RN (1982), Ten-Year Follow-Up Study of Total Hip Replacement with Particular Reference to Roentegenographic Loosening of the Components. J Bone Joint Surg 64A:970-82.

235. Steele GD and Bramblett CA (1988), The Anatomy and Biology of the Human Skeleton, Texas A & M University Press, College Station, pp. 190-215.

236. Stiehl JB, MacMillan E and Skrade DA (1991), Mechanical Stability of Porous-Coated Acetabular Components in Total Hip Arthroplasty. J Arthroplasty 6: 295-300.

237. Stromberg CN, Herberts P and Ahnfelt L (1988), Revision Total Hip Arthroplasty in Patients Younger than 55 Years Old. J Arthroplasty 3:47-59.

238. Sutherland CJ, Wilde AH, Borden LS and Marks KE (1982), A Ten Year Follow-up of One Hundred Consecutive Muller Curved-Stem Total Hip Replacement Arthroplasties. J Bone Joint Surg 64A:970-982.

239. Sutherland DH and Hagy JL (1972), Measurement of Gait Movements from Motion Picture Film. J Bone Joint Surg 54A:787-797.

240. Takedani H, Whiteside LA, White SE and Otani T (1991), The effect of Screws and Pegs on Cementless Acetabular Fixation. Trans Orthopedic Research Society 15:523.

241. Tallroth K, Slatis P, Ylinen P, Paavolainen P and Paavilainen T (1993), Loosening of Threaded Acetabular Components: Radiographic manifestations. J Arthroplasty 8:581-584.

242. Teinturier P, Terver S, Jaramillo CV and Besse JP (1983), La Biomechanique du cotyle. Rev. Chir. Orthop. 70:41-46.

243. Termote JL, Baert A, Crolla D, Palmers Y and Bulcke JA (1980), Computed Tomography of the Normal and Pathological Muscular System. Radiology 137:439-444.

244. Terver S, Dillingham M, Parker B, Bjorke A, Bleck EE, Levai JP, Teinturier P and Vaillet JF (1982), Etude de L'orientation Reelle du Cotyle Grace au Tomodensitometre Axial ou Scanner. J Radiol 63:167-173.

245. Tillmann B (1969), Die Beanspruchung des menschlichen Hüftgelenks. Z Anat Entwickl - Gesch 128: 329-349.

246. Tooke SM, Nugent PJ, Chotivichit A, Goodman W and Kabo JM (1988), Comparison of In Vivo Cementless Acetabular Fixation. Clin. Orthop. 235:253-260.

247. Van der Straaten JHM, Lohman AHM and van Linge B (1975), A Combined Electromyographic and Photographic Study of the Muscular Control of the Knee during Walking, J. Human Movement Studies 1:25-3l.

248. Vasu R, Carter DR and Harris WH (1982), Stress Distributions in the Acetabular Region - I. Before and After Total Joint Replacement. J Biomechanics l5:l55-l64.

249. Vrahas MS, Brand RA, Brown JD and Andrens JG (1990), Contribution of Passive Tissue to the Intersegmental Moments at the Hip. J Biomechanics 23:357-362.

250. Wagner M and Lawson TL (1982), Segmental Anatomy, Macmillan Publishing Co, New York.

251. Walmsley T (1928), The Articular Mechanism of the Diarthroses. J Bone Joint Surg 10B:40-45.

252. Wanivenhaus A, Zweymuller K (1988), 5-10-Jahresergebnisse mit einer Füßchenpfanne aus Keramik zur knochenzementfreien Implantation. Z Orthop 126:508-512.

253. Wasielewski RC, Cooperstein LA, Kruger MP, Rubash HE (1990), Acetabular Anatomy and the Transacetabular Fixation of Screws in Total Hip Arthroplasty. J Bone Joint Surg 72A:501-508.

254. Waters RL and Morris JM (1972), Electrical Activity of Muscles of the Trunk during Walking. J Anat 111:191-199.

255. White RE, Devlin TC and Teter KE (1994), Effect of Prosthesis and Instrument Manufacturing Tolerances on Surgical Technique of Bone Ingrowth Acetabulum, at "61st Annual Meeting of the Academy of Orthopedic Surgeons", New Orleans.

256. Wickiewicz TL, Roy RR, Powell PL and Edgerton VR (1983), Muscle Architecture of the Human Lower Limb. Clin Orthop 179:275-283.

257. Wilson-MacDonald J, Morscher E and Masar Z (1990a), Cementless Uncoated Polyethylene Acetabular Components in Total Hip Replacement. J Bone Joint Surg 72B:423-430.

258. Wilson-MacDonald J, Morscher E and Masar Z (1990b), Five-to-ten-year Results of 545 Cementless Polyethylene Acetabular Components in Total Hip Replacement. J Bone Joint Surg 72B:934-935.

259. Winter DA (1979), Biomechanics of Human Movement in "Kinesiological Electromyography", John Wiley & Sons, New York, Chichester, Brisbane, Toronto, Singapore, pp. 127-148.

260. Winter DA (1979), Overall Principle of Lower Limb Support During Stance Phase of Gait. J Biomechanics 13:923-927.

261. Winter DA and Marteniuk RG (1986), Is There a Normal Profile of EMG Activity in Gait?. Med Biol Eng Comput 24:337-343.

262. Winter DA and Yack HJ (1987), EMG Profiles During Normal Human Walking: Stide to Stride and Inter-Subject Variability, Electroenceph. Clin Neurophysid 67:402-411.

263. Yang JF and Winter DA (1985), Surface EMG Profiles during Different Walking Cadences in Humans. Electroencephalography and Clinical Neurophysiology 60:485-491.

264. Yochum TR and Rowe LJ (1987), Essentials of Skeletal Radiology. Williams and Wilkins, Baltimore, pp. 200-207.

265. Yoon YS and Mansour JM (1982), The Passive Elastic Moment at the Hip. J Biomechanics 15:905-910.

266. Zysset PK, Sonny M and Hayes WC (1994), Morphology-mechanical Property Relations in Trabecular Bone of the Osteoarthritic Proximal Tibia. J Arthroplasty 9:203-216

Appendix: COMPUTER DISK